

National Library  
of CanadaBibliothèque nationale  
du Canada

Canadian Theses Division    Division des thèses canadiennes

Ottawa, Canada  
K1A 0N4**PERMISSION TO MICROFILM — AUTORISATION DE MICROFILMER**

- Please print or type — Écrire en lettres moulées ou dactylographier

Full Name of Author — Nom complet de l'auteur

Kenneth Wayne Savigny

Date of Birth — Date de naissance

April 22, 1949

Country of Birth — Lieu de naissance

Canada

Permanent Address — Résidence fixe

Department of Civil Engineering  
University of Alberta  
Edmonton, Alberta T6G 2G7

Title of Thesis — Titre de la thèse

IN-SITU ANALYSIS OF NATURALLY OCCURRING  
CREEP IN ICE-RICH PERMAFROST SOIL

University — Université

University of Alberta

Degree for which thesis was presented — Grade pour lequel cette thèse fut présentée

Ph. D.

Year this degree conferred — Année d'obtention de ce grade

1980

Name of Supervisor — Nom du directeur de thèse

Dr. N. R. Morgenstern

Permission is hereby granted to the NATIONAL LIBRARY OF CANADA to microfilm this thesis and to lend or sell copies of the film.

L'autorisation est, par la présente, accordée à la BIBLIOTHÈQUE NATIONALE DU CANADA de microfilmer cette thèse et de prêter ou de vendre des exemplaires du film.

The author reserves other publication rights, and neither the thesis nor extensive extracts from it may be printed or otherwise reproduced without the author's written permission.

L'auteur se réserve les autres droits de publication; ni la thèse ni de longs extraits de celle-ci ne doivent être imprimés ou autrement reproduits sans l'autorisation écrite de l'auteur.

Date

May 13, 1980

Signature

K. Wayne Savigny

## NOTICE

The quality of this microfiche is heavily dependent upon the quality of the original thesis submitted for microfilming. Every effort has been made to ensure the highest quality of reproduction possible.

If pages are missing, contact the university which granted the degree.

Some pages may have indistinct print especially if the original pages were typed with a poor typewriter ribbon or if the university sent us a poor photocopy.

Previously copyrighted materials (journal articles, published tests, etc.) are not filmed.

Reproduction in full or in part of this film is governed by the Canadian Copyright Act, R.S.C. 1970, c. C-30. Please read the authorization forms which accompany this thesis.

**THIS DISSERTATION  
HAS BEEN MICROFILMED  
EXACTLY AS RECEIVED**

## AVIS

La qualité de cette microfiche dépend grandement de la qualité de la thèse soumise au microfilmage. Nous avons tout fait pour assurer une qualité supérieure de reproduction.

S'il manque des pages, veuillez communiquer avec l'université qui a conféré le grade.

La qualité d'impression de certaines pages peut laisser à désirer, surtout si les pages originales ont été dactylographiées à l'aide d'un ruban usé ou si l'université nous a fait parvenir une photocopie de mauvaise qualité.

Les documents qui font déjà l'objet d'un droit d'auteur (articles de revue, examens publiés, etc.) ne sont pas microfilmés.

La reproduction, même partielle, de ce microfilm est soumise à la Loi canadienne sur le droit d'auteur, SRC 1970, c. C-30. Veuillez prendre connaissance des formules d'autorisation qui accompagnent cette thèse.

**LA THÈSE A ÉTÉ  
MICROFILMÉE TELLE QUE  
NOUS L'AVONS REÇUE**



THE UNIVERSITY OF ALBERTA

IN SITU ANALYSIS OF NATURALLY OCCURRING  
CREEP IN ICE-RICH PERMAFROST SOIL

by



K. WAYNE SAVIGNY

A THESIS

SUBMITTED TO THE FACULTY OF GRADUATE STUDIES  
AND RESEARCH IN PARTIAL FULFILLMENT OF THE  
REQUIREMENTS FOR THE DEGREE OF  
DOCTOR OF PHILOSOPHY

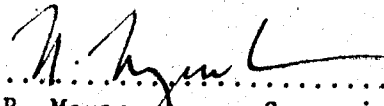
DEPARTMENT OF CIVIL ENGINEERING

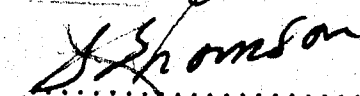
EDMONTON, ALBERTA

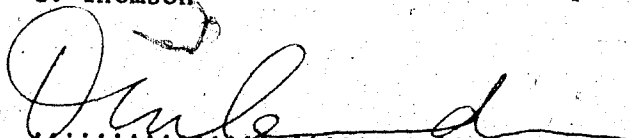
SPRING, 1980


THE UNIVERSITY OF ALBERTA  
FACULTY OF GRADUATE STUDIES AND RESEARCH

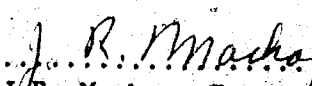
The undersigned certify that they have read, and recommend to the Faculty of Graduate Studies and Research, for acceptance, a thesis entitled 'IN SITU ANALYSIS OF NATURALLY OCCURRING CREEP IN ICE-RICH PERMAFROST SOIL' submitted by K. Wayne Savigny in partial fulfillment of the requirements for the degree of Doctor of Philosophy in Civil Engineering.

  
.....  
N.R. Morgenstern, Supervisor

  
.....  
S. Thomson

  
.....  
D.M. Cruden

  
.....  
N.W. Rutter

  
.....  
J.R. Mackay, External Examiner

Date .. April 14, 1980 .....

To Margie  
who made this possible

## ABSTRACT

This thesis provides the first documented, comprehensive, in situ study of naturally occurring creep in ice-rich permafrost soil.

The surficial geology of the Great Bear River area was studied in order to select the most suitable field site. A steep slope at km 7.2 of Great Bear River was chosen. The stratigraphy of the slope includes an anomalously thick section of ice-rich glaciolacustrine clay, and, coincidentally, it is situated at the proposed Arctic Gas Crossing of Great Bear River.

A field programme was undertaken in order to obtain continuous, undisturbed samples, and to install borehole inclinometers, piezometers and thermistors. Details of this programme are reported because many aspects were innovative and lacked precedence.

Deformation data, sub-permafrost pore pressure data and temperature data are reported and analysed. The scale of slope deformations was found to be marginally greater than the accuracy of the inclinometer system. The system accuracy was carefully verified and new data analysis techniques were developed. Steady state creep velocities in the order of 0.25 to 0.30 cm/year are indicated in the ice-rich glaciolacustrine clay.

The results of triaxial creep tests on undisturbed samples of glaciolacustrine clay, and non-linear finite element analysis of steady state creep deformations in the slope suggest that a simple power law with a coefficient of  $0.33 \times 10^{-8}$  year  $\text{kPa}^3$  and an exponent of 3.0 accurately simulates both the form and magnitude of in situ steady state creep deformations.

## ACKNOWLEDGEMENTS

The encouragement and unqualified support of my parents gave me the desire and the opportunity to undertake this work; to Mom and Dad, I am deeply grateful.

The research programme reported here was carried out in the Department of Civil Engineering, University of Alberta, under the supervision of Professor N.R. Morgenstern. I would like to express my sincere appreciation and thanks to Professor Morgenstern for proposing the thesis topic, and for his encouragement, guidance and seemingly endless enthusiasm.

I am grateful for the helpful suggestions and advice given by Professor D.M. Cruden, Professor Z. Eisenstein, Professor N.W. Rutter, and Professor S. Thomson on many occasions during the research programme. Professor J.R. Mackay, Dr. G.E. Green, Dr. O.L. Hughes and Dr. E.C. McRoberts also provided valuable contributions in specific areas.

I wish to thank the University of Alberta and the Transportation Development Agency for personal financial support between 1973 and 1978. The Geological Survey of Canada supported the geological mapping of the Great Bear River area. Northern Engineering Services Ltd. supported the site investigation activities. Northern Engineering Services Ltd. and the National Research Council of Canada jointly sponsored the many site visits for instrument monitoring. Laboratory testing and computer work were also carried out with the support of the National Research Council of Canada.

Thurber Consultants Ltd. provided assistance in typing,

drafting and duplication of the manuscript. This generous support, the encouragement of the staff, and especially the many extra hours given by Ms. M. McMann and Ms. C. Starr are greatly appreciated.

Special thanks are extended to the staff within the Department of Civil Engineering, in particular, Mr. A. Muir and Mr. O. Wood.

Many colleagues contributed through stimulating discussions. Notable among these are Dr. S. DaFontoura, Dr. M. Dusseault, Dr. P. Kaiser, Mr. J. Simmons and Dr. J. Weaver. Mr. P. Weerdenburg gave many hours of assistance and direction in the finite element analysis. To each of these individuals, and to others, unnamed, I extend my thanks.

Ms. Barbara Esdale edited the manuscript and provided many valuable comments and suggestions. Her contribution is greatly appreciated.

Dr. W.D. Roggensack provided guidance in the laboratory and Dr. D.C. Seago aided in the design of the laboratory equipment and assisted on several occasions in the field. Both individuals gave freely and unselfishly of their time whenever called upon, whether the task involved assistance or a listening ear over a cup of coffee. To both, who were and remain valued colleagues, I extend my utmost appreciation and thanks.

In closing, I would like to express profound thanks to my wife, Margaret, for her immense contribution over the past seven years. Many of the field and laboratory components could not have been completed without her assistance, many of the frustrations could not have been overcome without her patience and understanding, and many of the hurdles could not have been surmounted without her love and encouragement.

## TABLE OF CONTENTS

	Page
Release Form	i
Title Page	ii
Approval Sheet	iii
Dedication	iv
Abstract	v
Acknowledgements	vi
Table of Contents	viii
List of Tables	xiv
List of Figures	xv
List of Photographic Plates	xxiii
CHAPTER I	
INTRODUCTION	1
1.1 Scope of Thesis	3
CHAPTER II	
GEOLOGY OF THE GREAT BEAR RIVER AREA	5
2.1 Introduction	5
2.2 Historical Perspective	6
2.3 Physiography	7
2.3.1 Introduction	7
2.3.2 Mackenzie Plain	7
2.3.3 Franklin Mountains	8
2.4 Stratigraphy	9
2.4.1 Introduction	9
2.4.2 Paleozoic and Mesozoic	10
2.4.3 Cenozoic - Tertiary	11
2.4.4 Cenozoic - Quaternary	13

	Page
2.5 Geomorphic Development	25
2.6 Selection of the Field Instrumentation Site	29
CHAPTER III FIELD METHODS AND GEOTECHNICAL PROPERTIES OF GREAT BEAR RIVER AREA SOILS	44
3.1 Introduction	44
3.2 Site Description	45
3.3 Equipment and Materials for the Field Instrumentation Programme	47
3.3.1 Drill and Support Equipment	48
3.3.2 Sampling and Support Equipment	50
3.3.3 Helicopters	52
3.3.4 Drilling Fluid	53
3.3.5 Grout	56
3.4 Drilling and Instrumentation Programme	57
3.4.1 Mobilization	57
3.4.2 Hole Location and Site Preparation	58
3.4.3 Drilling and Sampling	59
3.5 Sample Handling and Logging	67
3.6 Instrument Installation Procedures	69
3.6.1 Inclimeters and Thermistor Strings	69
3.6.2 Piezometers	73
3.7 Surveys	75
3.8 Site Geology	75
3.9 Geotechnical Properties	78
3.9.1 Direct Shear (DS) Tests on Thawed Alluvial Clay	78



	Page
3.9.2 Consolidated Undrained Triaxial Compression (CUT) Tests on Thawed Glaciodeltaic Sand	79
3.9.3 CUT and DS Tests on Thawed Glaciolacustrine Clay	81
3.9.4 DS Tests on Frozen Glaciolacustrine Clay	83
<b>CHAPTER IV</b>	
<b>FIELD DATA AND DELINEATION OF <u>IN SITU</u> CREEP PROPERTIES</b>	114
4.1 Introduction	114
4.2 Thermistors	115
4.2.1 Specifications	115
4.2.2 Reading Procedure and Data	116
4.2.3 Hydration of Grout	117
4.2.4 Thermal Regime	118
4.3 Piezometers	121
4.3.1 Specifications	121
4.3.2 Reading Procedure and Data	122
4.3.3 Sub-permafrost Pore Pressures	123
4.4 Inclinometers	124
4.4.1 Introduction	124
4.4.2 Types of Inclinometers	124
4.4.3 Inclinometer Specifications	127
4.4.4 Monitoring Procedure	128
4.4.5 Data Analysis Procedure	130
4.4.6 Inclinometer Data	132
4.4.7 Inclinometer Accuracy	132
4.4.8 External Factors Affecting Measured Deformations	140

	Page
4.4.9 Delineation of Creep and Shear Deformations	150
<b>CHAPTER V CREEP BEHAVIOUR OF UNDISTURBED GLACIOLACUSTRINE CLAY SAMPLES UNDER SIMULATED FIELD CONDITIONS</b>	<b>192</b>
5.1 Introduction	192
5.2 Rheological Properties of Ice	193
5.3 Rheological Properties of Reconstituted Frozen Soils	197
5.4 Rheological Properties of Natural Permafrost Soils	199
5.5 Constant Stress Triaxial Creep Tests	202
5.5.1 Laboratory Equipment	203
5.5.2 Sample Description	205
5.5.3 Sample Preparation	206
5.5.4 Testing Procedure	208
5.5.5 Method of Analysis and Data Processing	209
5.5.6 Test Results	211
5.5.7 Physio-Mechanical Interpretation of Premature Failure	215
5.5.8 Assessment of Results	218
<b>CHAPTER VI IN SITU CREEP ANALYSIS</b>	<b>239</b>
6.1 Introduction	239
6.2 Finite Element Programme	239
6.2.1 Solution Method	240
6.2.2 Multiaxial Stress-Strain Relations	240
6.2.3 Solution Technique	242
6.2.4 Time Increment Determination	243

	Page	
6.3	Finite Element Mesh	244
6.4	Boundary Conditions	245
6.5	Material Properties	245
6.6	Elastic Analysis	246
6.7	First Creep Analysis - Uniform Creep Properties	246
	6.7.1 Material Properties	246
	6.7.2 Results of the First Creep Analysis	247
6.8	Second Creep Analysis - Uniform Creep Properties	248
	6.8.1 Material Properties	248
	6.8.2 Results of the Second Creep Analysis	249
6.9	Third Creep Analysis - Creep in Glacio-lacustrine Clay Lithofacies Only	250
	6.9.1 Material Properties	250
	6.9.2 Results of Third Creep Analysis	250
6.10	Assessment of Results	252
CHAPTER VII	CONCLUSIONS	265
7.1	Introduction	265
7.2	Conclusions and Recommendations of this Study	266
7.3	General Conclusions and Recommendations for Further Study	270
	7.3.1 Naturally Occurring Creep	270
	7.3.2 The Creep Process in Ice-Rich Permafrost Soils	272

	Page
REFERENCES CITED	276
APPENDIX A	
GEOLOGICAL FIELD DATA FROM THE GREAT BEAR RIVER AREA	287
A.1 Introduction	287
A.2 Field and Laboratory Technique	288
A.3 Permafrost Classification System	288
A.3.1 Introduction	288
A.3.2 Pore Ice	289
A.3.3 Segregated Ice	289
A.3.4 Reticulate Ice	289
A.3.5 Stratified Ice	289
A.4 Summary of Measured Sections, Test Hole Logs and Test Pit Logs from the Great Bear River Area	290
APPENDIX B	
DETAILED TEST HOLE LOGS FROM THE FIELD INSTRUMENTATION SITE	343
B.1 Explanation of Terms and Symbols Used on Test Hole Logs	343
B.2 Test Hole Logs	346
APPENDIX C	
THERMISTOR DATA	369
C.1 Thermistor Data from Hole GB1A	369
C.2 Thermistor Data from Hole GB2	375
C.3 Thermistor Data from Hole GB3	382
APPENDIX D	
SUMMARY OF LABORATORY TEST DATA	386
D.1 Direct Shear Tests	386
D.2 Triaxial Compression Tests	407
D.3 Triaxial Creep Tests	417

## LIST OF TABLES

Table	Description	Page
2.1	Guide to the location of test holes and measured sections along Great Bear River	31
2.2	Exposed bedrock formations in the Great Bear River area	33
2.3	Succession and lithology of Quaternary sediments in the Great Bear River area.	34
3.1	Drill rod and casing specifications	89
3.2	Specifications for drilling mud	89
4.1	Schedule of instrument monitoring	156
4.2	Thermistor installation data	157
4.3	Climatic data for Fort Norman, N.W.T.	158
4.4	Piezometer installation and calibration data	159
4.5	Inclinometer specifications	159
4.6	Example of statistical analysis of inclinometer data	160
B.1	Graphic soil symbols used on test hole logs	345
D.1	Summary of direct shear test data	387
D.2	Summary of consolidated undrained triaxial compression test data	408
D.3	Engineering properties of constant stress triaxial creep test samples	418
D.4	Summary of constant stress triaxial creep test data (primary stage)	419
D.5	Summary of constant stress triaxial creep test data (assumed secondary stage)	420

## LIST OF FIGURES

Figure	Description	Page
2.1	Physiography of the Great Bear River area	35
2.2	Field locations along Great Bear River	36
2.3	Field locations along Great Bear River in the Fort Norman to Brackett River area	37
2.4	Bedrock geology in the Great Bear River area	38
2.5	Cross-section of Tertiary and Quaternary stratigraphy between km 0 and km 16 of Great Bear River	39
2.6	Surficial geology in the Great Bear River area	40
2.7	Cross section of Quaternary stratigraphy between km 0 and 75 of Great Bear River	41
2.8	Plasticity chart for fine-grained soils from the Great Bear River area	42
2.9	Textural classification for the less than 2.0 mm size fraction of soils from the Great Bear River area	43
3.1	Site plan, proposed Arctic Gas crossing of Great Bear River (left bank)	90
3.2	Stratigraphic cross-section, proposed Arctic Gas crossing of Great Bear River (left bank)	91
3.3	Modified CRREL core barrel and assembly	92
3.4	Wire line core barrel assembly (base drawing courtesy Mobile Augers and Research Ltd., Edmonton, Alberta)	93
3.5	Types of sample boxes used to store and transport undisturbed frozen cores	94
3.6	Freezing point depression curve for KCl drilling mud additive	95
3.7	Mud system on the Heli Drill 500	96
3.8	Grout shoe assembly and grouting procedure for inclinometers	97
3.9	Installed piezometer assembly	98
3.10	Summary of textural data for hole GB1	99

Figure	Description	Page
3.11	Summary of basic engineering data for hole GB1	100
3.12	Summary of textural data for hole GB2	101
3.13	Summary of basic engineering data for hole GB2	102
3.14	Summary of textural data for hole GB3	103
3.15	Summary of basic engineering data for hole GB3	104
3.16	Peak strength envelope from direct shear tests on thawed alluvial clay	105
3.17	Residual strength envelope from direct shear tests on thawed alluvial clay	105
3.18	Peak strength envelope from consolidated undrained triaxial tests on thawed glaciodeltaic sand	106
3.19	Peak strength envelope from consolidated undrained triaxial tests on thawed glaciolacustrine clay	106
3.20	Peak strength envelope from direct shear tests on thawed glaciolacustrine clay	107
3.21	Residual strength envelope from direct shear tests on thawed glaciolacustrine clay	107
3.22	Peak strength envelope from direct shear tests on frozen glaciolacustrine clay	108
3.23	Apparent cohesion intercept as a function of time to failure	109
3.24	Residual strength envelope from direct shear tests on frozen glaciolacustrine clay	110
4.1	Temperature variation subsequent to grouting in hole GB1A	161
4.2	Temperature variation subsequent to grouting in hole GB2	162
4.3	Temperature variation subsequent to grouting in hole GB3	163
4.4	Temperature gradient for hole GB1A	164
4.5	Temperature gradient for hole GB2	165
4.6	Temperature gradient for hole GB3	166

Figure	Description	Page
4.7	Thermal cross-section, proposed Arctic Gas crossing of Great Bear River (left bank)	167
4.8	Sub-permafrost pore pressures as indicated by piezometer in hole GB3A	168
4.9	A-direction (parallel-to-slope) inclinometer data for hole GB1A	169
4.10	B-direction (traverse-to-slope) inclinometer data for hole GB1A	170
4.11	A-direction inclinometer data for hole GB2	171
4.12	B-direction inclinometer data for hole GB2	172
4.13	Inclinometer data for hole GB2 resolved into the true parallel-to-slope direction	173
4.14	Inclinometer data for hole GB2 resolved into the true transverse-to-slope direction	174
4.15	A-direction (parallel-to-slope) inclinometer data for hole GB3	175
4.16	B-direction (transverse-to-slope) inclinometer data for hole GB3	176
4.17	Results of repeatability tests in hole GB1A	177
4.18	Results of repeatability tests in hole GB3	178
4.19	Inclinometer calibration frame	179
4.20	Resolution test results - Test RE04	180
4.21	Resolution test results - mean values from all tests	181
4.22	Stabilization of inclinometer readings in response to a sudden step temperature	182
4.23	Temperature drift characteristics of inclinometer	183
4.24	Plots of standard deviation of SUMS <u>versus</u> time for each inclinometer casing	184
4.25	Rate of change of standard deviation of A-direction SUMS for each inclinometer casing	185
4.26	Plots of standard deviation of A-direction SUMS <u>versus</u> time for different lithofacies	186



Figure	Description	Page
4.27	Schematic representation of heave and settlement of inclinometer casing and grout column	187
4.28	Typical plots of deflection <u>versus</u> time at different depths in glaciolacustrine clay in GB1A	188
4.29	Velocity profiles for hole GB1A	189
4.30	Velocity profiles for hole GB2	190
4.31	Velocity profiles for hole GB3	191
5.1	Typical constant axial stress creep curves (after Vialov, 1965)	225
5.2	Schematic layout of specially designed triaxial cell used for creep tests	226
5.3	Schematic layout of creep testing system	227
5.4	Typical creep test data plotted to evaluate transient and steady state components (after Roggensack, 1977)	228
5.5	Results of creep test 8C on frozen glaciolacustrine clay	229
5.6	Creep rate data for ice-rich glaciolacustrine clay from the Great Bear River area	230
5.7	Creep rate data for ice-rich glaciolacustrine clay from various locations in the Mackenzie River Valley, N.W.T.	231
6.1	Finite element mesh	253
6.2	Orientations of principal stresses for elastic solution under gravity loading	254
6.3	Contours of effective stress (Odquist, 1966) for elastic solution under gravity loading	255
6.4	Comparison of measured and predicted steady state creep velocities in test hole GB1A	256
6.5	Comparison of measured and predicted steady state creep velocities in test hole GB2	257
6.6	Comparison of measured and predicted steady state creep velocities in test hole GB3	258

Figure	Description	Page
6.7	Comparison of creep relations used in numerical analysis	259
6.8	Deformed grid for steady state creep in both the sand and the medium to high plastic clay lithofacies	260
6.9	Contours of effective stress (Odqvist, 1966) for steady state creep in both the sand and the medium to high plastic clay lithofacies	261
6.10	Deformed grid for steady state creep in the medium to high plastic clay lithofacies only	262
6.11	Contours of effective stress (Odqvist, 1966) for steady state creep in the medium to high plastic clay lithofacies only	263
6.12	Contours of horizontal stress for steady state creep in the medium to high plastic clay lithofacies only	264
C.1	Thermistor 1 - hole GB1A	370
C.2	Thermistor 2 - hole GB1A	370
C.3	Thermistor 3 - hole GB1A	371
C.4	Thermistor 4 - hole GB1A	371
C.5	Thermistor 5 - hole GB1A	372
C.6	Thermistor 6 - hole GB1A	372
C.7	Thermistor 7 - hole GB1A	373
C.8	Thermistor 8 - hole GB1A	373
C.9	Thermistor 9 - hole GB1A	374
C.10	Thermistor 1 - hole GB2	375
C.11	Thermistor 2 - hole GB2	376
C.12	Thermistor 3 - hole GB2	377
C.13	Thermistor 4 - hole GB2	377
C.14	Thermistor 5 - hole GB2	378
C.15	Thermistor 6 - hole GB2	378

Figure	Description	Page
C.16	Thermistor 7 - hole GB2	379
C.17	Thermistor 8 - hole GB2	379
C.18	Thermistor 9 - hole GB2	380
C.19	Thermistor 10 - hole GB2	380
C.20	Thermistor 11 - hole GB2	381
C.21	Thermistor 12 - hole GB2	381
C.22	Thermistor 4 - hole GB3	383
C.23	Thermistor 5 - hole GB3	383
C.24	Thermistor 6 - hole GB3	384
C.25	Thermistor 7 - hole GB3	384
C.26	Thermistor 8 - hole GB3	385
D.1	Direct Shear Test 1 (frozen)	388
D.2	Direct Shear Test 2 (frozen)	389
D.3	Direct Shear Test 3 (frozen)	390
D.4	Direct Shear Test 4 (frozen)	391
D.5	Direct Shear Test 5 (frozen)	392
D.6	Direct Shear Test 6 (frozen)	393
D.7	Direct Shear Test 7 (multistage)	394
D.8	Direct Shear Test 8 (multistage)	395
D.9	Direct Shear Test 9 (multistage)	396
D.10	Direct Shear Test 10 (multistage)	397
D.11	Direct Shear Test 11 (multistage)	398
D.12	Direct Shear Test 12 (multistage)	399
D.13	Direct Shear Test 13	400
D.14	Direct Shear Test 14	401
D.15	Direct Shear Test 15	402

Figure	Description	Page
D.16	Direct Shear Test 16	403
D.17	Direct Shear Test 17	404
D.18	Direct Shear Test 18	405
D.19	Direct Shear Test 19	406
D.20	Triaxial Compression Test 1	409
D.21	Triaxial Compression Test 2	409
D.22	Triaxial Compression Test 3	410
D.23	Triaxial Compression Test 4	410
D.24	Triaxial Compression Test 5	411
D.25	Triaxial Compression Test 6	411
D.26	Triaxial Compression Test 8	412
D.27	Triaxial Compression Test 9	412
D.28	Triaxial Compression Test 10	413
D.29	Triaxial Compression Test 11	413
D.30	Triaxial Compression Test 12	414
D.31	Triaxial Compression Test 13	414
D.32	Triaxial Compression Test 14	415
D.33	Triaxial Compression Test 15	415
D.34	Triaxial Compression Test 16	416
D.35	Triaxial Compression Test 17	416
D.36	Triaxial Creep Test 3	421
D.37	Triaxial Creep Test 4	422
D.38	Triaxial Creep Test 5	423
D.39	Triaxial Creep Test 6	424
D.40	Triaxial Creep Test 7 (stage one of three)	425
D.41	Triaxial Creep Test 7 (stage two of three)	426

Figure	Description	Page
D.42	Triaxial Creep Test 7 (stage three of three)	427
D.43	Triaxial Creep Test 8 (stage one of three)	428
D.44	Triaxial Creep Test 8 (stage two of three)	429
D.45	Triaxial Creep Test 8 (stage three of three)	430
D.46	Triaxial Creep Test 9	431
D.47	Triaxial Creep Test 10 (stage one of two)	432
D.48	Triaxial Creep Test 10 (stage two of two)	433
D.49	Triaxial Creep Test 11	434
D.50	Triaxial Creep Test 12 (stage one of two)	435
D.51	Triaxial Creep Test 12 (stage two of two)	436
D.52	Triaxial Creep Test 13 (NES 3-11)	437
D.53	Triaxial Creep Test 14 (NES 3-8)	438
D.54	Triaxial Creep Test 15 (NES 3-10)	439

PHOTOGRAPHIC PLATES

Plate	Description	Page
3.1	Heli Drill 500 during assembly at test hole GB1	111
3.2	Assembled Heli Drill 500 in operation at test hole GB1	111
3.3	Severe desiccation resulting from an excess of drilling fluid remaining inside core wrapping during storage (GB2 Core 29).	112
3.4	Pre-thaw relationship of slickensided clay and ice vein (GB2 Core 18).	112
3.5	Slickensided surface of soil ped facing ice vein in Plate 3.4 (GB2 Core 18).	113
3.6	Steeply dipping ice vein in glaciodeltaic sand (GB1 Core 21)	113
5.1	Post-failure appearance of creep test 3 (GB1 Core 57).	232
5.2	Post-failure appearance of creep test 3 (GB1 Core 57). Failure planes generally follow the soil-ice interfaces of primary ice veins, with relatively little shear through frozen soil.	232
5.3	Post-failure appearance of creep test 4 (GB1 Core 56). The failure plane follows the soil-ice interface of a primary ice vein.	233
5.4	Post-failure appearance of creep test 5 (GB1 Core 58). The shear plane cuts through frozen soil at the top and bottom of the sample, but follows soil-ice interfaces of the primary ice vein through the middle portion of the sample.	233
5.5	The post-failure condition of creep test 5 (GB1 Core 58) indicates some deformation took place along secondary ice veins, leaving the sample with a blocky appearance.	234
5.6	Creep test 9 (GB1 Core 43) prior to assembly.	234
5.7	Post-failure condition of creep test 6 (GB1 Core 38). Deformation is evident along most secondary ice veins imparting a blocky, post-failure appearance. Shear planes developed as deformation along several secondary ice veins coalesced by shear through frozen soil.	235

Plate	Description	Page
5.8	Post-failure, close-up view of creep test 9 (GB1 Core 43) showing the magnitude of deformation along a secondary ice vein not associated with the main failure planes.	235
5.9	Post-failure appearance of creep test 7 (GB1 Core 43).	236
5.10	Creep test 12 (GB1 Core 60) prior to assembly.	236
5.11	Post-testing appearance of creep test 12 (GB1 Core 60) - longitudinal view. Vertical ice veins developed during testing as indicated by comparison with Plate 5.10.	237
5.12	Post-testing appearance of creep test 12 (GB1 Core 60) - cross-sectional view.	237
5.13	Sample of segregated ice (GB2 Core 4) similar to creep test 11 (GB2 Core 4).	238
5.14	Post-testing appearance of creep test 11 (GB2 Core 4).	238
7.1	Evidence of <u>in situ</u> deformation along secondary ice veins (GB1 Core 58).	275
7.2	Evidence of <u>in situ</u> deformation along a primary ice vein (GB1 Core 53 Sample 5).	275
7.3	Evidence of <u>in situ</u> deformation along secondary ice veins (GB1 Core 53 Sample 6).	275

## CHAPTER I

### INTRODUCTION

" We are now at our last frontier. It is a frontier that all of us have read about, but few of us have seen. Profound issues, touching our deepest concerns as a nation, await us there.

The North is a frontier, but it is a homeland too, the homeland of the Dene, Inuit and Metis, as it is also the home of the white people who live there. And it is a heritage, a unique environment that we are called upon to preserve for all Canadians..

The decisions we have to make are not, therefore, simply about northern pipelines. They are decisions about the protection of the northern environment and the future of northern peoples." (Berger, 1977, p.1 of introductory letter)

With these words, Mr. Justice Thomas R. Berger began his report of the Mackenzie Valley Pipeline Inquiry, a summary of evidence from 300 experts on northern conditions, northern environment and northern peoples, and from nearly 1000 northern residents in 35 communities across the Western Arctic. His report dealt an unprecedented blow to proponents of industrial development who viewed oil and gas resources of the Mackenzie Valley and the Arctic coastal region as a panacea for both the deteriorating North American energy supply and the economic ills of these northern regions. Many reasons may be cited as to why both Mr. Justice Berger and the National Energy Board (National Energy Board, 1977).



recommended against construction of a Mackenzie Valley Pipeline and an energy corridor across the Arctic coastal region, not the least of which were engineering and construction uncertainties.

The vast oil and gas potential and abundance of other minerals through the Canadian Arctic and other polar regions have been long established, however impetus for their development has been sporadic. When real demand for these resources became apparent in the 1970's, the technological challenges confronting designers and prospective builders were awesome. These were not limited to the scale of the megaprojects, their remote setting or harsh environment, but included aspects of the projects and their design which lacked any precedent and required innovative engineering concepts because of the presence of perennially frozen soils. One of the most important aspects to be addressed was that of naturally occurring creep in permafrost soil.

Knowledge that ice creeps under any sustained loading is fundamental. Since ice is present in pore spaces and, commonly, as disseminated structures in permafrost soil, it is a logical deduction that such soils should exhibit creep properties under conditions of sustained loading. Moreover, creep properties are likely to be more pronounced in soils with higher ice contents - especially those in which the volume of ice exceeds the volume of voids.

Some measure of industrial development is imminent in Northern Canada, and it will almost certainly require major structures to be founded on or within permafrost soils subject to

gravity loading. Design of these structures may have to accommodate existing in situ creep velocities. The objective of the research programme reported here is to provide the first documented, comprehensive, in situ study of naturally occurring creep in ice-rich permafrost soils. The components of the research programme include detailed surficial geology mapping to facilitate selection of the best possible field investigation site, a carefully planned and executed site investigation programme including drilling, sampling and instrumentation, a two year instrument monitoring period, extensive laboratory testing of undisturbed permafrost soils, and numerical analysis of in situ deformation patterns using empirical parameters from the laboratory programme.

1.1 Scope of Thesis

Chapter II presents the results of detailed surficial geology mapping along Great Bear River, N.W.T. This was carried out in order to determine the most suitable field site for in situ measurement of naturally occurring creep deformations.

The field investigation, which includes drilling, sampling, instrumentation and logistical procedures, is presented in Chapter III. A detailed site description and geotechnical properties of the soils are also presented in this chapter.

All field data are reported and analyzed in Chapter IV.

The results of laboratory creep tests on undisturbed permafrost soil are presented in Chapter V. In addition, an attempt is made to interpret the results of other laboratory programmes

4

carried out on similar materials. All data are considered in determining empirical relationships of creep behaviour.

Empirical relationships determined in Chapter V are used in non-linear finite element creep analyses in Chapter VI in an attempt to predict the observed field velocities.

A brief summary of the salient points from Chapters II through VI is given in Chapter VII. The overall conclusions from the study are presented, and recommendations for further study are outlined.

Field and laboratory data are appended.

## CHAPTER II

### GEOLOGY OF THE GREAT BEAR RIVER AREA

"The information which they gave respecting the river, ...that it would require several winters to get to the sea, and that old age would come upon us before the period of our return: we were also to encounter monsters of such horrid shapes and destructive powers as could only exist in their wild imaginations. They added, besides, that there were two impassible falls in the river, the first of which was about thirty days march from us."<sup>1</sup>

#### 2.1 Introduction

The surficial geology and limited bedrock geology in the Great Bear River area were mapped by the writer in 1973, with brief visits to specific locations in 1975, 1976, and 1977. There were two major objectives to this study. The first was to describe the stratigraphy of surficial deposits and the general scheme of major, late Quaternary events. The second was to select the most suitable site for in situ study of naturally occurring creep processes.

---

<sup>1</sup>Mackenzie, A. (1971 ed. pp. 33-34) This is an account of conditions along Mackenzie River between Ft. Norman, N.W.T. and the "Frozen" (Arctic) Ocean as related to Sir Alexander Mackenzie by natives at Ft. Norman during his descent of the Mackenzie in July, 1789. Sir Alexander Mackenzie was the first explorer to visit the Ft. Norman-Great Bear River area.

In this chapter, the results of the geological investigation are presented, and the criteria for selecting the field instrumentation site are outlined.

## 2.2 Historical Perspective

Early explorations in the Great Bear River area were carried out for geographical interest. The explorers included Sir Alexander Mackenzie, Sir John Franklin, and others of central importance in the history of the Canadian nation (Camsell and Malcolm, 1921; Robinson and Robinson, 1946; Hume, 1954).

Geological surveys of the area began in 1888 with investigations by R.G. McConnell of the Geological Survey of Canada. In 1914, Dr. J.O. Bosworth was the first to stake claims around local hydrocarbon shows. Since that time, exploration and development of the hydrocarbon deposits have provided a wealth of information on the local bedrock geology. (Hume and Link, 1945; Hume, 1954).

Regional geological surveys were undertaken by the Geological Survey of Canada beginning in 1957. These concentrated on bedrock geology, but also included significant surficial geological studies (Douglas and Norris, 1963; Norris et al., 1963; Aitken et al., 1969; Aitken et al., 1970; Cook and Aitken, 1971).

In 1968, the discovery of oil and natural gas on the North Slope of Alaska, together with encouraging results of wildcat drilling in the Mackenzie Delta, caused producers to look to the

Mackenzie Valley for the location of pipelines to carry petroleum products to southern consumers. In the early 1970's, numerous studies were initiated to resolve engineering complexities associated with the construction of pipelines and support facilities. Geological investigations, which formed part of these studies, concentrated on surficial geology, and involved mapping, describing, and explaining the unconsolidated deposits, landforms, permafrost, ground ice, and organic (muskeg) terrain present in map-sheets adjacent to Mackenzie River (Hughes et al., 1973; Hanley et al., 1973).

## 2.3 Physiography

### 2.3.1 Introduction

Two physiographic regions are represented in the study area: Mackenzie Plain, which is part of the Interior Plains; and Franklin Mountains, which is part of the Cordillera (Bostock, 1948). These are shown in Figure 2.1. The portion of each region which lies in the vicinity of Great Bear River is described below.

### 2.3.2 Mackenzie Plain

Mackenzie Plain is an area of low elevation and relief bordered on the northwest, north, and east by Franklin Mountains. It is drained by the Great Bear and two tributaries, Brackett River and St. Charles Creek. Otherwise drainage is very poorly developed, with myriads of small lakes, swampy inter-lake areas and few well-defined streams.

Near the Great Bear and Mackenzie confluence, the plain is underlain by Tertiary clastic rocks. These outcrop along Great Bear River to above the Brackett confluence, and upstream along the Mackenzie almost as far as Old Fort Point. Elsewhere, the plain is underlain by undifferentiated Tertiary-Cretaceous clastic rocks which rarely outcrop (Cook and Aitken, 1976). Till deposits of silty clay overlie bedrock throughout Mackenzie Plain. These are overlain by clays, silts, and sands of glaciolacustrine or glaciodeltaic origin. Glaciofluvial, alluvial, and eolian sediments are present in some locations.

Topographic elevations range from 52 m on the beach at Fort Norman to 150 m where Great Bear River crosses the trend of Franklin Mountains. Major streams are incised between 45 and 60 m below the featureless plain surface. Valley sides are commonly colluviated by active or remnant bimodal flows seated in ice-rich glaciolacustrine and occasionally morainic sediments.

### 2.3.3 Franklin Mountains

The Franklin Mountains region is represented by two mountain ranges: McConnell Range in the east; and Norman Range in the west. These merge north of Great Bear River defining a crescentic northern limit to Mackenzie Plain. The chain of lakes extending northwest from Brackett Lake through Kelly Lake marks their common boundary.

Paleozoic carbonates and shales are the dominant lithologies. Interbedded salt, gypsum, and anhydrite are important

components, but do not comprise significant thicknesses. Glacial drift is present throughout Franklin Mountains, but is thin or lacking in the highlands.

McConnell Range is a narrow ridge where it is crossed by Great Bear River at St. Charles Rapids. South of the river there are other topographic lows by which drainage passes into Mackenzie Plain. The ridge is more contiguous north of the river. Relief is 410 to 425 m.

Norman Range is wider and more rugged than McConnell Range, and forms a continuous drainage divide within Mackenzie Plain. Relief is 520 to 550 m.

## 2.4 Stratigraphy

### 2.4.1 Introduction

The bedrock geology of the Great Bear River area has been studied in detail during more than half a century of petroleum exploration. The stratigraphy of local rocks is well described in the literature. Specific properties which appear to affect the Quaternary stratigraphy are reviewed in this chapter.

Quaternary sediments are widespread throughout the area. They were examined in detail in the field and in the laboratory to facilitate selection of the best possible site to undertake the in situ programme, and to delineate any sedimentological and permafrost properties that could influence creep processes. In addition, their areal distribution was investigated to provide insight into regional geomorphic development.



The location of each measured section and drillhole from which data were obtained is given a code of the form GB followed by a number. The numbers have no particular order along the river; thus, any site referred to in the text may be found by determining its kilometre<sup>1</sup> location from Table 2.1, and then referring to Figures 2.2 or 2.3 for the location. A full description of each section and drillhole is given in Appendix A.

#### 2.4.2 Paleozoic and Mesozoic

Detailed study of Paleozoic and Mesozoic stratigraphy began soon after Bosworth's discovery of oil seeps in 1914. Camsell and Malcolm (1921) published the first detailed analysis, and Hume (1954) prepared what remains one of the most comprehensive. Operation Norman of the Geological Survey of Canada was aimed at updating geological knowledge and preparing 1:250,000 scale geological maps. Recent publications based on this programme, include: Aitken et al., 1969, 1970; Tassonyi, 1969; Fritz, 1970; Usher, 1970; Yorath, 1970; Balkwill, 1971; Aitken et al., 1973; Aitken and Cook, 1974; Norford and Macqueen, 1975; and, Cook and Aitken, 1976. A stratigraphic column is given in Table 2.2.

Paleozoic rocks are best exposed in Norman and McConnell Ranges (Figure 2.4). Several hard, resistant carbonate formations

---

<sup>1</sup> Kilometre 0 is arbitrarily defined as the confluence of Mackenzie and Great Bear Rivers. The kilometres accumulate upstream along Great Bear River.

make up most of the exposed rocks. Overlying shale formations outcrop on the west side of each range, and are well exposed along streams draining the highlands. Soluble evaporitic rocks make up thick zones of the Saline River and Bear Rock Formations (Tassonyi; 1964). Where the Bear Rock Formation is Quaternary subcrop, numerous sinkholes testify to Recent, and probably Pleistocene subsurface solution. Minor evidence of solution is also present in the Saline River Formation (Aitken and Cook, 1974).

Mesozoic rocks are made up of a succession of marine and non-marine clastic rocks of Cretaceous age. These are exposed on the flanks of Norman and McConnell Ranges, and in many valleys on Mackenzie Plain. The rocks are composed of interbedded medium to fine quartz sandstone and clay shale. Lignite is common as a minor constituent. Bentonite laminae up to 2.5 cm thick are also common, and most clay shales have a significant bentonite component (Tassonyi, 1969; Yorath, 1970; Yorath, in Aitken and Cook, 1974).

#### 2.4.3 Cenozoic - Tertiary

Tertiary rocks underlie most of Mackenzie Plain in the Great Bear River area (Yorath, 1970; Yorath in Aitken and Cook, 1974). They constitute an eastward thinning wedge of clastic rocks that pinches out near the western flank of McConnell Range (Figure 2.4).

The rocks are well exposed in the area of the Mackenzie and Great Bear confluence, and for several kilometres upstream along both rivers. Those along Great Bear River may be broken into two units, referred to here as the "lower unit" and the "upper unit".

### Lower Unit

The lower unit consists of a complex, upsection transition from undifferentiated shale and siltstone, through sandstone to conglomerate. These rocks are exposed intermittently along Great Bear River from Fort Norman to a short distance above the Brackett confluence (Figure 2.5).

Shale and siltstone appearing at the base of this unit, and therefore the locally exposed Tertiary System, are medium to highly plastic and bentonitic. They show varying degrees of fissuring and are more like heavily overconsolidated soils than rocks. They are weakly indurated, and may be excavated by hand and broken down with gentle finger pressure.

Sandstone is the most common rock exposed in the lower unit. This consists of medium to fine sand, of which 60% is quartz and 40% is argillite and chert. Exposures show well-developed cross-stratification and occasional joints. The degree of induration is low, and the material may be easily excavated with a shovel.

The conglomerate is approximately 80% gravel-sized clasts which consist mostly of quartzite and argillite with localized carbonaceous material. Cross-stratification is extensive and commonly associated with deep scour into underlying sandstone. Joints present in the sandstone also propagate through the conglomerate. The conglomerate is weakly indurated, and, like the sandstone, may be easily excavated with a shovel.

### Upper Unit

The upper unit consists of interbedded bentonitic siltstone and coal. The unit is exposed intermittently along Great Bear River from between 1 and 2 km above the Brackett confluence (Figure 2.5), but is truncated by the Pleistocene erosional surface below the confluence. It reappears in the hanging wall of a normal fault in contact with the lower unit at Fort Norman (see GB40, Appendix A).

Siltstone beds have a variable thickness and are separated by coal beds. The material is generally highly plastic and is composed of up to 45% montmorillonite, with an average of 20%. In outcrop the material is highly fissured and consistently soft to finger pressure. It is more appropriately described as an overconsolidated soil than a rock.

Coal beds and laminae are common. The coal is tentatively assigned a rank of lignite to sub-bituminous. It breaks down easily into angular peds 1 to 2 cm long and is easily recognized by the presence of plant fossils and amber.

#### 2.4.4 Cenozoic - Quaternary

The succession and basic lithology of Quaternary sediments in the environs of Great Bear River is given in Table 2.3. The regional surficial geology and geomorphology, modified from Geological Survey of Canada maps, are shown in Figure 2.6, and a composite stratigraphic section of surficial deposits along Great Bear River from km 0 to km 75 is shown in Figure 2.7.

Surficial sediments<sup>1</sup> pre-dating the last glaciation are present at two locations: sand and silty clay, which are considered alluvial, occupy a bedrock valley at km 7; and deltaic silt, sand, and gravel lie immediately west of McConnell Range, between km 45 and 53.

Till which is assumed to have been deposited during Wisconsin glaciation, is the lowest widespread unit in the Quaternary section. This is present throughout Mackenzie Plain, and to varying elevations in McConnell and Norman Ranges.

Glaciolacustrine silty clay and overlying glaciodeltaic sand are widespread on Mackenzie Plain. These accumulated in the proglacial environment of Wisconsin deglaciation.

Recent sediments are common throughout the area. Organic soils, lacustrine clay, silt and sand, and aeolian sand are present on the surface of the Mackenzie Plain. Alluvial silt, sand, and gravel are present on valley floors, and valley slopes are largely clayey and sandy colluvium. Recent sediments are typically thin and of little significance to this study, and are therefore not discussed further. For a detailed summary the reader is referred to Tarnocai (1973).

#### Pre-Wisconsin - Alluvial Clay and Sand

These deposits were only encountered at the proposed Arctic Gas crossing site (km 7.2, Figure 2.5). They consist of 6.7 m

---

<sup>1</sup> For the purposes of this thesis, "surficial sediments" refers to all sediments above the Tertiary bedrock surface.

of silty clay and sand, and separate Wisconsin till and Tertiary bedrock. They occur at and below river level in a bedrock valley that is identified by following the bedrock surface in exposures upstream and downstream of the site. The trend of this valley away from river is unknown, but it is likely north northwest parallel to bedrock structures (Figure 2.4).

Blue-grey to brown, highly plastic silty clay (CH) and clayey silt (MH) make up most of this alluvial deposit (Figs. 2.8 and 2.9). The beds are fissured and slickensided, and detrital coal fragments are found throughout. Clay minerals present include montmorillonite (60%), illite (30%), and kaolinite (10%).

Very uniform (SP), uncemented, salt and pepper sand in beds 20 to 30 cm thick makes up approximately 10% of the alluvial deposit. The grains are medium size, subangular, and consist of argillite (60%) and quartz (40%).

The remainder of the deposit is made up of a coal seam 30 cm thick. This is considered allogenic because of an increasing content of detrital coal in underlying silty clay, and because of thin clay laminae in the bottom of the coal itself.

Ground ice occurs where these strata lie within the permafrost zone. Thin films of ice coat most fissure surfaces, giving a pseudo-reticulate permafrost form<sup>1</sup>. Stratified ice is also present with veins up to 4 cm thick occurring at some contacts of silty clay with sand or coal beds.

---

<sup>1</sup>The classification system used in this thesis to describe permafrost is discussed in Section A.3.

### Pre-Wisconsin - Deltaic Silt, Sand, and Gravel

A sand and gravel complex underlies Wisconsin till on the west side of McConnell Range. The deposit has a typically deltaic morphology in cross section (Figure 2.7), with a steep, west-facing delta front at approximately km 42.

More than 20 m of silt, sand, and gravel belonging to this deposit outcrop at km 45.3 (GB9, Appendix A). Sand and gravel beds dominate the exposure. Clasts in the gravel represent up to 50% by volume and consist primarily of pebbles of crystalline and carbonate rocks. Cobbles and boulders are usually less than 1%, but locally as much as 5% and as large as 90 cm in diameter. The sand is medium to coarse, angular to subangular, and mostly quartz (80%) and feldspar (20%). Silt seams 15 to 25 cm thick are common, and make up 5 to 10% of the exposure.

Permafrost was not observed in the deposit.

### Wisconsin - Till

Till overlies Tertiary rocks, and locally pre-Wisconsin alluvial deposits, in the Brackett River to Fort Norman area (Figures 2.5 and 2.7). To the east, across Mackenzie Plain, the contact is buried, but it is assumed to be with Tertiary rocks to approximately km 35, and then with Cretaceous rocks to St. Charles Creek. From this point to the east side of McConnell Range, the unit rests on pre-Wisconsin sands and gravels. Over Mackenzie Plain the till is covered by glaciolacustrine clay, and through valleys in

McConnell Range, near Bennett Field, it is overlain by glaciofluvial outwash; elsewhere it comprises the surficial mineral soil.

Thicknesses of from 3 to 10 m are common for till in Mackenzie Plain. The till is thin or lacking in the highlands of Franklin Mountains, but the presence of glacial erratics indicate Laurentide glaciers advanced over the region (Hughes, 1969).

The till is compact, with very rare pockets and lenses of stratified material. The matrix is dark greyish brown (10YR4/2) to dark grey (10YR4/1), but becomes black near Tertiary lignite deposits. The structure of outcrops is dominated by fissures, with peds ranging from 2 to 6 cm. Joints are present, but are very indistinct.

Clasts are all subrounded and consist mainly of granite (40 to 50%) and carbonate (40%) with random sandstone, quartzite, syenite, and local siltstone and shale. The average size is 1 cm, with cobbles and boulders less than 1% of the total. The maximum size observed was 1 m in diameter. The long axes have a preferred east-west orientation, and most clasts have striae.

The matrix consists of a near-equal sand-silt-clay mixture, with local increases in sand content as shown in Figure 2.9. The plasticity characteristics summarized in Figure 2.8 give it a Unified Classification of low to medium plastic clay (CL to CI), and liquidity indices between 0 and -1 indicate overconsolidation. The unit weight averages  $22.1 \text{ KN/m}^3$ , and the specific gravity of the soil particles is 2.74. Clay minerals identified are illite (60 to



75%), kaolinite (20 to 25%), montmorillonite (0 to 15%), and chlorite (5%).

The deposit is everywhere within the permafrost zone, except in particularly deep sections in the valleys through McConnell Range. Ground temperatures at km 7.1 of Great Bear River range from -2.0 to -2.5°C. Pore ice is the most common permafrost form, but some reticulate ice occurs near the upper and lower contacts. Veins of ice in reticulate ice facies are limited to widely separated, sub-horizontal lenses 2 to 4 cm thick.

#### Wisconsin - Glaciolacustrine Clay

Fine-grained, glacial-lake-basin clay rests on till throughout its extent in Mackenzie Plain, except near km 37 where it overlies a small, coarse-grained, ice-contact deposit. Over most of Mackenzie Plain, it is overlain by glaciodeltaic sand (Figure 2.7), but in the east, near the lower Northern Transportation Company (NTCL) dock, it is covered by glaciofluvial sand and gravel. It has extensive organic-soil cover where it is the surficial mineral soil.

The thickness of the deposit is directly related to the morphology of the underlying till surface. Accumulations typically range from 5 to 10 m, but over highs this is reduced to 2 to 5 m, and in lows, such as the bedrock valley at km 7, it is up to 18 m thick.

The maximum elevation of the deposit is associated with strandlines at approximately el. 150 m near Big Smith Creek (Figure

2.6), 50 km southeast of Fort Norman. North of Great Bear River, on the west side of McConnell Range, the sediments reach approximately the same level, and on the east side of Bear Rock they reach el. 130 m. The estimated isostatic recovery from these data is 0.35 m/km in both east and southeast directions.

Outcrops are common in the headscarp of bimodal flows, many of which are active and provide fresh exposure of the clay and its contact with overlying sand. However, the operandi of these features commonly precludes exposure of the lower part of the clay, and is responsible for a paucity of field data in the lower portion of the clay section.

The lowest 1 m of glaciolacustrine sediments contain significant coarse sand and pebbles. The contact with the sand above is abrupt, and locally marked by a thin lens of pebbles and coarse sand. No gradation was found in the clay near this contact.

The clay is rhythmically laminated throughout the region, although only minor colour or texture difference exists between the "summer" and "winter" layers. The former are greyish brown (10YR4/2), average 0.2 cm thick, and range from 0.02 to 200 cm; the latter are very dark greyish brown (10YR3/2), average 2 cm thick, and range from 0.05 to 10 cm. The bedding structure is highly contorted, and individual laminae show rapid thickness variation, both of which make lateral correlation of more than a metre difficult. No diamicton deposits were found, and current-bedded

silt laminae were only observed at GB14 (Figure 2.2).

Preliminary grain-size analyses were planned to assess the textural difference between the "winter" and "summer" laminae. Owing to the difficulty in sampling each layer, and since the maximum difference was consistently less than reasonable experimental accuracy, this objective was abandoned and further samples were taken indiscriminately.

The lack of strong textural contrast between the components of each couplet is at least partially a manifestation of bedrock conditions in the Mackenzie Valley. Roggensack (1977) found that glaciolacustrine sediments from Fort Simpson and Norman Wells consisted of aggregates of clay minerals, and proposed that these were derived intact from the local Cretaceous System, transported, and deposited as silt-sized particles. His photomicrographs (Roggensack, 1977, p.400) illustrate a predominance of turbostratic fabric, which underscores the sedimentological importance of this model.

The photomicrographs also show a degree of edge-to-face structure indicating flocculation. Fraser (1929) showed experimentally that this process could occur in solutions with salinity as low as 1/90 that of normal sea water. The availability of electrolytes in local Paleozoic rocks, together with evidence of solution cited in Section 2.4.2, suggest that adjacent glacial lakes contained a sufficient electrolyte concentration to effect the observed flocculation. In the Great Bear River area, these

phenomena likely combined to produce silt-sized, clay-particle assemblages that settled from suspension at approximately the same rate as discrete silt grains. Therefore, clay sizes comprise a large percentage of the "summer" layers.

The results of 62 grain-size analyses are shown in Figure 2.9. The distribution shows the deposit is a silty clay. Plasticity characteristics illustrated in Figure 2.8 indicate a Unified Classification of medium to highly plastic clay (CI-CH). Liquidity indices are consistently near zero, indicating slight overconsolidation, bulk unit weights have an average of  $20 \text{ KN/m}^3$ , and specific gravity of the soil particles is generally 2.75.

X-ray analyses of the less than 0.002 mm fraction show between 15 and 20% clay minerals, 55% quartz, 10% calcite, 10% dolomite, and less than 10% each of gypsum and feldspar. The average composition of the clay minerals is 60% illite, 20% kaolinite, and 10% chlorite. Montmorillonite varied from 5 to 25% with a mode of 10%.

The deposits lie within the permafrost zone throughout Mackenzie Plain. Reticulate ice is the most common permafrost form. Veins of ice range up to 20 cm thick. Usually a primary vertical and secondary horizontal ice structure is evident, and the primary veins are almost always thicker. Segregated ice is also a common permafrost form. In general, the ground-ice to soil (volume) ratio is greater where the glaciolacustrine clay outcrops along valley sides, than it is at depth beneath adjacent uplands. Both reticulate ice and segregated ice facies are thaw unstable where

either is exposed to thawing conditions.

#### Wisconsin - Glaciodeltaic Sand

A thick blanket of glaciodeltaic sand covers Mackenzie Plain south of Great Bear River, southwest of Mackenzie River toward MacKay Range, and north of Great Bear River to el. 120 m. It rests on glaciolacustrine clay throughout the region, locally separated from it by a lens or thin bed of pebbles and coarse sand. Where the sand is thin, its surface is covered by peatland and fenland containing up to 4 m of organic soil. Peat palsas and plateaus 1 to 3 m high, separated by shallow lakes and frequently showing active thermokarst activity, form distinctive topographic features. Where the sand is thick, organic soil is generally between 0.5 and 1.0 m thick, lakes are less frequent, and swampy bogland is much less widespread. East of Brackett River and southeast and east of Fort Norman, the monotony of the plain is broken occasionally by sand dunes.

Sediment sources in the east and south are inferred from scattered paleocurrent data and general thickening of the sand facies in these directions. Incised glaciofluvial landforms, in gaps through McConnell Range (Figure 2.6) and adjacent to Mackenzie River at the Redstone River confluence, are further evidence that the sediment source areas were to the east and south.

Exposures of the sand are common in the headscarp of active and stable bimodal flows along Great Bear River and its tributaries. The unit shows a general northwestward thinning except where it fills topographic depressions originating in the till

surface and preserved through the glaciolacustrine clay. In the east, the deposit averages 20 m thick, at km 16.2 10 m, and near Fort Norman 5 m. A thickness of over 20 m successfully masks all evidence of the bedrock valley, at km 7.

Bedding structures are highly variable. The dominant sand bedforms are massive, horizontally bedded and laminated, and cross-laminated. Draped lamination is common and most often made up of discrete silt and sand-size coal grains. Thin, horizontal lenses of cohesive material, tabular cross-beds of sand, and thin, horizontal, pea-gravel lenses are each present in a few sections, but they represent an insignificant percentage of the overall sand facies.

The sand is vari-coloured, ranging from yellow-brown, to brown, to black. Quartz is the primary mineral, making up between 70 and 90%, while coal, argillite, and feldspar are secondary. Wood fragments are common near the top of the sand section. Quartz grains are angular to subangular, while other lithologies vary from subangular to subrounded. Moisture contents have an average of 27% and bulk unit weights  $18.2 \text{ KN/m}^3$ . The specific gravity of the soil grains is 2.68 and the void ratio ranges from 0.7 to 0.8.

The textural breakdown of the less than 2 mm fraction gives a pure sand classification (Figure 2.9). Gravelly lenses typically have up to 15% gravel sizes, with a maximum size of 6 cm and mode of less than 1 cm. Widely scattered, presumably ice-rafted clasts are as large as 58 cm in diameter.

The sand is within the permafrost zone, except beneath deep

lakes. The upper 3 to 10 m are within the zone of annual temperature fluctuation, and, depending upon the nature and thickness of organic soil cover, the active layer varies from 0.3 to 5 m thick. Pore ice is the dominant permafrost facies; vertical ice veins up to 2 cm thick are also present, but these are rare and zones containing them have not been assigned to any specific permafrost facies. Pore ice alone is sufficient to saturate the sand at its in situ void ratio, and any degree of shaking liberates abundant excess water. The sand is commonly thaw unstable. Natural slopes are generally 28 to 34°; precipitous slopes ranging up to 38° occur along much of Great Bear River, especially on the left (north facing) valley wall.

#### Wisconsin - Glaciofluvial Sand and Gravel

Glaciofluvial sediments were not examined by the writer. The following brief discussion is based on data from consulting reports, government sources, and airphoto interpretation.

Glaciofluvial sand and gravel occupy lowland gaps which traverse McConnell Range adjacent to inflowing rivers such as the Great Bear, and St. Charles and Big Smith Creeks (Figure 2.6). The kettled plains and terraces of the original landform are deeply incised. Evidence from immediately north of St. Charles Creek shows the coarse material was redeposited a short distance downstream, and sections along the Great Bear River show what is assumed to be the same material intercalated with glaciodeltaic sand. The deposits are composed of approximately equal quantities of sand and gravel

and give a Unified Classification of GW. They lie within the permafrost zone, and the impoundment of small lakes in kettles and in abandoned channels suggests the deposits contain ground ice.

## 2.5 Geomorphic Development

The earliest geomorphic record is the erosion and partial filling of a valley in Tertiary bedrock at km 7. Insufficient data are available to establish the local trend of this buried valley; on a regional scale, however, it is likely contiguous with the "Hare Indian - Mackenzie Trench" reported by Mackay and Mathews (1973). Attempts to date basal (alluvial) sediments lying in the valley on the basis of microflora are inconclusive. The presence of Alnus and cf. Ilex indicate the sediments are at least Tertiary, but the general lack of Tertiary taxa suggests Pliocene-Pleistocene Age<sup>1</sup>.

Deltaic deposits underlying glacial till at km 45 testify to a lacustrine phase prior to the last Wisconsin glaciation, and probably relate to deglaciation of an earlier glacial period. They were found to be barren of organic material and therefore could not be dated.

Flutings east of McConnell Range (Figure 2.6) indicate that

---

<sup>1</sup>Hopkins, W.S. Jr., 1977 personal communication. Identification of microflora revealed the following taxa: "Pleurocellasporites, Lycopodium, Selaginella, Osmunda, Laevigatosporites, Verrucosporites, Sphagnum, Pinaceae, Tsuga, Glyptostrobus-Taxodium, Sequoiapollenites, Liliacidites, Nuphar, Fibulapollis, Orbiculapollis, Aquilapollenites, Wodehouseia, Castanea-Type, ?Kurtzipites, Alnus, cf. Ilex."



the Classical Wisconsin Laurentide ice sheet entered the region from the southeast, but bifurcated east of McConnell Range (Hanley and Hughes, 1973). One lobe continued northwest in an arcuate pattern north of Mahoney Lake. The second lobe crossed McConnell Range and flowed northwest along Mackenzie Valley as far as Beavertail Mountain where the two lobes merged again and continued in a northwest direction (Mackay and Mathews, 1973). This last Wisconsin advance reached its maximum against the mountain front approximately 14,000 years ago (Hughes, 1969; Prest, 1970).

Large ice-dammed glacial lakes, occupying consequent valleys along the eastern front of Mackenzie Mountains, coexisted with the glacial maximum (Hughes, 1969). Ice-marginal channels indicate these glacial lakes stood at elevations greater than 300 m. During early retreat, the channels probably fed into a major meltwater system, which ultimately followed Mountain River into a glacial lake southwest of Fort Good Hope (Hughes, 1970; Mackay and Mathews, 1973); later the channels ended immediately north of MacKay Range, depositing coarse deltaic or outwash sediments east of Little Bear River. Retreat was accompanied by a steady decrease in lake level to an elevation of 150 m, where strandlines formed and below which glaciolacustrine sediments are widespread.

Near Sans Sault Rapids, equivalent lake-basin sediments show a gradational change to an overlying deltaic facies (Mackay and Mathews, 1973). In the Great Bear River area, however, this contact is abrupt, as described in Section 2.4.4, and may indicate that failure of an ice dam caused a sudden alternation to deltaic

sedimentation. Subtle differences in the elevation of glaciolacustrine sediments along the Mackenzie near the mouth of Little Bear River, and the presence of stream channels and strandlines near the mouth of Little Bear River as shown on Figure 2.6, suggest the ice dam was coincident with the glaciofluvial sediments east of Little Bear River in Mackenzie Plain. After breaching, glacial lakes above and below the barrier coalesced and a continuous body of water extended from the Ramparts-Ontaratué divide (Mackay and Mathews, 1973) to the area of the present Keele and Redstone River confluences with Mackenzie River.

Mackay and Mathews (1973) estimate that ice dams in the Fort Good Hope area had disappeared, and that the relative stability of ice-marginal conditions had become established at el. 95 m approximately 11,000 to 11,500 C<sup>14</sup> years ago. Assuming this is a reasonable estimate of when the ice dam near Little Bear River was breached, a minimum differential isostatic depression of 20 to 25 m was requisite to have maintained deltaic conditions in the Great Bear River area. This is considered reasonable in relation to the differential established across the basin (Section 2.4.4), and elsewhere in the area (Craig, 1965).

During this period, the ice front lay immediately east of McConnell Range and meltwater discharged through gaps now occupied by Great Bear River, and St. Charles and Big Smith Creeks (Prest, 1970; Hanley and Hughes, 1973). As the lake level fell, deltas adjacent to Mackenzie River near the mouths of Keele and Redstone Rivers, and deltas and outwash plains in the valleys through

McConnell Range became incised, and the new deltaic facies began to be as much as 30 m below the last. Systematic downcutting at coupled with decelerating isostatic readjustment in the basin facilitated northwestward progradation of the deltaic front. The low water environment, copious sediment supply, and abundance of uniform, fine to medium sand, derived from Cretaceous sandstones, combined to produce a fan-delta morphometry similar to the Hjulstrom model (Hjulstrom, 1952; Church and Gilbert, 1975).

As the ice retreated east of the McConnell Range, meltwater supply waned and became concentrated in Great Bear River. The river was established in its present course east of McConnell Range as early as 10,900 years ago (Craig, 1960; Prest, 1970), but wood fragments from gentle tabular cross-beds in the sand section at GB27 (Appendix A) indicate deltaic sedimentation continued in the central Mackenzie Plain after 10,600 C<sup>14</sup> years B.P.<sup>1</sup>. It seems likely that terrestrial conditions were established at el. 100 m in this area approximately 10,000 years ago, and further downcutting was in proportion to the outlet near Fort Good Hope as discussed by Mackay and Mathews (1973). A radiocarbon date reported by Roggensack (1977) indicates that the lake level had fallen to approximately el. 70 m by 3,290 C<sup>14</sup> years B.P.; and, wood fragments in colluvium, near the base of a stable, re-frozen bimodal flow at the proposed Arctic Gas Crossing site, indicate Great Bear River was incised

---

<sup>1</sup>Blake, W. Jr., 1976, personal communication. Geological Survey of Canada, Radiocarbon Sample Number 2328.

below approximately el. 68 m by 2,670 C<sup>14</sup> years B.P.<sup>1</sup>.

Glaciodeltaic sand in the uplands over Mackenzie Plain was locally modified by wind action shortly after terrestrial conditions were established, and before extensive vegetation cover developed. More recent modifications to upland topography have resulted from repeated aggradation and degradation of permafrost.

## 2.6 Selection of Field Instrumentation Site

On the basis of geological investigations reported in the foregoing sections, km 7.2 on Great Bear River emerged as the most suitable site for the in situ study of naturally occurring creep processes.

The location is near the thalweg of a buried valley. This topographic low was preserved after Wisconsin glaciation, and received an anomalously large thickness of fine-grained sediment when glacial lakes became impounded in the area. The sediments are presently within the permafrost zone and constitute a reticulate ice facies. They are overlain by a thick deposit of glaciodeltaic sand in the uplands, but they lie beneath a thin layer of organic soil on the steep slopes of the Great Bear River Valley.

The location is also on the proposed Canadian Arctic Gas pipeline route. In 1974, the Canadian Arctic Gas pipeline application was before the National Energy Board, and problems of naturally occurring creep were of central concern to the applicant.

---

<sup>1</sup>Blake, W. Jr., 1977, personal communication. Geological Survey of Canada, Radiocarbon Sample Number 2488.

As a result of these factors, a cooperative programme between the University of Alberta and Northern Engineering Services Limited was conceived in order to thoroughly investigate naturally occurring creep properties in ice-rich, fine-grained permafrost soil.

TABLE 2.1  
Guide to the location of drillholes and measured sections along  
Great Bear River

LOCATION CODE	KILOMETRE LOCATION ALONG RIVER	ELEVATIONS (METRES)		SOURCE S-Section DH-Drillhole CR-Consulting Rpt
		NEAREST RIVER LEVEL	TOP OF SECTION OR DRILL COLLAR	
GB1	7.1	56.3	101.5	DH GB1, 1A, 1B
GB2	7.1	56.3	80.2	DH GB2
GB3	7.1	56.3	70.4	DH GB3, 3A
GB4	7.1	56.3	56.3	CR DH N74-303
GB5	7.1	56.3	56.3	CR DH N74-304
GB6	7.1	56.3	87.5	CR DH N74-307
GB7	7.1	56.3	101.6	CR DH N74-308
GB8	46.3	80.1	86.2	S WS-73-2
GB9	45.4	79.5	125.5	S WS-73-3
GB10	42.5	78.0	125.7	S WS-73-4
GB11	41.1	77.3	109.7	S WS-73-5
GB12	40.0	76.9	82.6	S WS-73-6
GB13	39.6	76.7	116.8	S AR-73-4
GB14	37.1	75.5	118.4	S WS-73-8
GB15	35.1	74.8	120.5	S WS-73-9
GB16	34.8	74.7	82.5	S AR-73-5
GB17	32.6	73.2	80.0	S AR-73-6
GB18	31.1	72.2	113.6	S WS-73-11
GB19	29.0	71.2	86.2	S WS-73-12
GB20	24.1	68.8	108.8	S WS-73-14
GB21	27.25	70.3	116.9	S WS-73-15
GB22	25.6	69.5	76.3	S WS-73-16
GB23	24.1	68.8	95.8	S WS-73-17
GB24	21.1	67.3	99.1	S WS-73-18
GB25	20.3	67.0	80.0	S WS-73-19
GB26	18.9	66.2	107.2 (top sand)	S WS-73-20
GB27	18.1	65.7	79.3 (top clay)	S WS-73-21
GB28	16.2	64.7	99.2	S WS-73-22
GB29	11.8	61.3	100.6	S AR-73-7
GB30	11.5	61.0	86.4	S WS-73-23
GB31	11.2	60.9	N/A	S WS-73-24
GB32	10.3	59.8	110.9	S WS-73-25
GB33	8.0	57.8	N/A	S WS-73-26
GB34	6.5	56.5	101.8	S AR-73-8
GB35	6.6	56.6	66.6	S AR-73-8
GB36	3.3	53.3	87.3	S WS-73-28
GB37	0.4	51.4	83.4	S WS-73-27
GB38	57.6	97.7	130.82	S WS-73-1
GB39	65.2	110.6	213.4	CR DH B14

TABLE 2.1 continued  
Guide to the location of drillholes and measured sections along  
Great Bear River

LOCATION CODE	KILOMETRE LOCATION ALONG RIVER	ELEVATIONS (METRES)		SOURCE S-Section DH-Drillhole CR-Consulting Rpt
		NEAREST RIVER LEVEL	TOP OF SECTION OR DRILL COLLAR	
GB40	0 (Fort Norman)	51.0	N/A	S WS-75-8
GB41	56.5	96.0	135.3	CR DH M20
GB42	54.9	91.4	128.0	CR DH B15
GB43	53.0	91.4	147.8	CR DH M2
GB44	51.9	84.8	84.8	CR DH R2
GB45	8.7	58.4	UNKNOWN	CR DH 2FN13
GB46	8.0	57.8	UNKNOWN	CR DH 1FN30
GB47	5.9	56.0	UNKNOWN	CR DH 3FN10
GB48	3.9	54.2	UNKNOWN	CR DH 112
GB49	3.8	53.9	UNKNOWN	CR DH 113
GB50	N/A	N/A	UNKNOWN	CR DH 107
GB51	N/A	N/A	UNKNOWN	CR DH 122
GB52	N/A	N/A	UNKNOWN	CR DH C32FN8
GB53	3.1	N/A	UNKNOWN	CR DH 110
GB54	2.6	52.8	UNKNOWN	CR DH 111
GB55	2.3	52.7	UNKNOWN	CR DH 452
GB56	2.5	N/A	UNKNOWN	CR DH 1FN14
GB57	1.2	N/A	UNKNOWN	CR DH 465
GB58	1.4	N/A	UNKNOWN	CR DH 461
GB59	1.3	N/A	UNKNOWN	CR DH 522
GB60	outside map area	N/A	176.8	CR DH M14
GB61	outside map area	N/A	174.1	CR DH M18
GB62	10.4	59.9	61.1	CR DH R11
GB63	10.6	60.1	101.3	CR DH R21
GB64	12.3	61.4	102.3	CR DH R22
GB65	12.2	61.4	61.4	CR DH R20
GB66	5.5	55.8	97.5	CR DH R206
GB67	5.5	55.8	91.4	CR DH R207
GB68	5.7	55.8	57.3	CR DH R208
GB69	5.6	55.8	57.3	CR DH R209
GB70	5.2	55.4	91.4	CR DH R210
GB71	10.5	59.9	61.4	CR DH R201
GB72	10.2	59.6	61.4	CR DH R202
GB73	10.6	59.6	108.6	CR DH R203
GB74	10.7	N/A	111.2	CR DH R204
GB75	9.9	59.4	79.2	CR DH R205
GB76	71.0	N/A	234.8	CR DH M6
GB77	72.2	N/A	228.6	CR DH M7
GB78	61.2	N/A	182.9	CR DH M1

TABLE 2.2

## EXPOSED BEDROCK FORMATIONS IN THE GREAT BEAR RIVER AREA

ERA	PERIOD OR EPOCH	FORMATION AND MAXIMUM THICKNESS	LITHOLOGY	
CENO-ZOIC	EOCENE ?	UNNAMED 490	Gravel, conglomerate, sand, sandstone, minor beds of coal; nonmarine	
Unconformity				
MESOZOIC	CRETACEOUS	LITTLE BEAR AND EAST FORK FMS, undifferentiated: 300+	Sandstone, shale, minor coal; marine and nonmarine	
		Disconformity		
		SANS SAULT AND SLATER RIVER FMS, undifferentiated: 760	Shale, sandstone, local conglomerate at base; marine	
Unconformity				
PALEOZOIC	DEVONIAN	UPPER	IMPERIAL FORMATION 1,100	Shale, sandstone, minor limestone; marine
		Conformable Contact		
			CANOL FORMATION 90	Shale, black, siliceous, bituminous; marine
		Disconformity		
		MIDDLE	HARE INDIAN FORMATION 130	Shale, minor siltstone and limestone; marine
		Conformable Contact		
		HUME FORMATION 170	Limestone, fossiliferous; minor shale; marine	
	Disconformity			
	LOWER	BEAR ROCK FORMATION 300	Dolomite, dolomite solution-breccia, anhydrite and gypsum; marine. Equivalent to the Camell, Arnica and Landry Formations, jointly	
	Relationships Uncertain			
	SILURIAN		UNNAMED 200(?)	Dolomite, partly sandy or argillaceous; sandstone, dolomitic; marine. Equivalent to the Delorme Formation.
		Unconformity		
	ORDOVICIAN		MOUNT KINDLE FORMATION 310	Dolomite, fossiliferous, siliceous; minor chert; marine
		Unconformity		
	CAMBRIAN	LOWER		"Cherty member": dolomite, chert, drusy quartz; marine "Rhythmic member": alternation of very finely crystalline dolomite with finely to medium crystalline dolomite; marine
MIDDLE		FRANKLIN MOUNTAIN FORMATION 460	"Cyclic member": dolomite, conglomeratic, stromatolitic, and argillaceous, shaly, marine "Basal red beds": sandstone, red shales, conglomerate, dolomite, chert; marine and (?) nonmarine	
Conformable Contact				
U		SALINE RIVER FORMATION 841(?)	Red beds: shale, siltstone, sandstone, salt, gypsum, anhydrite, dolomite; marine	
Unconformity				
	M L	MOUNT CAP FORMATION 108	Shale, thin-bedded limestone, sandstone, siltstone; marine	



TABLE 2.3

SUCCESSION AND LITHOLOGY OF QUATERNARY  
SEDIMENTS IN THE GREAT BEAR RIVER AREA

ERA	PERIOD OR EPOCH	LITHOLOGY
CENOZOIC	QUATERNARY	Colluvium
		Lacustrine clay, silt and sand, organic deposits and marl, eolian sand, alluvium
		Glaciofluvial sand and gravel
		Glaciodeltaic silt, sand and gravel
		Glaciolacustrine silty clay
		Morainic till, and locally sand and gravel
		Deltaic silt, sand and gravel
	TERTIARY (PLIOCENE)	Alluvial clay and sand

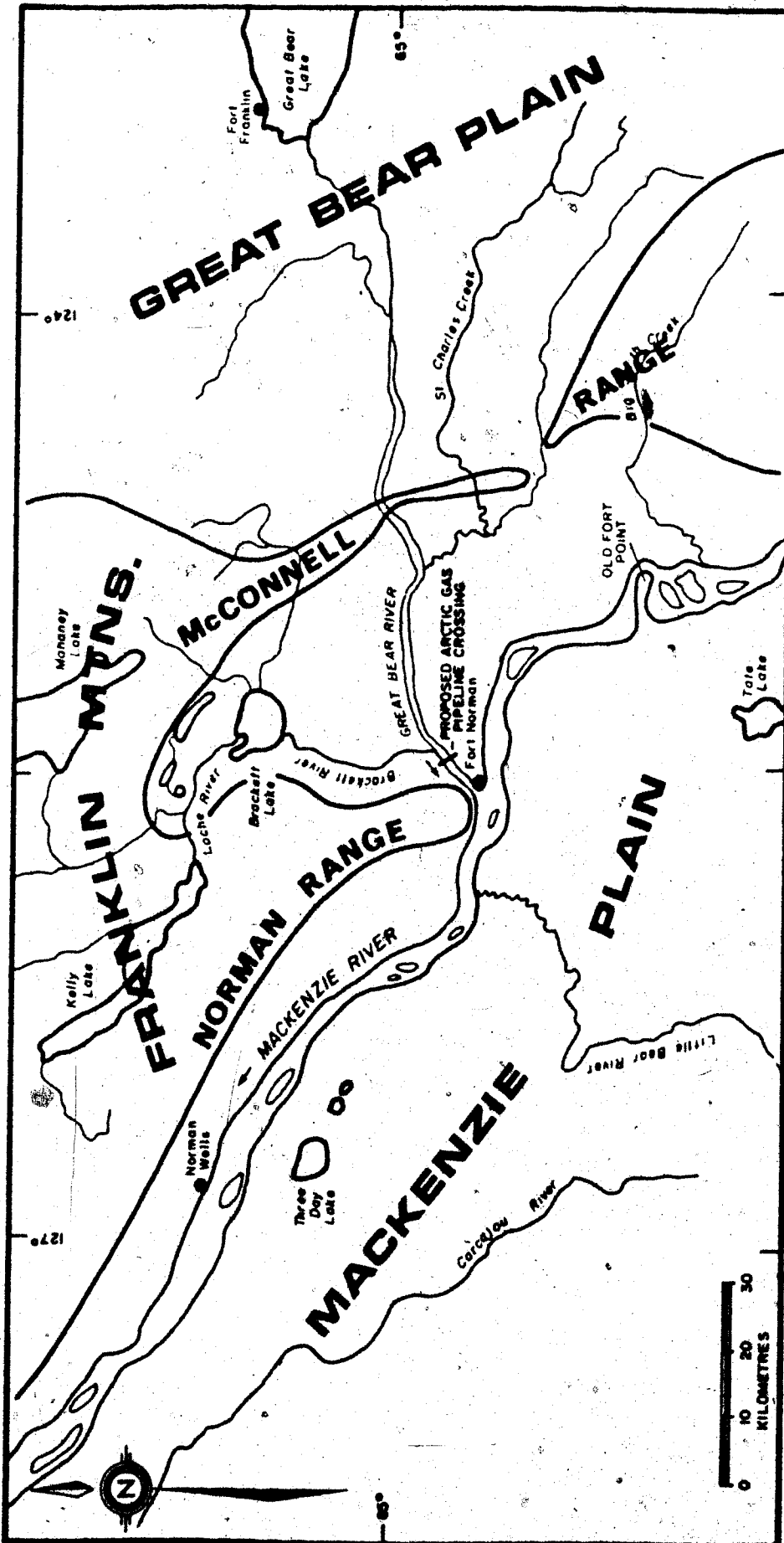


FIGURE 2.1 PHYSIOGRAPHY OF THE GREAT BEAR RIVER AREA

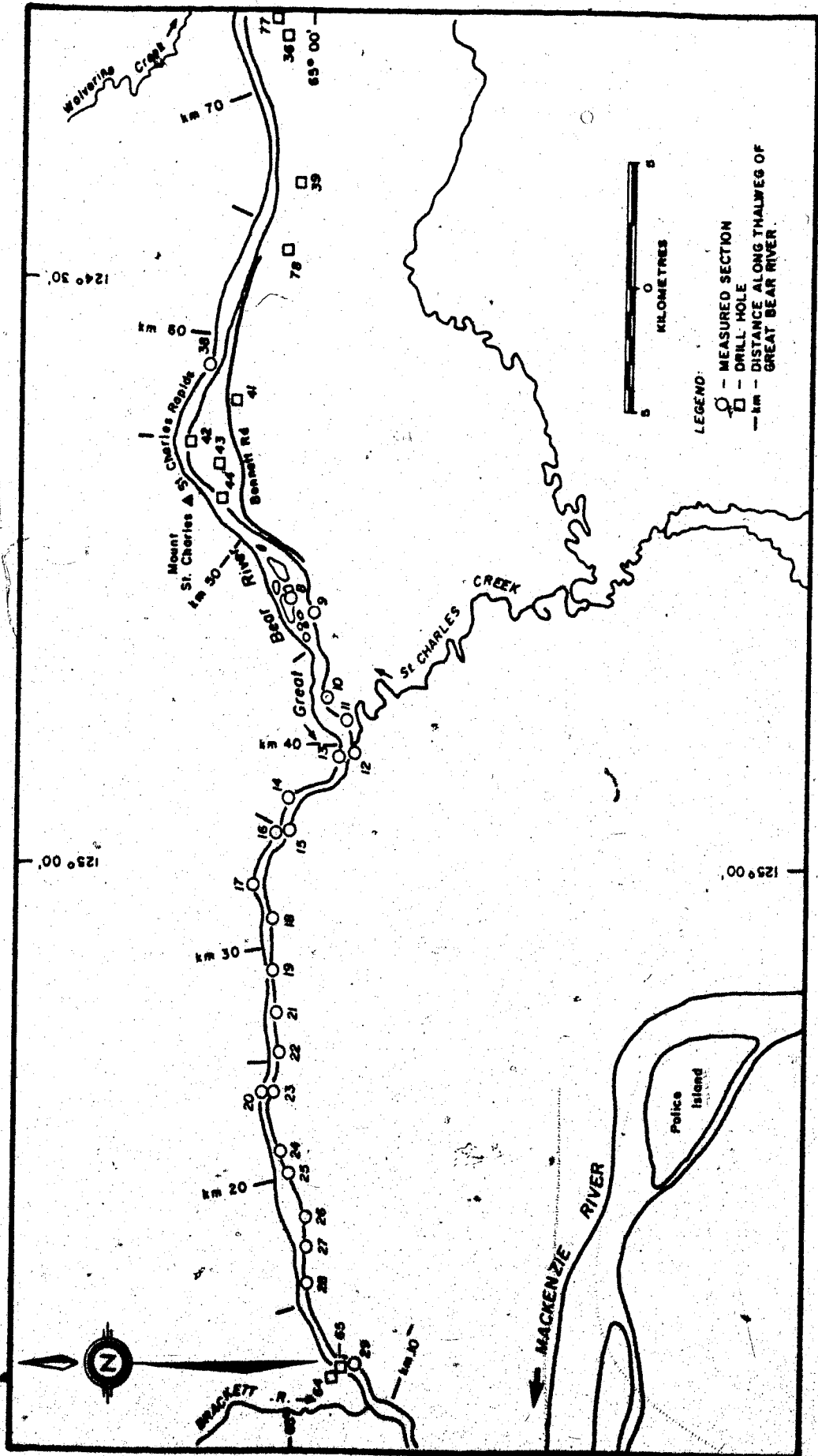
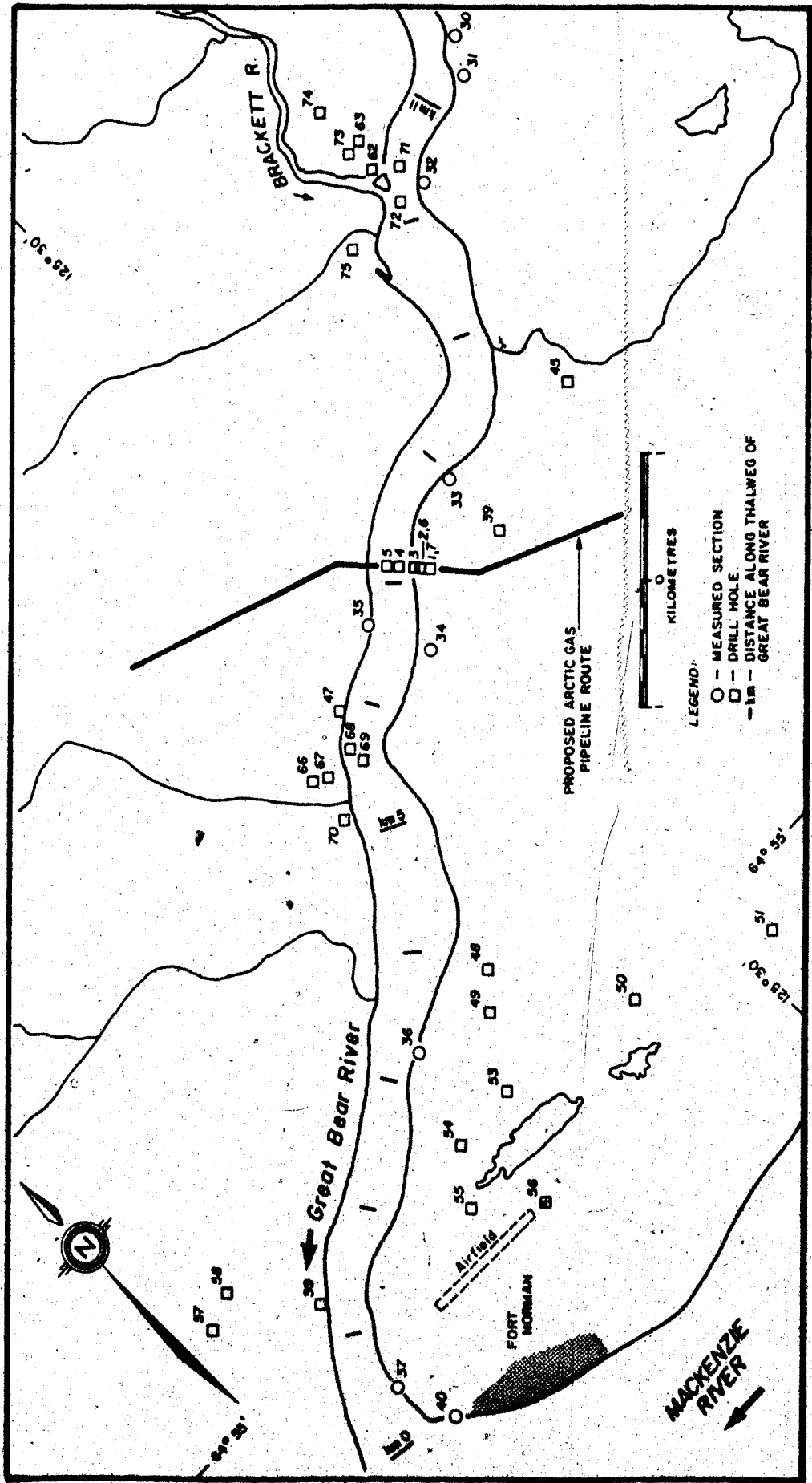


FIGURE 2.2 FIELD LOCATIONS ALONG GREAT BEAR RIVER



**FIGURE 2.3 FIELD LOCATIONS ALONG GREAT BEAR RIVER IN THE FORT NORMAN TO BRACKETT RIVER AREA**

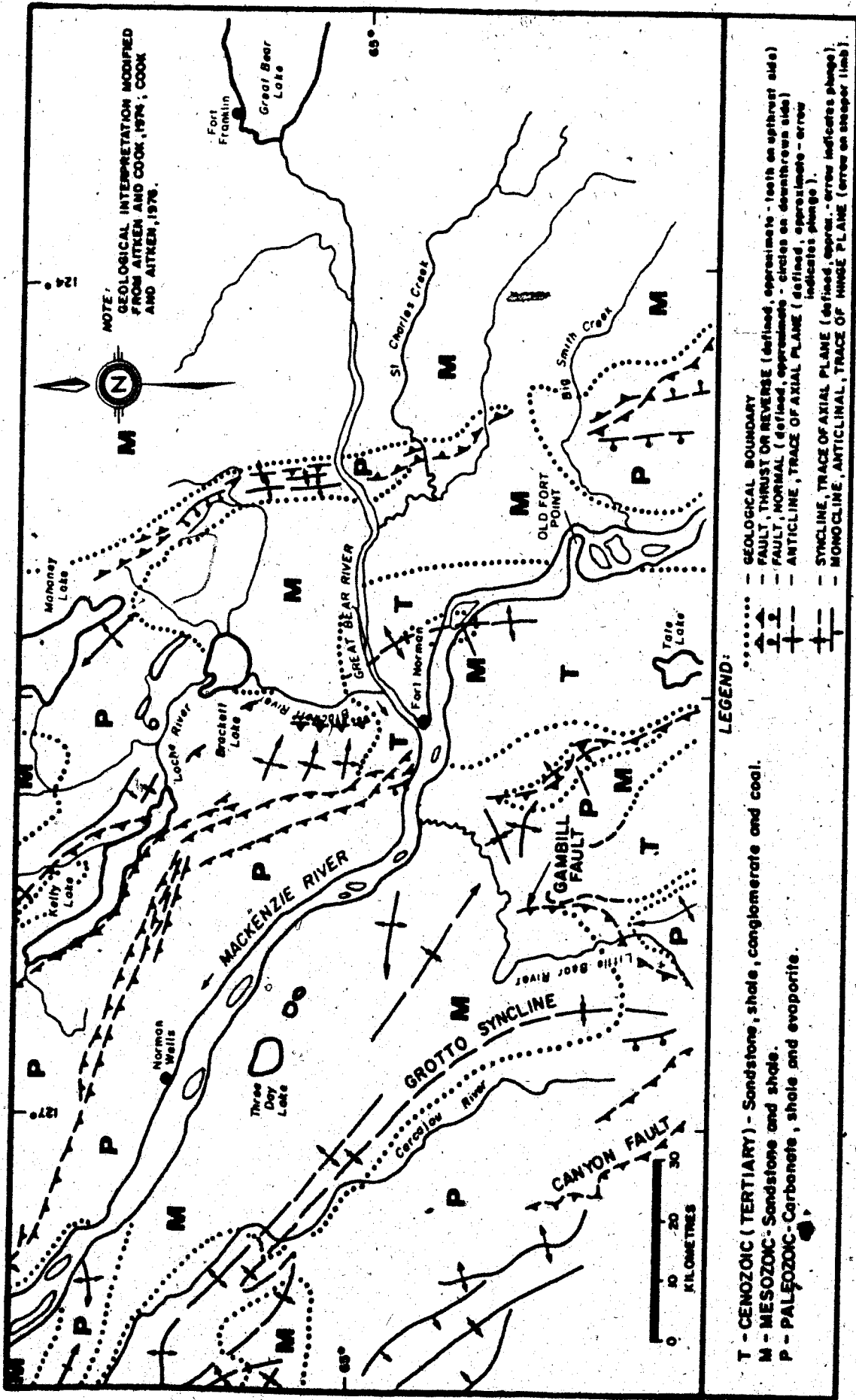


FIGURE 2.4 BEDROCK GEOLOGY IN THE GREAT BEAR RIVER AREA



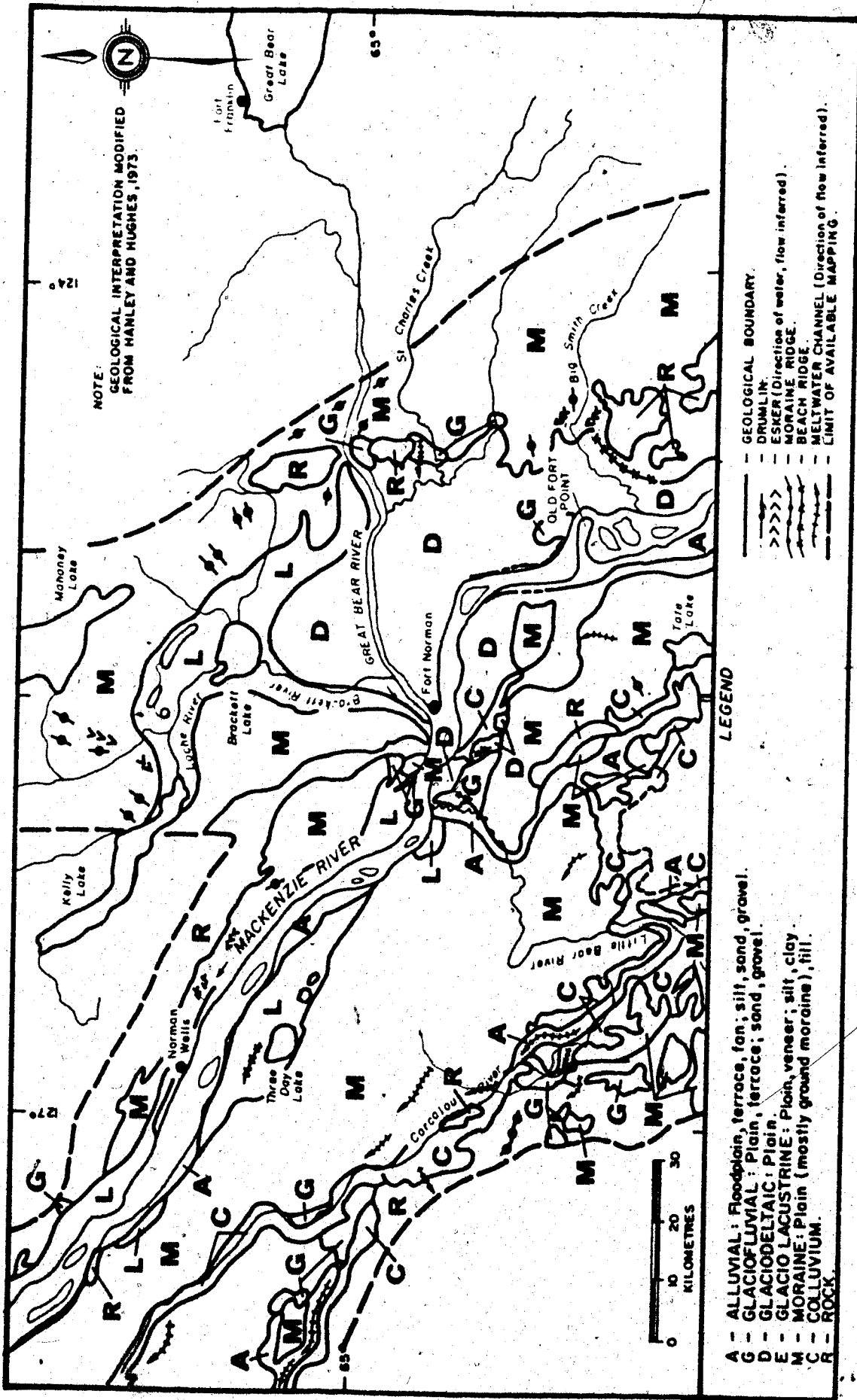
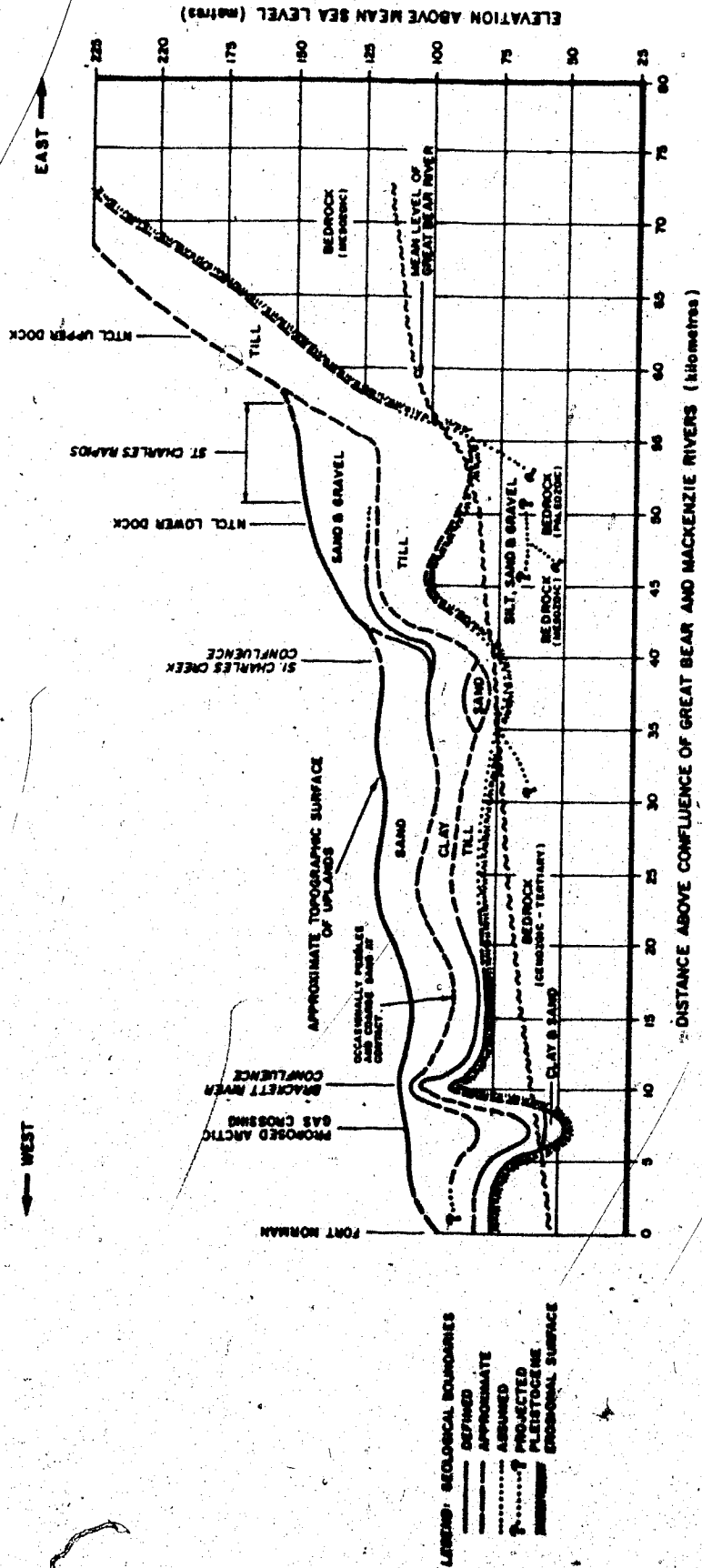


FIGURE 2.6 SURFICIAL GEOLOGY IN THE GREAT BEAR RIVER AREA



**FIGURE 2.7 CROSS-SECTION OF QUATERNARY STRATIGRAPHY BETWEEN KM 0 AND KM 75 OF GREAT BEAR RIVER**



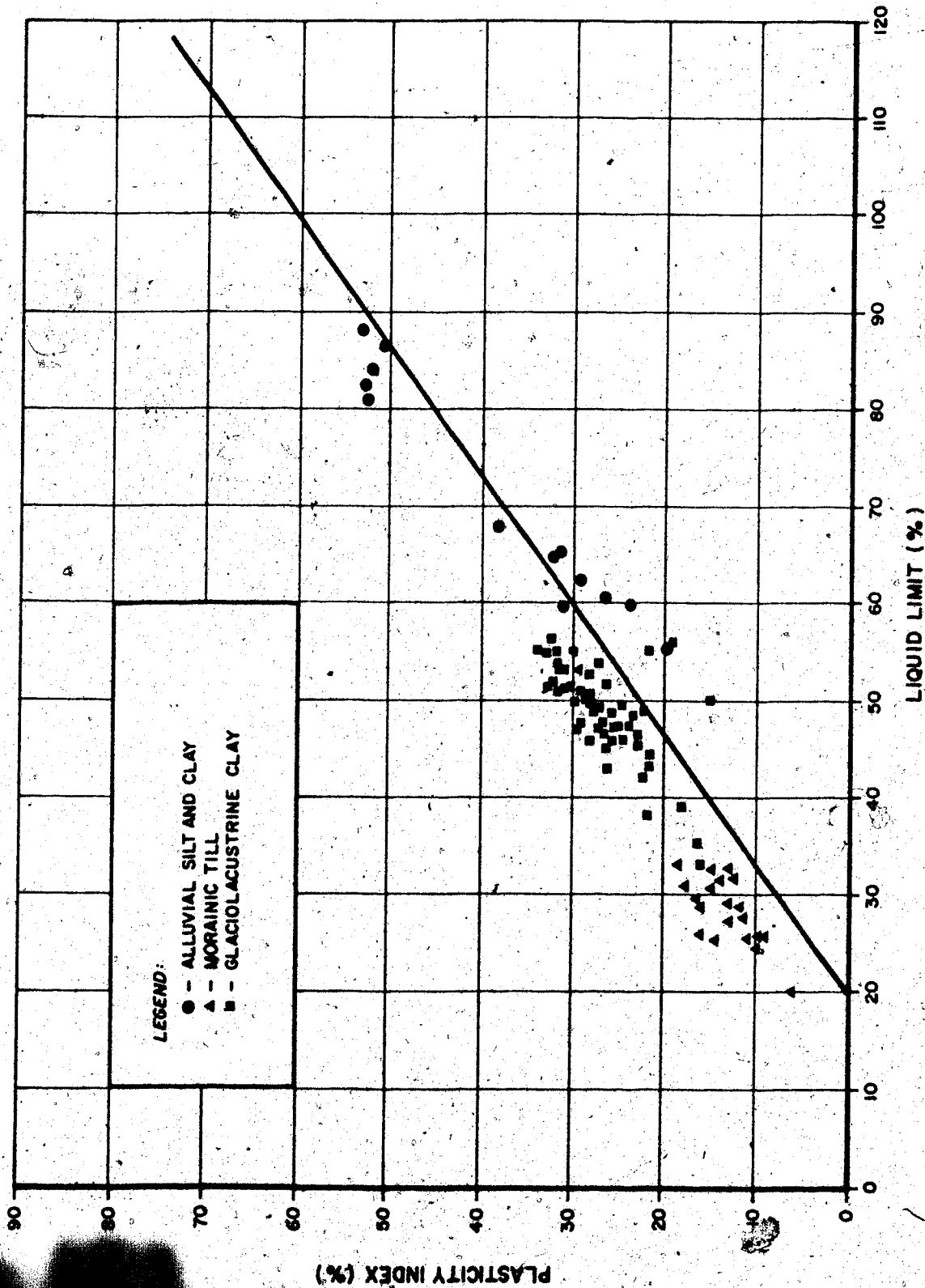
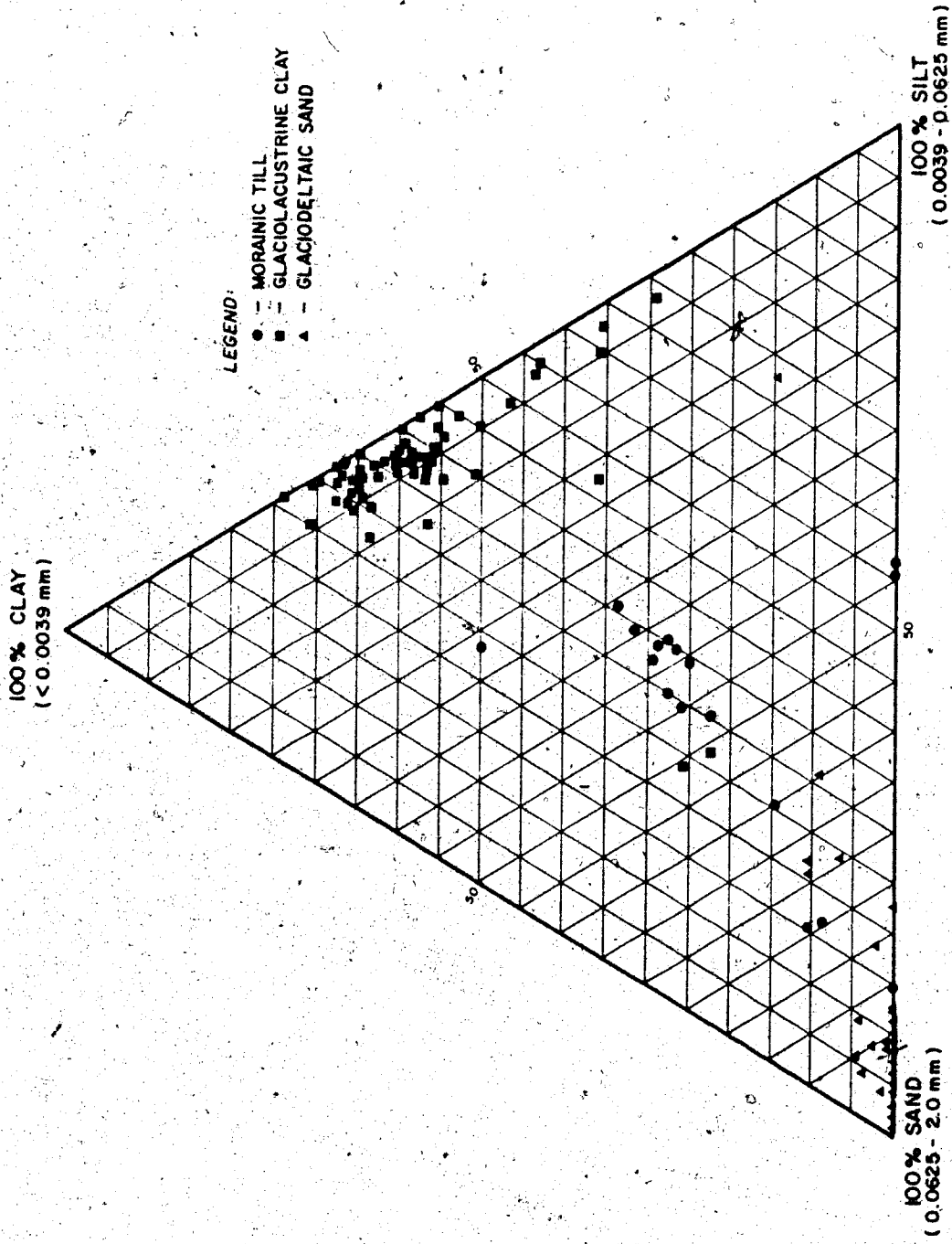


FIGURE 2.8 PLASTICITY CHART FOR FINE-GRAINED SOILS FROM THE GREAT BEAR AREA



**FIGURE 2.9** TEXTURAL CLASSIFICATION FOR THE LESS THAN 2.0 MM SIZE FRACTION OF SOILS FROM THE GREAT BEAR RIVER AREA

## CHAPTER III

### FIELD METHODS AND GEOTECHNICAL PROPERTIES OF GREAT BEAR RIVER SOILS

"Frank, as I have already indicated, had an inventive mind. He was always devising gadgets of one kind or another, and one winter, during a long spell of fifty-below weather, he made himself a stick-pin out of frozen mercury." (Berton, 1954, pp. 193)

#### 3.1 Introduction

The site investigation programme had four main objectives:

1. The installation of borehole inclinometers to measure in situ creep deformations in the ice-rich soils comprising the slope.
2. The installation of thermistor strings to establish the temperature gradient affecting each inclinometer casing.
3. The installation of piezometers below the lower permafrost table to assess the overall stability of the slope.
4. To obtain continuous undisturbed cores from each hole in order to establish the stratigraphy, to determine basic soil properties, and to facilitate detailed laboratory testing of deformation properties under simulated field conditions.

The field work was undertaken as a cooperative programme between the Department of Civil Engineering, University of Alberta (U of A), and Northern Engineering Services Company Limited (NES), acting for Canadian Arctic Gas Study Limited. NES coordinated all activities and provided supervisory and technical personnel. U of A planned the instrumentation, purchased and assembled the equipment, and completed the field installations, and as well provided supervisory and technical support throughout the programme.

In this chapter, all aspects of the field programme are summarized, and the site surveys, the detailed geology, and the geotechnical properties of the soils are reported.

### 3.2 Site Description

Great Bear River drains Great Bear Lake from its southwest end near Fort Franklin, flowing westerly for 115 km to its confluence with Mackenzie River at Fort Norman. Its flow is stable because of the high ratio of reservoir to catchment area of Great Bear Lake and a modest 25 to 30 cm annual precipitation in the region. Despite this apparent stability, evidence of ice-jams raising water levels 2 to 4 m is common, and during periods of high water on the Mackenzie, water levels at Fort Norman rise up to 10 m above normal and impound water as much as 15 km up the Great Bear Valley.

The proposed Arctic Gas crossing of Great Bear River is located at  $64^{\circ} 56' N$  latitude and  $125^{\circ} 29' W$  longitude,

approximately 7.2 km above the confluence of Mackenzie and Great Bear Rivers. On the proposed alignment, both banks are stable (Hollingshead and Sowa, 1974). The right bank shows no evidence of instability for several kilometres upstream or downstream. Over the same reach, the left bank is consistently steeper with abundant evidence of instability. Upstream, old multiple retrogressive slides completely encompass an abandoned meander terrace, and downstream recent slides and bimodal flow are common. The frequency of instability along the left bank, coupled with its relatively steeper slopes, made it the obvious choice as the field site for this study. A topographic plan and cross-section are shown in Figures 3.1 and 3.2 respectively. The following description refers to the site on the left bank.

The slope rises at an average of 22 degrees over 46 m from the river to local plain level. The steepest portions are near the toe and the crest where the slopes are 27 and 31 degrees respectively. Black spruce up to 9 m high are widespread, and birch and white spruce averaging 8 and 12 m respectively are common at the top. Shrubs, including labrador tea and alder, are abundant between the river and high water level, in natural clearings, and along seismic lines. Reindeer moss and lichens in a layer up to 0.6 m thick make up the near surface ground cover.

There is no evidence of erosion by the river at the toe of the slope, and a comparative study of aerial photographs between 1950 and 1975 gives no indication of lateral migration. The high

water level is approximately 6 m above the mean summer level and within this zone ice abrasion has locally removed the moss and lichen sufficiently for thermal degradation of the underlying frozen mineral soil. Such exposed areas are limited in extent and were observed to be self-healing within one or two thaw seasons.

As shown in Figure 3.1, sometime prior to 1974 a seismic line was cleared to the top of the slope. Further clearing over the upper third was completed in March of 1974 during site investigation associated with the crossing design (Hollingshead and Sowa, 1974).

### 3.3 Equipment and Materials for the Field Instrumentation Programme

The programme called for a helicopter-portable, wet drilling rig with minimum depth capabilities of 60 m. Dry sampling was to be carried out with modified CRREL ice augers at least to the limit of fine-grained sediments. Wet sampling was to commence with a 'PQ' wire-line core barrel, if and when the dry auger reached refusal in stoney sediments, and continued to the desired depth. Stringent environmental and technical regulations required the drilling fluid to be a non-toxic, biodegradable water-based mud chilled constantly to at least  $-2^{\circ}\text{C}$ . Inclometers were to be installed well below the deepest ice-rich zone encountered in Quaternary sediments, and grouted to the surface with a chilled, low heat of hydration grout. Piezometers were to be installed in holes advanced by mud-rotary drilling with sampling limited to grab samples.

This section describes the equipment and materials used for

drilling, sampling, and installation of the instruments. Actual instrument specifications are given in Chapter IV.

### 3.3.1 Drill and Support Equipment

The drill used was a modified Mayhew 200 owned and operated by Big Indian Drilling Company, Calgary. The basic machine was completely re-designed by Big Indian personnel to satisfy the depth and portability requirements of the programme. The modified version was referred to as a "Heli Drill 500".

The rig consisted of two units, each weighing approximately 1500 kg and fitted with hooks at four specific points to afford easy connection to a helicopter sling, and to ensure it remained in a secure horizontal position during suspended transport. The rig is shown during assembly in Plate 3.1. One unit was the drill frame, which housed the rotary table, draw works, mast assembly and drilling engine; the second was the power base on which the mud pump and circulation engines were mounted together with a 12 volt electric/hydraulic pump and three hydraulic legs for levelling. The two motors were Wisconsin VH4D, 30 h.p. air cooled gasoline engines; each operated independently. An optional light steel frame and nylon reinforced canvas cover (sock) enclosed the rig during operation (Plate 3.2). These were dismantled and transported apart from the two main units.

The casing and three types of drill rods used are listed with their dimensions in Table 3.1. The '2HIF' rods were used with the

modified CRREL barrel and for mud-rotary drilling. 'PQ' rods were used with the 'PQ' wire-line core barrel and 'A' rods were required to install the inclinometers. The casing was a contingency for sloughing sand and/or gravel zones, but was only used for protection of the inclinometer installations.

The support equipment included tanks for holding, mixing, and hauling water, a small water pump, and a steel mesh basket. The holding tank had a capacity of 1600 l and was used to store water required for mixing drilling fluids and grout. This was fitted with a fire-box and smoke stack to prevent freezing. Mixing was accomplished through an in-line Venturi mixing hopper and stored in a 700 l mixing tank. All water was drawn from an open channel in Great Bear River using a 350 l tank slung below a helicopter. The tank was made from segments of two 200 l drums. A small water pump, powered by a 2 h.p. Briggs and Stratton engine, was used to transfer water from the hauling to the storage tank and from the storage to the mixing tank.

The steel mesh basket was used to transport small heavy items such as the core extruder, subs, couplings, tools, and the frames and sock for the drill, as well as any miscellaneous equipment that could not be manually carried between sites. Some drill rods were also transported in the basket, but most were slung independently.



### 3.3.2 Sampling and Support Equipment

Dry coring was carried out with two identical modified CRREL ice augers (CRREL barrels) built in the U of A Machine Shop. Each was constructed according to specifications reported by Roggensack (1977), with the exception that a cutting shoe was added to limit abrasion of the fixed cutting foot. The CRREL barrel assembly is illustrated in Figure 3.3. The cutting teeth were made in the Technical Services Machine Shop, University of Alberta, and were also built according to the specifications given by Roggensack (1977). Tungsten carbide insert teeth were used exclusively in the sand. Oxy-acetylene welding equipment allowed the inserts to be adjusted or replaced as necessary in the field. Case-hardened teeth were used in the clay and, with limited success, in the till.

Two identical CRREL barrels were used throughout the project in order that drilling operations could continue while core was being extruded. This was also a contingency for possible loss or damage to one of the devices.

In hole GB3 a NES CRREL barrel was used. The basic structure was similar to the U of A barrel except the former had no cutting shoe and used slightly different tungsten carbide insert teeth. The NES barrel worked well in till and allowed continuous sampling until cobble-size rocks were encountered.

The presence of large rocks in the glacial till prevented continuous use of CRREL barrels. Despite many efforts, a change to wet drilling and sampling proved necessary within one or two metres

below the clay-till contact in each of the continuously sampled holes. A 'PQ' size wire-line core barrel was selected as the best device to facilitate continued coring, while at the same time maintaining optimum uphole quality for the inclinometer and providing the maximum core diameter possible (Hvorslev, 1949; Cumming, 1975).

The 'PQ' wire-line core barrel system was supplied by Big Indian Drilling Company. Specifications of the assembly are illustrated in Figure 3.4. The core barrel used a tungsten carbide insert bit that proved satisfactory in all lithofacies except the glacial till where considerable time was lost cutting through large rocks.

The inner barrel was fitted with a basket type core catcher and plastic liners. Use of the liners was discontinued because of difficulties in extruding the sample, and because on one occasion the liner buckled during coring. The reason for this problem remains unclear despite the fact that the sizes of the bit, core catcher, and liner were measured and found to be compatible, and great care was taken to ensure correct assembly prior to each coring run. Notwithstanding the possibility that the liners and bit sizes were in some way incompatible, it is assumed that the step temperature introduced by fluid circulation and/or stress release caused expansion in the sample between the times of cutting and entry into the liner.

An hydraulic extruder, with adaptors for the CRREL and inner

'PQ' wire-line core barrels, was built by Western Hydraulic and Machine Limited, Edmonton. Power was supplied from an electric-hydraulic pump used for the drill rig levelling system, but the extruder was fitted with independent controls. The stroke of the ram was 90 cm, which was sufficient for most dry cores. Plugs 40 cm long were built to accommodate the extra length of the 'PQ' cores, although without the plastic liners most of these were extruded by gravity after removal of the inner barrel shoe and core catcher.

Trays made from large diameter PVC pipe were used to hold and support the cores during visual inspection and photo logging. Each core was double wrapped in polyethylene sample bags, and stored and transported in one of the two types of boxes illustrated in Figure 3.5.

### 3.3.3 Helicopters

A Bell 204B helicopter was used to move all heavy equipment during mobilization from the Fort Norman air strip and operation at the site. The machine had a rated lifting capacity of 1800 kg and the cold ambient air temperatures during the programme made this a practical operating maximum, although attempts were made not to exceed 1600 kg in any haul. A Bell 206B with an external load capacity of 630 kg was used for ferrying personnel and slinging water and other light materials. Both were owned by Associated Helicopters Limited, Edmonton. The 204B was based in Norman Wells and the 206B in Fort Norman throughout the programme.

### 3.3.4 Drilling Fluid

In order to realize the sampling and instrumentation objectives of the field programme, the mud system had to comply with environmental regulations and satisfy several technical problems as well as the basic functions of a drilling fluid. Environmental regulations prohibited the use of oil-base muds because of the proximity of Great Bear River. In addition, the fluid had to be non-toxic and biodegradable since the only practical means of disposal was to discharge it near each site. The salient technical requirement was that mud be maintained at or below  $-2^{\circ}\text{C}$  in order to minimize in situ thermal disturbance, recover high quality ice-rich core samples, and maintain the stability of the ice and soil comprising the walls of the hole. Secondary technical considerations were that the mud chemicals should in no way corrode or otherwise degrade the ground ice, and that it should have filtrate capacity for zones where water loss was anticipated.

The mud system selected was developed with the assistance of Baroid of Canada Limited, Calgary. The basic components were KCl (potash), Aquagel and/or Zeogel, Kelzan XC-Polymer and Drispac. The proportions of each and the resulting standard properties of the mud are given in Table 3.2.

The use of KCl provided freezing point depression according to the relationship in Figure 3.6. It was considered superior to NaCl because it was much less corrosive.

Aquagel and Zeogel are trade names for sodium bentonite and

attapulгите respectively. When in contact with water, these colloidal size clay minerals readily hydrate (yield) to form stable colloids which then dominate the viscosity and gel strength properties of the mud. Aquagel was the principal clay used for the programme, and since it does not yield in brine solutions it was prehydrated in fresh water before the KCl was added. Zeogel hydrates to a stable suspension in salt water, and was added to mud already in use.

Kelzan XC-polymer, an industrial grade xanthan gum, is a high molecular weight linear polysaccharide. Water solutions of this polymer are extremely pseudoplastic; once the yield point has been exceeded the viscosity is inversely proportional to the amount of shear. Total viscosity is recovered almost immediately upon the release of shear. The solutions are unaffected by high concentrations of salts with monovalent cations, and show no viscosity alteration in sub-zero temperatures. Use of this additive allowed viscosity in the annulus to be controlled without adversely affecting the penetration rate, which is dependent upon viscosity at the bit. It also increased the yield point, which was important in order to suspend cuttings during periods of non-circulation when the core was being withdrawn.

Drispac is a high molecular weight polyanionic cellulosic polymer, which is much less degradable than Kelzan polymer. Many properties of the two additives are common, but of particular importance in the Drispac is its ability to control water loss. In

any water-based mud, regardless of salinity, it forms a thin impervious filter cake over porous zones to prevent fluid intrusion. At the Great Bear River site it was used for three important reasons: first, simple control of water loss reduced the cost of hauling water and minimized the mud requirements of the programme; second, because river-section observations had indicated the site was over a buried river channel, pervious ice-poor zones were expected; third, overall control of fluid intrusion assured optimum hole condition for the inclinometer.

The likelihood of thief zones was anticipated, but no special materials were acquired at the outset. When the problem developed repeatedly and thick slurries of Aquagel and Drispac were ineffective in recovering circulation, sawdust and bran additives were used. When these also proved ineffective, bentonite balls, made by hand from Aquagel, were poured into the hole from the surface. This technique was only moderately successful. Finally, Kwik-seal, a commercially available expansive plastic sealant was obtained and used successfully whenever circulation problems developed.

Support equipment included a Venturi mixing hopper which was used in-line with the mud pump and mixing tank as shown in Figure 3.7. All components were added through this in order to reduce the difficulty and time required for mixing. Other accessories included a mud balance and Marsh Funnel used to measure the density and viscosity of the mud respectively. The mud temperature was checked

frequently with a pocket thermometer.

### 3.3.5 Grout

Grout for the inclinometer casings had to satisfy stringent technical requirements, some of which were similar to those of the drilling fluid. It had to be placed and set under sub-zero ambient temperature conditions in order to prevent melting of ice in the walls of the hole. Similarly, it had to set without excessive or sustained liberation of heat from the hydration process. The curing time had to be rapid because the rig or other heavy objects could not be allocated as ballast on the buoyant casing for more than a few hours. Finally, it was essential that the volume expansion during set be minimal to avoid casing deformations or twist and to limit the introduction of anomalous stresses to ice-rich sediments around the orifice.

A cement meeting these requirements had been developed for oil exploration in the Mackenzie Delta and was available under the trade name "Permafrost Cement" from Halliburton Services Ltd., Edmonton. This is basically a gypsum-based cement with freezing-point depression to approximately  $-6.7^{\circ}\text{C}$ , and a minimum two hour pumping time and minimum 16 hour compressive strength of 72.5 kPa at this temperature. Expansion during hydration is limited to 0.1 to 0.3% and the heat liberated is only 41.9 J/gm compared to 214.2 J/gm in high aluminate cement alternatives<sup>1</sup>.

---

<sup>1</sup> McDonald, D., Halliburton Services Ltd., Edmonton, Alberta, personal communication, December 1976.

7

Assuming the most critical condition occurs when the grout is in contact with ice, it is a relatively simple exercise to show that the melted annulus around the grout in a 'PQ' size hole containing an empty inclinometer casing is slightly greater than 5 mm on the radius. This assumes the ice and grout temperatures are 0°C and the conduction of heat into the surrounding sediments is negligible. Since only random ice structures were expected at the site, it was considered that this amount of local melting would have no adverse effect on the installation. However, to provide an extra heat sink during set, diesel fuel, chilled to approximately -7°C, was added to the empty casing as soon as the attached thermistor strings indicated hydration had begun. In the short term the diesel fuel also reduced the buoyancy of the casing, and in the long term it prevented the build up of ice crystals inside and acted as a lubricant for the inclinometer.

### 3.4 Drilling and Instrumentation Programme

#### 3.4.1 Mobilization

Equipment and supplies were assembled in Calgary and Edmonton before being shipped by truck to Fort Simpson, N.W.T. on March 13 and 14, 1975. On March 16 and 17 they were airlifted to Fort Norman in three separate trips with a Bristol Freighter aircraft chartered from Norcanair of Prince Albert, Saskatchewan. All material was off-loaded at the Fort Norman Airstrip with a forklift D6 caterpillar hired locally. On March 18 it was staged by 204B



helicopter to the first drill site (GB1), which was designated as the staging area for the entire programme. The drilling equipment was placed over the first hole during this move.

All fuel for the programme had been obtained in Norman Wells and cached at the Fort Norman airstrip earlier in the winter. Gasoline and diesel fuel required for day to day operation were slung by helicopter to the site as needed. Refuelling and routine maintenance of the helicopters were carried out at the airstrip.

#### 3.4.2 Hole Location and Site Preparation

Holes GB1, 1A and 1B were located around site GB7 (Appendix A) at the top of the slope; GB2 and GB3 and 3A were located on the only two reasonably level benches between the crest of the slope and the river (Figure 3.1). The number two and three sites were checked by hand level in relation to GB6 and GB7 to ensure that at least several metres of glaciolacustrine clay would be present, and then clearing was begun.

As shown in Figure 3.1, a large clearing was present at the top of the slope prior to commencement of the programme. However, in order to accommodate the equipment and supplies, as well as the trailer and tents, while leaving enough hovering and landing area for the helicopters, it was necessary to expand the cleared area significantly. This was completed by several local residents between March 13 and 16. Later the same personnel cleared the second and third sites. Snow was removed from the number one site

by a D6 Caterpillar which was hired in Fort Norman and walked to the site via 9 km of seismic trails. Snow was removed by hand from the second and third sites.

### 3.4.3 Drilling and Sampling

Field logs summarizing the drilling and sampling records are given in Appendix B. The stratigraphy appearing with these data is improved following laboratory examination and testing of the samples. The remainder of this section is devoted to a brief discussion of the drilling and sampling schedule and methodology.

All operations were carried out around the clock with two twelve hour shifts, each composed of a minimum of one geotechnical engineer, one technician, one driller, and two driller's helpers. Rotations were made between 07:00 and 08:00 hours, and 19:00 and 20:00 hours. While wet-drilling operations were underway, water for night shift operations was hauled immediately after the night shift reached the field; during the day shift, water was hauled as required. Routine maintenance of the rig and support equipment was shared between shifts.

#### Hole GBI

Drilling activities commenced in hole GBI (Figure 3.1) on March 20, 1975. A hole approximately 30 cm in diameter was advanced 20 cm to facilitate easy mounting and disconnection of the CBREL barrel below the rotary table. Coring was straightforward to a

depth of 5.8 m using tungsten carbide insert teeth. After an unusually long run to this depth, the CRREL barrel became frozen in because of the accumulation of cuttings above it. A solution of KCl and later several litres of clean water were added to soften the cuttings. When coring continued, the fluid and sand cuttings quickly formed into a slurry which prevented core entry. To overcome this problem, it was necessary to perforate the top of each barrel to allow the fluid to escape as the sample entered. The slurry also occupied the inside clearance area of the barrel where it dilated during extrusion, generating very high shear stresses and causing difficulty in recovering the sample. Under these circumstances, it was necessary to combine pulsating force on the extruder, tapping the barrel with a hammer and intermittently heating the barrel with a torch. Such practice, together with the corrosive nature of the fluid adversely affected sample quality over the next 7 m, until most of the slurry had been bailed in successive coring runs. To prevent the freeze-in problem a practice of reaming the hole with a 15.9 cm diameter wing bit every 3 to 5 m was adopted, and individual coring advances were limited to between 0.5 and 0.7 m (approximately two thirds of the capacity of the CRREL barrels). In addition, the barrels were washed completely with water after each run to remove any frozen slurry and cuttings that could impair recovery and extrusion, or cause sample breakage because of torsional shear stresses after cutting. These procedures enabled superior recovery and sample quality through the remainder

of GB1 as well as GB2 and GB3 where dry coring techniques were used.

A thin pebble layer at 21.5 m caused no difficulty because the inclusions were small and friable. Case hardened steel teeth were mounted and coring was continued without difficulty through the clay. The length and coherence of each core was optimized by allowing only a fraction of the weight of the drill rod string as down hole pressure.

While pulling core 61, which had reached a depth of 36.9 m, a hammer was accidentally dropped down the hole. An attempt was made to continue tripping slowly enough that the hammer would not bridge the hole, but this was unsuccessful and the CRREL barrel had to be twisted by it at 18.3 m, which badly damaged the flites and resulted in loss of the hammer head. After core 61 was extruded an attempt was made to recover the object with the damaged barrel.

Approximately 20 cm of core were cut as a plug, but the hammer head was not recovered and both CRREL barrel teeth were lost. The fact that the head was missing suggested it had been pushed to the side of the hole, and on this basis a changeover to the 'PQ' system was made in order to continue sampling without concern for dislodging the object or damaging the last CRREL barrel.

The 'PQ' core barrel and drill rods had been set to the bottom of the hole and approximately 2000 l of drilling mud had been added before fluid loss to the gravel layer at 21.5 m was recognized. In an attempt to gain circulation, the core barrel was pulled to 24 m, and heavy mud with sawdust and bran additives was

circulated. When this proved unsuccessful, bentonite balls were prepared at the surface and dumped down the hole in a water slurry. This was a successful sealant, but caused the sand at 11 m to slough, and by the time the drill stem could be pulled above this zone circulation had been lost again. With the ability to continue the hole and its ultimate suitability as an inclinometer installation in question, the site was abandoned.

#### Hole GB1A

The rig was moved approximately 8 m south and drilling resumed on March 25, 1975. Since it was necessary to recover a portion of the time lost, and because the two holes were close together, GB1A was advanced by mud-rotary drilling, almost to the level GB1 had reached, before sampling operations commenced. The viscosity and filtrate components of the mud were increased shortly before reaching the gravel layer, and as a result, no circulation problems developed. However, as the mud weight began to increase naturally through the clay, it was necessary to watch the fluid temperature closely for anomalous increases associated with circulation.

Coring with the 'PQ' system commenced at 31.7 m and had reached 34.8 when circulation was lost to the gravel layer at 20.5 m. After several unsuccessful attempts to seal the zone by the methods outlined in GB1, Kwik-seal, which had been brought from Edmonton as soon as the problem was recognized, was used with

immediate success. Since no further time loss could be afforded, sampling operations were discontinued and the remainder of the hole was advanced with a 15.9 cm diameter wing bit.

The required depth was reached at 05:50, March 28, 1975. The hole was flushed with approximately 500 l of light mud immediately, and approximately the same volume four hours later when mud rings began to form. The inclinometer casing and an attached thermistor string were installed between 13:00 and 15:00 the same day.

Approximately 1000 l of cold water were pumped through the grout system to displace as much of the mud in the hole as possible.

Grouting followed immediately and pumping continued until all drilling mud and water had been displaced and the grout flowed cleanly at the surface. A significant amount of grout above 20.5 m was lost to the gravel bed immediately. A 4 m section of steel casing was pushed to 3 m leaving 1 m above ground to protect the exposed inclinometer casing. Ballast was applied to the inclinometer casing and the rig moved to GB1B on March 28, 1975. On March 30, 1975, the hole was again grouted to replace what was lost to the thief zone at 20.5 m during initial grouting.

#### Hole GB1B

The first piezometer installation was drilled to 40.5 m by mud-rotary advance on March 29 and 30. It was assumed on the basis of preliminary thermistor readings from GB1A, together with a reasonable estimate of remaining thermal recovery, that this depth would be several metres below the lower permafrost table. A 15.9 cm

diameter wing bit was used to 35.4 m where a concentration of boulders in glacial till necessitated a change to a 12.1 cm diameter rock bit. Circulation problems were encountered in the gravel zone but were quickly overcome with increased mud weights and the Kwik-seal additive. The piezometer assembly was installed and grouted between 09:00 and 10:45 March 30, 1975, with the tip at a depth of 40.4 m in glacial till. Approximately 200 l of grout were placed above the piezometer as outlined in Section 3.6.2, and the remainder of the hole was filled with sand from the surface. The rig was dismantled immediately and moved to GB2.

#### Hole GB2

The site for the second inclinometer was located on a bench near mid-slope, only a short distance below GB6. The hole was begun on March 31, 1975 in clay. Two CRREL barrels with case hardened steel teeth were used to 13.54 m, where bouldery till necessitated a change to PQ coring. Many thick zones of segregated ice were encountered in the clay, and despite great care during drilling and extrusion most of the ice was cloudy (fractured, but coherent) or completely broken. This problem was much more severe here than at any other site where the CRREL barrels were used.

'PQ' coring was used intermittently with a 17.07 cm diameter rock bit in the upper 4.5 m of till because of the presence of large boulders and the inability of the 'PQ' carbide insert bit to cut through them at a reasonable rate of progress. An attempt was made

to use the plastic liners with cores 24 and 25; however, these either buckled as the sample entered or caused great difficulty in extrusion, and therefore their use was discontinued. No large boulders were encountered below 20.90 m, which allowed wet coring and continuous sample recovery from the lower part of the till through interbedded clay, sand, and coal, and into the local bedrock. The required depth was reached at 09:20 on April 3, 1975.

The 'PQ' core barrel and drill rods were pulled immediately and '2HIF' stem with a rock bit was set to the bottom of the hole in order to complete the light-mud flushing. These were tripped at 11:45 and the installation of the inclinometer casing and two thermistor strings was carried out between 13:45 and 15:15. Soon after several lengths of casing had been installed, it was noticed that the axes were skewed slightly from true downslope and transverse to slope directions. No attempt was made to correct the orientation because spiralling and possible casing breakage were considered to be much more serious problems. Approximately 400 l of fresh water were pumped through the grout system at 15:45 and the grout was placed immediately after. A 4 m section of steel casing was pushed to 3 m and ballast was applied at 17:00.

After completion of GB2, the drilling rig and most equipment were used on a separate project in the same area for a period of one week. Operations resumed on April 11, 1975 when drilling commenced at GB3.



Hole GB3

The last inclinometer site was located on a narrow bench approximately two thirds of the way down the slope. The drill rig was placed on reasonably level ground, but all support equipment such as the tanks and drill stem had to be placed on timber cribs. Drilling began in clay, and sampling was carried out with two CRREL barrels according to the methods outlined in GB1 and GB2. One of the barrels, which was supplied by NES, was used in the till until large inclusions were encountered. This happened at 7.62 m, and a changeover to the 12.1 cm diameter rock bit and mud rotary drilling was made immediately. After advancing through the till an attempt was made to continue with the PQ coring system. However, the penetration rate was too slow and the hole had to be continued with a 12.1 cm diameter wing bit. The required depth of 28.4 m was reached at 14:45 on April 12, 1975. The hole was flushed with light mud before the drill rod string was tripped. Installation of the inclinometer and thermistor string was carried out between 15:30 and 16:15. Approximately 300 l of fresh water were flushed through the system at 16:30 and placement of the grout followed at 16:45. A 4 m section of steel casing was pushed to 3.5 m and ballast applied at 17:45. The drilling rig was quickly dismantled and moved to GB3A.

Hole GB3A

The final piezometer installation was located approximately 3 m southwest of GB3 on the same narrow bench. The hole was advanced to a total depth of 30.8 m by mud rotary drilling on April 12

and 13, 1975. A 12.1 cm diameter wing bit was used to approximately 6.0 m and between 15.5 to 30.5 m, while a 12.1 cm diameter rock bit was used in the boulder rich till between 6.0 and 15.5 m. The piezometer equipment was installed and grouted between 09:30 and 10:30 on April 13, 1975, with the tip placed at 30.5 m.

Demobilization to a staging yard at Fort Norman followed immediately.

### 3.5 Sample Handling and Logging

After each coring run drilling depths were recorded so that depths to the top and bottom of the core and percentage recovery could be accurately assigned. Cores were extruded directly into PVC holding trays and taken to a preparation area for examination and photo logging. Cores obtained during wet drilling were wiped to remove as much mud as possible (Plate 3.3). Visual inspection and the preparation of field logs involved scraping only enough of the core to identify the lithology and structure as well as ground ice characteristics and distribution. The remaining smear was then redistributed to cover the scraped area and the sample placed in a polyethylene bag. The core number and true top and bottom drilling depths were inscribed on the bag, air was sucked out, and the excess twisted, doubled over and taped near the ends of the core. A label showing the same basic information was taped near the centre of the core. It was then placed inside a second polyethylene bag which was also deaired and tied at each end before being wrapped in corrugated cardboard for packing and transport.

Wrapped samples were packed in snow inside insulated boxes in order to maintain a reasonably constant sub-zero temperature and a high vapour pressure. Once filled, the boxes were topped with snow before being securely closed. U of A containers were sealed with room-temperature-vulcanizing (RTV) silicone-rubber caulking compound to provide extra insulation around the lids. Full containers were stored in the shade or buried in snow until they could be taken by helicopter to Norman Wells. From there they were shipped "Priority Air Freight" on Pacific Western Airlines to cold storage laboratories at either the U of A or NES Engineering and Environmental Laboratories, Calgary.

Samples arriving at the latter facility were immediately unpacked, photographed, catalogued, repacked in polyethylene bags and stored in several different freezers. Those arriving the U of A were left in field wrapping and placed in several different freezers until detailed logging was started several months later. This was carried out in specially equipped cold rooms and involved several steps. First, cores were trimmed at each end perpendicular to the axis to obtain samples for textural analysis and the evaluation of basic engineering properties. The stratigraphy and nature of visible ground ice were described in detail, and the new measurements of core lengths and the dimensions and orientation of ice structures were recorded to facilitate a quick reference for planning the various testing requirements. Finally, the cores were sprayed with a light film of distilled water, wrapped and taped in

"Saran Wrap", wrapped in deaired polyethylene bags, and returned to freezers for storage. In order to complete the detailed logging, samples stored in the NES laboratories were examined in the same way during the winter and spring 1976.

### 3.6 Instrument Installation Procedures

#### 3.6.1 Inclinerometers and Thermistor Strings

The inclinometer casing, accessories and assembly tools were obtained directly from Slope Indicator Company (SINCO), Seattle, Washington. Specifications for all parts of the inclinometer system are given in Section 4.4.3. The grout shoe shown in Figure 3.8 was fabricated in the U of A, Machine Shop.

The string of inclinometer casing required for each hole was partially assembled several hours prior to installation to save time and reduce the risk of alignment errors. A large tent in the staging area at the top of the slope was used for this purpose. It was equipped with a diesel-fuel stove capable of holding the inside temperature at approximately 12°C. All materials were warmed in the tent before preliminary assembly was begun, and the temperature was maintained up to the time of installation to assist curing of the ABS cement.

In the preliminary assembly, the bottom of the lowest ABS section was trimmed immediately above the coupling recess, the grout shoe fitted inside, drilled in eight places and both surfaces were smeared with cement before being refilled and riveted in the

pre-drilled holes. At the opposite end a coupling was cemented and riveted in four places. The alignment tool was fitted into a pair of grooves inside this end of the first segment and its holding line was run through the inside of the second length of casing. While holding the line securely a pair of grooves on the second section was fitted over the tool and the new casing was pushed into position inside the coupling already attached to the first section. Four holes were drilled through the coupling and the casing section while the two segments were held tightly together. In addition, the outside of the casings were numbered and inscribed with felt markers to facilitate rapid alignment without the tool positioned inside. The alignment was subsequently checked with the tool in each pair of grooves before continuing. The remainder of the preparation involved systematically cementing and riveting couplings to the top of each section of casing, and aligning and drilling holes in the bottom of each respective section until a total length of at least 2 m greater than the drilling depth (to the nearest even casing length) had been assembled.

Once the required drilling depth was reached, heavy fluid was flushed from the hole to prevent the development of mud rings during installation. This was accomplished by pumping fresh light weight mud to the bottom of the hole and simply wasting the heavier fluid as it was displaced at the surface. The '2HIF' drill rods were used for this because they took much less time to trip out when flushing was completed. The prepared sections of ABS casing were brought to

the site and laid in order of installation while this procedure was underway.

Installing the string of inclinometer casing was begun by lowering a section of 'A' rod inside the bottom ABS section so that it slid over the inner projection of the grout shoe and rested securely on the rubber gasket at the bottom as shown in Figure 3.8. The lower end of the thermistor string was taped to the bottom of the ABS casing, and the whole assembly was lowered through the rotary table into the hole until about 30 cm of the ABS remained above the table. Two clamps were secured around the ABS casing and the lower of these was allowed to rest across the rotary table. The next section of 'A' rod was hoisted up the mast on a sand line and the second ABS casing slid over it. The two 'A' rods were connected, and both ends of the ABS casing were smeared with cement before being joined and riveted according to the inscribed alignment information. The new rivets were covered with cement and a small amount of heat was applied by passing a heat gun across the coupling. The assembly was left in this position for 5 to 8 minutes while the thermistor string was taped in several places along the assembled sections. When the cement showed definite signs that curing had begun, the second section was lowered to just above the rotary table as before, and the procedure was repeated. Between approximately 23 and 30 m in holes GB1A and GB2 the buoyancy of the assembled string required that it be pushed into the hole. If the necessary force became more than 75 to 100 N the 'A' rod was

connected to the swivel and was pushed by slowly lowering the draw works. When buoyancy was a factor, the ABS casing clamps were placed below the rotary table to prevent the assembled string from rising as successive sections were added.

Preparation of the grout began as soon as the installation activities were proceeding smoothly in order that it would be thoroughly mixed and chilled by the time it was required. When assembly of the casing string was complete, the last section of 'A' rod was securely connected to the swivel and the mud line intake was placed in water at 0°C. Several hundred litres were circulated through the grout shoe to clean the freezing point depressed fluids from the hole ahead of the grout column. The intake was then changed to the mixing trough and grout was pumped until the remaining drilling fluid and water were completely displaced and it returned cleanly to the surface around the ABS casing. The depth of the installation was determined on the basis of required embedment plus the volume of grout that would drain inside the casing as the 'A' rod was pulled. At the outset it was intended that each installation would be embedded approximately one meter into the till. However, when the till and underlying strata were found to contain ground ice, installations at GB2 and GB3 were placed as deep as possible within the time and budget constraints of the programme. As shown in Table 3-4, the desired embedment was achieved within a few centimetres in GB1A and GB3; however, almost one meter more than expected was lost in GB2. The reason for this

is uncertain but it is likely due to leakage of grout from within the pumping system before it was disconnected from the 'A' rod.

Before the 'A' rod string could be pulled it was necessary to ballast the ABS casing by tying several sections of '2HIF' drill rod just above the ground surface. Tripping began by disconnecting the top section of 'A' rod from the swivel and attaching it to the sand line for pulling. Excess ABS casing was cut off at the rotary table and removed with the first section of 'A' rod. A holding dog, bridging the rotary table, was used to secure the remaining 'A' rod string as individual sections were removed. When tripping was completed, the pump, hoses, and drill rods were flushed with clean water and carefully drained. Steel casing was fitted around the ABS casing and pushed until only about one metre remained above ground. The '2HIF' rods were resecured and all equipment was broken down and moved to the next site.

Completion of each installation followed removal of the drilling rig and equipment. When the thermistors indicated that hydration of the grout had begun, cold diesel fuel was poured into the ABS casing to act as a heat sink during hydration. Finally, an aluminium cap was taped over the end of the ABS casing for protection. A timber tripod was erected over the casing and the thermistor cable secured to one of the legs.

### 3.6.2 Piezometers

The piezometers were obtained from Terra Technology



Corporation, Seattle, Washington. For installation, each was fitted into a specially designed housing which was built in the Technical Services Machine Shop, University of Alberta (Figure 3.9).

The piezometer assembly consisted of 2 sections of galvanized steel pipe (Figure 3.9). The larger was '1.5 in.' nominal (at least 3.81 cm diameter) size approximately 1.5 m long. It was perforated over about 15 cm at one end, and 100 and 40 mesh screen were brazed in place over the holes. The piezometer tip was placed immediately above the perforated zone and the leads fitted through a recess machined in the opposite end below the bushing. The instrument and leads were then epoxied into the pipe; an 'O' ring, used initially to hold the instrument in place, prevented epoxy from leaking over the piezometer tip. The lower end of the assembly was fitted with a conical shaped aluminium head and an inverted traffic cone was attached approximately 45 cm above this. A 1.5 m length of '0.75 in' nominal (at least 1.91 cm diameter) size steel pipe was fitted into the open end of the bushing.

Installation of the assembly was very straightforward. The smaller steel pipe was pushed into the bottom of the first 'A' rod casing as far as the bushing and held in this position by pulling tightly on the leads while the 'A' rod was lowered into the hole with the sand line. The casing string was held at the rotary table with a holding dog as each successive section was added. At the bottom of the hole the 'A' rod string was lifted about 2 m and approximately 150 l of grout were placed above the traffic cone.

The casing was then tripped out and the hole backfilled with cuttings. The circulation system was flushed with clean water carefully drained, and all equipment was prepared for slinging to the next site. The installation was completed by erecting a timber tripod and securing the leads to one of the legs.

### 3.7 Surveys

On May 6 and 8, 1975, elevation relative to mean sea level was carried from bench mark 74T061 in Fort Norman, via approximately 9 km of seismic lines to the site. Closure was 5.5 cm. This allowed all surveys at the site to be referenced to mean sea level and also provided an opportunity to check the accuracy of the hand level surveys, which were referenced to the gradient of Great Bear River as described in Appendix A. Comparison of the two methods at the site showed the hand level elevations were within 60 cm of the true value.

Topography at the site was surveyed by stadia. The cleared area was completed on May 7, 1975 and the forested area and gully immediately downstream of the clearing on June 13 and 14, 1977.

### 3.8 Site Geology

The geology of the area has been dealt with in Chapter II, and to avoid unnecessary repetition, the treatment in this section is limited to a brief outline of the stratigraphy at the site, together with comments on its relation to the established regional

framework. The sequence of sediments encountered in each borehole has been projected into the cross-section presented in Figure 3.2. This illustration shows the slope is composed mainly of sand and clay. Till is exposed at river level and the channel has formed primarily in interbedded clay and sand which rest on bedrock.

The undifferentiated siltstone and shale bedrock belongs to the lithofacies of the same name in the lower Tertiary unit (see Section 2.4.3). These rocks are pale brown to brown (10 YR 6/3 to 5/3), laminated, highly arenaceous, and contain an abundance of carbonaceous material. They are weakly cemented, typically break down with moderate finger pressure, and soften only slightly when soaked in water. A near vertical joint set was evident in several of the core samples.

The bedrock is overlain unconformably by interbedded clay, sand, and coal. These strata are alluvial in origin and represent buried river channel deposits of Pleistocene age. They are predominately grey to very dark grey (10YR5/1 to 3/1), highly plastic, intensely fissured and slickensided clay. The bedding structures have been highly contorted by ice thrusting. Beds of dark grey (10YR4.1), poorly graded, argillite and quartz sand occur randomly and have no apparent gradational relationship with the clay strata. A thin allogenic coal bed was also found within the clay strata.

Glacial till deposited by the Classical Wisconsin Laurentide ice sheet rests unconformably on the alluvial deposits. It is

comprised of brown to very dark brown or grey (10YR5/3 to 3/1 or 4/3), low to medium plastic, fissured, silty clay, with rocks ranging up to boulder sizes. Pockets of medium-grained quartz sand are common. Reticulate ice facies occur near the till contacts.

Overlying the till with apparent conformity are thick deposits of glaciolacustrine clay. These accumulated in a glacial lake impounded at approximately el. 150 m during late Wisconsin deglaciation. The sediments are dark grey to dark grey-brown (10YR3/1 to 3/2), rhythmically laminated, medium to high plastic, silty clay. They are fissured throughout and commonly slickensided in association with ice veins, as shown in Plates 3.4 and 3.5. Reticulate ice, and to a lesser extent, segregated ice are the most common permafrost forms, with minor stratified ice near the till contact.

Glaciodeltaic sand, the upper-most lithofacies at the site, lies conformably on the glacial-lake-basin clays. A pebble unit at the bottom testifies to the sudden end of the glaciolacustrine phase. The sands are vari-coloured, medium to fine-grained, quartzose deposits, with horizontally bedded and laminated, and cross-laminated structures. Discrete low plastic, horizontal silt laminae occur in clusters throughout, and thin organic-rich cross-laminae are common near the top. Pore ice is the most common permafrost form; steeply dipping ice veins were also noted as shown in Plate 3.6.

### 3.9 Geotechnical Properties

An extensive programme of index testing to confirm soil classifications is reported with the borehole logs in Appendix B. These data are reproduced and combined with textural analyses in Figures 3.10 through 3.15, to provide a complete summary of the basic engineering properties of each lithofacies.

Laboratory studies of shear strength properties were carried out for the alluvial and glaciolacustrine clays and the glaciodeltaic sand. Data from these programmes are discussed briefly in the following sections to establish the strength properties of respective lithofacies.

#### 3.9.1 Direct Shear (DS) Tests on Thawed Alluvial Clay

Samples of alluvial clay from GB2 were tested in 6.35 cm diameter circular reversing direct shear boxes. Well advanced circumferential core desiccation caused by grout contamination precluded use of the more common 6.0 cm square boxes, and insufficient samples were obtained to allow for a triaxial testing programme. All samples were stage consolidated to 1,800 kPa before reducing the normal stress to commence shearing at displacement rates of 0.2 cm/day. Stage testing was carried out on several samples. The results of each test are given in Appendix D.

The peak strength envelope for alluvial clay is illustrated in Figure 3.16. For the range of normal stresses from 150 to 1350

kPa the effective friction angle is  $26^{\circ}$ <sup>1</sup> and the effective cohesion intercept 84 kPa. No curvature is evident, but the ubiquitous fissuring leaves little doubt that it would be significant over a lower stress range. Residual values shown in Figure 3.17 give an effective friction angle of  $19^{\circ}$ , but the data are much less consistent. The range among envelopes from each stage loaded sample is from  $13^{\circ}$  to  $21^{\circ}$ , reflecting the natural heterogeneity of the alluvial deposits and the difficulty of selecting similar samples because of contorted bedding structures. It is likely that lower strength parameters would have been obtained from samples of alluvial clay lying stratigraphically below those tested. The alluvial clays in these lower cores have higher plasticity and finer texture (Figure 3.12 and 3.13); however, desiccation during storage (Plate 3.3) rendered them unsuitable for strength testing. Based on the mineralogy reported in Chapter II, it is assumed that residual friction angles averaging  $10^{\circ}$  to  $12^{\circ}$  are realistic for these alluvial clays (Kenney, 1967).

### 3.9.2 Consolidated Undrained Triaxial Compression (CUT) Tests on Thawed Glaciodeltaic Sand

Strengths of the glaciodeltaic sand were measured in CUT tests. These were carried out on undisturbed 10 cm diameter cores, which were set up in the frozen state and thawed prior to

---

<sup>1</sup>The effective friction angles and cohesion intercepts quoted in this section are rounded from linear regression analyses.

consolidation and shearing. Sample preparation and testing procedures reported by Roggensack (1977) were followed with the exception that back pressure was used during consolidation. Zero back pressure was used during consolidation in three preliminary tests, but low saturation levels and the development of negative pore pressures during shear necessitated a change to high back pressures for the remainder of the programme. The void ratio of the samples averaged 0.79, and ranged from 0.68 to 0.85, which indicates a loosely packed structure by comparison with other uniform silty sands (Lambe and Whitman, 1969).

Distinct shear planes developed in all samples at failure, and test results shown in Appendix D indicate a slightly dilatant stress-strain behaviour in each test. The strength envelope in Figure 3.18 shows an effective friction angle of  $35^\circ$  and a cohesion intercept of approximately 0.

This friction angle is slightly high in comparison with other uniform silty sands having similar void ratios (Lambe and Whitman, 1969). Although the presence of a quasi-horizontal lamination structure likely accounts for this increased strength, experience in handling thawed sand samples indicates the presence of a weak cement which may also contribute to the higher-than-normal strength.

It has been established that deposition of the glaciodeltaic lithofacies occurred over a period of approximately 1500 years and that major thicknesses in any one place accumulated much more quickly as the delta front prograded. The periglacial climate

probably caused permafrost to develop soon after subaerial conditions were established at the prograding shoreline. Little time was available for cementation prior to the development of permafrost, and any weak cement would have been largely destroyed as the void ratio increased in proportion to the volume increase of water during freezing. The presence of salt concentrations in the depositional environment has been proven by flocculation of the clay materials, and it is proposed these same salts were concentrated in pore spaces of the sand by the freezing process and subsequently precipitated around particles and at their contacts. If this conjecture is accurate, it means the dissolving of this material at some time after thawing could lead to a significant loss in shear strength, where friction angles are reduced to between  $28^{\circ}$  and  $32^{\circ}$  (Lambe and Whitnam, 1969). Field evidence that this does in fact occur is widespread, because this range is consistent with the repose angle described for sand sections in Chapter II.

### 3.9.3 CUT and DS Tests on Thawed Glaciolacustrine Clay

Peak strengths for glaciolacustrine clay were measured in CUT tests similar to those described in Section 3.9.2. Samples were prepared in the frozen state from 10 cm diameter cores, and thawed prior to consolidation and shearing. Sample preparation and testing procedures reported by Roggensack (1977) were followed with the exception that back pressure was used during consolidation to ensure a reasonable level of saturation.



The DS tests were carried out in a conventional manner (Cullen and Donald, 1971) using 6.0 cm square undisturbed samples prepared in the frozen state with the aid of a small lathe and/or a milling machine. Samples were placed in the testing boxes at room temperature and allowed to stabilize under a small normal stress for approximately 48 hours. When the initial testing stress exceed 300 kPa, samples were stage consolidated to the desired normal stress before shearing was begun. Displacement rates of 0.05 to 0.2 cm/day were used. Once peak had been established, the rates were increased by approximately four times, and residual values measured at the initial load increment, and up to six decreasing load increments. The results of all tests are given in Appendix D.

Results from the CUT tests, using maximum deviator stress as a failure criterion, are shown in Figure 3.19. The envelope shows little scatter, and gives a peak effective friction angle of  $21^\circ$  and cohesion intercept of 36 kPa.

DS test envelopes illustrated in Figure 3.20 and 3.21 show the effective shear strength parameters include a peak friction angle of  $23^\circ$ , a cohesion intercept of 10 kPa and a residual friction angle of  $14^\circ$ . The data show little scatter, and even among individual envelopes of stage-loaded samples in Figure 3.21, there is good agreement.

The data for glaciolacustrine clay from both DS and CUT tests are in close agreement and are consistent with effective strength parameters reported by Roggensack (1977) for a similar soil from

Norman Wells. Close correspondence was also established between the consolidation properties and density water content relationships of the two soils as part of the CUT tests. The results shown here have been interpreted as a linear failure envelope because of the high effective stress range used for testing. They complement the data reported by Roggensack (1977) and clearly substantiate his conjecture that a linear failure envelope is established at effective stresses greater than 200 to 300 kPa. Moreover, the similarity in composition and macrostructure of samples from the two locations leaves little doubt that over a lower stress range the glaciolacustrine clay from this site would have a curved failure envelope and a geometric cohesion intercept approaching zero.

#### 3.9.4 DS Tests on Frozen Glaciolacustrine Clay

##### Laboratory Equipment

DS tests on frozen samples were carried out in a temperature controlled laboratory maintained between  $-1$  and  $-6^{\circ}\text{C}$ . Wykeham Farrance direct shear machines (model SB1) fitted with 6.0 cm square shear boxes were used for all testing. Extra temperature control was provided by fluid circulation from a controlled temperature bath, through the load cap and base of the shear box. The outer box was flooded with paraffin oil to damp out temperature fluctuations in the room and to prevent desiccation of the sample. Other details of the testing system have been reported by Roggensack (1977). Two minor modifications to the equipment described by Roggensack (1977)

are: a lever system was used to apply normal load; and, the thermistor was epoxied at the head of a stainless steel sheath and inserted into a pre-drilled hole in the upper shear box in order to monitor temperature as close to the shear plane as possible.

#### Sample Description

Samples were prepared from 10 cm diameter cores obtained between the 24.5 and 29.1 m drilling depth of hole GB1. Geotechnical index properties over this depth are summarized on the GB1 test hole log in Appendix B. Care was taken to ensure that the ground ice content was minimal (approximately 5% visible) and consisted of thin, feather-like ice veins. Individual samples ranged in height from 4 to 6 cm; their natural moisture content varied between 18.7 and 21.7%, and their bulk density varied between 2.02 and 2.09 Mg/m<sup>3</sup>.

#### Sample Preparation

All test samples were prepared in a soil preparation laboratory where the ambient temperature was maintained between -3° and -7°C. A length of core approximately 8 cm long was cut from the main core, and the test sample was trimmed roughly with a band saw. Final trimming to dimensions a few hundreds of a centimetre greater than the shear box was completed with an overhead milling machine fitted with a carbide insert cutter. After noting the dimensions and weight, and sketching visible ice structures, the test sample

was pushed into the shear box. The slight excess left on the sides during final trimming peeled off easily during insertion, facilitating the best possible fit. A nominal seating load of 50 kPa was applied and the controlled temperature fluid circulated while the sample was allowed to come to equilibrium.

#### Testing Procedure

Normal loads were increased in stages not exceeding 50 kPa normal stress, with vertical displacement allowed to stabilize between each loading increment. When the testing normal stress had been achieved, the retaining screws were removed, the upper shear box raised 0.4 mm, and the slowest possible rigid displacement rate of 0.07 cm/day was applied. This rate was chosen in order to minimize the affect of pore ice on strength properties (Sayles and Haines, 1974).

#### Test Results

All direct shear test results are given in Appendix D. Typical test results indicate that the shear stress increased quickly and reached a peak at relatively small shear displacements within the first cycle. During the second and subsequent cycles the maximum shear stress and the rate of change between successive maxima decreased, and a constant or residual shear stress value was approached at large displacements. After a maximum was reached in any one cycle, shear stress values decreased until the direction of

travel reversed. At large displacements the magnitude of this decrease also attenuated and the residual shear stress value was more clearly defined within each cycle.

Vertical deformation within each cycle was quite small and usually limited to less than 0.05 cm. A net decrease in sample height was indicated at the end of each test. This was primarily a result of extrusion, although some consolidation also occurred as indicated by the build up of ice in porous stones at the top and bottom of each sample.

Test temperatures were generally held within the range of  $-1.1$  to  $-1.3^{\circ}\text{C}$ . Two exceptions affected tests 1 and 2 where the first cycle was at temperatures of  $-1.7$  and  $-2.0^{\circ}\text{C}$  respectively.

Peak shear stress values for each test were selected within the first cycle. Data from the six tests are in close agreement as indicated on the peak strength envelope in Figure 3.22. A linear regression fit to these data indicates a friction angle of  $24^{\circ}$  and a cohesion intercept of 232 kPa.

The friction angle shows close agreement with the value of  $23^{\circ}$  determined for the same soil in the unfrozen state (Section 3.9.3). This clearly supports the theory that the presence of ice within a frozen soil matrix does not impede the full development of frictional strength, provided deformation takes place at a slow rate of strain (Vialov, 1962; Ladanyi, 1975).

The cohesion intercept is the component of shear strength supplied by ice. Test results reported by Sayles (1973) and

Roggensack (1977), and reproduced in Figure 3.23 demonstrate the time-dependency of this strength parameter. Since the data reported by Roggensack (1977) are based on similar material and testing procedures, it is logical that any change in the time to failure for direct shear tests reported here would cause an increase or decrease in cohesion in approximate proportion to the relation determined by Roggensack (1977).

Residual shear stress values were determined on the basis of maxima achieved in the last few cycles of shear. In some tests, however, there was still clear evidence of attenuation when the tests were terminated. In these cases it was necessary to use a projected estimate. Residual shear stress data shown in Figure 3.24 show significantly more variation than peak shear stress data. A linear regression fit through all data points provides a friction angle of  $25^\circ$  and cohesion intercept of 67 kPa. The friction angle is still in close agreement with the peak friction angle and the unfrozen angle of shearing resistance, but the cohesion intercept is approximately one quarter of its previous value. An alternative interpretation excludes data from tests 1 and 2. The remaining data points are amazingly consistent and indicate a residual friction angle of  $31^\circ$  with zero cohesion. There appears to be no physio-mechanical basis for such a dramatic increase in friction angle, however, and the interpretation is therefore discounted.

Further analysis of the residual strength data is beyond the scope of this thesis, but the implications of these findings are

worthy of note: although the data are scant and do not afford easy interpretation, they clearly show that accumulated deformation leads to a significant reduction of available shear strength in fine-grained soils. This may also limit the available shear strength along pre-existing shear planes in a soil medium through which permafrost has aggraded. Clearly, the subject of residual strength in frozen soils warrants further research.

TABLE 3.1  
DRILL ROD AND CASING SPECIFICATIONS

Code	O.D. (mm)	I.D. (mm)	wt. (kg/m)	Coupling I.D. (mm)	Threads (per 2.5cm)	Content (1/10m)
A	41.3	28.6	5.64	14.3	3	6.40
*2HIF	88.9	77.8	11.77	60.3	3	47.57
PQ	**117.5	103.2	15.33	flush	3	83.44
Casing	168.3	158.9	17.59	N/A	plain end	N/A

\* More commonly 'HW' size  
\*\* Coupling O.D.

TABLE 3.2  
SPECIFICATIONS FOR DRILLING MUD

Mud Composition:

Component	Quantity (g/l)*
Aquagel or Zeogel	2.91
Kelzan XC-Polymer	0.15
Drispac	0.15
KCl (Potash)	7.27

\* based on 1g/l = 3.44 #/bbl

Mud Properties: Density - 1.08 Mg/m<sup>3</sup> (9.0 ppg)

Viscosity - 47.6 Sec/1 (45.0 Sec/qt)

Filter Loss - 0.5 cc/min (15.0 m/s)



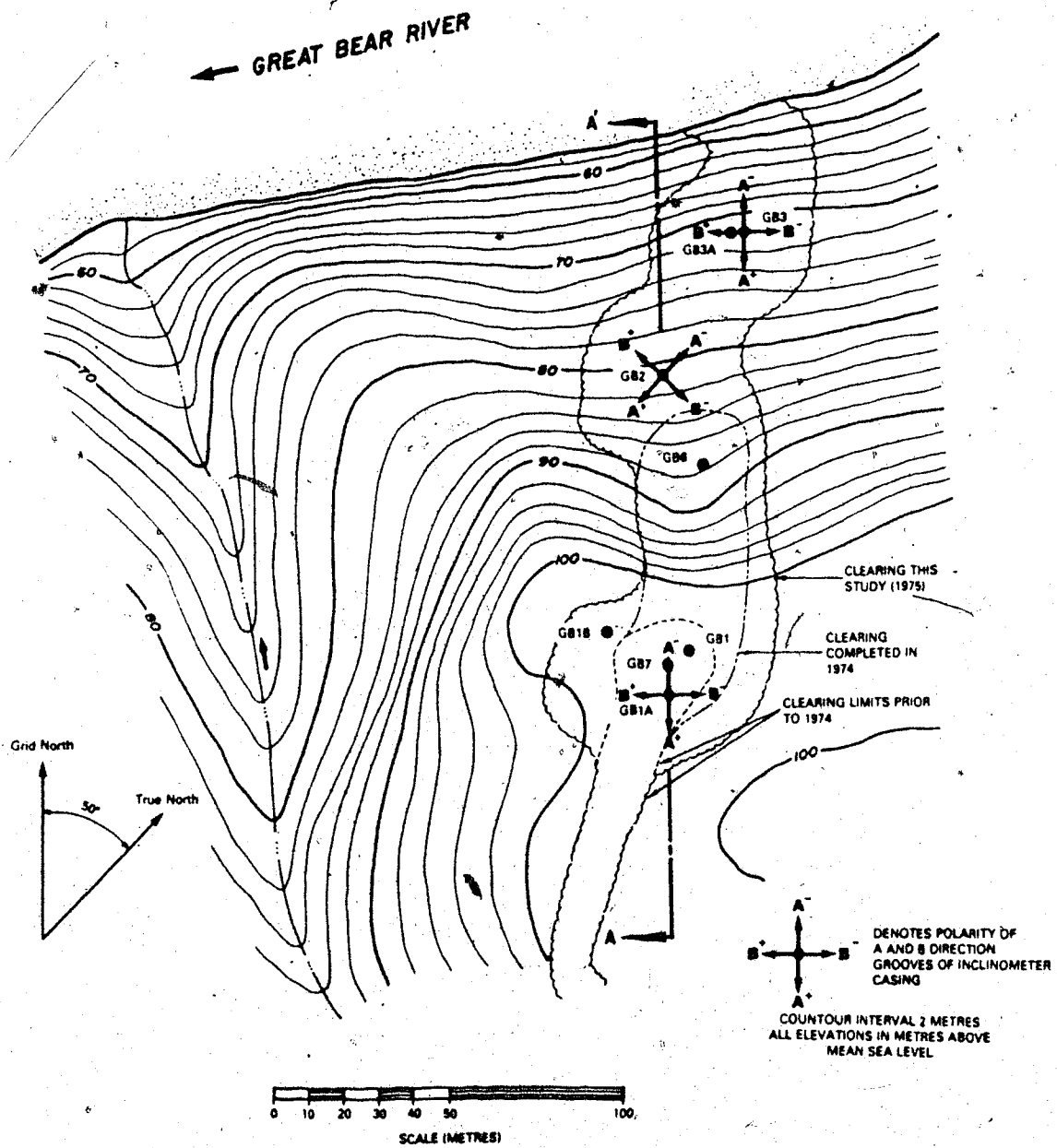
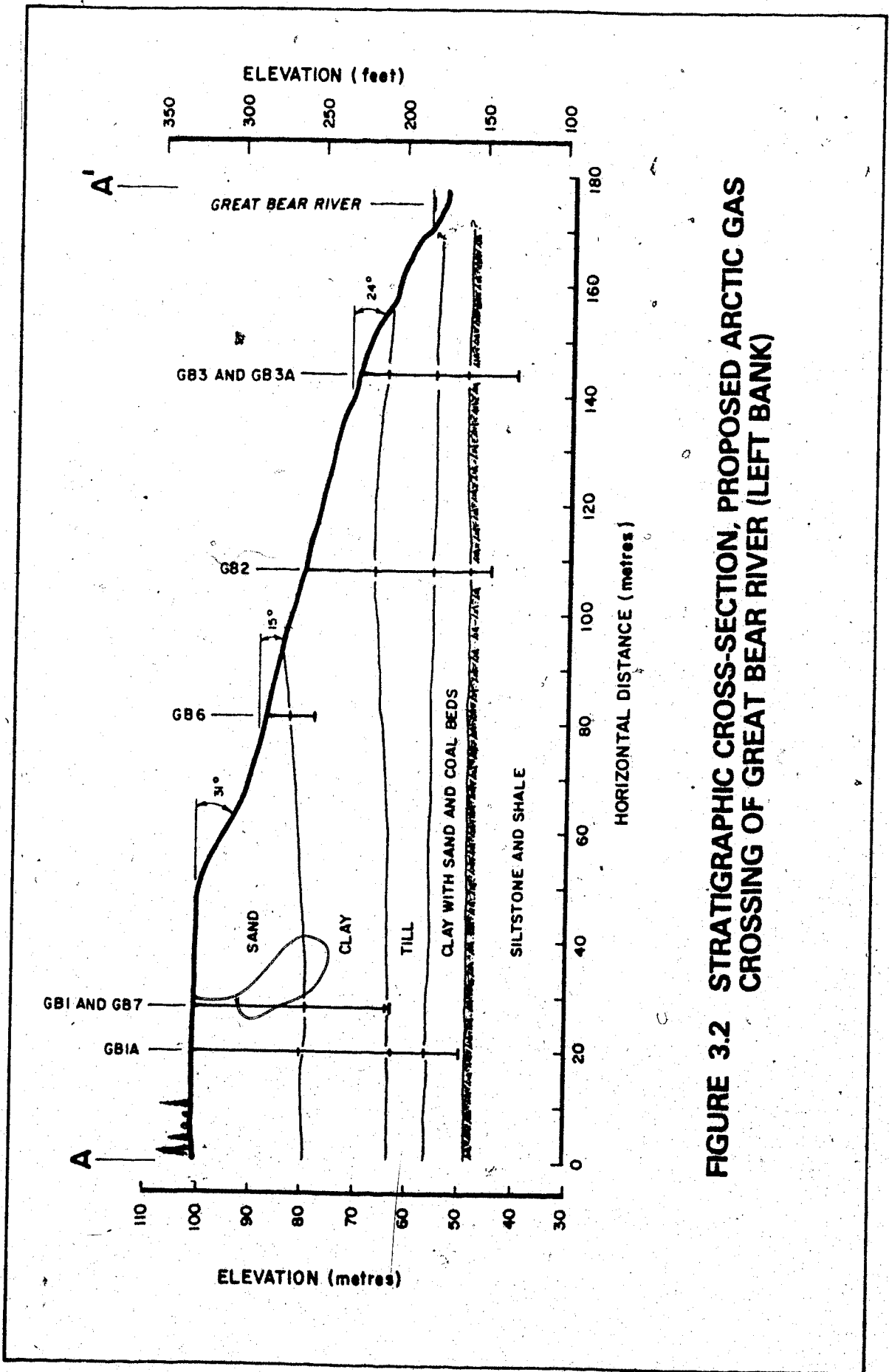


FIGURE 3.1 SITE PLAN, PROPOSED ARCTIC GAS CROSSING OF GREAT BEAR RIVER (LEFT BANK)



**FIGURE 3.2 STRATIGRAPHIC CROSS-SECTION, PROPOSED ARCTIC GAS CROSSING OF GREAT BEAR RIVER (LEFT BANK)**

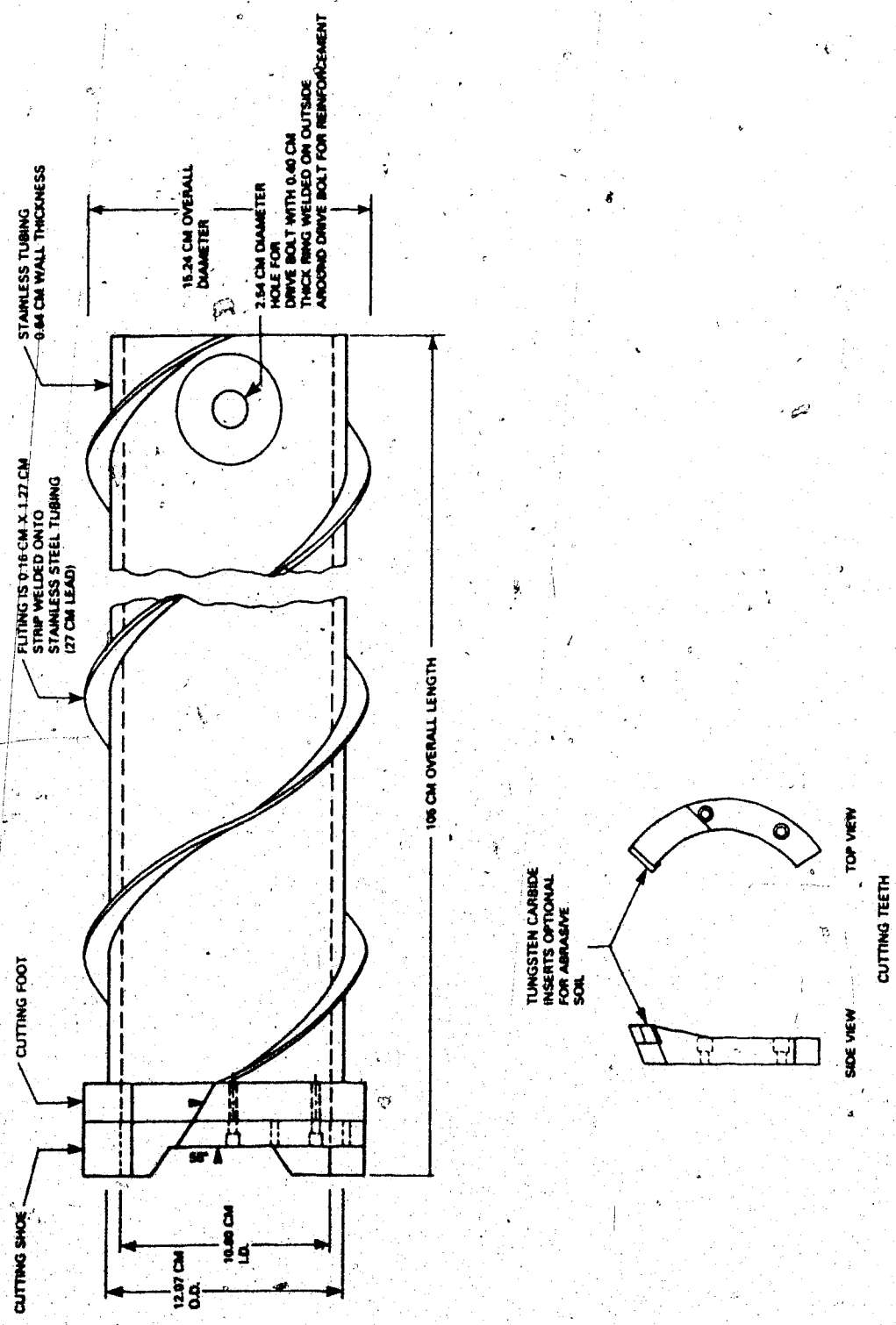


FIGURE 3.3 MODIFIED CRREL CORE BARREL ASSEMBLY (MODIFIED FROM ROGGENSACK, 1977)

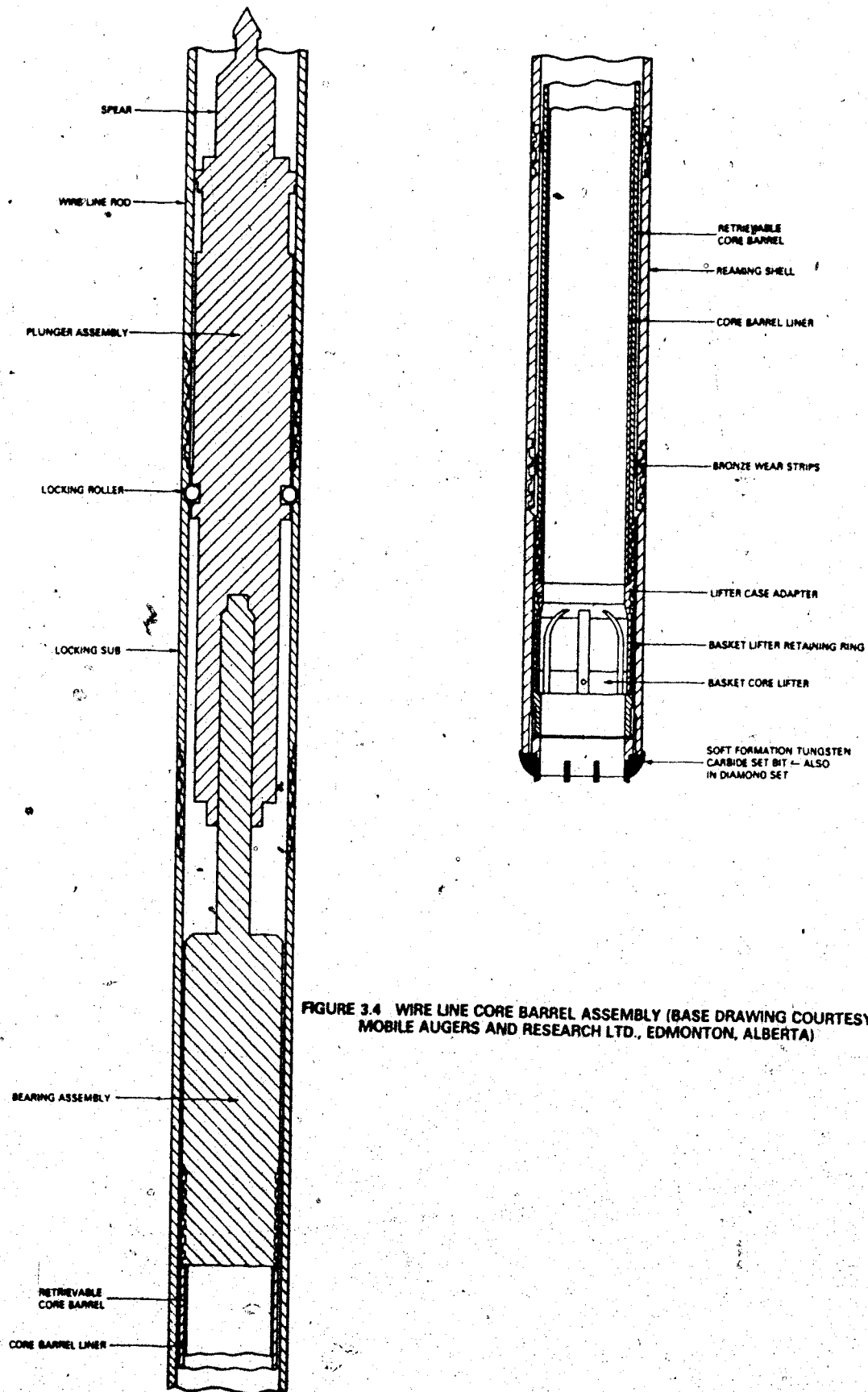
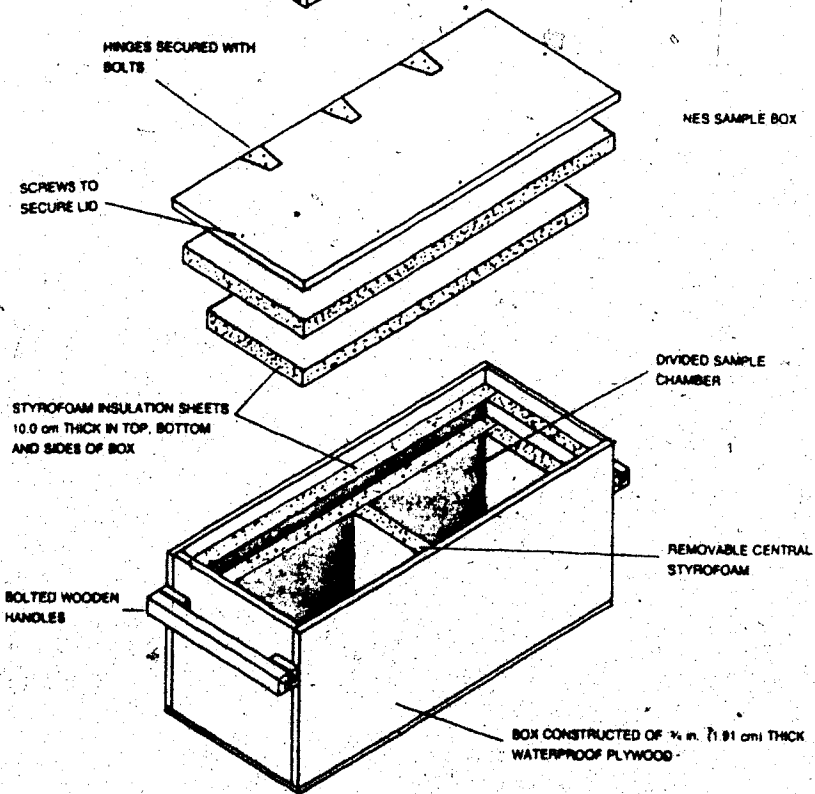
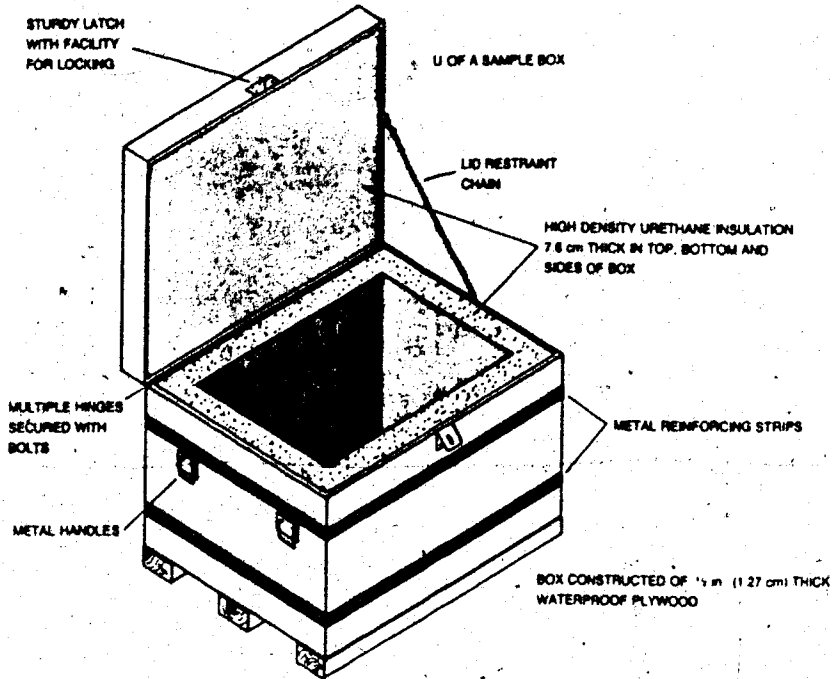
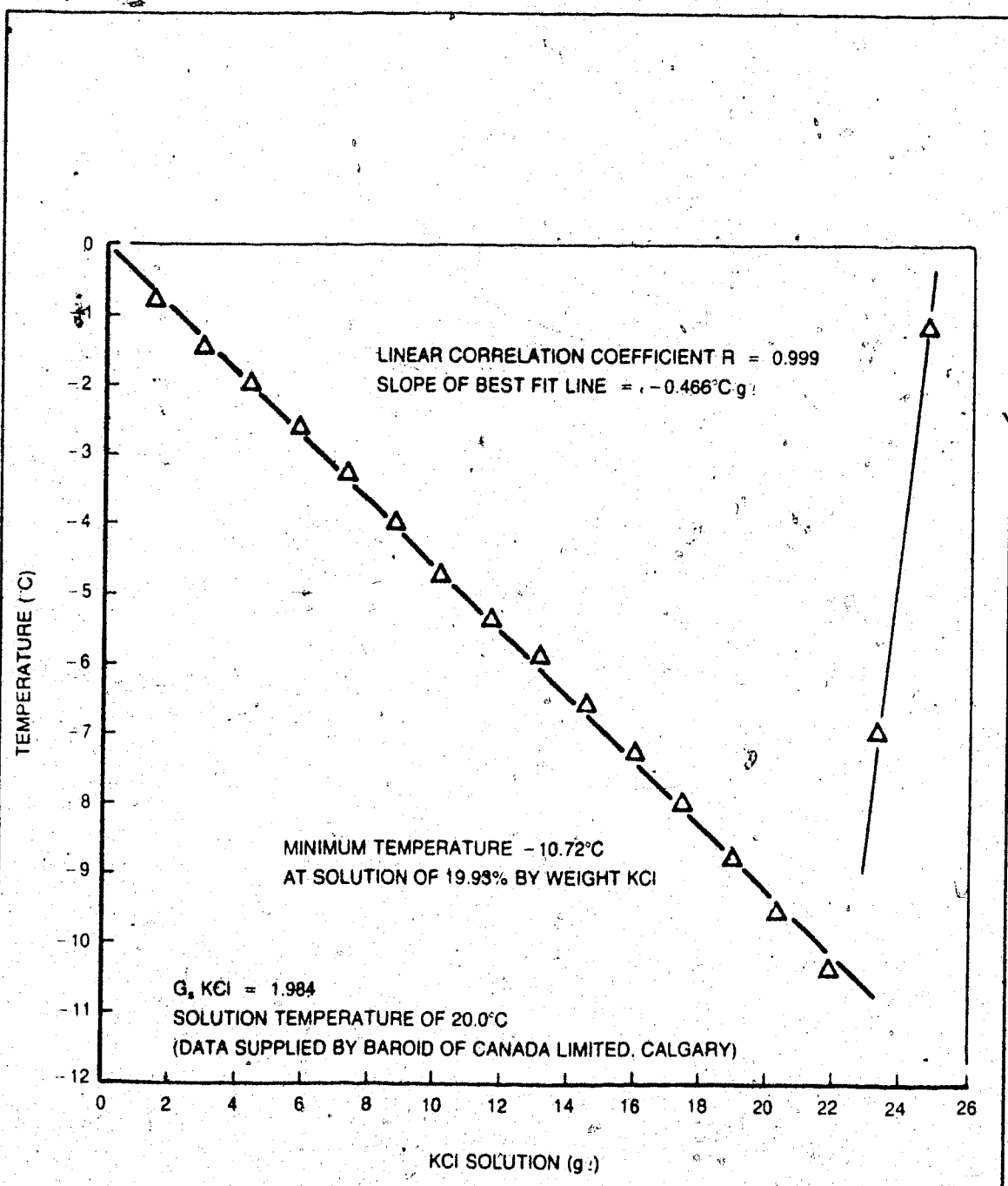


FIGURE 3.4 WIRE LINE CORE BARREL ASSEMBLY (BASE DRAWING COURTESY MOBILE AUGERS AND RESEARCH LTD., EDMONTON, ALBERTA)



**FIGURE 3.5 TYPES OF BOXES USED TO STORE AND TRANSPORT UNDISTURBED FROZEN CORES**



**FIGURE 3.6 FREEZING POINT DEPRESSION CURVE FOR KCl ADDITIVE DRILLING MUD**

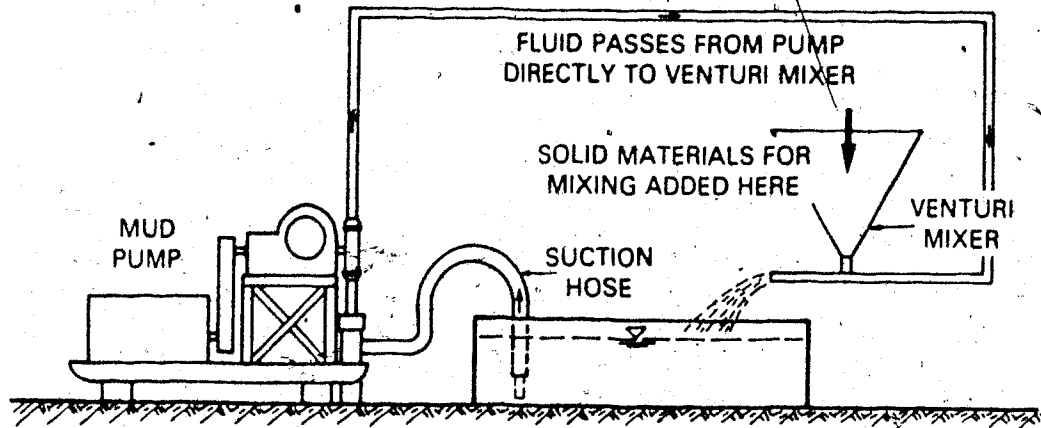


**FIGURE 3.7A MUD SYSTEM ON HELI DRILL 500 — SCHEMATIC REPRESENTATION OF MIXING ASSEMBLY**

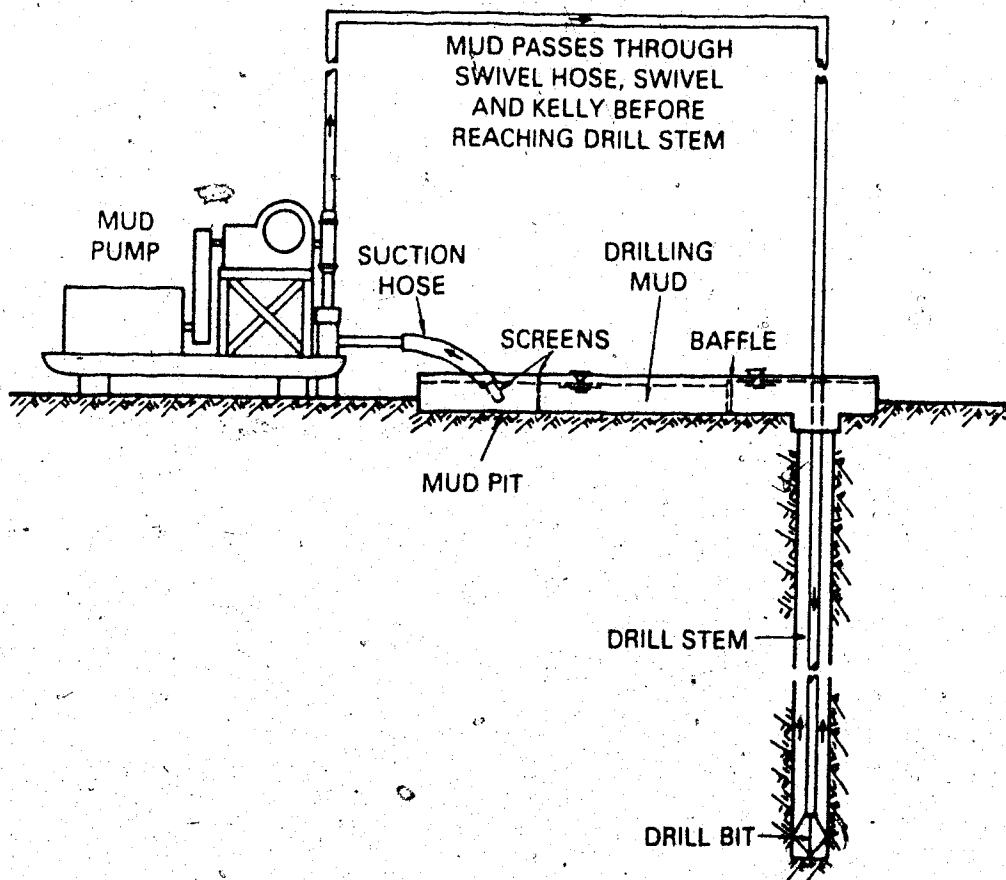
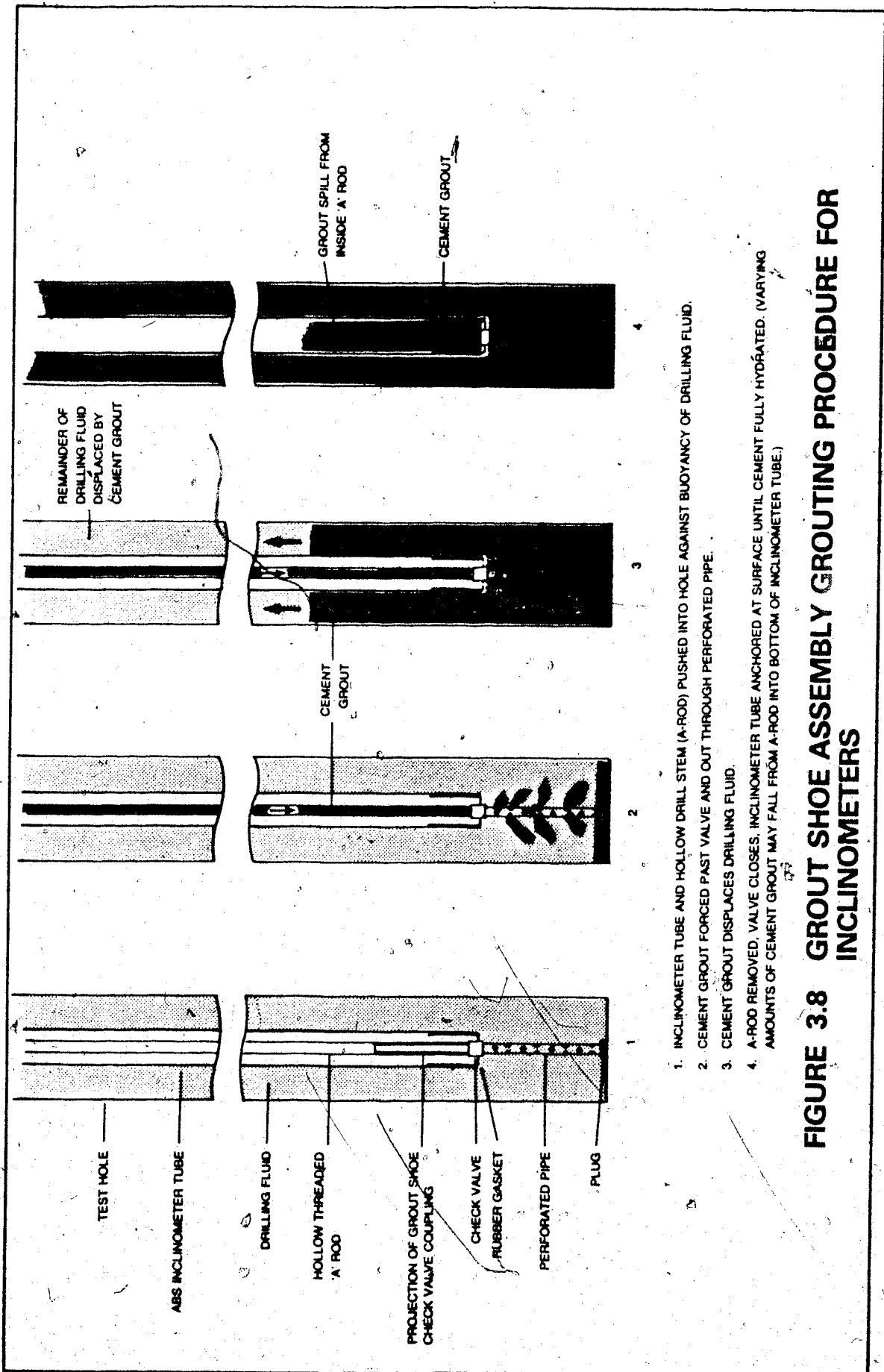


**FIGURE 3.7B MUD SYSTEM ON HELI DRILL 500 — SCHEMATIC REPRESENTATION OF CIRCULATING ASSEMBLY**



1. INCLINOMETER TUBE AND HOLLOW DRILL STEM (A-ROD) PUSHED INTO HOLE AGAINST BUOYANCY OF DRILLING FLUID.
2. CEMENT GROUT FORCED PAST VALVE AND OUT THROUGH PERFORATED PIPE.
3. CEMENT GROUT DISPLACES DRILLING FLUID.
4. A-ROD REMOVED. VALVE CLOSES. INCLINOMETER TUBE ANCHORED AT SURFACE UNTIL CEMENT FULLY HYDRATED. (VARYING AMOUNTS OF CEMENT GROUT MAY FALL FROM A-ROD INTO BOTTOM OF INCLINOMETER TUBE.)

**FIGURE 3.8 GROUT SHOE ASSEMBLY GROUTING PROCEDURE FOR INCLINOMETERS**



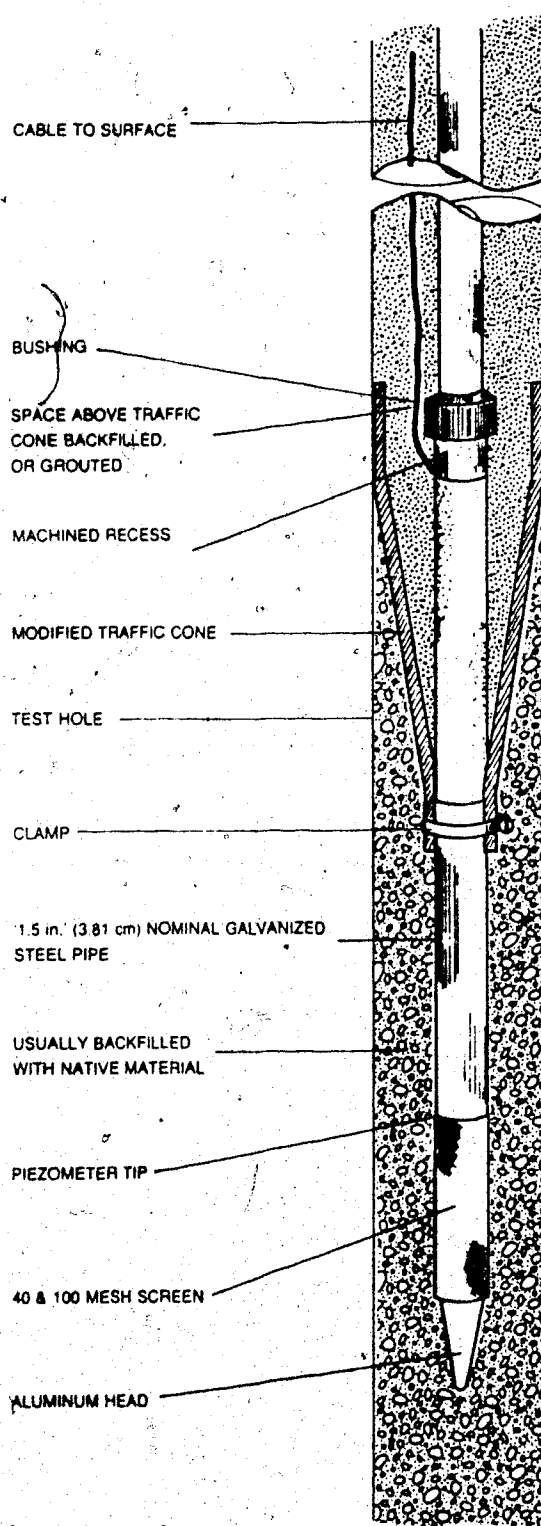


**FIGURE 3.9 INSTALLED PIEZOMETER ASSEMBLY**

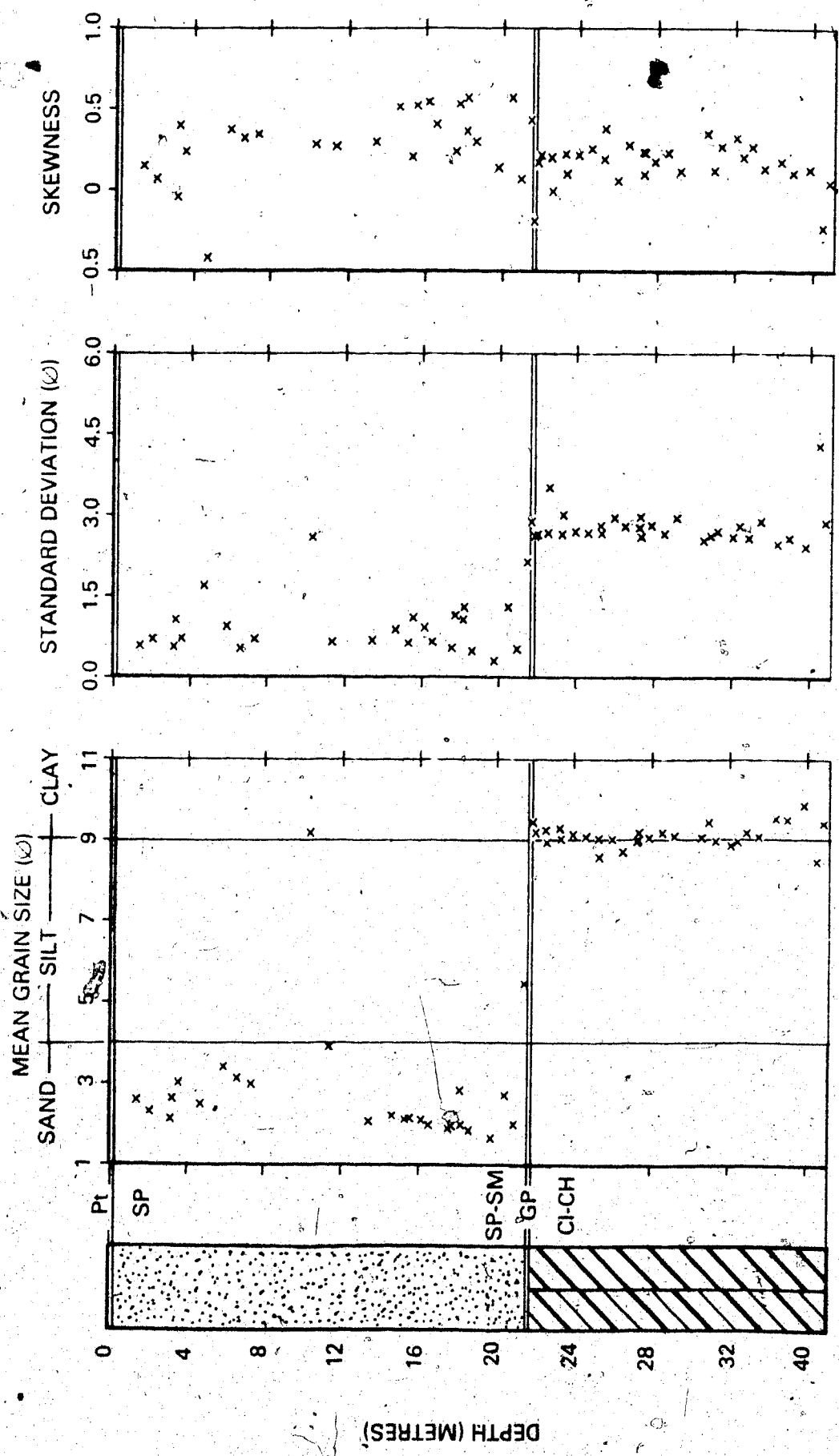


FIGURE 3.10 SUMMARY OF TEXTURAL DATA FOR HOLE GB1

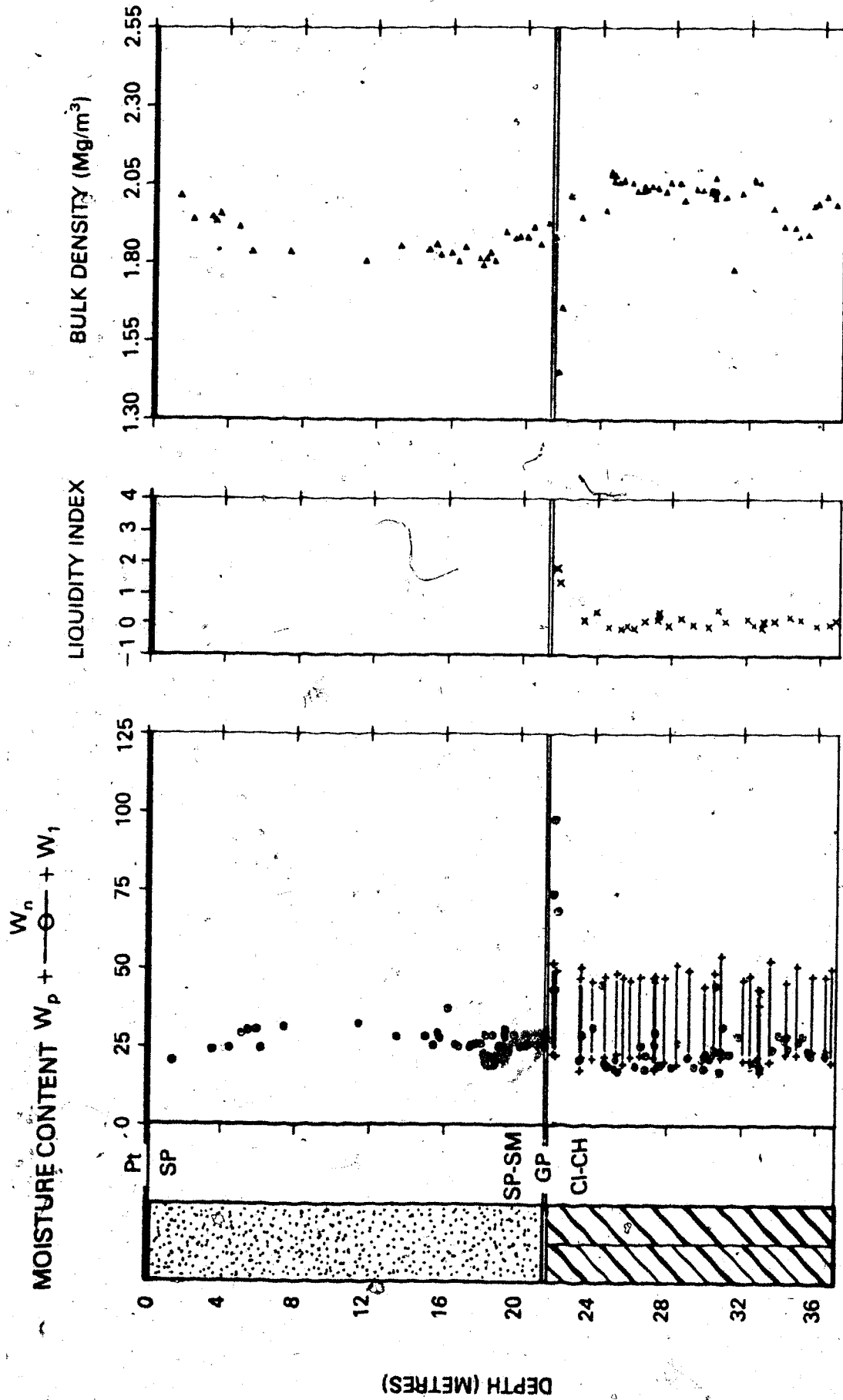


FIGURE 3.11 SUMMARY OF BASIC ENGINEERING DATA FOR HOLE GB1

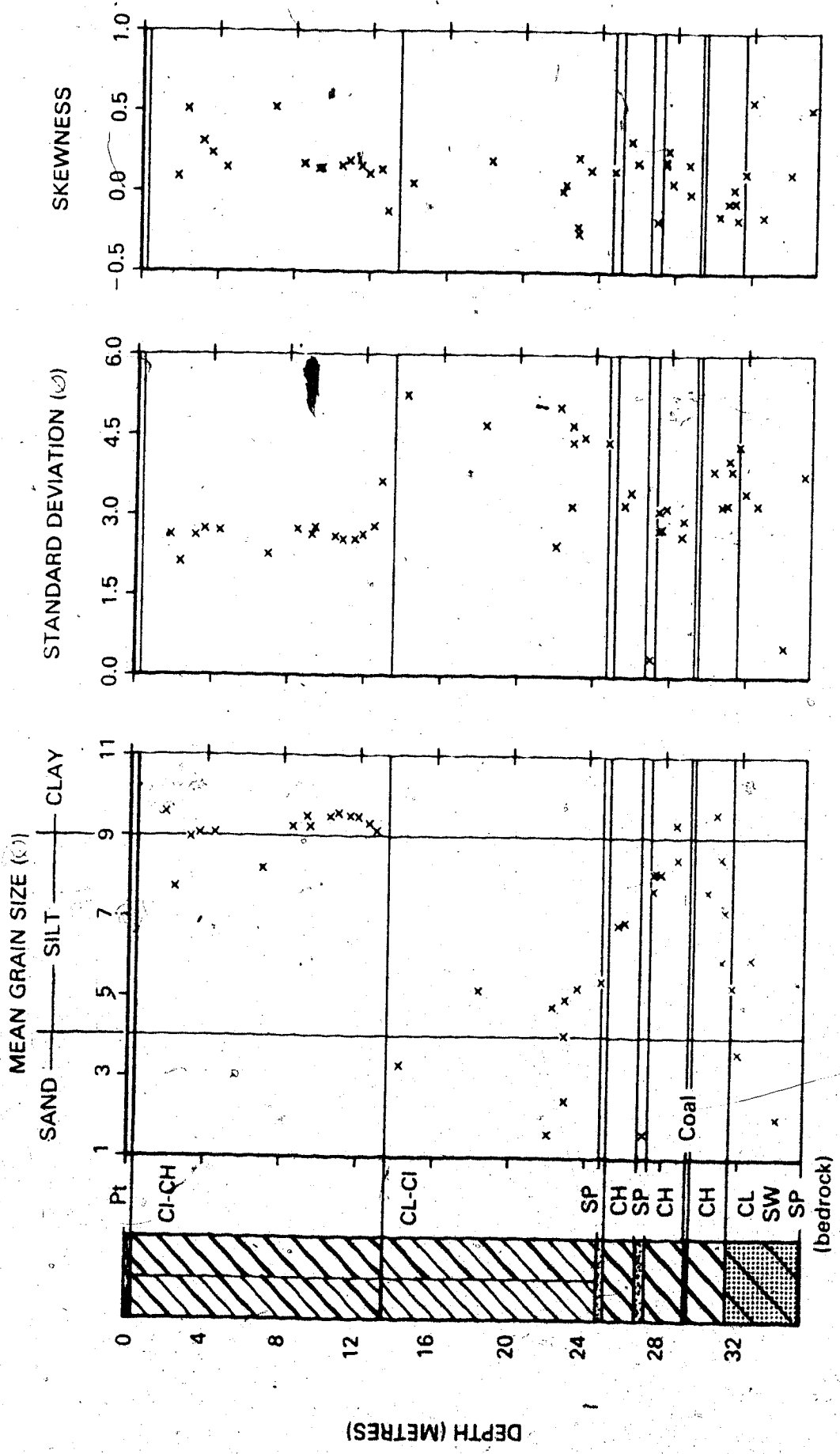


FIGURE 3.12 SUMMARY OF TEXTURAL DATA FOR HOLE GB2

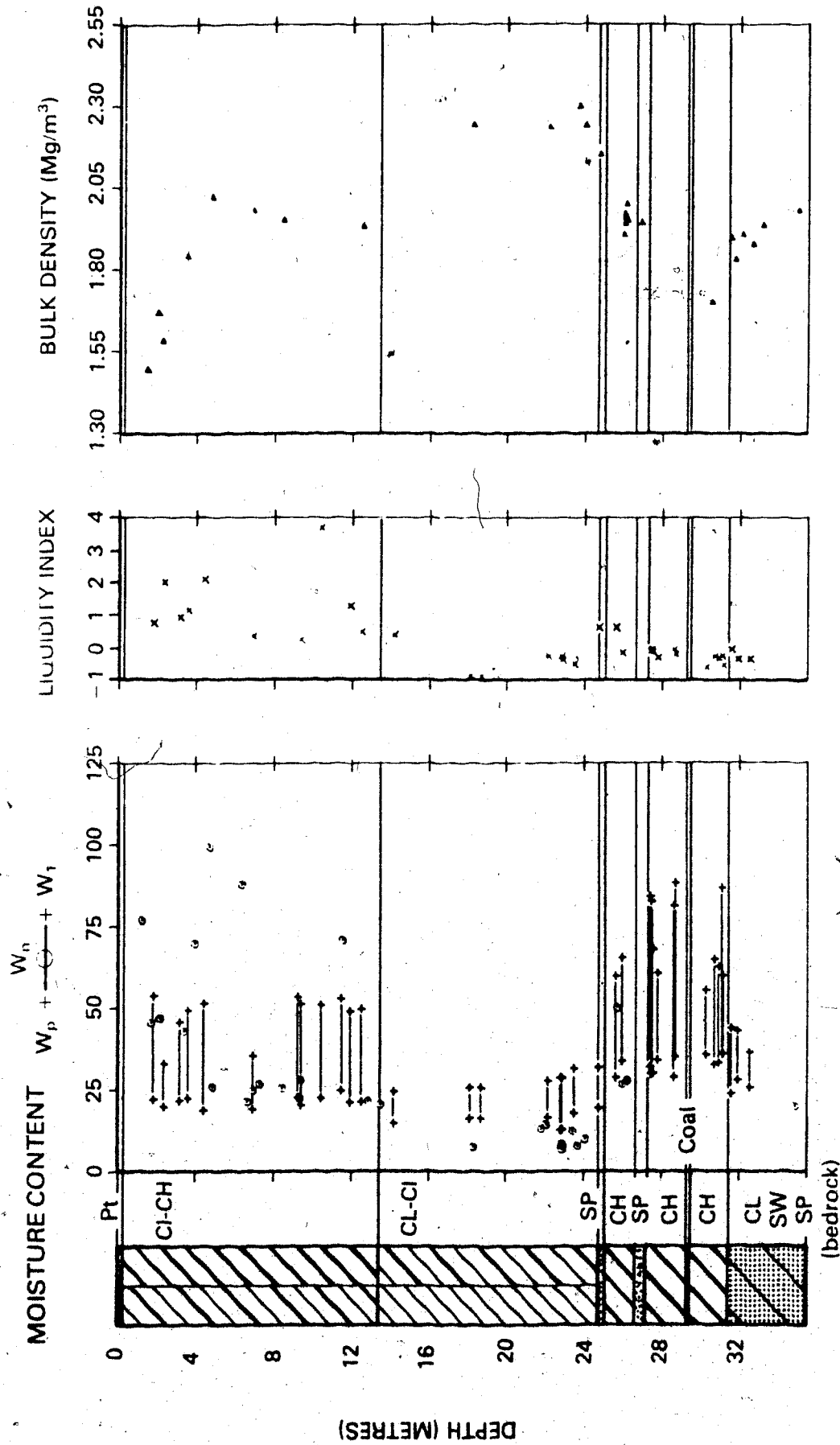


FIGURE 3.13 SUMMARY OF BASIC ENGINEERING DATA FOR HOLE GB2

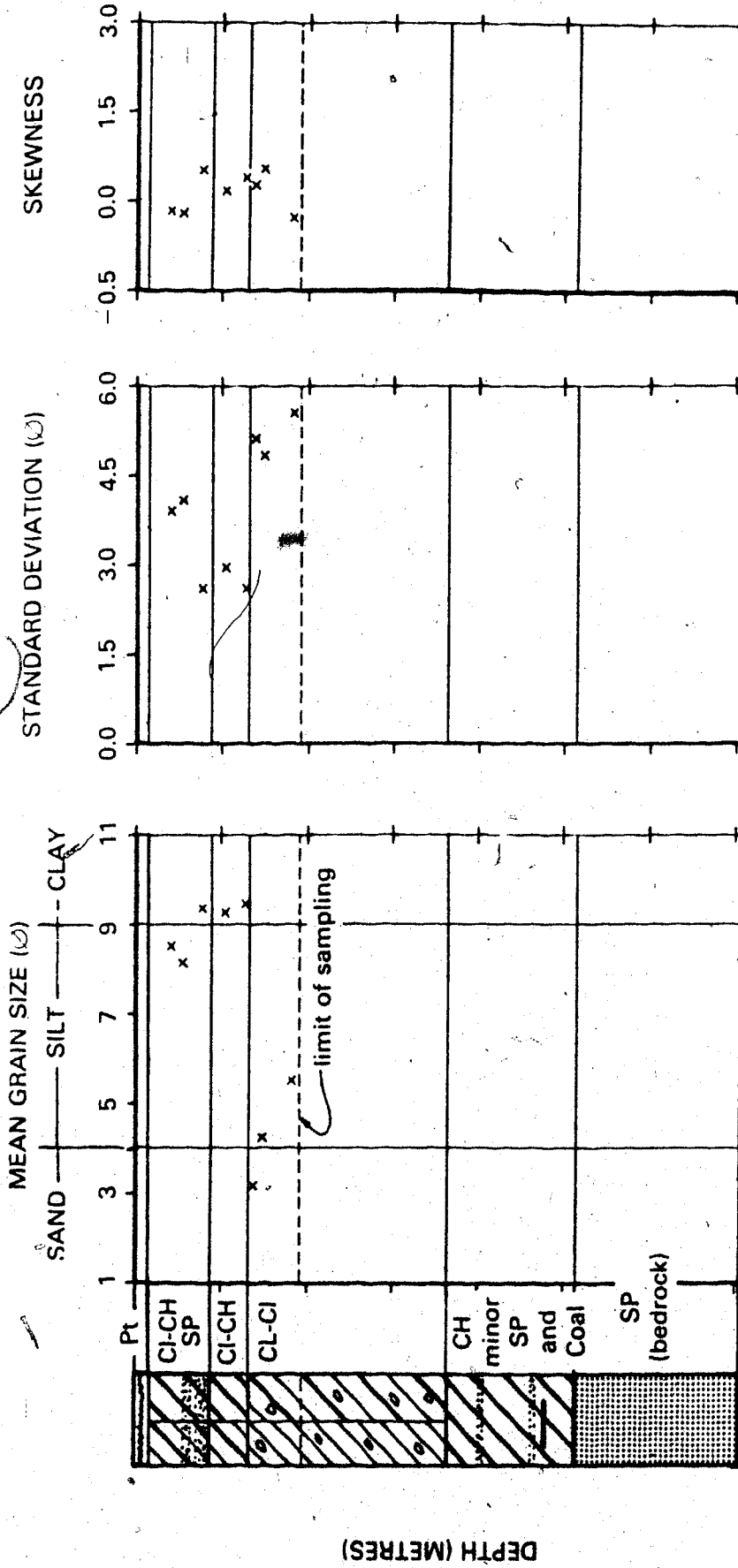


FIGURE 3.14 SUMMARY OF TEXTURAL DATA FOR HOLE GB3

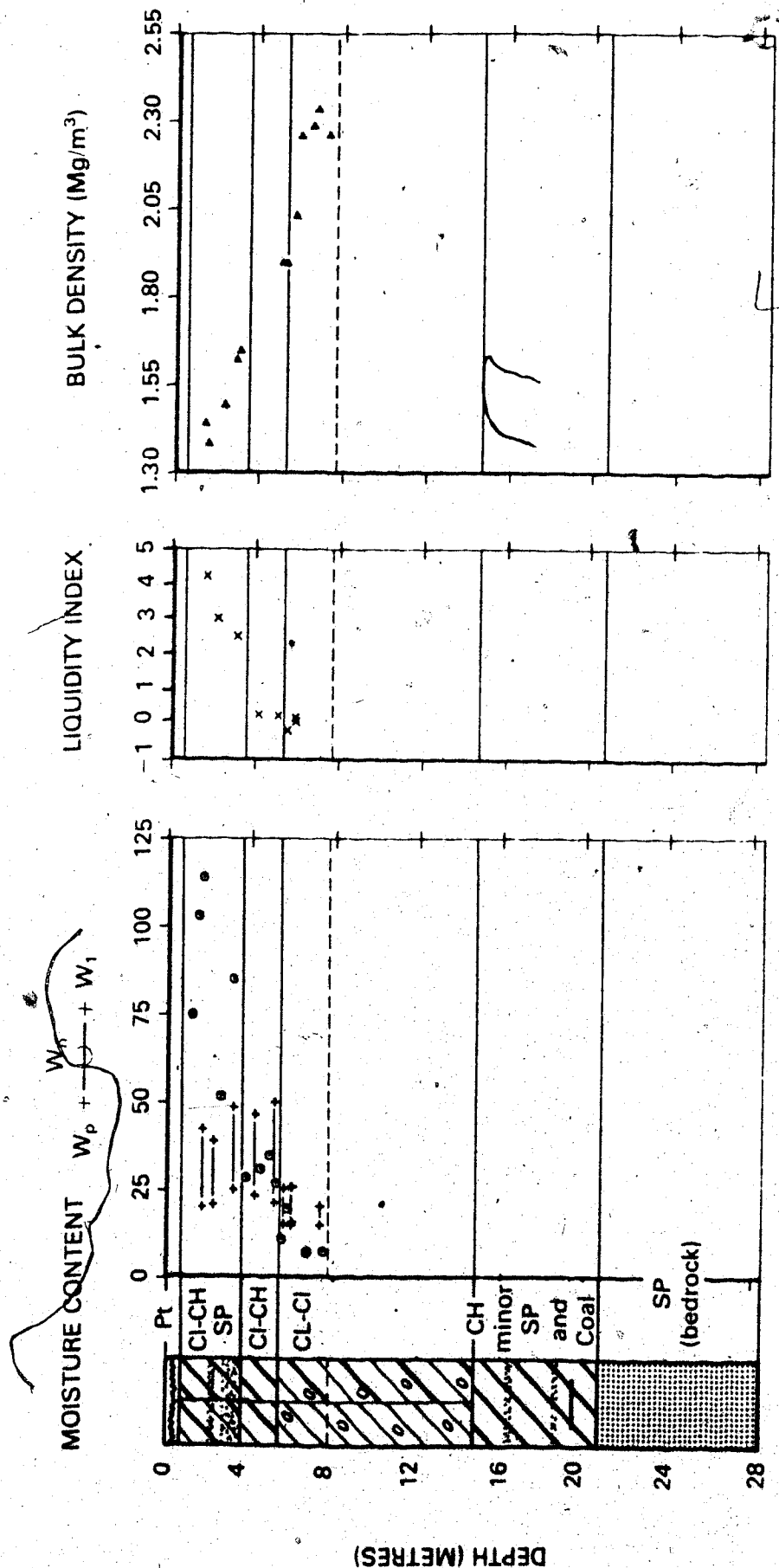
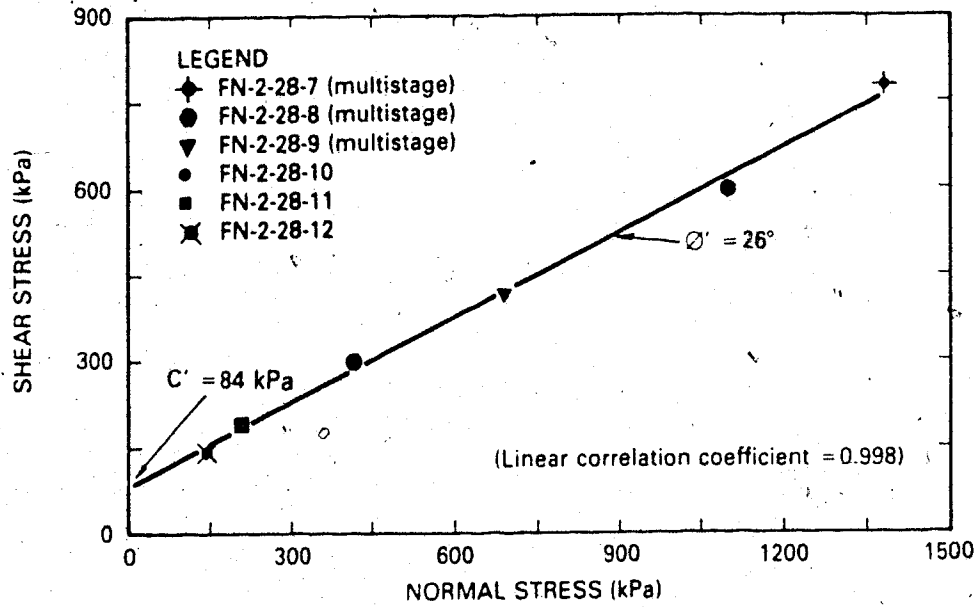
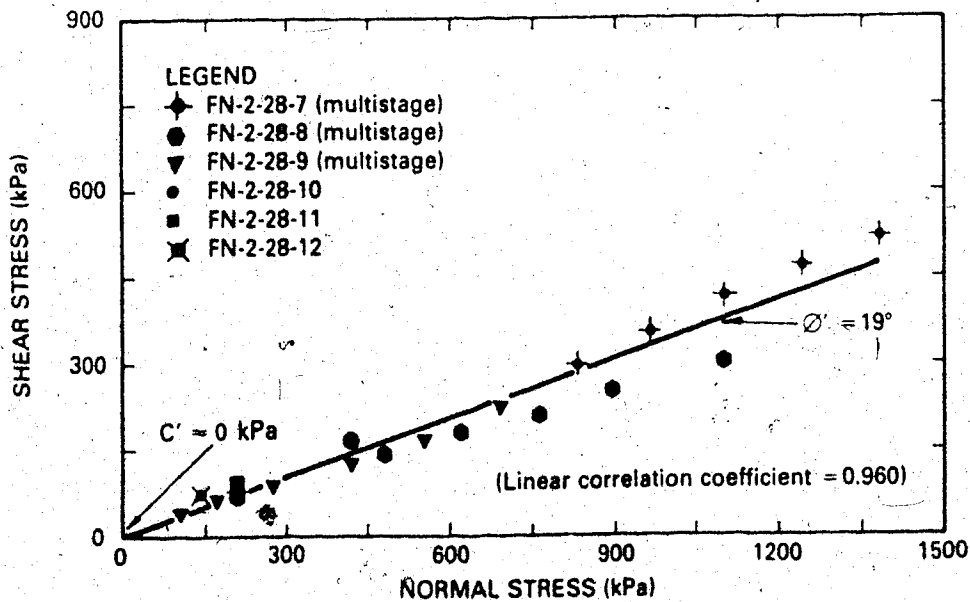


FIGURE 3.15 SUMMARY OF BASIC ENGINEERING DATA FOR HOLE GB3



**FIGURE 3.16 PEAK STRENGTH ENVELOPE FROM DS TESTS ON ALLUVIAL CLAY**



**FIGURE 3.17 RESIDUAL STRENGTH ENVELOPE FROM DS TESTS ON ALLUVIAL CLAY**



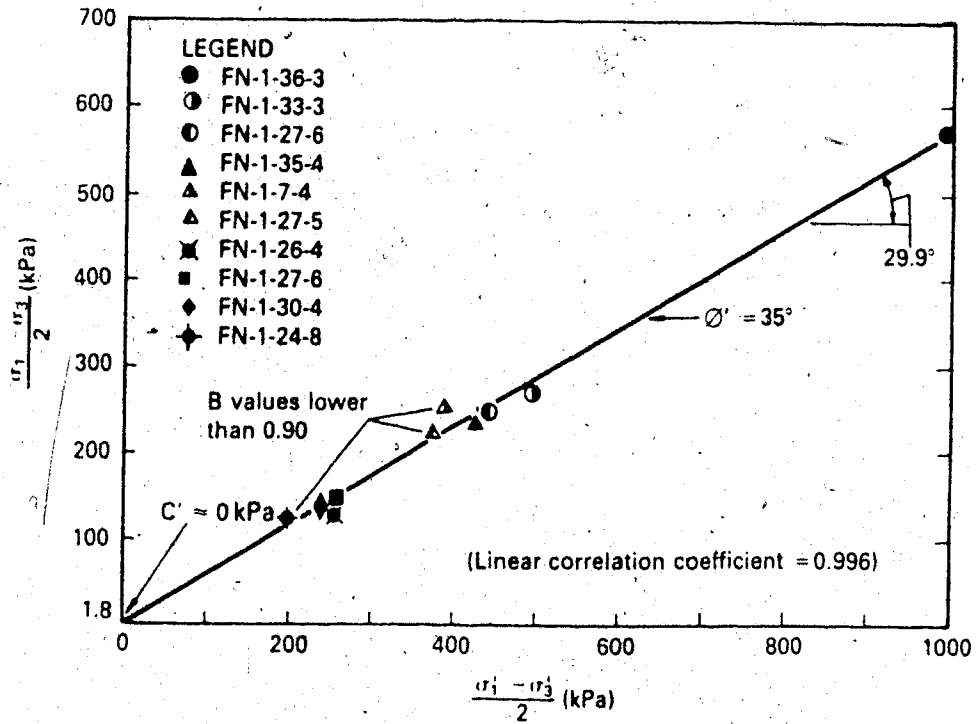


**FIGURE 3.18 PEAK STRENGTH ENVELOPE FROM CUT TESTS ON GLACIODELTAIC SAND**

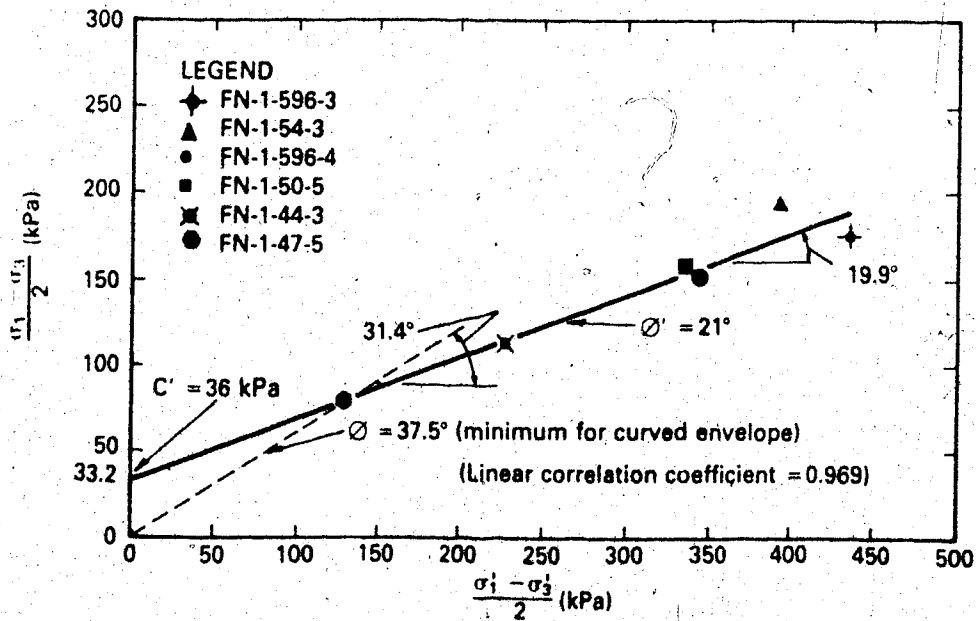


**FIGURE 3.19 PEAK STRENGTH ENVELOPE FROM CUT TESTS ON GLACIOLACUSTRINE CLAY**

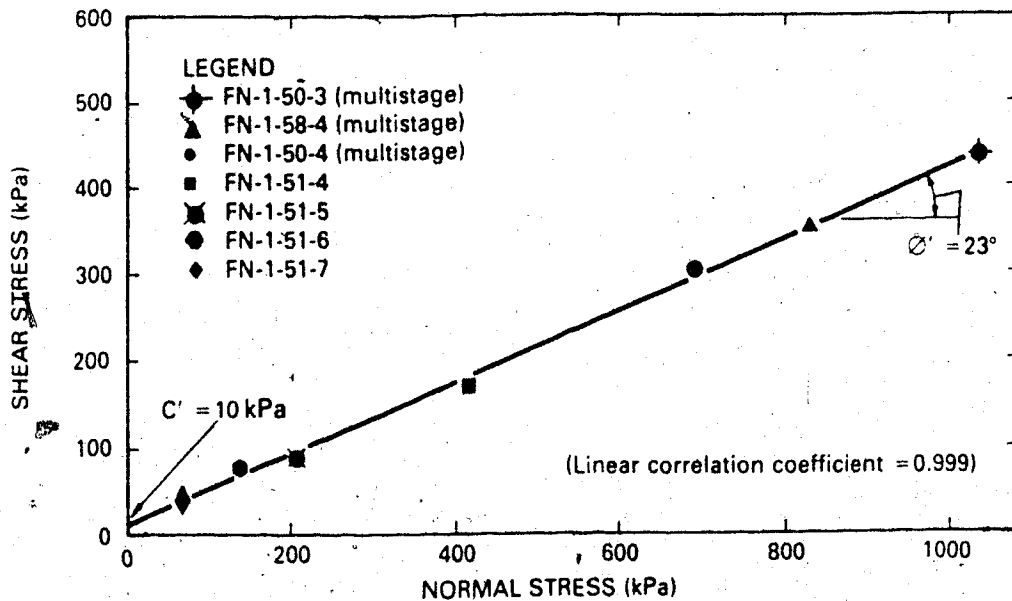


**FIGURE 3.20 PEAK STRENGTH ENVELOPE FROM DS TESTS ON GLACIOLACUSTRINE CLAY**

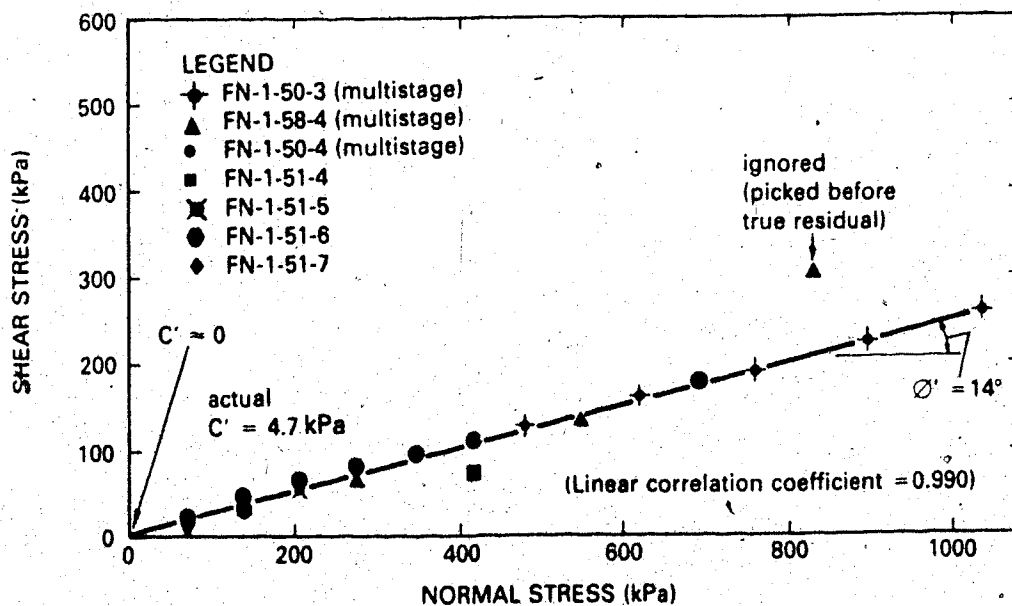


**FIGURE 3.21 RESIDUAL STRENGTH ENVELOPE FROM DS TESTS ON GLACIOLACUSTRINE CLAY**

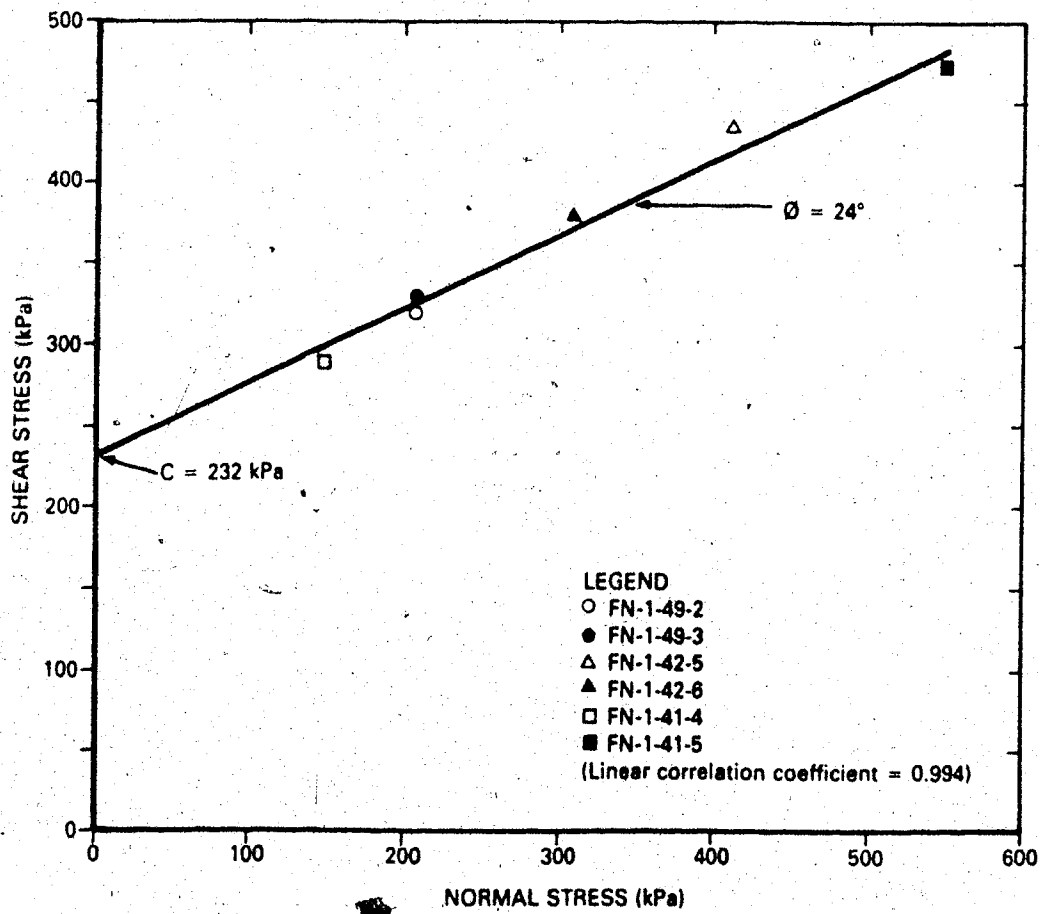


**FIGURE 3.22 PEAK STRENGTH ENVELOPE FROM DS TESTS ON FROZEN GLACIOLACUSTRINE CLAY**

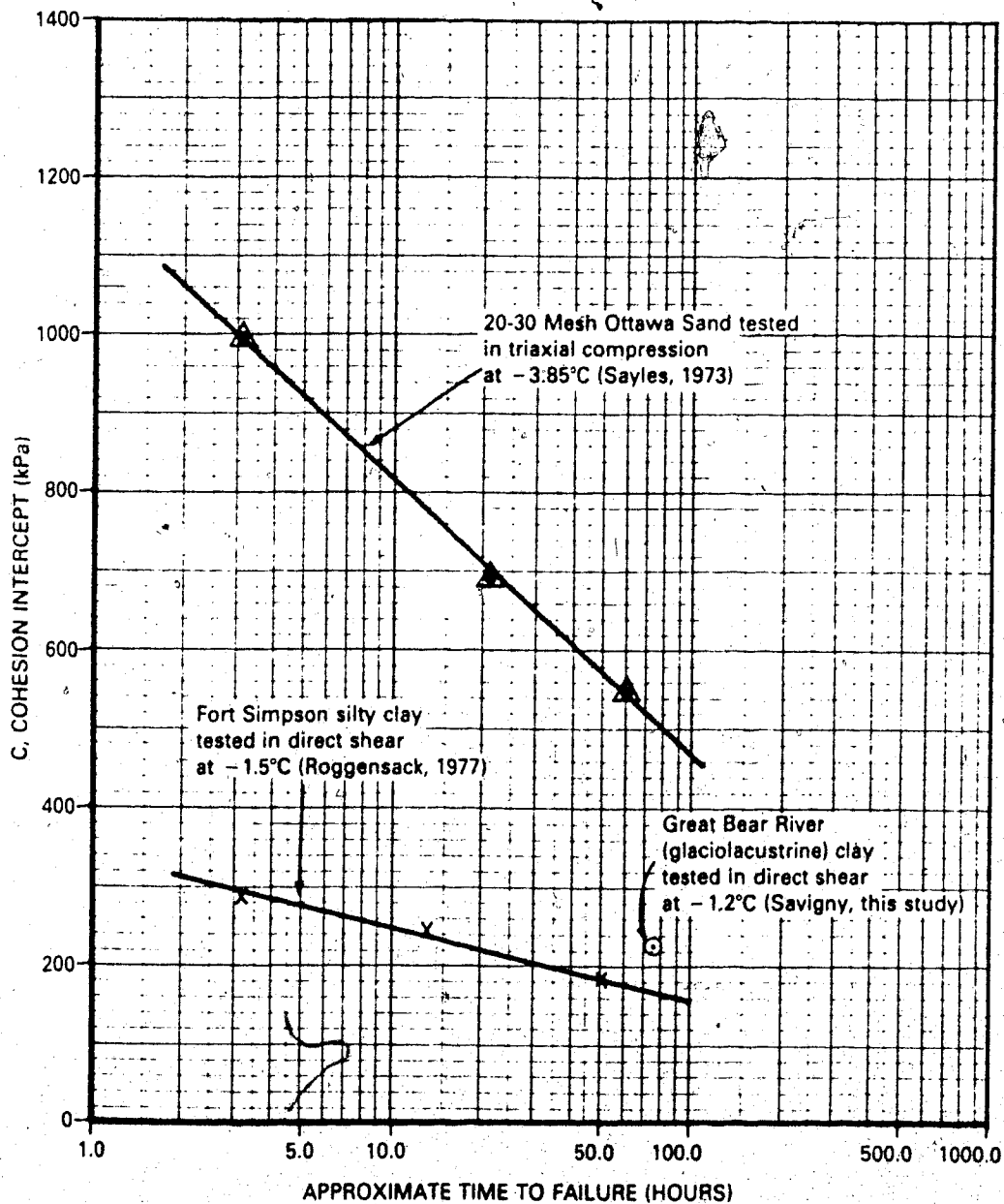


**FIGURE 3.23 APPARENT COHESION INTERCEPT AS A FUNCTION OF TIME TO FAILURE (MODIFIED FROM ROGGENSACK, 1977)**

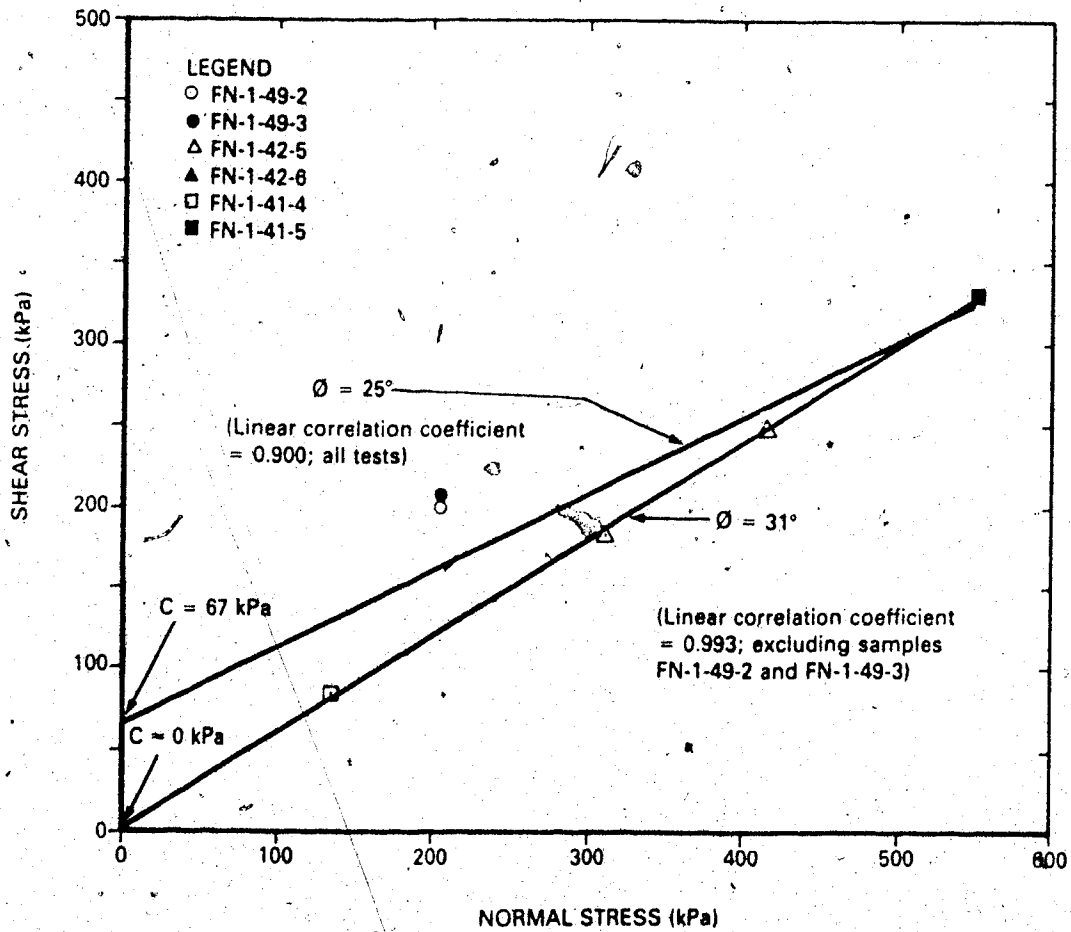


**FIGURE 3.24 RESIDUAL STRENGTH ENVELOPE FROM DS TESTS ON FROZEN GLACIOLACUSTRINE CLAY**



PLATE 3.1: Heli Drill 500 during assembly at test hole GB1.

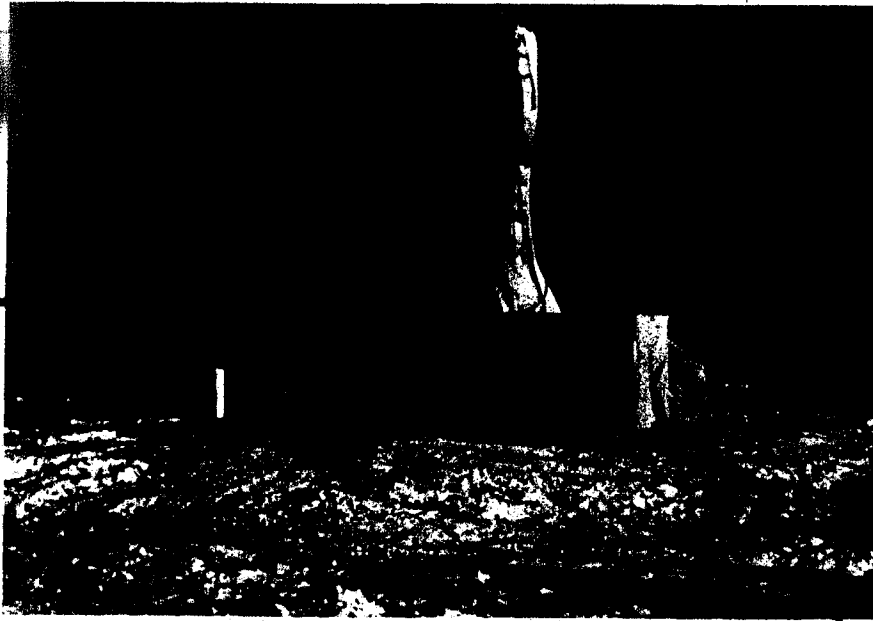
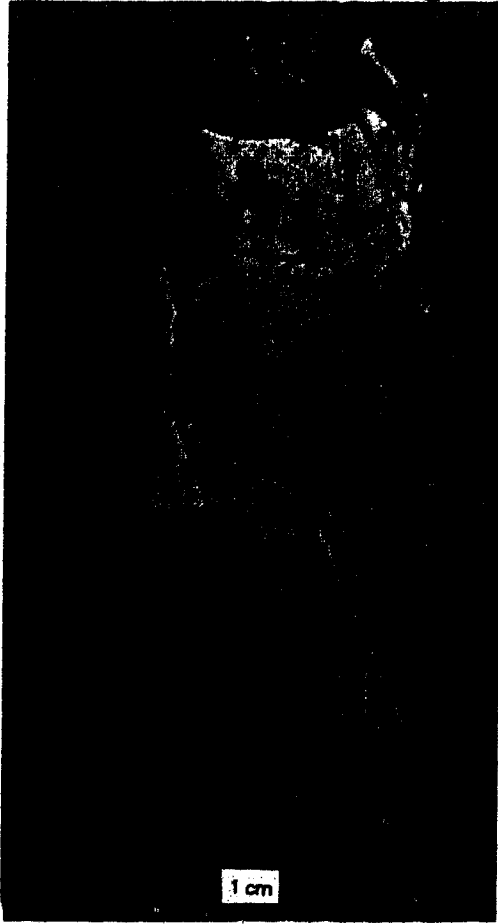
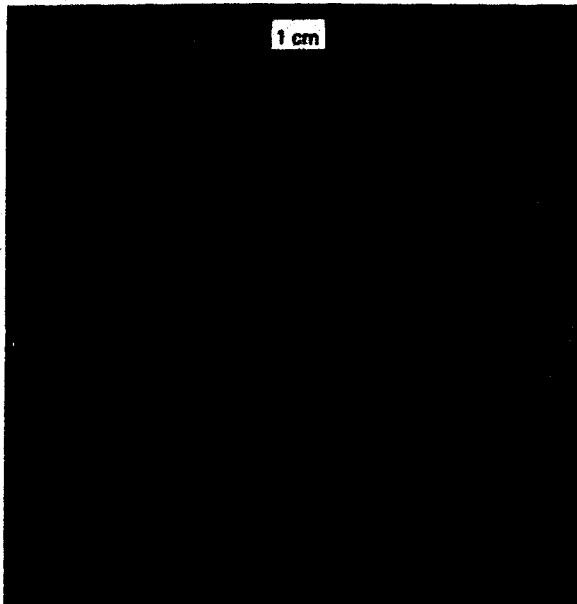


PLATE 3.2: Assembled Heli Drill 500 in operation at test hole GB1.



**PLATE 3.3:** Severe desiccation resulting from an excess of drilling fluid remaining inside core wrapping during storage (GB2 Core 29).



**PLATE 3.4:** Pre-thaw relationship of slickensided clay and ice vein (GB2 Core 18).

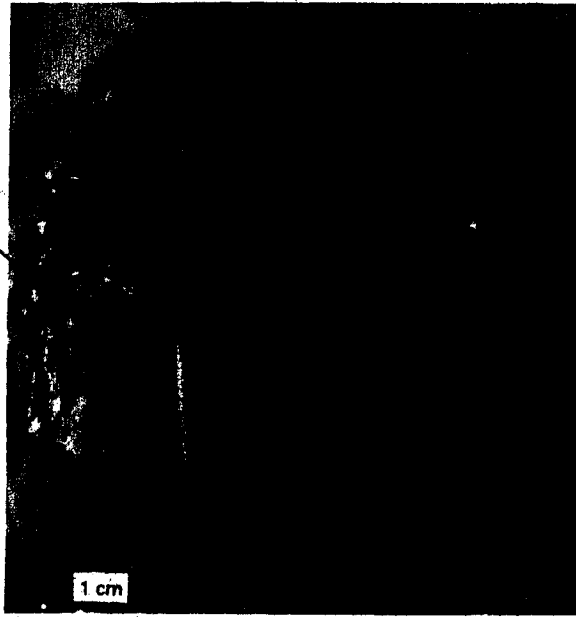


**PLATE 3.5:** Slickensided surface of soil ped facing ice vein in Plate 3.4 (GB2 Core 18).

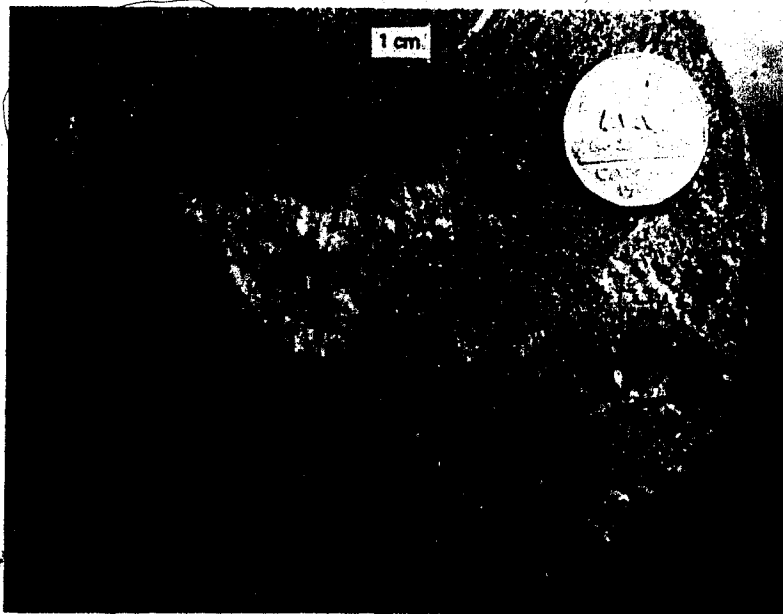


**PLATE 3.6:** Steeply dipping ice vein in glaciodeltaic sand (GB1 Core 21).



## CHAPTER IV

### FIELD DATA AND DELINEATION OF IN SITU CREEP PROPERTIES


"There's gold, and it's haunting and haunting;  
It's luring me on as of old;  
Yet it isn't the gold that I'm wanting  
So much as just finding the gold."  
(Service, The Spell of The Yukon)

#### 4.1. Introduction

Readings were taken on twelve occasions following completion of the field programme in April, 1975. Trips were scheduled in March and October of each year to coincide with the periods of maximum and minimum ground temperatures respectively. In addition, one trip was made during the winter and at least two through the summer. The dates of site visits, the activities carried out, the weather conditions, and other general information are given in Table

4.1.

Scheduled airlines were used to Norman Wells, for each site visit. Instruments were either carried or shipped as hand baggage to minimize the possibility of breakage or loss, and in order that the inclinometer batteries could be fully charged over the preceding night. Between June and October, a fixed wing charter was taken to Fort Norman where a local resident was hired to provide boat transport to the site. Between November and May, a helicopter



was chartered directly to the site. All instruments were read in the same order and on the same day, except in August, 1976 when readings were taken over two days.

The field instrumentation is described, and all field data are reported and analyzed in this chapter.

## 4.2 Thermistors

### 4.2.1 Specifications

Thermistors used were York Instruments Limited, glass-bead type P99-3. These were mounted at 6.1 m spacings on specified lengths of multiconductor cable by Cantech Controls Limited, Calgary. A switchbox with female connectors to both the thermistor string and the readout device was fabricated by the same company. A summary of the cable lengths and holes where each was installed is given in Table 4.2.

Each cable was calibrated against a quartz resistance thermometer and two Atkins Meters (Model 3F01-C46) using a constant temperature bath at 0°C and -3°C. The results, together with the industrial calibrations for the Atkins Meters, were integrated into a simple computer programme which was used to reduce field data as they were obtained.

Errors due to drift and resistance of the cable were considered insignificant (Judge, 1973). Repeatability tests on any one occasion showed accuracy to be  $\pm 0.05^{\circ}\text{C}$ ; however difficulty in setting the Atkins Meters to zero, and their extreme sensitivity to static electricity reduced overall accuracy to  $\pm 0.15^{\circ}\text{C}$  based on

readings from thermistors well below the depth of zero mean annual fluctuation. To overcome these difficulties it is recommended that future installations use a high sensitivity DC Wheatstone bridge for measurement of thermistor resistance.

The ends of each thermistor cable were placed in a plastic bag and tied to a large wooden tripod erected over or near each hole. This procedure is considered unsatisfactory for future installations because it does not adequately prevent ingress of water into the connector, and it is by no means a deterrent to curious animals. A more permanent installation, similar to that described by Judge (1973), is considered preferable.

#### 4.2.2 Reading Procedure and Data

The thermistors were read at the beginning of each site visit before the equilibrium temperature gradient of diesel fuel inside the ABS casing was disturbed by the inclinometer movement. Temperature change associated with movement of the tool was monitored concurrently with reading the inclinometer. This usually involved only one thermistor in each hole per trip so the more important task of reading the inclinometer could proceed uninterrupted.

All field data were reduced with a simple computer programme and plotted on a Calcomp C plotter. Figures 4.1, 4.2, and 4.3 show the data from each thermistor in holes GB1A, GB2, and GB3 respectively between the time grout was placed and the end of monitoring in June, 1977. Figures 4.4, 4.5, and 4.6 show the

trumpet curves for each of the respective holes based on those data obtained after approximate thermal stability had been recovered in May, 1975. A cross-section showing temperature contours in the slope is given in Figure 4.7. The data on this diagram represent averaged values from the trumpet curves for depths below that of zero mean annual temperature fluctuation (ZMTF).

The discontinuous nature of the data in Figures 4.1, 4.2, and 4.3 is a result of several factors: as shown in Table 4.1, some thermistors ceased to function at various times through the monitoring period; the Atkins Meter batteries went dead on October 8th, 1975 before the cables in GB1A and GB2 could be read; and, the end cover on one of the cables in GB2 was frozen on December 21st, 1976 and March 1st, 1977.

The apparent disagreement in the number of thermistors shown in Figures 4.3 and 4.6 is a result of three thermistor pods on the GB3 string being left exposed at the surface following installation. One of these was used to measure air temperature on each visit, and the other two were buried beside the hole in October, 1975 - one at a depth of 30 cm and one at 60 cm.

#### 4.2.3 Hydration of Grout

Figures 4.1, 4.2, and 4.3 show the temperature change induced by hydration of grout in each of the inclinometer holes, together with the systematic recovery of thermal stability as a function of time following placement. The most complete record was obtained in GB3 (Figure 4.3); the initial temperature increase was missed in

GB1A (Figure 4.1); and the entire hydration period was missed in GB2 (Figure 4.2). Pre-hydration temperatures that show an increase from the top of the hole to the bottom are directly related to the pumping and mixing procedure described in Section 3.6.1.

The data show that hydration began within 2 to 4 hours of placement and reached maximum temperatures of up to 13°C between 1 and 2 hours later. This time period varied slightly depending on how long the grout had been mixed. The chilled diesel fuel, which was added as soon as hydration began, had very little measurable effect, but this is considered to be a result of the location of the thermistor pods and in no way a measure of the fluid's effectiveness as a heat sink. The temperature increase stopped 6 to 7 hours after placement and between 75 and 80% of ultimate thermal recovery was achieved within 12 hours. Further temperature recovery continued until July, 1976. Thereafter, temperature changes below the depth of ZMTF were within the accuracy range of the Atkins Meter, or could be attributed to changing albedo at the site.

#### 4.2.4 Thermal Regime

The Mackenzie Valley climate is affected by warm maritime air of Pacific origin and cold Arctic air originating to the northeast. The relative interaction of these two systems causes the wide temperature range typical of the area. The tendency of the maritime troughs to frontalize northeast of Mackenzie Mountains provides a significant amount of precipitation (Burns, 1974).

The mean daily temperature over the year is -6.2°C.

January, the coldest month, has mean daily temperatures of  $-31.7^{\circ}\text{C}$ , and winter extremes reach as low as  $-54.4^{\circ}\text{C}$ . In contrast, the months of June, July, and August all have daily averages greater than  $13.3^{\circ}\text{C}$ , and summer maxima reach as high as  $35^{\circ}\text{C}$ . The mean annual precipitation of 33.3 cm is approximately equally distributed between rainfall and snowfall. Mean snowfall is 135.4 cm, and 42.6% of this falls before the end of November each year (Burns, 1974). The temperature and precipitation means and extremes for Fort Norman, N.W.T. are given in Table 4.3.

Surface conditions among the six drill sites may be described in two categories: one for all holes at the top of the slope; and one including GB2, GB3, and GB3A. The former has exposed light-coloured sandy soil over most of the cleared area with sticks, moss, and lichen providing only local cover. The second is represented by fallen black spruce trees lying on natural moss and lichen ground cover. In the area around each hole these ground flora are slightly compressed and the fallen trees are removed, but mineral soil is not exposed. At no time was there any evidence of ground ice degradation around the inclinometer installations.

Assuming Figures 4.4, 4.5, and 4.6 show typical temperature conditions beneath the cleared area, the generalized ground temperature regime for the two surface conditions described are as follows:

In the sandy area at the top of the slope the active layer is 3 m thick, and the depth of ZMTF is between 9 and 10 m. Data from thermistors 1 and 2 in GB1A (Figure 4.1) show clearly that a warming

trend has been in progress since monitoring began and was probably initiated by widespread clearing in 1974 (Section 3.2). Readings after October, 1976 indicate this has caused an inversion in the profile at a depth of approximately 19 m. This recent adjustment is superimposed on an earlier cooling trend which began in approximately 1950<sup>1</sup> and is manifest in the steep thermal gradient between 28 and 34 m (Figure 4.4). Ignoring the more recent change and projecting the mean gradient of the cooled zone to the surface, the mean annual ground surface temperature (MGST) prior to 1974 was  $-2.6^{\circ}\text{C}$ ; projecting the lower portion of the curve gives a MGST of  $-2.0^{\circ}\text{C}$ . Thus, the cooling trend was initiated by a change in mean annual air temperature of approximately  $0.6^{\circ}\text{C}$ . The depth of permafrost based on the gradient below 36 m (Figure 4.4) is estimated to be at least 61.3 m. If the cooling trend had persisted, ultimately this depth would have been at least 20 m more based on simple projection of the upper gradient.

Subsurface thermal conditions on the valley slope are slightly different because of the combined affects of aspect, vegetation cover (present and prior to clearing), and the micro-climate of the river valley. In GB2 the active layer is 1.2 m thick and the depth of ZMTF between 6 and 7 m (Figure 4.5). By taking an average thermal gradient, the MGST is  $-3.3^{\circ}\text{C}$  and the depth of permafrost 48 m. The cooling trend observed in GB1A is not evident and there is little possibility that it is present below the deepest

---

<sup>1</sup>Mackay, J.R., 1975, personal communication.

thermistor. In contrast, small warming trends of 0.1 to 0.2°C may be inferred: the first with an inflection point at approximately 17 m; the second over a low gradient section of the profile between 25 and 29 m. No regional records could be found in support of these. As a result they are considered local phenomena related to the microclimate within the Great Bear River Valley.

Data from GB3 show an active layer of 1.3 m and a depth of ZMTF between 6 and 7 m (Figure 4.6). The thermal gradient is uniform and indicates a MGST of -2.5°C and a permafrost depth of approximately 28 m. The higher MGST and steeper thermal gradient in GB3 relative to GB2 undoubtedly reflects the proximity of the former to Great Bear River. This is well illustrated in Figure 4.7, and is consistent with the findings of other authors (Johnson and Brown, 1964).

These results are in good agreement with those of other authors (Brown, 1967; Judge, 1973; Isaacs, 1974), for the region around Norman Wells, N.W.T. They indicate the area is correctly classified within the "widespread discontinuous permafrost zone" on the permafrost map of Canada (Brown, 1967).

#### 4.3 Piezometers

##### 4.3.1 Specifications

The piezometers used were Terra Technology Corporation, Model P2020 combination pneumatic/hydraulic. This model was chosen primarily because of the back-up hydraulic system in which light oil or ethylene glycol could be used in the event that the pneumatic



leads became damaged or frozen-off, or if verification of the pneumatic reading was required. The read-out console used was a Terra Technology Corporation, Model C6300. Dried carbon dioxide was used as the air source.

Calibration of each piezometer was carried out in a modified triaxial cell with pressure applied from a regulated source (air over water). Pressure was monitored with a 0 to 700 kPa pore pressure transducer and the field console. The final calibration curve and preload value were taken from a regression fit of ten data points over a range of 0 to 400 kPa. These data together with installation data are given in Table 4.4.

#### 4.3.2 Reading Procedure and Data

Readings were taken of each piezometer at the end of the field programme and as a matter of routine on each site visit up to June, 1976. The procedure outlined in the console operation manual was used on each occasion, with the exception that flow was maintained at 15.6 SLH (0.55 SCFH) instead of the suggested 42.5 SLH (1.5 SCFH).

No stable reading was obtained from the piezometer in GB1B in ten attempts between March, 1975 and June, 1976. With the console flowmeter stable at the specified value the read-out gauge varied over an irregular range between 0 and 310 kPa (75% of capacity). Variations in flow of  $\pm 25\%$  had no significant effect on this behaviour or range of fluctuation. Despite the fact that the piezometer tip was well inside the permafrost zone and any readings

would have been difficult to interpret, it is felt that the piezometer was damaged during installation.

The piezometer in GB3A was read on eight occasions between April and November, 1975. Attempts in March and June, 1976 were unsuccessful because of ice blockage in the pneumatic leads. Since data up to that time indicated pore pressures beneath the permafrost table were consistent and easily explained, no attempt was made to continue monitoring by using light oil in the piezometer.

#### 4.3.3 Sub-permafrost Pore Pressures

The pore pressures measured in GB3A are shown in relation to the elevation of Great Bear River on Figure 4.8. These data show close correspondence between the elevations of the river water and the hydrostatic head beneath the slope. In May, 1975, the single occasion when both were surveyed, the levels were almost identical. Subsequent pore pressures dropped off slightly. Since the May, 1975 river level was established within a few days of break-up, it is likely to have been up to 2 m above the mean flow level. This may account for the observed decrease in water pressure in the summer and autumn of 1975.

The interpretation of these pore pressure data is straightforward when the stratigraphy of the site is considered (Figure 4.8). Hollingshead and Sowa (1974) established that coarse river alluvium lay on bedrock beneath Great Bear River (see GB4 and GB5, Appendix A). The presence of highly arenaceous zones and discrete sandstone laminae in this bedrock provide a means of rapid pore pressure equalization.

#### 4.4 Inclinometer

##### 4.4.1 Introduction

Numerous instruments and techniques are available for the measurement of lateral movement, but only borehole inclinometers provide data over a full vertical profile with the accuracy necessary to resolve creep deformations. Moreover, these instruments have proven reliability from studies of the creep of soil in natural slopes (Wilson, 1970), and of particular relevance here, the creep of ice in glaciers and icecaps (Meier, 1960; Savage and Paterson, 1963; Wilson, 1970).

##### 4.4.2 Types of Inclinometers

Although several inclinometers have been developed (Kallstenius and Bergau, 1961; Wilson, 1962; Dunnicliff, 1971; Hanna, 1973), only one variety has suitable accuracy for this study. It consists of three components: a sensing device, a read-out console, and a connecting cable. The sensing device houses the tilt sensor in a watertight torpedo. This is lowered to the bottom of a near-vertical guide casing and then raised, with readings taken at equal depth intervals. The slope of the casing is determined by integrating slope readings from the bottom of the hole, which is embedded into a firm stratum and assumed to be free of translation (Hanna, 1973). Profiles show patterns of movement as a function of depth, and successive readings over a period of time provide a measure of velocity at respective depths.

Four basic types of inclinometer fall into this category, each characterized by the sensing element used to measure inclination. These include: the vibrating wire strain gauge type; the Wheatstone bridge type; the bonded electrical resistance strain gauge type; and the servo-accelerometer type.

#### Vibrating Wire Strain Gauge

Very little literature is available on this type of inclinometer and the only case history available is an indirect, uncorroborated statement by Dunicliff (1971). He reported precision<sup>1</sup> ranging from  $0.8 \times 10^{-4}$  to  $28.0 \times 10^{-4}$ , and high sensitivity to temperature and zero drift.

#### Wheatstone Bridge

The Wheatstone bridge type (Parsons and Wilson, 1956; Wilson and Hancock, 1959; Wilson, 1962) has had widespread use in bulkheads, earth and rockfill dams, embankments, foundations, and slope stability (Wilson and Hancock, 1959; Hakman and Buser, 1962; Henderson and Matich, 1962; Wilson, 1967; Wilson, 1970; Peters and Ellis, 1972). It combines a robust design with the simplicity of a pendulum-actuated, conventional Wheatstone bridge circuit. The pendulum tip contacts a precision-wound resistance coil subdividing it into two resistances which make up one half of the bridge. The

<sup>1</sup>The terminology of measurement accuracy used here follows that of Gould and Dunicliff, 1971, p. 314. Precision is given in units of shear strain, or simply metres of deflection per metre of depth (plus or minus is assumed).

remainder of the bridge and associated circuitry is contained in the control box. Based on controlled laboratory tests (Green, 1974), the precision is  $2.0 \times 10^{-4}$ , the calibration is linear, and the temperatures effects are negligible. Collective field experience (Peters and Ellis, 1972; Cornforth, 1974) shows actual precision ranges from  $1.7 \times 10^{-4}$  to  $8.3 \times 10^{-4}$ .

#### Bonded Resistance Strain Gauge

The sensing element in this type of inclinometer consists of a cantilever strip with a brass pendulum on the free end and the other rigidly fixed to prevent movement normal to the reference plane. When the instrument is inclined, the cantilever bends in proportion to the gravity component and this is monitored by four temperature-compensated electrical resistance strain gauges mounted on the strips. The housing is fitted with silicone-oil to damp the pendulum movement, and to insulate and protect the strain gauges (Phillips and James, 1974). The results of controlled laboratory tests indicate that precision ranges from  $0.3 \times 10^{-4}$  (Murray and Irwin, 1970) to  $2.0 \times 10^{-4}$  (Green, 1974), that certain instruments may be prone to non-linear calibration (Green, 1974; Phillips and James, 1974), and that zero drift and temperature drift are common problems (Dunnicliff, 1971; Green, 1974).

#### Servo-Accelerometer

This type of inclinometer utilizes a null-balance accelerometer as the sensing element. The gravity referenced sensor

is energized by an applied voltage and quickly stabilized in response to tilt by a change of current flow. The resulting voltage output is proportional to the sine of the angle of inclination and is monitored directly (Hanna, 1973). By virtue of the electrical balance design, the sensors have no significant inaccuracies associated with non-linearity, hysteresis, temperature change or zero drift. Laboratory calibrations reported by Bromwell et al. (1971) indicate precision of  $1.3 \times 10^{-4}$ . Field precision reported by the same authors is consistently better than  $1.0 \times 10^{-4}$  and for most cases better than  $0.4 \times 10^{-4}$ ; Peters and Ellis (1972) reported field precision of  $1.3 \times 10^{-4}$ .

#### 4.4.3 Specifications for the Digitilt Inclinator

After careful consideration of the various types of inclinometers described in Section 4.4.2, and solicitation of advice from several local consulting firms with experience in Arctic instrumentation, the SINCO Digitilt<sup>1</sup> inclinometer was selected as the most suitable. The governing criteria for this decision were:

1. Adequate accuracy and precision.
2. Negligible non-linearity, hysteresis, and temperature and zero drift.
3. Proven reliability.

The Digitilt system includes a sensor, cable, readout device and casing.

---

<sup>1</sup>Digitilt is the registered trade name for one slope indicator system sold by SINCO.

The torpedo-like sensor is 92.7 cm long and has an upper and lower wheel assembly, each consisting of one fixed wheel and one spring-loaded wheel; the gauge length or separation of the wheels is 61 cm. Two closed-loop, servo-accelerometer sensing elements, mounted at 90° to one another are housed in the sensor.

The tool is connected to the readout device by a 0.95 cm (outside diameter) neoprene-coated six-strand cable. Depths are measured by coloured neoprene markers vulcanized to the cable at 30.5 cm spacings.

The readout device is a digital voltmeter that indicates voltage in a four digit display. It contains a 6 volt rechargeable battery which operates continuously for up to eight hours at room temperature.

The casing is ABS plastic with four machined, longitudinal grooves equally spaced around the inside circumference. Casing sections are joined and sealed by riveted and cemented couplings. A pulley assembly with a cable clamp is fitted to the top of the casing string during reading.

Complete specifications for the inclinometer system are given in Table 4.5.

#### 4.4.4 Monitoring Procedure

Initial calibration of the inclinometers was completed on May 6th, 1975 (minimum of 23 days after placement of grout in GB3), but each was ignored when subsequent data indicated erratic deformations and further temperature recovery before the second inclinometer

readings were obtained on July 1st, 1975 (minimum of 79 days after placement of grout in GB3).

The inclinometers were read at least once on each site visit as outlined in Table 4.1. By June, 1976, when it could be established that lateral movements were marginally inside the specified accuracy of the Digitilt system, a decision was made to obtain as many readings as possible in order to define instrument accuracy and precision in each inclinometer casing.

Throughout the monitoring period, readings were taken in the same order (i.e. GB1A, GB2, and GB3), by the same personnel, on the same day, except August, 1976 when the holes were read in reverse order over a two day period. On each occasion the probe was set to the lowest reading depth and allowed to stabilize for approximately 20 minutes. On the initial run, the spring-loaded wheel was placed in the downslope-facing groove, and measurements were taken at increments equal to the gauge length as the instrument was raised. After the highest possible reading was recorded, the instrument was removed from the hole, checked, turned through 180°, re-set to the bottom of the hole, and the measuring procedure repeated at the same depths. Power was on at all times while the probe was in the hole.

Depths at which measurements were taken were established in May, 1975 and all subsequent readings were taken at the same levels. These depths were referenced to the clamp on the pulley assembly and the assembly itself was always mounted in the same position. Lengths of cable between the clamp reference point and the ground surface were accounted for during data processing so that



depths appearing with reduced data were corrected to the ground surface.

All equipment functioned perfectly during the monitoring period. The sensor and readout device required no service, but the cable was returned to the manufacturer for repairs to the neoprene jacket in October, 1976.

In GB2, tightness at the 10.5 m depth began to restrict movement of the probe in November, 1975. By October, 1976, the problem was sufficient to prevent free passage of the probe. This was overcome by assembling a string of flexible PVC pipe with couplings and fast setting cement, lowering it to the top of the sensor, and gently pushing the probe through the restrictive zone. This technique was also required in order to obtain readings in hole GB1A in June, 1977. Also in June, 1977, the casing in GB3 was found to be broken at approximately the 2.5 m depth. Some difficulty was encountered in lifting the sensor past this point; however a complete set of readings was obtained.

#### 4.4.5 Data Analysis Procedure

Reduction of the inclinometer data was carried out by computer. The programme was prepared according to the steps suggested in the Digitilt operations manual. These are as follows:

1. The algebraic difference (TOT) is determined from the A1 and A2 readings at each depth. Each TOT is proportional to the size of the angle from vertical.
2. The difference (DIFF) between the current TOT and the

calibration TOT is determined for each depth.

3. The deflection (DEFL) is computed by integrating the DIFF values from the bottom to the top, and multiplying by constants which correspond to the reading interval.
4. The same procedure is used to reduce the B direction readings.

All input and computed data were listed, and DIFF and DEFL plotted on a Calcomp C plotter as a function of true depth for both the A and B directions. In addition, plots of DEFL as a function of time at each depth were produced on the line printer for both A and B directions. Because of the skewness of grooves in the GB2 installation relative to true downslope and transverse to slope directions DIFF and DEFL were plotted in the skewed, and the true downslope and transverse to slope directions; line-printer plots of DEFL as a function of time were only produced for the true downslope and transverse to slope directions in GB2.

After each preliminary run with new data, computer listings were closely scrutinized for possible errors. Those originating from data entry were quickly corrected, and those originating in the field (typically reversed polarity, or reversing in the order of numbers) were corrected after careful consideration of earlier readings. No other changes were made to the data.

Statistical analysis was added to the basic data processing routine after sufficient data were available to justify a more comprehensive approach. These were developed to elucidate specific complexities in the data and will be discussed in Section 4.4.8.

#### 4.4.6 Inclinometer Data

Shapes of the inclinometer casing relative to vertical in the A and B reference planes are presented in Figures 4.9 through 4.16 inclusive. These show the inclination of the drillhole as well as any local curvature in the inclinometer casing at the time of calibration (July, 1975). Deflection data for the A and B directions of each installation are presented in the same diagrams. These include plots of true downslope and transverse-to-slope profiles for the GB2 casing (Figures 4.12 and 4.14).

The very complex pattern of movement indicated in Figures 4.9 through 4.16 inclusive, is a result of the degree to which deformations of the casing approach the minimum accuracy range of the Digitilt inclinometer. Therefore, in order to analyze the nature of deformations it is first necessary to know the accuracy of the system, and then to consider the influence of any external factors. These are discussed in Sections 4.4.7 and 4.4.8 respectively, and are followed by data analysis in Section 4.4.9.

#### 4.4.7 Inclinometer Accuracy

Tests to determine the accuracy of inclinometer systems have been outlined by Murray and Irwin (1970), and Green (1974). Similar tests are reported here to assess the repeatability, resolution, and temperature-drift characteristics of the U of A Digitilt inclinometer system. In addition, consideration is given to casing

spiral and sensor axis rotation error. Each is discussed separately in the following subsections:

### Repeatability Tests

Repeatability measurements demonstrate the accuracy with which the instrument can measure zero deformation. Hence, they are an important instrument performance test when dealing with small deformations. The data not only provide an independent check of the manufacturer's specifications, but, if used in situ, they also indicate locations in the inclinometer casing where slight separation of coupling joints, or irregularities in the tracking grooves cause anomalous behaviour.

The results of repeatability tests in GB1A and GB3 are shown in Figures 4.17 and 4.18 respectively. For each date and hole the mean values at each depth are plotted as the calibration values (straight line at zero deformation). The data show three important findings:

1. The poorest repeatability in the A direction (GB1A-June, 1976) is  $0.58 \times 10^{-4}$  while the repeatability at other times has an average of approximately  $0.25 \times 10^{-4}$ .
2. Repeatability in the B direction is typically poorer. The lowest value (GB1A-June, 1976) is  $0.65 \times 10^{-4}$ . Values typically vary more than in the A direction and average approximately  $0.43 \times 10^{-4}$ .

3. Anomalous behaviour of the GB1A casing at the 24 m depth corresponds to the location of a coupling. In June, 1976, it is assumed that one or both wheel assemblies left their grooves after passing the coupling, and returned after two depth intervals were read. On subsequent readings, great care was taken in passing this zone and the problem did not recur. For June, 1976 readings in the B direction, anomalies at the 34, 29, and 21 m depths in GB1A do not correspond to couplings or tight curvature. Extra care in raising the tool through these zones eliminated the problem.

The results of the repeatability tests demonstrate that the University of Alberta Digitilt inclinometer performs significantly better than the manufacturer's specifications (Table 4.5). The average performance is up to 10 times better, and even the poorest repeatability exceeded the specifications by approximately a factor of two. The A direction consistently shows better repeatability than the B direction, presumably because the latter is not controlled by a wheel assembly and is subject to a small amount of play in the bearings and bushings of the A direction tracking assemblies. This slack becomes a problem where irregularities in the tracking grooves, poor couplings, or tight curvature cause the assemblies to wobble. Finally, because the accuracy of the inclinometer system is apparently controlled by the tracking characteristics of the sensor, the accuracy varies from hole to hole. Moreover, it can be improved in any hole if careful regard is

given to zones in the inclinometer casing where irregularities are known to cause anomalous behaviour.

### Resolution Tests

Resolution tests were carried out to determine the accuracy with which the inclinometer can measure a known deflection. The tests were conducted in the calibration frame shown in Figure 4.19. This consists of a segment of standard ABS plastic inclinometer casing (Table 4.5) centred and clamped to a Palmgren milling head which is secured to a heavy steel levelling plate. The plastic casing is sealed at its lower end, and fitted with brass hose connectors and tubing so that controlled-temperature fluids can be circulated around the sensor. The casing and tubing are wrapped with 5 cm thick fibreglass insulation for improved temperature control. Temperatures are monitored on a digital thermometer with the thermistor secured to the sensor near the sensing elements.

Resolution tests were carried out in  $1^\circ$  increments through a range of  $\pm 7^\circ$  from vertical at an ambient temperature of  $21.6^\circ\text{C}$ . Tests were begun with the probe at a stable temperature, in a vertical position, in the A direction grooves. Angular measurements were taken in  $1^\circ$  increments while moving the probe from  $0^\circ$  to  $-7^\circ$ ,  $-7^\circ$  to  $+7^\circ$ , and  $+7^\circ$  to  $0^\circ$ . The probe was then set in the B direction grooves and the same procedure was used to measure deflection in the B direction.

The results of one resolution test are illustrated in Figure 4.20, where angles between  $-7^\circ$  and  $+7^\circ$  are plotted as a function of

the absolute voltmeter reading in dial units<sup>1</sup>. True values are shown as solid circles between the end members of each measurement. For example, 348.4 is the exact change in dial units from 3° to 4° deflection; therefore this value is the ordinate, and for convenience, 3.5° is the abscissa. Mean values are determined from the two readings obtained per direction at each angular deflection, to account for inaccuracies in setting the milling head. A total of four resolution tests were carried out. Mean values for the A and B directions from each test are given in Figure 4.21. The data show small scatter about true values indicating a linear calibration. They show that errors of up to 6 dial units ( $3.0 \times 10^{-4}$ ) may occur, but these are not cumulative and their overall affect is negligible.

#### Temperature Tests

Tests to determine the influence of temperature change on instrument accuracy were necessary because of the large variation in air temperatures on occasions when readings were taken (Table 4.1), and the small temperature gradient in each of the inclinometer casings. Two tests were carried out to simulate these natural conditions: the first measured stabilization of the dial reading following the application of a step temperature; the second

---

<sup>1</sup>Inclinometers are commonly read in values equivalent to  $10^4$  times the true reading to eliminate decimal places. These values are the "dial units" referred to throughout this chapter. Hence, dial units times  $10^{-4}$  is proportional to two times the sine of the deflection angle.

measured change in dial reading as a function of temperature change. Both tests were carried out in the calibration frame (Figure 4.19) with the probe held at constant inclinations, and a solution of ethylene glycol circulated for temperature control. For stabilization tests, the calibration system was brought to a constant temperature of approximately  $-7^{\circ}\text{C}$  before the instrument was set into position in the A-direction grooves. Variation of readings on the voltmeter was monitored for both the A and B directions until temperature stability<sup>1</sup> was achieved. Temperature change tests were carried out over a range from approximately  $-7$  to  $22^{\circ}\text{C}$  by increasing the temperature to pre-determined settings on the controlled-temperature bath. After the bath temperature stabilized, up to 30 minutes were allowed before readings were taken. Tests were carried out at inclinations of  $+4^{\circ}$ ,  $0^{\circ}$ , and  $-4^{\circ}$  in the A direction, and then repeated with the tracking system in the B-direction grooves and monitoring the B-direction sensor.

Results of the temperature stabilization test are illustrated in Figure 4.22. These show that the step temperature has a significant affect on both sensing elements, but the influence is more pronounced for the B-direction sensor. For both sensing elements, temperature stability is achieved within 20 minutes.

Results of the temperature change tests are given in Figure 4.23. These show that the sensor has a linear temperature drift in

---

<sup>1</sup>Temperature stability was assumed when variation of the voltmeter was limited to 1 dial unit on successive readings after a total of 60 minutes of monitoring.



both directions, but that of the B direction is consistently larger than the A direction. Neither is of significance to this study because of the very small temperature gradient in the installations (Figures 4.3, 4.4 and 4.5). Moreover, it is probable that movement of the probe causes some degree of equalization to the temperature gradient, which would further reduce possible error.

The readout device was protected from cold temperature extremes by holding it inside the reader's clothing during winter monitoring (November to March inclusive). The downhole cable and linkage cable could not be protected in the same way, but laboratory tests where the cable was varied through temperatures as cold as  $-7^{\circ}\text{C}$  showed no measureable affect on the readings.

### Casing Spiral

Spiralling of the inclinometer casing is a condition in which the tracking grooves become twisted, which causes errors in the direction and magnitude of observed movement. No attempt was made to determine the degree of spiralling, because equipment to measure it is large and insufficiently accurate for the purposes of the study<sup>1</sup>, and casing strings up to approximately 60 m in length are considered too short for spiralling problems to be significant<sup>2</sup>.

---

<sup>1</sup>Bumala, T.G., P.E., Slope Indicator Co., Seattle, WA., personal communication, May 1976.

<sup>2</sup>Green, G.E., P.E., Shannon and Wilson, Inc., Seattle, Wa., personal communication, May 1976.

### Sensor Axis Rotation Error

Inclinometer sensing elements cannot be mounted perfectly parallel and perpendicular to the tracking assembly. Therefore, with the instrument in a vertical position, a small but measurable apparent deflection is indicated in both the A and B directions. Similarly, if the instrument is inclined in either of the A or B planes, small apparent deflections make up a constant portion of the respective readings. Since the magnitude of these apparent deflections is constant among the calibration reading and successive readings, it is eliminated in the data reduction procedure. If a sensing element shifts, however, the difference between the magnitudes of apparent deflections from the new reading and the calibration reading is not eliminated, but constitutes an error that is proportional to the absolute profile of the inclinometer casing in the direction normal to the sensing element axis. On a depth versus deflection profile, which shows plots of corrected and uncorrected data from one reading of an inclinometer casing, the error causes the two plots to appear symmetric, but rotated about the lowest reading.

Sensing elements typically shift as a result of rough handling or when they are removed from the instrument for servicing. Since neither of these conditions occurred during the monitoring period, it is not surprising that the data show no obvious sensor axis rotation error. It was felt initially that erratic deformations between and including the March, 1976 and October, 1976 readings in the A-direction plane of GB1A were

indicative of this type of error; however, further study reported in Section 4.4.8, shows this to be a result of natural phenomena at the site.

#### 4.4.8 External Factors Affecting Measured Deformations

Several external factors related to the installation procedure and site conditions cause deformations. These include: recovery of equilibrium conditions around the casing; the effect of stratigraphy; and, settlement and heave of the casing. They are not unique to this study, but they are particularly important because the magnitude of associated movements is significant in relation to deflections shown in the deflection versus depth profiles (Figures 4.9 through 4.16 inclusive). These factors are discussed separately in the following subsections.

##### Recovery of Equilibrium Conditions

Drilling, sampling, and instrumentation procedures described in Chapter III caused a change in equilibrium temperature and stress conditions around each drillhole.

Temperature changes resulted from mud-rotary drilling, flushing, and placement and hydration of the grout. Mud-rotary drilling and placement of grout caused a decrease in ground temperatures, while flushing and hydration of the grout caused an increase. Although it is impossible to assess the significance of each procedure, it is likely that hydration was the most important. Data presented in Figures 4.1, 4.2, and 4.3 show that temperatures

after hydration were relatively warm, causing a negative temperature gradient which in almost all cases prevailed until the July, 1975 readings.

The stress field around each inclinometer casing changed as a result of drilling and sampling, placement and set of the grout, and frost heave associated with the negative temperature gradient mentioned above. Drilling and sampling activities disturbed the equilibrium stress field and doubtlessly caused high stress gradients around each opening. These stress gradients probably decreased as a result of placement and set of the grout, and decreased further as a result of frost heave associated with cooling temperatures which followed the hydration process.

It is assumed that these transient temperature and stress conditions caused small, random deformations which developed most rapidly in the several days immediately following placement and hydration of the grout, and continued to develop, at a decreasing rate, until recovery of stress equilibrium was complete. Moreover, it is assumed that erratic local deformations<sup>1</sup> in the inclinometer data are directly related to this recovery process. These deformations are most pronounced in May and July, 1975 readings and approach negligible magnitudes by the end of 1975. The small magnitudes, random occurrence, and erratic behaviour of these

---

<sup>1</sup>Erratic local deformations are those which impart a zig-zag or wavy appearance to the deflection versus depth profiles. They are rarely progressive with time, and may or may not appear in successive data sets.

measured deformations preclude the possibility of any direct analysis; however the same characteristics render the deformations suitable for statistical analysis<sup>1</sup>.

As background for the statistical analysis, it must be remembered that under ideal conditions the long axis of the digitilt inclinometer and that of the casing in which it runs are parallel, regardless of the inclination. When the casing deforms, in addition to the change in inclination, there is a slight distortion of the tracking grooves which effects a degree of non parallelism. The instrument records this non parallelism: A-direction readings are directly affected because the bottom of the tracking grooves, which control the A-direction sensor, is easily distorted; B-direction readings are less affected because the walls of the tracking grooves, which largely control the B-direction sensor, are much less sensitive. This is an apparent condition, however, because deformations associated with the recovery of equilibrium are randomly distributed around the casing, and the B-direction grooves, although not monitored, are doubtlessly affected in an identical way.

The non parallelism is manifest in the degree to which SUMS of opposing A or B-direction readings correspond in successive readings at respective depths. For example, Table 4.6 shows a complete set of inclinometer data for GB3. The SUMS have been determined at each depth, and the mean and standard deviation of SUMS have been calculated for each of the A and B directions. For

---

<sup>1</sup>A format for the statistical analysis was provided by Dr. G.E. Green, P.E., Shannon and Wilson, Inc., Seattle, Wa.

any subsequent set of data, increased non parallelism is reflected in a general increase in the absolute magnitude of the SUMS, and, therefore, an increase in the standard deviation of SUMS. Thus, an increase in the standard deviation is an index of a proportionate increase in the degree of non parallelism.

Plots of standard deviation versus time for the A and B directions of each inclinometer casing are shown in Figure 4.24. These indicate that from the time of grout placement, when the casing grooves are presumed to have been perfectly parallel, there is a change in the standard deviation with time. This change takes place at a decreasing rate, reaching a quasi-stable magnitude in the latter half of 1975. In each installation, approximately 50% of the long-term erratic movement occurs within a period of 25 to 50 days following placement of the grout, and approximately 75% within a period of 75 to 100 days. After approximately 75 to 100 days, the variation between successive sets of data is generally small enough that overall ground movement at the scale of creep deformations may be distinguished from erratic local deformations.

These results lead to several important conclusions:

1. The data appear to support the theory that recovery of temperature and stress equilibrium around inclinometer casings cause erratic local deformations.
2. As expected, the data reported in Figure 4.24 indicate that A-direction readings are much more sensitive to erratic deformations than B-direction readings. Since

these movements are randomly distributed, the A-direction measurements are representative of conditions around the entire circumference of the casing. .

3. The standard deviation of SUMS is a relative measure of non parallelism, but since the tracking grooves can have a reasonable degree of non parallelism and still give excellent reproducibility, it is the rate at which erratic deformations develop, relative to the rate of creep deformations, which is the most important criterion.

Figure 4.25 shows the rate of change of the standard deviation of A-direction SUMS for each of the inclinometer casings based on the data in Figure 4.24. The GB3 data show an almost constant decrease in rate as a function of time. The overall trend is similar for GB1A and GB2, although anomalous instrument behaviour in August, 1975 causes a significant departure.

On the basis of this work, it is concluded that a rate of change of 0,3 dial units/day is a maximum above which erratic deformations visually dominate deflection versus depth profiles to the extent that net ground movement at the scale of creep deformations are obscured. Data reported for GB2 in Figure 4.25 exceed this rate for approximately one quarter of the monitoring period, and this is one reason for difficulty in interpreting deformations in GB2, as discussed in Section 4.4.9.

4. When an inclinometer probe is not functioning properly, plots of the standard deviation SUMS as a function of time give an indication of this condition, and plots of rate of change of standard deviation of SUMS allow an assessment of whether or not the anomalous behaviour is of a sufficient scale to warrant rejection of the data.

### Stratigraphy

The distribution of erratic and progressive movements in the deflection versus depth profiles (Figures 4.9 through 4.16 inclusive) correlates with two aspects of the stratigraphy of the slope.

The first correlation, is the preponderance of erratic local deformations in certain lithofacies. To analyze this condition, inclinometer readings from within each discrete lithofacies (sand, clay, etc.) in each hole were studied statistically according to the format described in the preceding subsection. Not all data could be used because the number of readings within some lithofacies is too small to form a reasonable population for the necessary normal distribution.

The results illustrated in Figure 4.26 show that in each hole the largest standard deviation of A-direction SUMS generally occurs in the unit or units through which the most sampling and/or drilling difficulties were encountered. This includes the sand in GB1A, the till in GB2, and the clay with sand and coal beds in GB3. Values



for the clay are reasonably consistent among the three holes. This is probably a result of fairly consistent drilling and sampling conditions.

In general, the data indicate that a correlation exists between the standard deviation of A-direction SUMS and stratigraphy; however, this is considered coincidental, and the true correlation lies with drilling and sampling practice as it is affected by the stratigraphy. It is likely that difficulties in making hole, specifically because of washing or lost circulation in the granular soils, and cobbles and boulders in the till, caused increased disturbance around the hole, therefore increased frequency of erratic local deformations associated with recovery of equilibrium conditions. In addition, these difficulties probably caused significant variation in hole diameter, which led to unusually non-uniform stress distributions during grout set.

The second correlation is between deformations and ice-rich soils, especially those with pervasive ice lenses more than 2.5 cm thick. This is illustrated in Figures 4.9 through 4.16 inclusive, where A and B-direction deformation profiles are plotted adjacent to the moisture/ice content profile from the same, or a nearby hole.

Where single ice lenses or zones containing closely spaced ice lenses are separated by 2 m or more, movements are typically large and cause very sharp deflections. Examples of this occur at the 15 m depth and between 29 and 34 m in GB1A, at the 12.6 m depth in GB2, and it is assumed ice lenses are associated with the sharp deflections at the 11.0 and 15.5 m depths in GB3. In the A

direction, these movements are frequently, but not consistently progressive with time, contributing a net downslope deflection. In the B direction, movements are similar, but rarely cause any net deflection.

Where single ice lenses or zones containing closely spaced ice lenses are spaced at less than 1 m, and the natural moisture content of soil between the ice lenses is at least 25% to 30%, movements are typically smaller and much less abrupt. These are generally progressive with time in the A direction and cause net deflection in one direction, although the pattern is occasionally interrupted by a reversal in the sense of movement. Movements in the B direction tend to be slightly smaller in magnitude and show no significant net deflection. Examples where net downslope deflection occurs are between 20 m and 25 m in GB1A, above 4 m in GB2, and between 3 and 7 m in GB3. The only place where net (downstream) displacement occurs is between approximately 6 m and 8 m in GB2.

In summary, the data indicate a correlation between movement and ice lenses. Where ice lenses are widely spaced (greater than 1 to 2 m), movements are large and abrupt, causing sharp deflections in the deflection versus depth profile; where they are closely spaced (less than 1 m), movements are smaller. A-direction movements are frequently, although not consistently, progressive with time and generally cause net downslope deflection. In terms of homogeneous strain through any ice-rich section of the overall soil profile, the resulting deflection pattern approximates simple

shear. In the B direction, movements occur at similar depths, but are smaller in magnitude and rarely cause net movement in either direction.

#### Settlement and Heave of the Casing

The kinematics associated with settlement and heave are illustrated schematically in Figure 4.27. It is assumed compressive and tensile stresses seated in both the active layer and the zone of annual temperature fluctuation are transmitted through the inclinometer casing and grout column. Compressive stresses cause increased curvature by forcing the pile-like system laterally outward into the encompassing soil, tensile stresses pull or straighten the system and cause decreased curvature. Through the summer season, and up to approximately the culmination of warming of ground temperatures, lateral movement outward in response to settlement is progressive. Through the winter season, and up to the culmination of cooling of ground temperatures, lateral movements are progressively inward in response to heave.

Typical plots of deflection as a function of time for the A and B directions at four discrete measuring depths are shown in Figure 4.28 together with mean velocities determined from least-squares linear regression analysis. The data indicate that settlement and heave were active processes throughout the monitoring period. In the B direction, which is assumed to be free of overall ground deformation, each data set has a sinusoidal distribution

about its mean velocity with a wavelength of approximately 365 days. Lateral movement associated with settlement and heave is progressive, but opposite in direction during periods of ground warming and cooling respectively, and the net lateral movement after one year is small. In the A direction, conditions are identical, although the sinusoidal distribution is obscured because lateral movements resulting from settlement and heave are superimposed on natural ground deformations associated with creep.

Figure 4.28 also indicates that early data from the A and B directions show significant departure from their respective regression lines. This is a result of accelerated warming and anomalously large settlement in the zone of annual temperature fluctuation during the summer season immediately following installation of the inclinometers. On the basis of these observations, it is recommended that inclinometer installations in fine-grained permafrost soils be completed during, or shortly after the period of maximum cooling of ground temperatures. This ensures that settlement or heave-related loading is initially compressional, preserving the continuity of the inclinometer casing and grout column. It is also recommended that thick-walled plastic casing be used to complete the surface installation, in order to minimize heat conduction and associated heave during winter months.

Breakage of the GB3 casing at the 2.5 m depth between March and June, 1977 is considered to have been caused by heave and is further evidence that vertical deformations occurred in each

inclinometer installation. Removal of heat via the steel casing, and heave resulting from anomalously low ground temperatures probably lead to failure of the inclinometer casing and grout column, and separation of the two ends by an estimated 1 cm.

In summary, these data indicate that settlement and heave affect the entire length of the inclinometer casing. The process causes small movements which are progressive with time during the summer and winter season, but reverse their sense of movement as the season changes. This effects an apparent cessation or reversal to some patterns of progressive movement. After one year, the net movement induced by these processes is zero. Hence, the mean velocity determined from data for a one year period accurately represents the true rate of ground deformation.

#### 4.4.9 Delineation of Creep and Shear Deformations

Data presented in Section 4.4.7 demonstrated that the overall accuracy of the University of Alberta Digitilt inclinometer was, in general, better than the specifications given by the manufacturer, and easily sufficient to resolve deformations several times smaller than deflections shown in the deflection versus depth profiles (Figures 4.9 through 4.16). In Section 4.4.8 the influence of erratic local deformations emerged as a more serious concern than instrument accuracy, but with the aid of several special analytical techniques it was possible to distinguish between erratic local deformation and net ground movement.

Plots of deflection versus time (Figure 4.28) proved to be particularly useful for clearly delineating net ground deformation. Therefore, a computer analysis routine was prepared to generate line plots of this type, perform a linear regression fit, and determine velocity for each of the A and B direction at each measuring depth. The velocity data from this analysis are plotted as a function of depth for each inclinometer casing in Figures 4.29 through 4.31. These plots show deformation patterns much more clearly than the deflection versus depth plots (Figures 4.9 through 4.16).

Consideration of the deflection versus depth profiles and velocity versus depth profiles indicates that two deformation patterns cause net ground movement in the inclinometer casings. Moreover, each shows significant correlation with the distribution and size of ground ice structures.

The first deformation pattern is represented by net movement in one direction over depth intervals that are several metres thick. This deformation pattern is best developed through ice-rich sections of the soil profile. Strain<sup>1</sup> is commonly greatest near the bottom of the depth interval and decreases upward imparting a velocity profile which appears to attenuate to some degree near the top of the depth interval. Velocity gradients are however, pseudo-uniform over certain depth intervals. The second deformation pattern is represented by apparent shear through depth intervals that are typically less than 1 m thick. This deformation pattern

---

<sup>1</sup>Plane strain conditions are defined by the inclinometer data. Zero net vertical strain is assumed.

frequently occurs in the proximity of pervasive ice structures.

A discussion of these deformation patterns as they affect each of the inclinometer casings is given in the following subsections:

#### Casing GB1A

Figure 4.29 indicates net downslope (A direction) velocity through the medium to high plastic clay lithofacies. Although the data are scattered, the velocity at the top of the lithofacies is between 0.25 and 0.30 cm/year, and at the mid point is between 0.15 and 0.20 cm/year, indicating the strain rate through the lower half of the lithofacies is slightly higher than through the upper half. This is interpreted as creep deformation.

The creep pattern shows some relation to both the scale and the spacing of ground ice structures as inferred from the GB1 core logs (Figure 4.9). Above the 29 m depth where ice lenses are large and closely spaced the velocity gradient is pseudo-uniform. An approximate strain rate<sup>1</sup> through this zone is  $2.0 \times 10^{-4}$  year<sup>-1</sup>. Between approximately the 29 and 34 m depths, where large ice lenses are more widely separated, the velocity is erratic, with proportionally more movement associated with the large ice lenses. Below the 34 m depth, where only small ice lenses are present, the velocity gradient is again pseudo-uniform at an approximate rate of strain of  $0.4 \times 10^{-4}$  year<sup>-1</sup>.

---

<sup>1</sup>All values of strain rate are based on a linear regression fit to velocity data over the specified depth interval.

B-direction deflections through the same lithofacies oscillate about approximately zero deformation (Figure 4.10), with a small but insignificant constant downstream velocity (Figure 4.29).

No creep deformations are evident in the sand lithofacies. This does not preclude the possibility of creep deformation in the sand. Data quality is poor because of drilling and grouting difficulties as discussed in Sections 3.4.3 and 3.6.1, and this may obscure any evidence of creep deformation.

At the contact between the two clay lithofacies there is an indication of shear in the A direction which causes net downslope movement. Shear is also likely in the sand lithofacies between the 11 and 12 m depth. This may be related to the presence of a thick ice lens at between the 13 and 14 m depths in GB1<sup>1</sup>.

#### Casing GB2

Velocity data from this inclinometer casing are shown in Figure 4.30. Through the medium to high plastic clay, deformation rates range as high as 0.70 cm/year and are generally larger than in either of the other inclinometer casings. Over some depth intervals, a pseudo-uniform velocity gradient may be inferred with approximate shear strain rates of between  $8.0$  and  $12.0 \times 10^{-4}$  year<sup>-1</sup>, but correlations are typically poor and the values are not

---

<sup>1</sup>As part of another site investigation programme in the Great Bear River area (Northern Engineering Services Limited, alternate river crossings of Great Bear River) the author found steeply dipping ice lenses in association with shear planes through the sand lithofacies.



considered reliable. Moreover, between the ground surface and approximately the 3 m depth, correlation among deflection versus time data is so poor that meaningful velocities could not be determined.

The reason for difficulty in interpreting data through the medium to high plastic clay cannot be defined with certainty on the basis of this study, but the presence of numerous slickensided surfaces in cores (Appendix B), and progressive squeezing of the inclinometer casing at certain depths (Table 4.1) suggest a complex network of shear planes affect the inclinometer casing and probably cause the erratic deformation pattern. This is supported by data presented in Section 4.4.8 where it was shown that erratic deformation affected the GB2 inclinometer casing during most of the monitoring period to the extent that interpretation of net ground movements at the scale of creep deformation was expected to be difficult.

Although data from the low to medium plastic clay (till) were shown to be of poor quality in Section 4.4.8, data in Figure 4.30 indicate a pseudo-uniform downstream (true B direction) velocity gradient through this lithofacies. The approximate strain rate derived from these data is  $1.5 \times 10^{-4}$  year<sup>-1</sup>. Data through the same stratum in the true A direction show a small but insignificant constant upslope velocity.

Casing GB3

The deflection versus depth profile in Figure 4.15 indicates downslope (A direction) movement in both clay lithofacies above the 14.9 m depth. This movement is interpreted as creep deformation. Data in Figure 4.31 indicate that velocities associated with this movement range from approximately 0.10 cm/year at the 14.9 m depth to between approximately 0.25 and 0.30 cm/year at the 2.1 m depth. The velocity gradient over this depth interval is relatively uniform and indicates a shear strain rate of  $0.9 \times 10^{-4} \text{ year}^{-1}$ .

The creep pattern shows approximately the same relationship to ice structures as was described for casing GB1A. Between depths of 3.6 and 7.2 m, ice lenses are large and closely spaced, and the velocity gradient appears to be quite uniform. Between the 2.1 and 3.6 m depths, ice lenses are relatively smaller and more widely spaced, and deformations are sharper and associated with ice lenses.

B-direction deflections oscillate about zero deflection (Figure 4.16) between the 2.1 and 14.9 m depths, with zero net velocity (Figure 4.31).

Data in both the A and B directions above 2.1 m appear to be affected by the presence of the steel casing, and hence are not considered as reliable indicators of creep movement.

Some evidence of downslope (A direction) shear movement, is evident in Figure 4.15 between the 15.0 and 15.5 m depths. On the basis of grab samples and correlation with hole GB2, this shear zone appears to have developed in medium to high plastic alluvial clay.

TABLE 4.1  
SCHEDULE OF INSTRUMENT MONITORING

TRIP NUMBER	DATES		INSTRUMENT READINGS										GROUND SURFACE CONDITIONS	WEATHER		COMMENTS
	FROM	TO	INCLINOMETERS			THERMISTORS			PIEZOMETERS					AIR TEMP. (°C)	GENERAL	
			GB1A	GB2	GB3	GB1A	GB2	GB3	GB1B	GB2A	GB3A					
1	5/6/75	5/9/75	1	1	1	Yes	Yes	Yes	Dead	Yes	Dry	18	Sunny	Surveys at site and between Fort Norman and site.		
2	7/1/75	7/1/75	1	1	1	Yes	Yes	Yes	Dead	Yes	Dry	34	Sunny and Very Hot			
3	8/22/75	8/22/75	1	1	1	Yes	Yes	Yes	Dead	Yes	Dry at GB1A, wet elsewhere	23	Sunny but One Heavy Shower	Thunderstorm passed while moving from GB1A to GB2.		
4	10/8/75	10/8/75	1	1	1	No	No	Yes	Dead	Yes	Light Snow Cover	6	Sunny	Batteries dead in Actins Meter after reading GB3.		
5	11/21/75	11/21/75	1	1	1	Yes	Yes	Yes	Dead	Yes	45 cm of Snow Cover	-38	Sunny and Very Cold	Slight obstruction in GB2 at 11.6 m.		
6	3/3/76	3/3/76	1	1	1	Yes	Yes	Yes	Dead	Dead	50 cm of Snow Cover	-31	Sunny	Ice build up in GB3A piezo-meter leads - no reading possible. Obstruction in GB2 still present.		
7	6/8/76	6/8/76	3	1	1	Yes	Yes	Yes	Dead	Dead	Dry	21	Sunny	Obstruction in GB2 still present.		
8	8/11/76	8/12/76	2	1	2	Yes	Yes	Yes	N.R.A.	N.R.A.	Moist	21	Overcast	Obstruction in GB2 still present.		
9	10/4/76	10/4/76	1	1	1	Yes	Yes	Yes	N.R.A.	N.R.A.	Dry	14	Sunny	Forced to push inclinometer between 11.0 and 12.0 m in GB2.		
10	12/21/76	12/21/76	1	1	1	Yes	Part	Yes	N.R.A.	N.R.A.	25 cm of snow cover	-32	Sunny	Pushed inclinometer as above.		
11	3/1/77	3/1/77	1	1	1	Yes	Part	Yes	N.R.A.	N.R.A.	40 cm of snow cover	-24	Sunny	Cover on one thermistor cable in GB2 frozen. Pushed inclinometer as above.		
12	6/13/77	6/14/77	3	1	1	Yes	Yes	Yes	N.R.A.	N.R.A.	Dry	23	Sunny	Surveys at site. Pushed inclinometer as above in GB2, and between 11.6 and 12.2 m in GB1A.		

\* No Reading Attempted.

TABLE 4.2  
THERMISTOR INSTALLATION DATA

HOLE NUMBER	CABLE NUMBER	THERMISTOR NUMBER - DEPTH (metres)		
GB1A	1	1 - 4.27 4 - 22.56 7 - 40.84	2 - 10.36 5 - 28.65 8 - 46.94	3 - 16.46 6 - 34.75 9 - 53.04
GB2	2	1 - 4.57 4 - 21.03	2 - 10.67 5 - 22.86	3 - 16.76
GB2	3	1 - 0.91 4 - 19.20 7 - 31.39	2 - 7.01 5 - 25.30	3 - 13.12 6 - 28.96
GB3	4	1 - Surface 4 - 3.35 7 - 21.64	2 - 0.15 5 - 9.45 8 - 27.74	3 - 0.36 6 - 15.55

TABLE 4.3  
CLIMATIC DATA FOR FORT NORMAN, N.W.T.

CATEGORY	JAN.	FEB.	MAR.	APR.	MAY	JUNE	JULY	AUG.	SEPT.	OCT.	NOV.	DEC.	YEAR	TYPE*
Mean Daily Temperature	-27.6	-25.3	-18.5	-7.6	5.2	13.2	15.7	12.8	6.0	-3.8	-17.6	-26.2	-6.1	4
Mean Daily Maximum Temperature	-23.1	-21.0	-12.7	-1.3	11.4	19.6	22.1	18.8	10.7	-0.2	-14.2	-22.4	-1.0	4
Extreme Minimum Temperature Year	-53.9	-54.4	-50.0	-40.0	-23.9	-5.6	-3.3	-7.8	-15.6	-32.8	-43.9	-53.3	-54.4	1
	48	47	46	45	47	43	44	46	45	47	47	48		
Number of Days With Frost	31	28	31	30	18	2	1	3	12	29	30	31	246	4
Mean Total Precipitation (mm)	16.5	14.5	14.2	13.2	21.1	46.0	48.3	53.8	35.6	32.0	23.1	14.7	333.0	8
Mean Rainfall (mm)	0.0	0.0	0.0	3.0	14.2	45.2	48.3	53.8	28.7	4.3		0.0	197.5	8
Mean Snowfall (cm)	16.5	14.5	14.2	10.2	6.9	0.8	0.0	0.0	6.9	27.7	23.1	14.7	135.5	8
Greatest Precipitation in 24 Hrs (mm) Year	20.3	30.5	27.9	27.9	50.8	45.7	73.7	59.9	59.7	61.5	49.8	33.0	73.7	1
	49	49	48	47	50	46	47	48	48	48	46	47		
Greatest Rainfall in 24 Hrs (mm) Year	0.5	51	1.0	27.9	50.8	45.7	73.7	59.9	59.7	25.4	1.0	0.0	73.7	1
	49	49	48	47	50	46	47	48	48	50	49	49		
Greatest Snowfall in 24 Hrs (cm) Year	20.3	30.5	27.9	25.4	24.9	15.2	0.0	4.3	17.8	61.5	49.8	33.0	61.5	1
	49	49	48	47	50	49	49	49	48	48	46	47		
Number of Days with Measurable Precipitation	6	7	6	6	6	9	8	10	10	8	9	7	92	4
Number of Days with Measurable Rainfall	0	0	0	1	4	8	8	10	8	2	0	0	41	4
Number of Days with Measurable Snowfall	6	7	6	6	2	0	0	0	2	7	9	7	52	4

\*The actual period of record used to compute each category is given by the following:

Code Type of Normal

- 1 30 years between 1941 and 1970, or more
- 2 25 to 29 years between 1941 and 1970
- 3 20 to 24 years between 1941 and 1970
- 4 15 to 19 years between 1941 and 1970
- 5 10 to 14 years between 1941 and 1970
- 6 less than 10 years
- 7 combined data from 2 or more stations
- 8 adjusted
- 9 estimated

Note: All data obtained from Environment Canada, Atmospheric Environment Summary of Canadian Normals, Volumes 1-SI and 2-SI.

TABLE 4.4

## PIEZOMETER INSTALLATION AND CALIBRATION DATA

HOLE NUMBER	PIEZOMETER NUMBER	DEPTH OF PIEZOMETER TIP (metres)	PIEZOMETER CALIBRATION (kPa)
GB1B	644	40.4	$= (7.09 \times \text{Reading}) - 35.85$
GB3A	613	30.5	$= (7.12 \times \text{Reading}) - 28.96$

TABLE 4.5

## INCLINOMETER SPECIFICATIONS

SENSOR: Slope Indicator Company Model 50320

Sensitivity:	+ 0.0015 m per 30 m casing
Total System Accuracy:	+ 0.0076 m per 30 m casing
Wheel Base:	61 cm
Overall Length:	93 cm
Outside Diameter (not including wheels):	4.3 cm
Sensors:	Two 0.5 g closed loop force-balanced servo accelerometers
Operating Range:	0° to 30° (from vertical)

CABLE: Slope Indicator Company 1.07 cm O.D., six conductor with 0.16 cm stranded-steel core; waterproof neoprene cover with external marks at 0.31 m intervals.

INDICATOR: Slope Indicator Company Model 50306

Dimensions:	14.3 x 6.0 x 22.9 cm
Weight:	2.27 kg
Internal Power:	6V, 6 Ah
Charger:	External; 6 VDC
Operating Time on Batteries:	8 hours
Digital Display:	4 digits
Recording:	Manual

CASING: Slope Indicator Company ABS Plastic Casing & Couplings

Casing Length:	3.05 m
O.D.:	7.0 cm
I.D.:	5.9 cm
Coupling Length:	0.15 m
O.D.:	7.0 cm
I.D.:	6.5 cm

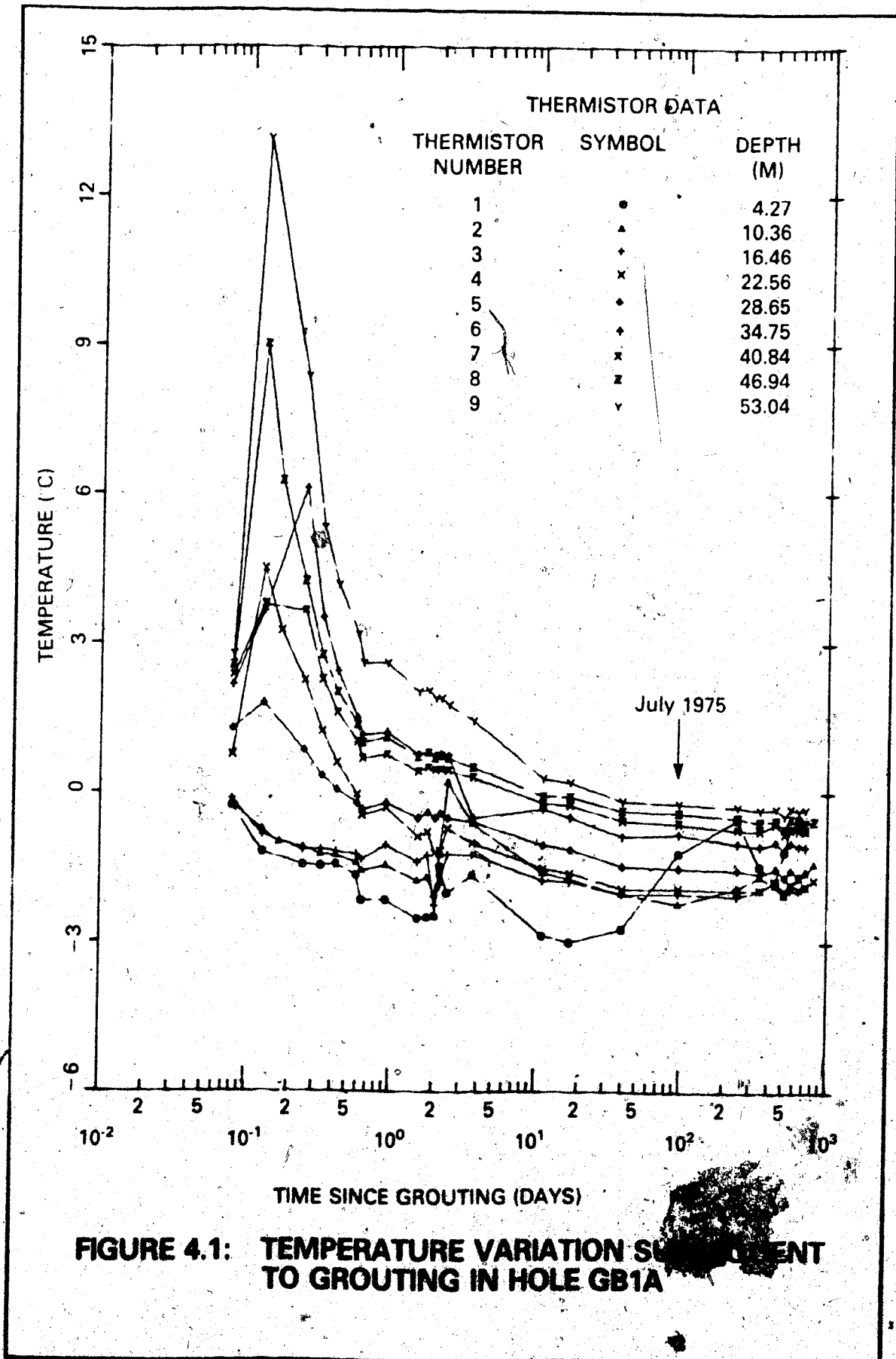
TABLE 4.6

EXAMPLE OF STATISTICAL ANALYSIS OF INCLINOMETER DATA  
HOLE GB3

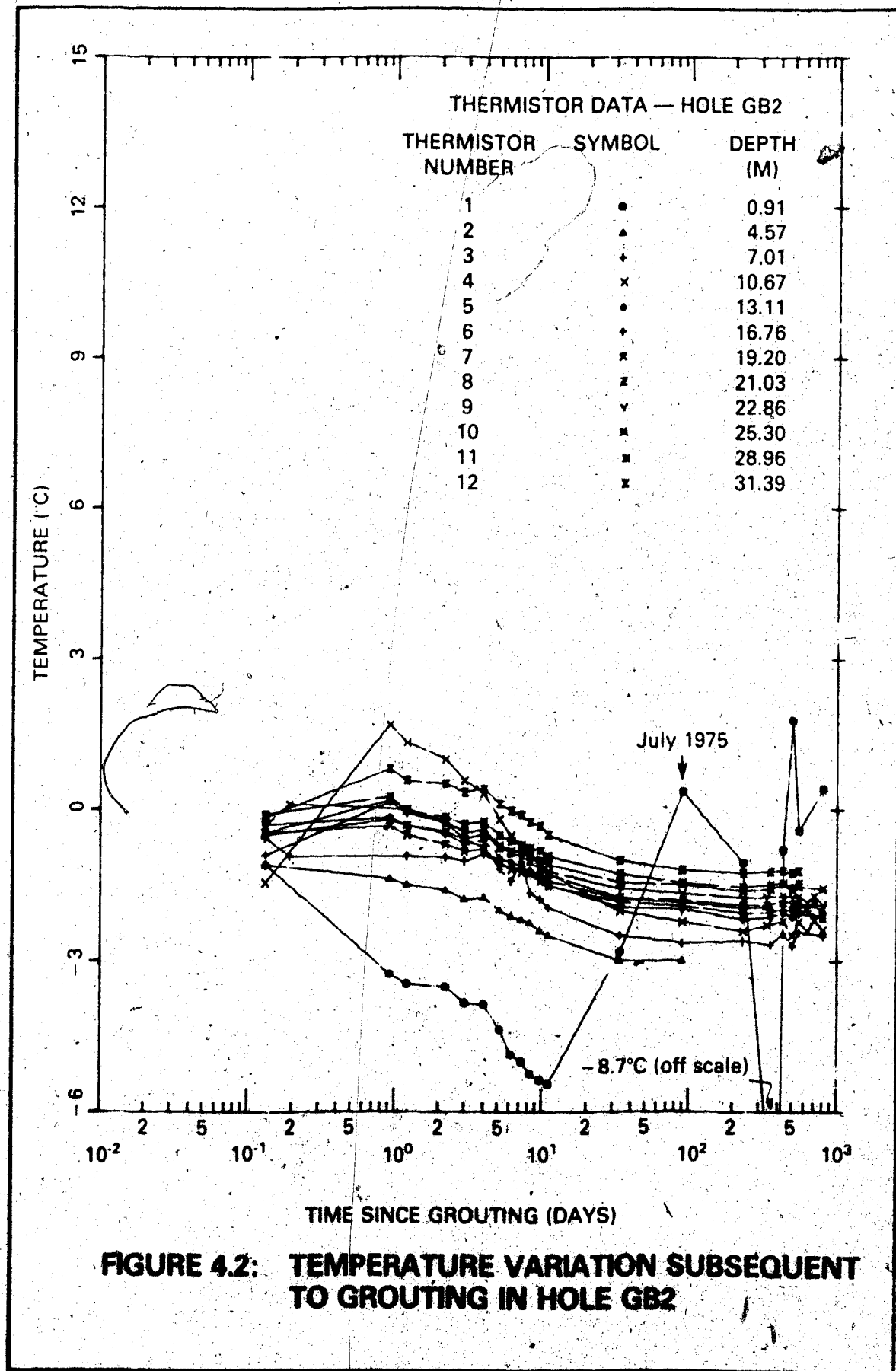
STATISTICAL ANALYSIS FOR DATA SET II OBTAINED ON MARCH 1, 1977						
DEPTH (metres)	A DIRECTION (dial units)			B DIRECTION (dial units)		
	A1	A2	SUM A	B1	B2	SUM B
21.03	215.	-60.	155.	409.	-486.	-77.
20.42	9.	-12.	-3.	417.	-483.	-66.
19.81	-172.	226.	54.	386.	-481.	-95.
19.20	-355.	454.	99.	250.	-323.	-73.
18.59	-461.	521.	60.	-22.	-68.	-90.
17.98	-491.	540.	49.	-90.	3.	-87.
17.37	-462.	522.	60.	-316.	227.	-89.
16.76	-228.	302.	74.	-287.	200.	-87.
16.15	-24.	82.	58.	-224.	158.	-66.
15.55	440.	-356.	84.	-54.	-44.	-98.
14.94	205.	-192.	13.	214.	-295.	-81.
14.33	603.	-494.	109.	268.	-359.	-91.
13.72	435.	-357.	78.	521.	-606.	-85.
13.11	306.	-229.	77.	427.	-500.	-73.
12.50	144.	-134.	10.	536.	-625.	-89.
11.89	-50.	126.	76.	510.	-591.	-81.
11.28	-64.	146.	82.	568.	-655.	-87.
10.67	-266.	290.	24.	458.	-529.	-71.
10.06	-287.	355.	68.	541.	-619.	-78.
9.45	-275.	334.	59.	191.	-276.	-85.
8.84	-381.	487.	106.	208.	-298.	-90.
8.23	-428.	471.	43.	-157.	69.	-88.
7.62	-392.	444.	52.	-305.	219.	-86.
7.01	-176.	229.	53.	-373.	290.	-83.
6.40	318.	-200.	118.	-456.	365.	-91.
5.79	629.	-626.	3.	-212.	145.	-67.
5.18	817.	-716.	101.	-192.	100.	-92.
4.57	870.	-841.	29.	42.	-129.	-87.
3.96	604.	-556.	48.	54.	-134.	-80.
3.35	500.	-431.	69.	466.	-543.	-77.
2.74	-33.	81.	48.	535.	-610.	-75.
2.13	-454.	535.	81.	141.	-216.	-75.
1.52	-716.	689.	-27.	762.	-864.	-102.
0.91	-502.	595.	93.	649.	-733.	-84.
0.31	-477.	576.	99.	661.	-737.	-76.

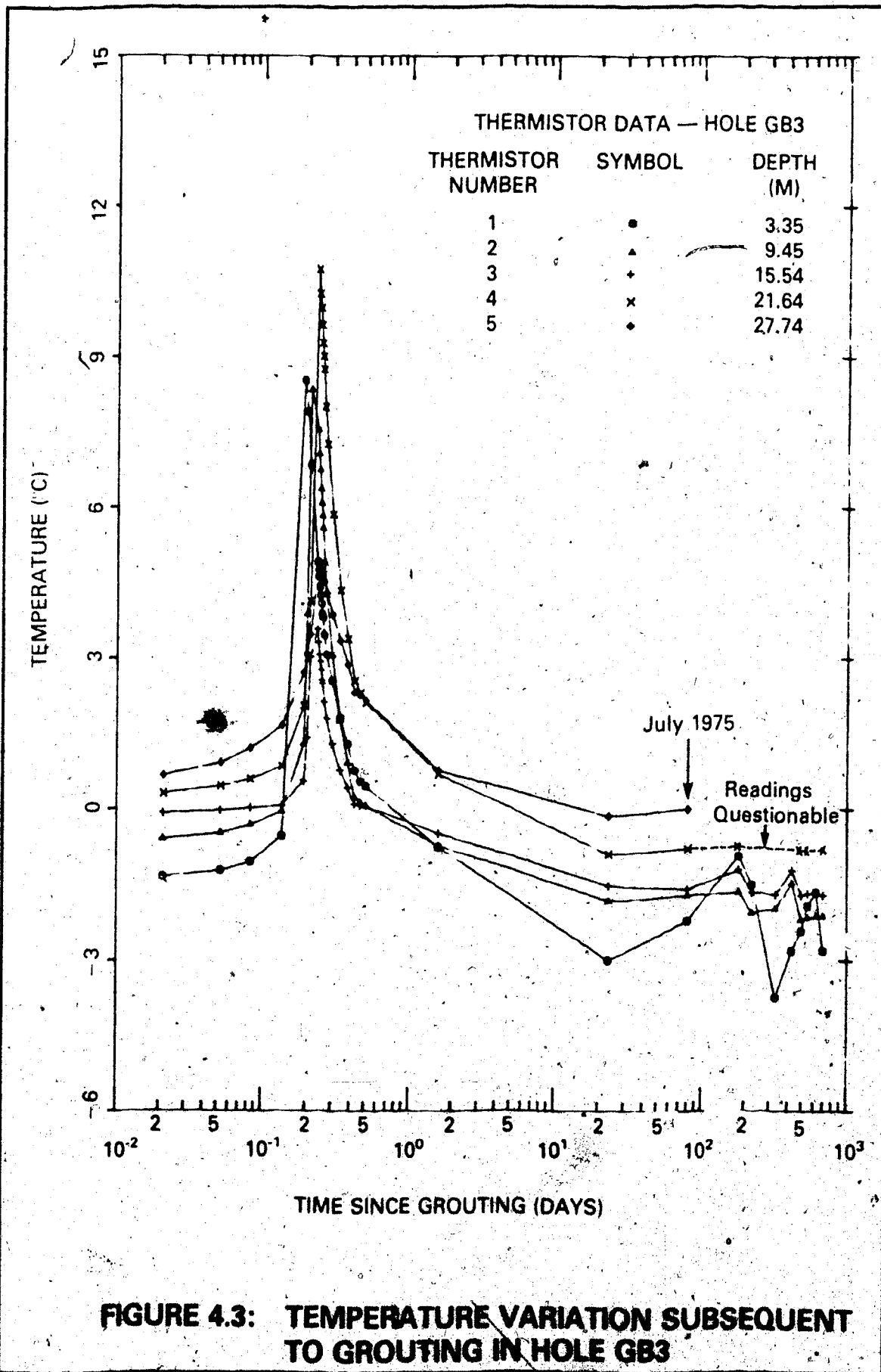
  

<p>From Sums of A:  Mean = 63 dial units  Standard Deviation:  = <math>\pm</math> 37 dial units</p>	<p>From Sums of B:  Mean = -83 dial units  Standard Deviation:  = <math>\pm</math> 9 dial units</p>
---	---









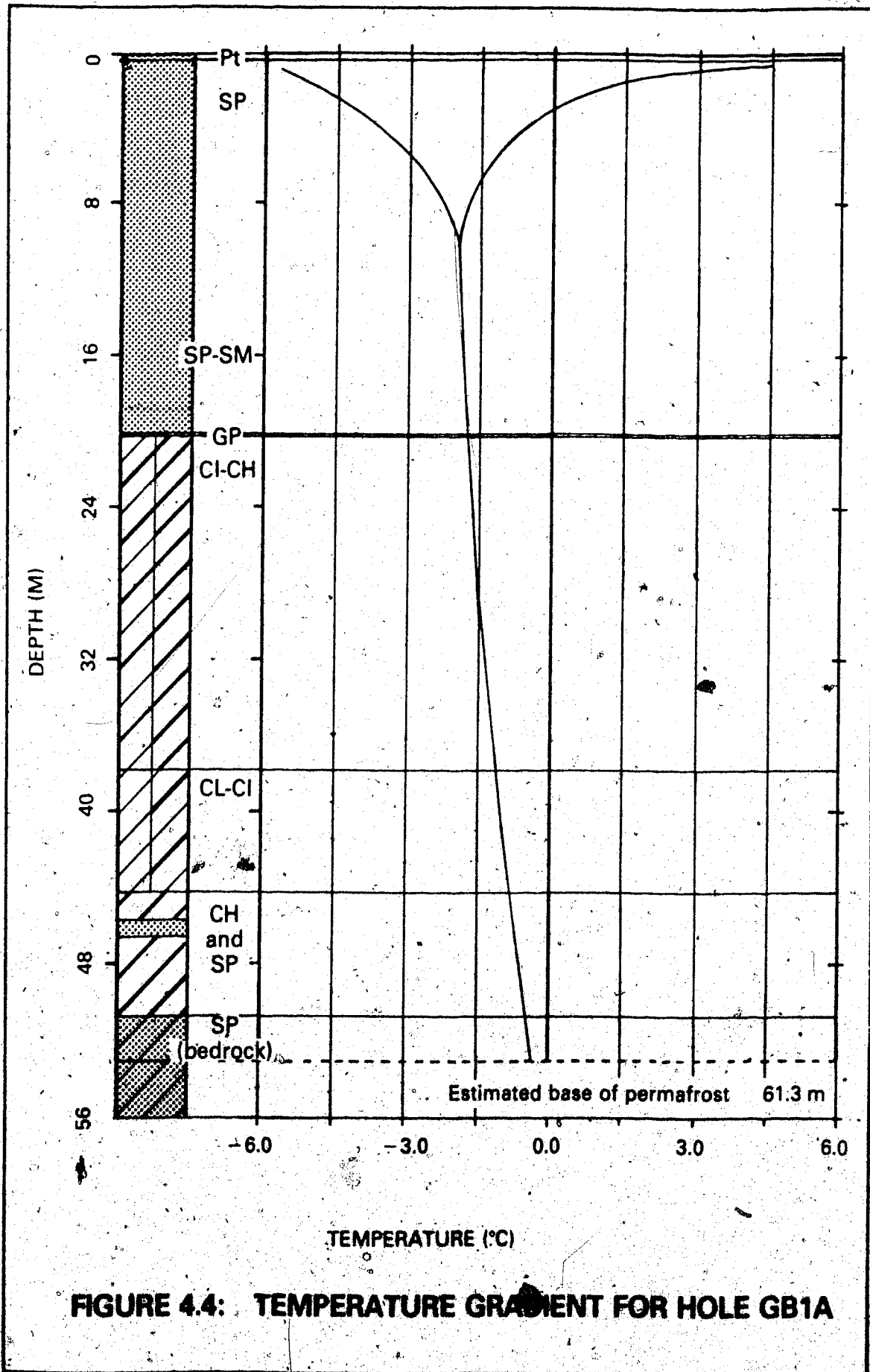


**FIGURE 4.4: TEMPERATURE GRADIENT FOR HOLE GB1A**

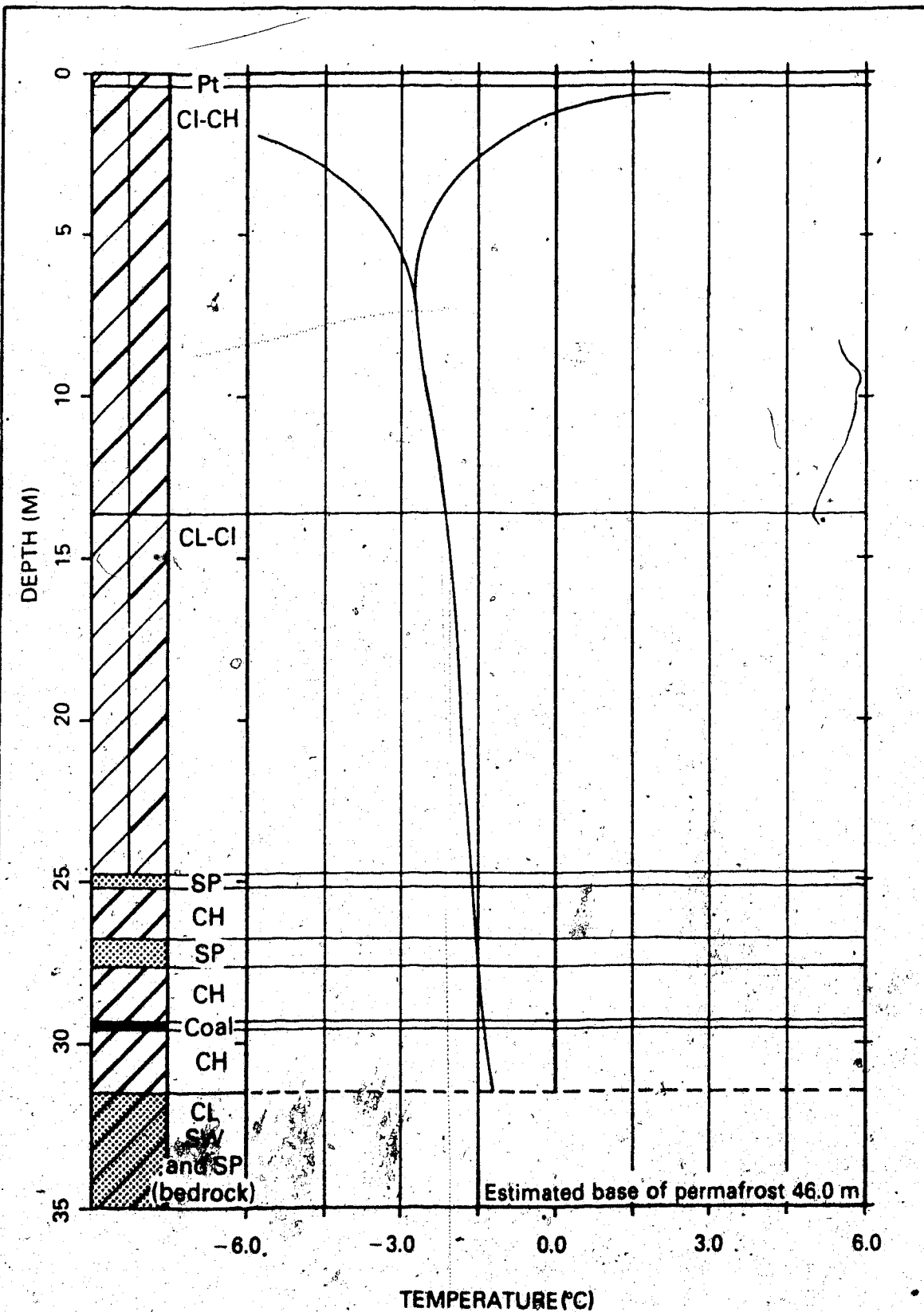


**FIGURE 4.5: TEMPERATURE GRADIENT FOR HOLE GB2**

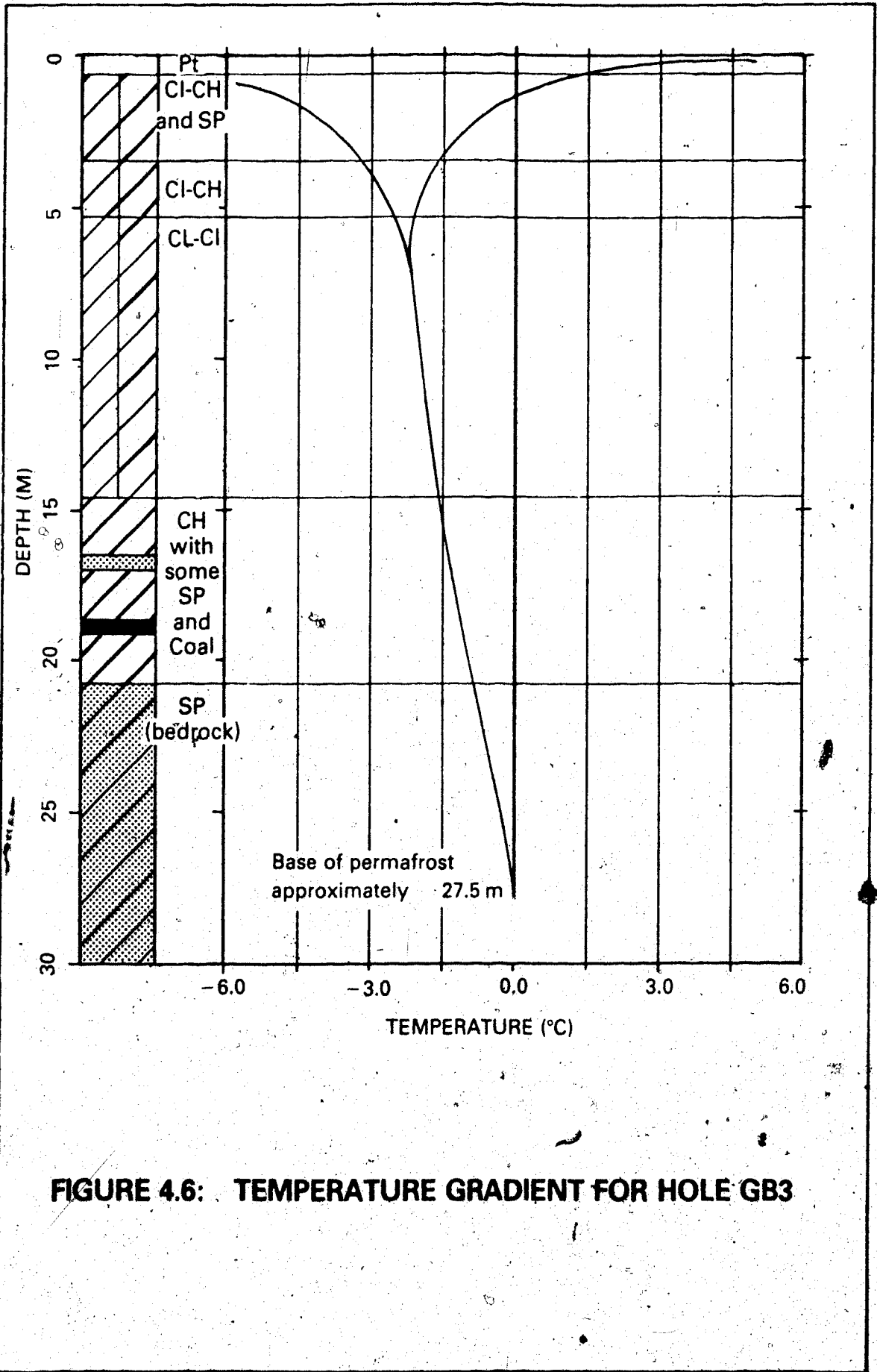


**FIGURE 4.6: TEMPERATURE GRADIENT FOR HOLE GB3**

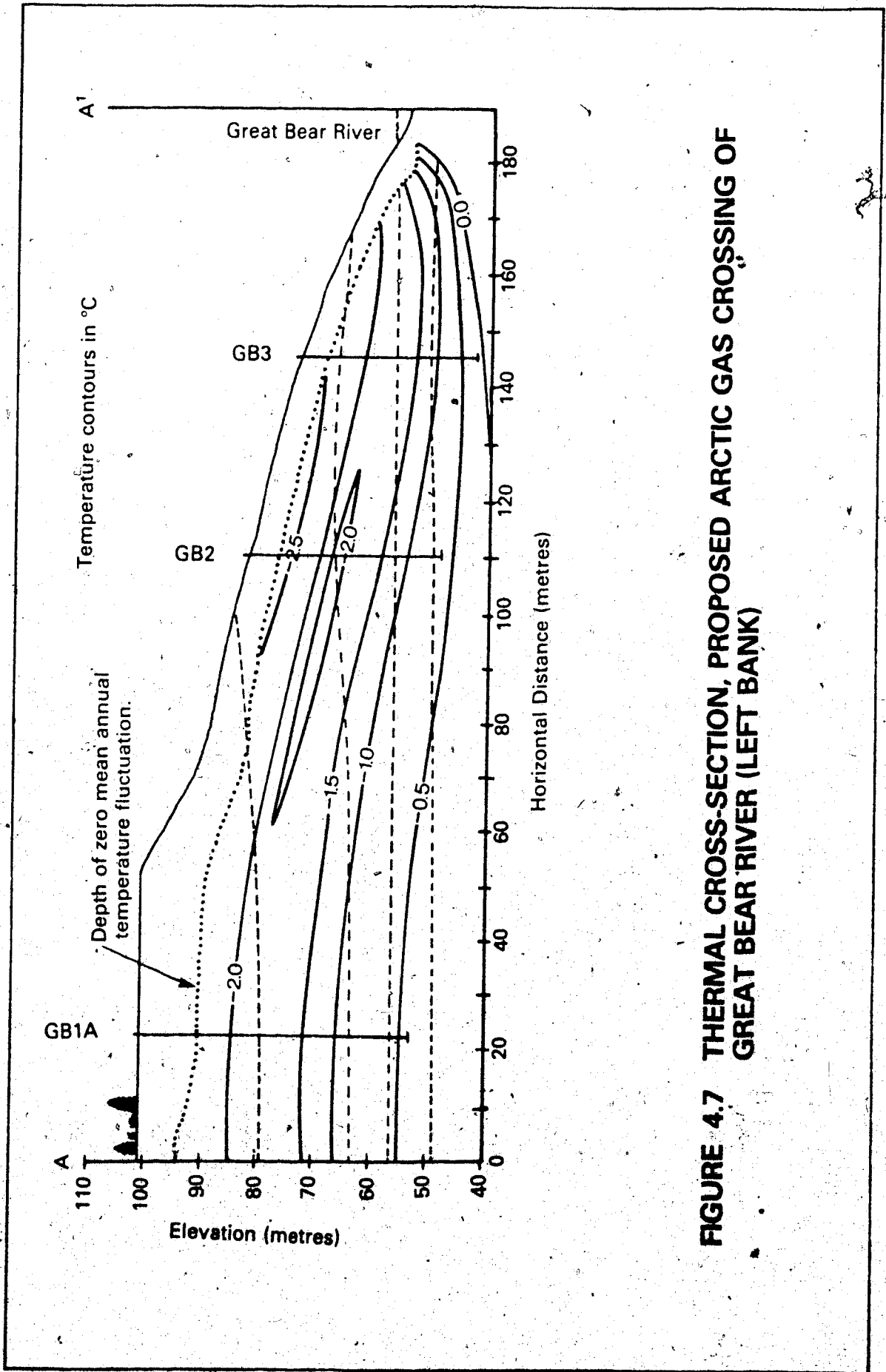


**FIGURE 4.7 THERMAL CROSS-SECTION, PROPOSED ARCTIC GAS CROSSING OF GREAT BEAR RIVER (LEFT BANK)**

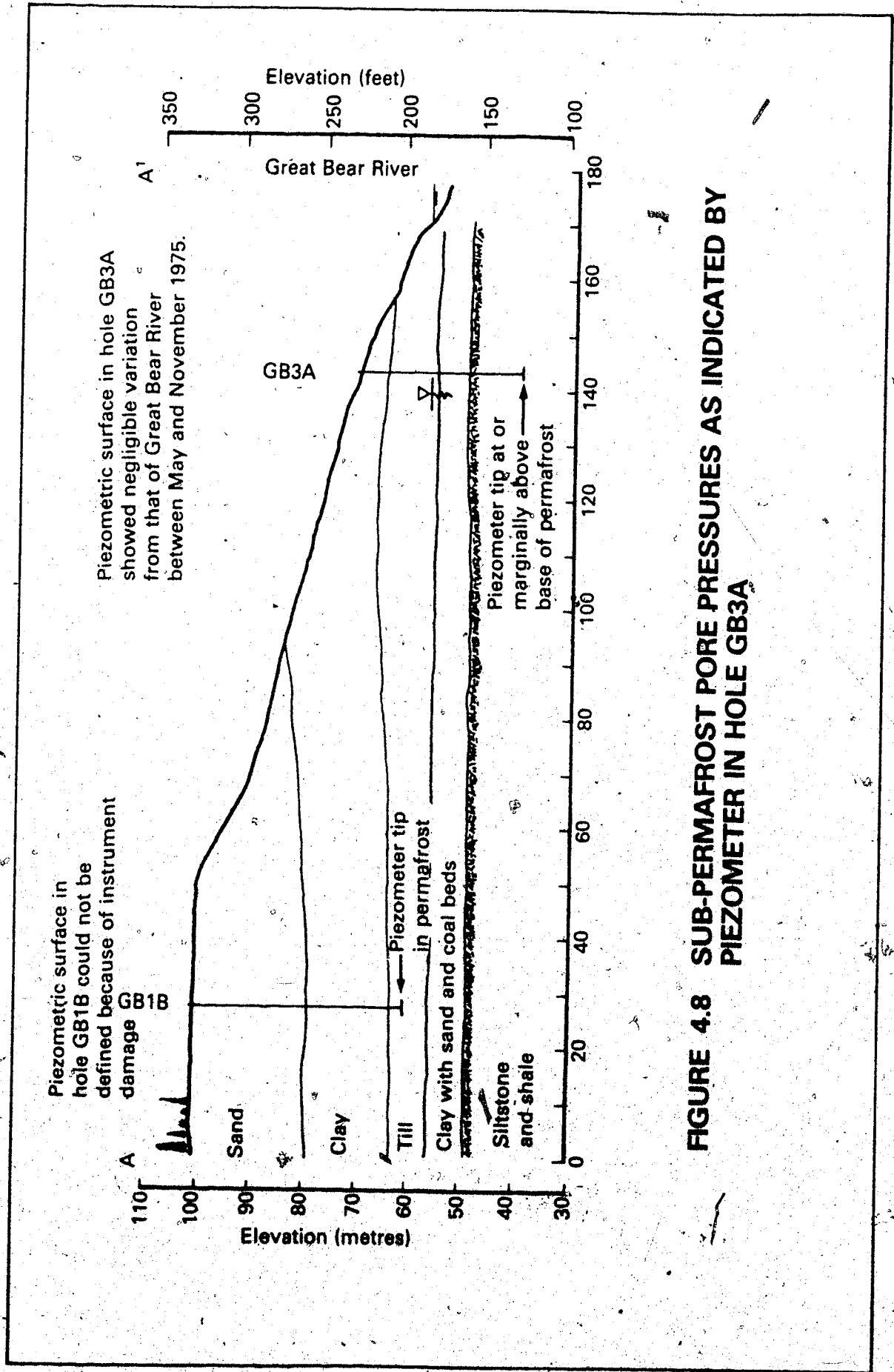
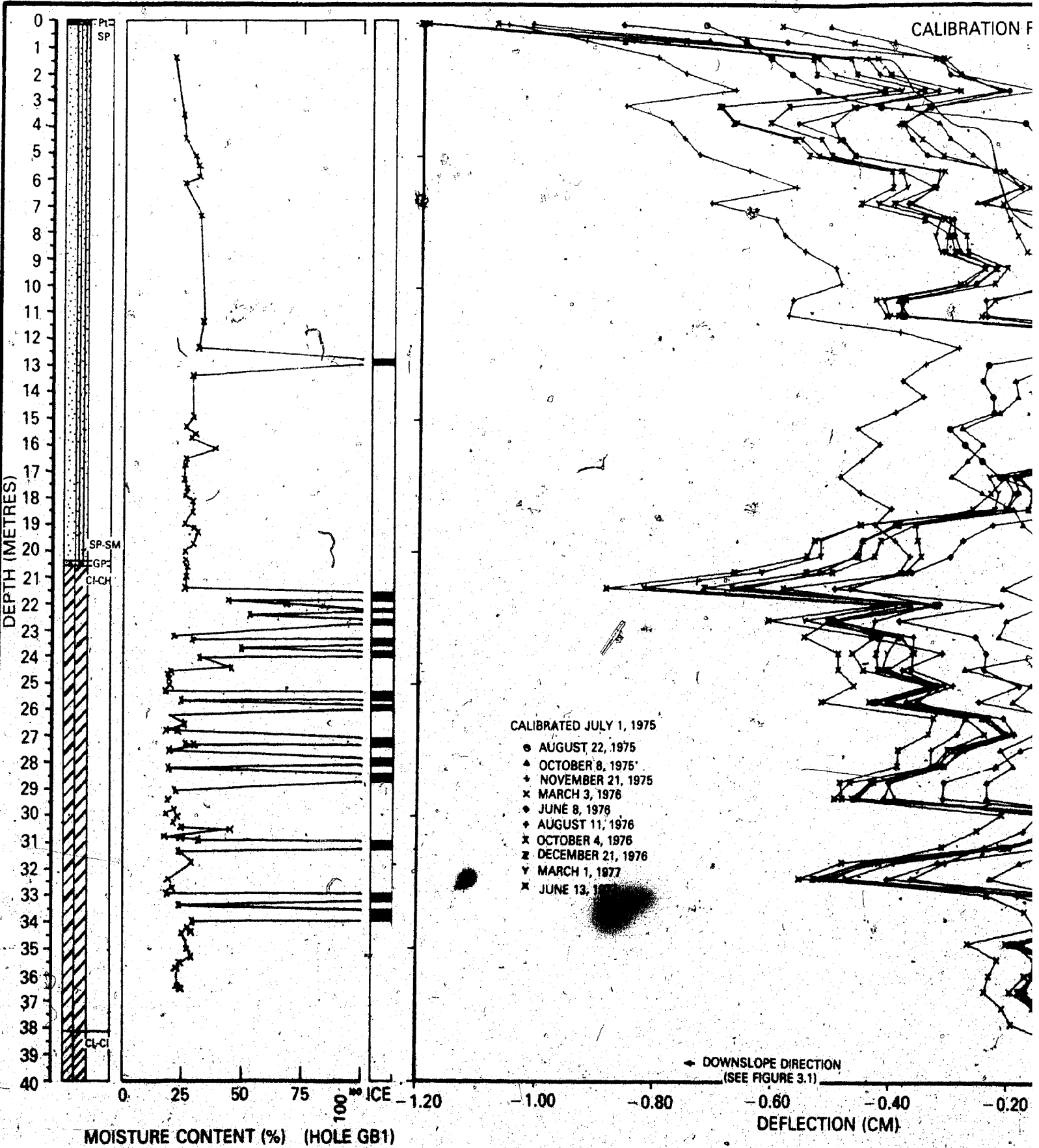
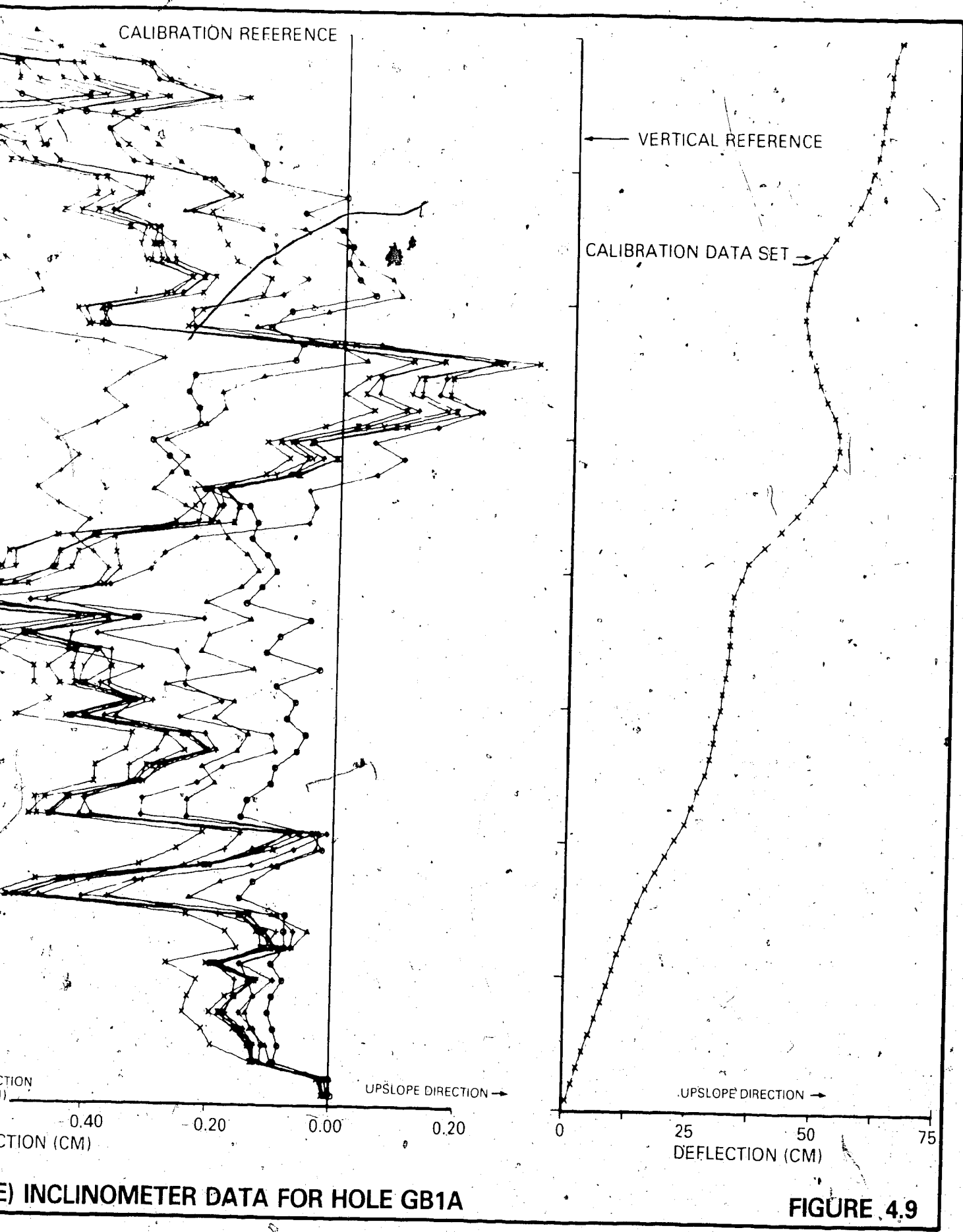


**FIGURE 4.8 SUB-PERMAFROST PORE PRESSURES AS INDICATED BY PIEZOMETER IN HOLE GB3A**



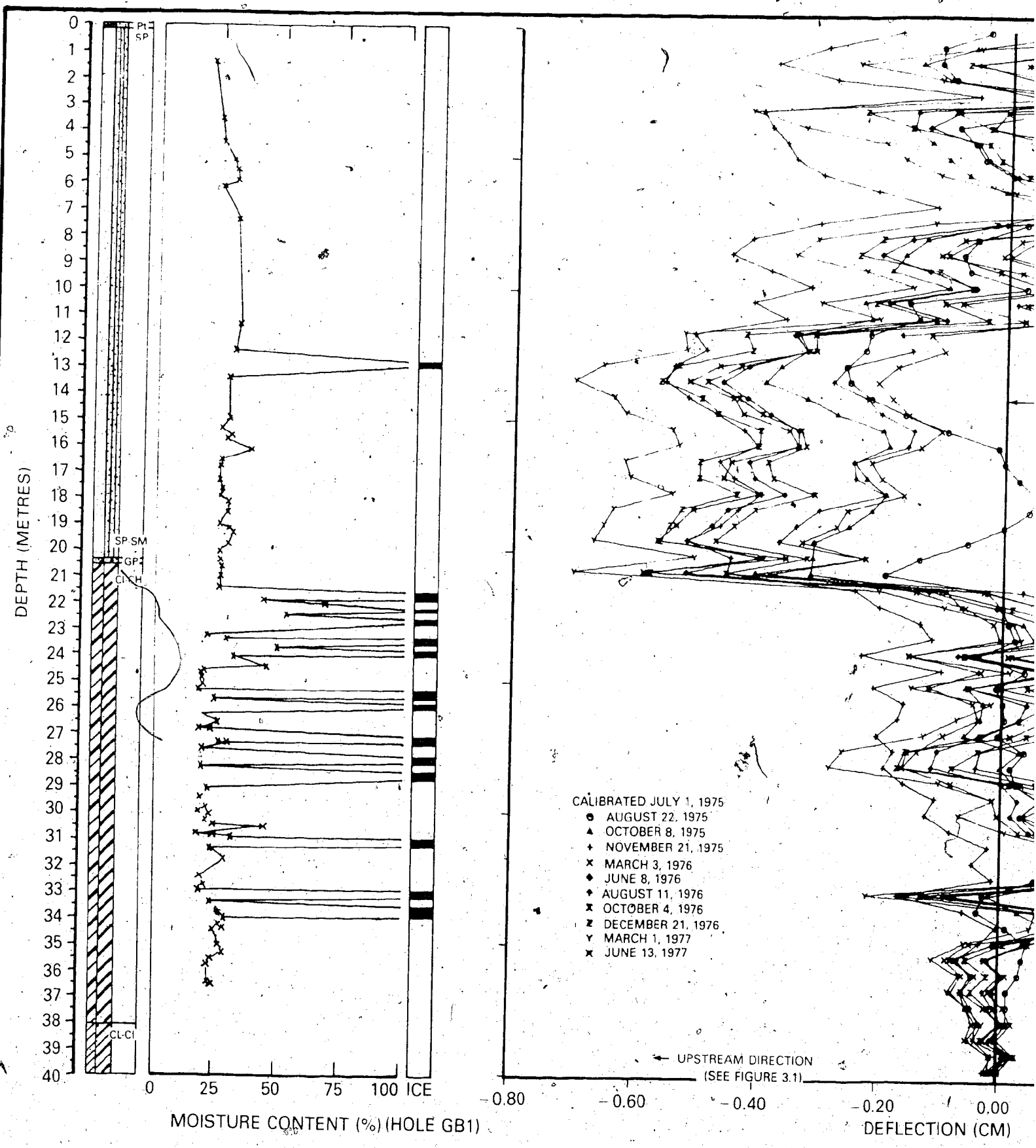
**A-DIRECTION (PARALLEL-TO-SLOPE) INCLINOMETER DATA**



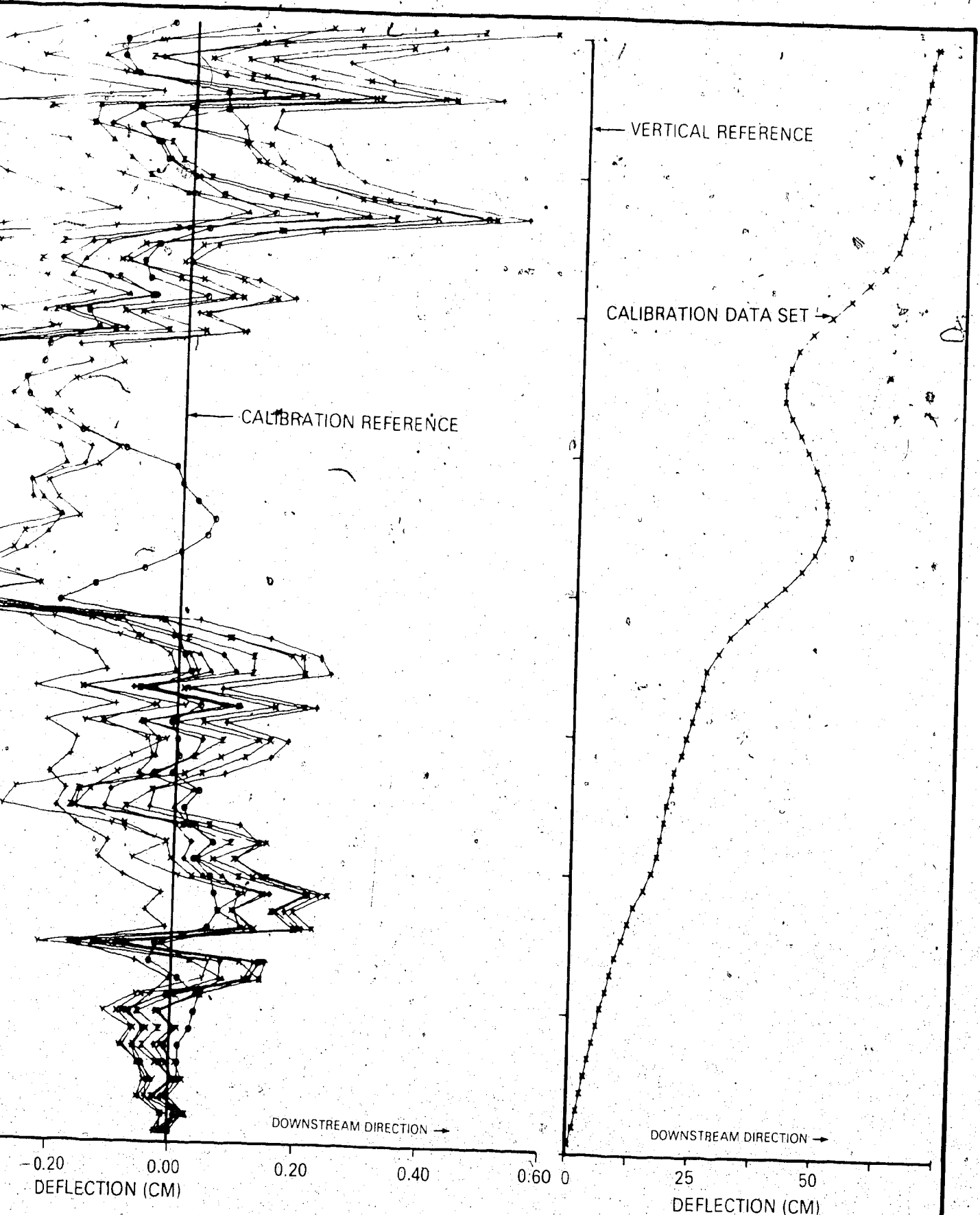


E) INCLINOMETER DATA FOR HOLE GB1A

FIGURE 4.9

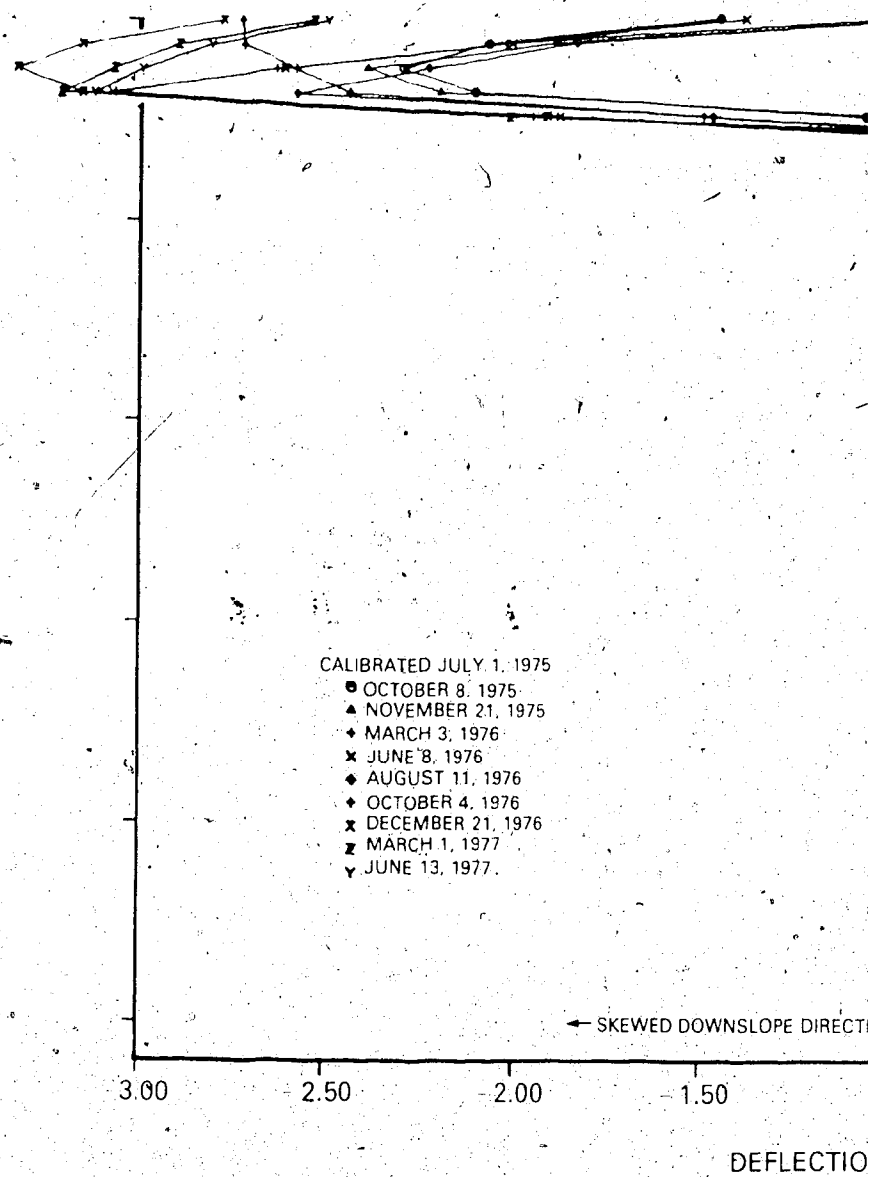
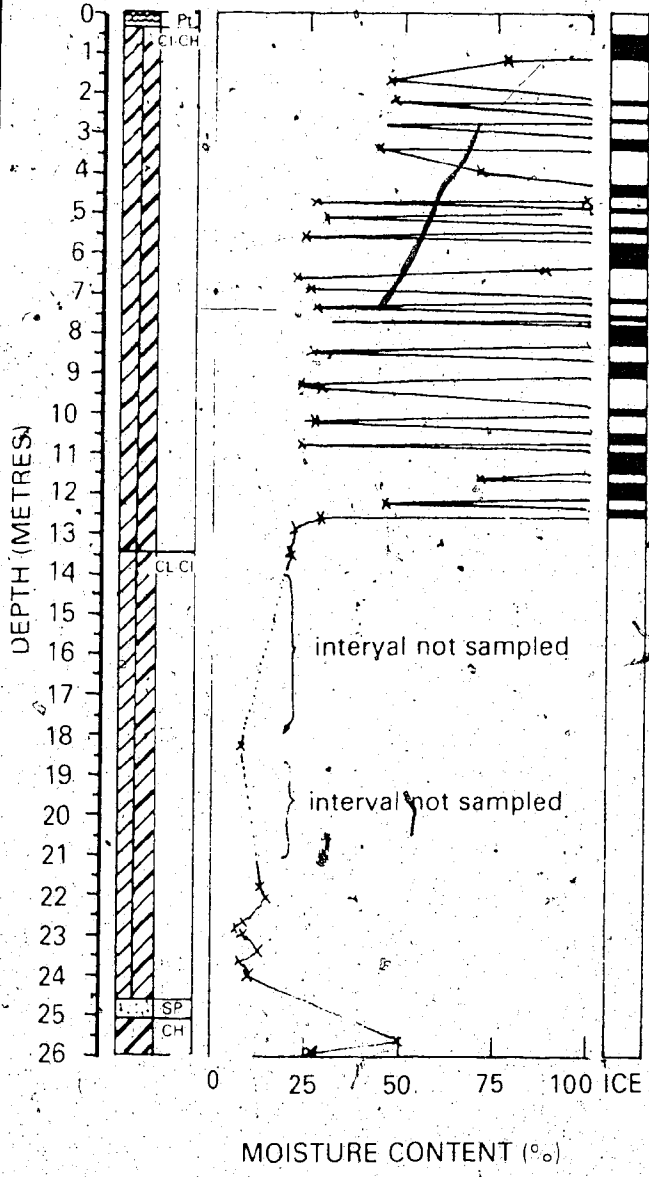


**B-DIRECTION (TRANSVERSE-TO-SLOPE) INC**

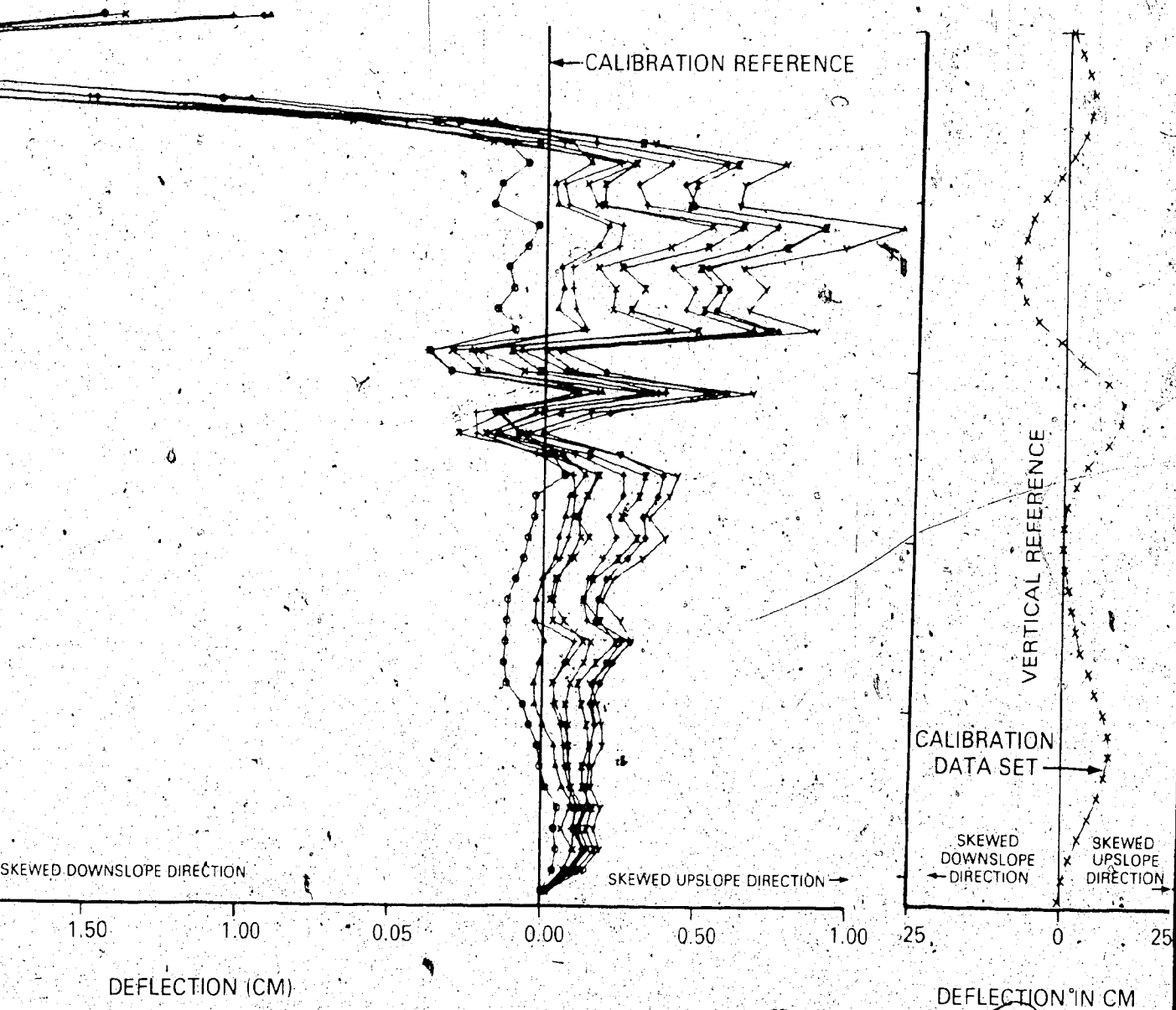


SE-TO-SLOPE) INCLINOMETER DATA FOR HOLE GB1A

FIGURE 4.10

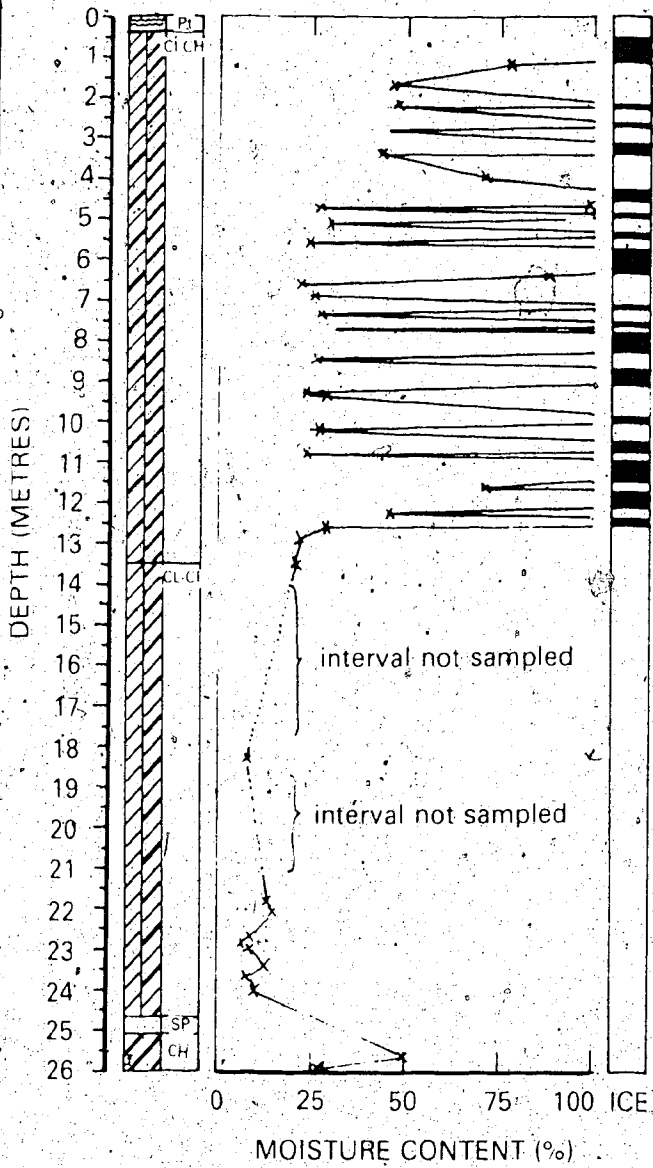


**A-DIRECTION INCLINOMETER DAT**

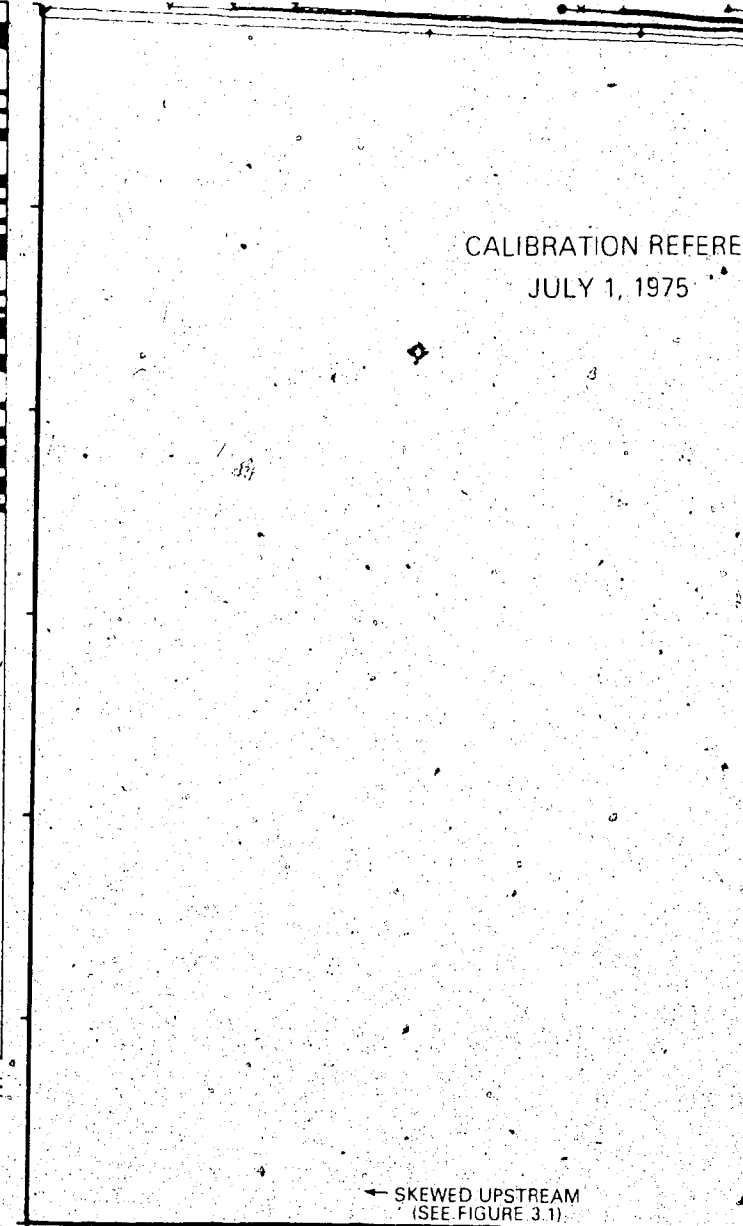


INOMETER DATA FOR HOLE GB2

FIGURE 4.11



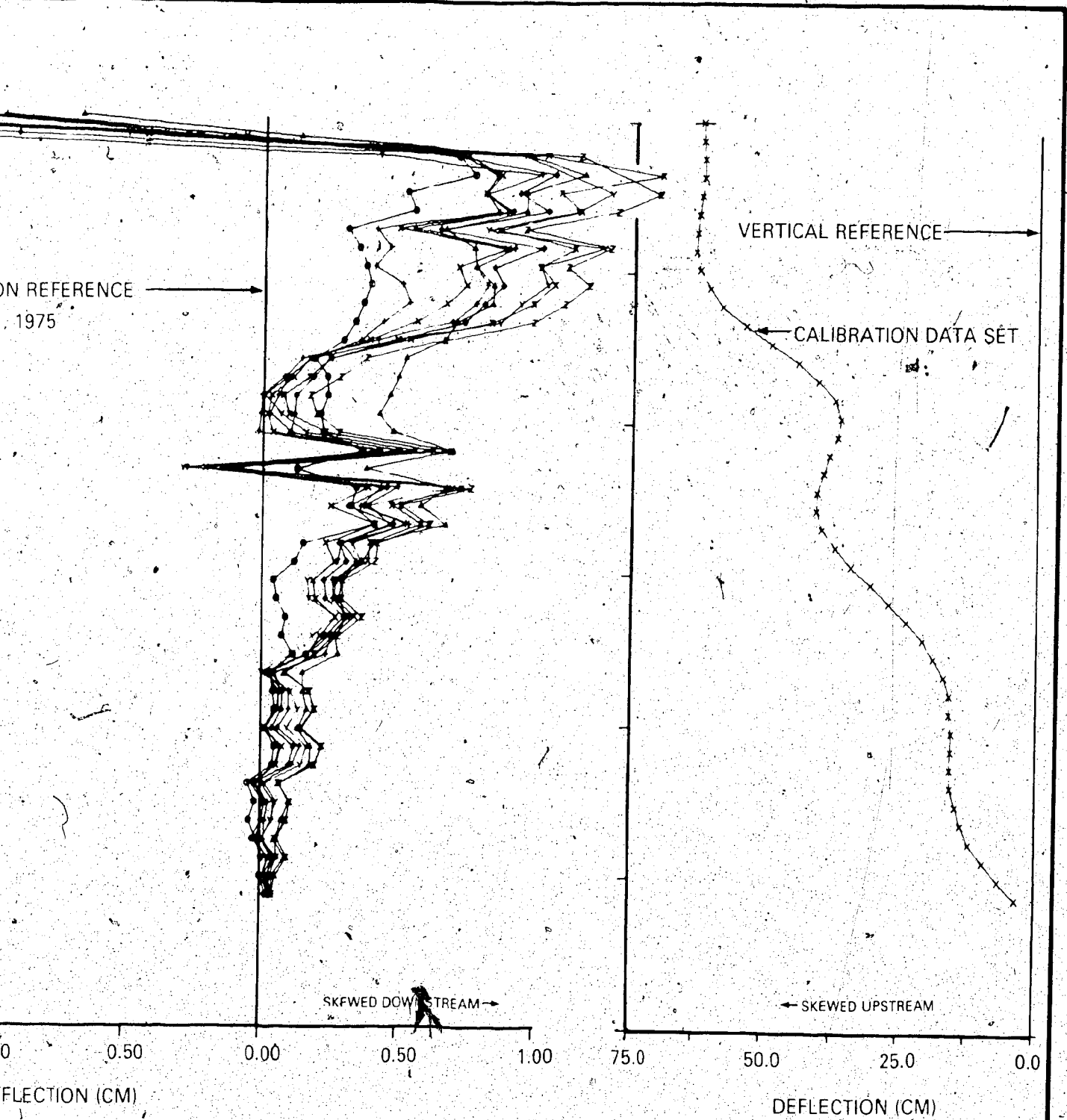
CALIBRATION REFERENCE  
 JULY 1, 1975



← SKEWED UPSTREAM  
 (SEE FIGURE 3.1)

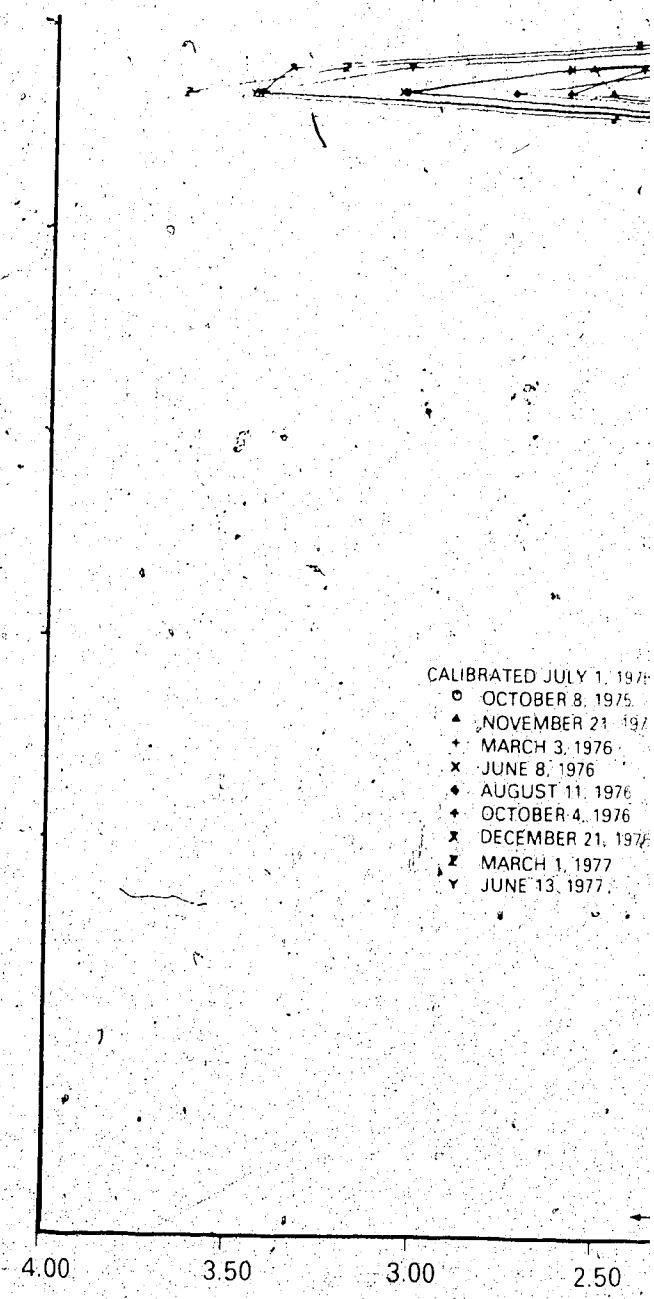
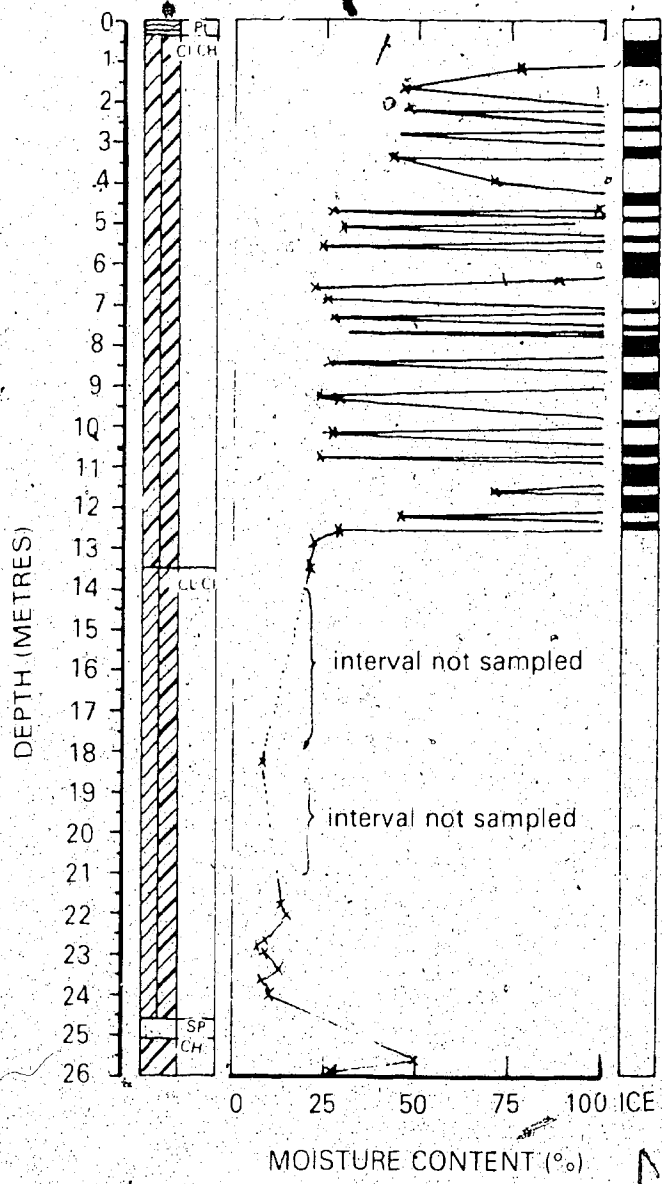
DEFLECTION

B-DIRECTION INCLINOMETER



INCLINOMETER DATA FOR HOLE GB2

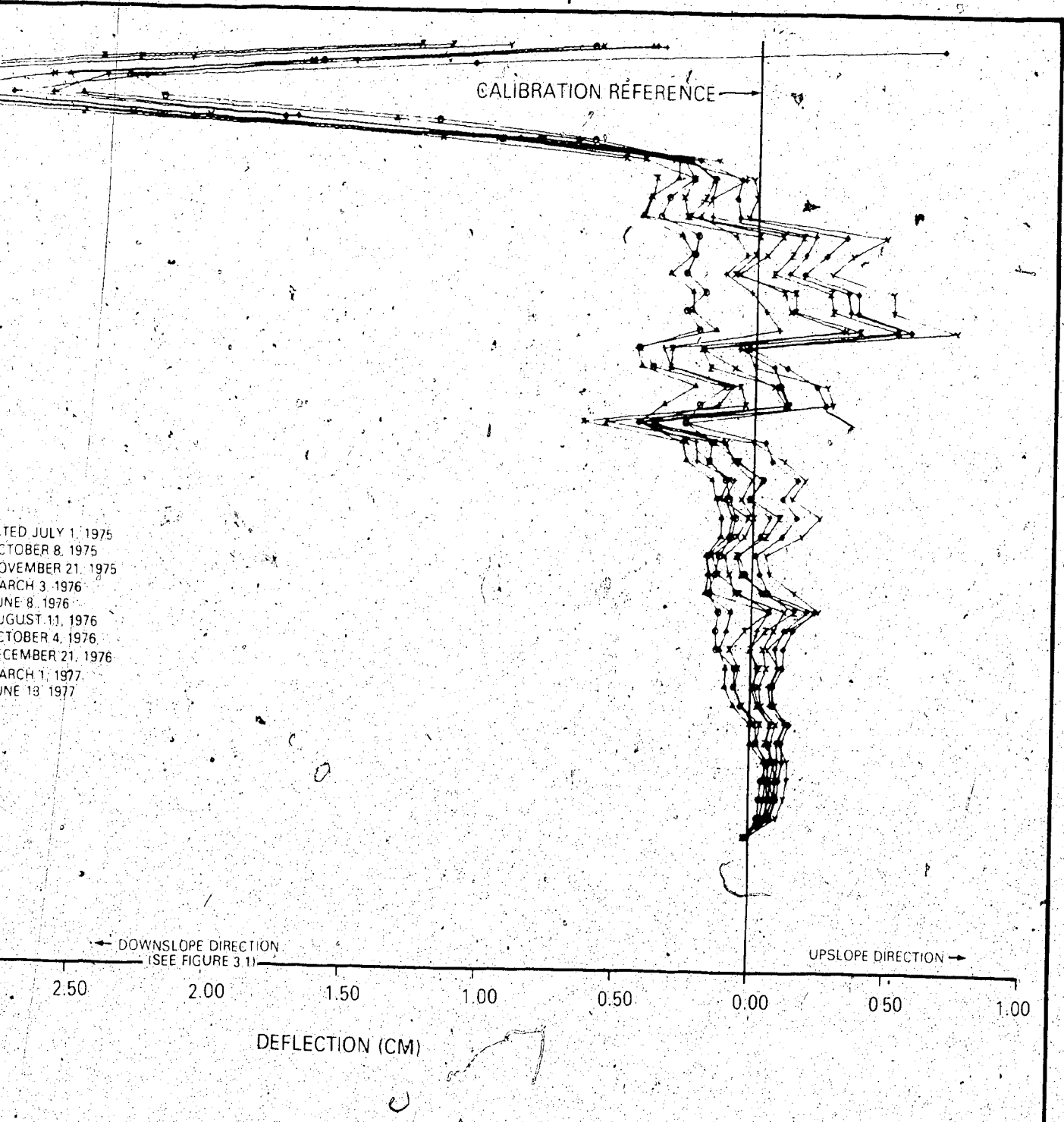
FIGURE 4.12



- CALIBRATED JULY 1, 1975
- OCTOBER 8, 1975
  - ▲ NOVEMBER 21, 1975
  - + MARCH 3, 1976
  - x JUNE 8, 1976
  - ◆ AUGUST 11, 1976
  - ⊕ OCTOBER 4, 1976
  - ⊗ DECEMBER 21, 1976
  - ⊠ MARCH 1, 1977
  - ▼ JUNE 13, 1977

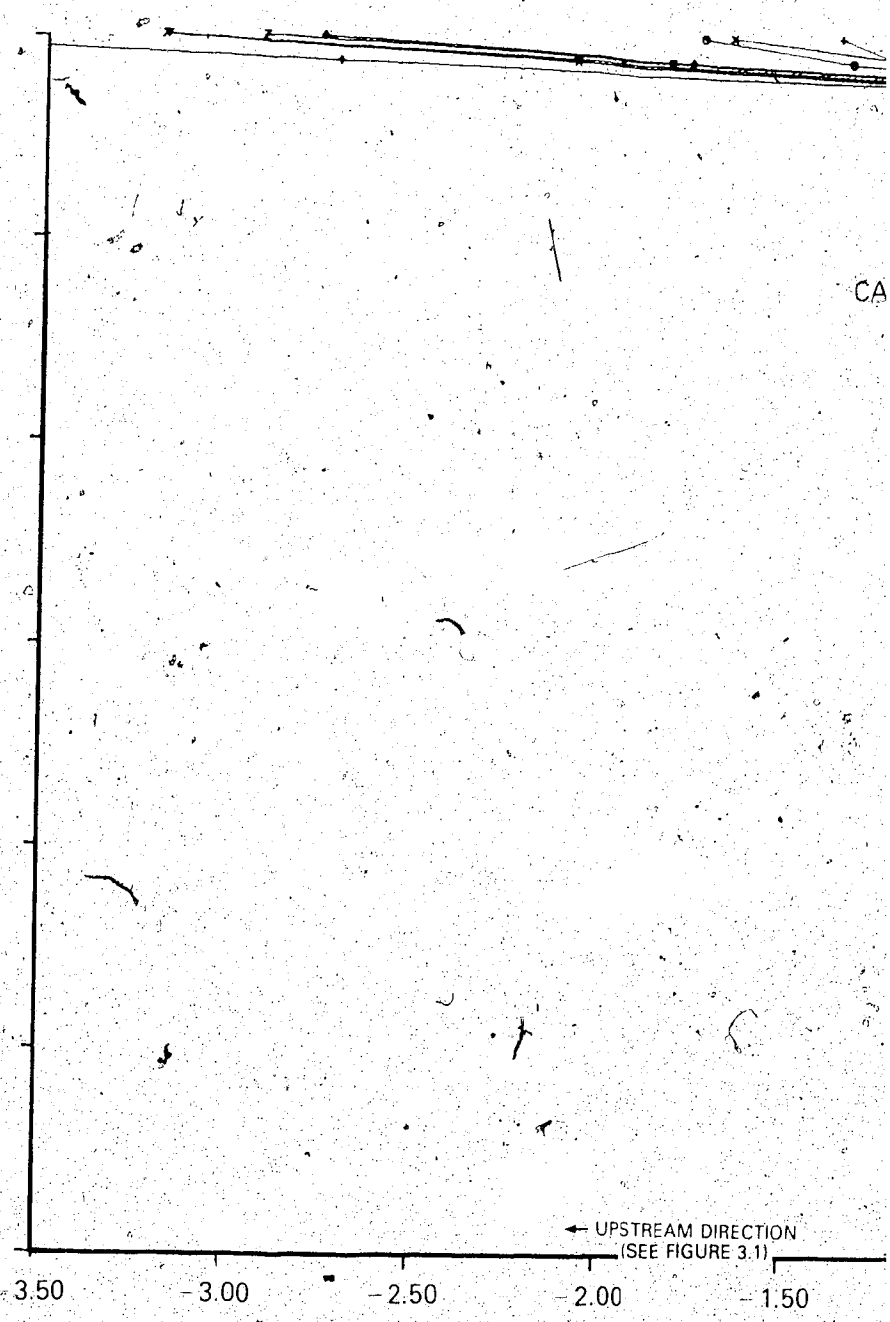
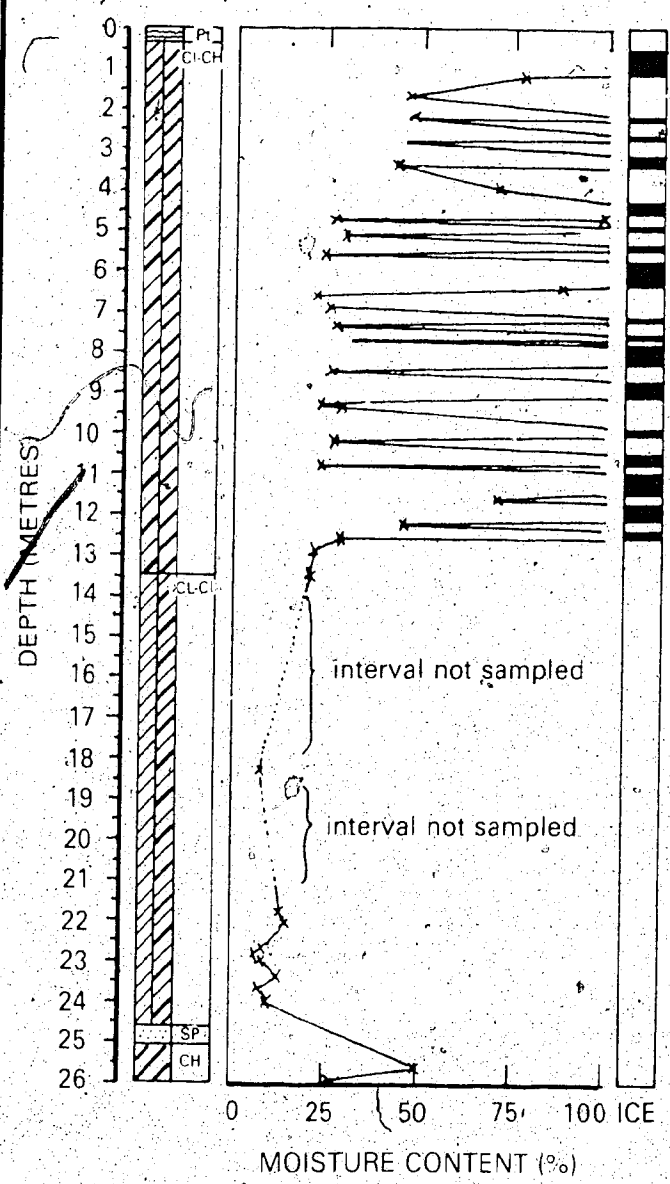
INCLINOMETER DATA FOR HOLE GB2 RESOLVE



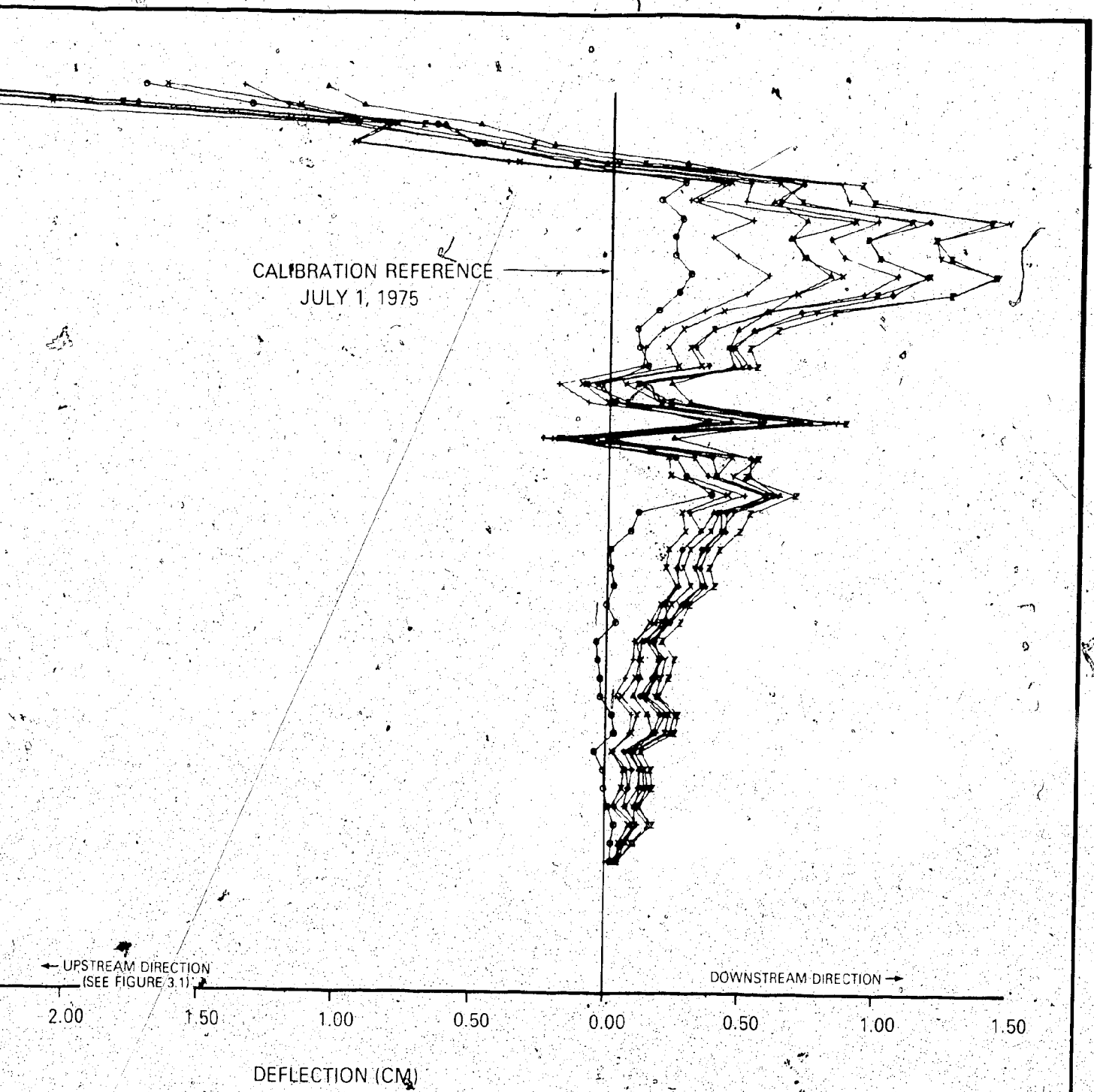


RESOLVED INTO TRUE PARALLEL-TO-SLOPE DIRECTION

FIGURE 4.13

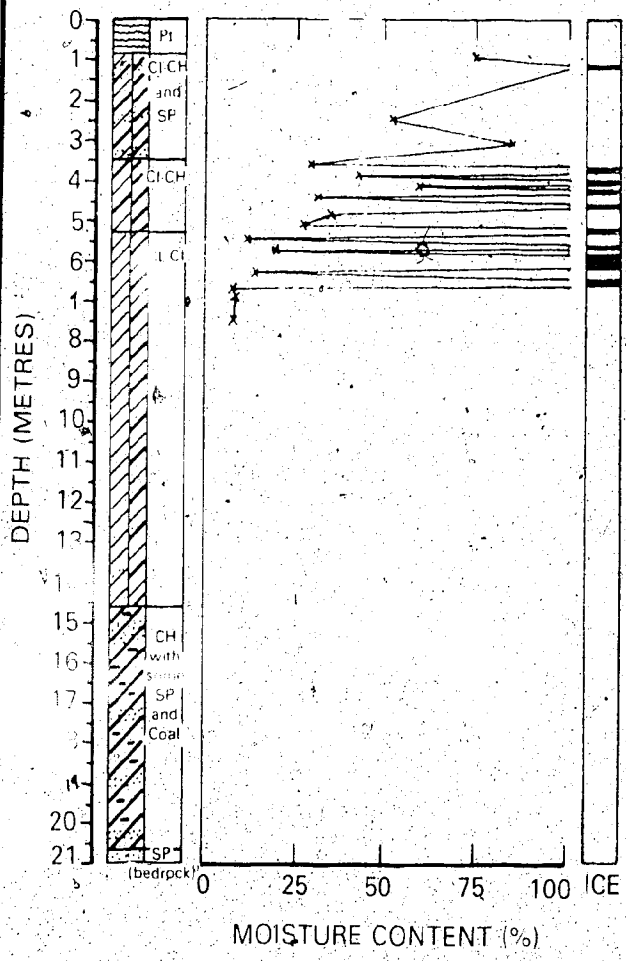


INCLINOMETER DATA FOR HOLE GB2 RESOLVED INTO TRUE TRA

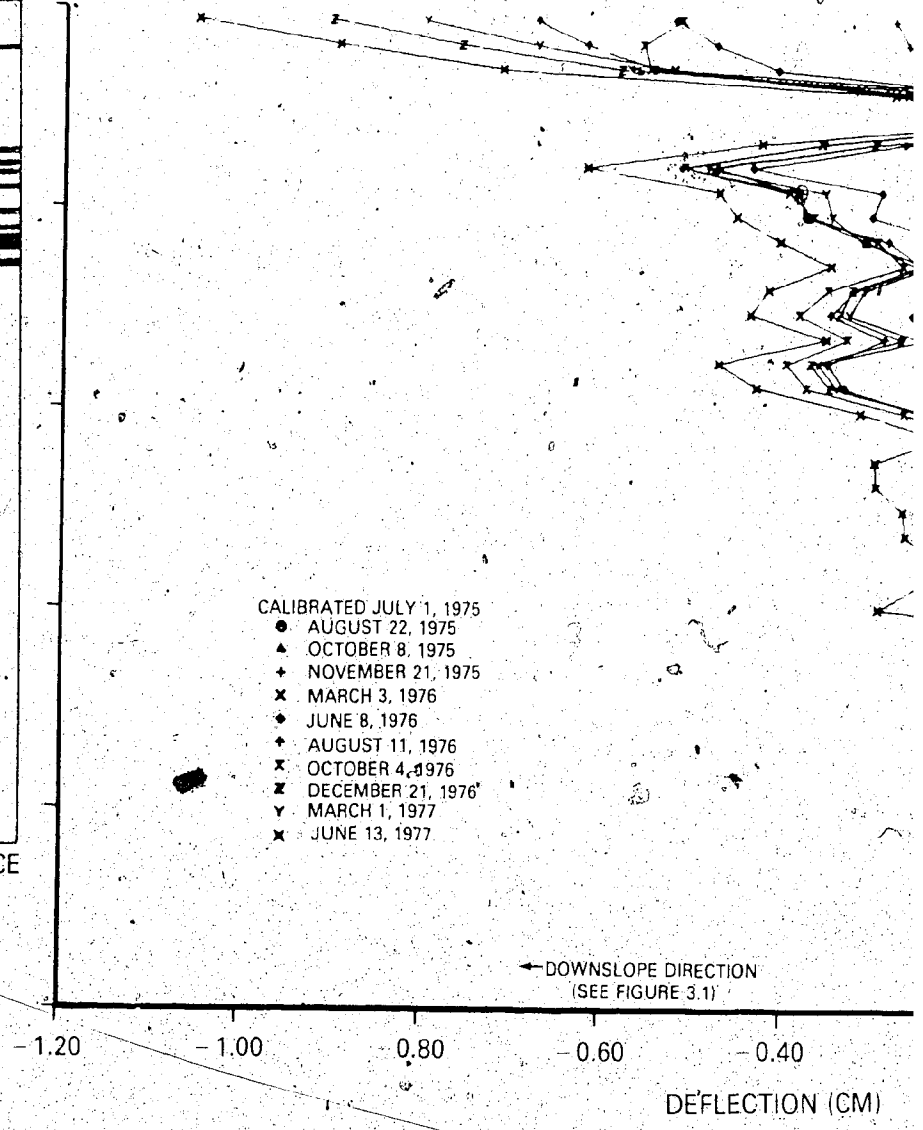


LVLED INTO TRUE TRANSVERSE-TO-SLOPE DIRECTION

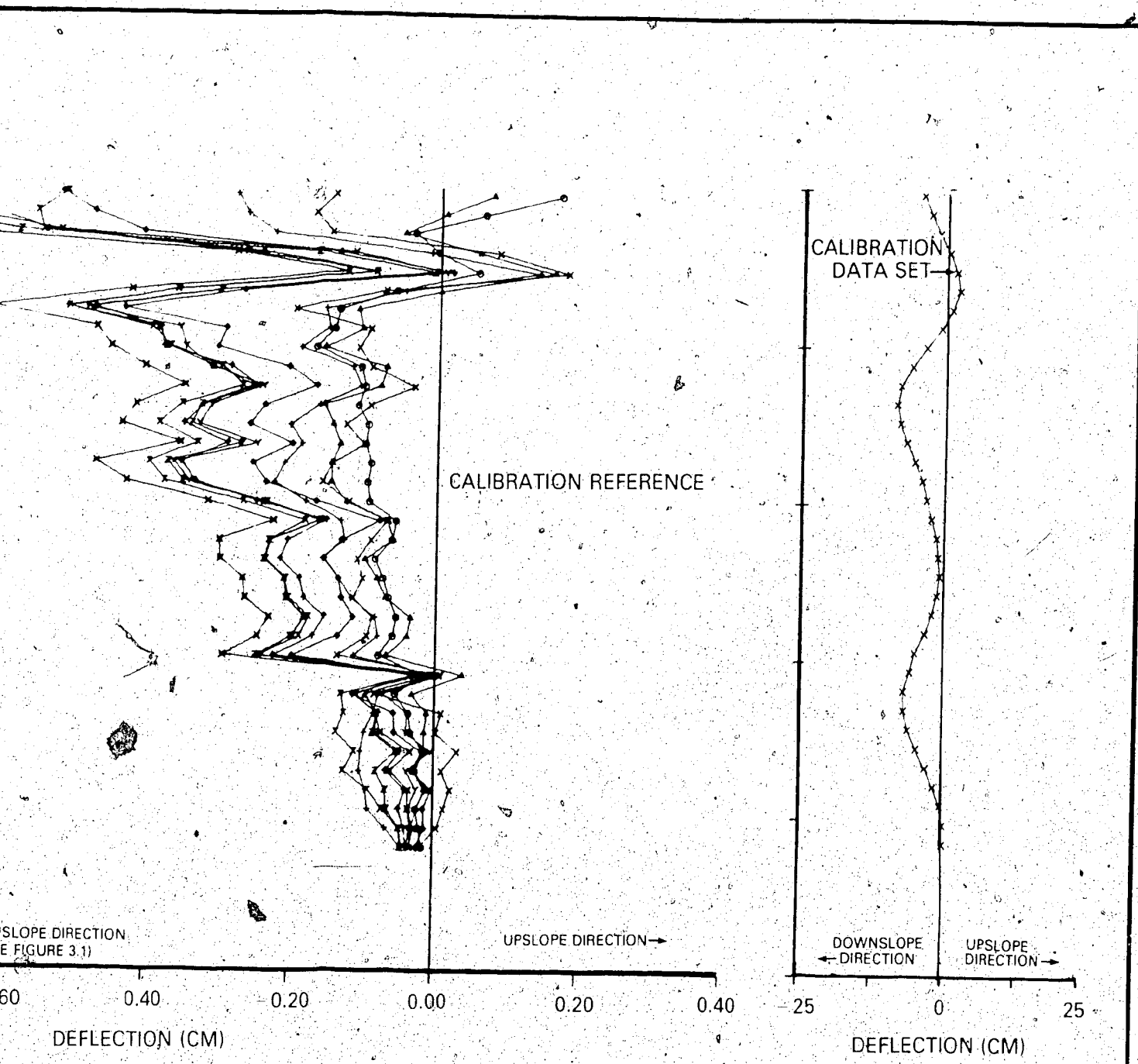
FIGURE 4.14



- CALIBRATED JULY 1, 1975
- AUGUST 22, 1975
  - ▲ OCTOBER 8, 1975
  - + NOVEMBER 21, 1975
  - x MARCH 3, 1976
  - ◆ JUNE 8, 1976
  - † AUGUST 11, 1976
  - x OCTOBER 4, 1976
  - z DECEMBER 21, 1976
  - y MARCH 1, 1977
  - x JUNE 13, 1977



**A-DIRECTION (PARALLEL-TO-SLOPE) INCLINOMETER**



SLOPE DIRECTION  
E FIGURE 3.1)

CALIBRATION REFERENCE

CALIBRATION  
DATA SET

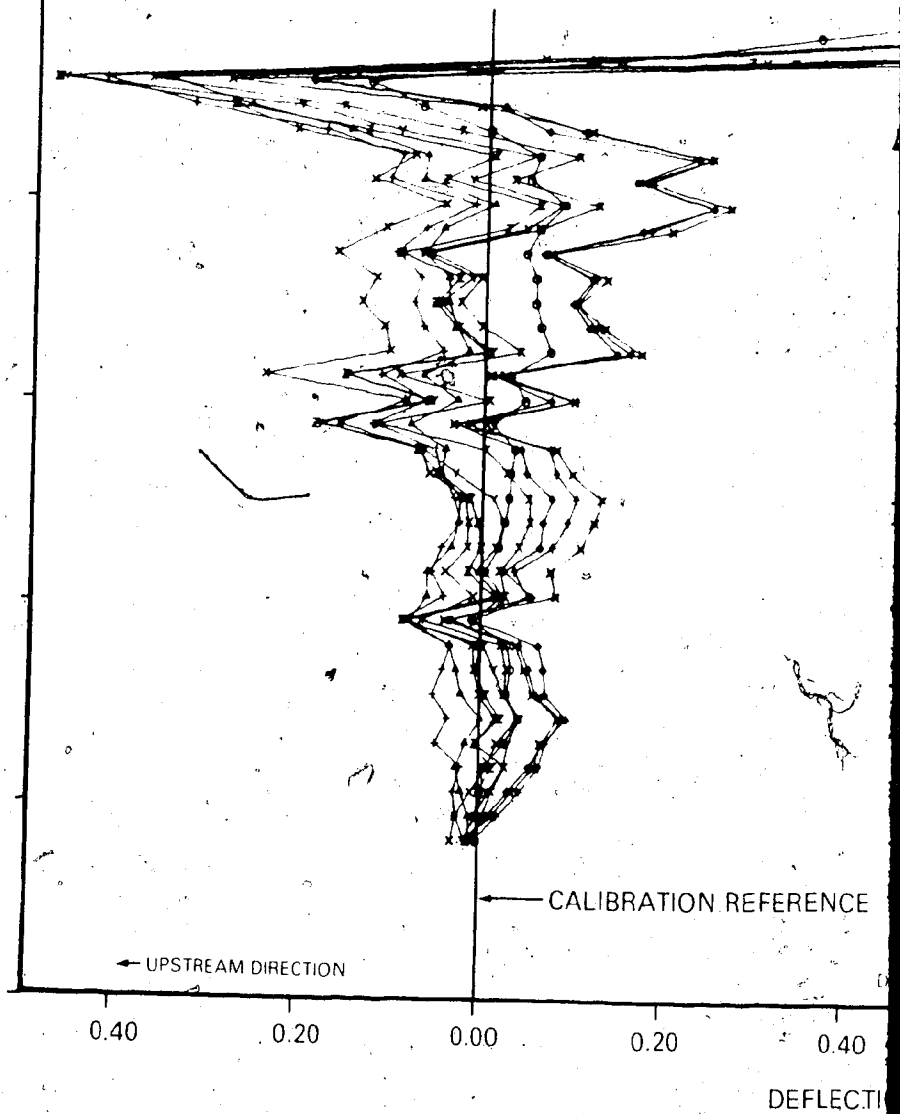
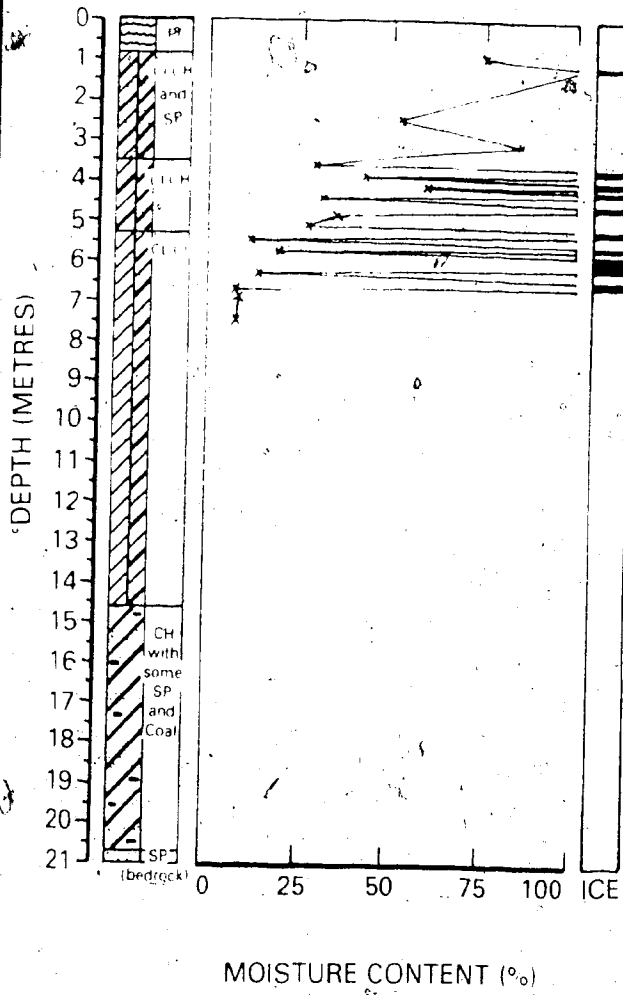
UPSLOPE DIRECTION →

DOWNSLOPE  
DIRECTION ←

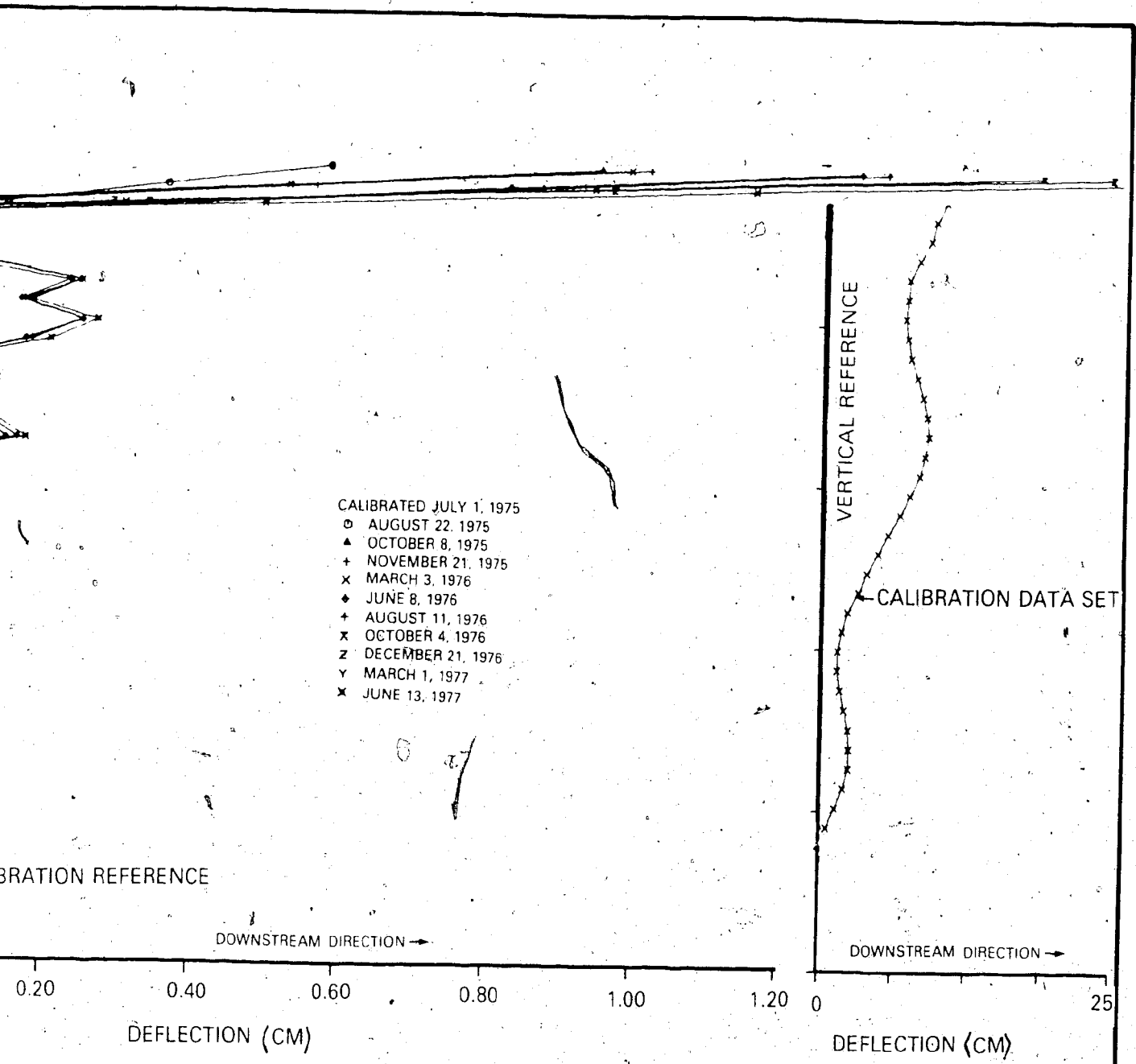
UPSLOPE  
DIRECTION →

D-SLOPE) INCLINOMETER DATA FOR HOLE GB3

FIGURE 4.15



B-DIRECTION (TRANSVERSE-TO-SLOPE) INCL



TO-SLOPE) INCLINOMETER DATA FOR HOLE GB3

FIGURE 4.16

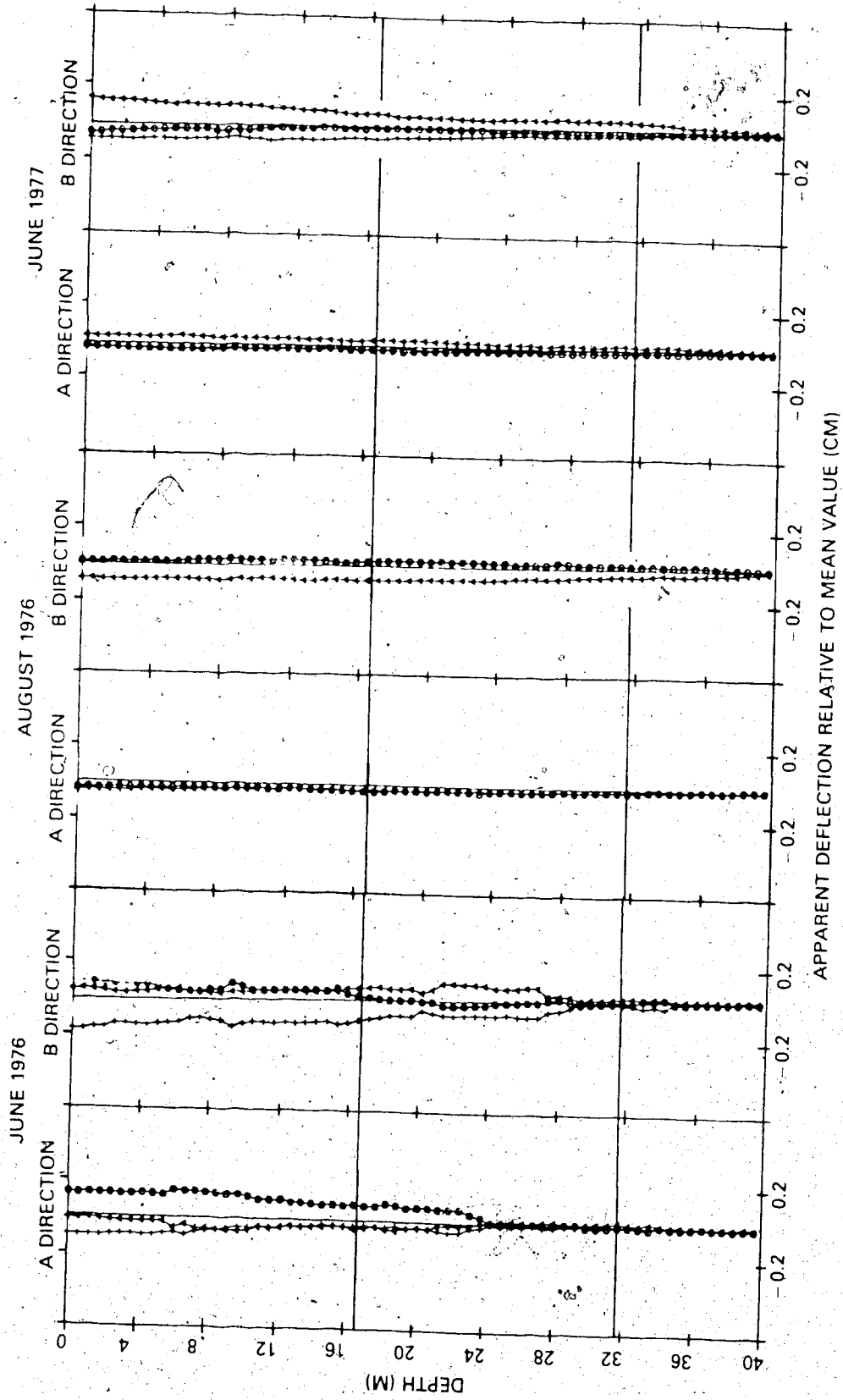
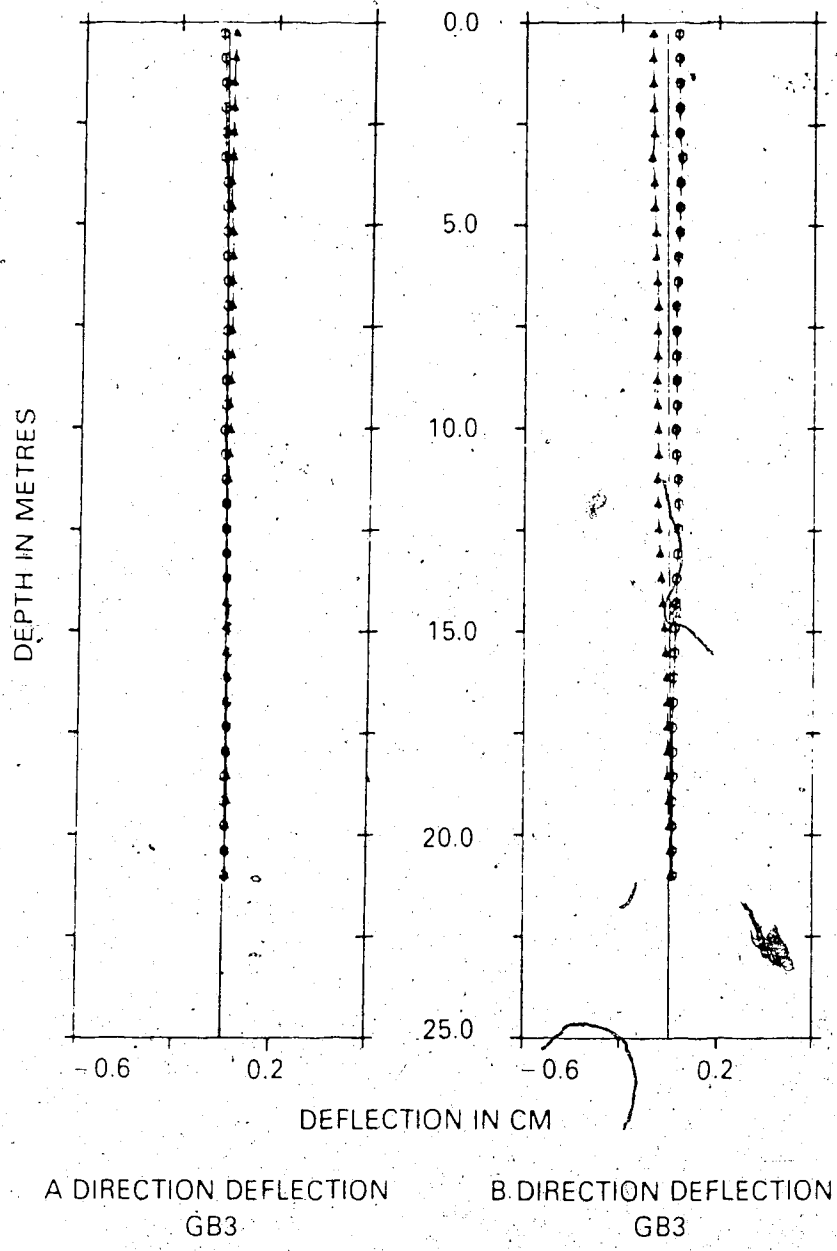


FIGURE 4.17 RESULTS OF REPEATABILITY TESTS IN HOLE GBIA





**FIGURE 4.18: RESULTS OF REPEATABILITY TESTS IN TEST HOLE GB3**

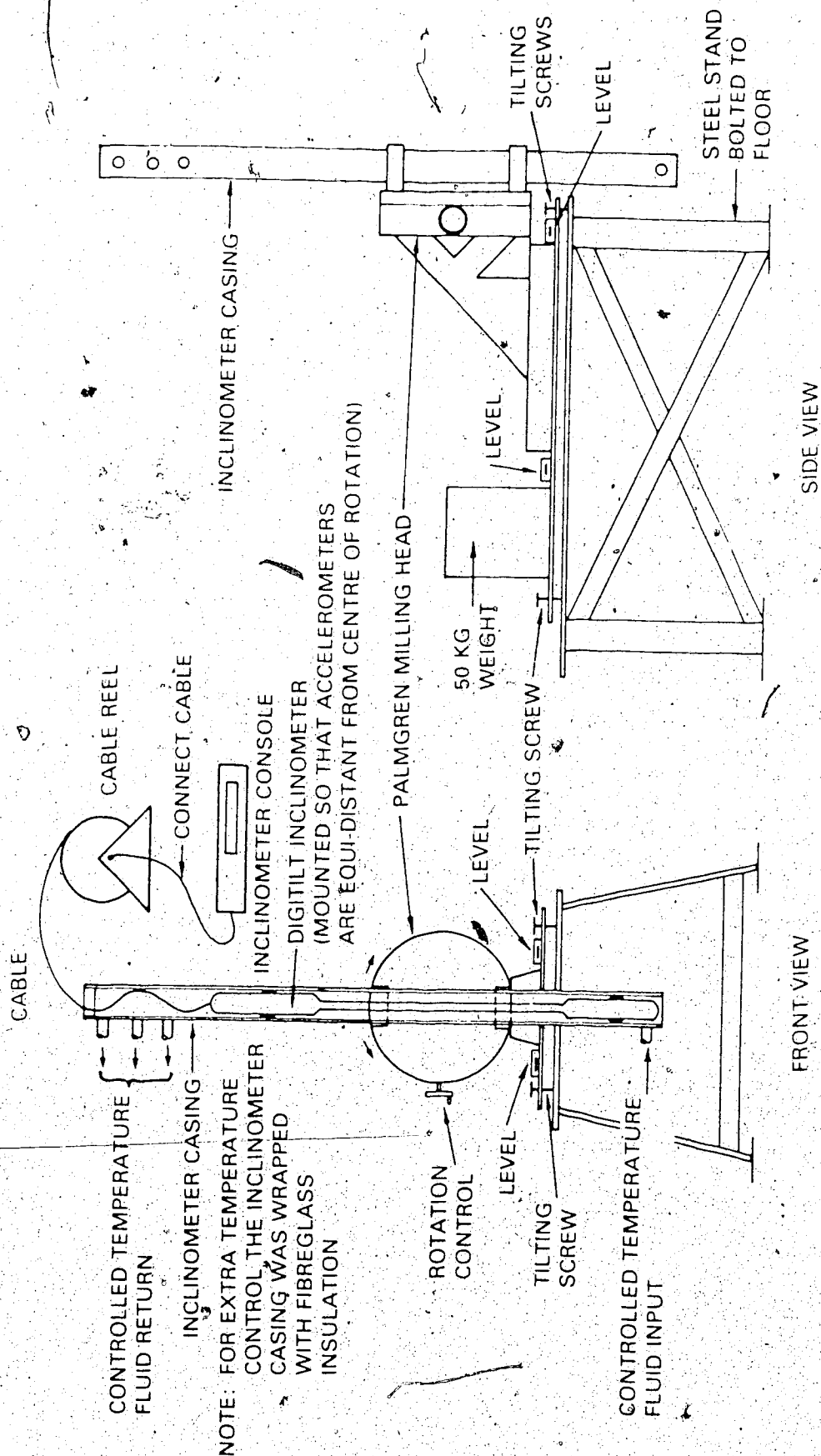


FIGURE 4.19 INCLINOMETER CALIBRATION FRAME

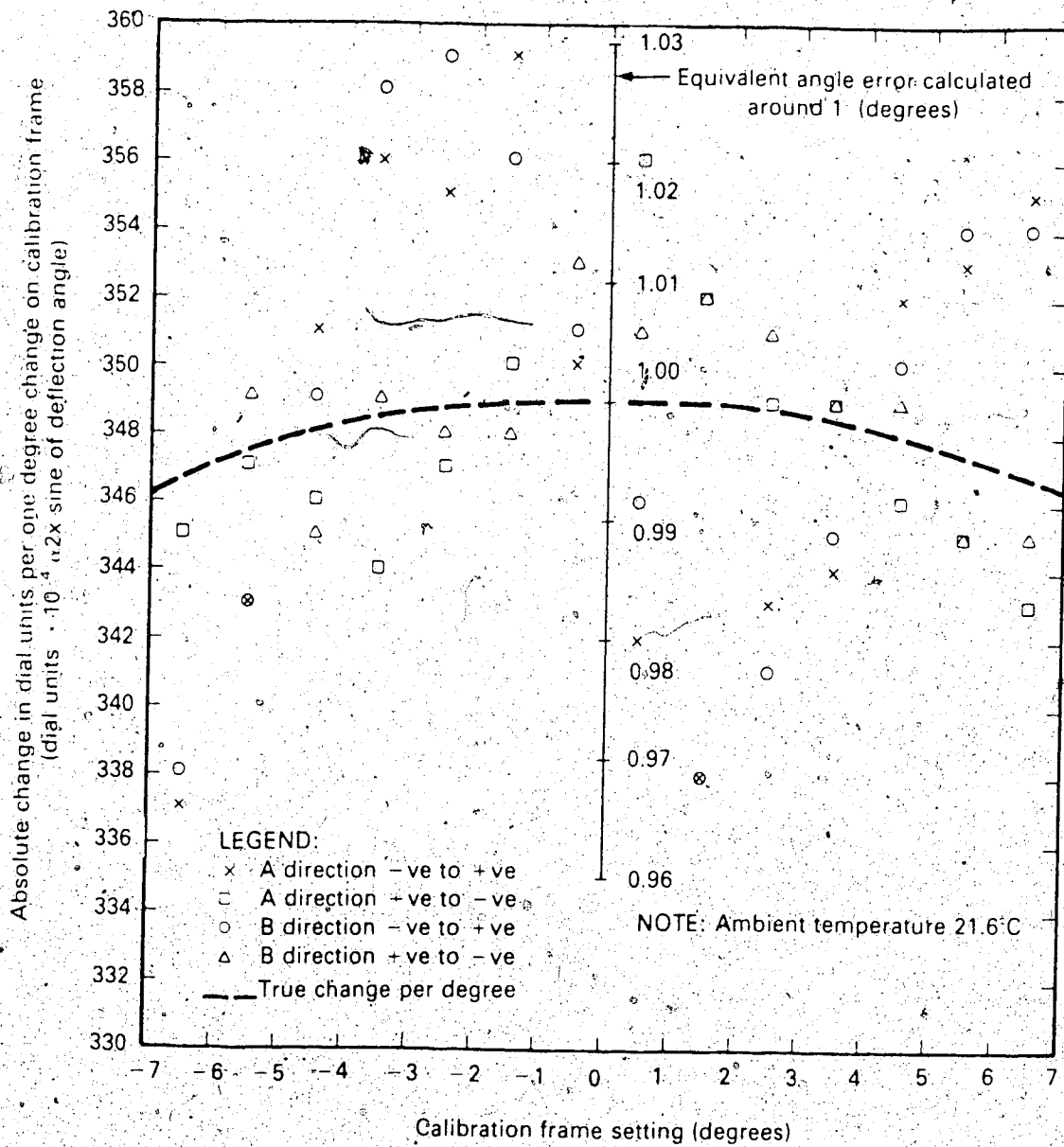
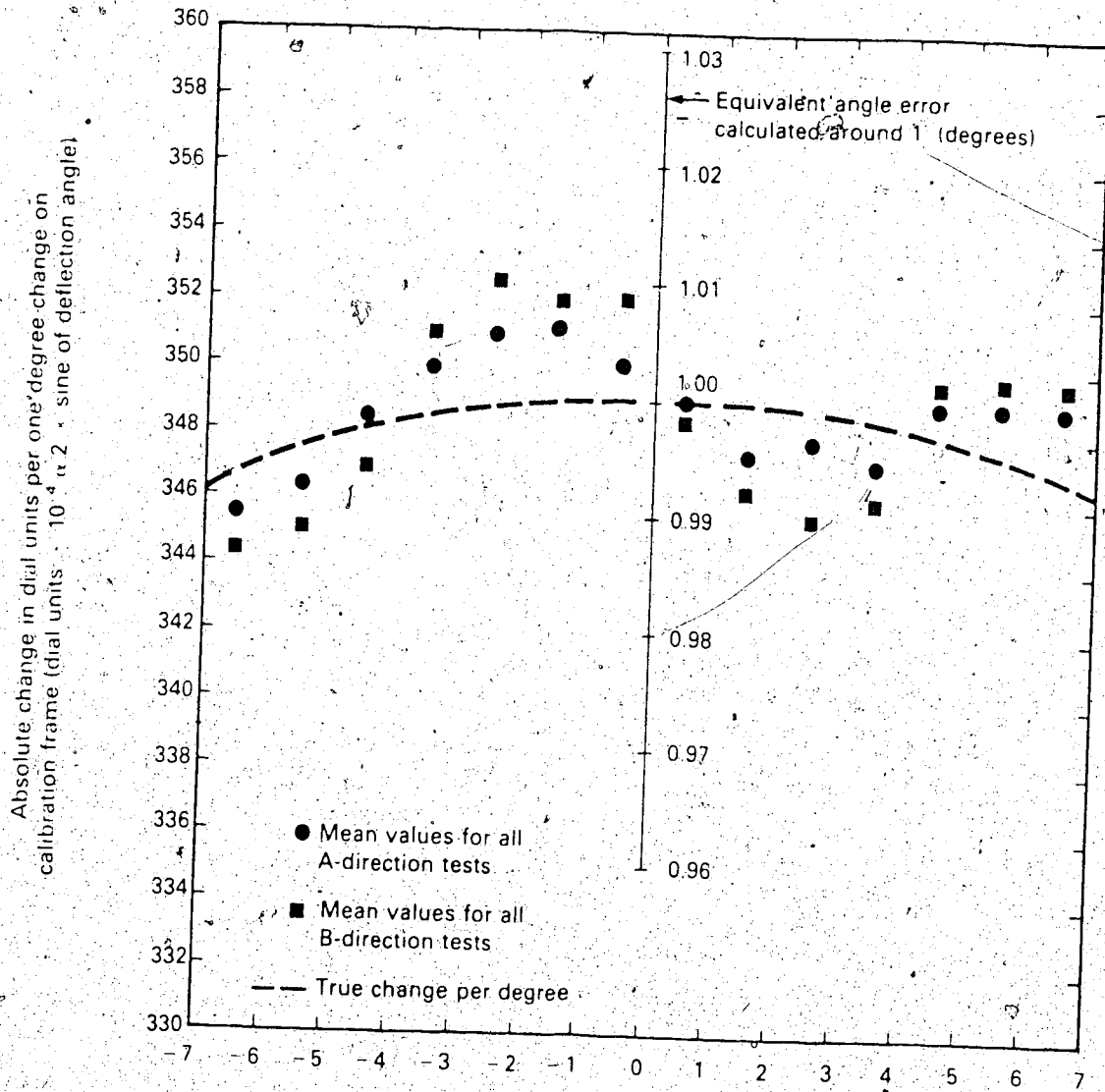


FIGURE 4.20 RESOLUTION TEST RESULTS — TEST RE04



NOTE: AMBIENT ROOM TEMPERATURE

FIGURE 4.21 RESOLUTION TEST RESULTS — MEAN VALUES FROM ALL TEST RESULTS

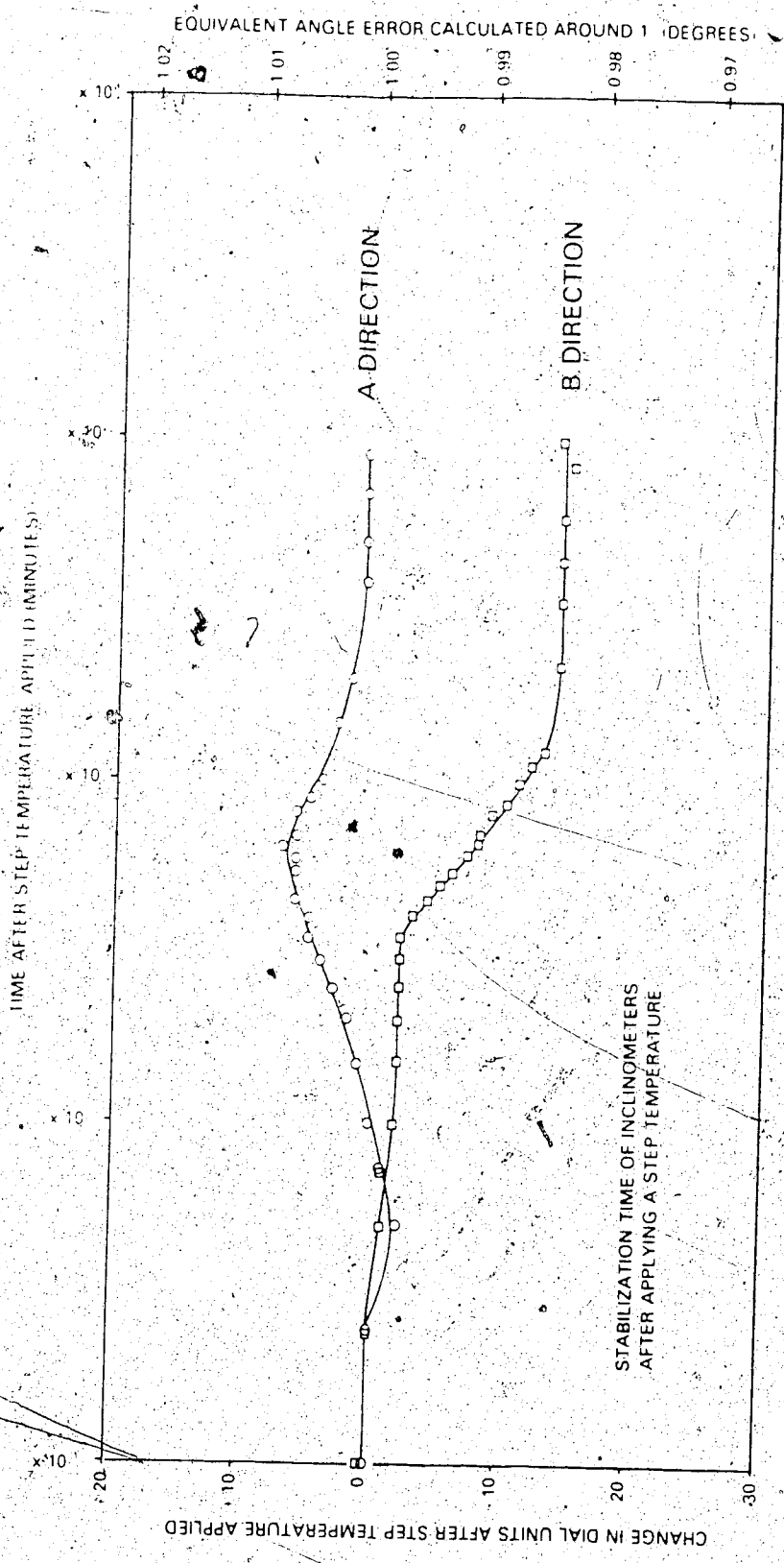
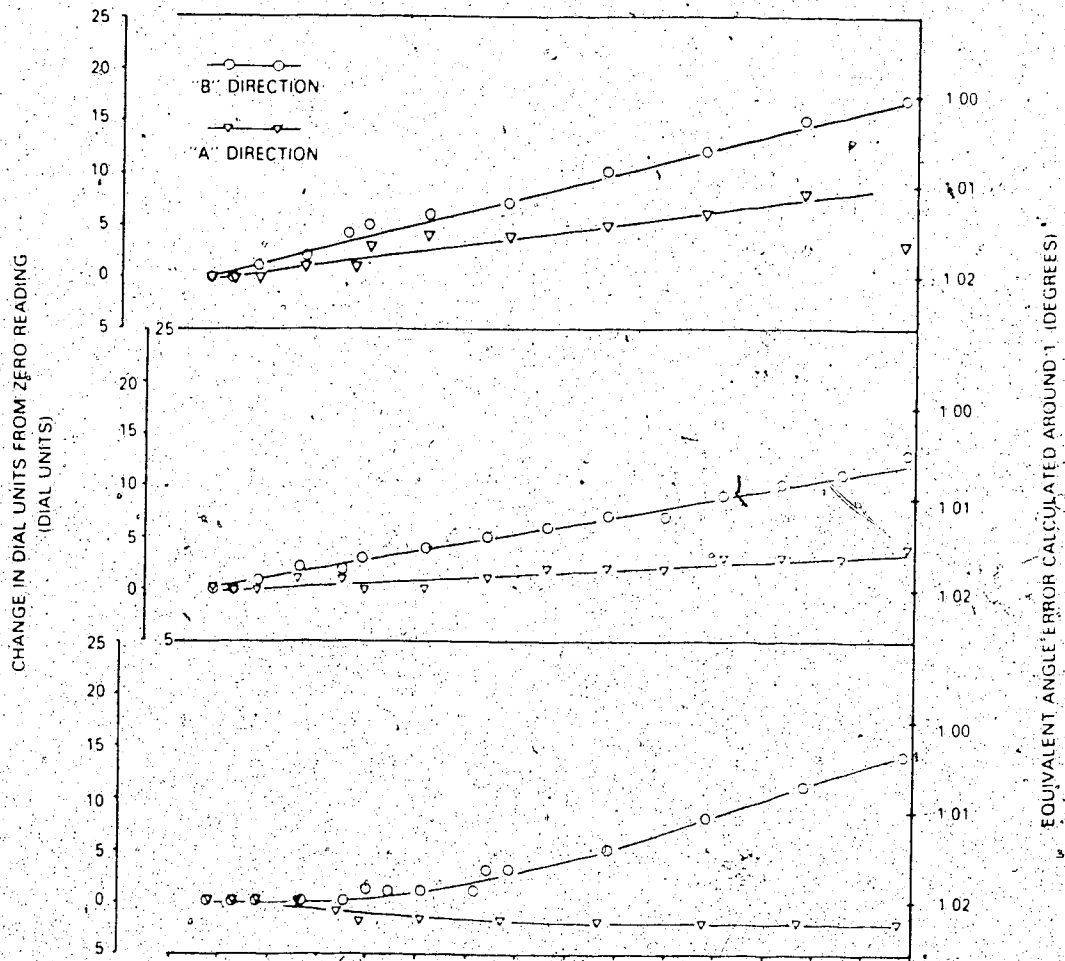


FIGURE 4.22 STABILIZATION OF INCLINOMETER READINGS IN RESPONSE TO A SUDDEN STEP TEMPERATURE



CHANGE IN DIAL READING AS A FUNCTION OF CHANGE IN TEMPERATURE — "A" & "B" DIRECTIONS — U OF A B336

FIGURE 4.23: TEMPERATURE DRIFT CHARACTERISTICS OF INCLINOMETER

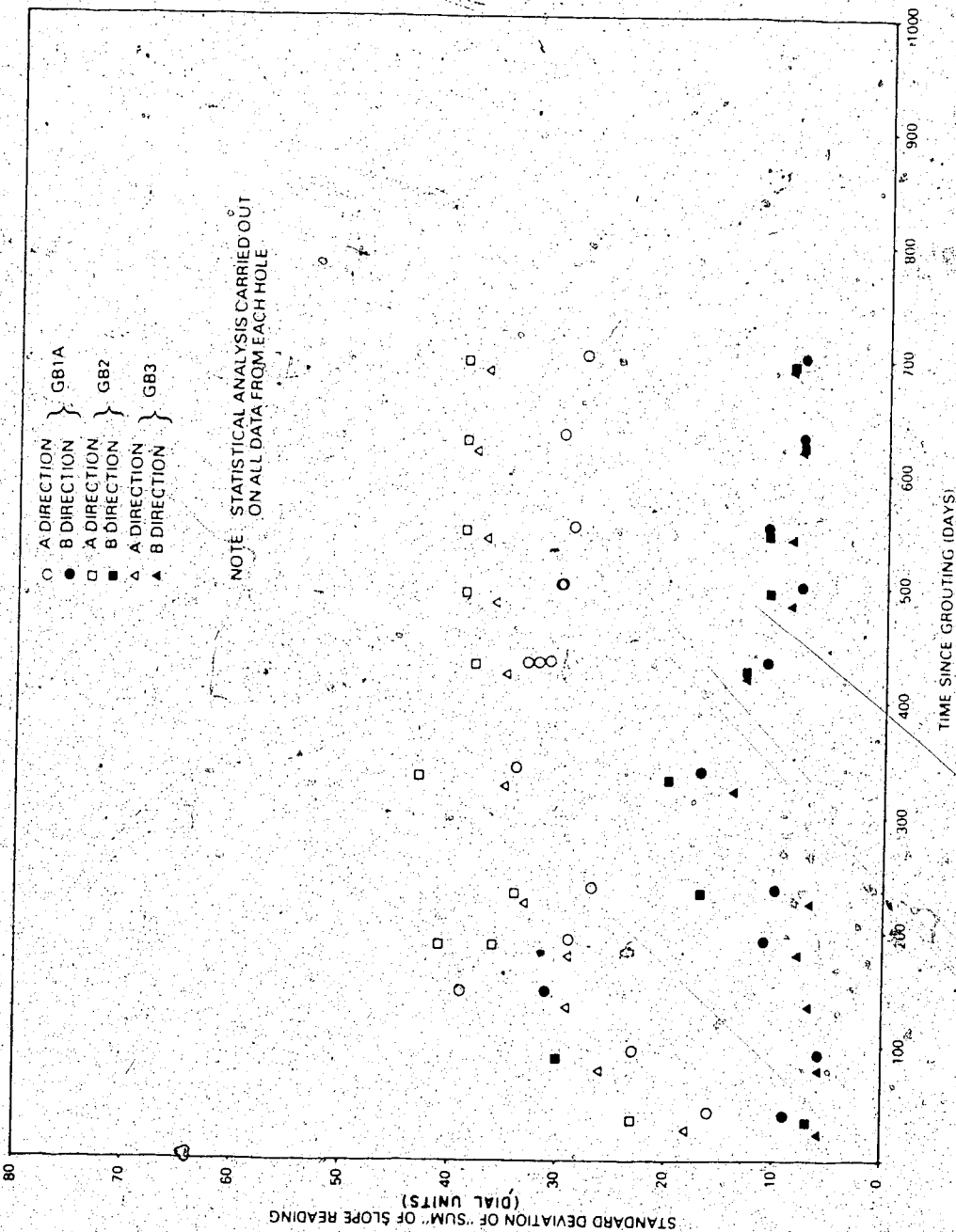
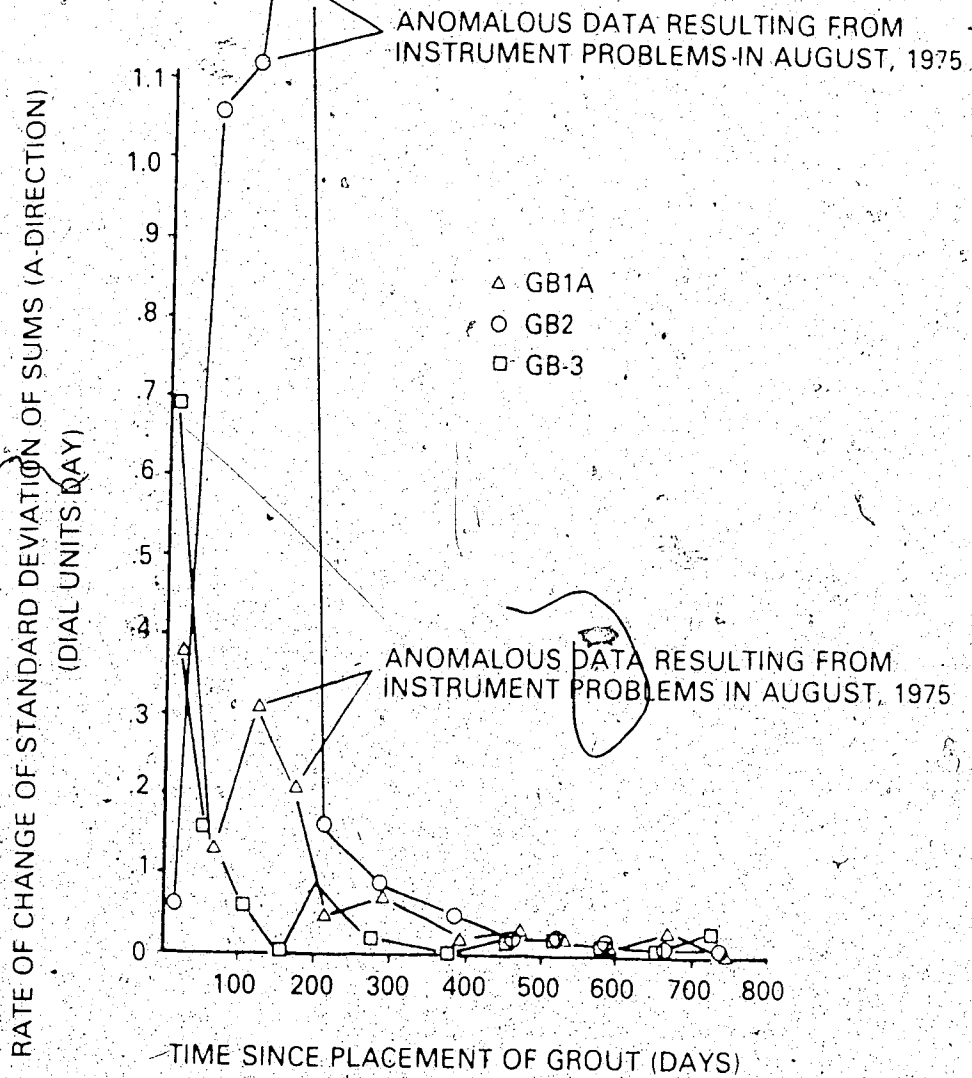


FIGURE 4.24 STANDARD DEVIATION OF SUMS AS A FUNCTION OF TIME



**FIGURE 4.25 RATE OF CHANGE OF STANDARD DEVIATION OF A-DIRECTION SUMS FOR EACH INCLINOMETER CASING**



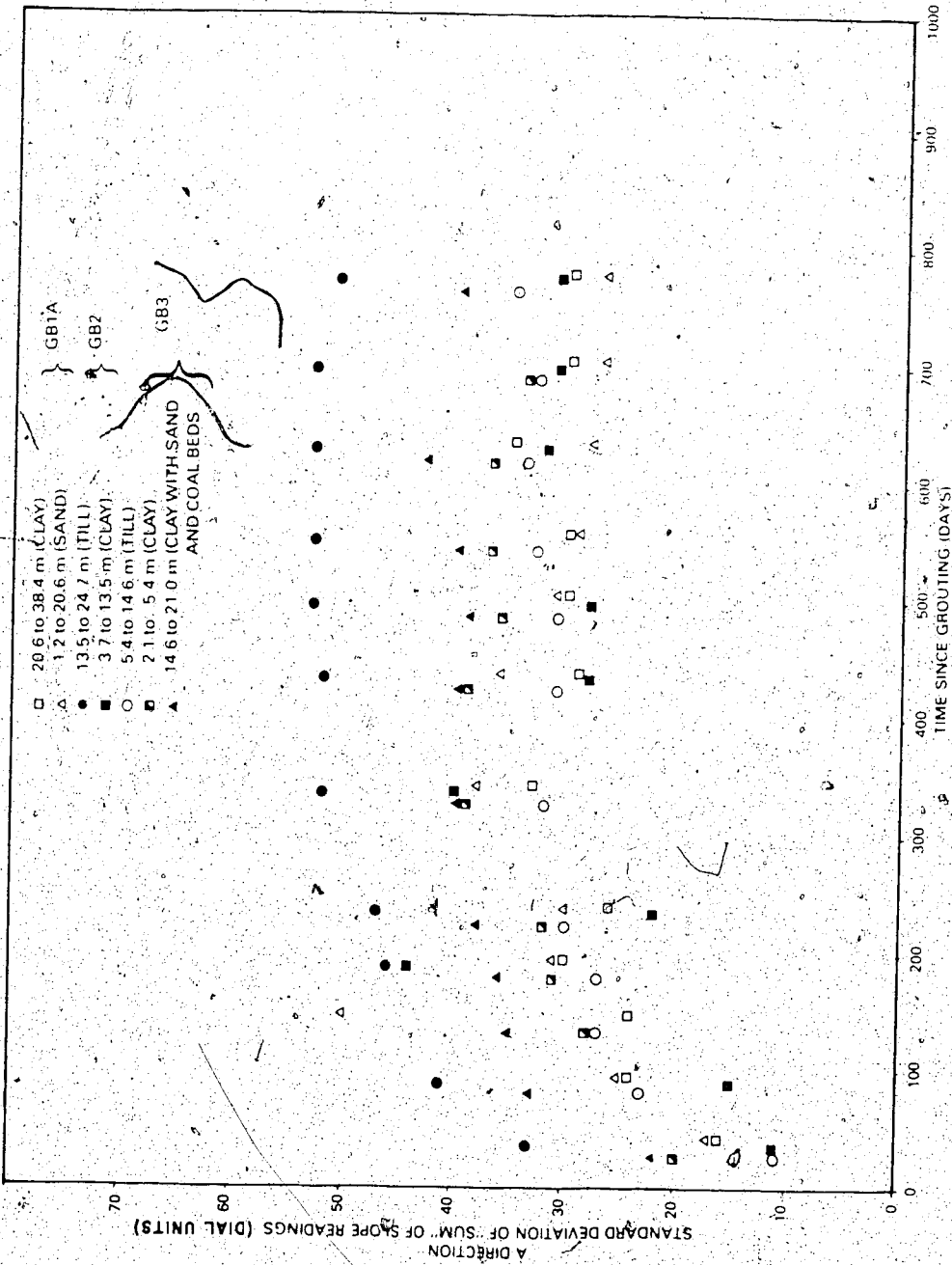
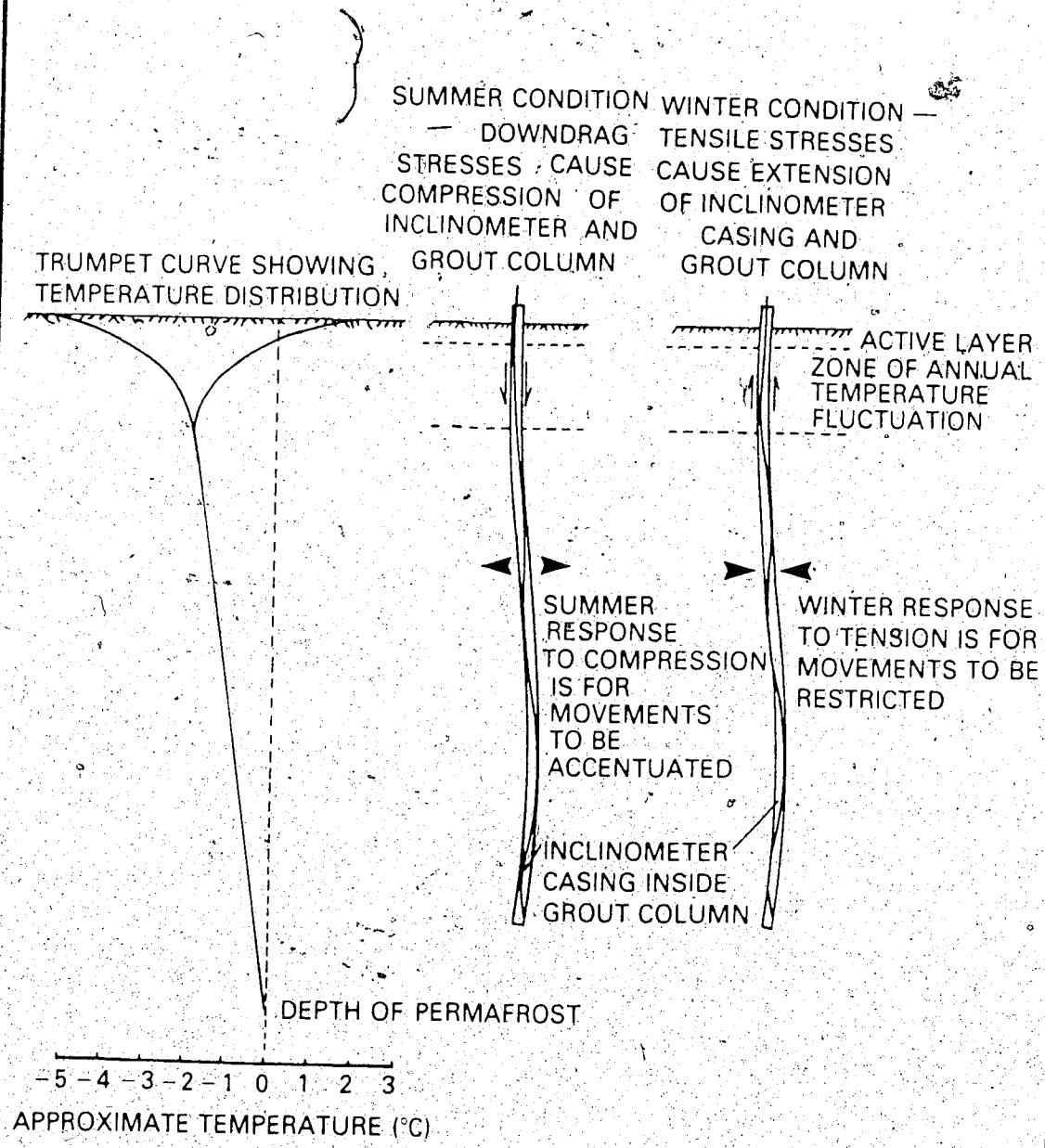
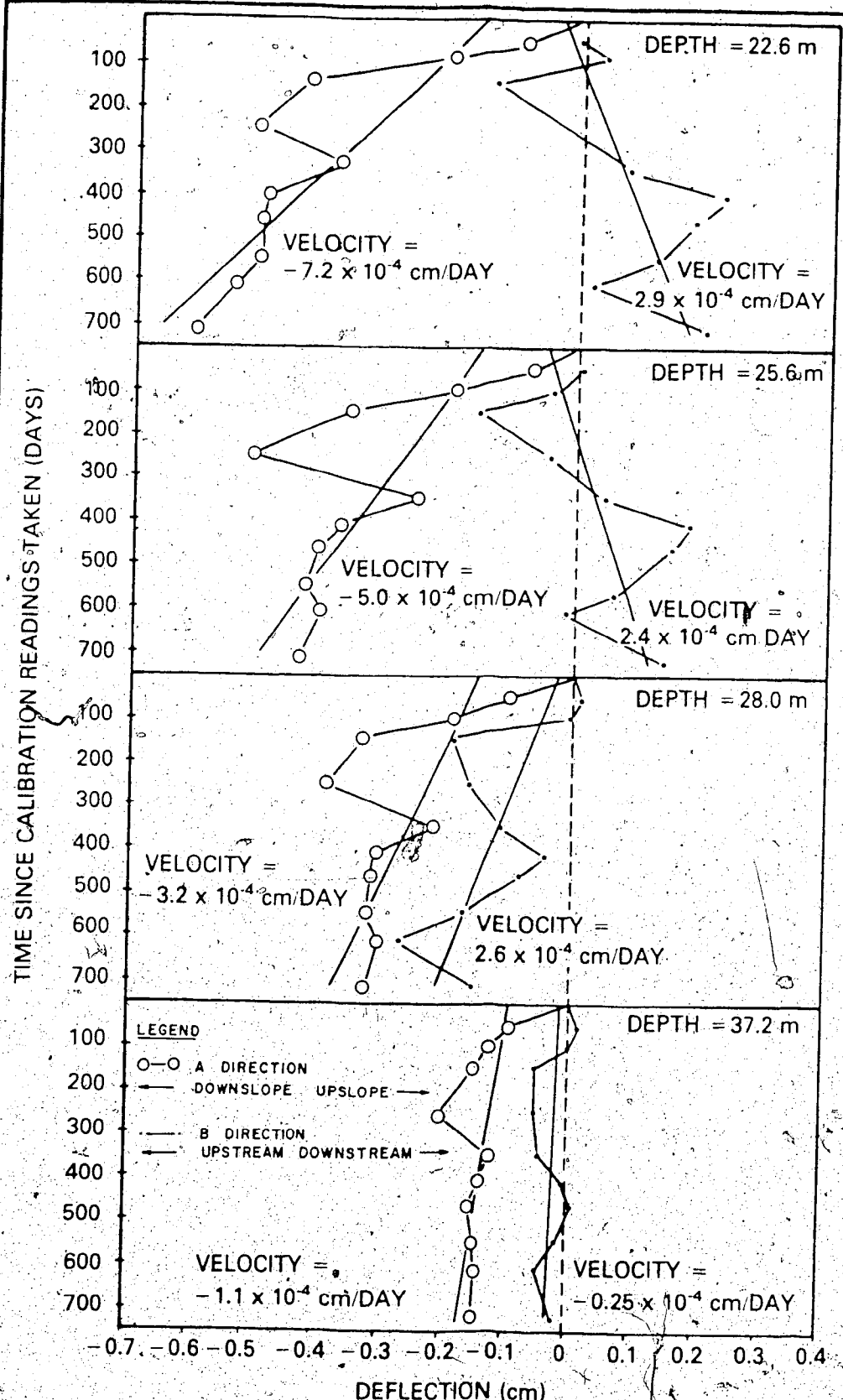


FIGURE 4.26 STANDARD DEVIATION OF SUMS AS A FUNCTION OF TIME FOR DIFFERENT LITHOFACIES



**FIGURE 4.27 SCHEMATIC REPRESENTATION OF HEAVE AND SETTLEMENT OF INCLINOMETER CASING AND GROUT COLUMN**



**FIGURE 4.28 TYPICAL PLOTS OF DEFLECTION VERSUS TIME AT DIFFERENT DEPTHS IN GLACIOLACUSTRINE CLAY IN HOLE GBIA**

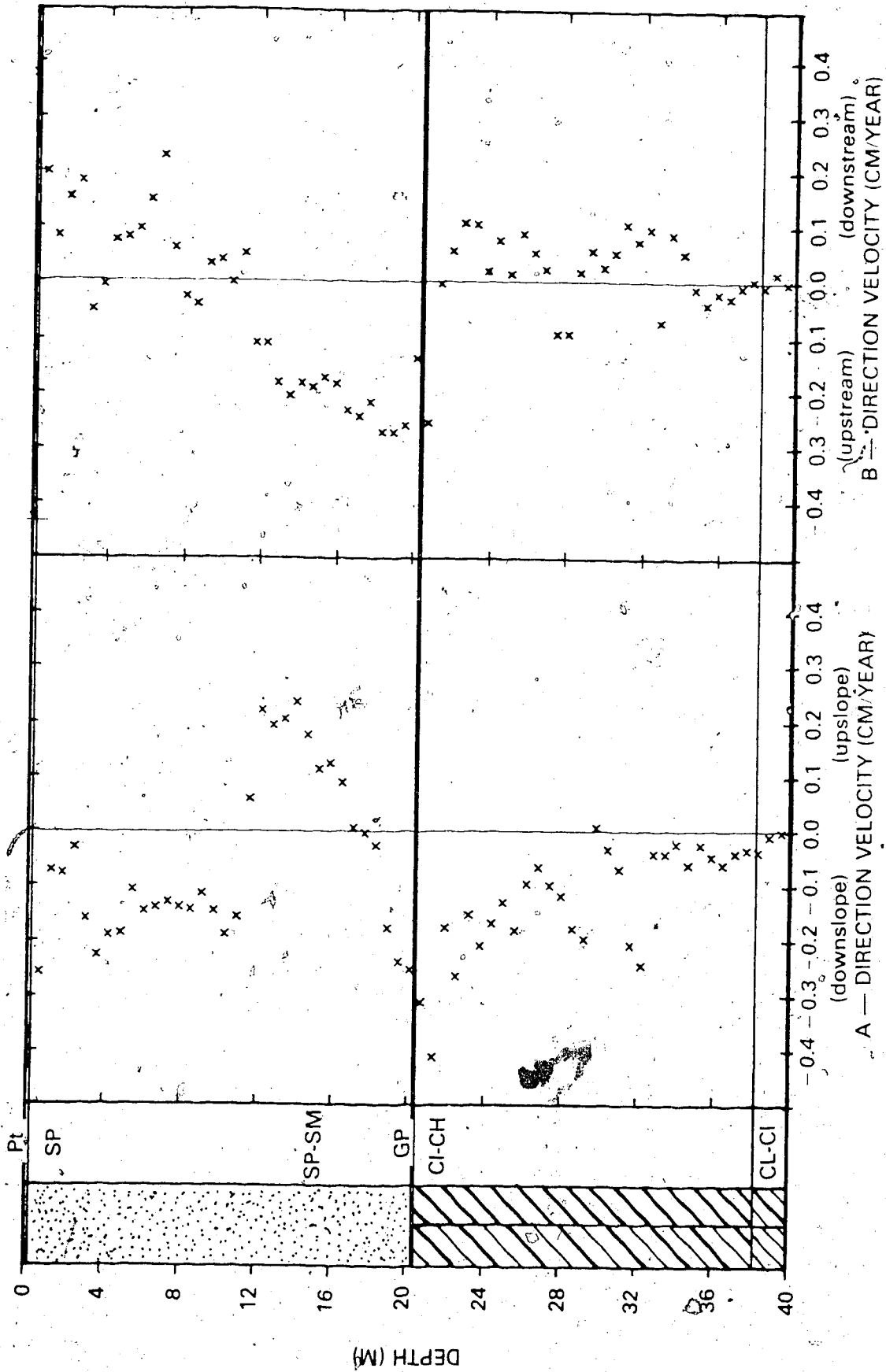


FIGURE 4.29 VELOCITY PROFILES FOR HOLE GB1A

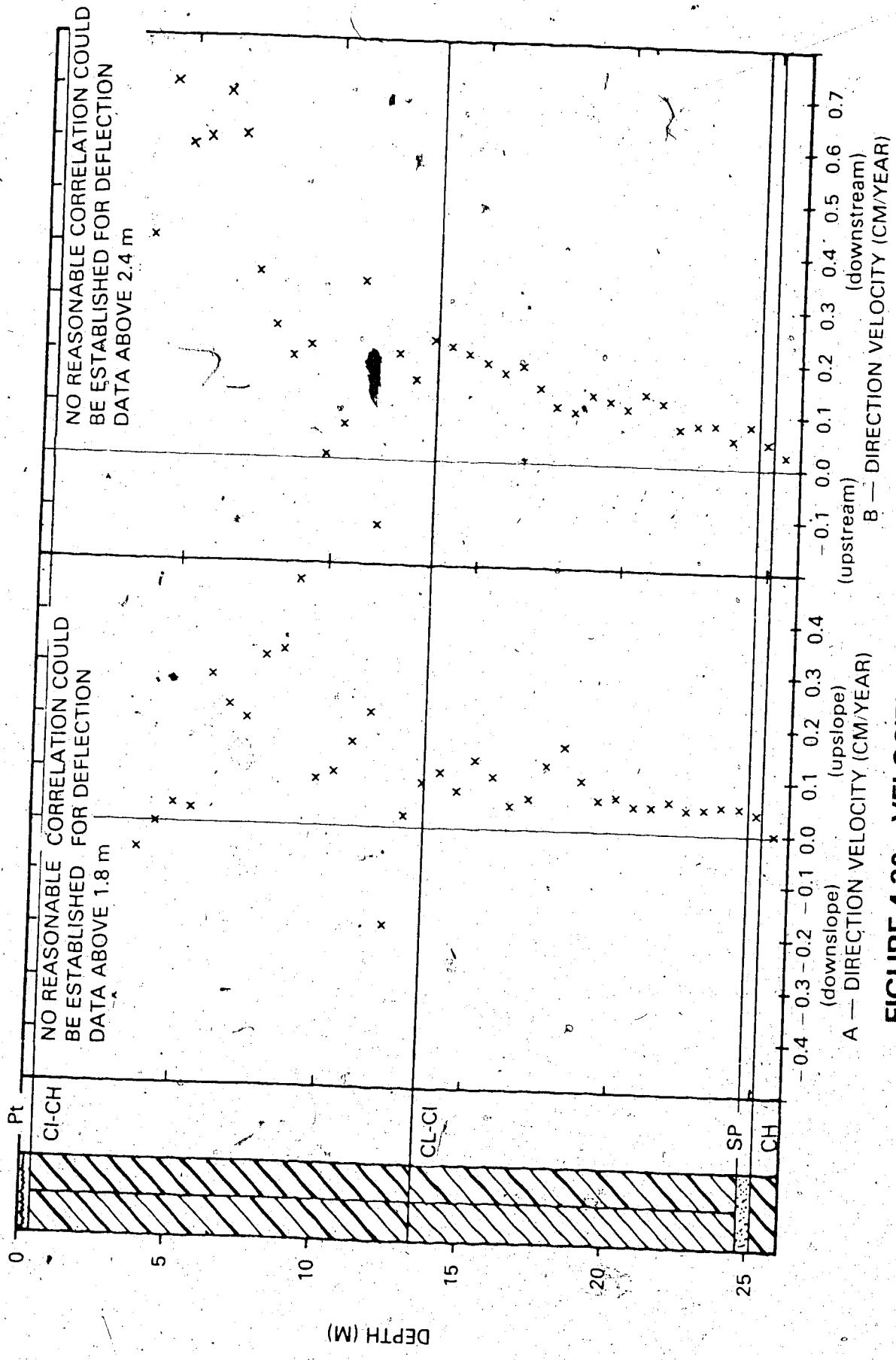


FIGURE 4.30 VELOCITY PROFILES FOR HOLE GB2

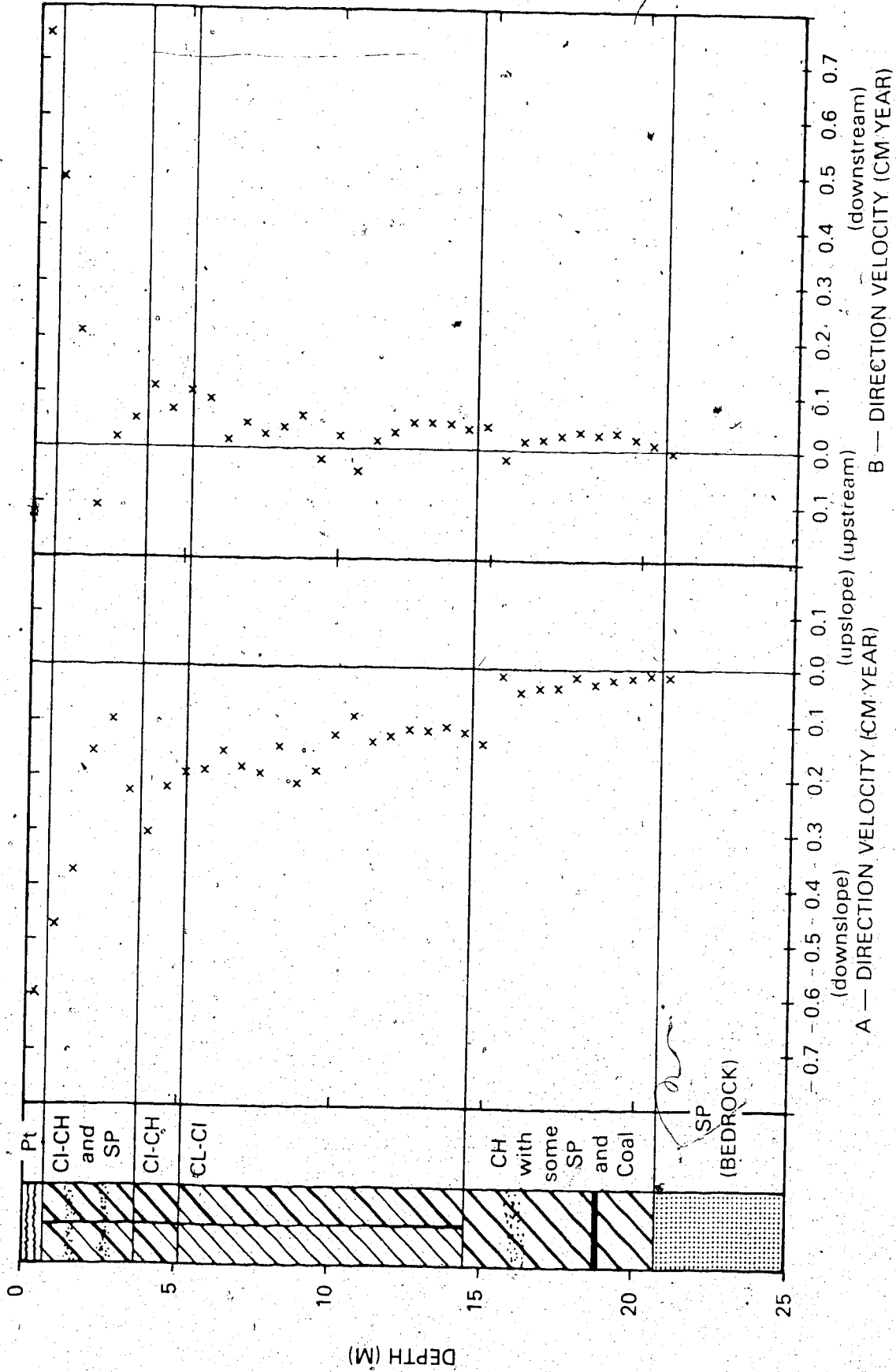


FIGURE 4.31 VELOCITY PROFILES FOR HOLE GB3

## CHAPTER V

### CREEP BEHAVIOUR OF UNDISTURBED GLACIOLACUSTRINE CLAY UNDER SIMULATED FIELD CONDITIONS

"...frozen slopes in very ice-rich soils may be expected to behave as if they were composed of pure ice, i.e., similar to natural glaciers." (Pipeline Application Assessment Group, Mackenzie Valley Pipeline Assessment, pp. 199)

#### 5.1. Introduction

In order to proceed with numerical analysis of steady state creep deformations in the slope at the proposed Arctic Gas crossing of Great Bear River, it is necessary to determine constitutive equations which describe the stress-strain-time behaviour of the materials. These equations require certain empirical parameters which are derived from laboratory tests.

Measurement of these parameters has been the focus of many recent studies, but significant fundamental disagreement remains because of a paucity of long-term field data with which to compare the laboratory results. This study afforded a unique opportunity to overcome this constraint, and hence a laboratory programme was undertaken in order to measure steady state creep behaviour of ice-rich core samples at temperatures and stresses which simulated field conditions. Inclinator data presented in the preceding chapter clearly showed that long-term creep deformations affect

fine-grained, ice-rich glaciolacustrine and morainic soils at the site. Only the medium to high plastic glaciolacustrine clay was tested in this programme, however, because sampling difficulties in the morainic soil precluded use of the few samples which were obtained.

Developments in the understanding of steady state creep properties in ice, reconstituted frozen soils and natural permafrost soils, are briefly surveyed in this chapter in order to establish a perspective with which to assess the laboratory data. This is followed by a discussion of the laboratory programme, and presentation and analysis of the results.

## 5.2 Rheological Properties of Ice

The rheology of permafrost soils is related to that of ice when ice forms disseminated structures or is present in the pore spaces of a soil mass. Excellent reviews of the deformation properties of ice have been prepared by Colbeck (1970), Glen (1975), Hobbs (1974), and Paterson (1969). The following discussion summarizes portions of these reviews that relate to the creep of frozen soils. A temperature and stress range of interest in geotechnical engineering is implicit in this discussion.

The fundamental crystalline form of ice is hexagonal. Each crystal may be imagined as a series of hexagonal-shaped plates aligned concentrically along a single axis known as the optic or 'C' axis. The face of each hexagonal plate (normal to the 'C' axis) is referred to as a basal plane.



The basal plane is the only pervasive structural weakness in the lattice. Single crystals deform most easily along this basal plane by a process referred to as basal glide. They also deform when oriented for non-basal glide, but stresses must be in the order of 20 times greater to achieve the same deformation. In this case, movement occurs along structural irregularities in the lattice known as dislocations. These two conditions are referred to as easy glide and hard glide respectively (Glen 1958; 1963).

It is generally accepted that ground ice in frozen soil is made up of polycrystalline ice. Deformation processes in polycrystalline ice are much more complex than in single crystals because movements are restricted by the confinement of individual crystals. Barnes *et al.* (1971) suggested that hard glide dominates creep deformation below temperatures of  $-8^{\circ}\text{C}$ . At warmer temperatures, they proposed that deformation is associated with cracks opening between crystals, grain boundary sliding and diffusion of water along grain boundaries into dilating zones, and as temperatures approach the freezing point (especially above  $-1^{\circ}\text{C}$ ), pressure melting and regelation dominate the overall deformation process.

The creep behaviour of polycrystalline ice in response to the application of load may be represented by four deformation processes. Each is illustrated schematically in Figure 5.1 and described below; collectively they represent undamped creep behaviour (Vialov, 1965):

- 1) OA - Instantaneous (elastic) and primarily recoverable strain
- 2) AB - Primary or transient creep at a decreasing rate of strain
- 3) BC - Secondary or steady state creep at a constant and minimal rate of strain
- 4) CD - Tertiary creep at an increasing rate of strain culminating in failure

Creep tests in compression, tension, shear, and other more specialized conditions have been carried out to determine a constitutive relationship for polycrystalline ice in the secondary creep mode. The most common flow law determined is a simple power law of the form (Glen, 1953; 1975):

$$\dot{\epsilon} = B\sigma^n \quad [5.1]$$

where  $\dot{\epsilon}$  is the uniaxial creep rate;

$\sigma$  uniaxial stress,

B a constant with dimensions of  $(\text{time})^{-1}(\text{stress})^{-n}$ ,  
and

n a dimensionless constant

Morgenstern et al. (1979) completed an extensive review of published secondary creep rates and determined the following values for the constants B and n:

Temperature (°C)	B (kPa <sup>-3</sup> year <sup>-1</sup> )	n
-1	4.5 x 10 <sup>-8</sup>	3.0
-2	2.0 x 10 <sup>-8</sup>	3.0
-5	1.0 x 10 <sup>-8</sup>	3.0
-10	5.6 x 10 <sup>-9</sup>	3.0

In order to relate this empirical flow law to more complex stress systems encountered in field applications, many authors (Emery and Nguyen, 1974; Ladanyi, 1972; and Roggensack, 1977) have adopted effective stress and strain rates as defined by Odqvist (1966). Roggensack (1977) reported these as:

$$\sigma_e = \sqrt{3} \sqrt{I_2}, \text{ and } = \sqrt{\frac{3}{2} \sigma'_{ij} \sigma'_{ij}} \quad [5.2]$$

$$\dot{\epsilon}_e = \frac{2}{\sqrt{3}} \sqrt{J_2}, \text{ and } = \sqrt{\frac{2}{3} \dot{\epsilon}_{ij} \dot{\epsilon}_{ij}} \quad [5.3]$$

Where

- $\sigma_e$  is the effective stress,
- $I_2$  the second invariant of deviatoric stress,
- $\sigma'_{ij}$  the deviatoric part of the stress tensor (the stress deviator)
- $\dot{\epsilon}_e$  the effective strain rate,
- $J_2$  the second invariant of strain rate, and
- $\dot{\epsilon}_{ij}$  the creep rate tensor.

These relations assume the material is isotropic and incompressible, creep rates are unaffected by the hydrostatic part of the stress tensor, and the tensors of stress and strain rate are coaxial. In the special case of uniaxial loading the simple power law expression in Equation 5.1 is recovered.

### 5.3 Rheological Properties of Reconstituted Frozen Soils

Frozen soil is a multicomponent system made up of assemblages of solid granular minerals and/or organic matter, polycrystalline ice, water containing solute, and air or other gases. This heterogeneity, coupled with the many physical and thermodynamic variables which collectively control the interrelationship of the components, causes considerable complexity in geotechnical analysis.

Creep processes in frozen soils are complex. In North America, the main process is thought to involve localized pressure melting of ice caused by a build up of stresses at soil-ice contacts. This water moves under a pressure gradient induced by external loading and internal surface tension, to regions of lower stress where it recrystallizes. At the same time, ice remaining in the pore spaces deforms in the manner described in Section 5.2. Both of these conditions facilitate particle rearrangement which is effectively creep deformation of the soil mass (Andersland et al., 1978). In the Soviet Union, the initiation and development of creep behaviour in frozen soils is presently linked to the growth of microcracks along structural defects in the soil mass. Water moves into these dilatant zones where it refreezes. Deformation of pore ice and particle rearrangement, although not clearly accounted for, seem implicit in this deformation model.

When load is applied to frozen soil it responds with either damped or undamped creep behaviour as illustrated schematically in Figure 5.1. Damped creep is characterized by two processes (Vialov, 1965):

- 1) OA - Instantaneous and primarily recoverable strain.
- 2) AE - Primary or transient creep with decreasing strain rate which attenuates to a limiting strain.

Undamped creep is characterized by the four processes described for ice in Section 5.2.

The stress level above which undamped creep occurs is not well defined. Polycrystalline ice creeps at small stresses, and hence it generally forms an upper bound for undamped creep. As the soil concentration increases, creep deformations are ultimately inhibited by the mobilization of frictional resistance in the soil mass. The soil-ice concentration where this occurs is a function of ambient temperature, soil composition and texture, and loading conditions.

Anderson and Morgenstern (1973), Andersland et al. (1978), and Roggensack (1977) have reviewed numerous published laboratory studies on the creep behaviour of reconstituted frozen soils. These provide a good overall assessment of the relative influence of factors such as soil type, ice content, temperature and stress on creep behaviour. Because creep testing is very time consuming, and because the results are sensitive to small temperature changes when ambient conditions are near the freezing point, most testing programmes have been undertaken at temperatures and stresses extreme to those encountered in practice. Despite this constraint, some of the conclusions reported by these authors are relevant to the present study.

Secondary creep rates may exceed those of clean

polycrystalline ice in a medium where granular soil is dispersed thinly through an ice matrix. Increases in soil concentration, however, ultimately cause an exponential decrease in creep rate. At void ratios representative of sand deposits at the proposed Arctic Gas crossing of Great Bear River, creep behaviour in compression is damped provided the frictional strength of the sand is not exceeded (Hooke *et al.*, 1972; Sayles, 1968; 1973).

Ice-rich, fine-grained soils typically show undamped creep behaviour. Most authors (Perkins and Ruedrich, 1973; Sayles and Haines, 1974; Vialov, 1963) interpret secondary creep data in terms of a simple power law of the form given in Equation 5.1; however, many of the tests reported appear to have been terminated before strain rates reached a minimum, and hence empirical values of the exponent in the flow law are, in general, higher than for true steady state conditions. The exponent values converge on 3 as test duration and data quality improve indicating close correspondence with exponent values for polycrystalline ice. Tests generally show a relationship between confining stress and strain rate indicating some frictional response. In ice-poor, fine-grained soils only damped creep behaviour is indicated provided the frictional strength of the soil is not exceeded (Sayles and Haines, 1974).

#### 5.4 Rheological Properties of Natural Permafrost Soils

Creep properties determined for reconstituted frozen soils cannot be indiscriminately applied to natural permafrost soils because the cryogenic textures typically show some degree of

difference. In pore ice facies, the differences are of relatively little significance because ice is only present through the soil matrix. In situ void ratios can be measured and then re-generated in artificial samples relatively easily, and therefore ice structures are representative. In reticulate, segregated and stratified ice facies, however, ice is present through the soil matrix as well as in complex arrays of veins. Vialov (1965) reported that the strength between soil particles and an ice matrix exceeded that between soil particles and adjacent ice veins. It may be inferred from this that under certain loading conditions deformations are localized along ice veins. Since the cryogenic textures of reticulate and segregated ice facies, and to a certain extent stratified ice facies cannot be recovered in artificial samples, it is therefore necessary to undertake testing of natural permafrost soils.

Johnson and Sayles (1972) investigated the steady state creep behaviour of very ice-rich Fairbanks silt in association with in situ monitoring of deformations in a tunnel partially excavated through the same material. Samples were tested at temperatures of  $-1.7^{\circ}\text{C}$  in unconfined compression at stress levels between approximately 250 and 2000 kPa. The results showed surprisingly close agreement with a flow law of the same form as Equation 5.1 with an exponent of 4. Numerical analysis using this relation accurately predicted tunnel deformations.

Roggensack (1977) reported creep tests on ice-rich fine-grained glaciolacustrine sediments from the Mackenzie River Valley. The tests were carried out in modified triaxial cells at

varying confining pressures and at temperatures of approximately  $-1.0^{\circ}\text{C}$ . Deviatoric stresses were varied from 20 to approximately 400 kPa. The data showed considerable scatter, but appeared to define a bilinear flow law of the form:

$$\dot{\epsilon} = A\sigma^{n_1} + B\sigma^{n_2} \quad [5.4]$$

where

$\dot{\epsilon}$  is the uniaxial strain rate,

$\sigma$  is the deviatoric stress, and

A, B,  $n_1$  and  $n_2$  creep parameters dependent upon temperature and stress.

Roggensack (1977) considered that the departure from non-linearity was related to differences in cryogenic texture among the various test samples, and difficulties in picking a steady state rate in the low stress range<sup>1</sup>. He therefore ignored some of his data and used strain rates determined from tests at higher stress levels, together with results from other sources to define a flow law of the form given in Equation 5.1 with an exponent of 2.75.

McRoberts et al. (1978) tested glaciolacustrine silts from the Mackenzie Valley in a similar manner to that reported by Roggensack (1977). The results were interpreted in terms of a bilinear flow relation. In the low stress range they determined an exponent value of 3, which is similar to that defined by Roggensack (1977). At higher stresses, however, because of the bilinear relation, they determined an exponent value of 6.

<sup>1</sup> Deviatoric stresses below 100 kPa are arbitrarily defined as the low stress range.



Nixon (1978) reviewed the results reported by Roggensack (1977) and McRoberts et al. (1978), before endorsing the latter interpretation.

Roggensack (1977) and McRoberts et al. (1978) also reported preliminary findings on the effect of changes in temperature and confining pressure on secondary creep rates. Their results indicated that an increase in temperature caused an increase in strain rate, and fluctuations in temperature were of greater significance near 0°C where the amount of unfrozen water increased proportionately more for any given temperature change. Increases in confining pressure caused modest decreases in strain rate, but the effects were minimal and much less than in frozen granular soils.

In conclusion, it is clear that there is no agreement on the form of a constitutive relationship for steady state creep behaviour in laboratory samples. A linear relation with an exponent of approximately 3 is generally accepted in the low stress range, but is disputed at stresses above 100 kPa where data indicate the relation becomes bilinear with a new exponent of approximately 6.

The laboratory programme reported in the remainder of this chapter was undertaken in an attempt to resolve these discrepancies, and define a flow law and empirical parameters which could be used for numerical analysis of secondary creep deformations at the field instrumentation site.

### 5.5 Constant Stress Triaxial Creep Tests

Tests were undertaken concurrently in laboratories at the

University of Alberta (U of A), and Northern Engineering Services Limited, Calgary (NES). Results from both testing programmes are analyzed and reported here.

Temperature and stress conditions for the testing programmes were selected in order to simulate field conditions.

#### 5.5.1 Laboratory Equipment

Creep tests at the U of A were carried out in specially designed triaxial cells fabricated in the U of A Civil Engineering machine shop. The cell details are illustrated schematically in Figure 5.2. Samples were tested without membranes in a confining medium of light paraffin oil, a technique which has been shown to have no adverse affect on sample quality (Iverson and Moum, 1974; Roggensack, 1977). Temperature of the oil was monitored by a thermistor bead embedded at the head of a stainless steel tube inserted through the cell cover to approximately mid-height beside the sample. The sample temperature was assumed to be identical to that of the oil. Temperature control was provided by a solution of ethylene glycol regulated in a temperature control bath and circulated through heat-exchange coils wrapped in a circumferential pattern around the sample.

Details of the overall apparatus are shown schematically in Figure 5.3. The cell was placed on a bakelite centering plate inside an insulated cabinet. The cabinet was mounted on a frame of channel iron and the entire apparatus was situated in a controlled temperature laboratory maintained at between  $-3$  and  $-7^{\circ}\text{C}$ . A Hot

Pack Model 603340 temperature control bath was elevated over a row of four apparatuses. The unit was equipped with a manifold and the four cells connected in parallel with taigon tubing. A special pump was used in order to adequately service each cell.

A lever-assisted, dead-load loading frame was used to apply constant load. This was transferred to the upper platten via a frame narrowly fitted outside of the insulated box. The entire load transfer system was aligned during fabrication to ensure no eccentric loads affected the load ram.

Confining pressure was supplied by an air over paraffin oil, pressure-regulated supply reservoir. The regulator and air supply were situated outside of the controlled temperature laboratory to eliminate the possibility of water vapour condensing and freezing in the lines. The pressurized oil line was connected to a manifold inside the laboratory, from which each cell was supplied and could be independently controlled. The cells were filled by connection to a larger, pressure-regulated supply reservoir.

The instrumentation for each apparatus included a thermistor and a linearly variable differential transducer (LVDT); an electrical resistance strain-gauge diaphragm pressure transducer was mounted in the central pressure line outside of the laboratory. The thermistor was an Atkins PR99-3 calibrated against a quartz resistance thermometer<sup>1</sup>, and mounted in stainless steel tubing as described earlier in this section. The LVDT was a Hewlett-Packard

---

<sup>1</sup>See Segó (1980, Appendix B) for specifications of this thermistor and details of the calibration procedure.

24 DCDT capable of measuring displacements as small as  $1.0 \times 10^{-4}$  cm. It was mounted so as to measure the displacement of the load ram relative to the top of the cell. The pressure transducer was capable of measuring pressure changes as small as 0.15 kPa. Both the LVDT and pressure transducer were calibrated with equipment of local design.

Data were recorded on a Techtran cassette recorder attached to a data acquisition system.

Details of the Northern Engineering Services Ltd. testing apparatus have been reported by McRoberts *et al.* (1978). The only significant difference from the University of Alberta equipment described above was that a bellofram system was used to apply axial load.

#### 5.5.2 Sample Description

Natural permafrost cores, 10 cm in diameter, from holes GB1, GB2, and GB3 were used in the testing programme. Those selected had the following characteristics:

- (1) The core had a useable length to diameter ratio not less than one and one-half and not more than three.
- (2) A pervasive ice structure was present. Veins of ice in reticulate and stratified ice ranged from fractions of a millimetre to 25 mm thick, and from 10 to 30 mm thick in segregated ice; soil layers in reticulate ice ranged from 40 to 100 mm thick, and in segregated ice from 10 to 30 mm thick. Ice structures were variable among the

different samples, and occasionally within individual samples. Although this was considered undesirable, there was no alternative in view of the number of available samples of suitable length.

- (3) The core was visibly of high quality, with no desiccation and no planes of fracture in either the ice or soil medium.

Index properties of all samples tested are given in Table D.3.

#### 5.5.3 Sample Preparation

Samples were prepared in a soil preparation laboratory where the ambient temperature was maintained between  $-3^{\circ}\text{C}$  and  $-7^{\circ}\text{C}$ . The ends were trimmed with a band saw before the sample was mounted in a soil lathe and turned to an outside diameter of approximately 10 cm. Finally, the ends were trimmed parallel on an overhead milling machine.

The dimensions and weight of the sample were noted and photographs taken to record the ice structure. Engineering properties were routinely determined from the several centimetres of core trimmed at each end. These are reported in Table D.3. Since the presence of varying amounts of ice precluded any possibility of obtaining representative water contents, bulk density is reported for the purpose of comparing the relative ice content of different samples.

When trimming was completed, holes for centering pins were drilled into the top and bottom of the sample and it was put in

place on the lower platten. The upper platten was set in place and the loading ball set in the recess at the top of the platten. The upper part of the cell was lowered over the sample, and when in place, the position of the loading ball was inspected through the load-ram annulus at the top of the cell. On two occasions this inspection showed the top platten to be slightly off centre and further trimming was required before continuing. Otherwise, the upper portion of the cell was bolted to the base.

Light paraffin oil was introduced to the cell through the load-ram annulus until the upper load platten was covered. The cell was then placed in the insulated box, and while topping of the paraffin oil continued, the load ram, instrumentation, confining pressure lines, and temperature control lines were assembled. When paraffin oil began to displace through the pressure relief valve at the top of the cell, all valves were closed, the supply line was disconnected, and the insulated cabinet was closed. The lever and load transfer system were put in place, and a nominal axial load, marginally greater than the reaction of the load ram to the planned confining pressure, was applied. Finally, circulation of the temperature control fluid was begun and the confining pressure was applied.

The system was allowed between 24 and 36 hours to come to temperature and stress equilibrium. Within the first few hours a check was made inside the cabinet to ensure that all equipment had been assembled correctly and that no hose connections were leaking. Monitoring was carried out throughout the stabilization period to

check instrument performance.

Samples tested by NES were prepared in a similar manner.

#### 5.5.4 Testing Procedure

By the end of the stabilization period zero readings for the LVDT, pressure transducer, and thermistor were well established.

The load requirement for the desired axial stress was placed on the lever arm which was supported by an hydraulic jack. The jack was lowered and monitoring commenced at time zero. Loading took place over a period of between 3 and 5 seconds.

Readings during the first hour were recorded by hand through remote monitoring of the data acquisition system. All subsequent readings were recorded on the Techtran recorder. At least one reading was obtained within the first 45 seconds and approximately 15 within the first hour. From the second to at least the sixth hour the reading interval was set at 10 minutes and thereafter 1 hour.

Data were transferred at regular intervals to the IBM 360 computer. The results were processed intermittently by computer so the test progress could be accurately monitored.

As vertical deformation accumulated, the lever was maintained in a horizontal position by adjusting the reaction device on the lever assembly. For tests which extended for more than approximately 2 days, adjustments to the load were made at intervals of 0.5% strain to maintain constant stress conditions.

For tests where secondary creep behaviour was well

established over a 50 to 70 day period with no indication of acceleration into tertiary mode, the samples were stage loaded to at least one higher axial stress level following the same procedure outlined earlier in this section.

Cells were dismantled within a few hours of sample failure or termination of the test. All instrumentation and pressure and temperature regulation lines were disconnected, and a dummy heat-exchange coil was installed inside the insulated cabinet to minimize thermal disturbance to other in-line tests.

Similar procedures were followed by NES.

#### 5.5.5 Method of Analysis and Data Processing

The distinction between damped and undamped creep is difficult to define at low stress levels, and within the practical time frame available for laboratory programmes. What appears to be a secondary creep mode may be attenuating transient creep, and vice versa.

Roggensack (1977) considered this problem and concluded that the principal of superposition (Conway, 1967), which assumes transient and steady state deformations occur concomitantly from the time of stress application, should be adapted in order to clearly delineate secondary creep rates from laboratory data. He proposed a modified Cottrell-Aytenkin relation in which the strain  $\epsilon$  at time  $t$  is given by the sum of the elastic, transient, and secondary deformations, according to the following equation:

$$\epsilon = \epsilon_0 + Bt^m + \epsilon_{st} \quad [5.5]$$



where  $\epsilon_0$  is the instantaneous strain,  
 $\epsilon_s$  the true secondary creep rate,  
 $B$  a constant dependent upon stress and  
 temperature, and  
 $m$  a constant approximately equal to 1/3.

Differentiating Equation 5.5 with respect to time gives the strain rate  $\dot{\epsilon}$  at any time  $t$  as follows:

$$\dot{\epsilon} = At^a + \epsilon_s \quad [5.6]$$

where  $A$  is a constant equal to  $Bm$ , and

$a$  an exponent equal to  $m-1$ .

By systematically calculating strain rate from creep data and plotting the calculated data as  $\log \dot{\epsilon}$  versus  $\log t$ , the constants  $A$ ,  $a$  and  $\theta$  can be determined as shown in Figure 5.4. The constants  $B$  and  $m$  may also be calculated for substitution into Equation 5.5. This graphical relationship affords a reliable means of assessing whether or not creep deformations are associated with a steady state process. If so, the secondary strain rate may be read directly as the minimum ordinate value (Roggensack, 1977).

All data obtained in laboratory tests were processed by computer and the output given in printed and plotted form. Typical graphical test results are shown in Figure 5.5, and include the following: the classical plot of conventional axial strain as a function of time; temperature as a function of time; and  $\log$  axial strain rate<sup>1</sup> as a function of  $\log$  time, which is the same form as

<sup>1</sup>Because of the thousands of data points for each test, a method had to be devised to systematically limit the data. This was accomplished by using a deformation interval which was a function of test duration and which was similar among the different tests. Strain rate was determined from a moving, three-point, linear regression fit to these data points.

### Reticulate Ice

Samples 3, 4, and 5 contained distinctive primary and secondary ice veins. Primary veins ranged from 8 to 25 mm thick, and were an average of approximately 10 times thicker than secondary veins. Each sample failed in times which ranged from 1 to 230 hours. The post-failure appearance of each sample is shown in Plates 5.1 through 5.5, inclusive. These indicate that shear developed principally along the soil-ice interface of pervasive, primary ice veins. Closer examination reveals some shear along secondary veins, and relatively little through frozen soil. Plate 5.5 shows that in Test 5, which deformed for the longest time before failure, significant movement also occurred along secondary ice veins, causing the sample to have a blocky appearance.

Samples 6 through 10 contained only secondary veins as shown in Plate 5.6. These ranged in thickness up to 3 mm and were rarely pervasive. The test results varied from short-term failure, as described above, to deformation which lasted for periods of up to 6 months, with no indication of the onset of tertiary processes. All samples except one failed. Typical post-failure conditions are illustrated in Plates 5.7 and 5.9. Shear planes typically developed along secondary ice veins, especially ones with significant thickness and length, which could coalesce with minimum shear of frozen soil to become pervasive. Secondary ice veins outside of the main shear zone in samples which failed, and throughout sample 8 which did not fail, showed some evidence of movement, leaving the sample with a blocky appearance. An example of this is illustrated

in Plate 5.9.

#### Stratified Ice

Sample 10 contained numerous veins of ice ranging in thickness up to 4 mm and oriented approximately horizontally as shown in Plate 5.10. The deformation behaviour was unique in that an unusually large amount of strain accumulated within a short period of load application. This attenuated to more reasonable rates after approximately 200 hours; in a subsequent loading stage, the sample also behaved normally. The post-failure condition of the sample shown in Plate 5.11 indicates that significant radial movement occurred in frozen soil between ice veins. This appears to have been facilitated by shear at the soil-ice interfaces. The magnitude of movement varies in apparent proportion to the thickness of soil between horizontal ice veins. The cross-section of the sample shown in Plate 5.12 indicates that radial movement was associated with tensile failure of the soil, and concomitant growth of ice veins in the dilating zones.

#### Segregated Ice

Sample 11 consisted of segregated ice. Ice formed irregular shaped veins up to 25 mm thick, and comprised approximately 35% of the sample volume. Soil peds were more contiguous, but could also be found floating in the ice matrix. Typical ice structure is illustrated in Plate 5.13 for a portion of core stratigraphically below the one tested. The sample deformed at a quasi-steady-state

rate almost from the time of loading, reaching approximately 15% strain in 40 hours. Following termination of the test, the sample showed no evidence of failure (Plate 5.14); however the blocky nature of the surface indicated that movement occurred at most soil-ice interfaces. Some of these contacts were separated and dilated up to 0.5 mm.

#### 5.5.7 Physio-Mechanical Interpretation of Premature Failure

Creep tests carried out at U of A were dominated by failure processes. Failure occurred at much lower deviatoric stresses than had been anticipated on the basis of documented testing programmes by Thompson and Sayles (1972), Roggensack (1977), and McRoberts et al. (1978). Shear planes consistently developed at soil-ice interfaces. The sample failed quickly where these planes were pervasive; otherwise failure occurred more slowly, with shear development along several ice structures coalescing by shear through frozen soil. Samples which did not fail still showed evidence of shear along soil-ice interfaces.

Tests conducted by NES as part of this programme were carried out on samples of reticulate ice with large primary ice structures oriented at approximately  $40^\circ$  to the core axis. Based on the behaviour of U of A samples, these should have failed soon after the application of deviatoric stress, but they did not. It is not known whether or not there was visible indication of shear along the ice veins at the end of these tests.

Two variables which may account for the difference in creep

behaviour between the two testing programmes are sample disturbance and the affect of confining pressure:

The presence of ice veins in permafrost soil renders it a non-homogeneous continuum. Therefore, stress release during coring causes non-uniform stress fields to develop in samples (Tsytoich, 1975). Although these likely dissipate by creep or microsheading along ice veins during prolonged storage, sample disturbance is the net result. All U of A samples, with the exception of number 11, came from depths of 22 to 36 m in GB1, while the NES samples came from depths of 3 to 5 m in GB3. Hence, more significant disturbance in U of A samples correlates with the premature failure.

Applying confining pressure as part of a confined triaxial creep test causes sample disturbance in the same way as stress release during coring. Since the non-uniform stress fields generated by the application of confining pressure probably dissipate largely by creep deformation, a significant time period is required between the times of confining and deviatoric stress application in order for the sample to reach stress equilibrium. NES specimens were tested without the use of a confining pressure. The strain rate versus log time plots for NES tests (Appendix D) show that the primary creep stage lasted approximately 500 hours. U of A samples, which were loaded within a few hours of the application of a 400 kPa confining pressure, either failed prior to 500 hours or were undoubtedly still in transient creep<sup>1</sup>.

---

<sup>1</sup>This refers to the initial (A) loading stage only.

Therefore, the use of confining pressure also correlates with premature failure.

Sample 11 was the only U of A sample obtained from a comparable depth (1.5 m) with NES samples. Although the cryogenic textures were dissimilar, the overall ice contents were comparable. Under the same confining pressure and stabilization conditions used in other U of A tests, sample 11 failed at a very fast rate. Since sample disturbance insofar as it relates to the NES samples was not a contributing factor, it can be concluded that premature failure of the U of A samples was, in all probability, caused by the confining pressure.

Tests reported by Roggensack (1977) also lend support to this conclusion. These were carried out on ice-rich, fine-grained permafrost samples where "... each specimen contained a similar, evenly-distributed network of thin, reticulate ice lenses..." (ibid, p.123). He used confining pressures and deviatoric stresses similar to those used for U of A samples reported here. He found distinct behavioural differences with different ground ice structures and reported that several samples failed along soil-ice interfaces.

In conclusion, it is proposed that the use of confining pressure in the U of A tests caused high shear stress gradients in soil adjacent to ice veins. Because insufficient time was allowed for these stresses to dissipate, shear stresses in the permafrost soil samples after loading were much higher than would have been the case at zero confining pressure. This caused deformation along all ice lenses. When the only disseminated ice structures present were

closely spaced secondary ice veins, this deformation resulted in soil peds rearranging themselves within the array of ice veins, and this occasionally led to sample failure. However, when primary ice structures were present, deformation took place along a pervasive plane and quickly led to sample failure.

It is recommended that a laboratory programme be undertaken in order to clearly resolve this apparent transient influence of confining pressure.

#### 5.5.8 Assessment of Results

In order to use laboratory results from the U of A and NES programmes to determine a constitutive relationship and empirical parameters for field modelling, it is necessary to assess the degree to which minimum observed strain rates represent steady state conditions. The physio-mechanical deformation behaviour discussed in the preceding section provides important guidelines for this assessment.

Sample 11 had unusually high ice content with random and reasonably uniform distribution. Deformations at minimum strain rate were localized along soil-ice interfaces, and only the anastomosing ice network prevented development of a pervasive failure plane. The deformations represent a rupture process rather than uniform deformation, and the apparent rate of strain exceeds that of true steady state behaviour.

For samples 3, 4, and 5 which had large, pervasive ice structures, minimum strain rates appear to represent an inflection

point where localized shear movements along soil-ice interfaces began to propagate and coalesce along smaller ice structures and through frozen soil to form a through-going failure plane. Little or no uniform deformation of the sample occurred, and the rates are clearly much higher than those of steady state creep behaviour.

Relatively large secondary ice structures were closely aligned with planes of maximum shear stress in samples 6 and 9. In both cases failure occurred along some of these ice structures. Although secondary veins throughout the sample showed evidence of deformation, it is likely that movements along the ultimate failure planes dominated, and the minimum strain rates are significantly faster than true secondary rates. Similarly, for the last loading stage of samples 7 and 10 (7C and 10B) the failure process likely dominated deformation behaviour, and minimum strain rates exceed steady state rates.

For samples 7, 8, 10, and 12 with smaller secondary or stratified ice structures, it was observed that deformation occurred along most soil-ice interfaces. Moreover, these were randomly, and to a great extent, uniformly distributed through the sample. It is likely that most of these deformations occurred during A loading stage, but persisted at least into the B loading stage. In samples 7 and 10, deformation along secondary ice structures coalesced, resulting in failure during the last loading stage. It is unlikely that any of the minimum rates from test stages for samples 7 and 10 represent true steady state rates. For samples 8 and 12, however, it appears that at some time in the B loading stage, deformation



rates along secondary ice structures abated to an equilibrium rate controlled by pseudo-uniform strain through the entire sample.

Hence, minimum strain rates for tests 8B, 8C, and 12B are considered to be reasonably representative of steady state creep rates.

Examination of the log strain rate versus log time plots for these tests (Appendix D) indicates that only test 8C shows clear evidence of steady state behaviour. In both 8B and 12B there is reason to argue that transient conditions prevailed, and the minimum rates exceed those of true steady state behaviour.

The log strain rate versus log time plots for tests NES 3-11 and NES 3-8 (Figures D.52 and D.53 respectively, Appendix D) suggest that steady state conditions were achieved after approximately 500 hours. The minimum rate for test NES 3-8 is expected to be representative of steady state creep rates. A minimum rate for test NES 3-11 is more difficult to define because strain rates vary over nearly two orders of magnitude; a minimum value has been determined but its reliability is subject to question. Test 3-10 reached a minimum value, but immediately began a slow, systematic increase in response to increasing ambient temperature. There is no well-defined steady state strain rate, and the minimum may represent an inflection point and transient processes.

In summary, although the testing programme reported here has contributed to a mechanistic understanding of creep behaviour in ice-rich permafrost, and exposed probable limitations to the use of confining pressure in creep testing, it has done little to elucidate a constitutive relationship or empirical parameters for use in field

modelling. In view of the fact that relatively few reliable creep data have been determined, it is necessary to consider other test results on ice-rich, fine-grained permafrost soils to find a suitable relationship.

Thompson and Sayles (1972) reported unconfined creep tests on very ice-rich Fairbanks silt. The tests reported by these authors typically reached true strains in excess of 40% within 8 days. The magnitude of these strains suggests a complete loss of strain compatibility at soil-ice interfaces and localized brittle fracture of ice. This is analagous to the behaviour of sample 11 from the U of A testing programme reported earlier in this section. Minimum strain rates are faster than would be representative of steady state creep and the value of 4 determined for the exponent is therefore high.

Testing programmes reported by Roggensack (1977) and McRoberts et al. (1978) were carried out on ice-rich, fine-grained glaciolacustrine sediments of similar age and with similar sedimentological and permafrost characteristics. The results of these programmes, together with all data from the present study, are presented in Figure 5:7. In addition, four relevant flow relationships are shown. These include:

- (1) The flow law for polycrystalline ice (Morgenstern et al., 1979).
- (2) A tentative upper bound proposed by Nixon (1978) for steady state creep in ice-rich permafrost soils (extended here into a higher stress range).

(3) A regression fit to a simple power law using all data shown.

(4) A regression fit to a simple power law using data from tests on loading stages where failure did not occur.

The data appear to be most consistent in the high stress range. Minimum strain rates are typically faster than ice for any given stress, and almost all samples reached failure. In the low stress range, the data show considerably more scatter. Samples 3, 4, 5, 6, and 11<sup>1</sup> lie outside the general range of values determined from other programmes, but they do not represent steady state behaviour as discussed earlier in this section. The remainder of data in the low stress range still show significant scatter. Where minimum strain rates exceed those of polycrystalline ice at comparable stress levels, there is relatively more variation, for which the limiting condition appears to be failure.

It is of interest to reflect on a review of creep properties of polycrystalline ice completed by Roggensack (1977). He observed that creep test data displayed similar characteristics to those described above. Specifically, at high stresses data were in relatively close agreement, while at low stresses there was significantly more scatter. By reanalysis of several laboratory programmes, and assessment of field studies of glaciers and ice shelves, he demonstrated that minimum rates in the low stress range were frequently representative of transient creep processes. On

---

<sup>1</sup>These sample numbers are identified in Figure 5.6.

this basis he concluded a linear constitutive relationship, which excluded many of these data, best represented actual steady state behaviour.

It is obvious that the same argument could be applied in order to define an upper bound for steady state creep deformations in ice-rich permafrost soil. Nixon (1978) proposed an upper bound, as shown in Figure 5.7, for a stress range up to 100 kPa. Above this stress level, Nixon (1978) and McRoberts *et al.* (1978) considered that the constitutive relation was bilinear and the exponent value changed from 3 to 6. Many of the tests on which these authors based their interpretation of a bilinear relation ultimately failed. On the basis of the physio-mechanical interpretation presented in this thesis, these data were in all likelihood dominated by transient processes, and therefore the minimum rates exceed steady state values.

Extending the upper bound relation proposed by Nixon (1978) into the stress range above 100 kPa provides, with few exceptions, a valid upper bound for steady state data derived from tests which did not fail. It would be an arduous and possibly impossible task to reprocess the data shown in Figure 5.7 in order to exclude all tests where no clear evidence of steady state behaviour was evident. For the moment, it seems obvious that reliable secondary creep data are limiting to an upper bound of the form predicted by Nixon (1978). In light of new generalizations reported by Morgenstern *et al.* (1979) it seems this upper bound may be the flow law of polycrystalline ice. This implies that steady state creep in

ice-rich permafrost soils is less than polycrystalline ice at low stress levels, which is consistent with McRoberts et al. (1978) who reported that "... samples .. tested at stress levels which did not lead to failure, exhibit secondary creep rates considerably slower than published information on the flow laws for ice at the same stresses and temperatures".

It can be concluded that the flow law of polycrystalline ice represents an upper bound for steady state creep deformations in ice-rich, fine-grained, permafrost soils at the proposed Arctic Gas crossing of Great Bear River. The constitutive relation is in the form of the simple power law given in Equation 5.1, with an exponent of 3.0 and a coefficient of  $2.0 \times 10^{-8}$  year  $\text{kPa}^3$ . The actual in situ secondary creep relation is in all likelihood best represented by a flow law of the same form and with the same exponent, but with a slightly lower coefficient representing a uniform<sup>1</sup> decrease in strain rate for any given stress relative to polycrystalline ice.

---

<sup>1</sup>The uniform decrease is in terms of a log versus log relationship.

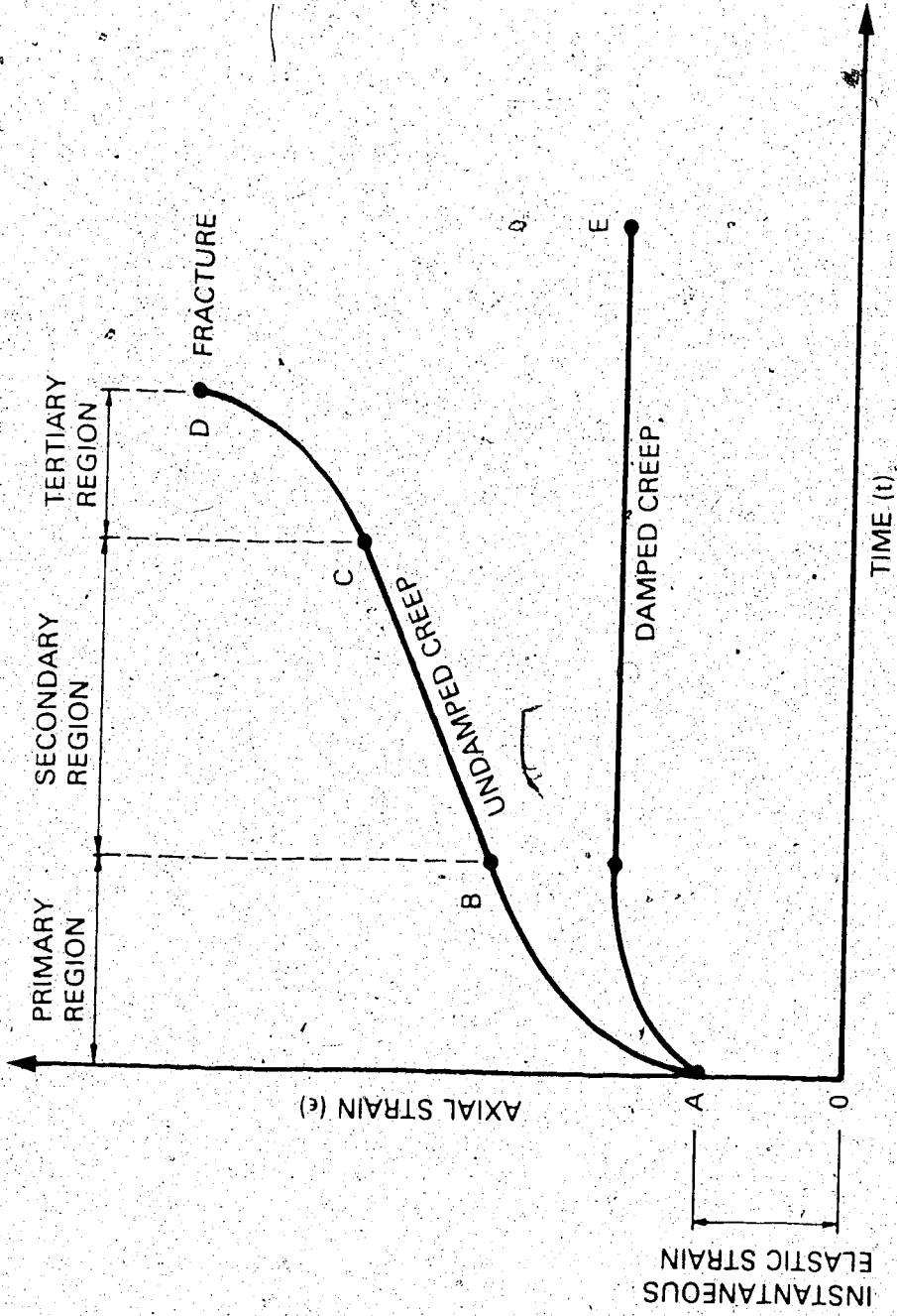
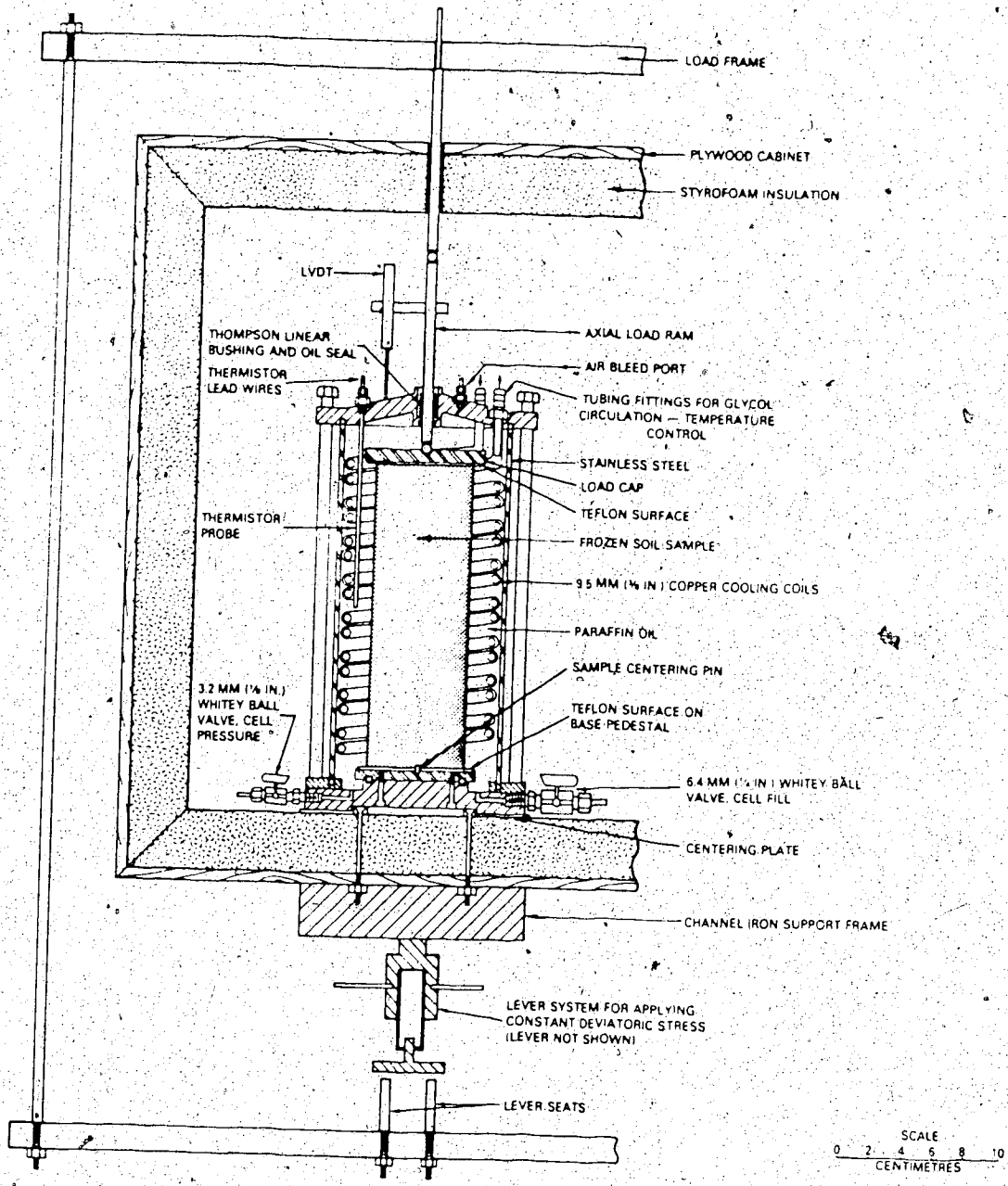


FIGURE 5.1 TYPICAL CONSTANT AXIAL STRESS CREEP CURVES  
(AFTER VIALOV, 1965)



**FIGURE 5.2: SCHEMATIC LAYOUT OF SPECIALLY DESIGNED TRIAXIAL CELL USED FOR CREEP TESTS**

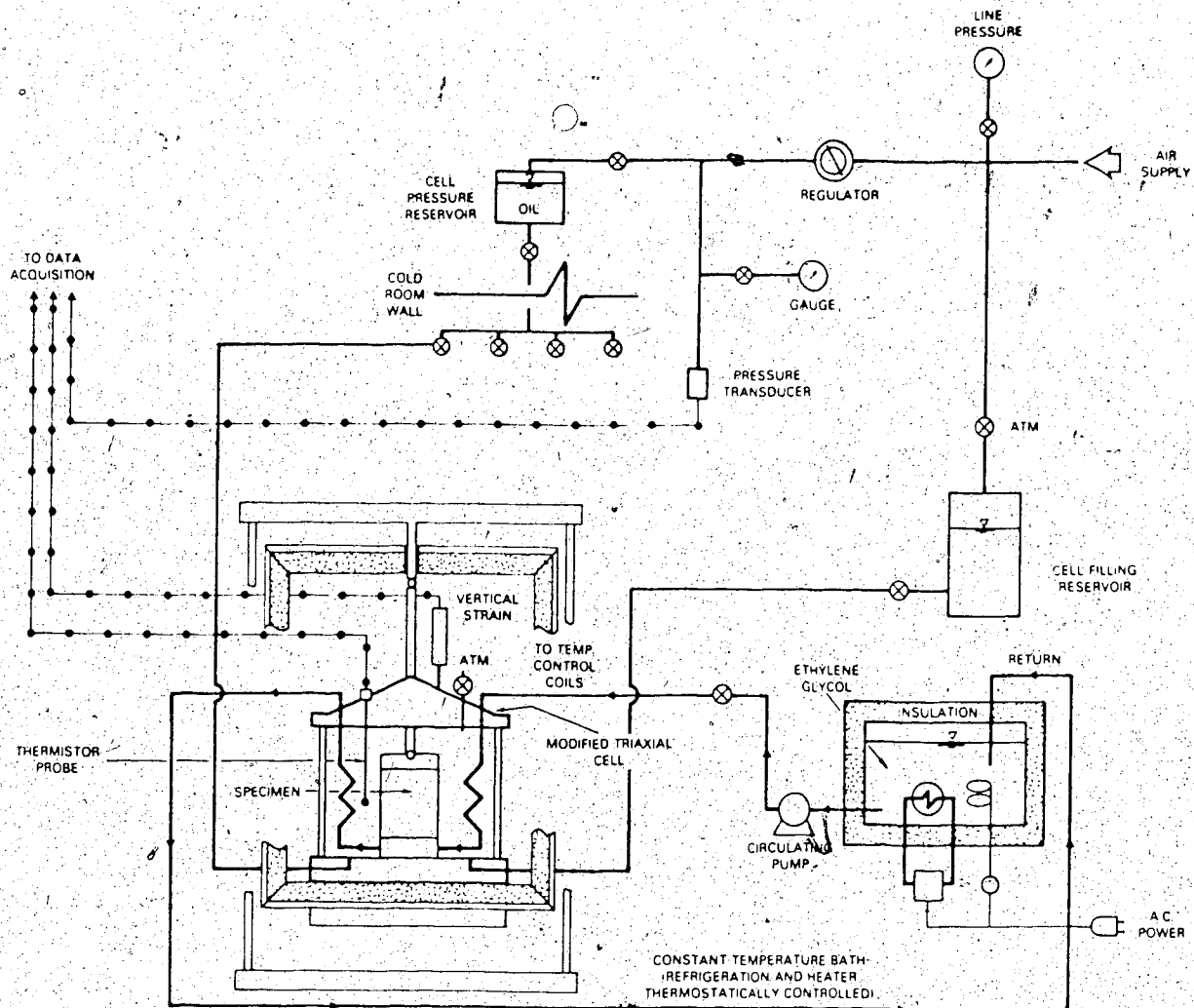


FIGURE 5.3 SCHEMATIC LAYOUT OF CREEP TESTING SYSTEM



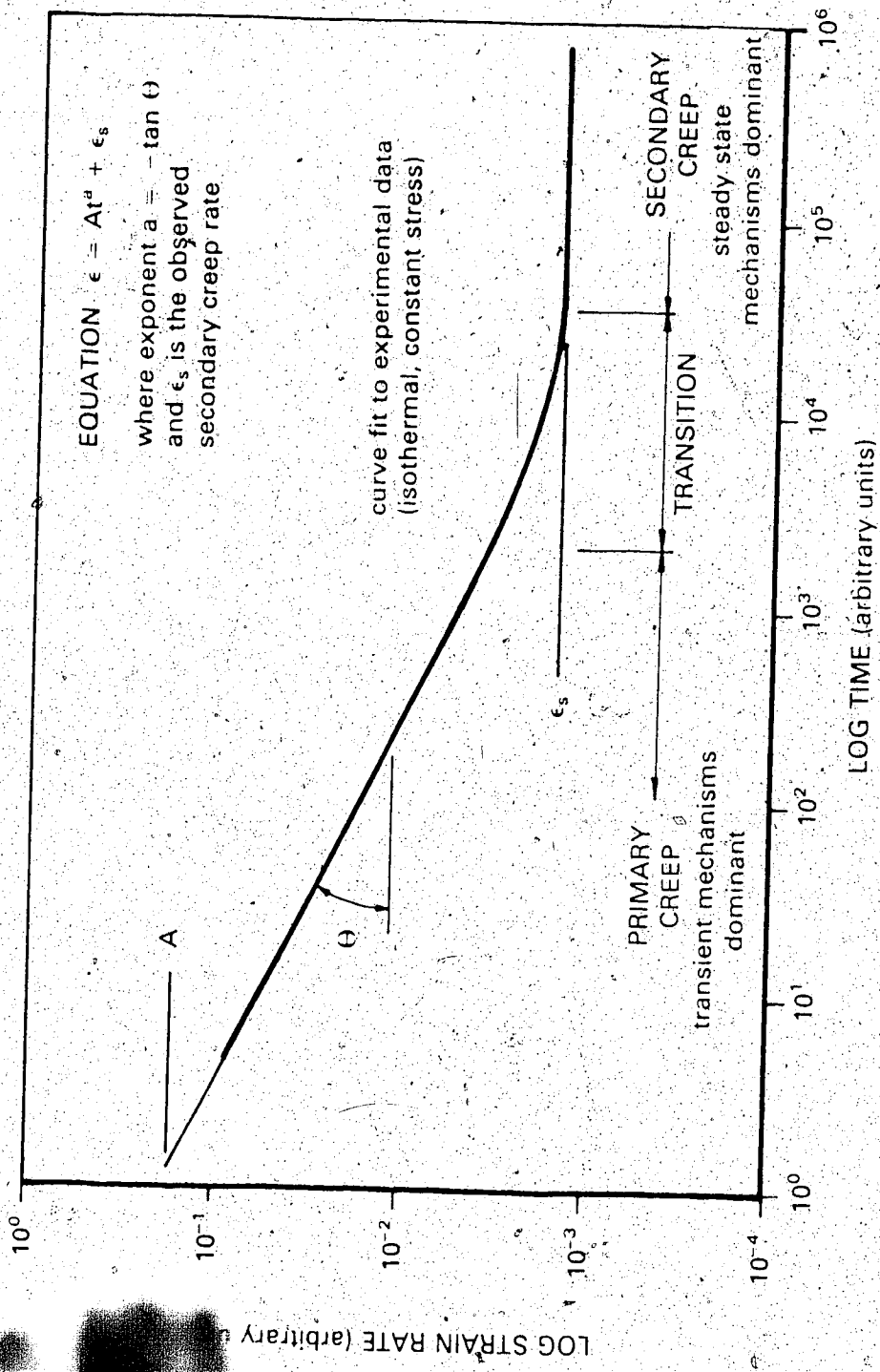


FIGURE 5.4: TYPICAL CREEP TEST DATA PLOTTED TO EVALUATE TRANSIENT AND STEADY STATE COMPONENTS (AFTER ROGGENSACK, 1977)

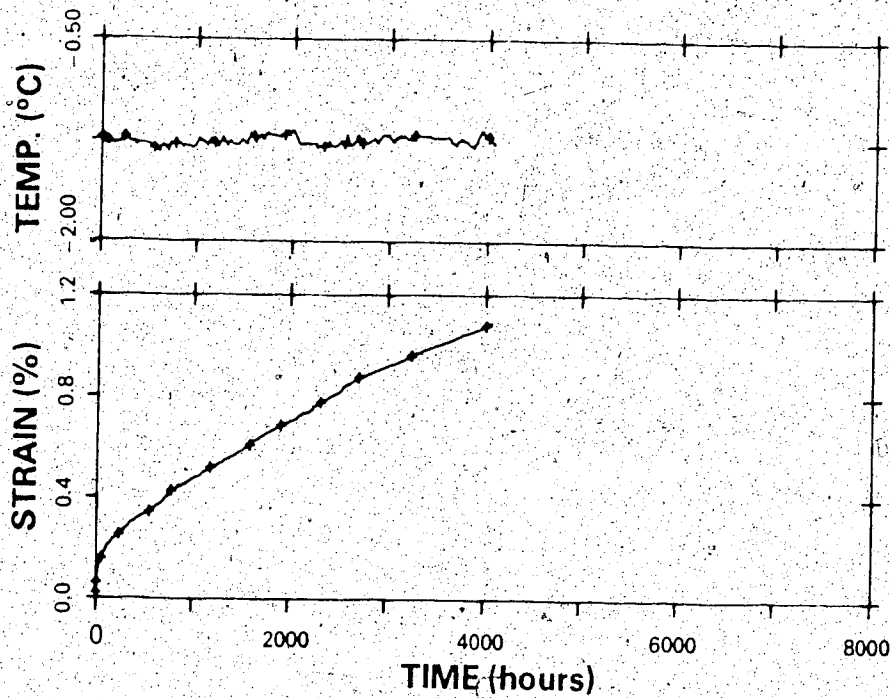
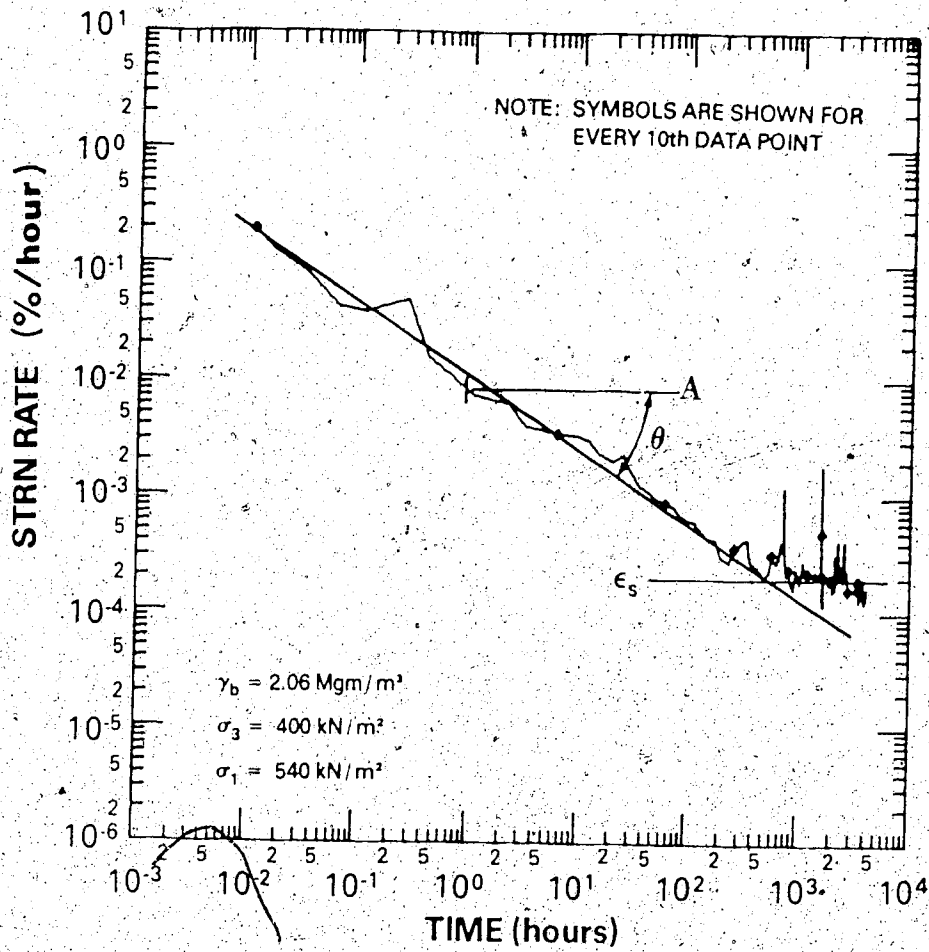
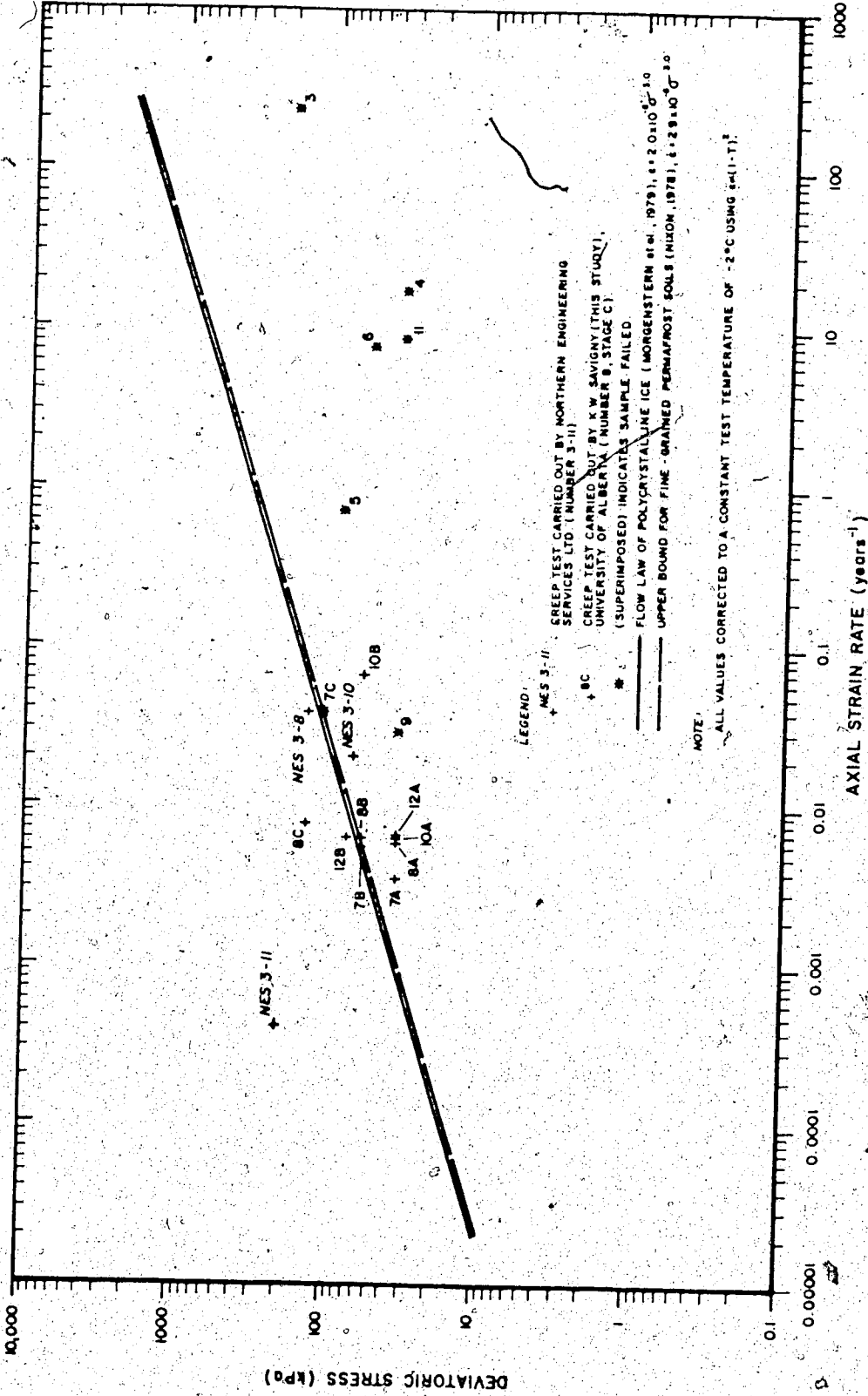
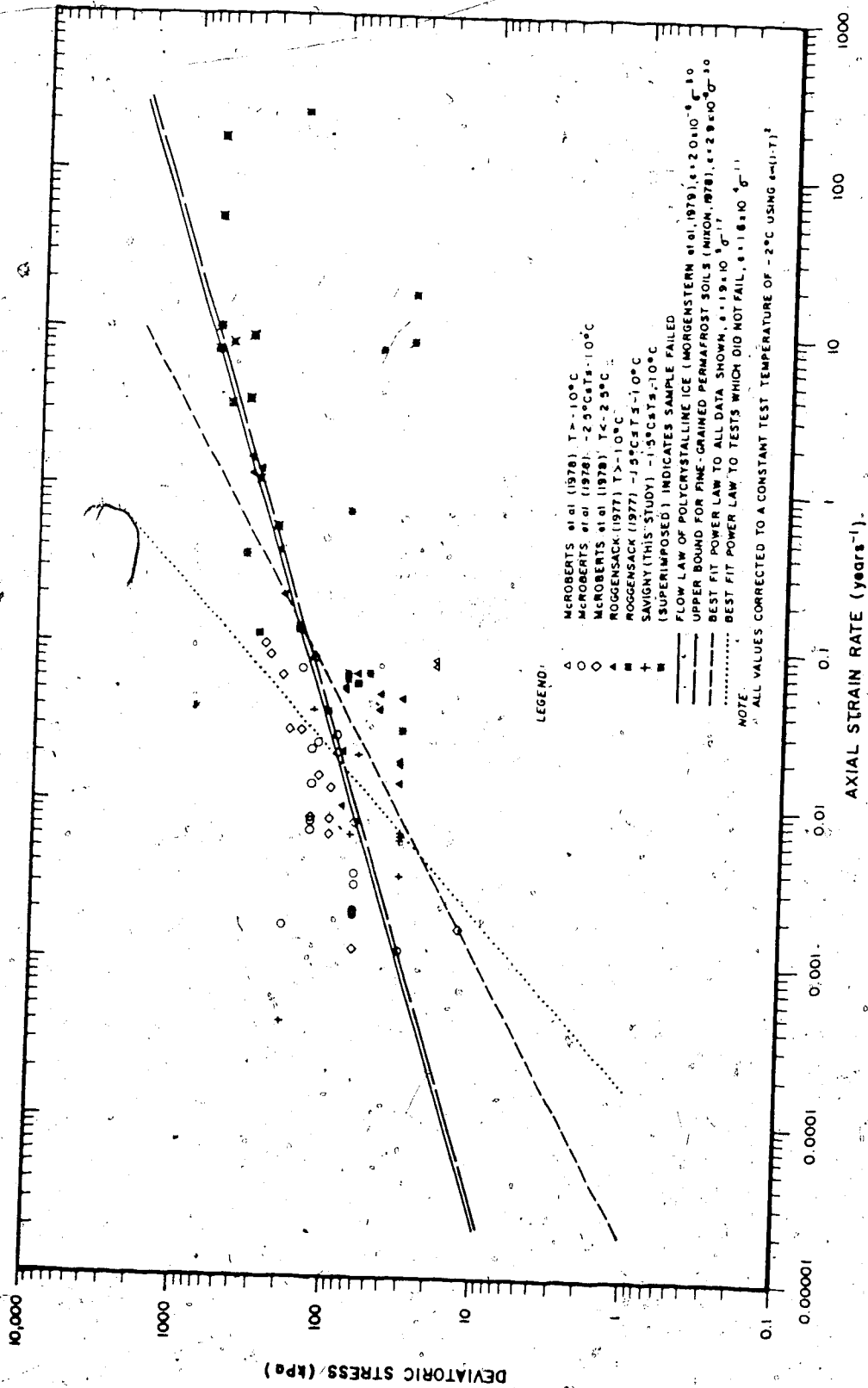


FIGURE 5.5: RESULTS OF CREEP TEST 8C ON FROZEN GLACIOLACUSTRINE CLAY



**FIGURE 5.6 STEADY STATE CREEP RATE DATA FOR ICE-RICH GLACIOLACUSTRINE CLAY FROM THE GREAT BEAR RIVER AREA**



**FIGURE 5.7** STEADY STATE CREEP RATE DATA FOR ICE-RICH GLACIOLACUSTRINE CLAY FROM VARIOUS LOCATIONS IN THE MACKENZIE VALLEY, N.W.T.

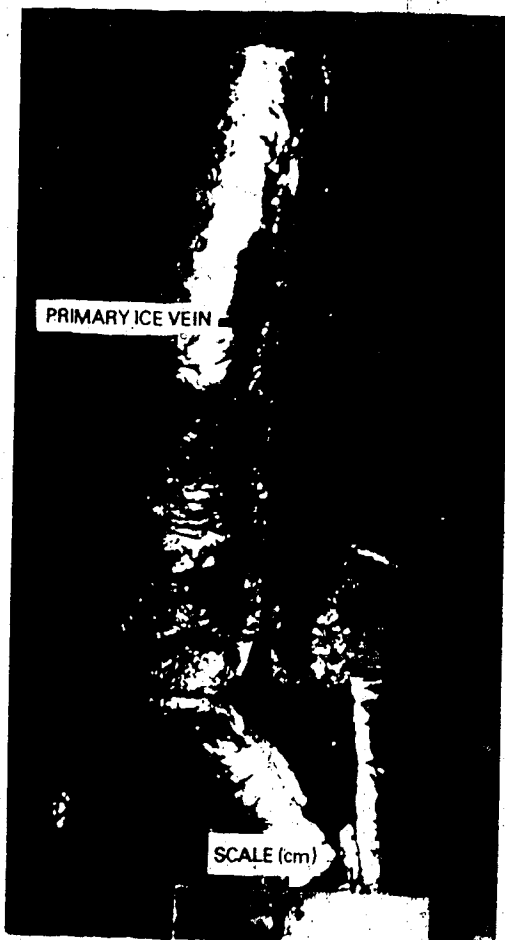


**PLATE 5.1:** Post-failure appearance of creep test 3 (GB1 Core 57).



**PLATE 5.2:** Post-failure appearance of creep test 3 (GB1 Core 57). Failure planes generally follow the soil-ice interfaces of primary ice veins, with relatively little shear through frozen soil.

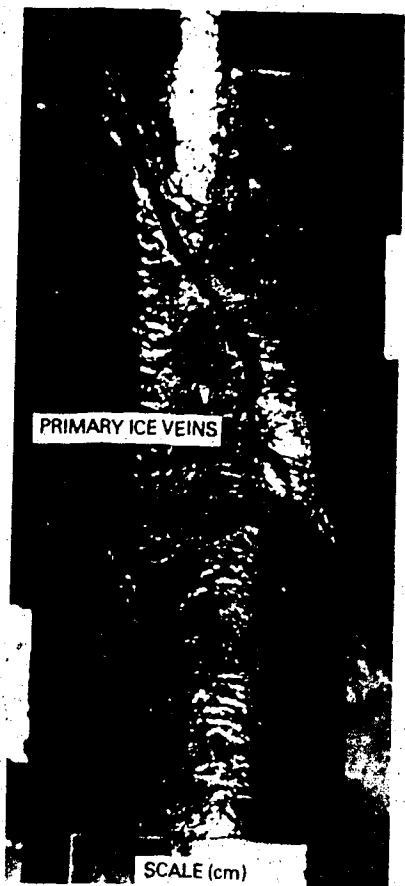


**PLATE 5.3:** Post-failure appearance of test 4 (GB1 Core 56). Failure plane follows the soil-ice interface of a primary ice vein.

**PLATE 5.4:** Post-failure appearance of creep test 5 (GB1 Core 58). The shear plane cuts through frozen soil at the top and bottom of the sample, but follows soil-ice interfaces of the primary ice vein through the middle portion of the sample.

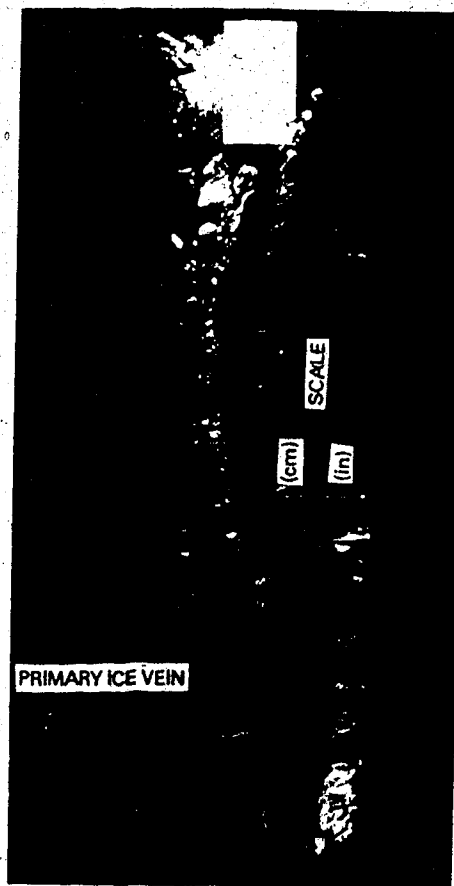


**PLATE 5.5:** The post-failure condition of creep test 5 (GB1 Core 58) indicates some deformation took place along secondary ice veins, leaving the sample with a blocky appearance.

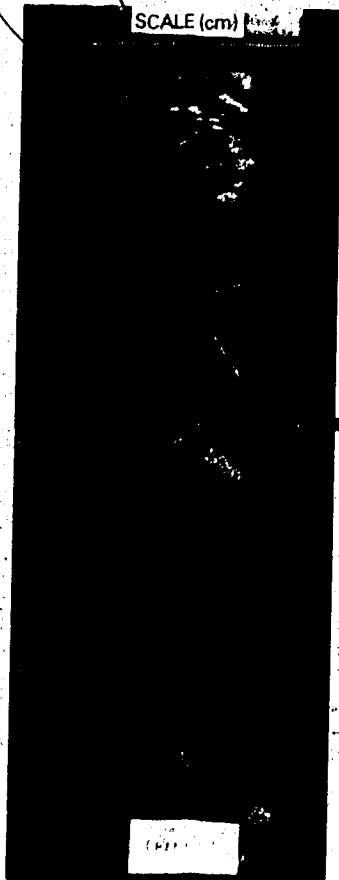
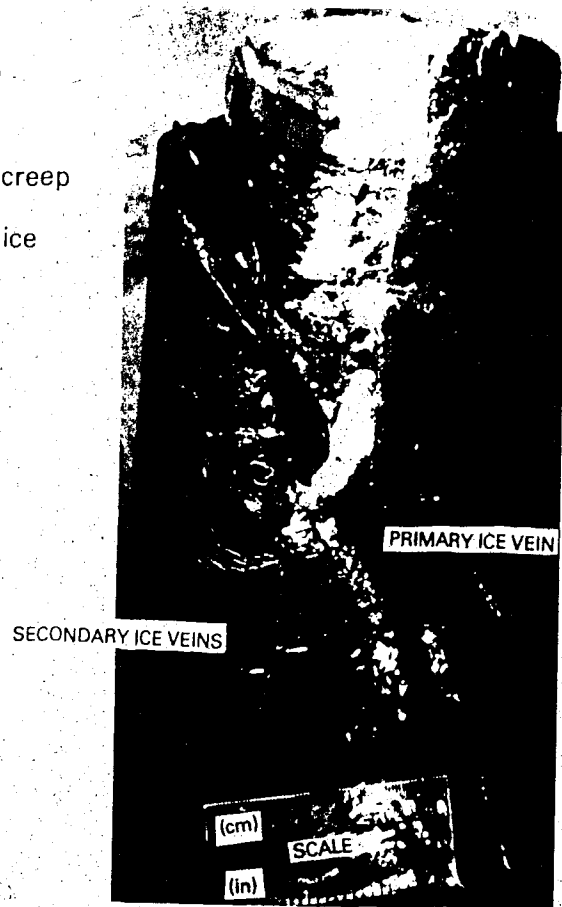


**PLATE 5.6:** Creep test 9 (GB1 Core 43) prior to assembly.

SECONDARY ICE VEIN SHOWN IN PLATE 5.8



**PLATE 5.7:** Post-failure condition of creep test 6 (GB1 Core 38). Deformation is evident along most secondary ice veins imparting a blocky, post-failure appearance. Shear planes developed as deformation along secondary ice veins coalesced by shear through frozen soil.

**PLATE 5.8:** Post-failure, close-up view of creep test 9 (GB1 Core 43) showing the magnitude of deformation along a secondary ice vein not associated with the main failure planes.

SECONDARY ICE VEIN  
(SHOWN PRIOR TO TESTING IN PLATE 5.6)

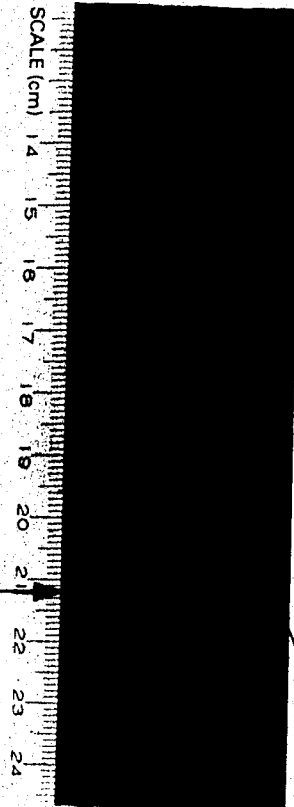




**PLATE 5.9:** Post-failure appearance of creep test 7 (GB1 Core 43).



**PLATE 5.10:** Creep test 12 (GB1 Core 60) prior to assembly.





PLATE 5.11: Post-testing appearance of creep test 12 (GB1 Core 60) — longitudinal view. Vertical ice veins developed during testing, as indicated by comparison with Plate 5.10.



PLATE 5.12: Post-testing appearance of creep test 12 (GB1 Core 60) — cross-sectional view.

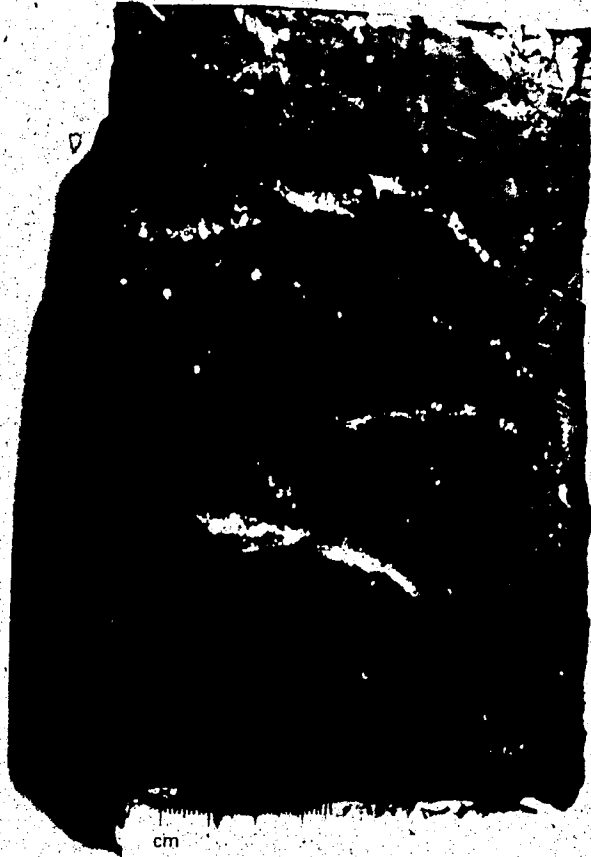
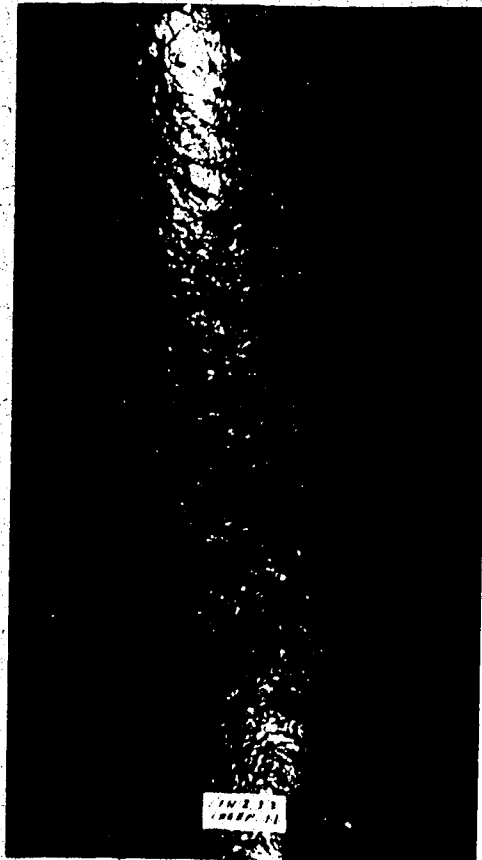


PLATE 5.13: Sample of segregated ice (GB2 Core 4) similar to creep test 11 (GB2 Core 4).

PLATE 5.14: Post-testing appearance of creep test 11. (GB2 Core 4).



1 cm

## CHAPTER VI.

### IN-SITU CREEP ANALYSIS

"Science moves, but slowly slowly,  
Creeping on from point to point." (Tennyson, Locksley Hall)

#### 6.1 Introduction

The results of a plain strain finite element analysis of in situ, steady state creep deformations at the proposed Arctic Gas crossing of Great Bear River are presented in this chapter. In particular, the validity of the simple power law (Equation 5.1) in predicting the form of creep movement, and the accuracy of empirical parameters determined in Chapter V in predicting the magnitude of creep velocities are assessed.

#### 6.2 Finite Element Programme

The finite element programme used in this thesis was developed at the University of British Columbia for non-linear creep analysis of axisymmetric, plane strain and plane stress problems (Emery, 1971). In 1979, the programme was obtained by the University of Alberta from Dr. J.J. Emery, Professor of Civil Engineering, McMaster University. Minor input-output changes were made when the programme was entered into the University of Alberta computer. An instruction manual for the University of Alberta version of the programme has been prepared by Weerdenburg (1979a).

### 6.2.1 Solution Method

The method of analysis used in the finite element programme is known as the direct stiffness or displacement method.

Descriptions of this method may be found in text books on finite element analysis by Zienkiewicz and Cheung (1967), and Desai and Abel (1972).

The analysis of non-linear creep behaviour follows the incremental initial strain procedure. A description of this technique and its development, together with a review of its application in creep behaviour of various soil and rock masses, is given by Weerdenburg (1979b, 1980).

### 6.2.2 Multiaxial Stress-Strain Relations

In order to relate uniaxial creep data to a multiaxial stress condition, it is necessary to formulate multiaxial stress-strain relationships in terms of effective stress ( $\sigma_e$ ) and effective creep strain ( $\epsilon_e^c$ ). Analytical derivations of these effective components from the stress and strain tensors has been described by Odqvist (1966), Greenbaum and Rubinstein (1968), Sutherland (1970) and Weerdenburg (1979b). Using the format given by Sutherland (1970), the following assumptions are made:

1. Creep strain causes no volume change.
2. The hydrostatic state of stress has no affect on creep rate.
3. The principal strain rate and stress tensors are coaxial.

4. The stress-strain relationship for the multiaxial state of stress reduces to a uniaxial relationship for a uniaxial loading conditions.

Stress-strain relationships which satisfy these conditions are as follows:

$$\Delta \epsilon_{ij}^c = \frac{3}{2} \frac{\Delta \epsilon_e^c}{\sigma_e} \sigma'_{ij} \quad [6.1]$$

where the effective stress ( $\sigma_e$ ), the effective incremental creep strain ( $\Delta \epsilon_e^c$ ) and the stress deviator tensor  $\sigma'_{ij}$  are defined by:

$$\sigma_e = \sqrt{\frac{3}{2} \sigma'_{ij} \sigma'_{ij}} \quad [6.2]$$

$$\Delta \epsilon_e^c = \sqrt{\frac{2}{3} \Delta \epsilon_{ij}^c \Delta \epsilon_{ij}^c} \quad [6.3]$$

$$\sigma'_{ij} = \sigma_{ij} - \frac{1}{3} \delta_{ij} \sigma_{kk} \quad [6.4]$$

These stress-strain relationships indicate effective stress and effective incremental creep strain are equivalent to uniaxial stress and creep strain, and hence constitutive relations derived from uniaxial creep tests can be expressed in terms of effective components. In general, the effective incremental creep strain is a function of the effective stress ( $\sigma_e$ ), the total effective creep strain ( $\epsilon_e^c$ ), the temperature ( $T$ ), time ( $t$ ), and the strain history of the material. The generalized form of this relation is as follows:

$$\Delta \epsilon_e^c = f(\sigma_e, \epsilon_e^c, T, t) \quad [6.5]$$

In chapter 5 it was shown that the specific form of this relation is that of the simple power law given in Equation 5.1.

### 6.2.3 Solution Technique.

The solution technique described by Greenbaun and Rubinstein (1968), Emery (1971) and Weerdenburg (1979b) is summarized in the following paragraph.

The solution of the creep problem begins with an elastic solution under the imposed boundary conditions. At time zero, the elastic solution is used as the starting point for the creep solution. In the first and subsequent time increments the solution procedure follows five basic steps:

1. The effective stress ( $\sigma_e$ ) is determined from the stresses ( $\sigma_{ij}$ ) accumulated to the end of the previous time increment, or defined by the elastic solution in the first time increment. The stresses are assumed constant throughout the small time increment.
2. The effective stress ( $\sigma_e$ ) is substituted into an empirical relation of the general form given by Equation (6.2) to determine the effective incremental creep strain ( $\Delta\epsilon_e^c$ ).
3. The effective incremental creep strain ( $\Delta\epsilon_e^c$ ) is expressed in terms of creep strain increments in each direction ( $\Delta\epsilon_{ij}^c$ ).

4. The directional creep strain increments ( $\Delta\epsilon_{ij}^c$ ) are treated as initial strains, and using appropriate constitutive equations, boundary conditions and equilibrium equations, the incremental stresses ( $\Delta\sigma_{ij}$ ) at the end of the time interval are calculated.
5. The incremental stresses ( $\Delta\sigma_{ij}$ ) from the current time interval are added to initial stresses ( $\sigma_{ij}$ ) at the beginning of the current time interval to obtain a new stress distribution to be used in step 1 of the next time interval.

These steps are repeated for each time interval until either the final time is reached or until a steady state condition is achieved where  $\Delta\sigma_{ij} \rightarrow 0$ .

#### 6.2.4 Time Increment Determination

Stresses change very rapidly in the early stages of the creep analysis and it is necessary to select very small time increments in order to satisfy the assumption that stresses remain approximately constant through a single time increment. The time increment is then increased as the solution approaches a steady state condition (Greenbaun and Rubinstein, 1968).

Experience reported by Sutherland (1970), Emery (1971) and Weerdenburg (1980) showed that the maximum time increment was such that the change in effective incremental creep strain could not exceed the total elastic strain; where this limit was exceeded, the numerical solution diverged from the correct solution.



On the basis of this experience the first time increment is found by setting the initial effective incremental creep strain ( $\Delta \epsilon_e^c$ ) equal to 1/25 the maximum value of the effective elastic strain ( $\epsilon_e^e$ ) max., i.e.

$$\frac{\Delta \epsilon_e^c}{(\epsilon_e^e)_{\max}} \leq \eta \quad [6.6]$$

where  $\eta = 1/25$

Subsequent time intervals ( $\Delta t_{i+1}$ ) are computed on the basis of a fractional change in the current or first time increment ( $\Delta t_i$ ), i.e.

$$\Delta t_{i+1} \leq 1.2 \Delta t_i \quad [6.7]$$

In the new time increment, the ratio of strains from Equation 6.6 is checked using  $\eta = .1$  (Weerdenburg, 1980).

### 6.3 Finite Element Mesh

The finite element mesh is based on the stratigraphic cross-section in Figure 3.2. The mesh used is shown in Figure 6.1.

The following criteria were considered in mesh design:

1. Only the sand and clay lithofacies were discretized; the sand and clay were classified as material 1 and material 2 respectively. Creep movements were reported in the till lithofacies (Chapter 4), however those occurring in till in GB2 were transverse-to-slope and could not be considered in this plane strain analysis, and those occurring in till in GB3 were too localized to warrant integration into the analysis. Contacts between the

three major Quaternary lithofacies were simplified for the purposes of this analysis. Therefore, actual contacts differ slightly from those of the finite element grid at the GB1A, GB2 and GB3 test hole locations.

2. Triangle aspect ratios were kept as low as possible.
3. Finer mesh divisions were used through the clay lithofacies and in regions where high stress gradients were anticipated.
4. The mesh length was greater than the length of the slope and several times the slope height.

#### 6.4 Boundary Conditions

Boundary conditions are illustrated in Figure 6.1. Pin-type constraints were used as basal boundaries because of the expected high in situ modulus of the till lithofacies and the fact that generally little or no deformation occurred through the till in the parallel-to-slope inclinometer profiles. Side boundaries consisted of roller-type constraints and the surface boundary was stress free.

#### 6.5 Material Properties

Bulk unit weights were assigned on the basis of core examination reported in Chapter 3. Mean values assigned for the sand and clay lithofacies are shown in Figure 6.1.

Elastic values for the sand and clay lithofacies were defined on the basis of data reported at similar temperatures over a similar stress range. The values shown in Figure 6.1 were obtained from

Tsytoovich (1975) for an assumed average temperature of  $-2^{\circ}\text{C}$ .

Creep properties for the sand and clay lithofacies were varied in order to obtain the best approximation of observed in situ behaviour. These properties are given in subsequent sections where the creep analyses are discussed.

## 6.6 Elastic Analysis

The elastic parameters shown in Figure 6.1 were used in each creep analysis, and hence the initial elastic solution was common for each creep analysis.

The results of this elastic solution are presented here for purposes of comparison with steady state creep solutions in later sections. The orientation and sense of the principal elastic stresses is shown in Figure 6.2. Effective stress contours from the elastic solution are illustrated in Figure 6.3.

## 6.7 First Creep Analysis - Uniform Creep Properties

### 6.7.1 Material Properties

It was concluded in Chapter 5 that the constitutive relation describing steady state creep behaviour in polycrystalline ice (Morgenstern et. al., 1979) represents an approximate upper bound for creep deformations in ice-rich, fine-grained permafrost soil. Although this was expected to overestimate the in situ creep rate, of the clay lithofacies it was considered the best creep relation to use for an initial evaluation of in situ behaviour. The creep parameters for this relation are shown in Figure 5.7. These include

an exponent of 3.0 and a coefficient of  $2.0 \times 10^{-8}$  year kPa<sup>3</sup>.

The selection of a suitable constitutive relation for the sand lithofacies was more difficult. Creep in the clay lithofacies was expected to cause tensile stresses in the overlying sand. Review of available creep data from similar reconstituted sands left doubt as to whether or not the sand would creep under small compressive stresses (Section 5.3), but, under the influence of tensile stresses, it was assumed the sand would creep. Since all tensile stresses would be transmitted through the ice phase, and since the creep properties of polycrystalline ice are similar in tension and compression (Steinman 1954, 1958), the creep relation and parameters for polycrystalline ice were also used to obtain the sand lithofacies for an initial evaluation of in situ behaviour.

#### 6.7.2 Results of the First Creep Analysis

Creep velocities predicted by the preliminary finite element analysis for each of the GB1A, GB2 and GB3 inclinometer casings are shown in Figures 6.4, 6.5, and 6.6 respectively. A-direction velocity data for each of the inclinometers are also plotted on these diagrams.

The predicted velocity profiles for the GB1A and GB3 (Figures 6.4 and 6.6 respectively) inclinometer casings indicate generally good agreement in form with the observed velocity profiles, however the magnitude of the predicted velocities is approximately six times greater than those observed. There appears to be no correspondence between measured and predicted values for the GB2 (Figure 6.5)

inclinometer casing. Field velocity data for the GB2 inclinometer casing are not considered reliable indicators of creep velocities because of drilling, sampling, instrumentation and monitoring difficulties, and evidence of in situ shear planes through the soil profile (Sections 3.4.3 and 4.4.4). Therefore, critical assessment of the finite element results is limited to the GB1A and GB3.

The close agreement in form between the observed and predicted velocity profiles for the GB1A and GB3 inclinometer casings indicates that in situ behaviour of the material is accurately represented by a simple power law of the form given in Equation 5.1. Although the magnitude of the observed and predicted velocity profiles differ, the difference is a constant factor, and hence a proportional change in the coefficient of the creep relation is sufficient to facilitate agreement between the two profiles in both form and magnitude.

## 6.8 Second Creep Analysis - Uniform Creep Properties

### 6.8.1 Material Properties

In order to confirm that any change in the coefficient in the creep relation would have a proportional change in the magnitude of the velocity profile, a second creep analysis was carried out. In the first analysis a coefficient of  $2.0 \times 10^{-8}$  year  $\text{kPa}^3$  provided velocities which were approximately six times greater than observed velocities. Therefore, in the second creep analysis it was decided to use a coefficient of  $0.33 \times 10^{-8}$  year  $\text{kPa}^3$ , or one sixth the original value. This new coefficient was used in both the

sand and clay lithofacies. The exponent value in the creep relation was left at 3.0 in both lithofacies. The creep relations from the first and second creep analyses are compared in Figure 6.7.

#### 6.8.2 Results of the Second Creep Analysis

Creep velocities predicted by the second finite element analysis are shown in Figures 6.4, 6.5, and 6.6 for the GB1A, GB2 and GB3 inclinometer casings respectively. The predicted velocity profile in GB1A (Figure 6.4) corresponds closely with the observed velocity profile through the clay lithofacies. Through the sand lithofacies, however there appears to be little similarity; this is attributed to drilling and grouting difficulties (Section 3.4.3). The predicted velocity profile in GB3 (Figure 6.6) is also in close agreement with observed velocities, although some discrepancy exists in the top 2 to 3 m because of the influence of the steel casing (Section 4.4.9). There appears to be little correspondence between measured and predicted velocities in GB2 (Figure 6.5), as discussed in Section 6.7.2.

Accumulated creep deformations after a one year period are shown over the original finite element grid in Figure 6.8. Contours of effective stress for steady state creep are shown in Figure 6.9.

Data from the second creep analysis indicate that the steady state creep equation

$$\dot{\epsilon} = 0.33 \times 10^{8.0} \sigma^{3.0}$$

[6.8]

accurately represents in situ creep behaviour through the ice-rich glaciolacustrine clay lithofacies. Through the glaciodeltaic sand lithofacies in GB1A (Figure 6.4) there is much less agreement.

Although this discrepancy is attributed to drilling and grouting difficulties, there remains some doubt as to the validity with which Equation 6.8 represents creep deformation in the sand, and indeed, whether the sand actually creeps or not. In an attempt to gain further insight into these factors, a third creep analysis was undertaken in which the sand was not allowed to creep.

### 6.9 Third Creep Analysis - Creep in Glaciolacustrine Clay Lithofacies Only

#### 6.9.1 Material Properties

The third creep analysis was carried out to investigate the condition where movements in the glaciodeltaic sand were limited to elastic deformation. Elastic properties of the sand lithofacies were consistent with those described in Section 6.3. Creep properties of the clay lithofacies were similar to the second creep analysis, as given in Equation 6.8.

#### 6.9.2 Results of the Third Creep Analysis

Predicted velocity profiles for the GB1A, GB2, and GB3 inclinometer casings are shown in Figures 6.4, 6.5, and 6.6 respectively. Accumulated creep deformations after a one year period are shown over the original finite element grid in Figure

6.10. In general, limiting the sand to elastic deformation, appears

to retard creep deformations in the clay lithofacies. This influence is most pronounced beneath the complete glaciodeltaic sand lithofacies (Figure 6.10), and decreases beneath the Great Bear River Valley slope, where the sand thins and ultimately pinches out. The resulting deformation pattern suggests the clay lithofacies is being extruded. Predicted velocity profiles for the GB1A and GB2 inclinometer casings do not appear to correspond in form or magnitude to observed velocities. The predicted velocity profile from the third creep analysis for the GB3 inclinometer casing shows good agreement with both the results of the second creep analysis and the observed velocity profile, but this appears to be because it is largely beyond the influence of the sand lithofacies which pinches out at least 35 m upslope.

On the basis of comparison between predicted and observed velocity data, it appears that limiting the sand to elastic deformation does not accurately represent in situ creep behaviour. This conclusion also emerges from examination of effective stress and horizontal stress distribution for steady state creep in Figures 6.11 and 6.12. Figure 6.10 indicates very high effective stresses develop in the sand lithofacies. This is likely a result of the high tensile horizontal stress build up through the sand lithofacies as this medium restricts steady state deformation of the underlying clay lithofacies. The magnitude of the tensile horizontal stresses suggests that failure would propagate through the glaciodeltaic sand before effective stresses reached those shown in Figure 6.11.



#### 6.10 Assessment of Results

The results of the finite element analysis indicate that in situ creep behaviour in ice-rich glaciolacustrine clay at the proposed Arctic Gas crossing of Great Bear River is adequately represented by a simple power law of the form given in Equation 5.1. This relation also appears to be satisfactory as a first approximation for creep behaviour of the glaciodeltaic sand, although further information is required in order to confidently and accurately represent its deformation behaviour under tensile stress conditions.

Creep parameters which provide the best fit between predicted and observed data are given in Equation 6.5. The exponent is the same as that of polycrystalline ice (Morgenstern et. al., 1979), while the coefficient is lower by a factor of six. These data support predictions made on the basis of laboratory analysis in Section 5.5.8.)

Treating the sand lithofacies as an elastic medium appears to be an incorrect approximation. It is likely that the clay lithofacies creeps at a faster rate than the sand. The build up of tensile stresses as a result of this condition would, in all likelihood, lead to failure in the sand. Therefore, inclusion of a failure criterion in the sand lithofacies appears to be a requirement in order to accurately model in situ behaviour.

Extension of the finite element analysis to this capacity is beyond the scope of this thesis, but it is recommended as a fruitful area for further research.

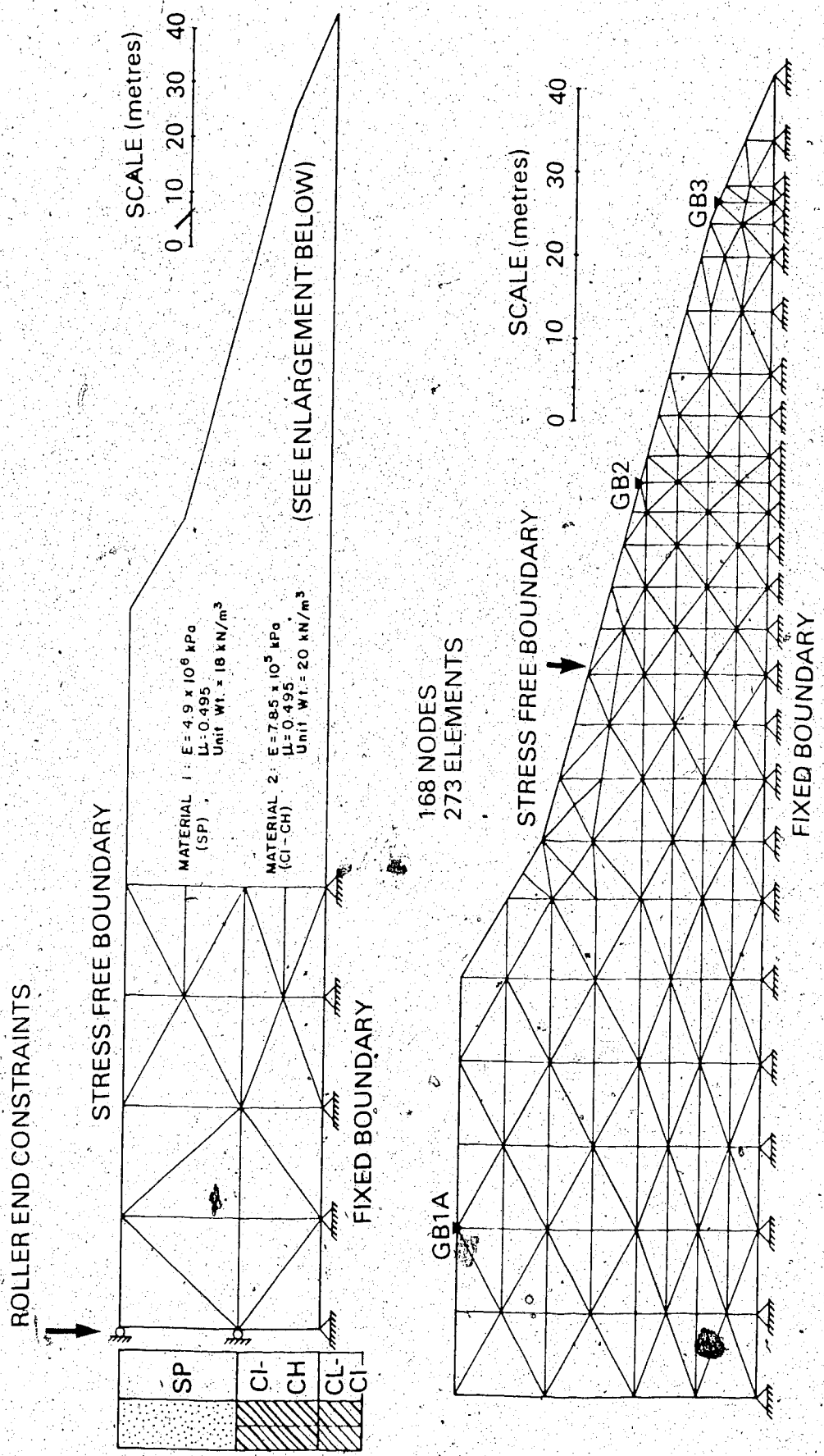
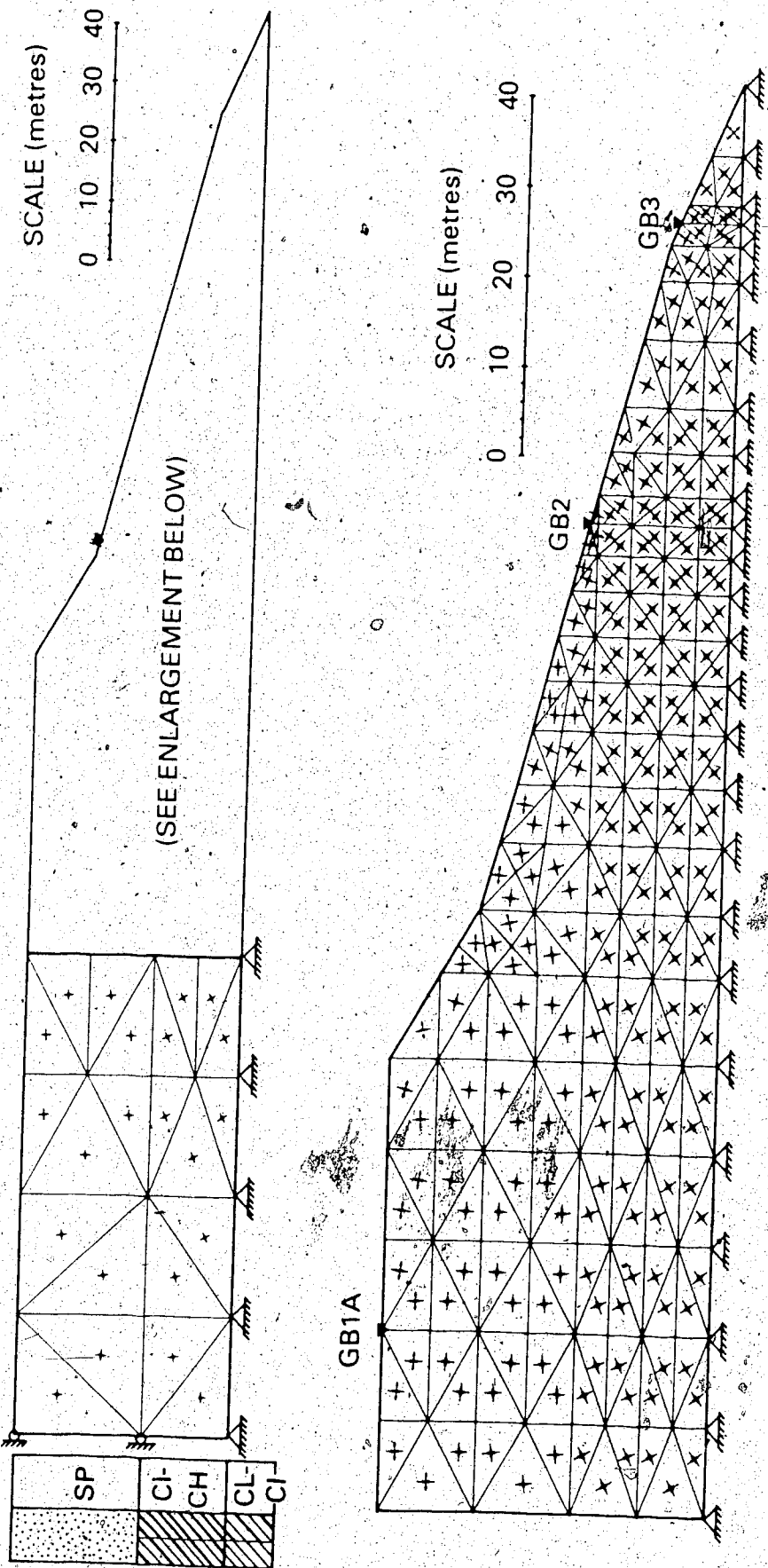


FIGURE 6.1: FINITE ELEMENT MESH



**FIGURE 6.2: ORIENTATIONS OF PRINCIPAL STRESSES FOR ELASTIC SOLUTION UNDER GRAVITY LOADING**

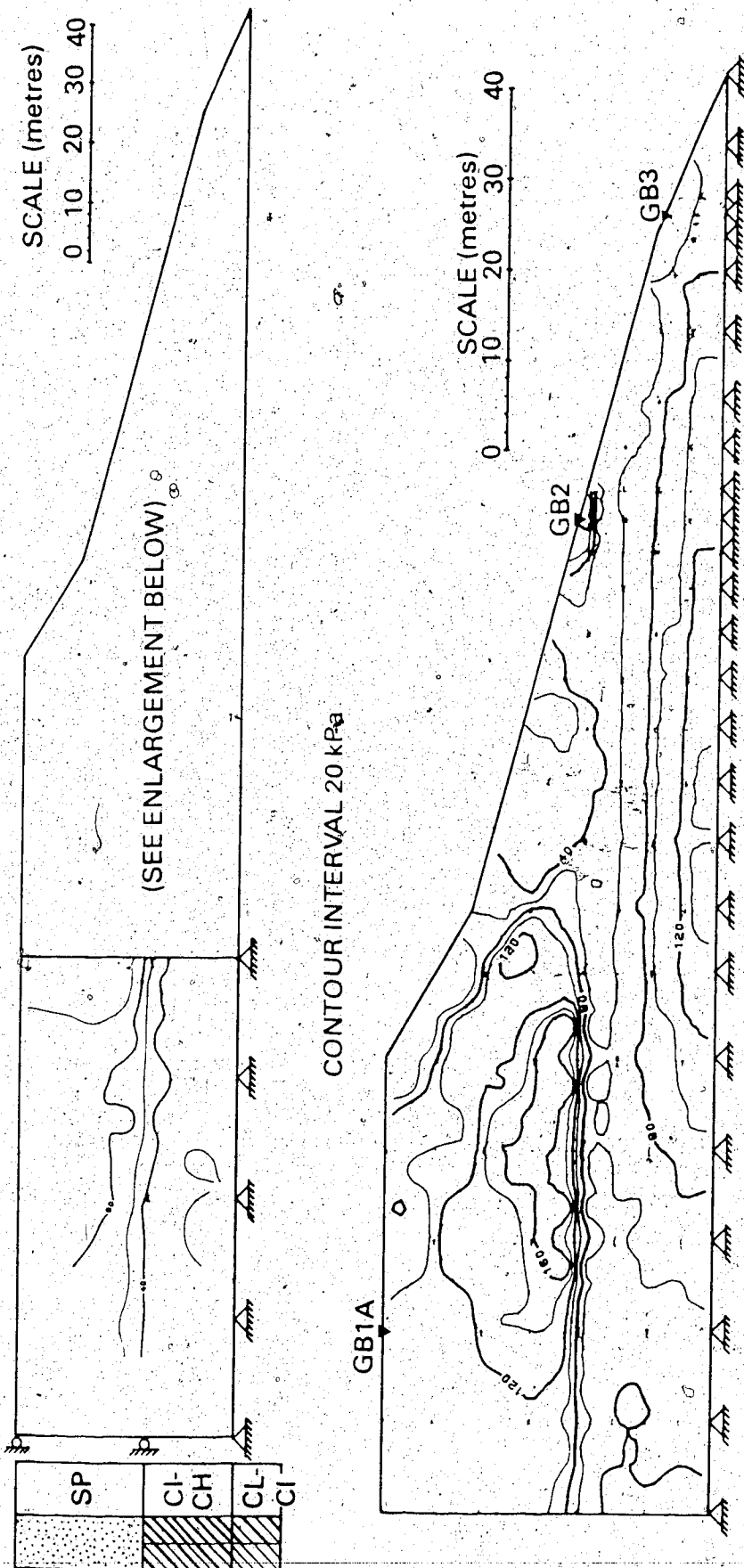
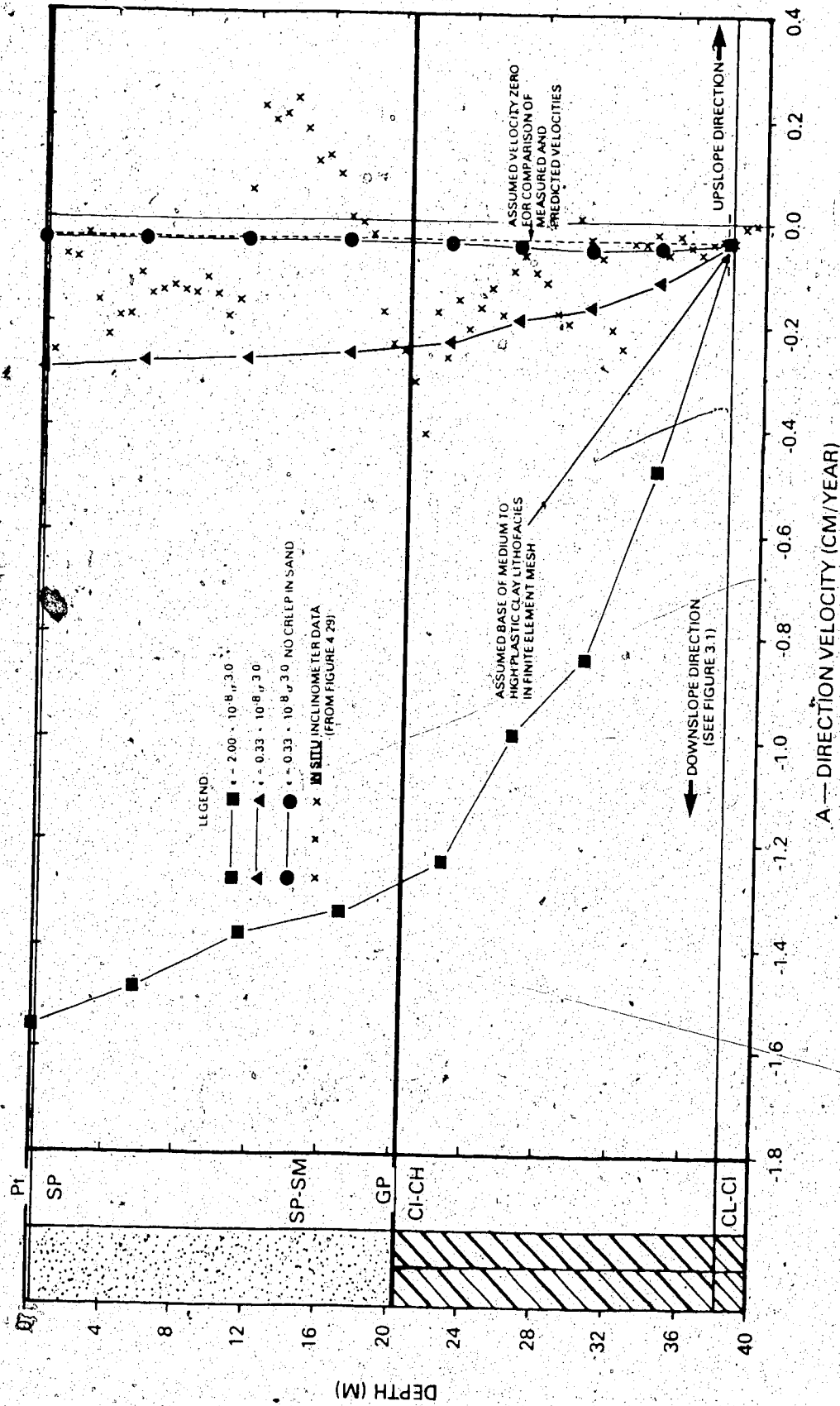


FIGURE 6.3: CONTOURS OF EFFECTIVE STRESS (ODQVIST, 1966) FOR ELASTIC SOLUTION UNDER GRAVITY LOADING



**FIGURE 6.4: COMPARISON OF MEASURED AND PREDICTED STEADY STATE CREEP VELOCITIES IN TEST HOLE GB1A**

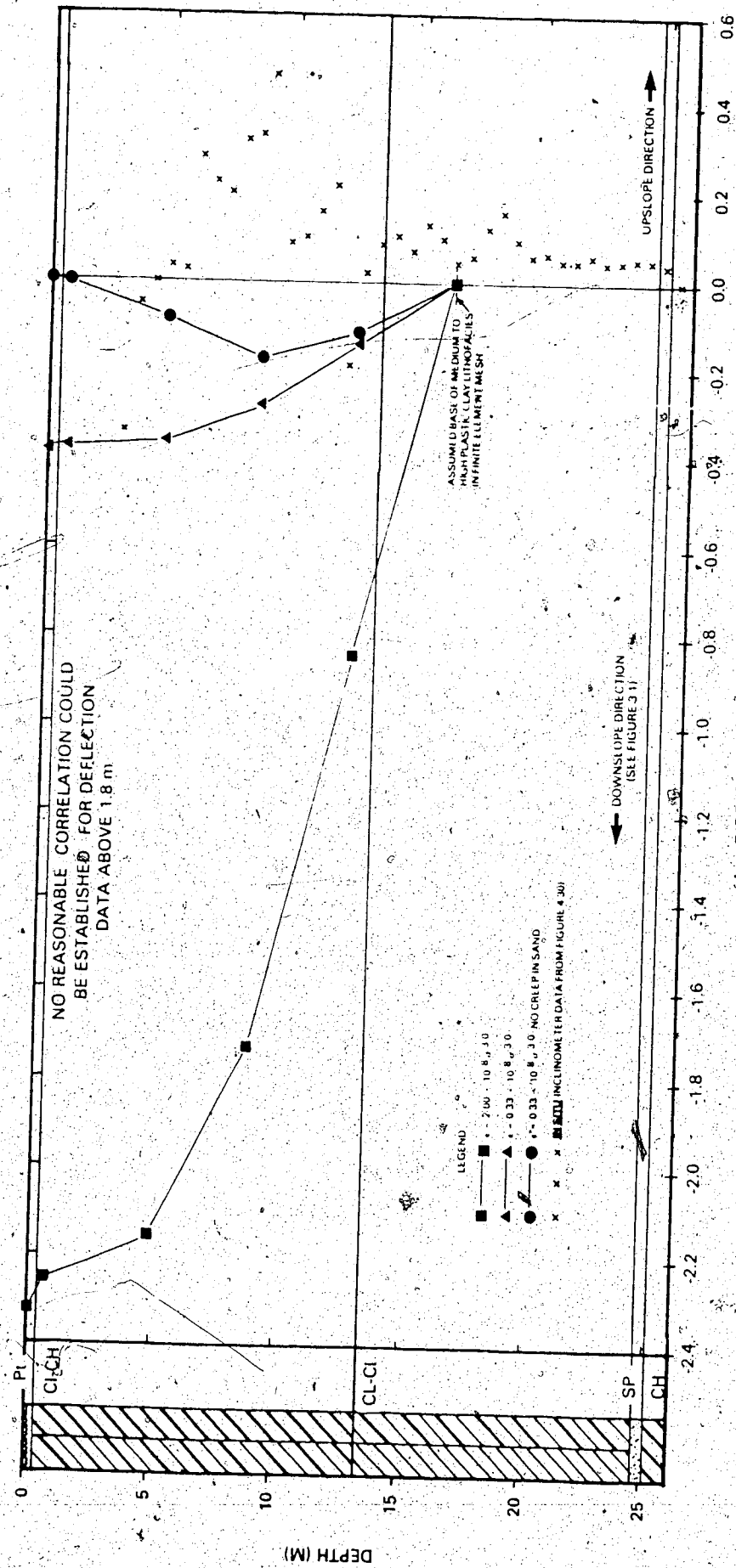


FIGURE 6.5: COMPARISON OF MEASURED AND PREDICTED STEADY STATE CREEP VELOCITIES IN TEST HOLE GB2

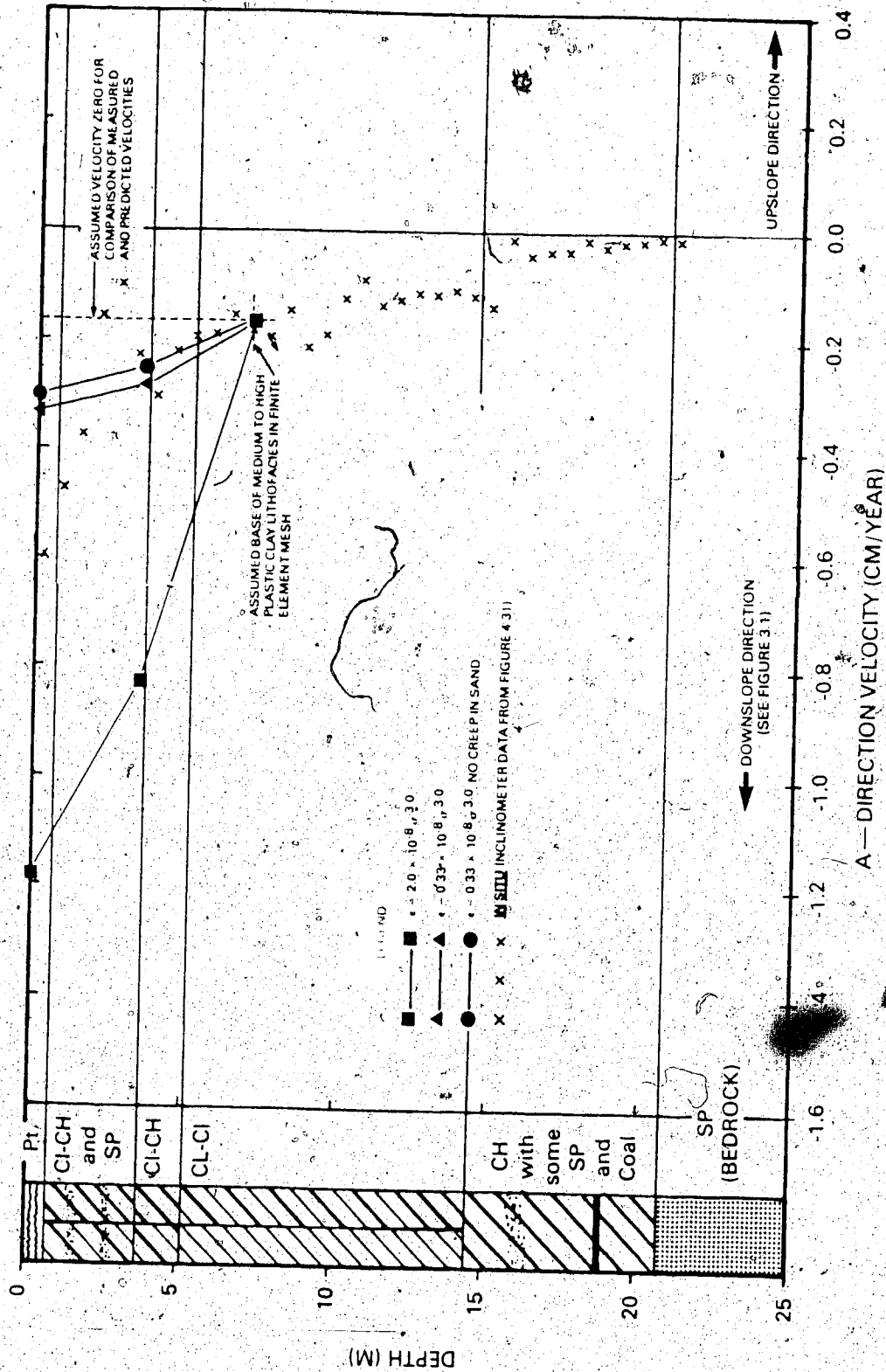


FIGURE 6.6: COMPARISON OF MEASURED AND PREDICTED STEADY STATE CREEP VELOCITIES IN TEST HOLE GB3

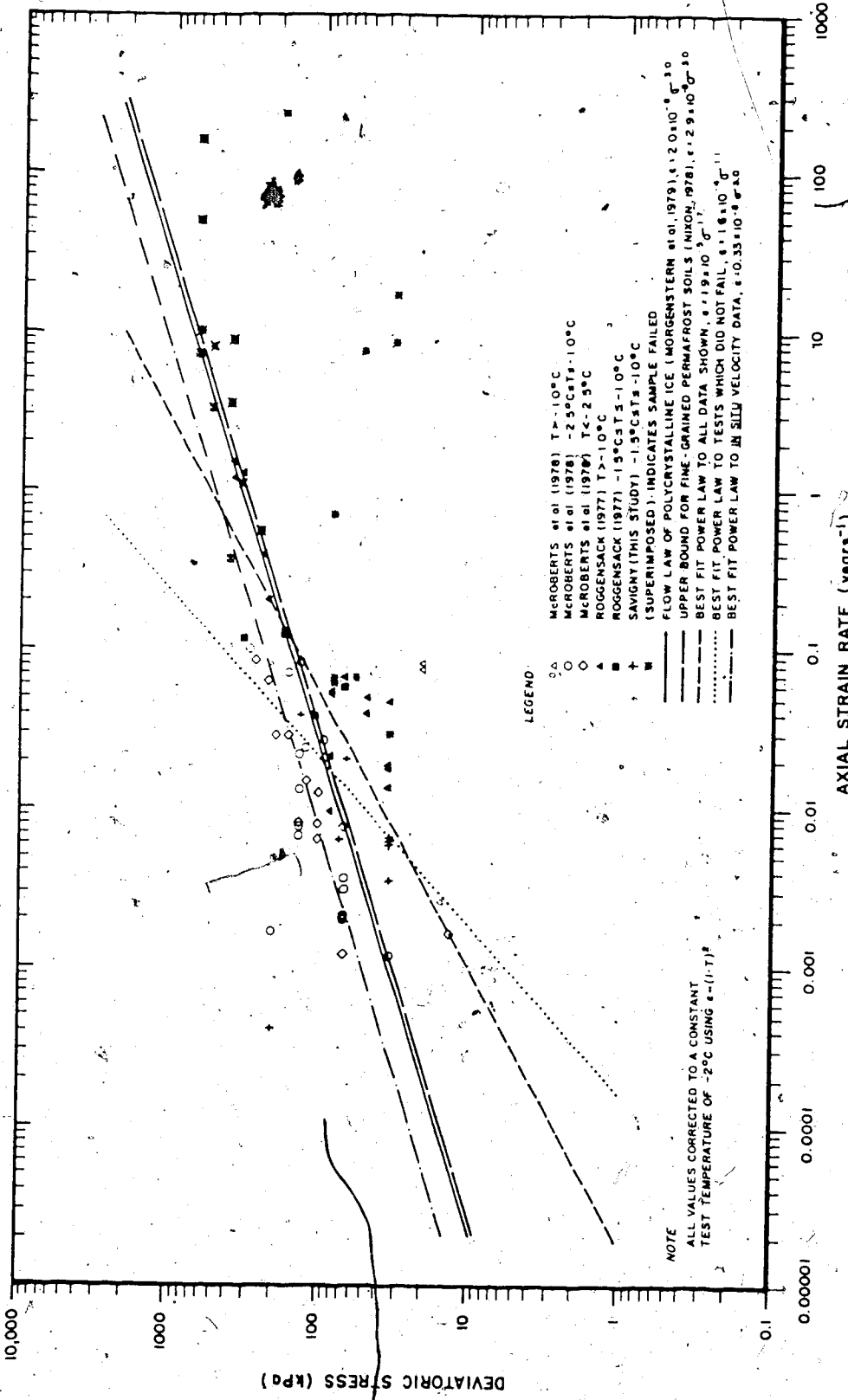
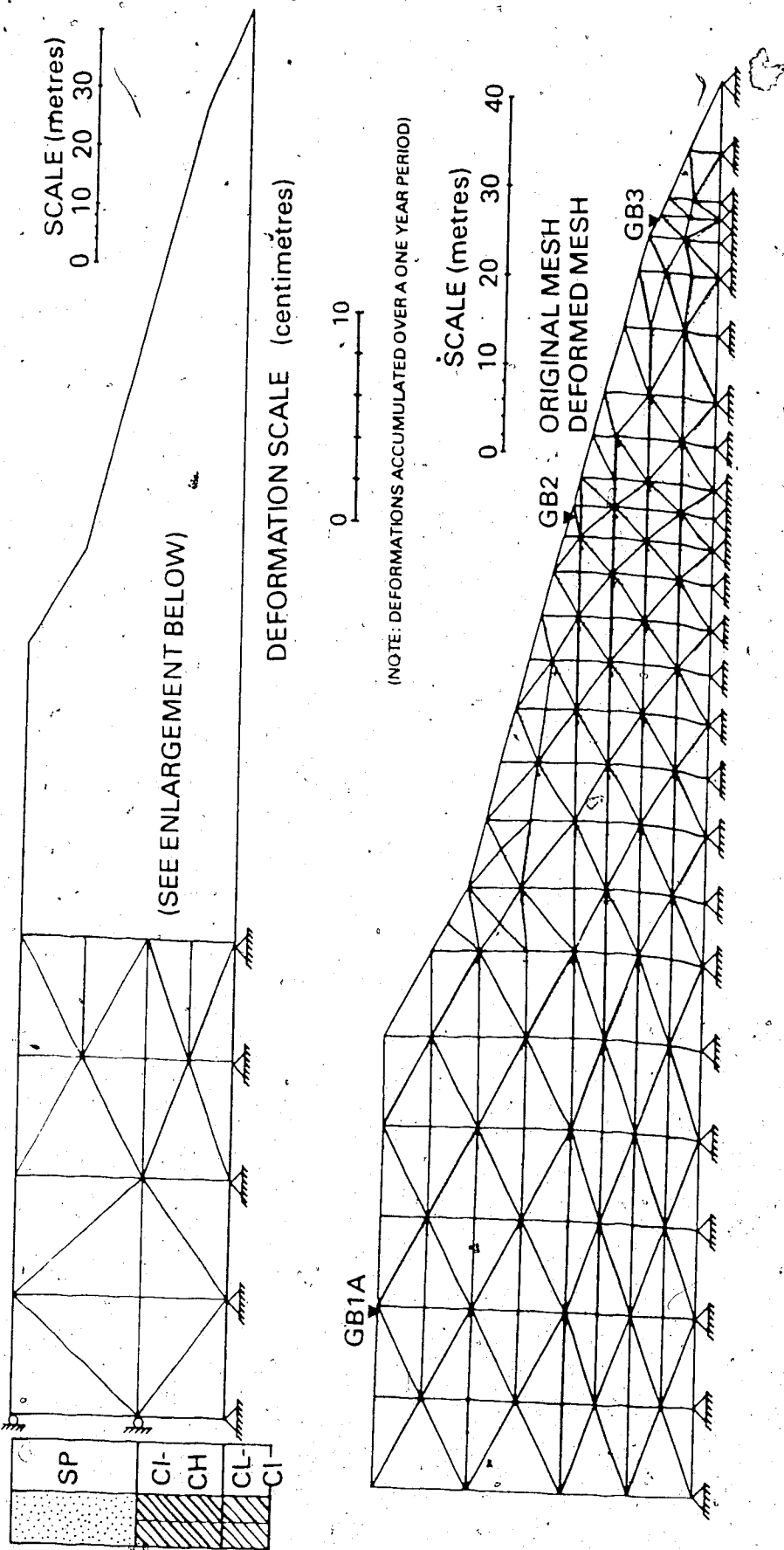
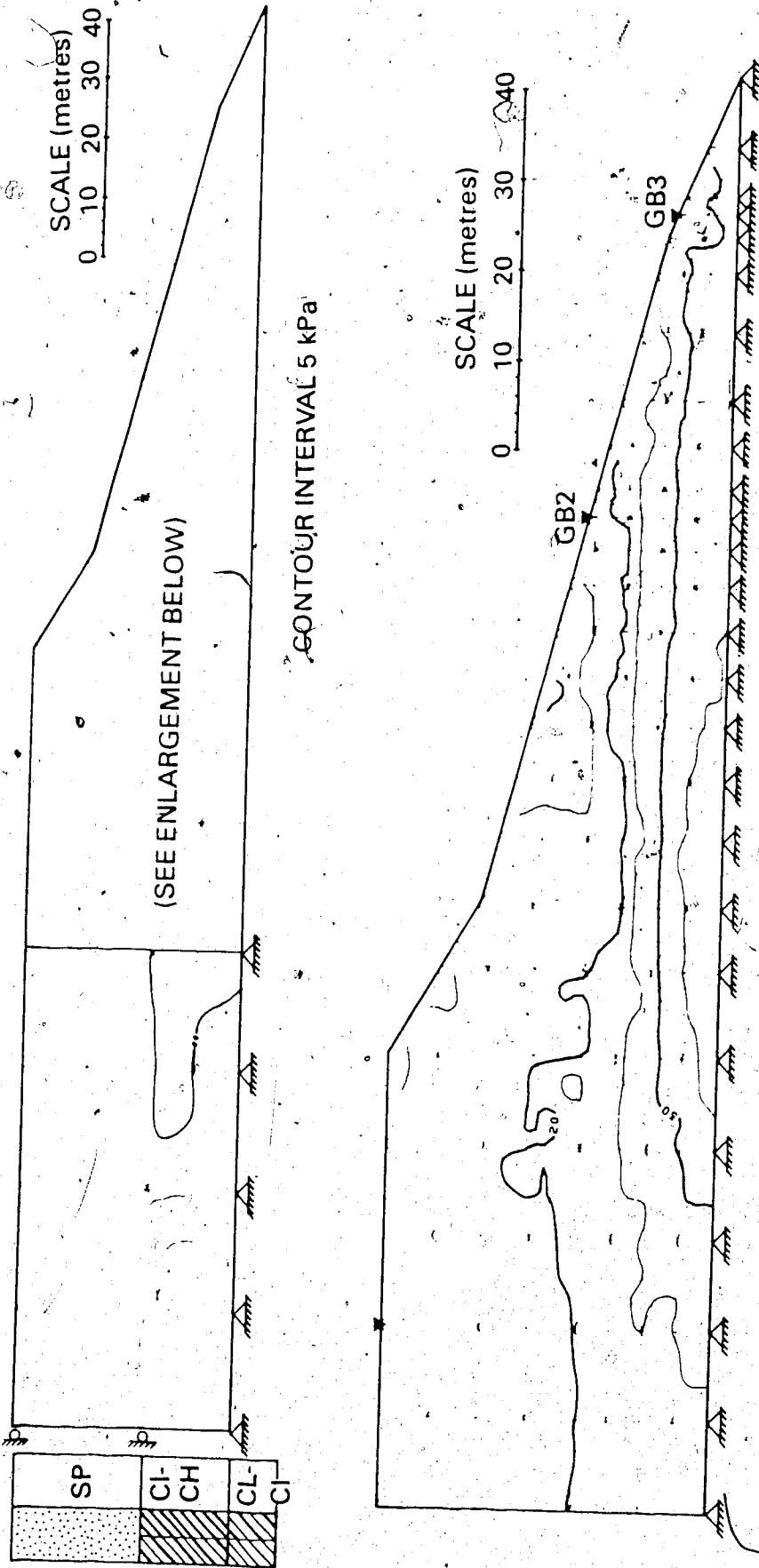


FIGURE 6.7: COMPARISON OF CREEP RELATIONS USED IN NUMERICAL ANALYSIS





**FIGURE 6.8: DEFORMED GRID FOR STEADY STATE CREEP IN BOTH THE SAND AND THE MEDIUM TO HIGH PLASTIC CLAY LITHOFACIES**



**FIGURE 6.9: CONTOURS OF EFFECTIVE STRESS (ODQVIST, 1966) FOR STEADY STATE CREEP IN BOTH THE SAND AND THE MEDIUM TO HIGH PLASTIC CLAY LITHOFACIES**

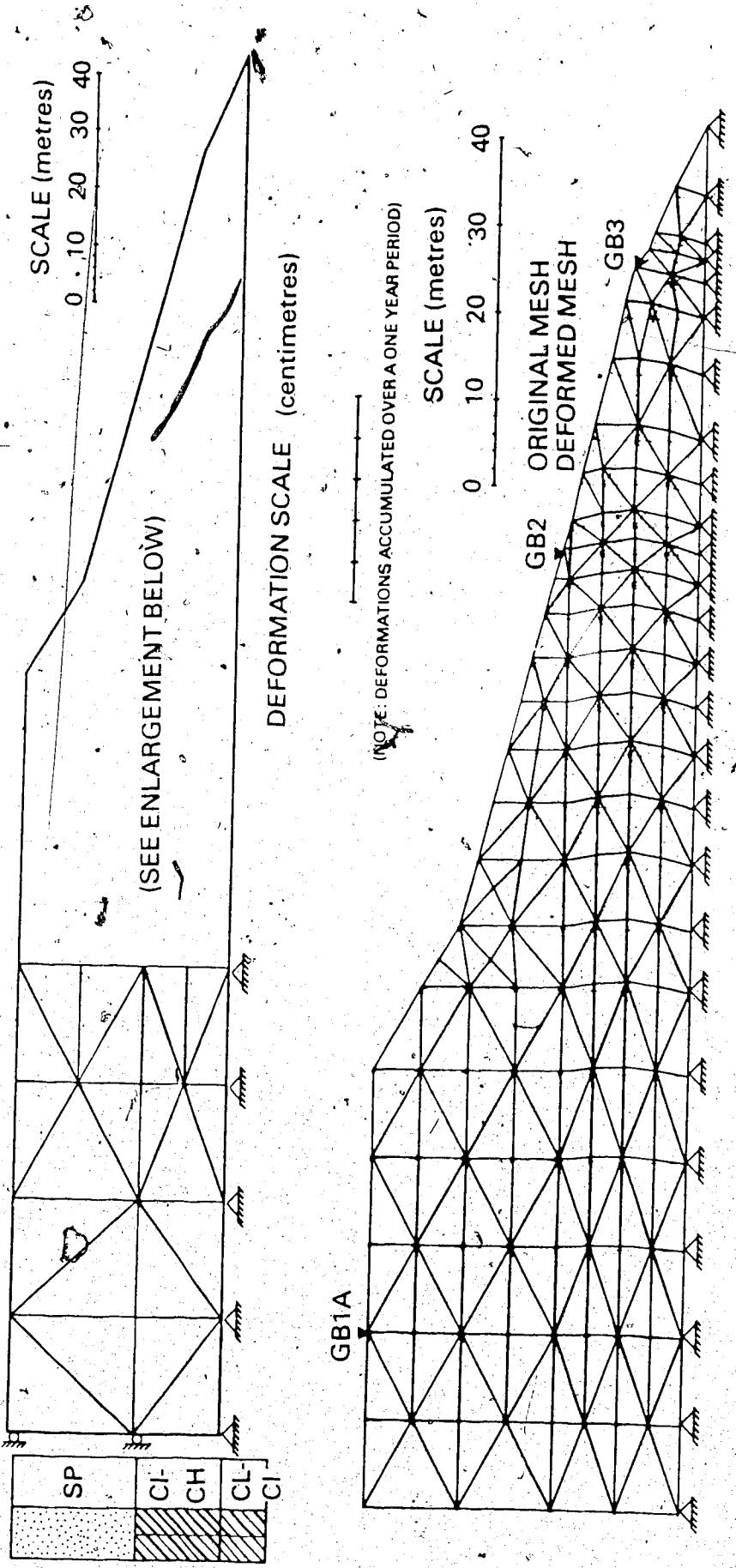
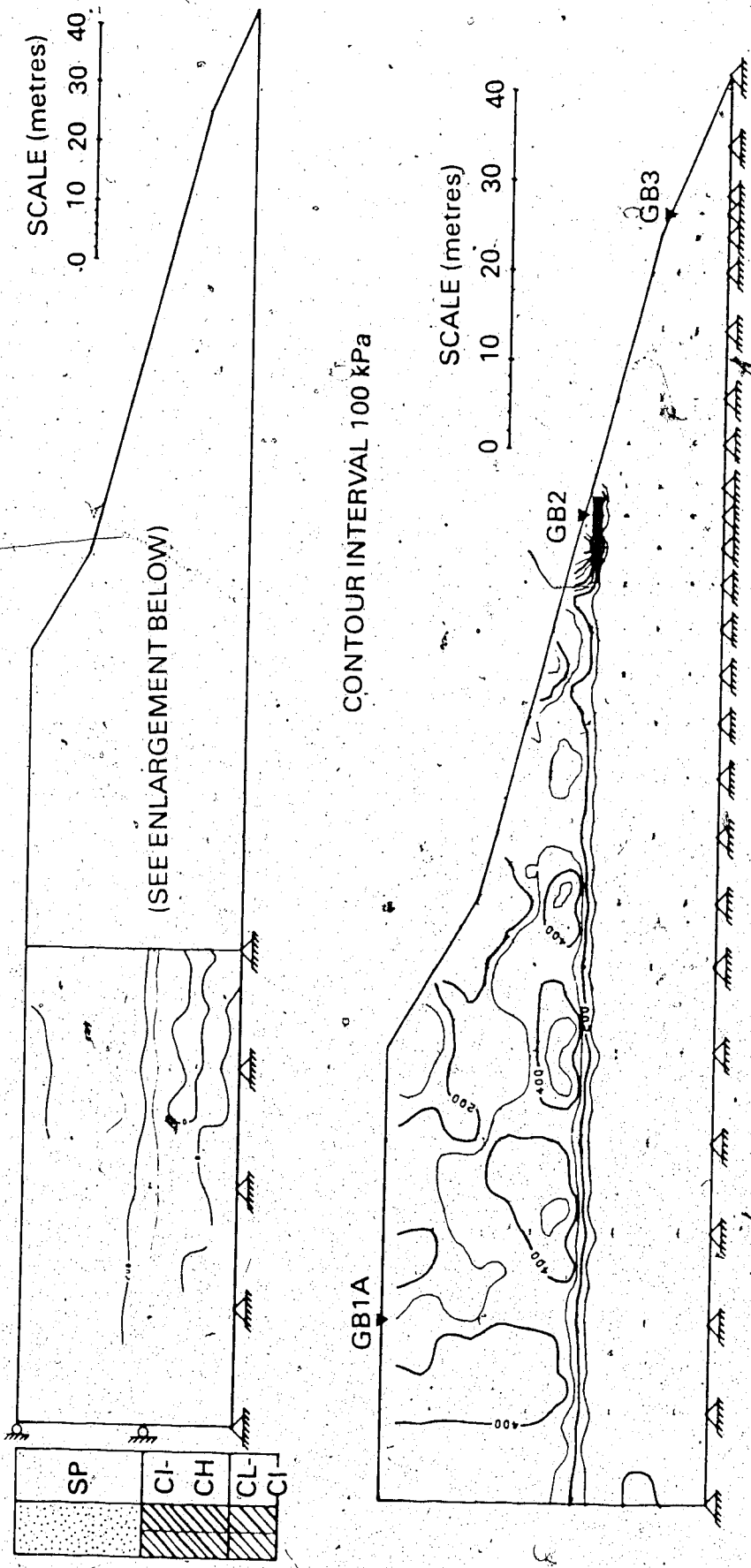


FIGURE 6.10: DEFORMED GRID FOR STEADY STATE CREEP IN THE MEDIUM TO HIGH PLASTIC CLAY LITHOFACIES ONLY



**FIGURE 6.11: CONTOURS OF EFFECTIVE STRESS (ODQVIST, 1966) FOR STEADY STATE CREEP IN THE MEDIUM TO HIGH PLASTIC CLAY LITHOFACIES ONLY**

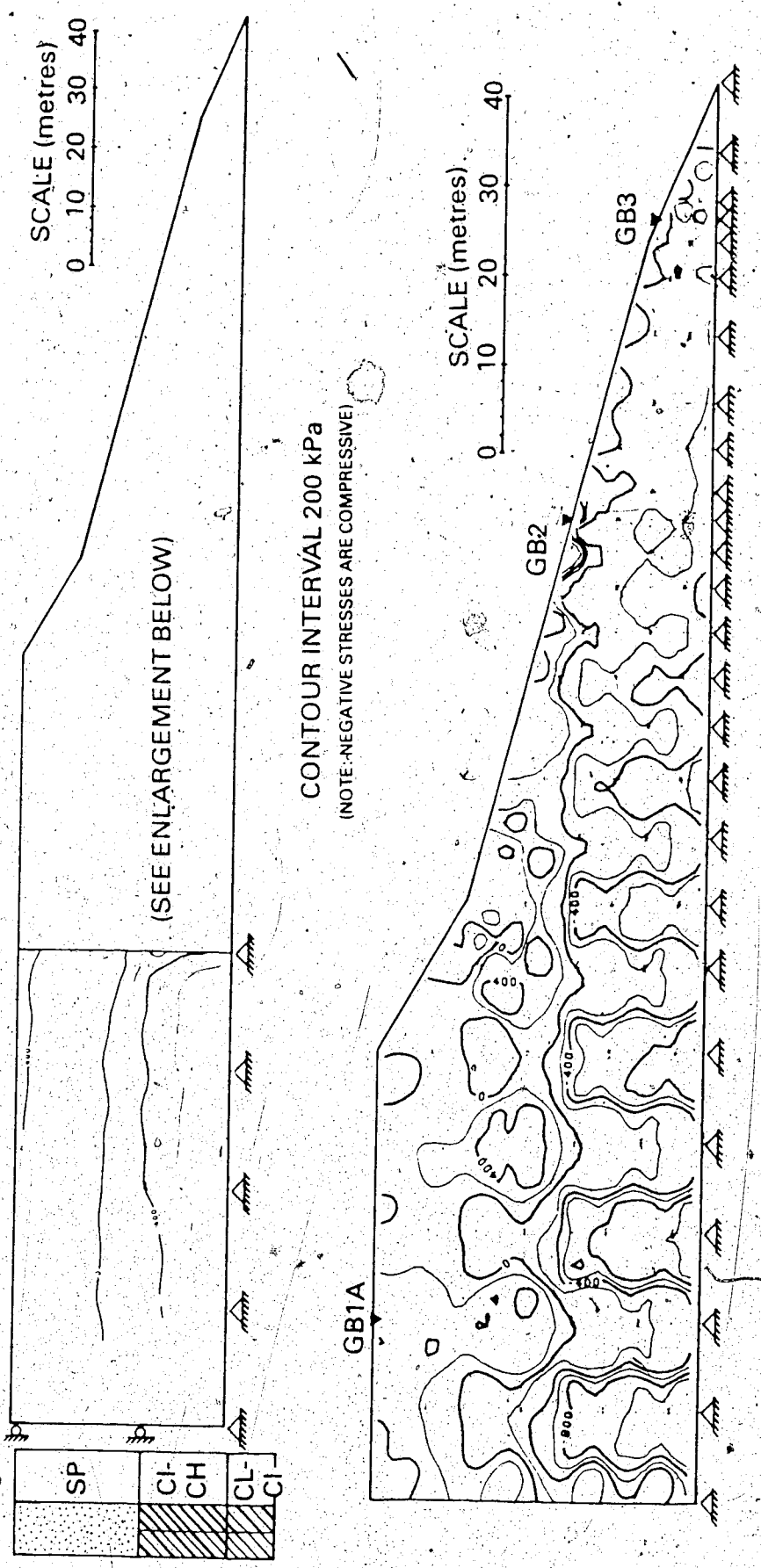


FIGURE 6.12: CONTOURS OF HORIZONTAL STRESS FOR STEADY STATE CREEP IN THE MEDIUM TO HIGH PLASTIC CLAY LITHOFACIES ONLY

## CHAPTER VII

### CONCLUSIONS AND RECOMMENDATIONS

"There's a land where the mountains are nameless,  
And the rivers all run God knows where;  
There are lives that are erring and aimless,  
And deaths that just hang by a hair;  
There are hardships that nobody reckons;  
There are valleys unpeopled and still;  
There's a land - oh, it beckons and beckons,  
And I want to go back - and I will."  
(Service, The Spell of the Yukon.)

#### 7.1 Introduction

The objective of this research programme was to complete the first documented, comprehensive, in situ study of naturally occurring creep in ice-rich permafrost soils. In order to optimize the huge expenditure necessary for support of the in situ study, the research programme began with surficial geology mapping to facilitate selection of the best possible site for field monitoring. Each facet of the field drilling, sampling and instrumentation activities was carefully planned and scheduled prior to commencement of field operations in March, 1975. The field drilling, sampling and instrumentation programme lasted five weeks. Monitoring of the field instruments extended between May, 1975 and June, 1977. Laboratory testing of undisturbed samples was undertaken concurrently with monitoring. Careful qualitative

analysis of laboratory creep behaviour enabled selection of a constitutive relationship for use in non-linear finite element analysis of the in situ, steady state creep behaviour.

Conclusions stemming directly from this research programme, general conclusions, and recommendations for further study are presented in this chapter.

## 7.2 Conclusions and Recommendations of this Study

Surficial sediments in the Great Bear River area include three main lithofacies, viz., morainic silty clay till, glaciolacustrine silty clay, and glaciodeltaic sand. The till overlies Tertiary clastic rocks throughout most of the area, but locally rests on Plio-pleistocene alluvial sediments that appear to lie in a buried river valley. The morphology of this buried valley is preserved through the till lithofacies creating a paleo-topographic depression where accumulations of glaciolacustrine and glaciodeltaic sediments are anomalously thick in relation to general accumulations elsewhere across Mackenzie Plain. Where the thalweg of this buried valley is cut by Great Bear River at km 7, these anomalously thick sequences are present in the valley slopes. With the proposed Arctic Gas crossing of Great Bear River at almost the same location, this represented an ideal field instrumentation site.

All drilling, sampling and instrumentation objectives were achieved during the field programme, despite several drilling

difficulties caused mainly by unexpected soil conditions. Details of the drilling, sampling and instrumentation programme are reported in detail in Chapter 3 because many facets were innovative and, therefore, they may be of benefit to those planning similar undertakings.

The thermistors used at the field site performed well and facilitated measurement of grout hydration, recovery of thermal equilibrium, and the quasi-stable thermal regime around each drill hole. These data are presented in graphic form in Chapter 4.

Of the two piezometers installed, one was assumed to have been damaged during installation and provided no readings. The other functioned normally for several months until moisture in the leads became frozen. Data from this piezometer suggest sub-permafrost pore pressures at the site are controlled by the level of Great Bear River. The combination pneumatic/hydraulic piezometer appears to be suitable for monitoring sub-permafrost pore pressures, however, it is recommended that future piezometer installations through permafrost use light oil or glycol to overcome the problem of moisture ingress and freeze-off of the leads.

The Digitilt inclinometer system performed exceedingly well throughout the monitoring period. Inclinometer data were difficult to interpret, however, because the magnitude of ground movements approached the minimum accuracy range of the inclinometer. Specific tests were carried out in order to verify the reliability of the measurements. These tests included in situ measurement of temperature effects and resolution. The test results demonstrated



that the accuracy of the Digitilt system was easily sufficient to delineate ground movements at the scale of those observed.

With the reliability of the inclinometer readings proven, it became necessary to separate movements related to steady state creep from other movements affecting the inclinometer casing. New data analysis techniques were developed and by reprocessing the inclinometer data it was found that the following external factors affected each of the inclinometer casings:

- 1) recovery of equilibrium conditions;
- 2) the stratigraphy, insofar as it influenced drilling and sampling, and therefore caused different levels of disturbance; and,
- 3) settlement and heave caused by seasonal temperature change above the level of zero mean annual temperature fluctuation.

Patterns of creep movement and localized shear movement became clear when external factors were accounted for. Creep movements occur in ice-rich sections of the glaciolacustrine silty clay, and to a limited extent through ice-rich sections of the till. Localized shear movements occur in both of these lithofacies and in the glaciodeltaic sand, and are typically associated with widely separated, pervasive ice structures. Creep velocities in the GB1A and GB3 test holes range from 0.25 to 0.30 cm/year. Strain rates are typically highest near the bottom of creeping zones and decrease upward. An approximate order of magnitude for strain rates is  $10^{-4}$  year<sup>-1</sup>. Deformations in the GB2 test hole are generally

larger in magnitude than those in GB1A or GB2 but they appear to be associated with a complex array of shear planes, and hence are not consistent with steady state creep behaviour.

An extensive laboratory creep testing programme was undertaken to assess steady state creep properties of undisturbed ice-rich, fine-grained soils. The results were generally poor because the use of a high confining pressure caused a non-uniform stress distribution that should have been allowed to dissipate prior to application of the deviatoric stress. Nevertheless, careful consideration of the results and critical assessment of other documented creep testing programmes lead to the important conclusion that the steady state deformation behaviour of ice-rich, fine-grained permafrost soils is expressed by a simple power law (Equation 5.1) where strain rate is a function of stress to a power of 3.0. The same form of this equation describes steady state creep in polycrystalline ice (Morgenstern *et. al.*, 1979), however the coefficient of  $2.0 \times 10^{-8}$  year  $\text{kPa}^3$  in the creep equation for polycrystalline ice represents an upper bound for strain rates in soil at any given stress. On the basis of the few reliable laboratory data available, the value of the coefficient which describes steady state creep in ice-rich, fine-grained permafrost soil is several times smaller than that of ice.

The reliability of this constitutive relationship and the empirical parameters was verified by non-linear finite element analysis of steady state creep in the slope. Using the simple power law (Equation 5.1) as the constitutive relationship, with an

exponent of 3.0 and a coefficient of  $0.33 \times 10^{-8}$  year  $\text{kPa}^3$ , good agreement was found between observed and predicted values, except through the glaciodeltaic sand lithofacies. In a subsequent analysis, the sand was treated as a non-creeping material with the hope of improving correlation between observed and predicted values. This assumption proved invalid, however, because significantly less correlation was found and unreasonably high horizontal tensile stresses were indicated through the sand lithofacies.

### 7.3 General Conclusions and Recommendations for Further Study

#### 7.3.1 Naturally Occurring Creep

On the basis of this study it can be concluded that ice-rich permafrost soils subjected to gravity loading exhibit in situ steady state creep behaviour. Natural evidence of this process is doubtlessly obscure because the magnitude of deformation rates associated with creep is generally less than rates associated with other natural processes in the periglacial environment.

Nevertheless, elucidating natural evidence of in situ creep processes is recommended as a logical and exceedingly important extension of this research programme.

Deformation of bedform structures by apparent flow of a frozen soil mass has been identified in association with ice wedges and bimodal flows in the MacKenzie Delta<sup>1</sup>, and in association with gently sloping ground in MacKenzie Plain at a location southeast of

---

<sup>1</sup>Mackay, J.R., 1978 personal communication

Arctic Red River<sup>1</sup>. These may be a product of creep in response to either local stress gradients or gravity loading.

Bimodal flows may also be indirect indicators of naturally occurring, steady state creep processes. These features are very common in ice-rich permafrost soils, (McRoberts and Morgenstern, 1974 a), however they frequently develop for no apparent reason. It is proposed that one of the main causes may be slow, steady exposure of the ice-rich soils as a result of creep deformation. This increased exposure causes local thickening of the active layer to the extent that ablation processes take over.

Cambering and valley bulging (Higginbottom and Fookes, 1971; Horswill and Horton, 1976) may, however, be the best evidence of naturally occurring creep. Valley bulging involves valley-ward displacement of incompetent strata, and cambering is deformation of overlying competent strata to accommodate this movement. Competent blocks of cambered strata may be partially detached or wholly detached with a debris filled crack or gull parallel to the valley crest. These deformation characteristics are similar to those observed in the Great Bear River area. The glaciolacustrine clay is analagous to the incompetent material, and it has been shown to move valley-ward by steady state creep deformation. The overlying sand is the more competent continuum and, although cambering and gulls have not been identified, the finite element analysis in Chapter 6 clearly showed tensile stress development which could lead to

---

<sup>1</sup>Illustrated in Zoltai and Pettapiece (1973, pp. 65), and examined by this writer in the field on July 18, 1973 (location: 134° 34'W longitude, 67° 51'N latitude).

fracture and detachment of a block. Moreover, examination of aerial photographs in the area clearly shows lineaments in uplands adjacent to the valley slopes and trending parallel to the valley crests, and tensile deformation fabric is clearly visible in natural exposures of the sand (see GB20, Appendix A).

In order to fully substantiate the hypothesis that cambering and valley bulging are caused by steady state creep movement under periglacial conditions, further numerical modelling of the Great Bear site should be attempted. To accomplish this, more must be learned about creep properties of frozen sand in tension. With these data, more meaningful numerical analyses of the slope may be performed. These analyses will also require integration of a rate dependent failure criterion for both the sand and clay lithofacies.

### 7.3.2 The Creep Process in Fine-Grained Permafrost Soils

Close examination of core samples of ice-rich glacio-lacustrine clay from the Great Bear River site shows evidence of deformation along ice lenses. This varies from a fraction of a centimetre off-set as shown in Plate 7.1, to several centimetres as shown in Plates 7.2 and 7.3. Inclinator data and observations of creep test samples both indicate that creep deformations are localized to a large extent along ice lenses, and hence the deformation fabric observed in undisturbed core samples is probably primarily a result of creep deformation. This leads to the conclusion that creep deformations in ice-rich, fine-grained permafrost soil occur preferentially along ice lenses. Whether

these deformations occur at soil-ice interfaces or through ice lenses, or both, is unclear and should be resolved through further research. Slickensides are common along soil-ice interfaces (Plates 3.4 and 3.5) in undisturbed soil. It is believed that these are a product of the creep process, originating when deformations associated with two or more separate ice lenses coalesce by shear through frozen soil. Ice lenses develop along the failure plane in response to continued shearing (Roggensack, 1977). This creep process would effect a decrease in spacing between ice lenses through a creeping soil mass. It would also cause locally high pore pressure gradients which would facilitate movement of unfrozen water to areas of active creep deformation. Therefore, the operandi of the creep process may itself cause the deformation rate to accelerate with time. The limiting condition, and hence the upper bound for design purposes would therefore appear to be the steady state creep relation for polycrystalline ice.

It is recommended that further research be undertaken to assess the validity of this apparent creep process. Laboratory testing of artificial samples with uniform ice structures would be the most desirable approach, but this type of research would be difficult and some aspects would be exceedingly time consuming. Numerical modelling of the composite soil-ice medium is also recommended.

In summary, this research programme has contributed to the field of permafrost engineering by proving that ice-rich, fine-grained permafrost soils exhibit in situ creep properties, and

by showing that these properties can be measured in carefully controlled laboratory tests. The success of the research programme is largely attributed to careful observation of natural phenomena in the field and in the laboratory. On many occasions when instrument, laboratory or numerical data seemed difficult to interpret, the key element of the interpretation emerged from these observations.

Therefore, as the geotechnical community proceeds with further research in this field, it is highly recommended that equal emphasis be given to the study of naturally occurring phenomena, laboratory study and numerical study.

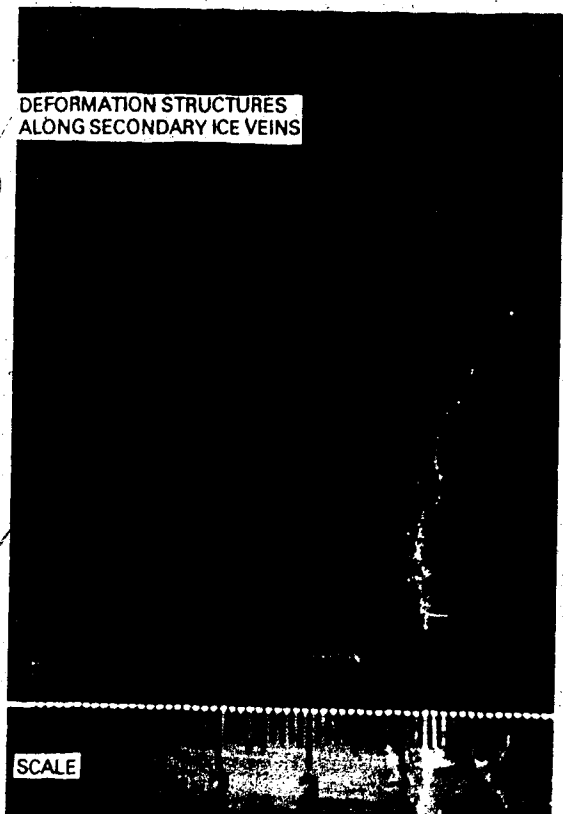


PLATE 7.1: Evidence of in situ deformation along secondary ice veins (GB1 Core 58).



PLATE 7.2: Evidence of in situ deformation along a primary ice vein (GB1 Core 53 Sample 5).

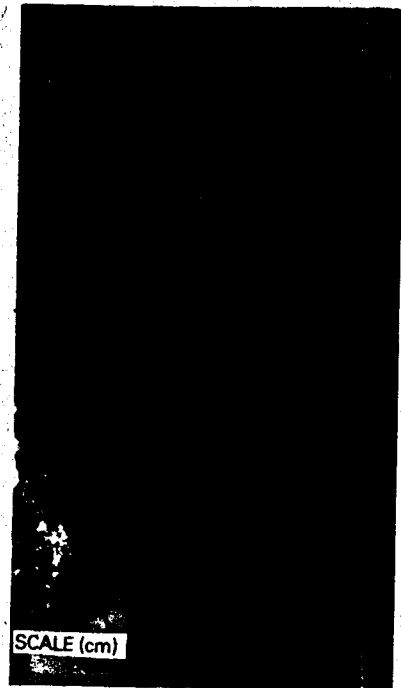


PLATE 7.3: Evidence of in situ deformation along secondary ice veins (GB1 Core 53 Sample 6).



## REFERENCES CITED

- Aitken, J.D., Yorath, C.J., Cook, D.G., and Balkwill, H.R.  
 1969: Operation Norman, District of Mackenzie, Northwest Territories; in Report of Activities, May to October, 1968, R.G. Blackadar, ed.; Geol. Surv. Can., Paper 69-1A, pp. 223-229.
- Aitken, J.D., Cook, D.G., and Balkwill, H.R.  
 1970: Operation Norman, District of Mackenzie, Northwest Territories; in Report of Activities, April to October, 1969, R.G. Blackadar, ed.; Geol. Surv. Can., Paper 70-1A, pp. 202-206.
- Aitken, J.D., Macqueen, R.W., and Foscolos, A.E.  
 1973: A Proterozoic sedimentary succession with traces of copper mineralization, Cap Mountain, Southern Franklin Mountains, District of Mackenzie (95-0); in Report of Activities, April to October 1972, Geol. Surv. Can., Paper 73-1A, pp. 243-246.
- Aitken, J.D., and Cook, D.G.  
 1974: Carcajou Canyon map-area, District of Mackenzie, Northwest Territories; Geol. Surv. Can., Paper 74-13, 28 p.
- Andersland, O.B., Sayles, F.H., and Ladanyi, B.  
 1978: Mechanical properties of frozen ground; in, Geotechnical Engineering for Cold Regions, O.B. Andersland and D.M. Anderson (eds.), McGraw-Hill Book Company, New York, pp. 216-275.
- Anderson, D.M., and Morgenstern, N.R.  
 1973: Physics, physical chemistry and mechanics of frozen ground, The North American Contribution to the 2nd Int. Conf. on Permafrost, Yakutsk, USSR, pp. 257-288.
- Balkwill, H.R.  
 1971: Reconnaissance geology, southern Great Bear Plain, District of Mackenzie; Geol. Surv. Can., Paper 71-11, 47 p.
- Barnes, P., Tabor, D., and Walker, J.C.F.  
 1971: The friction and creep of polycrystalline ice; Proc. Roy. Soc. London, v. 324A, pp. 127-155.
- Berger, T.R.  
 1977: Northern Frontier Northern Homeland, The Report of the MacKenzie Valley Pipeline Inquiry: Vol. 1; Minister of Supply and Services Canada, 213 p.
- Berton, L.B.  
 1954: I Married the Klondike; McClelland & Stewart Ltd., 240 p.

- Bostock, H.S.  
1948: Physiography of the Canadian Cordillera, with special reference to the area north of the fifty-fifth parallel; Geol. Surv. Can., Mem. 247.
- Bromwell, L.G., Ryan, C.R. and Toth, W.E.  
1971: Recording inclinometer for measuring soil movement; Proc. Fourth Panamerican Conf. on Soil Mechanics and Foundation Engineering, San Juan, Vol. 2, pp. 333-343.
- Brown, R.J.E.  
1967: Permafrost in Canada; Map prepared as joint project of Geol. Surv. Can. and Nat. Res. Council Can., NRC 9769.
- Burns, B.M.  
1974: The climate of the Mackenzie Valley - Beaufort Sea; Environment Canada, Climatological Studies Number 24, 2 volumes.
- Camsell, C., and Malcolm, W.  
1921: The Mackenzie River Basin (revised edition); Geol. Surv. Can., Mem. 108.
- Church, M., and Gilbert, R.  
1975: Proglacial fluvial and lacustrine environments, in Glaciofluvial and Glaciolacustrine Sedimentation, A.V. Jopling and B.C. McDonald (eds.), Society of Economic Paleontologists and Mineralogists, Spec. Pub. No. 23, pp.
- Colbeck, S.C.  
1970: The flow law for temperate glacier ice; Unpubl. Ph.D. Thesis, Univ. of Washington, Seattle, Wa., 149 p.
- Conway, J.B.  
1967: Numerical Methods for Creep and Rupture Analyses; Gordon and Breach Science Publishers, New York, 204 p.
- Cook, D.G., and Aitken, J.D.  
1971: Operation Norman, District of Mackenzie, Northwest Territories; in Report of Activities, April to October, 1970, R.G. Blackadar, ed.; Geol. Surv. Can., Paper 71-1A, pp. 197-201.
- Cook, D.G., and Aitken, J.D.  
1976: Geological Maps of Blackwater Lake (96B) and Fort Norman (96C), District of Mackenzie, Geol. Surv. Can., Open File 402.
- Cornforth, D.H.  
1974: Performance characteristics of the slope indicator series 200-B inclinometer. Proc. of a symposium on Field Instrumentation in Geotechnical Engineering, Butterworths, London, pp. 126-135.

- Craig, B.G.  
1960: Surficial geology of north-central District of Mackenzie, Northwest Territories; Geol. Surv. Can., Paper 60-18, 8 p.
- Craig, B.G.  
1965: Glacial Lake McConnell, and the surficial geology of parts of Slave River and Redstone River map-areas, District of Mackenzie, Geol. Surv. Can., Bull. 122, 33 p.
- Cullen, R.M., and Donald, I.B.  
1971: Residual strength determination in direct shear; Proc. First Australian New Zealand Conference on Geomechanics, Melbourne, 1971.
- Desai, C.S., and Abel, J.F.  
1972: Introduction to the Finite Element Method - A Numerical Method for Engineering Analysis; Van Nostrand Reinhold Company, New York, 477 p.
- Douglas, R.J.W., and Norris, D.K.  
1963: Dahadini; and Wrigley map-areas, Northwest Territories; Geol. Surv. Can., Paper 62-33, p.
- Dunnicliff, C.J.  
1971: Equipment for field deformation measurements. Proc. Fourth Pan American Conf. on Soil Mechanics and Foundation Engineering, v. 2, pp. 319-332.
- Emery, J.J.  
1971: Finite Element Analysis of Creep Problems in Soil Mechanics; Unpubl. Ph.D. Thesis, Univ. of British Columbia, Vancouver, British Columbia.
- Emery, J.J., and Nguyen, T.Q.  
1974: Simulation of ice flow problems; in Applications of Solid Mechanics, 2nd Symp. (CSME-CSCE-ASME) McMaster Univ., v. 1, pp. 30-45.
- Fraser, H.J.  
1929: An experimental study of varve deposition; Trans. Roy. Soc. Canada, v. 23, no. 4, pp. 49-60.
- Fritz, W.H.  
1970: Cambrian biostratigraphy in the Canadian Cordillera; in Report of Activities; April to October, 1969, R.G. Blackadar, ed.; Geol. Surv. Can., Paper 70-1A, pp. 110.
- Glen, J.W.  
1952: Experiments on the deformation of ice; J. Glaciology, v. 2, pp. 111-114.

- Glen, J.W.  
1955: The creep of polycrystalline ice; Proc. Royal Soc., Ser. A., v. 228, pp. 519-538.
- Glen, J.W.  
1956: Measurement of the deformation of ice in a tunnel at the foot of an ice fall; J. Glaciology., v. 2, p. 735-745.
- Glen, J.W.  
1958: The mechanical properties of ice; Advances in Physics, Vol. 7, no. 26, pp. 254-265
- Glen, J.W.  
1963: The rheology of ice; in Ice and Snow, Proc. of Conference held at the Mass. Inst. of Tech., W.D. Kingery, ed.; the M.I.T. Press, Cambridge, Massachusetts, pp. 3-7
- Glen, J.W.  
1975: The mechanics of ice; U.S. Army CRREL Monograph II-C2.
- Green, G.E.  
1974: Principles and performance of two inclinometers for measuring horizontal ground movements. Proc. of a symposium on Field Instrumentation in Geotechnical Engineering, Butterworths, London, pp. 166-179.
- Greenbaum, G.A., and Rubinstein, M.F.  
1968: Creep analysis and axisymmetric bodies using finite elements; Nuclear Engineering and Design, v. 7, pp. 379-397.
- Hakman, A., and Buser, W.M.  
1962: Bulkhead test program at Port of Toledo, Ohio. Journal of the Soil Mechanics and Foundations Division, ASCE, v. 88, no. SM3, pp. 151-184.
- Hanley, P.T., and Hughes, O.L.  
1973: Surficial geology and geomorphology of 96C, 96D (part), 96E (part), 106H, District of Mackenzie, N.W.T. (preliminary drafts); Geol. Surv. Can., Open File 155.
- Hanna, T.H.  
1973: Foundation instrumentation; Trans. Tech. Publications, Series on Rock and Soil Mechanics, pp. 187-193.
- Henderson, R.P., and Matich, M.A.J.  
1962: Use of slope indicator to measure movements in earth slopes and bulkheads; ASTM STP 322, Field Testing of Soils, pp. 166-185.
- Higginbottom, I.E. and Fookes, P.G.  
1971: Engineering aspects of periglacial features in Britain; Q.J. Eng. Geol., v. 3, pp. 85-117

- Mackenzie A.
- 1971: Voyages from Montreal Through the Continent of North America to the Frozen and Pacific Oceans in 1789 and 1793 with an Account of the Rise and State of the Fur Trade (First Published in London in 1801). Reprint, M.G. Hurtif Ltd. Booksellers and Publishers, Edmonton.
- McRoberts, E.C.
- 1975: Some aspects of a simple secondary creep model for deformations in permafrost slopes; Cdn. Geotech. J., v. 12, no. 1, pp. 98-105.
- McRoberts, E.C. and Morgenstern, N.R.
- 1974a: The stability of thawing slopes; Cdn. Geotech. J., v. 11, no. 4, pp. 447-469.
- McRoberts, E.C. and Morgenstern, N.R.
- 1974b: Stability of slopes in frozen soil, Mackenzie Valley, N.W.T.; Cdn. Geotech. J., v. 11, no. 4, pp. 554-573.
- McRoberts, E.C., Law, T.C., and Murray, T.K.
- 1978: Creep tests on undisturbed ice-rich silt; Proc. Third Int. Conf. on Permafrost, Edmonton, Canada, pp. 539-545.
- Meier, M.F.
- 1960: Mode of flow of Saskatchewan Glacier, Alberta, Canada; U.S. Geol. Surv., Prof. Paper 351, 70 p.
- Morgenstern, N.R., Roggensack, W.D., and Weaver, J.S.
- 1979: Pile creep in ice-rich soils; in press.
- Murray, R.T., and Irwin, M.J.
- 1970: The performance of an inclinometer for measuring lateral movements in soil; Road Research Laboratory, Report L.R. 332.
- Nixon, J.F.
- 1978: Foundation design approaches in permafrost areas; Cdn. Geotech. J., v. 15, no. 1, pp. 96-112.
- Nixon, J.F., and McRoberts, E.C.
- 1976: A design approach to pile foundations in permafrost; Cdn. Geotechn. J., v. 13, no. 1, pp. 40-57.
- Norford, B.S., and Macqueen, R.W.
- 1975: Lower Paleozoic Franklin Mountain and Mount Kindle Formations, District of Mackenzie; Their type sections and regional development; Geol. Surv. Can., Paper 74-34, 37 p.
- Norris, D.K.
- 1963: Geology northern Yukon Territory and northwest District of Mackenzie; Geol. Surv. Can., Map 10-1963.

- Odqvist, F.K.G.  
1966: Mathematical Theory of Creep and Creep Rupture; Oxford Mathematical Monograph, Clarendon press, Oxford, 268 p.
- Parsons, J.D., and Wilson, S.D.  
1956: Safe loads on dog-leg piles. Trans. ASCE, v. 121, pp. 695-721.
- Paterson, W.S.B.  
1969: The physics of glaciers; Pergamon Press, Oxford, 250 p.
- Perkins, T.K., and Ruedrich, R.A.  
1973: The mechanical behaviour of synthetic permafrost; J. Soc. Petroleum Engineers of AIME, v. 13, no. 8, pp. 211-220.
- Peters, N. and Ellis, J.H.  
1972: Instrumentation for Gardiner Dam; Proc. 25th Can. Geotech. Conf., Ottawa.
- Phillips, S.H.E., and James, E.L.  
1974: An inclinometer for measuring the deformation of buried structures with reference to multi-tied diaphragm walls; Proc. of a symposium on Field Instrumentation in Geotechnical Engineering, Butterworths, London, pp. 359-369.
- Pinlainen, J.A., and Johnston, G.H.  
1963: Guide to a field description of permafrost for engineering purposes; Nat. Res. Council. Can., Tech. Mem. 79, NRC 7576.
- Pipeline Application Assessment Group  
1974: Mackenzie Valley Pipeline Assessment, Environmental and Socio-Economic Effects of the Proposed Canadian Arctic Gas Pipeline on the Northwest Territories and Yukon; Issued under the authority of the Minister of Indian Affairs and Northern Development, Ottawa.
- Prest, V.K.  
1970: Quaternary Geology, in Geology and Economic Minerals of Canada, R.J.W. Douglas (ed.); Geol. Surv. Can., Economic Geology Report No. 1.
- Robinson, M.J., and Robinson, J.E.  
1946: Exploration and settlement of Mackenzie District, N.W.T., Can. Geog. J., v. 66, no. 3.
- Roggensack, W.D.  
1977: Geotechnical properties of fine-grained permafrost soils; Unpublished Ph.D. Thesis, University of Alberta.
- Savage, J.C., and Paterson, W.S.B.  
1963: Measurements of the Athabasca Glacier relating to the flow of ice; J. Geophys. Res., v. 68, no. 15, pp. 4521-4543.

- Savigny, K.W.  
1977: A method for determining the bulk moisture content of cores and natural exposures of segregated ice; Nat. Res. Council, Tech. Memo. 124, pp. 8-13.
- Sayles, F.H.  
1968: Creep of frozen sand; U.S. Army CRREL Tech. Report 190, 54 p.
- Sayles, F.H.  
1973: Triaxial constant strain rate tests and triaxial creep tests on frozen Ottawa sand; The North American Contribution to the 2nd Int. Conf. on Permafrost, Yakutsk, USSR, pp. 384-391.
- Sayles, F.H., and Haines, D.  
1974: Creep of frozen silt and clay, U.S. Army CRREL Tech. Report 252, 50 p.
- Sego, D.C.  
1980: Deformation of ice under low stresses; Unpublished Ph.D. Thesis, University of Alberta, 450 p.
- Steinemann, S.  
1954: Flow and recrystallization of ice; Union Geodesique et Geophysique Int. Assoc. d'Hydrologie Scientifique. Comptes Rendus Ass., Rome, v. 4, pp. 449-462.
- Steinemann, S.  
1958: Experimental investigation of the plasticity of ice; U.S. Airforce, Cambridge Research Laboratory, Research Translation AMST-G-166+.
- Sutherland, W.H.  
1970: AXICRP - finite element computer code for creep analysis of plane stress, plane strain and axisymmetric bodies; Nuclear Engineering and design, v. 11, pp. 269-285.
- Tarmocai, C.  
1973: Soils of the Mackenzie River area; Environmental - Social Committee Northern Pipelines, Task Force on Northern Oil Development, Report No. 73-26.
- Tassonyi, E.J.  
1969: Subsurface geology, lower Mackenzie River and Anderson River area, District of Mackenzie; Geol. Surv. Can., Paper 68-25.
- Thompson, E.G., and Sayles, F.H.  
1972: In situ creep analysis of a room in frozen soil; J. Soil Mech. Found. Div., ASCE, v. 98, no. SM9, p. 899-915.

Tsyrovich, N.A.

1975: The Mechanics of Frozen Ground; The McGraw-Hill Book Company, New York, 427 p.

Usher, J.L.

1970: Upper Proterozoic to Mid-Cambrian stratigraphy, District of Mackenzie (96D, 106A, G, H); in Report of Activities, April to October, 1969, R.G. Blackadar, ed., Geol. Surv. Can., Paper 70-1A, pp. 240-242.

Vialov, S.S.

1962: Strength and creep of frozen soils and calculations for ice soil retaining structures; U.S. Army CRREL Tech. Trans. No. 76.

Vialov, S.S.

1965: Rheological properties and bearing capacity of frozen soils; U.S. Army CRREL Tech. Trans. No. 74, 219 p.

Weerdenburg, P.

1979a: Utilization of underground space in frozen ground; Inter-Departmental Note, Department of Civil Engineering, University of Alberta, 19 p.

Weerdenburg, P.

1979b: CREEP user's manual; Inter-Departmental Note, Department of Civil Engineering, University of Alberta, 15 p.

Weerdenburg, P.

1980: M.Sc. thesis in preparation.

Williams, P.J.

1966: Pore pressures at a penetrating frost line and their prediction. Geotechnique, v. 16, no. 1, p. 187-208.

Wilson, S.D.

1962: The use of slope measuring devices to determine movements in earth masses. ASTM STP 322, Field Testing of Soils, pp. 187-197.

Wilson, S.D.

1967: Investigation of embankment performance; J. Soil Mechanics and Foundation Division, ASCE, v. 93, no. SM4, pp. 135-156.

Wilson, S.D.

1970: Observational data on ground movements related to slope instability; J. Soil Mech. Found. Div., ASCE, v. 96, no. SM5 pp. 285-310.



- Wilson, S.D., and Hancock, C.W., Jr.  
1959: Horizontal displacement of clay foundations. Proceedings, First Pan. American Conf. on Soil Mechanics and Foundation Engineering, v. 1, pp. 41-57.
- Wilson, S.D., and Hancock, C.W., Jr.  
1965: Instrumentation for movements within rockfill dams. ASTM STP 392, Instruments and Apparatus for Soil and Rock Mechanics, pp. 115-130.
- Yorath, C.J.  
1970: Cretaceous and Tertiary Stratigraphy, District of Mackenzie (96C, D, E; 106G, H); in Report of Activities April to October, 1969, R.G. Blackadar, ed.; Geol. Surv. Can., Paper 70-1A, pp. 243-245.
- Zienkiewicz, O.C. and Cheung, Y.K.  
1967: The Finite Element Method in Structural and Continuum Mechanics, McGraw-Hill, London, 521 p.
- Zoltai, S.C. and Pettapiece, W.W.  
1973: Studies of vegetation, landform and permafrost in the Mackenzie Valley: terrain, vegetation and permafrost relationships in the northern part of the Mackenzie Valley and Northern Yukon; Environmental - Social Committee, Northern Pipelines, Task Force on Northern Oil Development, Report No. 73-4, 105 p.

## APPENDIX A

### GEOLOGICAL FIELD DATA FROM THE GREAT BEAR RIVER AREA

#### A.1 Introduction

Quaternary and limited Tertiary stratigraphy in the Great Bear River area were mapped during the summer of 1973 as part of a larger mapping programme supported by the Geological Survey of Canada. Data collected along Great Bear River were intended to supplement surficial geology mapping of map-area 96F (Mahoney Lake) and supply base-line data for evaluation of several proposed dam sites along Great Bear River. When the study reported in this thesis was conceived, the data also served as a basis for selecting the most suitable field instrumentation site.

Geological studies were carried out in the following steps:

1. Preliminary airphoto interpretation.
2. Field reconnaissance via helicopter.
3. Detailed field checking by boat traverse along Great Bear River.
4. Final airphoto interpretation.
5. Compilation.

The work was supplemented by stratigraphic data obtained from test hole and test pit logs included in the following geotechnical reports:

1. G.E. Crippen and Associates Ltd., report to Northern Canada Power Commission on Great Bear River Power Development, October 1972.
2. Pemcan Services "72", report to Department of Indian Affairs and Northern Development on Granular Materials Inventory, Fort Norman, N.W.T. Community Study Area; 1973.
3. R.M. Hardy and Associates Ltd.; report to Department of Public Works on Geotechnical Investigations along Mackenzie Highway, Mile 544 to Mile 635, Volumes 1 to 7, April 1973.
4. R.M. Hardy and Associates Ltd., report to Northern Engineering Services Company Ltd. on 1974 Drilling and Sampling Programme at the Proposed Arctic Gas Pipeline Great Bear River Crossing, 1974.

Survey data along Great Bear River were obtained from the Crippen report. Supplementary information was also gathered from specific field checks carried out in association with visits for instrument monitoring.

Comments on field and laboratory technique follow in Section A.2 and a discussion of the permafrost classification system used in this thesis is given in Section A.3. Sections measured at natural exposures along Great Bear River are summarized in Section A.4. Test hole and test pit logs are also summarized in Section A.4. In

some cases the original lithologic designation in these logs has been altered (i.e. GRAVELLY CLAY would be described as TILL, and the change clearly indicated as in GB61), but the original lithologic description has not been changed.

## A.2 Field and Laboratory Technique

In the initial phase of field checking a helicopter reconnaissance was made over the Great Bear River area. Natural exposures along the river and for short distances upstream along its major tributaries were located on aerial photographs and subsequently measured and described during a boat traverse along the river. Vertical distances were measured with a brunton compass and referenced to approximate elevations along Great Bear River as given in the Crippen report.

Disturbed samples were taken and later analysed to determine moisture content, Atterberg limits, specific gravity and grain size distribution. All laboratory tests were carried out according to ASTM standards. Moisture content data are reported as a percentage of dry weight. Where high ice contents precluded the possibility of obtaining sufficiently large samples for representative moisture content determination, remote sensing techniques were used to obtain the values according to a procedure described by Savigny (1977).

## A.3 Permafrost Classification System

### A.3.1 Introduction

The most commonly used classification system for ground ice structures was developed jointly by the National Research Council of Canada (NRC) and the Cold Regions Research and Engineering Laboratories of the United States Army. In Canada this is referred to as the NRC system (Pihlainen and Johnston, 1963). It is based upon the presence or absence of ground ice and the scale of ice structures.

A large portion of the geological data reported in this thesis is based upon field observations of large exposures of permafrost soil, many with complex ground ice structures. While describing these exposures, it became obvious that ice structures would appear more variable in core samples than was actually the case through the soil mass, and hence descriptions based on the NRC system would be inconsistent for the same permafrost soil.

To overcome this problem a facies classification, where the soil and ice components in permafrost soil were collectively referred to as one medium or facies, was developed and used in conjunction with the NRC system. Ground ice structures may change in successive core samples according to the NRC system, but each may be characteristic of a discrete facies which would be obvious at the scale of a field exposure. Hence the facies concept maintains greater continuity between field and laboratory descriptions of

---

<sup>1</sup>Soil in this context implies mineral particles, air and water as in thawed soil mechanics.

permafrost soil.

Facies classes are based upon ground ice form because this factor is readily discernable and affords a preliminary assessment of engineering behaviour. For convenience, contemporary names of ground ice forms have been adopted as facies class names. Those likely to be encountered include: pore ice, segregated ice, reticulate ice and stratified ice. The following is a brief description of each class.

#### A.3.2 Pore Ice

Pore ice is an almost ubiquitous permafrost soil facies. It is a medium where ice is present as a cement or bond in interstices between mineral particles.

#### A.3.3 Segregated Ice

Segregated ice is a medium where impure, irregularly shaped ice structures are dispersed randomly through the soil mass. Typically neither the ice or the soil component exhibits any preferred orientation. The distinction between segregated ice and pore ice becomes somewhat arbitrary as the scale of ice structures decreases to approximately that of interstitial dimensions.

A similar definition for segregated ice was proposed by Mackay (1966).

#### A.3.4 Reticulate Ice

In reticulate ice, the ice component comprises a network of veins which impart an overall reticulate (brick-like, as defined by Mackay, 1974) structure to the soil-ice medium. Usually, veins are through-going in one direction and are referred to as primary veins. Other veins intersect these at varying angles near 90° and are called secondary veins.

#### A.3.5 Stratified Ice

Stratified ice, as the name implies, is a medium where discrete ice strata lie along stratigraphic contacts and appear to be an integral part of the sedimentary profile.

L  
L

A.4 Summary of Measured Sections, Test Holes Logs, and Test Pit logs from the Great Bear River Area

		Thickness (metres)	Depth of base (metres)
March & April/75			
GB 1			
GB 1A			
GB 1B	Test holes drilled as part of this study. See Appendix B for detailed logs.		
GB 2			
GB 3			
GB 3A			
March 26 & 27/74			
GB 4	Northern Engineering Services Ltd., test hole N74-303 (km 7.1, river course) <sup>1</sup> .		
ICE:	Estimated ice surface el. 56.7 m.	1.68	1.68
1			
WATER:		1.07	2.75
2			
CLAY and SAND:	Interbedded; grey, medium to high plasticity, sandy clay; and fine to medium grained, locally cemented, sand; unfrozen (originally described as SILTSTONE over SANDSTONE).	2.59	5.34
3			
SILTSTONE and SHALE:	Dark grey; trace of fine sand throughout; hard; blocky except for occasional fissile lenses; varies from a silty clay with medium plasticity to a clay and silt with low plasticity; unfrozen (originally described as CLAY SHALE).	6.23	11.57
4			
March 23 - 25/74			
GB 5	Northern Engineering Services Ltd., test hole N74-304 (km 7.1, river-course).		

<sup>1</sup> Where the sections or test holes are near the banks of Great Bear River, the location is given by the kilometre location along the river followed by R or L signifying right or left bank respectively or "river course" if drilling took place in the channel. If the location is more than a few 100 m from the banks it is given with latitude and longitude.

		Thickness (metres)	Depth of base (metres)
ICE 1	Estimated ice surface el. 56.7 m.	1.37	1.37
WATER: 2		1.68	3.05
CLAY and SILT 3	Grey; some fine to medium sand; low plasticity; unfrozen.	0.61	3.66
SILTSTONE and SHALE 4	Dark grey; overall clay-silt classification; high plasticity components; fine sand throughout; carbonaceous; hard; laminated; unfrozen (originally described as CLAY SHALE).	0.15	3.81
SILTSTONE and SHALE: 5	Dark grey, fine-grained silty clayey sand; laminated; some cementation, well cemented below 3.66 m; occasional thin layers of interbedded shale; variable plasticity (originally described as SANDSTONE).	9.39	13.20
SILTSTONE and SHALE: 6	Hard; sandy; interbeds of sand- stone as above unit 4 (originally described as CLAY SHALE).	0.51	13.71

April 3 &amp; 4/74

GB 6 Northern Engineering Services Ltd., test hole N74-307  
(km 7.1, L).

Collared at el. 87.5 m.

PEAT (Pt): 1	Woody, coarse fibrous peat containing scattered wood; ground ice Vx with 70% excess.	0.27	0.27
SAND (SP): 2	Brown to grey; trace of silt; fine to medium grained; ground ice Vs & Vx with ice lenses to 1 cm thick and an excess of 50%.	0.95	1.22

		Thickness (metres)	Depth of base (metres)
PEAT (Pt): 3	Coarse fibres criss-crossing fine fibrous peat; ground ice Vs & Vx with an excess of 60%.	0.73	1.95
SAND (SM): 4	Brown with rust stains throughout; fine grained; calcareous; occasional small coal inclusion; ground ice Vs & Vx at top changing to Vx at bottom, excess decreases from 50% to 15% with depth, one 6 cm ice lens at 0.79 m.	2.47	4.42
SILT (ML): 5	Trace of fine sand; low plasticity; ground ice Vx with excess of 5%.	0.18	4.60
CLAY (CI-CH): 6	Grey; silty; calcareous; stiff when thawed; high unfrozen water content (based on deformability in frozen state); stratified below 1.19 m; medium plasticity; ground ice Vx, Vr and Vs throughout with excesses ranging from 10% to 30% and ice lenses up to 27 cm.	4.54	9.14
7	Estimated distance from bottom of hole to local river level.	21.95	31.09
			Mar. 27/74 to Apr. 2/74
GB 7	Northern Engineering Services Ltd., test hole N74-308 (km 7.1, L).		

Collared at 101.50 m a.m.s.l.

SAND (SM): 1	Medium brown; trace of silt; random fine gravel zones; generally fine grained, becoming medium to coarse in zones with fine gravel; calcareous; ground ice Nbn to 6.86 m (unfrozen between 0.61 m and 1.22 m), Vx and Vr between 6.86 m and 9.45 m, Nbn thereafter; excess varies from 10% to 40%, one ice lens @ 11.43 m, 18 cm thick.	17.68	17.68
-----------------	---	-------	-------



		Thickness (metres)	Depth of base (metres)
CLAY and SILT (CL): 2	Brown; low plasticity; unfrozen to 0.31 m, ground ice Nbn thereafter; sloughing suggests other unfrozen areas.	1.52	19.20
SAND (SM): 3	As above unit 1; some silt and clay interbeds below 2.13 m.	3.20	22.40
CLAY (CI-CH): 4	Grey; silty, some silt partings; calcareous; medium plasticity; stiff when thawed; very deformable in frozen state suggesting high unfrozen water content; small ice partings and ice lenses up to 50% outside of pure ice zones.	15.70	38.10
TILL (CL-CI): 5	Grey; silty, trace of fine sand, trace of medium gravel; medium to low plasticity.	1.86	39.96
6	Estimated distance from bottom of hole to local river level.	5.15	45.11

July 23/73

GB 8 This section is representative of the alluvial plains below St. Charles Rapids (km 46.3, R).

COVERED 1		1.16	1.16
SAND: 2	Greyish brown (10YR5/2) fresh; silty 30% to 40%, increasing with height; plasticity and dry strength negligible; grain size ranges from silt size to coarse sand size, sand is angular, quartz and feldspar; overall structure is massive.	.94	2.10
SAND & GRAVEL: 3	Sand 70%, as above unit 2; gravel 30%; up to 6 cm, mode 2.5 cm, subrounded to rounded, 90% granites and other crystalline rocks, 5% each of sandstones and carbonates.	.1	2.2

		Thickness (metres)	Depth of base (metres)
SAND: 4	As above unit 2; gravel 5% to 10%, up to 10 cm, mode 5 cm, subrounded, predominately crystalline rocks esp. granites.	.8	3.0
BEACH: 5	A loose boulder and cobble pavement; maximum size 80 cm, mode 20 cm to 40 cm; matrix sand, medium to coarse as above unit 2.	3.16	6.16

## RIVER LEVEL

July 23/73

GB 9 First good exposure of glacial deposits below the St. Charles rapids. The section has a 45° slope and is unstable. The river is eroding the toe and debris is continually falling from the face. Small bimodal flows have developed in an ice-rich stratum overlying the till. Although largely covered, this unit appears to be a silty clay. All units dip slightly westward (km 45.4, L).

COVERED: 1	Organic sand as Unit 2 below.	.28	.28
SAND: 2	Medium to coarse grained, mode coarse; angular; moderately sorted; quartz and feldspar; gravel 5% to 10%, maximum size 2 cm, mode 1 cm, subrounded to rounded, predominantly crystalline; lowest third stratified, beds average 5 cm thick and range from 1 cm to 13 cm, bedding control is between medium and coarse grained sorting. (AR-73-3 @ .8 m)1.	1.37	1.65

- 1 Where samples were taken from a particular unit the sample number appears at the end of the description together with the sampling depth (when known) below the top of the unit.

		Thickness (metres)	Depth of base (metres)
CLAY: 3	Very dark greyish brown (10YR 3/2) fresh; silty 40% to 50%; firm consistency undisturbed; medium dry strength; medium plasticity; massive; upper contact cryoturbated with overlying sand; very moist, high ground ice content is suspected (AR-73-2 @ 0.25 m and WS-73-3a @ 0.2 m).	.35	2.0
COVERED: 4	Assumed similar to unit 3 above. Together with unit 3, this interval is the seat of bimodal flows. The lower boundary is defined at a break in slope.	5.8	7.8
COVERED: 5	Below the break in slope mentioned above (unit 4) the covered interval is assumed as unit 6 below.	2.48	10.28
TILL: 6	Dark greyish brown to very dark greyish brown (10YR 4/2 to 3/2) fresh, light grey (10YR 7/2) dry; moderately sandy, becoming very sandy with depth; hard undisturbed consistency; very low dry strength; low plasticity; inclusions 20% to 30%, maximum size 38 cm mode 1 cm, boulders 1% subrounded, predominately crystalline, very rarely stratified by sand lenses, 1 cm to 7 cm thick, never greater than 1 m laterally; moderate fissuring throughout; no permafrost within 1 m of face and no evidence of this unit failing. (WS-73-4b @ 2 m, WS-73-3c @ 12 m).	14.12	24.40
SILT: 7	Very dark grey (10YR 3/1) fresh; clayey 20% to 30%; stiff consistency undisturbed; low dry strength; low to medium plasticity; massive; moderate fissuring.	2.0	26.40

	Thickness (metres)	Depth of base (metres)
8 SAND & GRAVEL: Sand is medium grained; angular to subangular, well sorted; quartz 90%, feldspar 10%; 50% of total unit; well stratified and moderately cross-bedded. Course sand and fine gravel beds up to 30 cm thick make up 35% of total unit; gravel only pebble size. Silt beds up to 15 cm thick; 15% of total unit, usually fringed by a few centimetres of fine-grained, very well sorted, sand.	4.45	30.85
9 SAND & GRAVEL: Coarse grained; angular to sub-angular, angular mode; well sorted; 70% quartz, 30% feldspar; gravel 10% to 40%, mode 15% to 20%, maximum size 90 cm, mode 0.5 cm, boulders and cobbles 1%; stratified with minor cross-bedding, bedding controlled by sorting of gravels.	7.74	38.59
10 SAND & SILT: Unit 9 above; interbedded with silt and fine sand; these beds are 15 cm to 50 cm thick and represent 50% of the unit; the beds are saturated, there is very slow seepage which evaporates from the face; no evidence of ground ice or permafrost within 1.5 m of face.	1.6	40.19
11 SAND & GRAVEL: As unit 9 above; maximum size of gravel 20 cm, mode 4 cm, approximately 5% larger than pebble sizes.	5.85	46.04

RIVER LEVEL

Thickness      Depth of base  
(metres)      (metres)

July 23/73

GB 10      Major failure area, good exposure is limited to the top. The feature is a bimodal flow with its toe extending into the river. The backscarp angle is 21°. Permafrost is within one half metre of the backwall and is actively degrading (km 42.5, L).

COVERED:      Root strength is very high. In      .18      .18  
1      some cases the organic mat has folded 3 m over the face and has remained intact.

SILT or      Dark brown (10YR 3/3) fresh; light      .46      .64  
LOESS:      grey (10YR 7/1) oxidized; stiff  
2      to hard consistency undisturbed; negligible dry strength and plasticity; very well sorted; no structure.

SAND:      Coarse grained; angular; well      6.88      7.52  
3      sorted; quartz and feldspar; top 32 cm oxidized; gravel up to 6 cm, mode 0.8 cm; stratified and cross-bedded throughout; lignite common in lowest 1 m; permafrost at 48 cm below the face.

CLAY:      Very dark greyish brown (10YR 3/2)      2.6      10.12  
4      fresh; silty (20% to 30%); firm consistency undisturbed; medium to low dry strength; fissured; upper contact cryoturbated with overlying sand. (WS-73-4a @ 0.5 cm)

COVERED:  
5

RIVER LEVEL

Thickness      Depth of base  
(metres)      (metres)

July 23/73

GB 11	This section is similar to GB 10 but is less well exposed. The failure is mildly active but the seat of melting is not visible. It is not affecting river hydraulics in any way. The backscarp angle is 27°. Permafrost is present at 1.2 m in the upper sand (km 41.05, L).		
COVERED: 1	Organic sand as Unit 2 below.	.67	.67
SAND: 2	Dark greyish brown (10YR 4/2) fresh; silty, 10% to 30% except in last 2 cm where it is 50%; fine to medium grained, mode fine; angular to subangular; moderately to well sorted; predominantly quartz; stratified throughout, most beds 1 cm to 2 cm thick, thickest bed is bottom 2 m of unit; zones of high silt content appear wet.	3.14	3.81
SAND: 3	Coarse grained; angular; moderately to well sorted; quartz 50%, feldspar 40%, dark minerals 10%; gravel 5% to 10% maximum size 4 cm, mode 1 cm, sub-rounded, predominately crystalline; gentle cross-bedding; bedding controlled by sorting of gravel.	2.0	5.81
COVERED: 4	A break in slope at the lower boundary of this unit is assumed to be a sand clay contact.	4.0	9.81
COVERED: 5		22.6	32.41
RIVER LEVEL			

Thickness      Depth of base  
(metres)      (metres)

July 23/73

GB 12      An alluvial plain section similar to GB 8. The high water mark is 3 m above the top of this section (km 40.0, about 75 m up St. Charles Creek on its left bank).

COVERED:      Organic cover immediately above exposure.      .05      .05  
1

SILT:      Dark greyish brown (10YR 4/2)      4.41      4.46  
2      fresh; sandy 20% to 40%; hard consistency undisturbed; negligible dry strength and plasticity; sand; fine grained, angular, quartz and feldspar; occasional horizontal clay and silt lenses (10% of unit) up to 1.8 cm thick and up to 5 m long; mode 1.5 m long.

SAND & GRAVEL:      Oxidized; sand 50% to 60%,      1.19      5.65  
3      medium and coarse grained, angular, moderately sorted; gravel, maximum size 80 cm, 10% to 15% boulders, 20% cobbles, mode 2 cm, predominately crystalline rocks.

RIVER LEVEL

July 24/73

GB 13      An old bimodal flow now stable and vegetated. No permanent frost found although it is suspected at between 2 and 5 m (km 39.55. R).

COVERED:      Organic cover immediately above exposure      0.31      0.31  
1

SAND:      Medium to coarse grained; angular; moderately to well sorted; quartz 70%, feldspar 20%, dark      17.48      17.79  
2

		Thickness (metres)	Depth of base (metres)
	minerals 10%; gravel 10% to 15%, maximum size 2 cm, modes 0.3 cm to 0.4 cm; stratified; bedding controlled by different grain sizes of sand and by sorting of gravel; bedding horizontal.		
GRAVEL:	Pebbles and small cobbles; maximum size 9 cm, mode 1.5 cm; rounded; predominately crystalline.	.15	17.94
3			
CLAY:	Dark grey (10YR 4/1) fresh; silty 30%; firm consistency undisturbed; medium dry strength and plasticity; massive; moderately fissured (AR-73-4 @ 3 m).	12.73	30.67
4			
COVERED:		9.4	40.07
5			
RIVER LEVEL			

July 24/73

GB 14	Steep section exposed on the river bank. It is being cut back by the river. Permafrost is not a factor in this exposure and was not observed; it is estimated at 3 m to 5 m below the face. Several pits were dug above the top of the exposure in a slope leading up to the local plain. Based on these pits, the stratigraphy above the section is estimated. The high water mark at this location is 2.75 m above present river level (km 37.1, R).		
COVERED:	Considered sand and silt based on very random holes.	18.0	18.0
1			
COVERED:	Considered to be clay based on very random holes.	9.15	27.15
2			
COVERED:	Organic cover immediately above exposure.	.20	27.35
3			
CLAY:	Light brownish grey (10YR 6/2) fresh; silty 20% to 30%; firm consistency undisturbed; medium dry strength; medium plasticity; massive and fissured.	2.62	29.97
4			



		Thickness (metres)	Depth of base (metres)
CLAY: 5	Mottled rhythmites; silty 30% to 40%; stiff to hard consistency undisturbed; low dry strength; low plasticity; stratified by dark lenses of clay frequently containing traces of fine to medium-grained sand; bedding is consistently 10% off parallel with lower contact (dips 10° northeast). Approximately 20 rhythmites present.	.41	30.38
SAND: 6	Fine, medium and coarse grained; trace of silt; angular; very poorly sorted; quartz 80%, feldspar 15%, dark minerals 5%; gravel 10% to 20%, maximum size 42 cm, mode 5 cm; boulders 1%; well stratified and crossbedded, mode of bedding thickness 10 to 25 cm, bedding controlled by sorting.	10.48	40.86
COVERED: 7		2.0	42.86

## RIVER LEVEL

July 24/73

GB 15 Section exposed in stream cut high on bank and well back from river. Stable, vegetated, with no permafrost observed but estimated between 2 and 5 m below the surface. (km 35.1, L).

COVERED: 1		13.0	13.0
COVERED: 2	Organic cover immediately above exposure.	.35	13.35
SAND: 3	Very pale brown (10YR 7/3) dry; silty 20% to 40%; angular; well sorted; quartz and feldspar; massive.	7.4	20.75

		Thickness (metres)	Depth of base (metres)
COVERED: 4		25.0	45.75
RIVER LEVEL			
July 24/73			
GB 16	Small, well-exposed section almost at river level. No permafrost was observed but it is assumed between 1 m and 4 m from the surface. The natural moisture content is high in both major units. The section is stable (km 34.8, R).		
COVERED: 1	Organic cover immediately above exposure.	.3	.3
CLAY: 2	Very dark grey (10YR 3/1) fresh; silty 20%; firm consistency undisturbed; medium dry strength; medium plasticity; massive; moderately fissured throughout (AR-73-6 @ 0.6 m).	1.2	1.5
TILL: 3	Very dark greyish brown (10YR 3/2) fresh; sandy texture; hard consistency undisturbed; dry strength negligible; low to negligible plasticity; inclusions 20% to 30%, boulders and cobbles 1%, maximum size 28 cm, mode 4 cm; moderately fissured (AR-73-5 @ 0.75 m).	1.5	3.0
COVERED: 4		4.75	7.75
RIVER LEVEL			
July 24/73			
GB 17	Small section almost at river level. No permafrost observed but assumed between 1 m and 4 m from the surface. The natural moisture content is high. The section is stable (km 32.6, R).		
COVERED: 1	Organic cover immediately above exposure.	0.3	0.3

		Thickness (metres)	Depth of base (metres)
TILL: 2	Very dark greyish brown (10YR 3/2) fresh; sandy 10% to 15%; hard consistency undisturbed; negligible; dry strength and plasticity; inclusions 15% to 20%, maximum size 1.52 m, boulders and cobbles 1%, mode 3 cm to 5 cm; moderately fissured.	1.0	1.3
COVERED: 3		5.48	6.78
RIVER LEVEL			

July 24/73

GB 18 Steep sand section forming backwall of bimodal flow. The angle of the backwall is 52°, the flow angle of the bank is 28°. The section appears stable, however, small streamlets emerging near the base and its bimodal character suggest degradation of ground ice in a unit below the exposed sand. No permafrost found but it is suspected at between 1 m and 3 m below the face (km 31.1, L).

COVERED: 1		6.52	6.52
COVERED: 2	Organic sand as unit 3 below	4.8	7.00
SAND: 3	Fine and medium grained, fine mode; angular; well sorted; quartz 85%, feldspar 10%, dark minerals 5%; frequently interbedded with silt, silt beds range from 10 cm to 50 cm thick.	10.0	17.0
COVERED: 4	Assumed same as unit 3	4.38	21.38

		Thickness (metres)	Depth of base (metres)
COVERED: 5	There is a distinct break in slope at the top of this unit. Within several metres below this break, small streamlets are observed coming through the colluvium. This is assumed to be a sand clay contact and the water is from degrading ground ice within the clay.	20.0	41.38
RIVER LEVEL			
July 24/73			
GB 19	Small exposure in the backwall of a bimodal flow. The backwall angle is 55° and the flow angle is 29°. Permafrost ranges between 14 cm and 35 cm below the face at the top and bottom of the exposure respectively (km 29.0, L).		
COVERED: 1	Root strength is high. The organic mat folds up to 2.4 m over the face.	.48	.48
TILL: 2	Very dark grey (7.5YR 3/2) fresh; silty, sandy texture; hard consistency undisturbed; low dry strength; low plasticity; inclusions 10% to 20%, maximum size 45 cm, mode 1 cm, boulders 1%, subrounded to rounded, predominantly crystalline; reticulate ice, maximum thickness of ice veins 0.4 cm, mode 0.1 cm to 0.2 cm, 10% to 20% excess. (WS-73-12a)	2.0	2.48
COVERED: 3		12.52	15.00
RIVER LEVEL			

Thickness      Depth of base  
(metres)      (metres)

July 25/73

GB 20      Excellent exposure in the backwall of an active bimodal flow. The slope of the backwall is  $59^\circ$  and from the base of the backwall to the river is  $26^\circ$ . High ice content in the lower clay and groundwater movement along the permafrost table in the overlying sand contribute to the unusually high activity of this flow. The top of the plain is 3.0 m above the top of the exposure and has been recently burned. (km 24.1, R).

COVERED:

1

.16

.16

SAND:

2

Silty with distinct silt bands; medium and fine grained, mode fine; well sorted; quartz 90%, feldspar 10%, dark minerals 1%; stratified, bedding controlled by silt bands and sorting of dark minerals; silt lenses up to 1 cm thick, mode 0.2 cm to 0.4 cm, 50% silt, 50% sand; frequently small extension faults showing downslope movement of exposure (toward river) in apparent frozen state; permafrost 10 cm to 75 cm below face; frequently ground water flow over permafrost table causes sand to slough off exposure (WS-73-14a @ 1.0 m).

3.59

3.75

CLAY:

3

Dark grey (10YR 4/1) fresh; silty 20% to 30%; soft consistency undisturbed; high dry strength; highly plasticity; reticulate ice ranging from 10% excess at the top to 80% excess at the base of the exposure.

2.0

5.75

		Thickness (metres)	Depth of base (metres)
COVERED: 4	The sloughing material leading to the river is moist with numerous streamlets leading from the back-wall. It is deeply gouged indicating recent large mass movement toward the river.	34.34	40.09

## RIVER LEVEL

July 25/73

GB 21 Several small active bimodal flows provide random exposures for approximately 45 m above the river. All of the contacts given are inferred except for the clay-sand contact. Limited permafrost was observed and is considered to be between 1 m and 4 m below the surface (km 27.35, L).

COVERED: 1	Vegetation mat is quite strong. In several cases backwall ablation has ceased because of the insulating effect of overhanging organic cover.	0.3	0.3
---------------	--	-----	-----

SAND: 2	Locally silty; medium and fine grained, mode is medium; angular; well sorted; quartz 85%, feldspar 10%, dark minerals including lignite 5%; gravel 1%; maximum size 58 cm (ice rafted); stratified and gently cross-bedded; bedding control is grain size sorting; silty areas have high moisture content.	17.5	17.8
------------	--	------	------

CLAY: 3	Silty 10%; soft consistency undisturbed; high dry strength; high plasticity; moderately fissured; reticulate ice, up to 40% excess ice, mode 20% to 30%.	12.8	30.60
------------	--	------	-------

		Thickness (metres)	Depth of base (metres)
TILL: 4	Very dark greyish brown (10YR 3/2) fresh; sandy silty texture; hard consistency undisturbed; low dry strength; low plasticity; inclusions 10% to 20%, maximum size 20 cm; mode 3 cm; fissured throughout.	16.0	46.60

## RIVER LEVEL

July 25/73

GB 22 Small active bimodal flow. Permafrost at 0.8 m (km 25.6, L).

COVERED: 1	Thin organic soil mat partially covering top of exposure.	0.3	0.3
---------------	---	-----	-----

TILL: 2	Very dark greyish brown (10YR 3/2) fresh; silty; hard consistency undisturbed; low dry strength; low plasticity; inclusions 10% to 15%, maximum size 38 cm, mode 3 cm; 1% boulders; reticulate ice, 10% to 15% excess ice, ice lenses 0.1 cm to 0.2 cm thick.	1.3	1.3
------------	---	-----	-----

COVERED: 3		5.2	6.8
---------------	--	-----	-----

## RIVER LEVEL

July 25/73

GB 23 Section is opposite large bimodal flow described in section GB 20. It is poorly exposed but till can be defined up to 17 m above the river (km 24.1, L).

COVERED: 1	Based on sections a short distance upstream, this is assumed to be clay (thickness given is not to the top of the bank).	10.0	10.0
---------------	--	------	------

		Thickness (metres)	Depth of base (metres)
TILL: 2	Dark grey (10YR 4/1) fresh; sandy and silty; hard consistency; undisturbed; very low dry strength; low plasticity; inclusions 10% to 20%, maximum size 26 cm, mode 4 cm, subrounded, crystalline; fissured throughout.	17.0	27.0
RIVER LEVEL			
July 25/73			
GB 24	Good exposure of sand. The sand appears to have been deposited in a channel eroded into underlying clay (km 21.1, L).		
SAND: 1	Silty 10%; medium and fine grained, medium mode; angular; moderately to well sorted; quartz 30%, feldspar 15%, dark minerals and lignite 5%; stratified and gently cross-bedded, bedding control is grain size sorting.	10.25	10.25
CLAY: 2	Silty 10% to 20%; firm consistency undisturbed; medium dry strength; high plasticity, fissured throughout; reticulate ice, 20% to 30% excess ice, ice veins vary from 1 mm to 3 mm thick.	1.0	11.25
COVERED: 3	Assumed clay as above unit 2.	10.5	21.75
COVERED: 4	Assumed till as described in sections GB 22 and GB 23.	10	31.75
RIVER LEVEL			



	Thickness (metres)	Depth of base (metres)
July 25/73		
GB 25	Examined a number of poorly exposed bimodal flows. Based largely of observations of colluvium the section is clay over till with a contact 13 m above the river (km 20.3, L).	
July 25/73		
GB 26	Steep section with sand exposed from 41 m (the top of the section) to 27 m, then colluvium to river level. A trickle of water and a slight break in slope at 23 m may indicate the approximate position of a sand-over-clay contact (km 18.9, L).	
July 25/73		
GB 27	Several small quasi-stationary bimodal flows. Exposure is poor but digging revealed several units. Clay is present at 11.6 m and rises at least 2 m above. No good evidence of the till was found, however pebbles and cobbles of crystalline rocks in colluvium at lower elevations in the flows suggest its presence (km 18.1, L).	
July 25/73		
GB 28	Bedrock appears as bluffs rising sharply out of the river, capped by Pleistocene deposits which are exposed in small bimodal flows. Permafrost is present throughout the section. Reticulate ice was observed in the siltstone (km 16.2, L).	
SAND: 1	This is a minimum thickness, thick bush and lack of time did not allow a thorough investigation of the extent of the sand. Silty 10%; medium and fine grained, mode is medium; angular; well sorted; quartz 85%, feldspar 10%, dark minerals including lignite 5%; several ice rafted cobbles observed, maximum size 34 cm; stratified and gently cross-bedded, bedding control through grain size	

Thickness      Depth of base  
(metres)      (metres)

	several permafrost expected between 2 m and 3 m below the fa		
CLAY: 2	The contact was not located and is inferred with a possible error of 2 m. Silty 20% to ; soft consistency undisturbed; high dry strength; medium to high plasticity; moderately fissured; reticulate ice, 20% to 30% excess ice.	10	20
TILL: 2	ity; very dark greyish brown (10YR 3/2) fresh; stiff to hard consistency undisturbed; very dry strength; low plasticity; inclusions 5%, maximum size 17 cm, mode 1 cm, crystalline 80%, shale and siltstone in various weathering stages 20%; fissured through- out; reticulate ice, 10% to 15% excess ice, active layer 80 cm to 120 cm thick (WS-73-22a @ 6.5 m)	7	27
SILTSTONE: 4	Very dark greyish brown (10YR 3/1) fresh; loose; non-calcareous; heavily fissured rendering it unstable and crumbly; carbonaceous material common and in various stages of decomposition to lignite; massive except for a 20 cm coal seam at 4.8 m; breaks down easily when wet, permafrost present, critical active layer thickness is 90 cm to 100 cm before localized fall type failures occur; reticulate ice, 10% to 15% excess ice; (WS-73-22b @ various levels in siltstone, WS-73-22c coal @ 4.9 m above river level).	7.5	34.5

RIVER LEVEL

		Thickness (mètres)	Depth of base (mètres)
July 26/73			
GB 29	Excellent exposure of Pleistocene sand over bedrock. The sand banks extend almost to river level but the unit itself seems perched on one or several units which are failing, causing the whole bank to regress. Tertiary bedrock dipping steeply southwest is exposed at river level. This attitude does not reflect regional trends rather it seems related to local instability (km 11.8, L).		
COVERED: 1	Thin organic rich sand at top of exposure.	0.3	0.3
SAND: 2	(The basal contact is estimated approximately 14 m of fresh exposure were examined at the top of the section). Medium and fine grained; mostly quartz; subangular to rounded, finer grains show greater roundness; subangular grains represent the medium fraction; lignite beds common, up to 3 cm thick, mode 0.3 cm; traces of undecomposed organics; bedding control is with lignite beds, limited cross-bedding; permafrost estimated between 2 m and 3 m below the face (AR-73-7 @ 8 m).	17.38	17.68
COVERED: 3	Assumed to be clay overlying till as described in section GB 28.	18.08	35.76
COAL: 4	Fissured, peds up to 3 cm in diameter; sand and silt content up to 40%, mode 10% to 20%; frequently plant fossils are well preserved; amber crystals common up to 0.1 cm in diameter; no distinct bedding.	1.22	36.98

		Thickness (metres)	Depth of base (metres)
SILTSTONE: 5	Greyish brown (10YR 5/2) fresh; loose; non-calcareous; fissured throughout, maximum diameter of peds 3 cm, mode 2 cm; traces of plant fossils in various stages of decomposition to lignite; no distinct bedding; breaks down easily when wet.	2.30	39.28

## RIVER LEVEL

July 26/73

GB 30 — Exposure of Pleistocene deposits over bedrock in a west-facing stream cut approximately 700 m upstream from the confluence of Brackett River. Between this section and GB 29 the stratigraphy is obscured by cover while in a western direction through GB 31 and GB 32 the stratigraphy is well exposed (km 11.5, L.)

CLAY: 1	Silty 40 to 50%; firm consistency undisturbed; medium dry strength; medium plasticity; fissured; believed to contain ground ice, permafrost not observed within 0.75 m (thickness given is not to the top of the bank; WS-73-23a @ 2.0 m).	3.8	3.8
------------	--	-----	-----

TILL: 2	Silty 20%; sandy 40%, very poorly sorted, quartz 50%, lignite 20%, other minerals 30%; subangular to subrounded; gravelly 40%, very poorly sorted, maximum size 14 cm, mode 1 cm, sub-rounded, frequently coated with a fine-grained, non-calcareous precipitate; unit is massive and dark in colour; it becomes very dusty (coal dust) when dried; coal grains are angular to subangular and rarely exceed 1 cm in diameter. The till described here is unlike any other exposure of till found along Great Bear River (WS-73-23b @ various levels).	5.8	3.8
------------	---	-----	-----

		Thickness (metres)	Depth of base (metres)
COAL: 3	Fissured; maximum diameter of peds 2 cm, mode 1 cm; sand and silt content up to 30%, mode 10% to 20%; abundant plant fossils; amber crystals common up to 0.1 cm in diameter; white siltstone bands common, up to 5 cm thick and extending 3 m laterally (WS-73-23c, at various levels).	2.89	12.49
SILTSTONE: 4	Very pale brown (10YR 8/4) weathered; sand 26% (74% passed #200 sieve); soft; non-calcareous; highly fissured, commonly breaks in egg-shaped peds; well oxidized along fissures; anastomosing bedding 6 cm to 23 cm thick (WS-73-23d @ various levels). Laboratory analysis indicated high plasticity silt classification (MH) and high montmorillonite content (this clay mineral comprised almost 100% of material passing, the #200 sieve).	4.1	16.59
COVERED: 5		8.84	25.43
RIVER LEVEL			

July 26/73

GB 31 For the purpose of correlation with the same stratigraphic location as the top of unit 4 section GB 30, the difference in elevation to river level is now 15 m (km 11.2, L).

Thickness      Depth of base  
(metres)      (metres)

July 26/73

GB 32      Excellent exposure of Pleistocene and Tertiary deposits opposite the Brackett River confluence. The upper part shows localized bimodal flow development. The lower portion is protected from large scale river erosion by the accumulation of colluvium in the river course. Permafrost is suspected at between 2 m and 3 m below the face. Significant ground ice is likely only in the Pleistocene clay and till (km 10.3, L).

COVERED: 1		3.0	3.0
SAND: 2	Silty 10% to 20%; medium to fine grained, medium mode; subangular; moderately to well sorted; 80% quartz, 20% dark minerals and lignite; noticeably low in feldspar; no inclusions observed; minor cross-bedding, otherwise bedding indistinct; lower contact is covered but is inferred with an accuracy of 1 m.	4.07	7.07
CLAY: 3	Silty 20% to 30%; firm consistency undisturbed; medium dry strength; medium plasticity; fissured; substantial ground ice is suspected; many bimodal flow scars appear around the bluff.	3.0	10.07
TILL: 4	Black (SY 2.5/2) fresh; silty texture; hard consistency undisturbed; low dry strength; low plasticity; inclusions 10% to 20%, maximum size 96 cm, mode 0.8 cm, boulders and cobbles 1%; well developed fissures; (WS-73-25a @ 5.0 m).	10.07	20.14

		Thickness (metres)	Depth of base (metres)
SANDSTONE: 5	Very poorly indurated; easily broken down by sampling or rubbing between fingers; medium grained; subangular; very well sorted; quartz 50%, dark minerals 50%, no feldspar observed; stratified, beds range from 3 cm to 20 cm, bedding controlled by sorting of dark minerals; no permafrost observed; upper contact with till is undulatory (WS-73-25b @ various levels).	1.3	21.44
CONGLOMERATE: 6	Poorly indurated; easily broken down with a shovel and can be broken down by rubbing between fingers; maximum inclusion size 21 cm, mode 1 cm to 2 cm, subrounded and subangular; predominantly dark siliceous igneous rocks; gravel sizes 60% to 70% sand sizes 30% to 40%; stratified, bedding controlled by beds of sandstone (as above unit 5) up to 1.3 m thick (WS-73-25d @ 11 m).	13.75	35.19
SILTSTONE: 7	Light grey (10YR 7/1) weathered; slightly sandy 10%; loose; non-calcareous; fissured; breaks down very easily when wet; sand is 50% quartz, 50% dark minerals, subrounded; fissured structure; no permafrost observed (WS-73-25e @ 4.0 m).	6.0	41.19
CONGLOMERATE: 8	As above unit 6; very irregular thickness, never exceeding 0.6 m and sometimes pinching out completely.	0.6	41.79

		Thickness (metres)	Depth of base (metres)
SANDSTONE: 9	Light olive brown (2.5 Y 5/6) fresh and weathered; poorly indurated; easily broken down by sampling or rubbing between fingers; medium and fine grained; subangular to sub-rounded; very well sorted; quartz 50%, dark minerals 50%, no feldspar observed; massive but well cross-bedded; vertical joints spaced at between 0.5 m and 1.0 m throughout (WS-73-25f @ various levels).	9.32	51.11
RIVER LEVEL			
GB 33	Observed coarse alluvial deposits overlying Tertiary sandstone. Contact approximately 6 m above river level (km 8.0, L).		
July 26/73 and July 1/75			
GB 34	Very similar to GB 30. Pleistocene sand over tertiary bedrock. Failure of one or more units beneath the sand is hidden by colluvium. Tertiary bedrock is almost totally covered with colluvium but its top can be picked at a prominent break in slope with an estimated accuracy of 3 m (km 6.5, L).		
COVERED: 1	Organic sand immediately above exposure.	0.3	0.3
SAND: 2	Clean; fine grained; subangular and angular; very well sorted; quartz 75%, lignite 10%, dark minerals and feldspar 5%; lignite usually occurs in beds 2 cm to 3 cm thick; bedding control is by lignite beds, low angle cross-beds common; permafrost estimated at between 2 m and 3 m below the face (AR-73-8 @ various levels; C14 sample HH-WS-7527-1 sampled July 1, 1975 @ 5.0 m).	20	20.30



		Thickness (metres)	Depth of base (metres)
COVERED: 3	The base of this covered interval is a prominent break in slope. This is assumed to be a contact of clay overlying till as described in GB 32.	18	38.30
COVERED: 4	This interval is assumed to be Tertiary bedrock probably the basal sandstone mentioned in GB 32. This sandstone unit is observed across the river in GB 35.	7	45.30
RIVER LEVEL			
July 26/73			
GB 35	Section on the north side of the Great Bear facing GB 34. Approximately 10 m of section are visible; 2 m of till overlying 6 m of sandstone and siltstone to a well developed boulder pavement which extends for a further 2 m to river level (km 6.6, R).		
July 26/73			
GB 36	A long exposure of Pleistocene deposits over Tertiary bedrock. The following observations were made from a boat in the river. One or more recessive units (probably sand over clay) occupy the top of the section and are largely hidden from view, their thickness is estimated at 13 m. Till is the first resistant unit. It underlies the recessive units, and is estimated at 6 m thick. Bedrock is approximately 20 m thick and extends to river level. The recessive units show signs of recent bimodal flow activity (km 3.3, L).		
July 26/73			
GB 37	A Pleistocene and Tertiary section on the left bank of the Great Bear immediately off the west end of the Fort Norman air strip. The following observations were made from a boat in the river. The Pleistocene deposits consist of 6 m of sand over 7 m of till. Tertiary bedrock consists of 20 m of sandstone with beds of conglomerate. All units appear stable (km 0.4, L).		

	Thickness (metres)	Depth of base (metres)
--	-----------------------	---------------------------

July 22/73

GB 38

This section is measured in Cretaceous bedrock on the north side of Great Bear River about mid-point in the St. Charles Rapids. A similar exposure on the opposite side of the river was inspected from a helicopter.

These rocks are placed in the Cretaceous Little Bear Formation. Upstream approximately two kilometres random exposures of a black very fissile shale, probably the Cretaceous East Fork Formation, were observed. No definite contact could be found between the East Fork and Little Bear Formations. Downstream approximately two kilometres there is evidence in stream cuts and along the river bank of still another shale. No good exposures of this shale were found.

The strata in the measured section dip  $5^{\circ}$  to  $73^{\circ}$  azimuth. At least two joint sets are visible. The averages of these joint sets give strikes of  $122^{\circ}$  and  $203^{\circ}$ , both with vertical dips. The range was as much as  $20^{\circ}$  from these averages.

(Measuring down in the section)

The section can be divided into units of similar thickness. The top unit is a siltstone while the bottom unit is dominantly siltstone with interbeds of arenaceous shale (km 57.6, R.).

---

TOP UNIT

COVERED: 1	Mostly peat and organic material.	0.5	0.5
SILTSTONE: 2	Very pale brown (10YR 7/4) weathered, pale yellow (5Y 7/3) fresh; moderately well cemented, grains may be rubbed off with fingers, but the rock can only	12.1	12.6

		Thickness (metres)	Depth of base (metres)
	be broken with a hammer; non-calcareous; cement is often oxidized; fine sand represents about 30% of the rock; bedding resembles a thin brickwork, it is thinly bedded and broken; cross-bedding is present and ripple marks common on bedding planes; the dominant mineral is quartz with feldspar and carbonaceous content 5%; iron-rich blotches on bedding planes are common.		
SILTSTONE: 3	As above unit 2. Arcaceous, fissile shale interbeds up to 2 cm thick. Siltstone bedding planes show frequent but random iron stain.	1.0	13/6
SILTSTONE: 4	As above unit 2.	8.25	21.85
<u>BOTTOM UNIT</u>			
SILTSTONE & SHALE 5	Siltstone as above unit 2; fine sand content 10% to 20%; shale partings 0.1 cm thick run through siltstone beds; the shale is very arenaceous, fissile, and friable; beds vary in thickness from 1 cm to 2 cm; increasing near base to 3 cm to 5 cm thick; ironstone concretions are present in both the siltstone and shale beds; minor evidence of ripple marks on the siltstone bedding planes; minor burrowing in the siltstone; shale content increases with depth from 30% to 50%.	8.68	30.53
COVERED: 6		2.59	33.12
RIVER LEVEL	Estimated river surface el. 97.7 m.		

		Thickness (metres)	Depth of base (metres)
Aug. 30/72			
GB 39	G.E. Crippen & Associates Ltd. test hole B14 (65°01'N, 124°25'W).		
	Collared at el. 213.4 m.		
TILL: 1	Grey; sandy 50%, fine to coarse sand with boulder chips (originally called CLAY).	15.55	15.55
TILL: 2	Sandy, fine to coarse, subangular; 25% rock chips; clayey 10% (originally called SAND).	3.36	18.91
TILL: 3	Clayey 25%; rock chips; boulders likely every 60 cm to 90 cm where drill slowed down and vibrated (originally called CLAY (TILL)).	40.55	59.46
Oct. 7/75			
GB 40	Exposure of Pleistocene sediments over Tertiary bedrock. A normal fault present in bedrock. Orientation of fault plane is obscured by colluvium. Southwest side is down; bentonitic siltstone (see Unit 5, GB 30) in the hanging wall, against siltstone and sandstone (see Units 7 and 9, GB 32) in the footwall. This supports the correlation established in GB 30 and GB 31 above the Brackett River confluence (km 0, beach level along Mackenzie River at the northwest end of Fort Norman).		
Sept. 5/71			
GB 41	G.E. Crippen & Associates Ltd. test hole number M20 (65°02'N, 124°38'W).		
	Collared at el. 135.3 m.		
TILL: 1	Encountered silt, sand, gravel, cobbles and boulders; boulders granitic, well rounded; silty material between 3.36 m and	32.00	32.00

		Thickness (metres)	Depth of base (metres)
	5.80 m; hole logged from wash water; began losing circulation at 30.50 m.		
2	Estimated distance from the bottom of this hole to river level.	7.30	39.30
Sept. 5/71			
GB 42	G.E. Crippen & Associates Ltd. test hole M20 (65°02'N, 124°38'W).		
	Collared at el. 128.0 m.		
SAND: 1	Yellow-brown; very fine.	2.44	2.44
GRAVEL: 2	Sandy; many boulders, rounded.	5.80	8.24
TILL: 3	Grey; clayey, 50% passed the #200 sieve. Estimated river level is at 29.46 m in this interval (36.59 m below collar).	34.45	42.69
GRAVEL: 4	Sandy.	12.20	54.89
Sept. 6/71			
GB 43	G.E. Crippen & Associates Ltd. test hole M2 (65°03'N, 124°50'W).		
	Collared at el. 147.8 m.		
SAND:	Gravelly; poorly sorted; occasional rounded boulders on surface, maximum size 60 cm diameter.	4.88	4.88
SAND: 2	Medium to coarse; some gravel and fines; sloughing in hole.	8.84	13.72

		Thickness (metres.)	Depth of base (metres)
Aug. 20/71			
GB 44	G.E. Crippen & Associates Ltd. test hole R2 (km 51.9, L).		
RIVER WATER: 1	Water surface at el. 84.80 m.	0.23	0.23
BOULDERS: 2	Granitic composition.	0.45	0.68
GRAVEL: 3	Few boulders; no finer material recovered.	8.53	13.48
SAND: 4	Few granitic boulders; no fines, fines possibly washed away by drill water.	8.53	13.48
SILT: 5	Grey; fine sand particles in drill water and a small amount in core barrel.	9.75	23.23
Feb. 2/73			
GB 45	Pemcan Services test hole 2, site number FN13 (64°57'N, 125°26'N).		
TOPSOIL: 1	Dark brown; little silt; fibrous; ground ice described as Vx, 10% to 50% by volume.	0.31	0.31
SAND: 2	Grey; little silt; fine grained; poorly graded; ground ice described as Vx and Vs; bottom 0.61 m contains some gravel, ground ice described as Vx, 10% to 50% by volume.	3.66	3.97
GRAVEL: 3	Brown; sandy; trace of silt; poorly graded; pebbles 2.5 cm to 4 cm, subangular to subrounded, occasional cobbles, mainly limestones and quartzites; ground ice described as Vx, 10% to 50% by volume.	1.52	5.49

Thickness      Depth of base  
(metres)      (metres)

Feb. 2/73

GB 46      Pemcan Services test hole 1, site number FN30C (64°5'N,  
125°28'W).

TOPSOIL:      Dark brown to black; little silt;      0.15      0.15  
1      organic and fibrous; ground ice  
described as Vx, 10% to 50% by  
volume.

SAND:      Grey; trace of silt; fine grained;      5.34      5.49  
2      poorly graded; silt pockets  
common below 3.20 m; ground ice  
throughout, described as Vx,  
10% to 50% by volume.

Jan. 30/73

GB 47      Pemcan Services test hole 3, site number FN 10 (km 5.9, L).

SILT:      Dark brown; organic; ground ice      0.46      0.46  
1      described as Vx, 10% to 50% by  
volume.

SILT:      Medium brown to grey; little sand;      2.59      3.05  
2      low plasticity; ground ice des-  
cribed as Vs, to 1.68 m greater  
than 50% by volume, below 1.68 m  
10% to 50% by volume; change in  
ice content correlates with  
increase in sand content at  
1.68 m.

GRAVEL:      Medium brown; some sand; little      0.92      3.97  
3      silt; ground ice described as  
Vx, 10% to 50% by volume.

SILT:      Blue-grey; little sand; ground      0.92      4.89  
4      ice described as Vs, 10% to 50%  
by volume.

		Thickness (metres)	Depth of base (metres)
December 12/72			
GB 48	R.M. Hardy & Associates Ltd. test hole 112 approximately mile 582, Mackenzie Highway (km 3.9 L).		
PEAT: 1	Amorphous-granular peat containing woody, fine fibres; ground ice described as Nbn.	0.31	0.31
SAND: 2	Brown; variable silt and clay content throughout (non-plastic); ground ice described as Nbn; $w_n$ 13% to 35%.	6.70	7.32
CLAY: 3	Grey; high plasticity; ground ice described as Vx, 10% to 50% by volume; $w_n$ 38%.	0.31	7.32
Dec. 12/72			
GB 49	R.M. Hardy & Associates Ltd. test hole 113 approximately mile 582, Mackenzie Highway (km 3.8 L).		
PEAT: 1	Amorphous-granular peat containing woody, fine fibres; ground ice described as Nbe.	0.15	0.15
SAND: 2	Brown; very silty, becoming less silty with depth; fine grained; non-plastic except between 1.37 m and 3.20 m where low plasticity; ground ice described as Nbe to 1.18 m, Nbn thereafter; $w_n$ 25% rising to 33% at base.	6.86	7.01
CLAY: 3	Grey; high plasticity; ground ice described as Vx, 10% to 50% by volume; $w_n$ 24%.	0.31	7.32



		Thickness (metres)	Depth of base (metres)
Dec. 12/72			
GB 50	R.M. Hardy & Associates Ltd. test hole 107 approximately mile 581, Mackenzie Highway (64°54'N, 125°32'W).		
PEAT: 1	Amorphous-granular peat; ground ice described as Nbn.	0.31	0.31
SILT: 2	Sandy, organic; ground ice described as Nbn; $w_n$ 66%.	0.31	0.62
SAND: 3	Brown; slightly silty; fine grained; non-plastic; ground ice described as Nbn; $w_n$ near 80% at top levelling off quickly to 25%.	2.74	3.36
SILT: 4	Grey; clayey; medium plasticity; ground ice described as Nbn; $w_n$ 25% (originally described as CLAY).	1.07	4.43
SILT: 5	Grey; clayey; medium plasticity; ground ice described as Vx, 30% by volume to 0.21 m, thereafter 5% by volume (sample RMH B3).	2.90	7.33
Dec. 12/72			
GB 51	R.M. Hardy & Associates Ltd. test hole 122 approximately mile 579, Mackenzie Highway (64°54'N, 125°29'W).		
SAND: 1	Brown; silty; fine grained, non-plastic; ground ice described as Nbn to 1.83 m, thereafter it is described as Vx, ice content rises with depth from 1% to 60% by volume; $w_p$ increases with depth from 8% to 74%.	5.18	5.18
CLAY: 2	Grey; silty; high plasticity; ground ice described as Vx, excess by volume 15% to 20%; $w_n$ 32% to 38%.	2.14	7.32

		Thickness (metres)	Depth of base (metres)
date not given			
GB 52	Pemcan Services test hole C32, site number FN8 (drilled by R.M. Hardy & Associates Ltd; 64°53'N, 125°22'W).		
PEAT: 1	Ground ice described as Nbn.	0.62	0.62
SAND: 2	Brown; very silty; clayey through bottom 30 cm; fine grained; low plasticity; ground ice described as Nbn.	1.52	2.14
CLAY: 3	Brown to grey, becoming grey, silty and sandy, becoming less with depth; medium plasticity; sandy high plasticity at depth; ground ice described as Nbn.	2.74	4.98
Dec. 12/72			
GB 53	R.M. Hardy & Associates Ltd. test hole 110 mile 582, Mackenzie Highway (km 3.1 L).		
PEAT: 1	Amorphous-granular peat; ground ice described as Nbn.	0.15	0.15
SAND: 2	Brown; trace of silt at top, increasing slightly downward; non-plastic; ground ice described as Nbn; $w_n$ varies from 13% to 26%.	2.44	2.59
SILT: 3	Brown; sandy; low plasticity; ground ice described as Nbn; $w_n$ 28%.	1.37	3.96
SAND: 4	Brown; silty; non-plastic; ground ice described as Nbn; $w_n$ 28%.	0.46	4.42
SILT: 5	Brown; sandy; low plasticity; ground ice described as Nbn; $w_n$ 24%.	0.76	5.18

		Thickness (metres)	Depth of base (metres)
CLAY: 6	Grey; medium plasticity; ground ice described as Nbn; $w_n$ 26%.	0.31	5.49
CLAY: 7	Grey; silty; medium plasticity; ground ice described as Nbn.	1.83	6.32
Dec. 12/72			
GB 54	R.M. Hardy & Associates Ltd. test hole 111 mile 582, Mackenzie Highway (km 2.6, L).		
SAND: 1	Brown, becoming grey with depth; silty, becoming clayey with depth; ground ice described as Nbn; $w_n$ 14% to 30%.	6.10	6.10
CLAY 2	Slightly silty; trace of sand; ground ice described as Nbn; $w_n$ 25%.	2.22	8.32
Feb. 3/73			
GB 55	R.M. Hardy & Associates Ltd. test hole 452 approximately mile 582, Mackenzie Highway (km 2.3 L).		
SILT: 1	Dark brown; sandy; organic with organic inclusions and peat inclusions below 0.61 m; ground ice described as Nbn; $w_n$ 58% to 100%.	1.52	1.52
SAND: 2	Light brown to grey; silty; fine grained; non-plastic; ground ice described as Nbn; $w_n$ varies from 24% plus at the top to 29% with depth.	3.66	5.18
CLAY: 3	Dark grey brown; slightly sandy; medium plasticity; ground ice 20% excess; $w_n$ increases from 30% to 44% with depth.	0.92	6.10

		Thickness (metres)	Depth of base (metres)
			date not given
GB 56	Pemcan Services test pit TP1 site number FN-14. (All deposits in the test pits are assumed to be unfrozen (km 2.5 L).		
TOPSOIL: 1	Black, organic, roots.	0.12	0.12
SILT: 2	Light brown; some clay; moist.	0.12	0.24
SAND: 3	Low in silt; fine grained; dry.	0.67	0.91
			Feb. 5/73
GB 57	R.M. Hardy & Associates Ltd. test hole 465 approximately mile 538, Mackenzie Highway (km 1.2 R)..		
SILT: 1	Organic.	0.31	0.31
SILT: 2	Brown; slightly clayey; low plasticity; ground ice described as Nbn; $w_n$ varies from 38% to 25% with depth (originally described as TILL).	1.22	1.53
SAND: 3	Grey; slightly silty (silt and clay sizes 7%, sand sizes 93%); fine grained; low plasticity to non-plastic; ground ice described as Nbn; $w_n$ 12% to 26% (originally described as TILL).	2.74	4.27
SILT: 4	Grey; sandy; pebbles to 0.6 cm; low plasticity; ground ice described as Nbn; $w_n$ 12% to 26% (originally described as TILL).	1.22	5.49

		Thickness (metres)	Depth of base (metres)
SAND: 5	Grey; slightly silty (silt and clay sizes 11%, sand sizes 89%); fine grained; non-plastic; ground ice described as Nbn; $w_n$ 20% to 25% (originally described as TILL).	0.61	6.10
Feb. 5/73			
GB 58	R.M. Hardy & Associates Ltd. test hole 461 approximately mile 583, Mackenzie Highway (km 1.4 R).		
PEAT: 1		0.15	0.15
SILT: 2	Brown; clayey; low to medium plasticity; ground ice described as Nbe to 0.31 m, unfrozen thereafter; $w_n$ at top of unfrozen zone 28%.	0.76	0.91
TILL: 3	Brown; becoming silty at 0.92 m, then clayey at 2.42 m; pebbles up to 1.25 cm in the silty zone; generally non-plastic but exhibits low plasticity in clayey zone; unfrozen to top of silty zone, thereafter ground ice defined as Nbn; $w_n$ 10% and 20%.	3.28	4.19
TILL: 4	Grey; sandy; pebbles to 0.75 cm; fine grained; non-plastic; rust specks below 2.74 m; ground ice described as Nbn; $w_n$ 18% to 24%.	4.57	9.37
Feb. 12 & 13/73			
GB 59	R.M. Hardy & Associates Ltd. test hole 522 approximately mile 583, Mackenzie Highway (km 1.3, R).		

		Thickness (metres)	Depth of base (metres)
PEAT: 1	Predominantly amorphous-granular, containing fine woody fibres, held in a woody, coarse-fibrous framework; ground ice described as Vx with an excess of up to 65% in the top 0.31 m, and Vr with an excess of 5%; $w_n$ 40% to 100% plus; the bulk unit weight is 7.43 kN/m <sup>3</sup> (47.3 pcf), the dry unit weight 1.81 kN/m <sup>3</sup> (11.5 pcf).	0.46	0.46
CLAY: 2	Dark brown; sandy; becoming slightly silty below 1.98 m; high plasticity; ground ice described as Vr to 1.07 m, Nbn thereafter; excess ice ranges from 49% to 55% in Vr zone; $w_n$ drops from a high of 66% near the top to 10% at the bottom, overall it is variable; the bulk unit weights vary from 13.35 kN/m <sup>3</sup> (78.6 pcf) to 16.90 kN/m <sup>3</sup> (107.5 pcf), the dry unit weights vary from 8.16 kN/m <sup>3</sup> (51.9 pcf) to 12.21 kN/m <sup>3</sup> (77.7 pcf). Estimated river level 5.0 m.	5.50	5.96
TILL: 3	Brown; sandy (silt and clay sizes 9%, sand sizes 41%, gravel sizes 50%); non-plastic; ground ice described as Nf; $w_n$ generally 8% increasing slightly near the bottom (originally described as GRAVEL).	2.42	8.38
CLAY SHALE: 4	Grey; arenaceous; rust specks; ground ice described as Nbn; $w_n$ 22%.	5.64	14.02

		Thickness (metres)	Depth of base (metres)
SANDSTONE: 5	Grey; poorly indurated; non-plastic; trace of argillaceous material below 6.10 m (silt, and clay sizes 27%, sand sizes 73%) low plasticity; ground ice described as Nbn; $w_n$ 19% to 26%.	13.10	27.12
CLAY SHALE: 6	Grey; arenaceous; high plasticity; ground ice described as Nbn; $w_n$ 23%.	0.61	27.73
SANDSTONE: 7	Grey; trace of argillaceous material; poorly indurated; low plasticity; ground ice described as Nbn; $w_n$ decreases from 22% to 18% with depth.	1.22	28.95
GREY SHALE: 8	Grey; arenaceous; high plasticity; ground ice described as Nbn; $w_n$ decreases from 18% to 15% with depth.	2.74	31.69

Sept. 12/71

GB 60 G.E. Crippen & Associates Ltd. test hole M14, 4.88 km (16,000 feet) east northeast of the confluence of the Porcupine River and the Great Bear River (outside of area shown in Figs. 2.2 and 2.3).

Collared at el. 176 m.

TILL (CL): 1	Clayey; generally sand, gravel and boulders in a silty clay matrix; $w_n$ 17% (sample GEC 43 @ 3.66 m, sample GEC @ 54.9 m).	62.5	62.5
-----------------	--	------	------

Estimated river level at 25.9 m in this hole.

		Thickness (metres)	Depth of base (metres)
Aug. 31/71			
GB 61	G.E. Crippen & Associates Ltd. test hole M18, 3.05 km. (10,000 feet) west northwest of the confluence of Rosalie Creek and Great Bear River (outside of area shown in Figs. 2.2 and 2.3).		
Collared at el. 174.1 m.			
TILL: 1	Contains about 25% brown clay; sand, medium, subangular (originally described as GRAVELLY CLAY).	3.35	3.35
SAND AND GRAVEL: 2	Pea gravel with medium to fine sand. Very few fines.	6.10	9.45
TILL: 3	Clay matrix; some sand; gravel, few boulders. River level is estimated at 3.08 m beneath the top of this unit (originally described as GRAVELLY CLAY).	24.07	33.52
SAND AND GRAVEL: 4	Few fines.	5.18	38.70
TILL:	Clay matrix; some sand and gravel (originally described as CLAY).	23.79	62.49
Aug. 29/71			
GB 62	G.E. Crippen & Associates Ltd. test hole R11 (km 10.4 R, at Brackett River confluence).		
Collared at el. 61.1 m.			
BOULDERS: 1	Estimated river level at 1.20 m of this unit.	4.57	4.57



		Thickness (metres)	Depth of base (metres)
SILTSTONE and SHALE: 2	Salt and pepper colour; very fine grained; argillaceous matrix; often soft; generally oxidized; 0.75 cm laminations; core recovered in 2.5 cm to 7.5 cm lengths (originally described as SANDSTONE).	3.50	8.07
SILTSTONE and SHALE: 3	Brown; sandy; weathered; core recovered in 7.5 cm lengths (originally described as SILTSTONE).	0.15	8.22
SILTSTONE and SHALE: 4	Grey; argillaceous; 0.35 cm tabular coal lenses, 1% of total unit; rock generally weak; core recovery in 0.31 m lengths, machine breaks; no visible alteration (originally described as ARGILLACEOUS SILTSTONE).	2.14	10.36
Sept. 26/71			
GB 63	G.E. Crippen & Associates Ltd. test hole R21 (km 10.6, R).		
SAND: 1	Brown; medium to coarse; very little fine material; poorly graded.	4.57	4.57
CLAY: 2	Grey; silty; no sand or gravel; very firm; no ice observed in core; good core recovery.	1.52	6.09
TILL: 3	Sandy; subangular boulders, very few fines (originally described as GRAVEL).	4.57	10.66
SANDSTONE: 4	Grey; fine; no recovery except for return in wash water (originally described as SILTY SAND).	7.62	18.28

		Thickness (metres)	Depth of base (metres)
5	CONGLOMERATE: Grey; sandy, approximately 4% is 1.25 cm well rounded gravel (originally described as GRAVELLY CLAY).	0.31	18.59
6	CONGLOMERATE Well rounded; igneous rocks (originally described as SANDY GRAVEL).	3.05	21.64
7	Estimated distance from bottom of hole to river level.	19.56	41.20
Sept. 28/71			
GB 64	G.E. Crippen & Associates Ltd. test hole R22 (km 12.25,R).		
Collared at el. 102.4 m.			
1	SAND: Grey; more than 50% passed #200 sieve; gravel, subangular (originally described as SILTY CLAYEY TILL).	4.27	4.27
2	CLAY: Grey; till-like; more than 80% passed #200 sieve; clay becomes very firm after thawing and drying; ice lenses in core (originally described as CLAYEY SILT).	12.20	16.47
3	TILL: Grey; cobbles up to 10 cm, angular to subangular; approximately 50% passed #200 sieve. Average core recovery for hole 62%.	3.36	19.83
4	Estimated distance from bottom of the hole to river level.	21.07	40.90
Sept. 24/71			
GB 65	G.E. Crippen & Associates Ltd. test hole R20 (km 12.25,R).		
1	RIVER WATER: Surface el. 59.89 m.	1.50	1.50

		Thickness (metres)	Depth of base (metres)
BOULDERS: 2	Sandy gravel mixed with boulders; no recovery.	4.40	5.90
SANDSTONE: 3	Grey; medium; (originally des- cribed as SAND).	7.90	13.80
April 8/72			
GB 66	G.E. Crippen & Associates Ltd. test hole R206 (km 5.5, R).		
	Collared at el. 96.5 m		
SAND: 1	Brown; fine to coarse; frozen; wet.	3.05	3.05
SILT: 2	Grey; frozen; wet.	13.72	16.77
GRAVEL: 3		2.93	18.90
TILL: 4	Grey; sandy, small percentage of gravel (originally described as SILT).	11.58	30.48
SILTSTONE and SHALE: 5	Light grey; poorly indurated; breaks down when soaked; very sandy; indication of vertical jointing (Estimate local river level at 11.22 m).	17.68	48.16
April 8/72			
GB 67	G.E. Crippen & Associates Ltd. test hole R207 (km 5.5, R).		
	Collared at el. 91.4 m		
SAND: 1	Brown; fine to medium; frozen.	3.96	3.96
GRAVEL: 2	Sandy; maximum gravel size 1.92 cm.	0.61	4.57

		Thickness (metres)	Depth of base (metres)
SILT: 3	Frozen; wet when thawed.	7.01	11.58
TILL: 4	Silt 50%, sand 25%, gravel 25%; maximum gravel size 2.54 cm, angular; low moisture content (originally described as SILT).	17.37	28.95
SHALE: 5	Soft; sandstone interbeds near bottom (Estimated local river level at 6.65 m, 34.74 m below collar).	7.62	36.57
April 8/72			
GB 68	G.E. Crippen & Associates Ltd. test hole R208 (km 5.7, river course).		
ICE: 1	Ice surface el. 58.6 m. Estima- ted water surface el. 58.3 m.	1.52	1.52
WATER: 2		0.20	1.72
SAND: 3	Silty, some gravel.	1.20	2.92
SILT: 4	Grey.	0.90	7.82
SILTSTONE and SHALE: 5	Light grey with some greenish grey layers up to 0.64 cm thick; latter are higher in clay content; a few 0.64 cm layers of silty sandstone orthogonal to core axis; cement breaks down when soaked in water (originally described as SILTSTONE).	6.10	13.92

		Thickness (metres)	Depth of base (metres)
April 9/72			
GB 69	G.E. Crippen & Associates Ltd. test hole R209 (km 5.6 river course).		
ICE: 1	Ice surface el. 58.5 m. Estimated water surface el. 58.1 m.	1.52	1.52
WATER: 2		0.70	2.22
GRAVEL: 3	Few cobbles and boulders.	0.30	2.52
SILT: 4	Sandy; occasional boulders.	5.80	8.32
SILTSTONE and SHALE: 5	Dark with layers of light, soft, silty material (originally described as SHALE).	2.70	11.02
SILTSTONE and SHALE: 6	Light grey with some greenish grey layers up to 0.64 m thick; latter are higher in clay content; generally soft; may be broken down by hand; random siltstone interbeds; a 0.31 m bed of calcareous sandstone near bottom; all disintegrate when soaked in water except calcareous sandstone; some evidence of jointing; maximum core length 17.8 cm with 30% less than 2.5 cm (originally described as SILTY SANDSTONE).	18.30	29.32
April 10/72			
GB 70	G.E. Crippen & Associates Ltd. test hole R210 (km 5.2 R).		
	Collared at el. 91.4 m.		
SILT: 1	Grey; sandy; frozen.	1.84	1.84

		Thickness (metres)	Depth of base (metres)
SAND: 2	Fine to coarse; some subangular gravel; ice lenses.	4.30	6.14
CLAY: 3	Frozen; ice lenses (originally described as SILT).	9.10	15.24
TILL: 4	Occasional boulder; angular; loss of drill mud reported (originally described as SILT, SAND and GRAVEL)	7.60	22.84
SILTSTONE AND SHALE: 5	Soft; coring impossible (Estimated river level at 13.2 m (originally described as SHALE)	21.40	44.24
SILTSTONE AND SHALE: 6	Dark grey; fine grained; very soft, may be broken by hand; disintegrates when soaked; core recovered in lengths to about 2.5 cm; drill mud loss reported (originally described as SILTY SANDSTONE)	4.50	48.74

April 5/72

GB #71 G.E. Crippen & Associates Ltd. test hole R201 (km 10.5, river course).

ICE: 1	Ice surface el. 62.6 m. Estimated water surface el. 62.3 m.	1.83	1.83
WATER: 2		2.76	4.59
GRAVEL: 3	Sand, some silt and a few boulders.	2.14	6.73
SILTSTONE and SHALE: 4	Slightly arenaceous; stiff; core could not be recovered (originally described as SILT).	16.75	23.48

		Thickness (metres)	Depth of base (metres)
SILTSTONE and SHALE: 5	Light grey with some greenish grey layers up to 0.64 m thick; latter are higher in clay content; silty; brittle but may be easily broken down by hand; disintegrates when soaked in water; longest piece of core recovered 15 cm, 50% less than 5 cm (originally described as SILTY SHALE).	6.09	29.57
April 6/72			
GB 72	G.E. Crippen & Associates Ltd. test hole R202 (km 10.2, river course).		
ICE: 1	Ice surface el. 62.2 m. Estimated water surface el. 61.9 m.	1.83	1.83
WATER: 2		2.30	4.13
GRAVEL: 3	Sandy with small percentage silt and boulder sizes.	2.70	6.83
SILTSTONE and SHALE: 4	Grey; slightly arenaceous; stiff, core could not be recovered (originally described as SILT).	14.60	21.43
SILTSTONE and SHALE: 5	Light grey with some greenish grey layers up to 0.64 cm thick; latter are higher in clay content; soft and easily broken in hand; disintegrate when soaked in water; longest piece of core recovered 15 cm; indications of vertical joints (originally described as SILTY SHALE).	26.60	48.03

Thickness      Depth of base  
(metres)      (metres)

April 3/72

GB 73      G.E. Crippen & Associates Ltd. test hole R203 (km 10.6,R).

Collared at el. 108.6 m.

SAND over CLAY (undif- ferentiated) 1	Stiff; low moisture content (originally described as SILT).	12.19	12.19
TILL: 2	Small percentage of sand and gravel, subangular (originally described as SILT).	7.62	28.95
SILTSTONE and SHALE: 3	Light grey with some carbonaceous seams; very soft and may be bro- ken by hand; disintegrates when soaked in water; longest piece of core recovered 15 cm, 90% longer than 2.5 cm.	7.62	28.95
4	Estimated distance from bottom of hole to river level.	20.05	49

April 3/72

GB 74      G.E. Crippen & Associates Ltd. test hole R204 (km 10.6,R).

Collared at el. 111.3 m.

SAND: 1	Brown; fine to medium grained; moist.	6.10	6.10
CLAY: 2	Clean; moist (originally described as SILT).	7.93	14.03
TILL: 3	Sandy; small percentage sub- angular gravel (originally described as SILT).	5.79	19.82



		Thickness (metres)	Depth of base (metres)
SILTSTONE and SHALE: 4	Drilling indications were that (the rock was soft and became harder with depth (originally described as SHALE).	3.66	23.48
April 7/72			
GB 75	G.E. Crippen & Associates Ltd. test hole R205 (km 9.9, R).		
	Collared at el. 79.3 m.		
SILT: 1	Grey; sandy; frozen, wet when thawed; below 18.29 m drier and firmer; few ice lenses (Esti- mate river level at 19.82 m).	20.42	20.42
SILTSTONE and SHALE: 2	Greenish grey; contains few 0.64 cm carbonaceous seams and few sandy seams; very soft and easily broken by hand; dis- integrates when soaked in water; core lengths all less than 5 cm (originally described as SILT).	32.92	53.34

## APPENDIX B

### DETAILED TEST HOLE LOGS FROM THE FIELD INSTRUMENTATION SITE

#### B.1 Explanation of Terms and Symbols used on Test Hole Logs

General information, indicating test hole number, date started, date finished, surface elevation and sheet number of the overall log, is given along the bottom of each form.

Two types of forms are used: A detailed log for intervals where test holes were advanced by continuous sampling; and a simplified log for intervals where test holes were advanced by conventional rotary drilling.

The detailed log is presented in columnar form. Sheet 1 for test hole GB1 is an example of this format. A description of each column used is given below:

- Columns 1 and 6 - Depth scale giving increasing depth of drillhole below the existing ground surface.
- Column 2 - Unified Classification indicating the abbreviated material classification in accordance with the Unified Soil Classification System.
- The interface between different soil strata is shown as a single continuous line. A change in sampling technique from continuous sampling to grab sampling or vice versa is shown as a single dashed line.
- Column 3 - Graphic soil log shows soil strata in accordance with symbols in Table B.1.
- Column 4 - Soil description provides the engineering description of each soil stratum.
- Colour codes refer to Munsell Soil Colour Charts.
  - Permafrost facies are described in Section A.3.
  - The interface between soil strata and changes in sampling technique from continuous sampling to grab sampling are shown as a single continuous line.
- Column 5 - National Research Council of Canada classification of ground ice following Pihlainen and Johnston (1963). The volume of ground ice is estimated visually and expressed as a percentage of the total volume of soil and ice.
- The location and approximate orientation of ice structures greater than 2.5 cm thick is shown as black shading. Orientations of planar ice structures relative to the core axis (CA) are given.

- The interface between different soil strata is shown as a single continuous line. A change in sampling technique from continuous sampling to grab sampling or vice versa is shown as a single dashed line.
- Column 6 - The results of laboratory determinations of moisture content, Atterberg limits and bulk density are plotted at sampling depths. Moisture content data are expressed as a percentage of dry weight.
- Column 7 - The length of core recovered is expressed as a percentage of total length attempted.  
- The depth at the top and bottom of each core run is shown as a solid continuous line.
- Column 8 - The condition of each core or segment of core is designated by one of the following symbols extending over the appropriate depth interval:
- Column 9 - Mud temperatures applicable to 'PQ' wire line sampling and conventional mud rotary drilling are shown at the drilling depths where measurements were taken. In all cases measurements were taken by immersing a pocket thermometer in the mud pit.
- Column 10 - Additional pertinent information such as in situ drilling conditions, drilling and sampling criteria, date and time are noted in this column.

The simplified log is also presented in columnar form. Sheet 1 for test hole GB1A is an example of this format. A graphic soil log shows soil strata in accordance with symbols in Table B.1. A depth scale showing increasing depth of drillhole below the existing ground surface is given on the right side of the graphic soil log. The soil description determined largely from grab samples, and other pertinent information such as in situ drilling conditions, drilling and sampling criteria, date and time are given on the right side of the depth scale. The interface between different soil strata is shown as a single continuous line.

TABLE B.1 GRAPHIC SOIL SYMBOLS USED ON TEST HOLE LOGS		
UNIFIED SOIL CLASSIFICATION SYMBOL	GRAPHIC SYMBOL	TYPICAL MATERIALS
<b>GW</b>		Well graded gravels, and gravel-sand mixtures, little or no fines.
<b>GP</b>		Poorly graded gravels, and gravel-sand mixtures, little or no fines.
<b>SW</b>		Well graded sands, gravelly sands, little or no fines.
<b>SP</b>		Poorly graded sands, little or no fines
<b>SM</b>		Silty sands, sand-silt mixtures.
<b>SC</b>		Clayey sands, sand-(silt) clay mixtures
<b>ML</b>		Inorganic silts and very fine sands, rock flour, silty sands of slight plasticity.
<b>MH</b>		Inorganic silts, micaceous or diatomaceous, fine, sandy, or silty soils.
<b>CL</b>		Inorganic clays of low plasticity, gravelly sandy, or silty clays, lean clays.
<b>CI</b>		Inorganic clays of medium plasticity, silty clays.
<b>CH</b>		Inorganic clays of high plasticity, fat clays.
<b>Pt</b>		Peat and other highly organic soils.

B.2 Test Hole Logs

DEPTH (m)	UNIFIED CLASSIFICATION	GRAPHIC SOIL LOG	SOIL DESCRIPTION	NRC ICE CLASSIFICATION (VISUALICE-%)	MOISTURE CONTENT (%)		BULK DENSITY (Mg/m <sup>3</sup> )	CORE NUMBER (% RECOVERY)	CORE CONDITION	MUD TEMP (°C)	DATE & TIME - COMMENTS
					W <sub>p</sub>	W <sub>L</sub>					
0	PE		PEAT: dark brown to black.		0	0	1.50				
1	SP		SAND: pale brown (10YR6/3); poorly graded; fine grained; sub-angular; quartz (80-90%), lignite and argillite (10-20%); horizontal and subhorizontal laminae. Occasional reticulate ice veins, usually near vertical, average 1.0 cm thick; pore ice present throughout; commonly excess water when thawed and remoulded.	Nf	20	25	1.80	C1 (53)		N/A	09:00 Two CRREL barrels used alternately. Each fitted with tungsten carbide insert teeth (changed as required).
2					50	55	1.90	C2 (100)			10:15
3			Horizontal silt-rich laminae.	Nbn	75	80	2.00	C3 (94)			10:35 Extrusion extremely difficult; became necessary to gently heat barrel and tap it with a hammer to facilitate extrusion.
4				Nf	100	105	2.10	C4 (100)			
					125	130	2.20	C5 (100)			
					135	140	2.30	C6 (100)			
					145	150	2.40	C7 (100)			
					155	160	2.50	C8 (100)			12:00 Frozen in hole. With G8 potash solution added to free barrel.

LOG NUMBER: GBI  
 STARTED 3/20/75  
 FINISHED 3/23/75  
 SURFACE ELEVATION 101.5 m  
 SHEET 1 OF 8

DEPTH (m)	UNIFIED CLASSIFICATION	GRAPHIC SOIL LOG	SOIL DESCRIPTION	NRC ICE CLASSIFICATION (VISUALICE %)	MOISTURE CONTENT (%)	BULK DENSITY (Mg/m <sup>3</sup> )	Δγ <sub>i</sub>	CORE NUMBER (% RECOVERY)	CORE CONDITION	MUD TEMP (°C)	DATE & TIME - COMMENTS
6.0	SP		SAND: as above. Sudden (downward) change to sub-horizontal lamination structure at 5.10 m.	Nbn	25	1.80	2.30	C8 (97)	Diagonal hatching	N/A	Core barrel heated in order to extrude C8. Sample badly disturbed at 15:00 ends.
6.5			Samples between 4.72 m and 7.77 m locally desiccated because of potash contamination inside of field wrapping.		25	1.80	2.30	C9 (90)	Diagonal hatching		Core barrel heated in order to extrude C9.
7.0					25	1.80	2.30	C10 (100)	Diagonal hatching		
7.5					25	1.80	2.30	C11 (100)	Diagonal hatching		
8.0			Samples between 7.77 m and 11.64 m badly disturbed during core recovery and extrusion.	Nbn & Vt	25	1.80	2.30	C12 (70)	Diagonal hatching		Build up of cuttings in the potash solution seriously impaired core recovery and core quality between 7.77 m and 11.64 m.
8.5					25	1.80	2.30	C13 (100)	Diagonal hatching		
9.0					25	1.80	2.30	C14 (90)	Diagonal hatching		17:00

LOG OF TEST HOLE NUMBER: GBI      STARTED: 3/20/75      FINISHED: 3/23/75      SURFACE ELEVATION: 101.5 m      SHEET 2 OF 8

DEPTH (m)	UNIFIED CLASSIFICATION	GRAPHIC SOIL LOG	SOIL DESCRIPTION	NRC ICE CLASSIFICATION (VISUAL ICE %)	MOISTURE CONTENT (%)	BULK DENSITY (Mg/m <sup>3</sup> )	Δ · δ <sub>i</sub>	CORE NUMBER (% RECOVERY)	DEPTH OF BASE	CORE CONDITION	MUD TEMP (°C)	DATE & TIME - COMMENTS
11	SP		SAND: as above  Horizontal silt-rich laminae.	Nbn	0-100	130-230	Δ · δ <sub>i</sub>	C15 (60)		X	N/A	Core barrel heated in order to extrude C15. Top of core barrels perforated to improve sample recovery
12			Gentle sub-horizontal lamination structure increasing slightly with depth.					C16 (60) C17 (90) C18 (90) C19 (30)		X	22:30	Extrusion difficulty still a problem. Began washing each barrel in water on alternate runs when it was not in use.
13			Regular sub-horizontal lamination structure at 70° to core axis between 13.80 m and 15.00 m.	Ice @ 30 to core axis				C20 (100) C21 (65) C22 (90) C23 (100) C24 (90)		X	03/21/75 00:30 00:45 01:45	Hole reamed with a 15.9 cm (6.25 in.) dia. wing bit (all reaming was with this bit unless otherwise indicated)

LOG OF TEST HOLE NUMBER: GBI

STARTED 3/20/75

FINISHED 3/23/75

SURFACE ELEVATION: 101.5 m

SHEET 3 OF 8

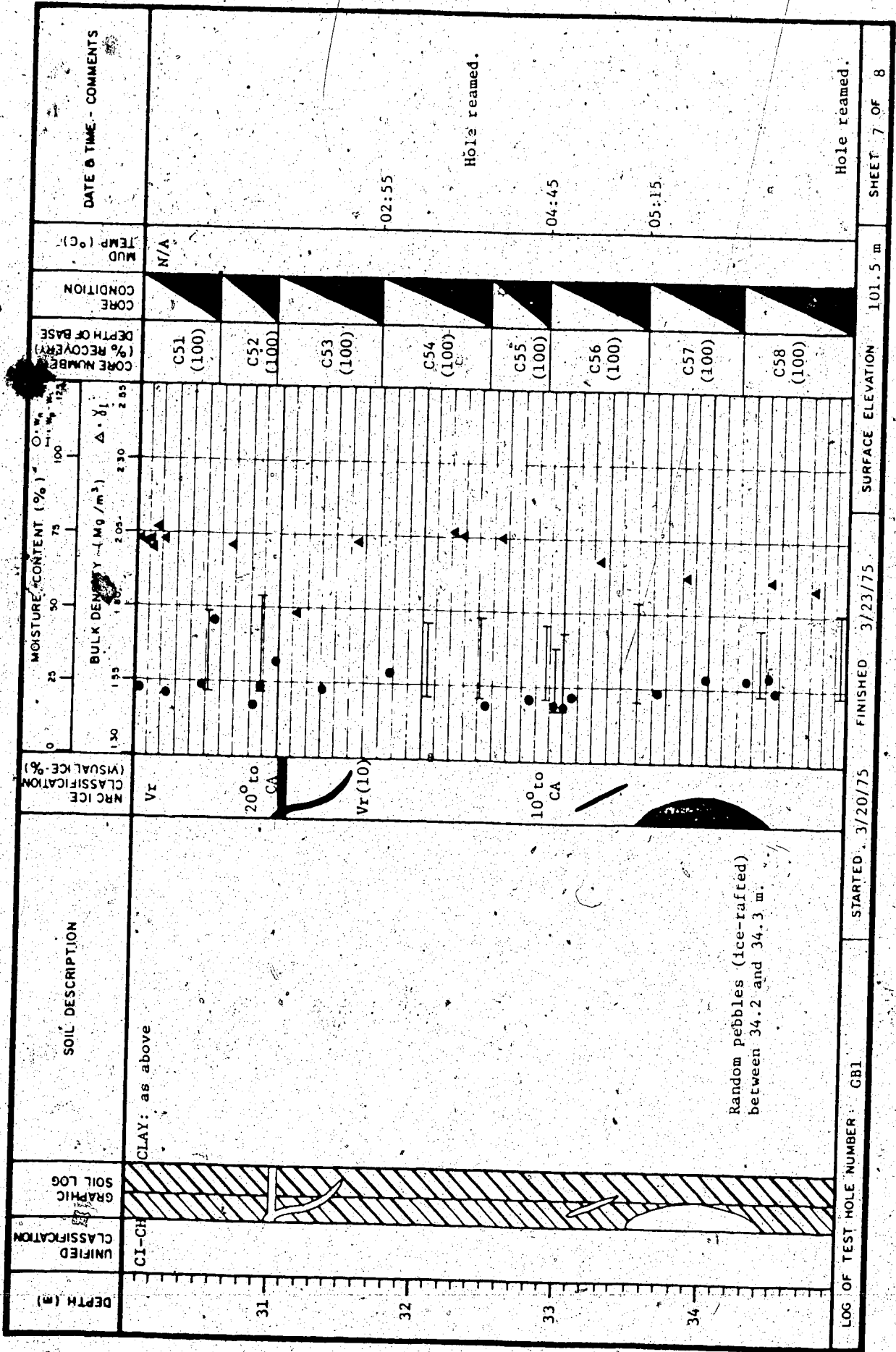


DEPTH (m)	UNIFIED CLASSIFICATION	GRAPHIC SOIL LOG	SOIL DESCRIPTION	NRC ICE CLASSIFICATION (VISUAL ICE %)	MOISTURE CONTENT (%)		BULK DENSITY (Mg/m <sup>3</sup> )	CORE NUMBER (% RECOVERY)	CORE CONDITION	MUD TEMP (°C)	DATE & TIME - COMMENTS
					w <sub>L</sub>	w <sub>p</sub>					
15.0 - 16.0	SP		SAND: as above	Nbn	25	50	1.50	C25 (100)		N/A	03:20
16.0 - 17.0			Horizontal lamination structure.		25	50	1.50	C26 (95)			03:40
17.0 - 18.0			Silt content increases steadily below 17.50 m.	Nbn	25	50	1.50	C27 (100)			04:00
18.0 - 19.0			Structure remains horizontal, but laminae thicken to faint beds.	Vr(10)	25	50	1.50	C28 (90)			04:20
19.0 - 20.0					25	50	1.50	C29 (90)			05:10
20.0 - 21.0					25	50	1.50	C30 (100)			06:15
21.0 - 22.0					25	50	1.50	C31 (90)			Drilling halted temporarily at 19.90 m to prepare all equipment for wet drilling (continued at 12:40 with CRREL bar-logs)
22.0 - 23.0					25	50	1.50	C33 (95)			

LOG OF TEST HOLE NUMBER: GBI      STARTED: 3/20/75      FINISHED: 3/28/75      SURFACE ELEVATION: 101.5 m      SHEET 4 OF 8

DEPTH (m)	UNIFIED CLASSIFICATION	SOIL LOG GRAPHIC	SOIL DESCRIPTION	NRC ICE CLASSIFICATION (VISUAL ICE %)	MOISTURE CONTENT (%)	BULK DENSITY (Mg/m <sup>3</sup> )	DEPTH OF BASE	CORE NUMBER	CORE CONDITION	MUD TEMP (°C)	DATE & TIME - COMMENTS
21	SP & SM		SAND: as above SAND: as above; increasing silt content.	Nbn & Vr(10)	0-100	1.30-2.35	C34 (100)		N/A		Hole reamed.
22	SM & GP		SAND: as above; horizontal bedding; very silty. GRAVEL: pebble size; sub-rounded; quartz (80%), carbonate (20%).	Nbe (10), Nf, Vc, Vr(35)	0-100	1.30-2.35	C35 (100), C36 (90)			14:00	Rig bounced 14:50 lightly when pebble layer encountered. RPM and pull-down pressure cut to minimum to avoid damaging teeth on CRREL barrel.
23	CI-CI		CLAY: dark grey to dark greyish brown (10YR3/1 to 3/2); medium to high plastic; silty; pseudo-rhythmic with anastomosing lamination structure. Ice up to 25 cm thick; reticulate ice throughout, primary veins near vertical to 35.35 m below which they change abruptly to horizontal, average 1.0 cm thick; secondary veins average 0.2 cm thick.	Vr(30), Vr(10)	0-100	1.30-2.35	C37a (100), C37b (100), C38 (95)			16:15	Pull-down pressure kept light to avoid breaking ice veins.
24				Vr(10), Vr(10), 20° to CA	0-100	1.30-2.35	C39 (100), C40 (100), C41 (100), C42 (100)				Case hardened steel teeth mounted at 21.87 m (changed as required) 16:50 Extrusion of clay proved much simpler than sand. 18:15 Hole reamed.

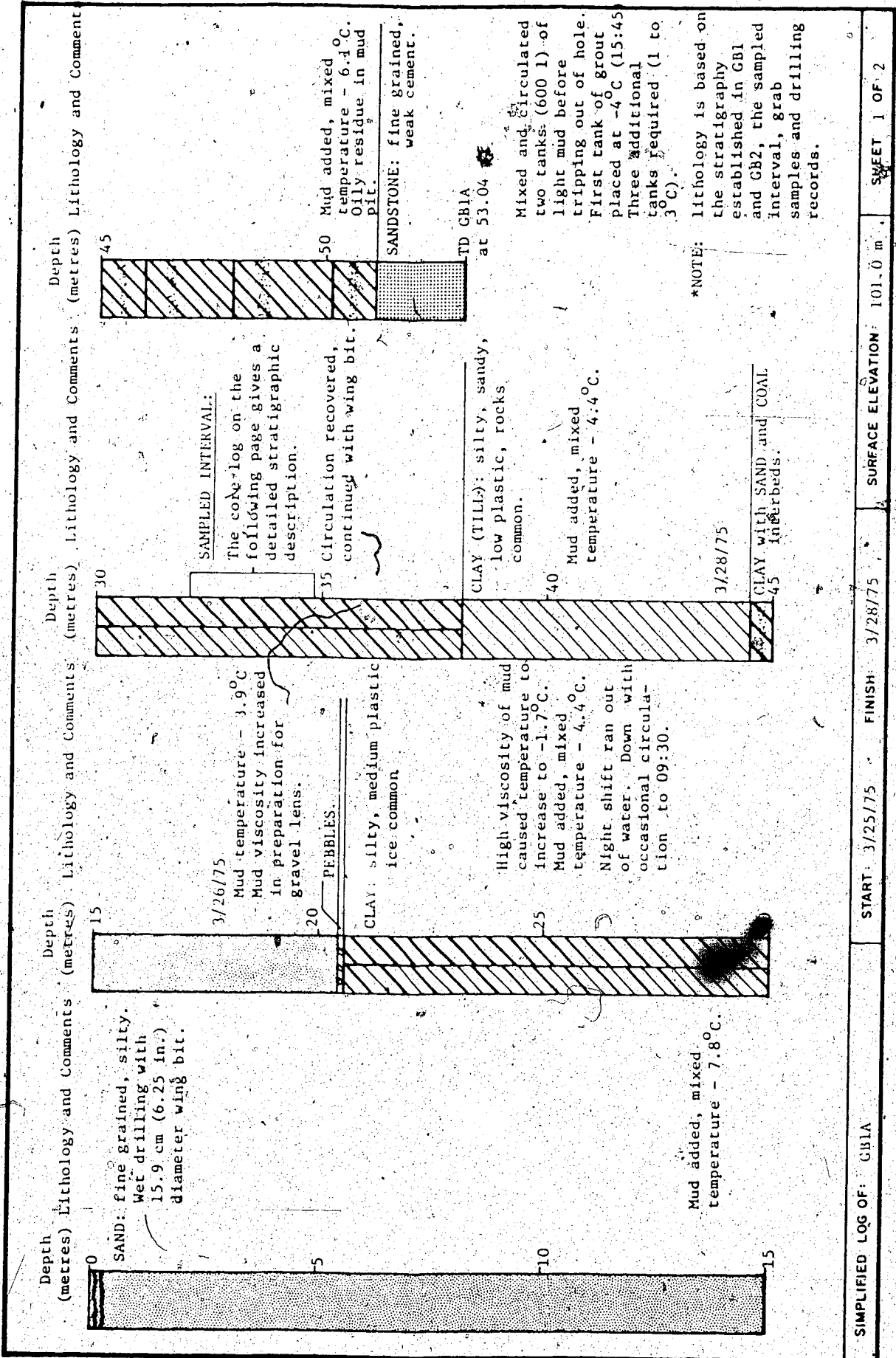
DEPTH (m)	UNIFIED CLASSIFICATION	GRAPHIC SOIL LOG	SOIL DESCRIPTION	NRCS CLASSIFICATION (VISUAL - %)	MOISTURE CONTENT (%)	BULK DENSITY (Mg/m <sup>3</sup> )	CORE NUMBER (% RECOVERY)	DEPTH OF BASE	CORE CONDITION	MUD TEMP (°C)	DATE & TIME - COMMENTS
26.0 - 26.5	CI-CH	[Hatched pattern]	CLAY: as above	VI (10) 20° to CA	~25	~1.55	C43 (100)			N/A	19:20
26.5 - 27.0		[Hatched pattern]		VI	~25	~1.55	C44 (100)				Hole reamed.
27.0 - 27.5		[Hatched pattern]		20° to CA	~25	~1.55	C45 (100)				21:45
27.5 - 28.0		[Hatched pattern]		VI	~25	~1.55	C46 (100)				
28.0 - 28.5		[Hatched pattern]		20° to CA	~25	~1.55	C47 (100)				
28.5 - 29.0		[Hatched pattern]		VI	~25	~1.55	C48 (100)				22:30
29.0 - 29.5		[Hatched pattern]		VI	~25	~1.55	C49 (100)				03/22/75
29.5 - 30.0		[Hatched pattern]		VI	~25	~1.55	C50 (100)				01:15
LOG OF TEST HOLE NUMBER: GBI      STARTED: 3/20/75      FINISHED: 3/23/75      SURFACE ELEVATION: 101.5 m      SHEET 6 OF 8											



LOG OF TEST HOLE NUMBER: GB1      STARTED: 3/20/75      FINISHED: 3/23/75      SURFACE ELEVATION: 101.5 m      SHEET 7 OF 8

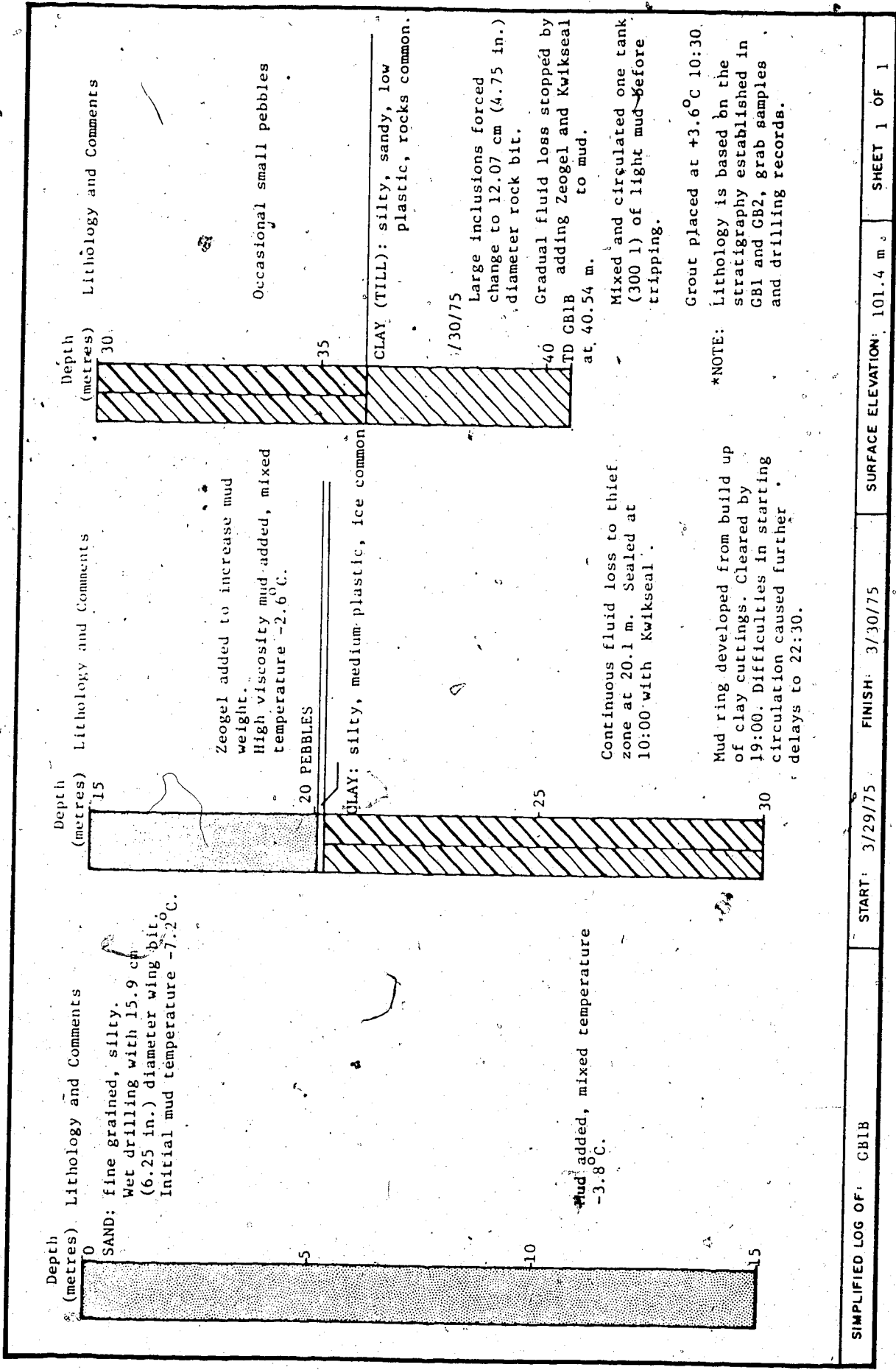
DEPTH (m)	UNIFIED CLASSIFICATION	GRAPHIC SOIL LOG	SOIL DESCRIPTION	NRCICE CLASSIFICATION (VISUAL %)	MOISTURE CONTENT (%)		BULK DENSITY (Mg/m <sup>3</sup> )	CORE NUMBER (% RECOVERY)	CORE CONDITION	MUD TEMP (°C)	DATE & TIME - COMMENTS
					$\frac{O.W.}{L.W.} \times 100$	$\Delta \cdot \delta t$					
36	CI-CH		Between 35.2 and 35.5 m gradual change in primary ice-structure from vertical to horizontal. Pebbles (ice-rafted) common below 35.5 m; less than 1.5 cm dia.; siliceous and carbonate varieties found.	Vr(10)	25	1.55	1.80	C59 (100)		N/A	-09:00
37					25	1.55	1.80	C61 (100)			-09:30 Hammer dropped down hole while pulling C61. Barrel forced up past the hammer at 18.3 m, barrel badly damaged and hammer head lost. Attempts to recover the head with C62 as a plug were unsuccessful and two case hardened steel teeth were lost.
					25	1.55	1.80	C62 (80)			-12:00
					25	1.55	1.80				-16:00
					25	1.55	1.80				-16:30 Attempts to mud up and continue with the PQ system were unsuccessful because of a thief zone at 21.5 m. Sand began sloughing.
					25	1.55	1.80				-17:30
					25	1.55	1.80				-18:30 Hole abandoned.

LOG OF TEST HOLE NUMBER: GBI STARTED: 3/20/75 FINISHED: 3/23/75 SURFACE ELEVATION: 101.5 m SHEET 8 OF 8



SIMPLIFIED LOG OF: G81A | START: 3/25/75 | FINISH: 3/28/75 | SURFACE ELEVATION: 101.0 m | SHEET 1 OF 2

DEPTH (m)	UNIFIED CLASSIFICATION	GRAPHIC SOIL LOG	SOIL DESCRIPTION	NRC ICE CLASSIFICATION (VISUALICE-%)	MOISTURE CONTENT (%)			CORE NUMBER (% RECOVERY)	CORE CONDITION	MUD TEMP (°C)	DATE & TIME - COMMENTS
					0-25	25-50	50-100				
31					130	155	180	205	230	255	
32	CI-CH		CLAY: dark grey to dark greyish brown (10YR3/1 to 3/2); medium to high plastic; pseudo-rhythmic with anastomosing lamination structure; occasional lamina pebble (ice-rafter) throughout. Reticulate ice common; primary veins near vertical; average 0.8 cm thick; secondary veins average 0.3 cm thick.	Vr(10)					N/A	-4.5	3/26/75 Continued from preceding page. Drilling with 15.9 cm (6.25 in.) diameter wing bit. Mud added, mixed temperature - 5.6°C. Reached 32.06 m at 14:45 and began change over to 'PQ' coring system.
33										-2.0	14:45 Two tanks of mud added, mixed temperatures of -10.5°C and -2.2°C. Coring started at 18:10.
34				20° to CA						-3.6	Continuous fluid loss to thief zone at 20.5 m. Night shift ran out of water attempting to regain circulation.
										-3.2	18:45 to 19:30
										-3.2	19:45 to 12:00 3/27/75
LOG OF TEST HOLE NUMBER: GBTA (30 to 35m)					STARTED 3/25/75	FINISHED 3/28/75	SURFACE ELEVATION 101.0 m		SHEET 2 OF 2		



SIMPLIFIED LOG OF: CB1B	START: 3/29/75	FINISH: 3/30/75	SURFACE ELEVATION: 101.4 m.	SHEET 1 OF 1
-------------------------	----------------	-----------------	-----------------------------	--------------



DEPTH (m)	UNIFIED CLASSIFICATION	GRAPHIC SOIL LOG	SOIL DESCRIPTION	NRC ICE CLASSIFICATION (VISUAL ICE %)	MOISTURE CONTENT (%)		BULK DENSITY (Mg/m³)		CORE NUMBER (% RECOVERY)	CORE CONDITION	MUD TEMP (°C)	DATE & TIME - COMMENTS
					w <sub>p</sub>	w <sub>L</sub>	ρ <sub>s</sub>	ρ <sub>w</sub>				
1	Pt CI-CH		PEAT: dark brown (10YR4/3) CLAY: dark grey to dark greyish brown (10YR3/1 to 3/2); medium to high plastic; pseudo-rhythmic with anastomosing lamination structure; frequently (70) because of widespread ice structures. Segregated ice abundant, especially in top 1.5 m, average 30% ice by volume; reticulate ice common throughout, primary veins near vertical, average 1.5 to 2.0 cm thick, secondary veins average 0.5 cm thick.		2.55	1.80	2.30	C1 (100)		N/A	11:50 Two CRREL bat- rels used al- ternately. Each fitted with case hardened 12:45 steel teeth (changed as required). Ice cloudy and broken at 0.75 m. 13:05	
2				Vr(40)	2.55	1.80	2.30	C2 (95)				
3				Vr(40)	2.55	1.80	2.30	C3 (100)				
4				Vr(40)	2.55	1.80	2.30	C4 (100)				
				Vr(40)	2.55	1.80	2.30	C5 (100)				
				Vr(40)	2.55	1.80	2.30	C6 (90)				
				Vr(30)	2.55	1.80	2.30	C7 (100)				
				Vr(20)	2.55	1.80	2.30	C8 (95)				
				Vr(20)	2.55	1.80	2.30	C9 (100)				
				Vr(20)	2.55	1.80	2.30	C9 (100)				

LOG OF TEST HOLE NUMBER: GB2      STARTED: 3/31/75      FINISHED: 4/3/75      SURFACE ELEVATION: 80.5 m      SHEET 1 OF 8

Ice cloudy and slightly broken during drilling. No adjustment to drilling technique seemed to improve condition of ice.

Ice cloudy and broken during drilling.

DEPTH (m)	UNIFIED CLASSIFICATION	GRAPHIC SOIL LOG	SOIL DESCRIPTION	NRC ICE CLASSIFICATION (VISUAL ICE %)	MOISTURE CONTENT (%)		CORE NUMBER (% RECOVERY)	CORE CONDITION	MUD TEMP (°C)	DATE & TIME - COMMENTS
					W <sub>p</sub>	W <sub>L</sub>				
6.00	CL-CH	[Hatched pattern]	CLAY: as above	Vr(20)	130	135	C10 (90)	[Hatched pattern]	N/A	16:25
6.07		[Hatched pattern]	Slickensides (soil-ice contacts) between 6.07 and 6.22 m.	Vr(15)	130	135	C11 (100)	[Hatched pattern]		17:40 Ice cloudy and badly broken.
6.22		[Hatched pattern]		Vr(15)	130	135	C12 (100)	[Hatched pattern]		
6.38		[Hatched pattern]		Vr(15)	130	135	C13 (95)	[Hatched pattern]		
6.84		[Hatched pattern]	Slickensides (soil-ice contacts) between 8.38 and 8.84 m.	Vr(15)	130	135	C14 (100)	[Hatched pattern]		Ice cloudy and badly broken.
8.38		[Hatched pattern]		Vr(15)	130	135	C15 (100)	[Hatched pattern]		Ice in C15 and C16 cloudy and broken in several places.
8.84		[Hatched pattern]		Vr(15)	130	135	C16 (100)	[Hatched pattern]		21:00 Hole reamed with 15.9 cm (6.25 in.) diameter wing bit.
9.00		[Hatched pattern]		Vr(15)	130	135	C17 (100)	[Hatched pattern]		

LOG OF TEST MOLE NUMBER CB2      STARTED 3/31/75      FINISHED 4/3/75      SURFACE ELEVATION 80.5 m      SHEET 2 OF 8

DEPTH (m)	UNIFIED CLASSIFICATION	GRAPHIC SOIL LOG	SOIL DESCRIPTION	NRC ICE CLASSIFICATION (VISUAL ICE %)	MOISTURE CONTENT (%)		CORE NUMBER (% RECOVERY)	DEPTH OF BASE	CORE CONDITION	MUD TEMP (°C)	DATE & TIME - COMMENTS
					W	L					
11	CI-CR		CLAY: as above Random pebbles (ice-rafterd) below 10.30 m.	Vr(15)	0	100	C18 (100)		N/A		21:45 Ice in C18 and C19 cloudy and totally pulverized.
11			Intense distribution of slickensides (soil-ice contacts) between 10.87 and 11.10 m.	Vr(15)	0	100	C19 (100)				22:15
12			Distinct, slickensided shear plane (soil-soil contact), centered at 11.74 m, cuts core at 60° to axis; slickensides (soil-ice contacts) common between 11.56 and 11.79 m.	Vr(15)	0	100	C20 (100)				22:45 Ice cloudy and badly broken.
13			Slickensides (soil-ice contact) between 12.14 and 12.30 m. Contact with underlying clay till is sharp.	Vr(10)	0	100	C21 (100)				23:10
13					0	100	C22 (100)				23:35 Two teeth on CRREL barrel lost taking C23
14	CI-CI		CLAY TILL: brown to very dark grey (10YR5/3 to 3/1); low to medium plastic; silty and locally very sandy; crystalline, carbonate and sandstone inclusions common; fissured. Well bonded with no excess ice. Grab samples only between 14.25 and 18.08 m.	Nbn	0	100	C23 (100)				23:55 Night shift stopped at 13.54 m to prepare rig for PQ system.
14					0	100	C24 (80)				22:00 4/1/75 Mud added, mixed temperature -5°C. Hole reamed with 15.9 cm (6.25 in.) diameter wing bit.

LOG OF TEST HOLE NUMBER: GB2      STARTED: 3/31/75      FINISHED: 4/3/75      SURFACE ELEVATION: 80.5 m      SHEET 3 OF 8

DEPTH (m)	UNIFIED CLASSIFICATION	GRAPHIC SOIL LOG	SOIL DESCRIPTION	MRC ICE CLASSIFICATION (VISUALICE-%)	MOISTURE CONTENT (%)		BULK DENSITY (Mg/m <sup>3</sup> )		CORE NUMBER (% RECOVERY)	DEPTH OF BASE	CORE CONDITION	MUD TEMP (°C)	DATE & TIME - COMMENTS
					0-25	25-50	50-75	75-100					
16	CL-CI		CLAY TILL: as above Grab samples only between 14.25 and 18.08 m. One or more large granite inclusions between 15.20 and 15.55 m.	assumed Nbn								-3.4	Cobbles and boulders very common. Coring difficult and sample quality poor. Therefore coring ceased at 14.25 m and with 12.07 cm (4.75 in.) diameter rock bit to 18.08 m. Mud added at 15.2 m, mixed temperature -5.8°C. Rate of advance very slow between 15.20 and 15.55 m. 23:45 m.
18	CL-CI		CLAY TILL: as above; coal fragments up to 0.3 cm.	Nbn					C25 (40)			-3.4	Changed from rock bit to PQ system. Slight obstruction at 15.50 m. Mud added, mixed temperature -6.0°C.
19	CL-CI		Grab samples only between 19.07 and 20.90 m.	assumed Nbn								-3.1	Liner buckled as C25 entered. Seemed to be size problem so use of liners discontinued. Hole advanced with rock bit between 19.07 & 20.90 m. Mud added, mixed temp

LOG OF TEST HOLE NUMBER: GB2

STARTED: 3/31/75

FINISHED 4/3/75

SURFACE ELEVATION 80.5 m

SHEET 4 OF 8

DEPTH (m)	UNIFIED CLASSIFICATION	GRAPHIC SOIL LOG	SOIL DESCRIPTION	NRC ICE CLASSIFICATION (VISUALICE %)	MOISTURE CONTENT (%)	BULK DENSITY (Mg/m <sup>3</sup> )	CORE NUMBER (% RECOVERY)	DEPTH OF BASE	CORE CONDITION	MUD TEMP (°C)	DATE & TIME - COMMENTS
21	CL-CI		CLAY TILL: as above. Grab samples only between 19.07 and 20:90 m.	Nbn	25.5	2.30	C26 (90)			10:25	11:00 Mud added, mixed temperature unknown.
22	CI		CLAY TILL: as above.  Medium to coarse-grained sand bed.	Nbn	25.5	2.30				14:50 to 15:35	14:00 Changed from rock bit to PQ system.
23			Below 22.30 m only pebble size inclusions; crystalline and carbonate sizes average 1.5 cm and 2.5 cm respectively; angular coal fragments up to 0.4 cm common.		25.5	2.30	C27				Mud records incomplete between 20.00 m and 26.21 m.
24	SP		Contact with underlying sand sharp.  SAND: very dark grey (10YR 3/1); very poorly graded; medium grained; subrounded; quartz and argillite. Well-bonded with no excess ice.	Nbn	25.5	2.30	C28			16:35 to 18:40	

LOG OF TEST HOLE NUMBER: GB2      STARTED 3/31/75      FINISHED 4/3/75      SURFACE ELEVATION 80.5 m      SHEET 5 OF 8

DEPTH (m)	UNIFIED CLASSIFICATION	GRAPHIC SOIL LOG	SOIL DESCRIPTION	MRC ICE CLASSIFICATION (VISUALICE %)	MOISTURE CONTENT (%)	BULK DENSITY (Mg/m <sup>3</sup> )	CORE NUMBER (% RECOVERY)	DEPTH OF BASE	CORE CONDITION	MUD TEMP (°C)	DATE & TIME - COMMENTS
26.00	CH	[Hatched pattern]	SAND: as above CLAY: grey to very dark grey (10YR5/1 to 3/1); high plastic; sandy, silty; sand size coal fragments common; bedding highly contorted (ice thrusting); fissured. Thin (0.1 cm thick) ice veins on fissure planes, no excess when thawed. Contact with underlying sand sharp.	Nbn	25	1.80	C28			-2.9	19:20 Core barrel to temporarily 23:20 jammed inside PQ drill rod.  Mud added, mixed temperature -5.0°C.
27.00	SP	[Dotted pattern]	SAND: dark grey (10YR4/1) salt and pepper like; very poorly graded; medium grained subrounded; argillite (60%), quartz (40%). Well bonded with no excess ice.	Vr	30	2.05	C29			-3.1	23:59 Mud added, mixed temperature 01:30 ed temperature 4/3/75 -5.2°C.
28.00	CH	[Hatched pattern]	CLAY: as above (25.09 to 26.67 m); no significant sand, silty, organic fragments, highly fissured; slickensides present on most fissure planes.	Vr	35	2.30	C30			-2.9	Brown residue appeared in mud pit.
29.00	Coal	[Solid black]	Contact with underlying coal sharp but irregular due to ice thrusting.	Nf	40	2.50					
29.49	CH	[Hatched pattern]	CLAY: as above (27.33 to 29.49 m)	Vr	45	2.55					

LOG OF TEST HOLE NUMBER GB2      STARTED 3/31/75      FINISHED 4/3/75      SURFACE ELEVATION 80.5 m      SHEET 6 OF 8

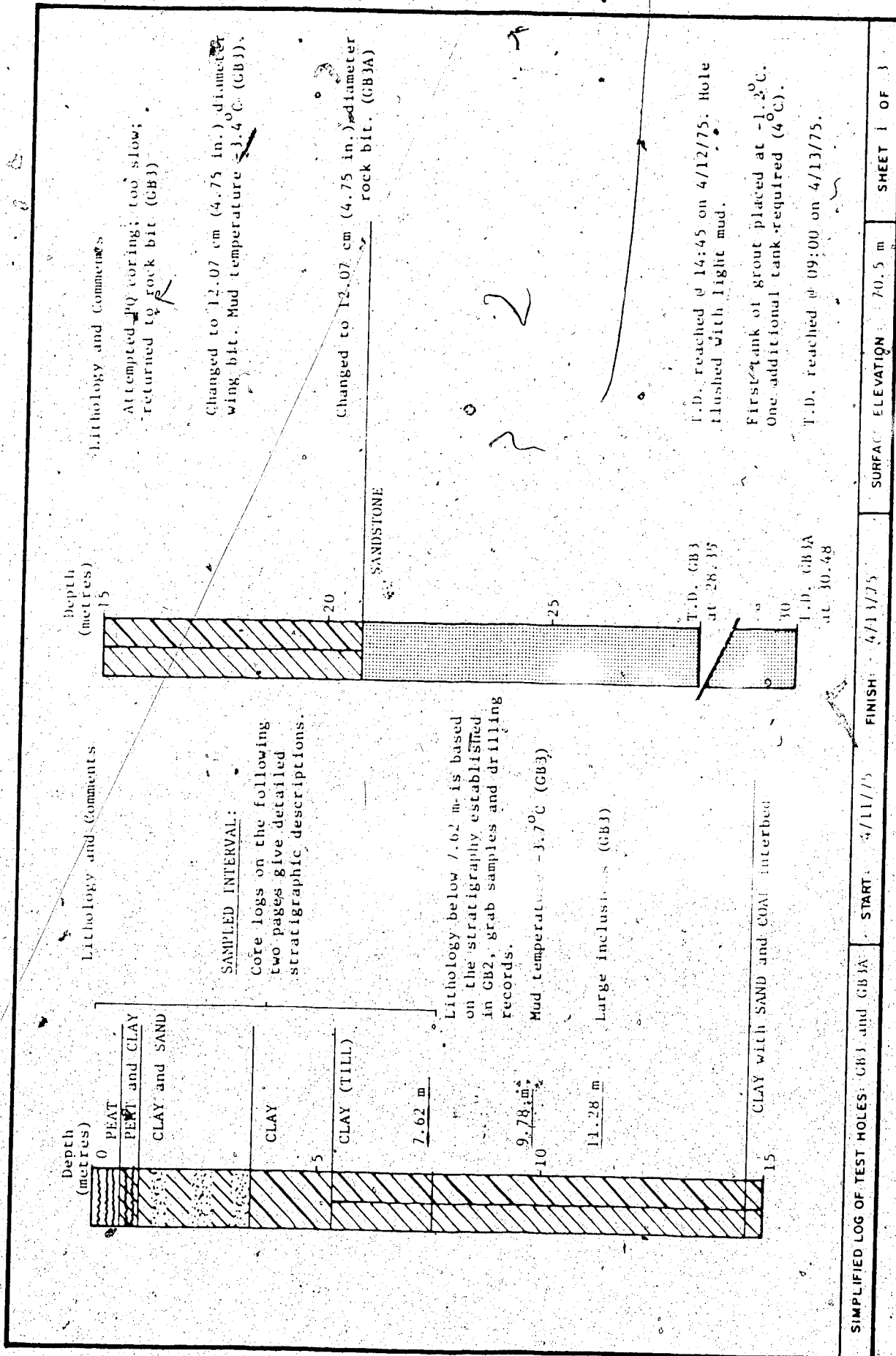
DEPTH (m)	UNIFIED CLASSIFICATION	GRAPHIC SOIL LOG	SOIL DESCRIPTION	MRCICE CLASSIFICATION (VISUALICE %)	MOISTURE CONTENT (%)	BULK DENSITY (Mg/m <sup>3</sup> )	CORE NUMBER (% RECOVERY) DEPTH OF BASE	CORE CONDITION	MUD TEMP (°C)	DATE & TIME - COMMENTS
31	CH		CLAY: as above  Contact with underlying bedrock not easily distinguishable.	Vr	100	1.80	C30		-3.2	02:45 Mud added, mixed temperature 04:00 -5.4°C.
32	CL		SILTSTONE and SHALE: pale brown to brown (10YR6/3 to 5/3); very sandy throughout, carbonaceous fragments common in sand rich zones; non-to high plastic; contacts gradational and two units very difficult to distinguish between; opaque, milky, soft cement, breaks down partially when soaked in water; vertical joint set with rusty precipitate. Well bonded with no excess ice.	Nbn	100	1.80	C31		-2.6	05:15 Extruder required to remove C31. 08:20 remove C31.
33	SW				100	1.80				
34	SP				100	1.80	C32			

LOG OF TEST HOLE NUMBER: GB2      STARTED: 3/31/75      FINISHED: 4/3/75      SURFACE ELEVATION: 80.5 m      SHEET 7 OF 8

DEPTH (m)	UNIFIED CLASSIFICATION	GRAPHIC SOIL LOG	SOIL DESCRIPTION	NRC ICE CLASSIFICATION (VISUALICE %)	MOISTURE CONTENT (%)		BULK DENSITY (Mg/m <sup>3</sup> )	δ (	CORE NUMBER (% RECOVERY) DEPTH OF BASE	CORE CONDITION	MUD TEMP (°C)	DATE & TIME - COMMENTS
					w <sub>p</sub>	w <sub>L</sub>						
36	SP		SILTSTONE and SHALE: as above	Nbn					C32			T.D. reached at 09:20.
37			Total Depth 35.36 m.						35.36			10:45 PQ drill rod and core barrel out of hole.
38												11:30 2HIF drill rods and rock bit tripped in and hole flushed with light mud.
39												13:00 Hole ready for installation of inclinometer casing and thermistors.
												16:00 First tank of grout placed at -2.2°C. Three additional tanks required (1 to 3°C).

LOG OF TEST-HOLE NUMBER: GB2      STARTED: 3/31/75      FINISHED: 4/3/75      SURFACE ELEVATION: 80.5 m      SHEET 8 OF 8





DEPTH (m)	UNIFIED CLASSIFICATION	GRAPHIC	SOIL DESCRIPTION	NRC ICE CLASSIFICATION (VISUALICE %)	MOISTURE CONTENT (%)	BULK DENSITY (Mg/m <sup>3</sup> )	CORE NUMBER (% RECOVERY)	CORE CONDITION	MUD TEMP (°C)	DATE & TIME - COMMENTS
0					0	0				
1	Pt		PEAT: dark reddish brown (5YR3/4); woody and mossy with numerous roots near top.	Nbe	130	1.30	C1 (100)		N/A	10:45 One U of A CRREL barrel with case hardened steel teeth and one NES CRREL barrel with tungsten carbide insert teeth used alternately.
1	Pt and CI		PEAT: as above; no roots. CLAY: yellowish brown (10YR5/4); medium plastic; silty; sand pockets; blocky structure.	Vr(40)	155	1.55	C2 (100)			
2	CI-CI and Sp.		CLAY: dark greyish brown (10YR4/2); medium to high plastic; silty blocky structure contorted with sand (described below) - probably colluvium from a date stabilized bimodal flow. 2670+ 130 YK B.P. and SAND: pale brown (10YR6/3); poorly graded; medium grained; sub-angular to subrounded; quartz (80%), lignite and argillite (20%); in discrete beds with organic material and as coating on clay (described above) blocks.	Vr(10)	175	1.75	C3 (100)			
3					200	2.00	C4 (100)			
3					230	2.30	C5 (100)			
3					255	2.55	C6 (100)			
3					270	2.70	C7 (100)			11:50
4	CI-CI		CLAY: as above 1.07 to 3.56 m; except no evidence of sand. Well developed, parallel, ice veins oriented at 40° to CA. Rusty precipitate at soil-ice interfaces. Ice is pitted and locally absent forming a honeycomb structure.	Vr(40)	285	2.85	C8 (100)			
4					300	3.00	C9 (100)			
4					315	3.15	C10 (100)			

LOG OF TEST HOLE NUMBER CB3 (0 to 10 m) STARTED 4/11/75 FINISHED 4/12/75 SURFACE ELEVATION 70.5 m SHEET 2 OF 3

DEPTH (m)	UNIFIED CLASSIFICATION	GRAPHIC SOIL LOG	SOIL DESCRIPTION	NRC ICE CLASSIFICATION (VISUALICE %)	MOISTURE CONTENT (%)	BULK DENSITY (Mg/m <sup>3</sup> )	CORE NUMBER (% RECOVERY)	DEPTH OF BASE	CORE CONDITION	MUD TEMP (°C)	DATE & TIME - COMMENTS
6.0			CLAY TILL: brown to dark brown (10YR5/3 to 4/3); low plastic; silty and locally sandy; crystalline, carbonate and sandstone inclusions common; lightly fissured. Reticulate ice common, primary veins near vertical, average 0.6 cm thick, decreasing content downward.	VI (30)	100	1.80	C11 (100)			N/A	NES CRREL barrel only used below 5.03 m.
6.5					75	1.85	C12 (100)				
7.0					50	1.90					Too many rocks - use of CRREL barrel discontinued.
7.5					25	1.95					
8.0			Grab samples only below 7.62 m.		0	2.00				-3.8	Rig prepared for wet drilling 14:20 with 12.07 cm (4.75 in.) diameter rock bit. 18:00 meter rock bit.
8.5						0	2.05				
9.0					0	2.10				-3.1	20:00 Hole reamed with 15.9 cm (6.25 in.) diameter wing bit. Began to advance hole with rock bit.

LOG OF TEST HOLE NUMBER CB3 (0 to 10 m) STARTED 4/11/75 FINISHED 4/12/75 SURFACE ELEVATION 70.5 m SHEET 3 OF 3

APPENDIX C

THERMISTOR DATA

C.1 Thermistor Data from Hole GB1A

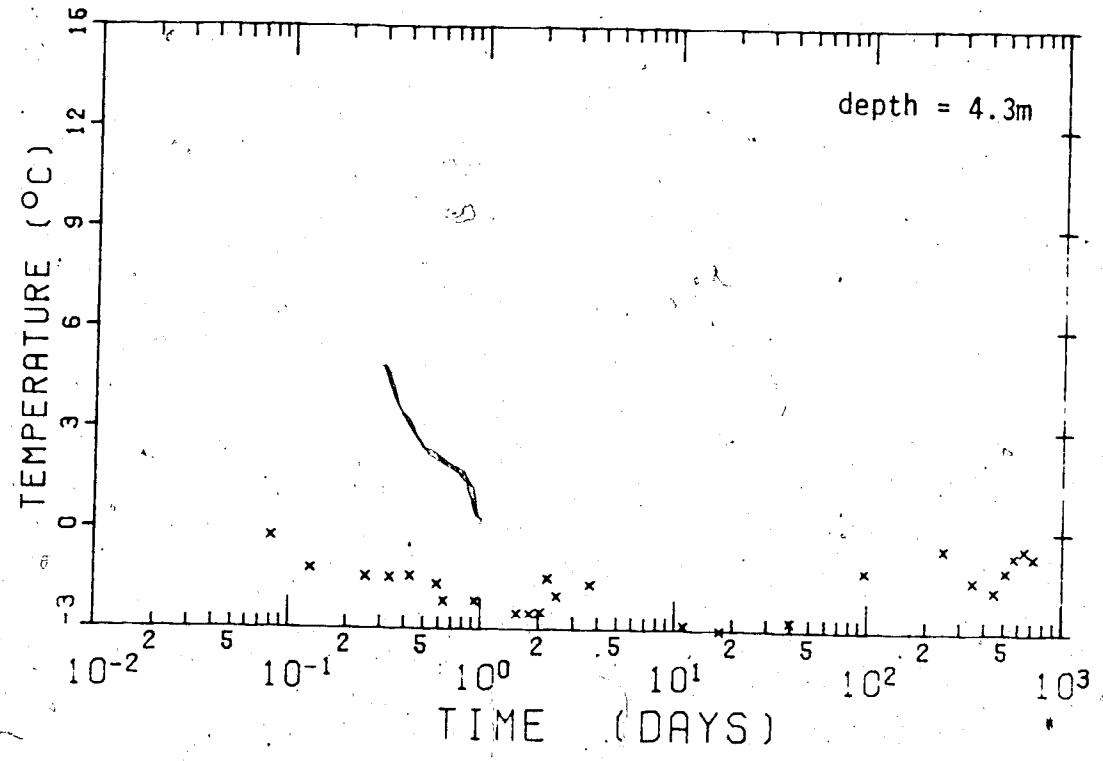


Figure C.1 Thermistor 1 - hole GB1A

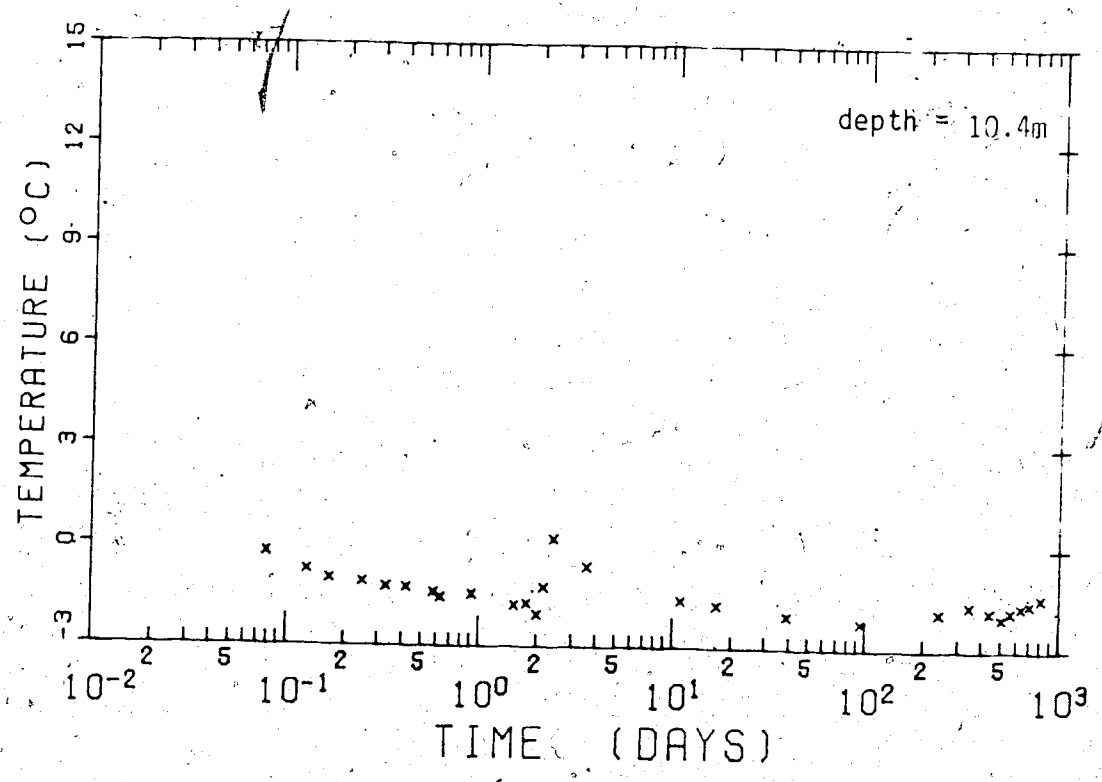


Figure C.2 Thermistor 1 - hole GB1A

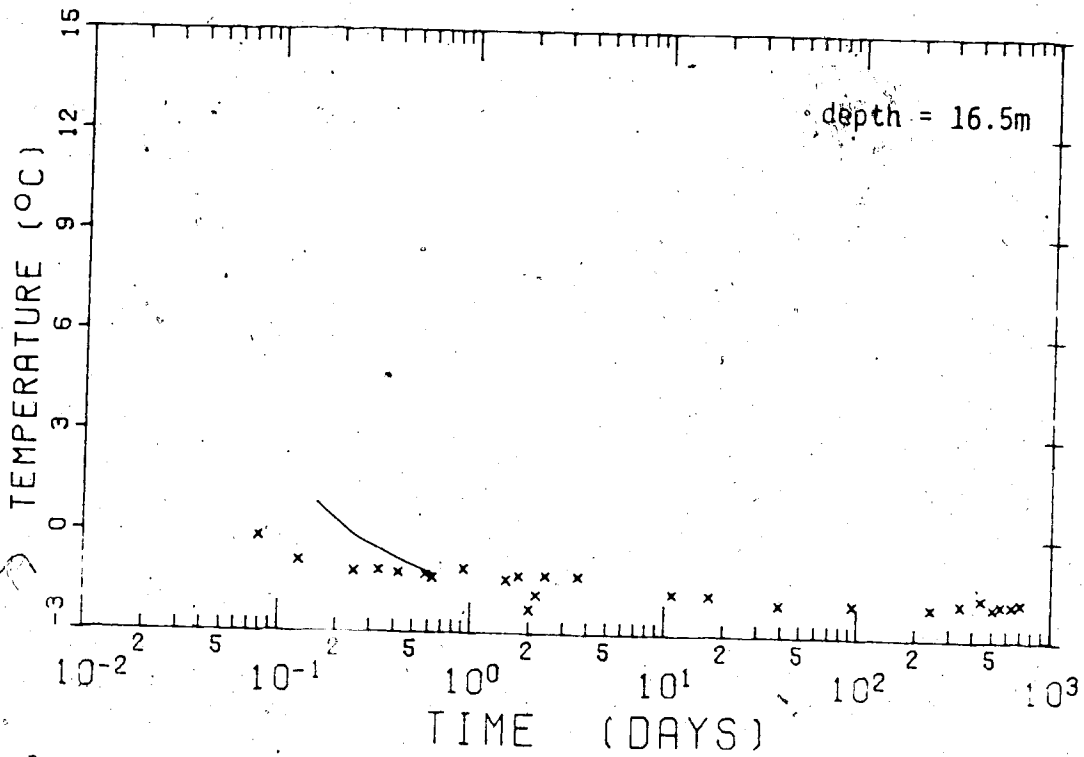


Figure C.3 Thermistor 3 - hole GB1A

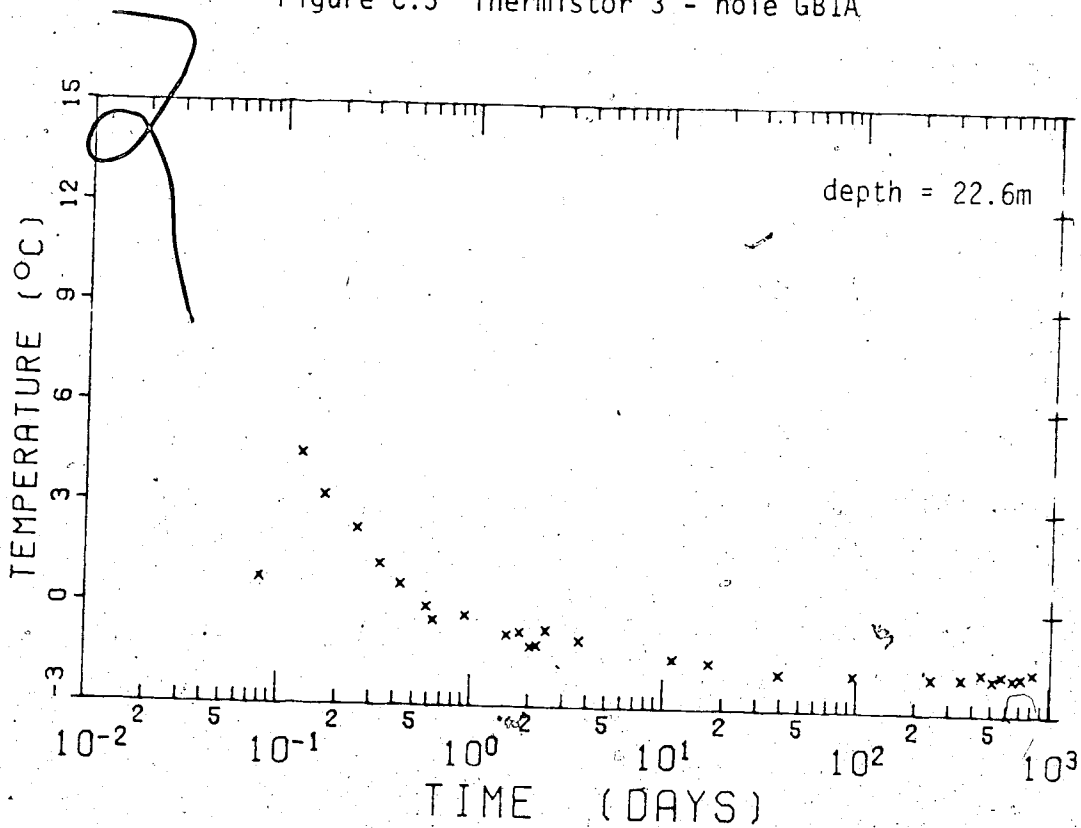


Figure C.4 Thermistor 4 - hole GB1A

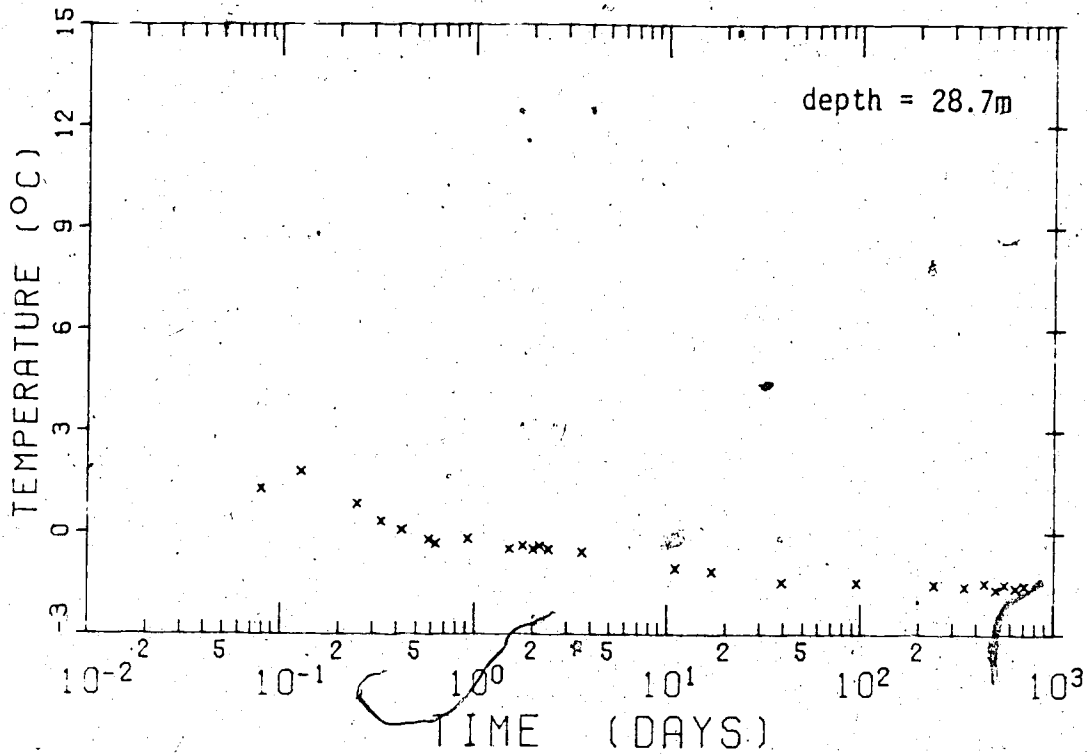


Figure C.5 Thermistor 5 - hole GB1A

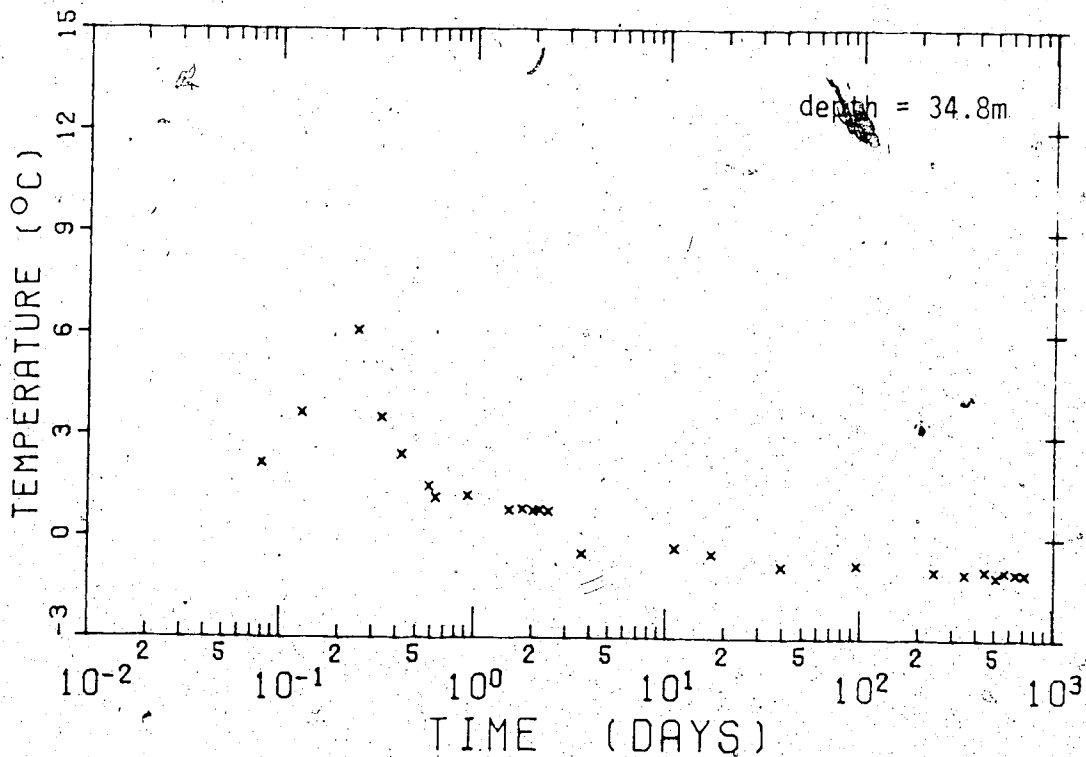


Figure C.6 Thermistor 6 - hole GB1A

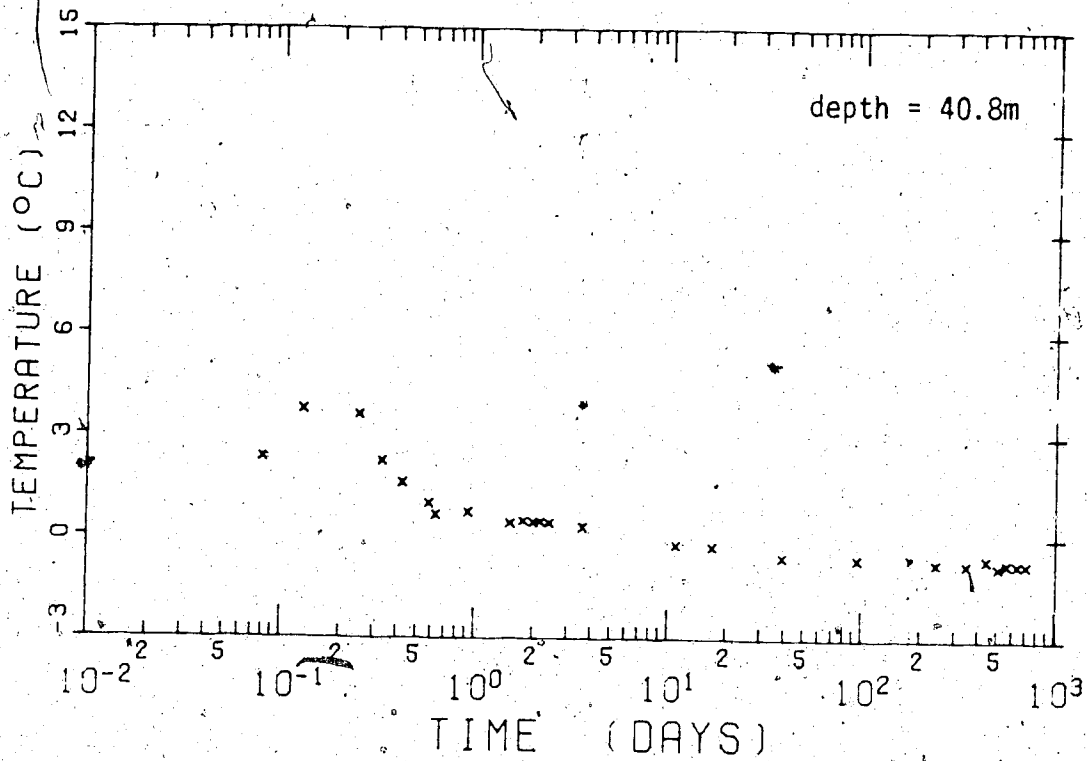


Figure C.7 Thermistor 7 - hole GB1A

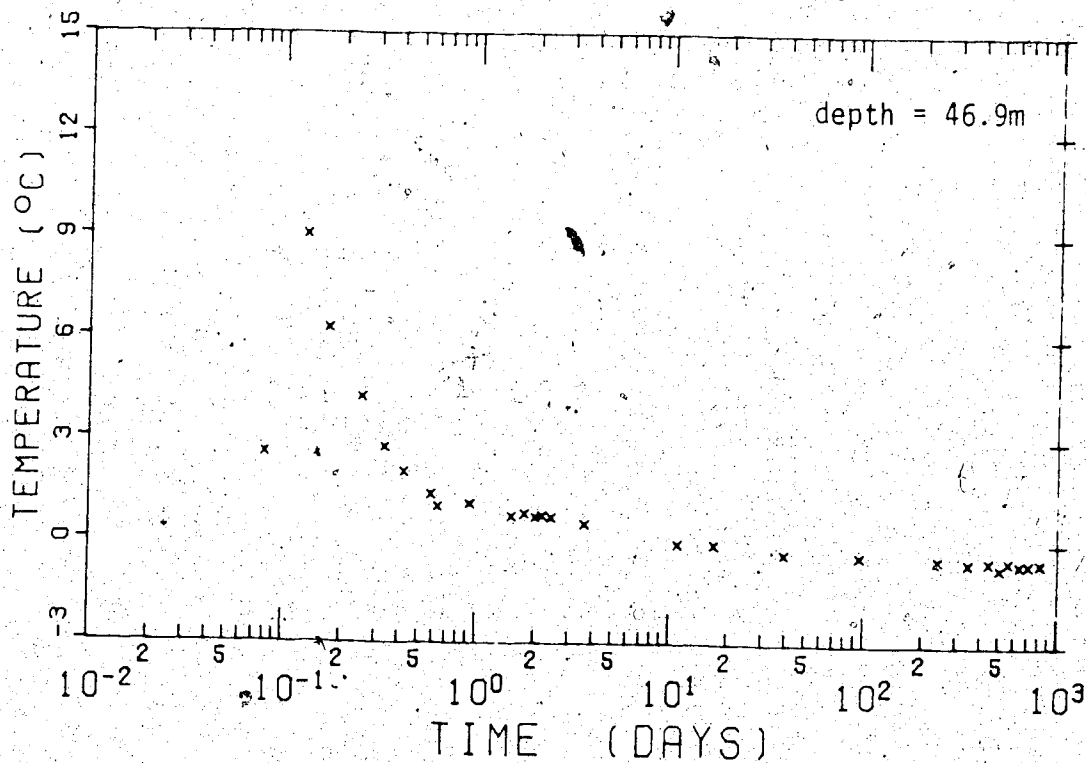


Figure C.8 Thermistor 8 - hole GB1A



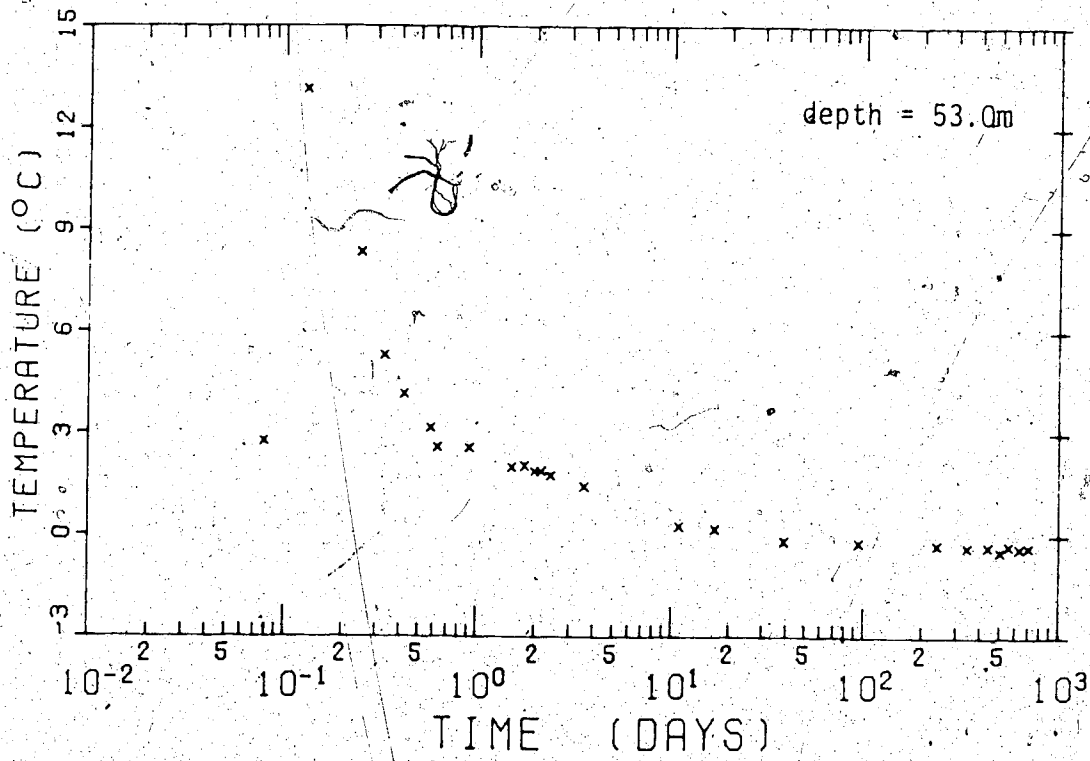


Figure C.9 Thermistor 9 - hole GB1A

C.2 Thermistor Data from Hole GB2

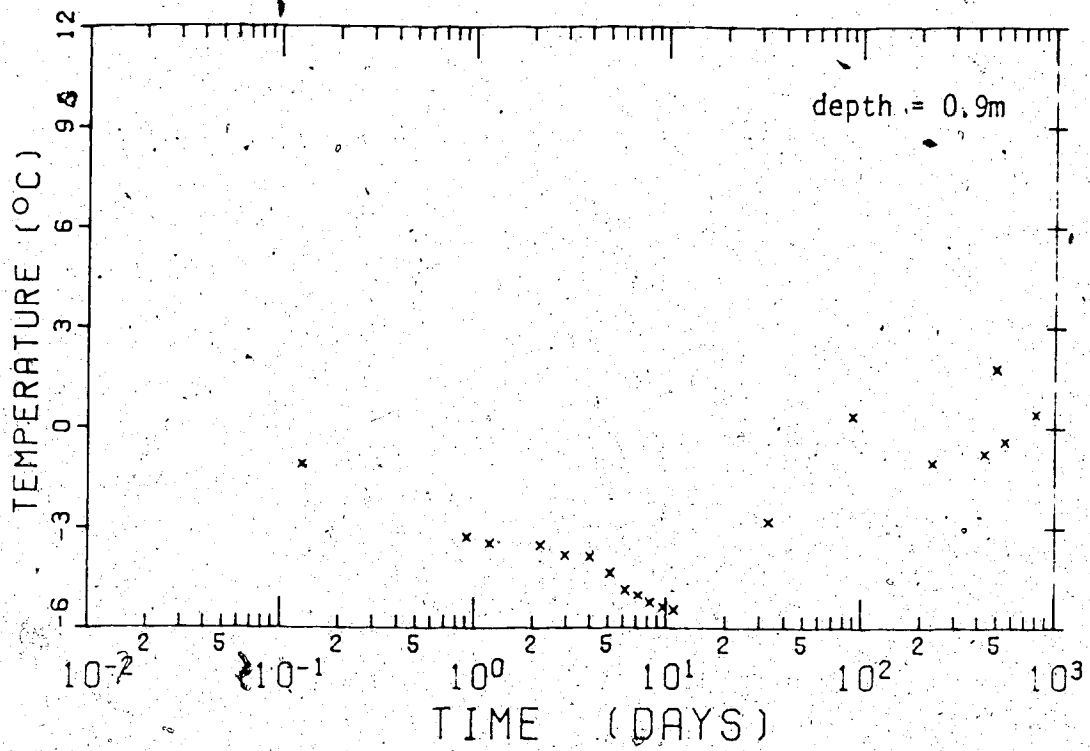


Figure C.10 Thermistor 1 - hole GB2

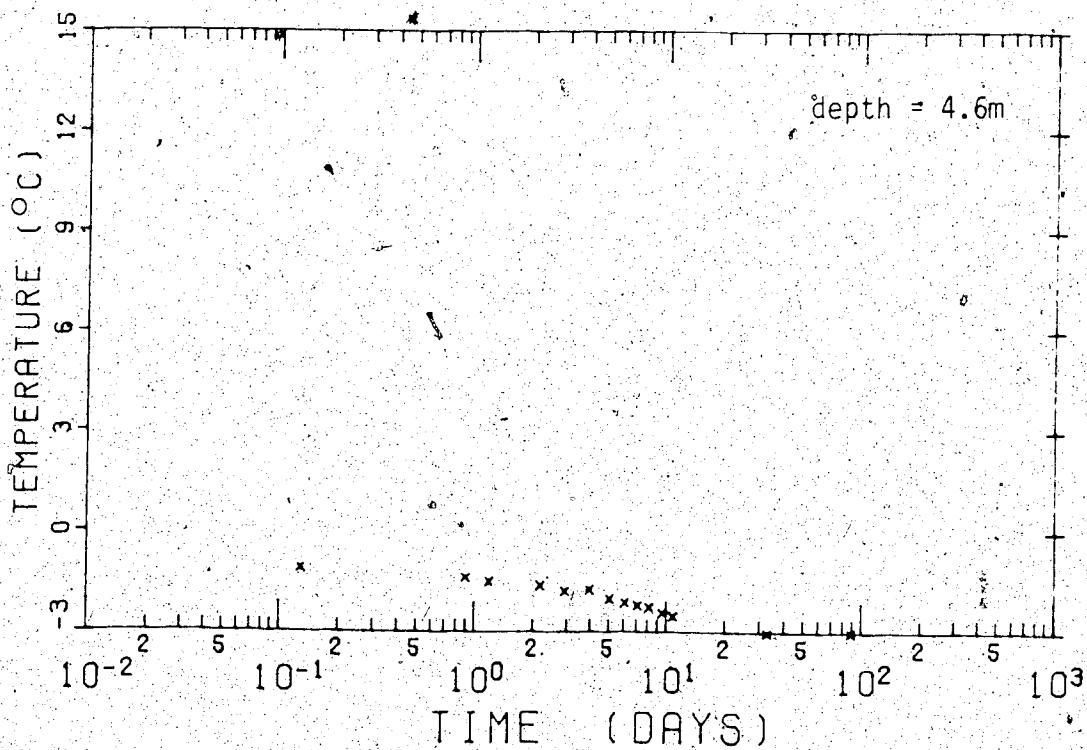


Figure C.11 Thermistor 2 - hole GB2

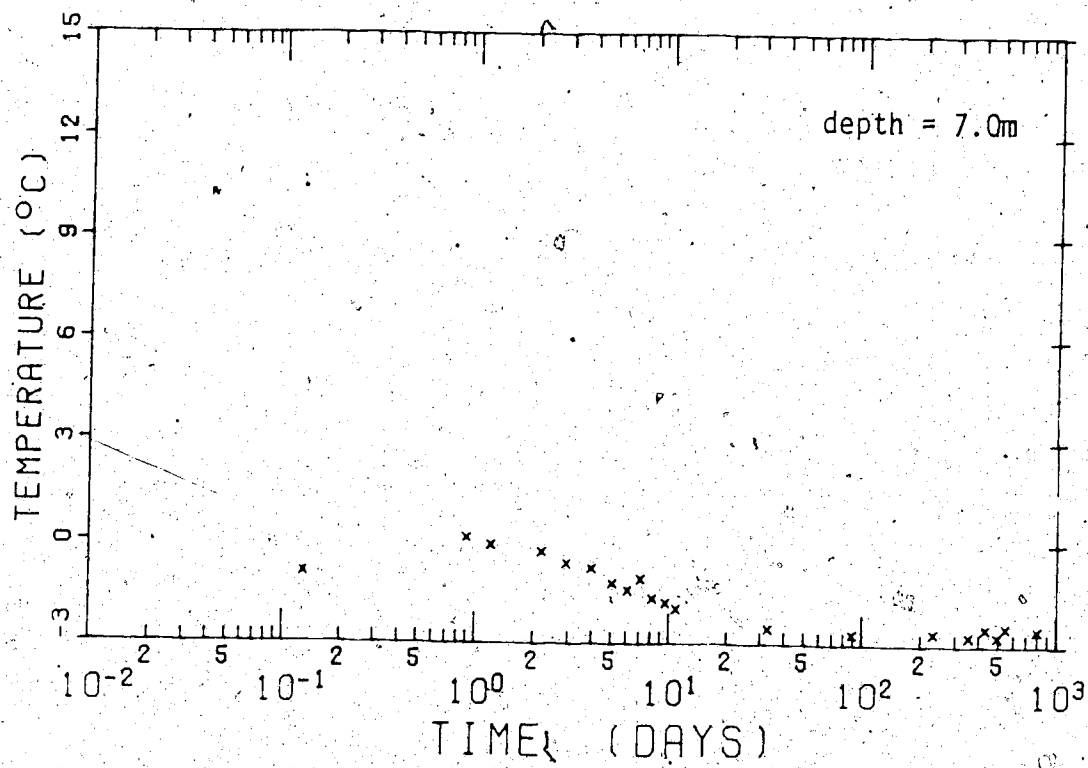


Figure C.12 Thermistor 3 - hole GB2

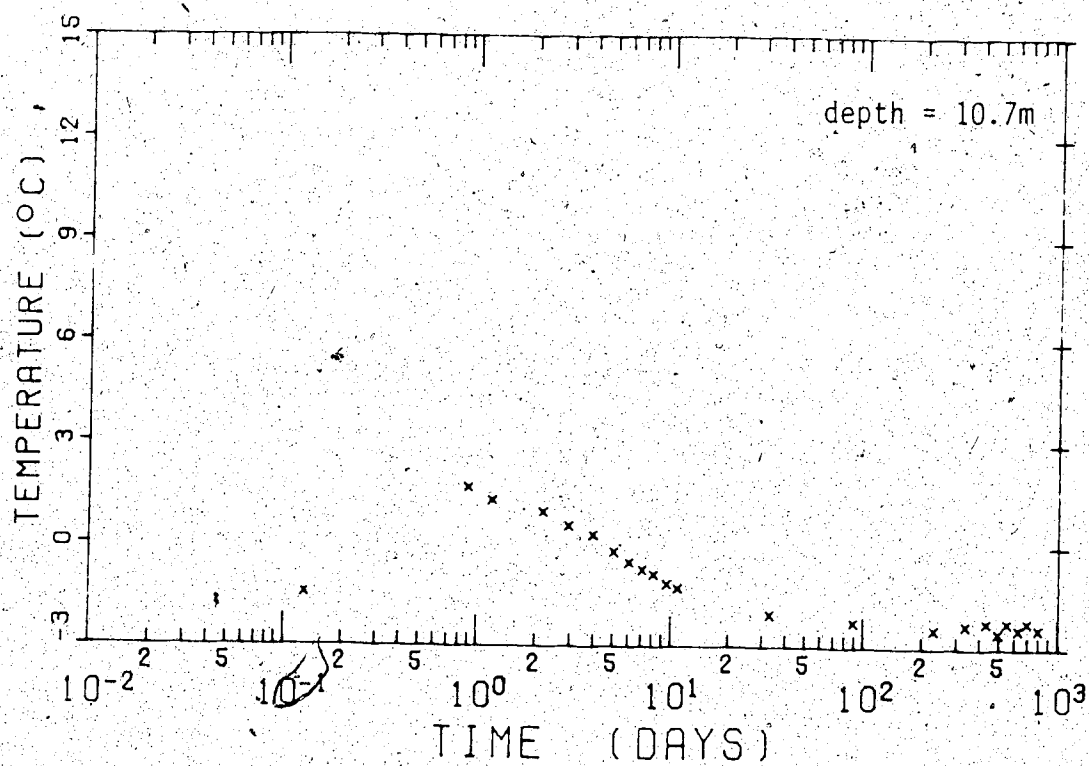


Figure C.13 Thermistor 4 - hole GB2

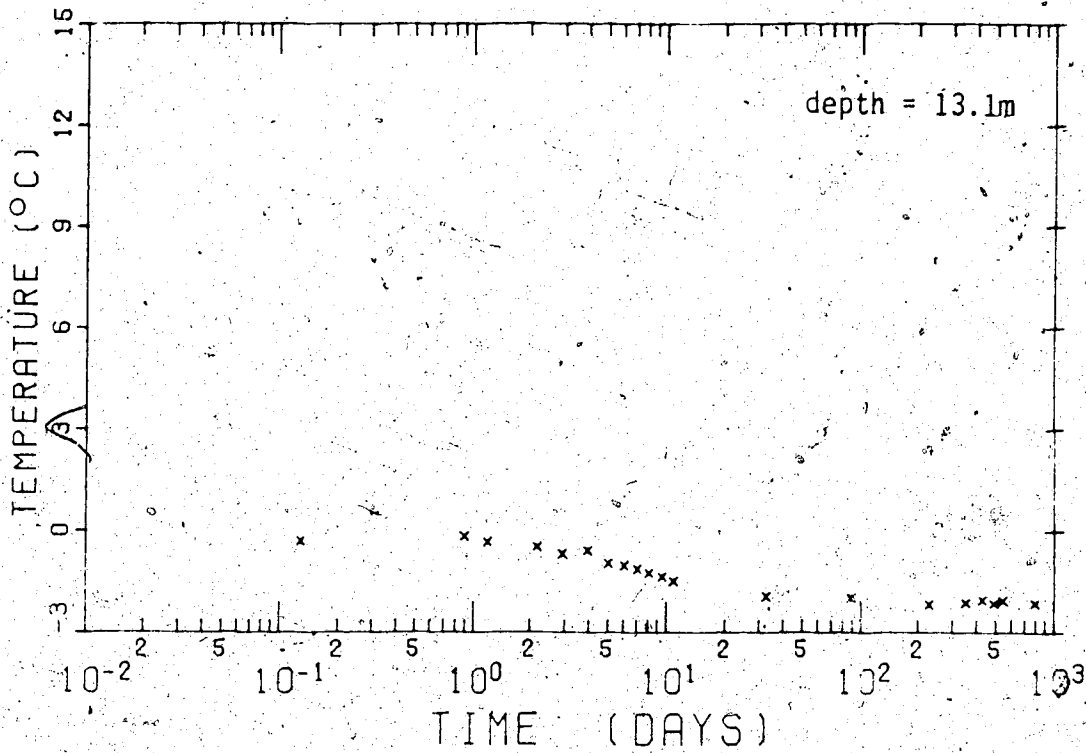


Figure C.14 Thermistor 5 - hole GB2

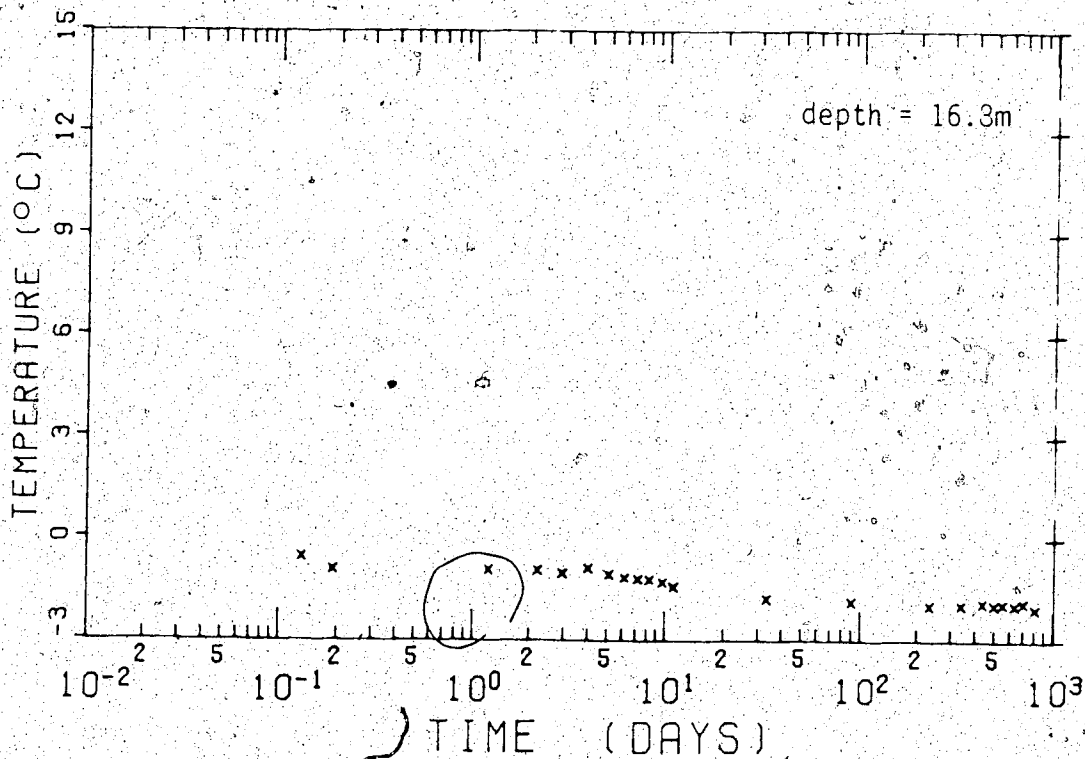


Figure C.15 Thermistor 6 - hole GB2

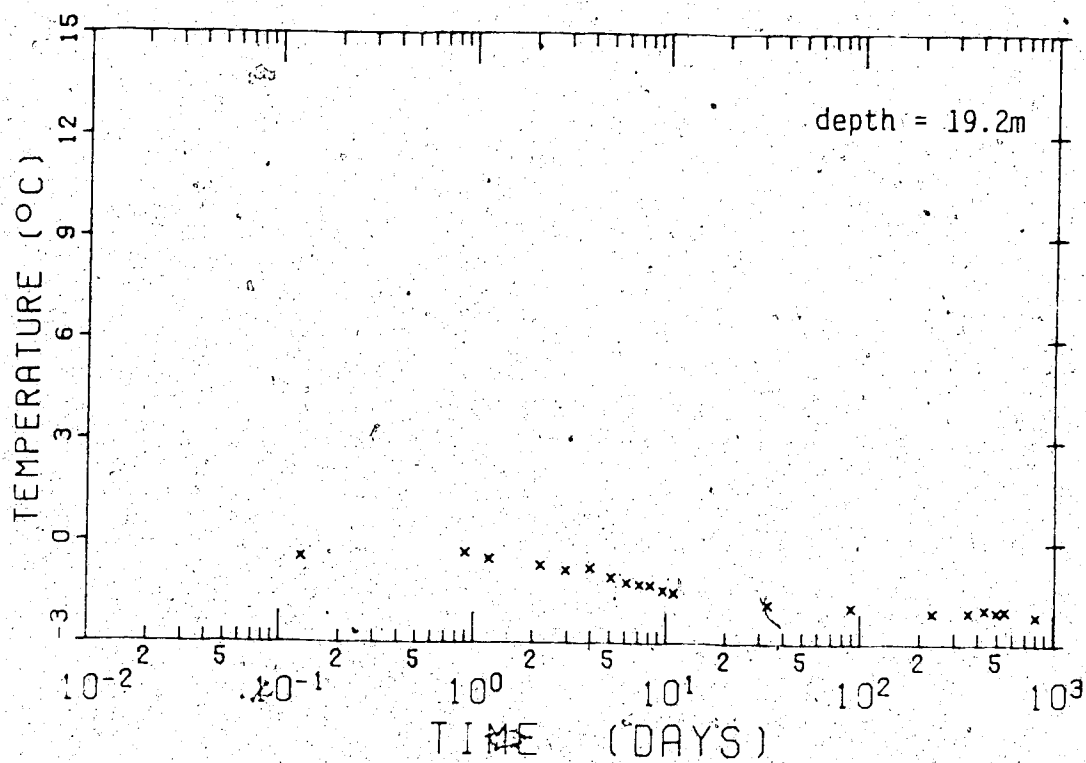


Figure C.16 Thermistor 7 - hole GB2

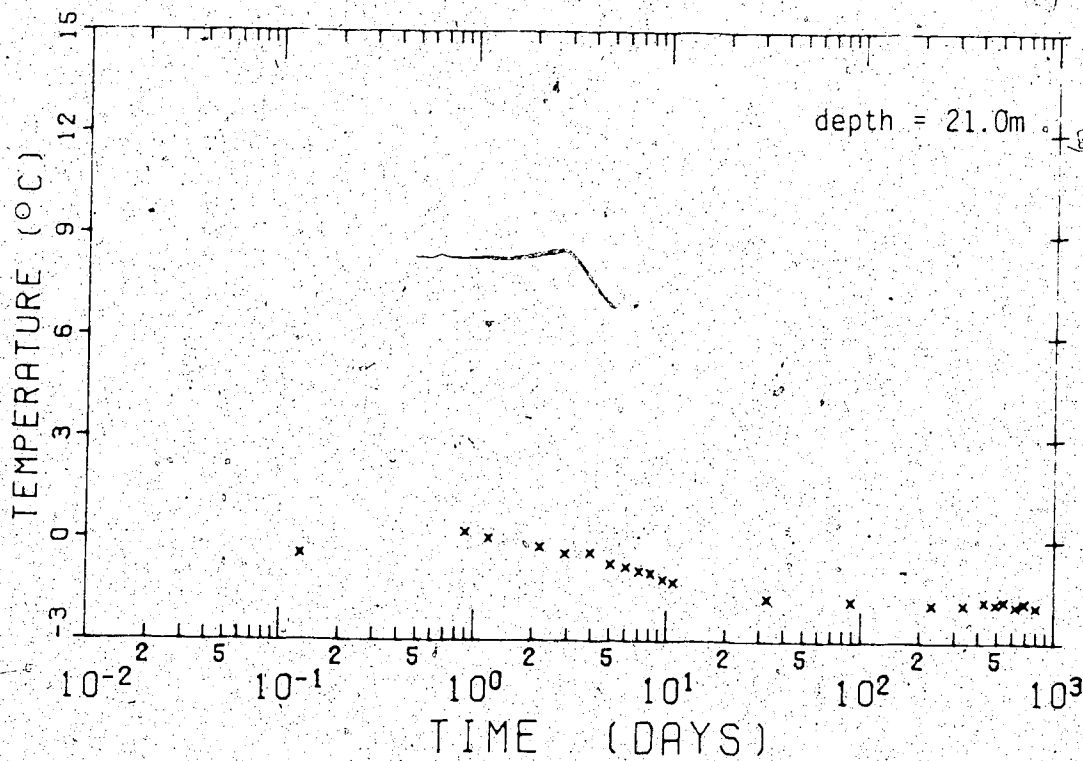


Figure C.17 Thermistor 8 - hole GB2

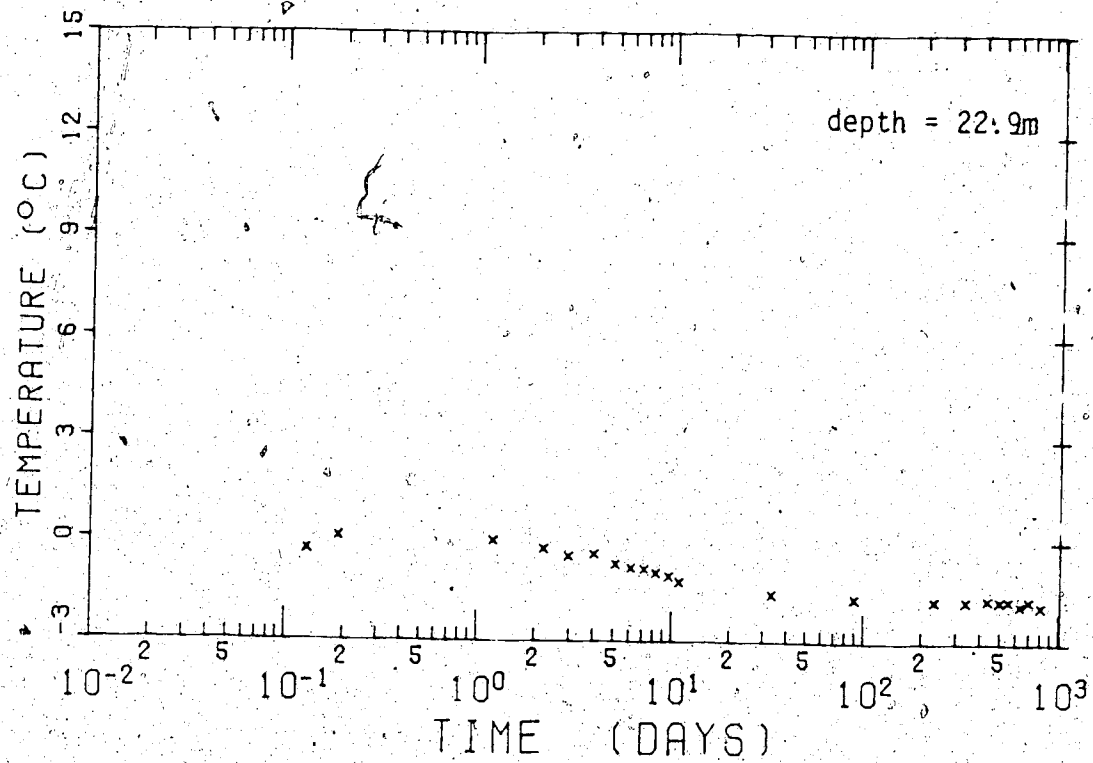


Figure C.18 Thermistor 9 - GB2

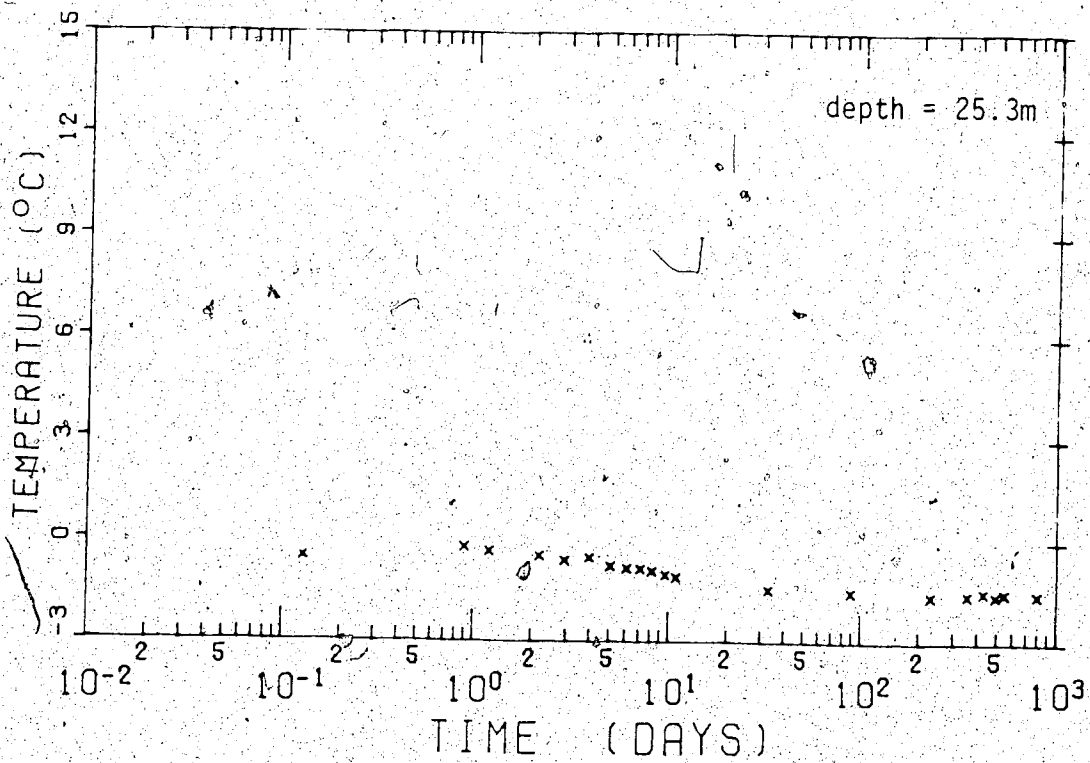


Figure C.19 Thermistor 10 - GB2

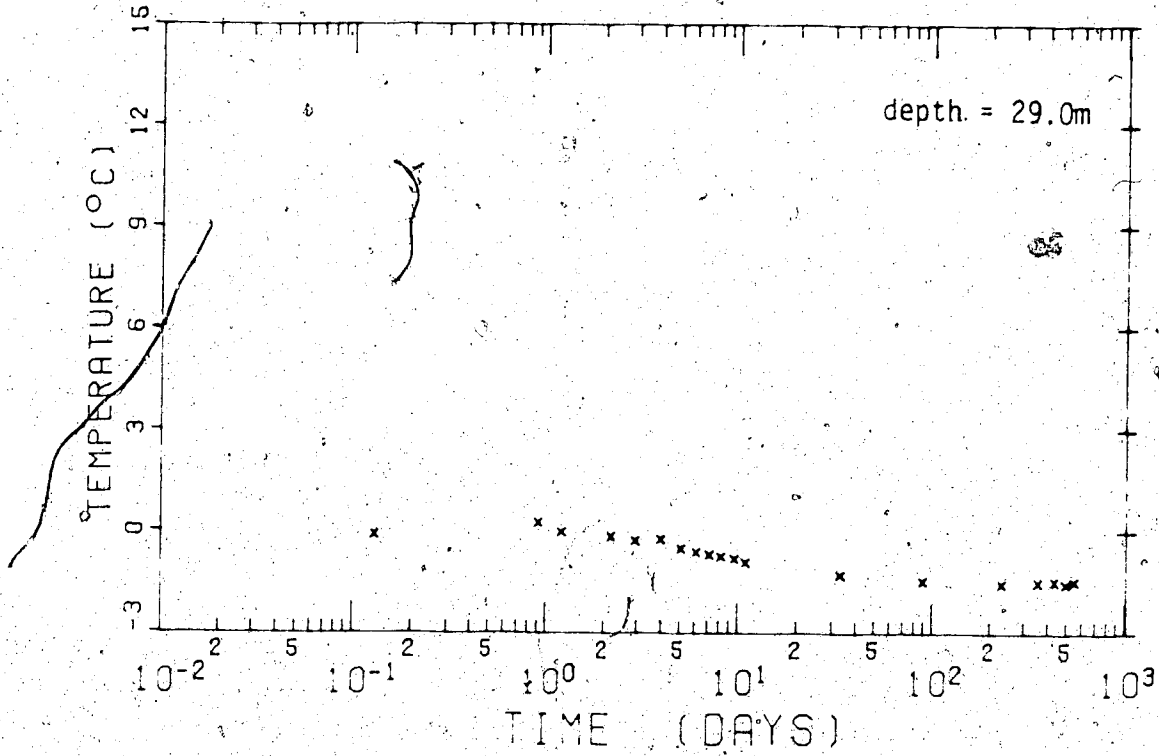


Figure C.20 Thermistor 11 - hole GB2

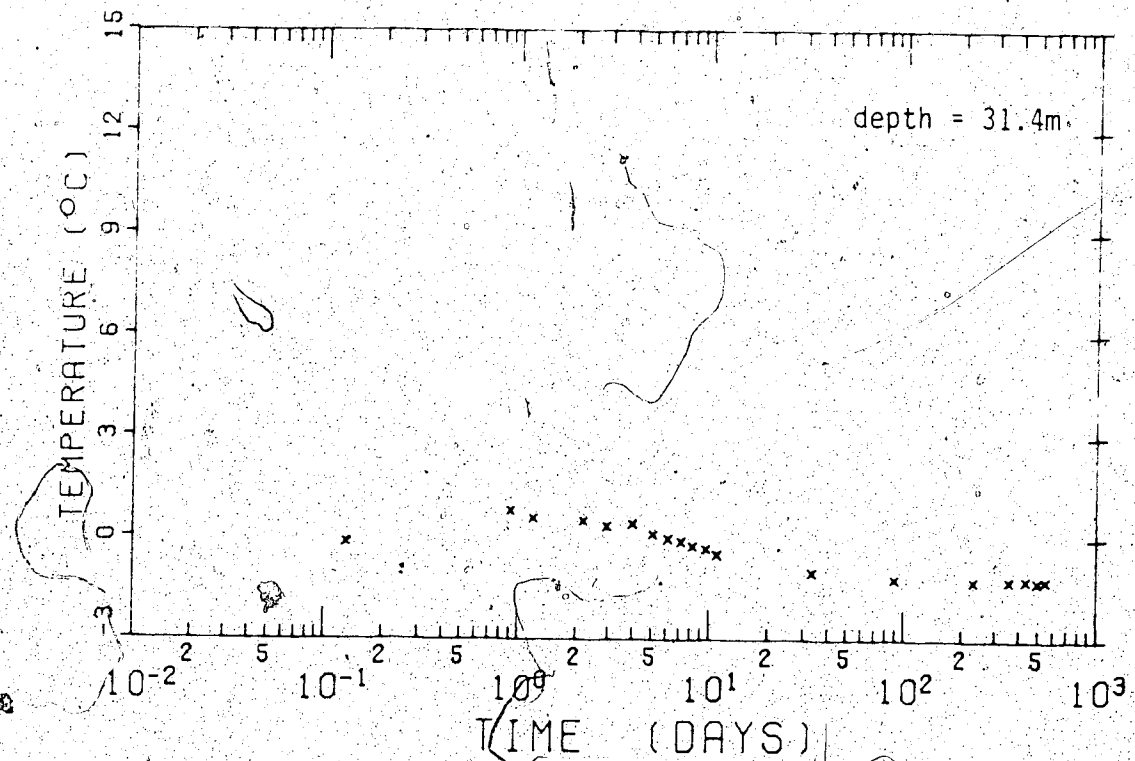


Figure C.21 Thermistor 12 - hole GB2



C.3 Thermistor Data from Hole GB3

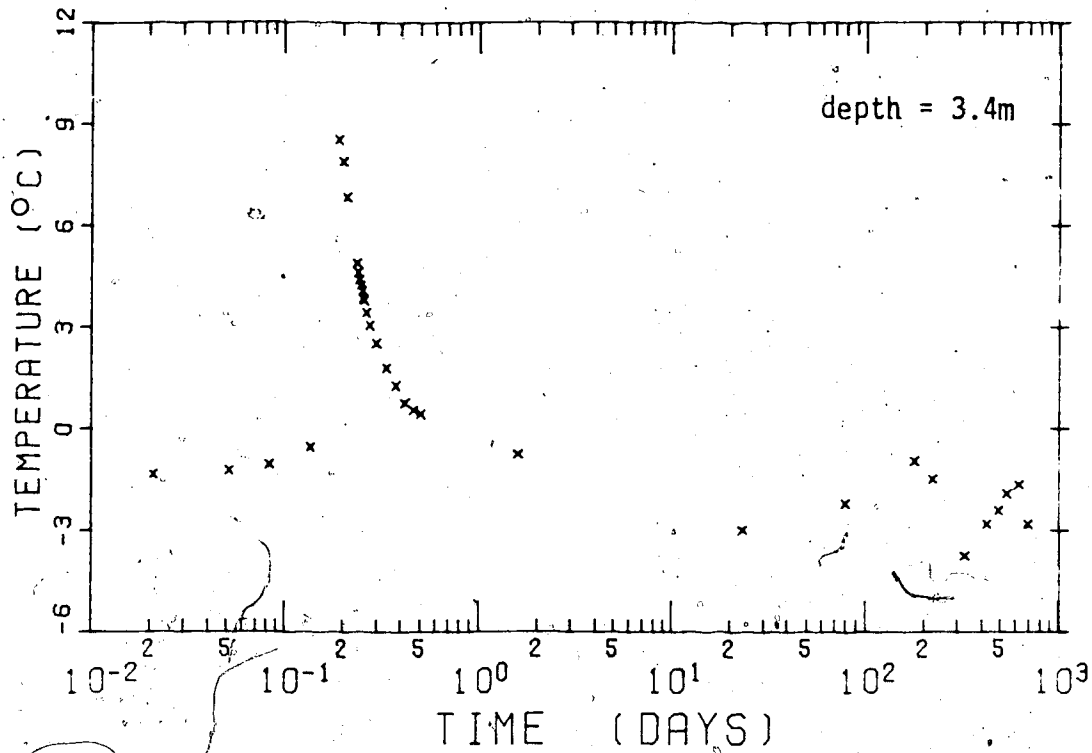


Figure C.22 Thermistor 4 - hole GB3

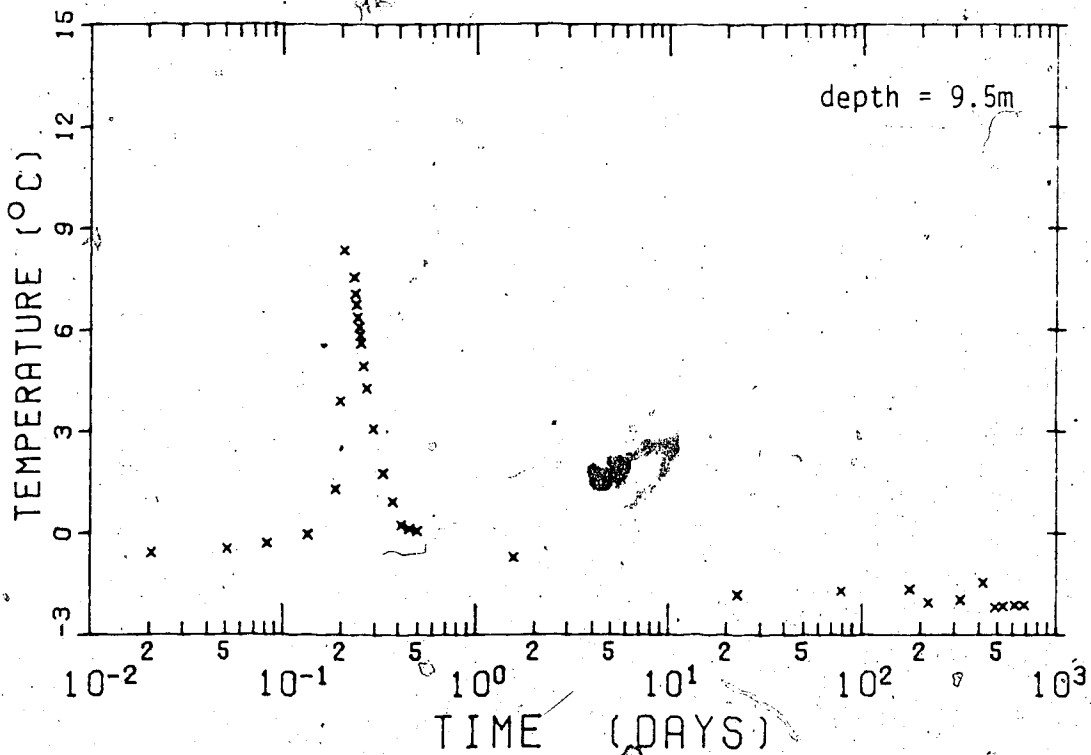


Figure C.23 Thermistor 5 - hole GB3

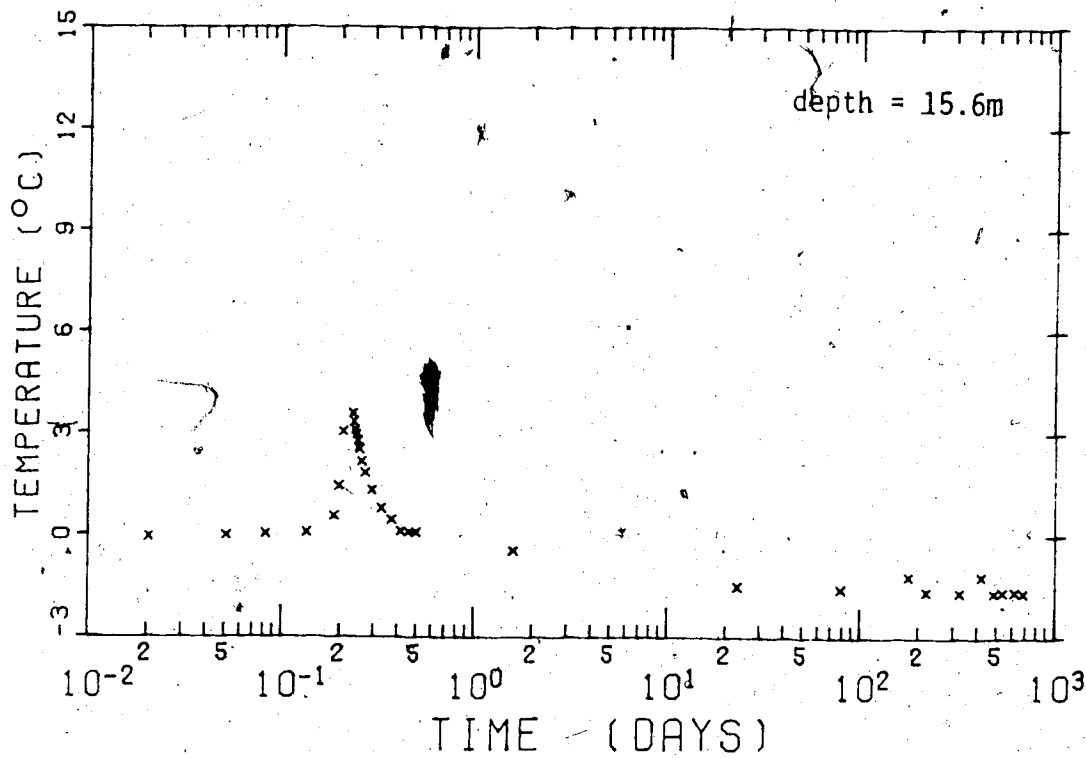


Figure C.24 Thermistor 6 - hole GB3

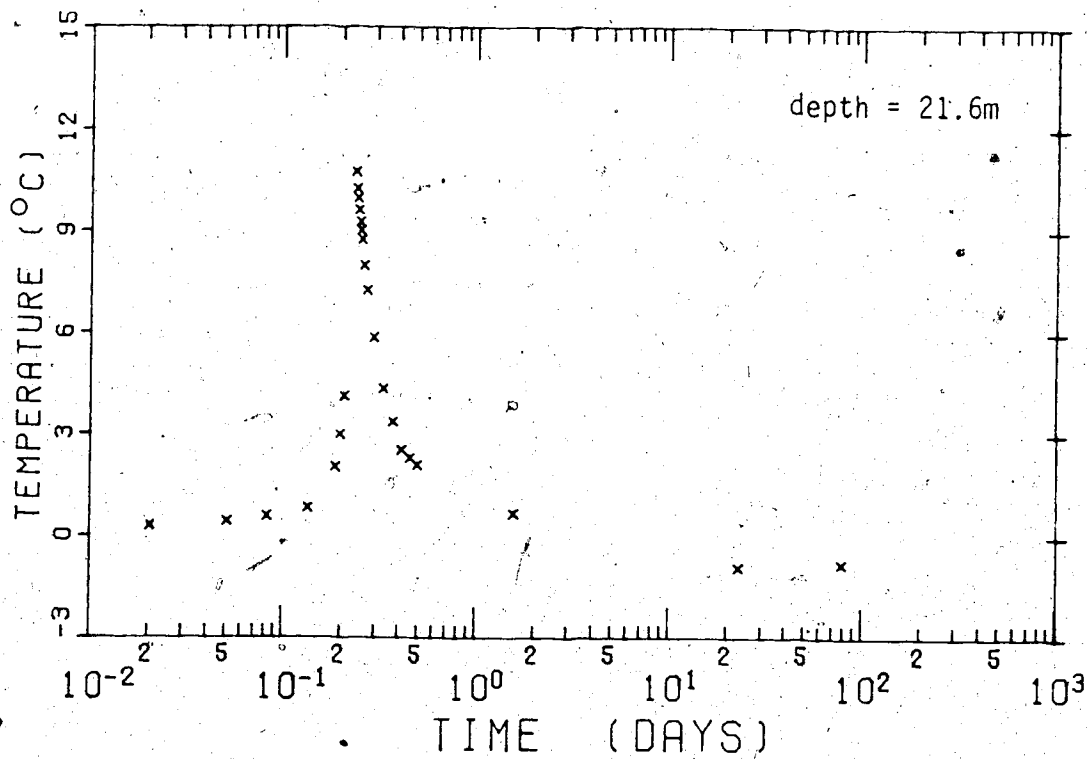


Figure C.25 Thermistor 7 - hole GB3

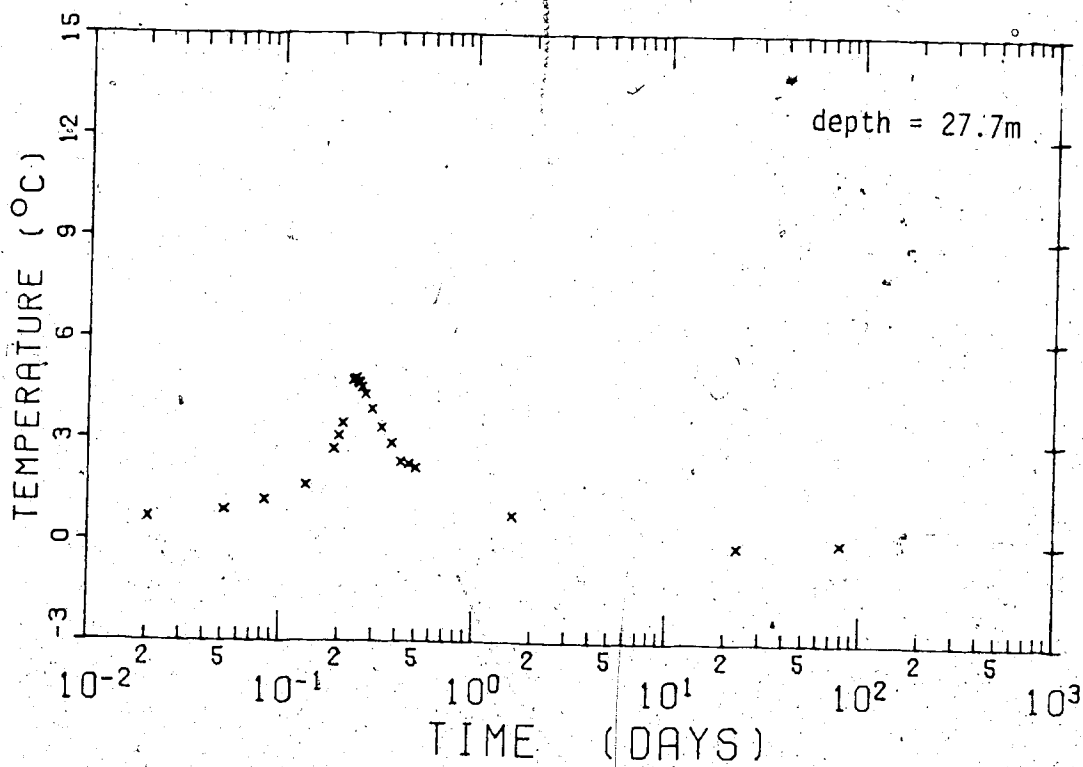


Figure C.26 Thermistor 8 - hole GB3

APPENDIX D

SUMMARY OF LABORATORY TEST DATA

D.1 Direct Shear Tests

TABLE D.1  
SUMMARY OF DIRECT SHEAR TEST DATA

SAMPLE NUMBER	SOIL	TEST NO.	STATE NO.	WATER CONTENT (%)	FROZEN BULK DENSITY (Mg/m <sup>3</sup> )	TEST TEMP. (°C)	INITIAL DISPLACEMENT RATE (cm/day)	σ <sub>v</sub> (kPa)	τ (kPa)	τ (RESIDUAL) (kPa)
PH-1-49-2	glaciolacustrine clay	1	M/A	21.7	2.02	-1.1 to -1.3	0.070	707	321	200
		2	M/A	21.2	2.03	-1.1 to -2.1	0.070	707	328	206
		3	M/A	18.7	2.06	-1.3	0.150	410	433	249
		4	M/A	18.4	2.08	-1.3	0.070	310	478	184
		5	M/A	1	2.09	-1.2	0.070	138	270	86
		6	M/A	1	2.09	-1.2	0.070	550	421	311
		7	M/A	24.8	1.91	room	0.20	830	351	131
PH-1-50-3	glaciolacustrine clay	8	3	21.2	2.02	room	0.20	275	440	260
		9	3					1035		223
		10	3					895		191
PH-1-50-4	glaciolacustrine clay	11	3	21.2	2.03	room	0.20	620	160	150
		12	3					480		127
		13	3					690		179
		14	3					415		112
		15	3					345		98
		16	3					275		82
PH-2-28-7	alluvial clay	17	6	26.7	1.94	room		205		67
		18	6					140		49
		19	6					70		26
		20	6					1380		518
		21	6					1260		470
		22	6					1100		418
PH-2-28-8	alluvial clay	23	5	26.7	1.96	room	0.070	965	354	301
		24	5					830		288
		25	5					205		80
		26	5					1100		600
		27	5					895		250
		28	5					620		211
PH-2-28-9	alluvial clay	29	5	27.0	1.94	room	0.070	480		179
		30	5					205		161
		31	5					690		224
		32	5					550		224
		33	5					415		153
		34	5					275		88
PH-2-28-10	alluvial clay	35	6	26.7	1.92	room	0.070	170		65
		36	6					105		40
		37	6					415		167
		38	6					205		90
		39	6					140		74
		40	6					415		72
		41	6					205		55
42	6					140		32		
PH-1-51-4	glaciolacustrine clay	43	M/A	22.6	2.07	room	0.20	70	41	18
		44	M/A	26.7	2.00	room	0.070	105	301	65
		45	M/A	26.7	2.00	room	0.070	415	145	167
		46	M/A	22.7	2.03	room	0.070	205	145	90
		47	M/A	22.7	2.03	room	0.070	140	145	74
		48	M/A	22.7	2.03	room	0.070	415	171	72
		49	M/A	23.0	2.04	room	0.20	205	89	55
50	M/A	22.6	2.07	room	0.20	140	76	32		

1. The sample numbers may be interpreted as follows: Example: PH-1-49-2  
 PH - indicates this study  
 1 - Hole number (among CB1, CB2 and CB3)  
 49 - Core number  
 2 - Sample number from core

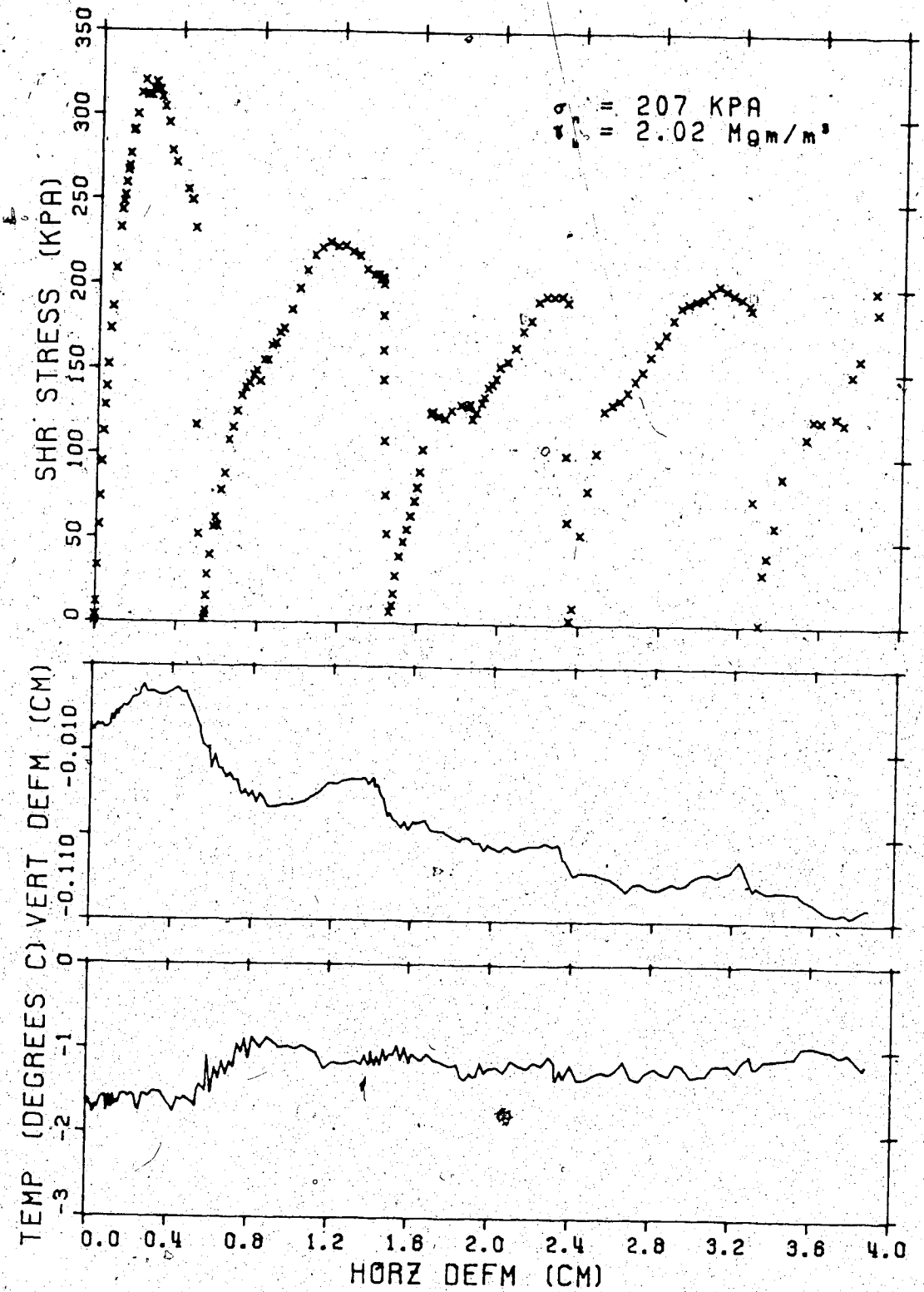


Figure D.1 Direct Shear Test 1 (frozen)

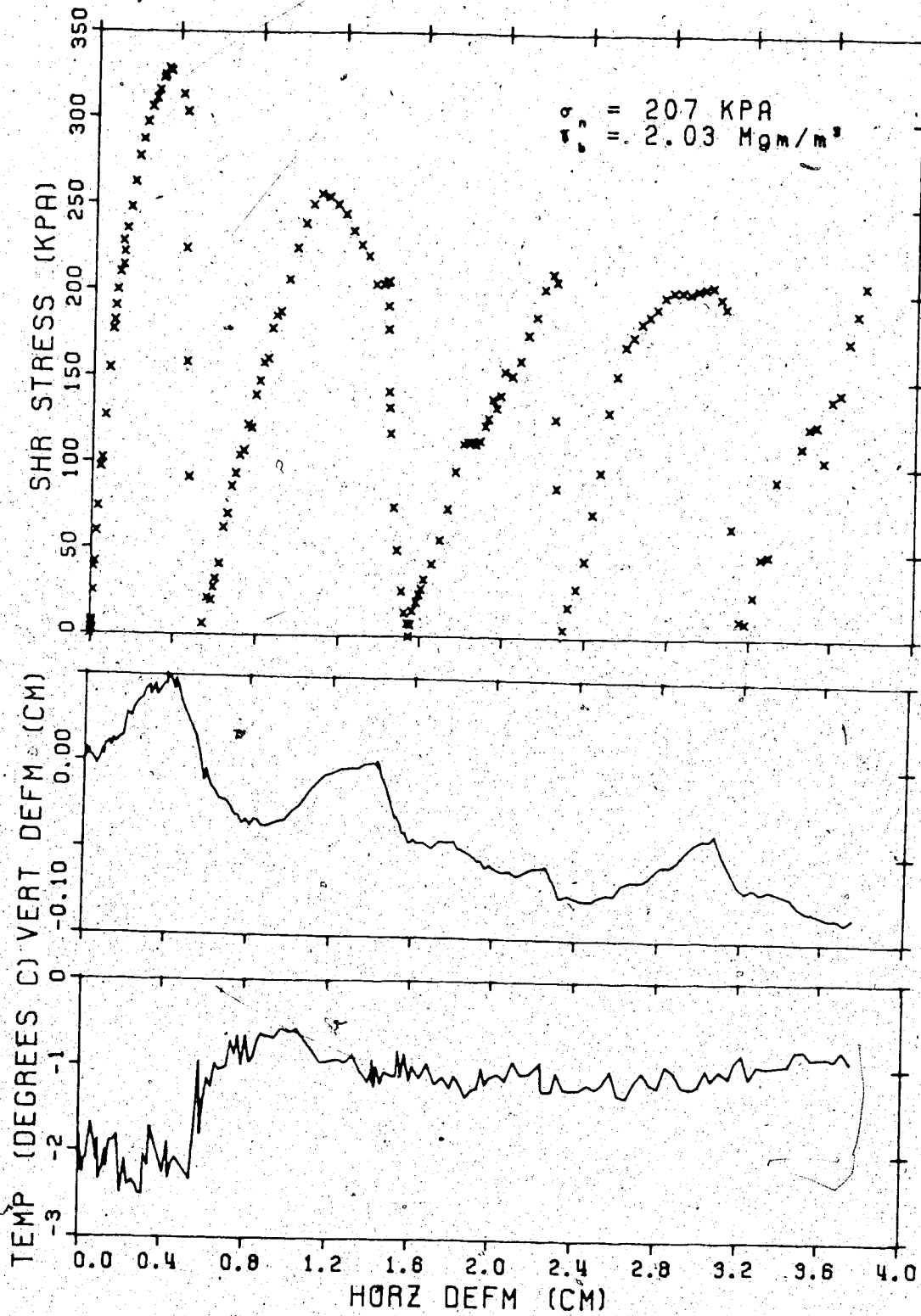


Figure D.2 Direct Shear Test 2 (frozen)



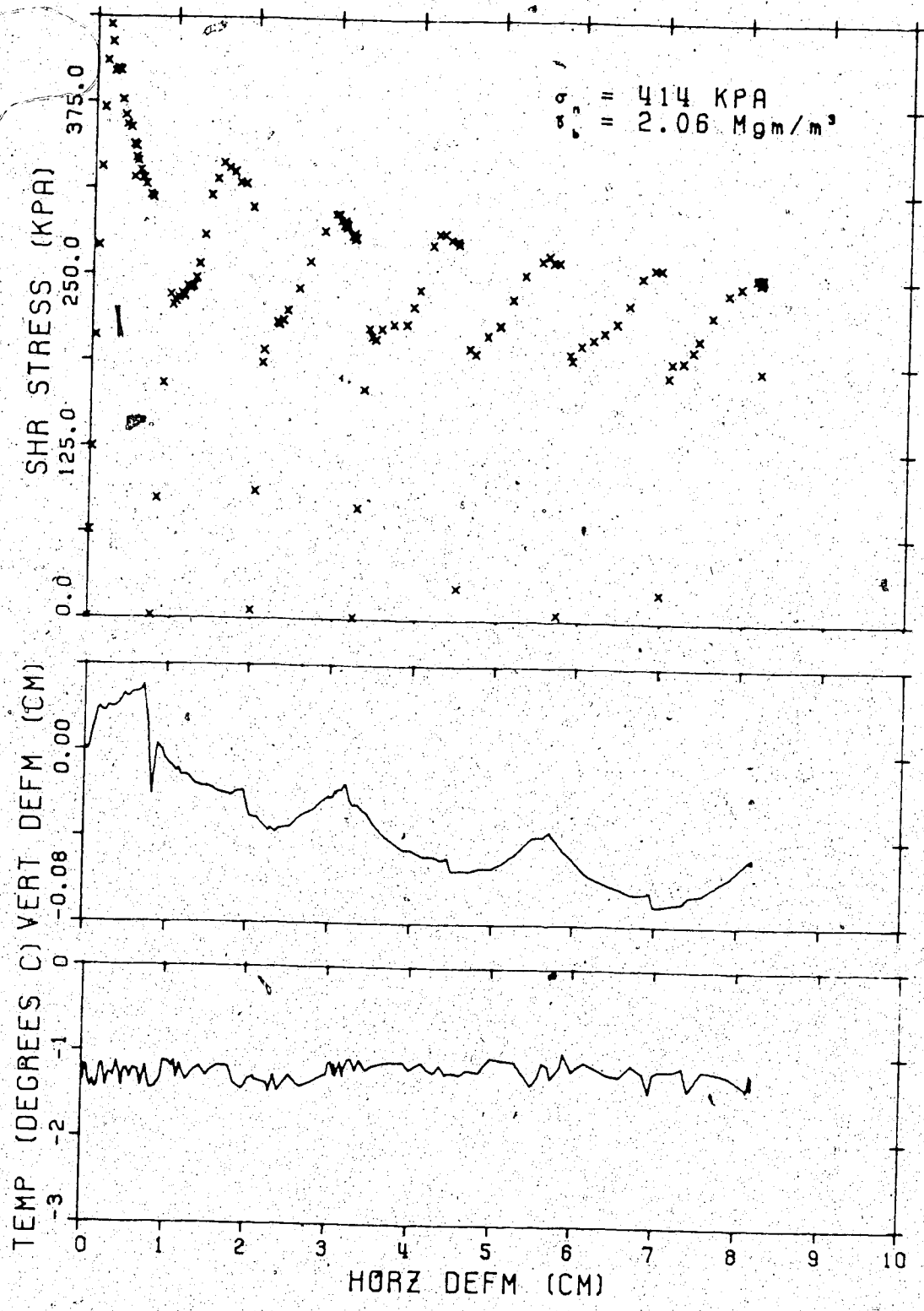


Figure D.3 Direct Shear Test 3 (frozen)

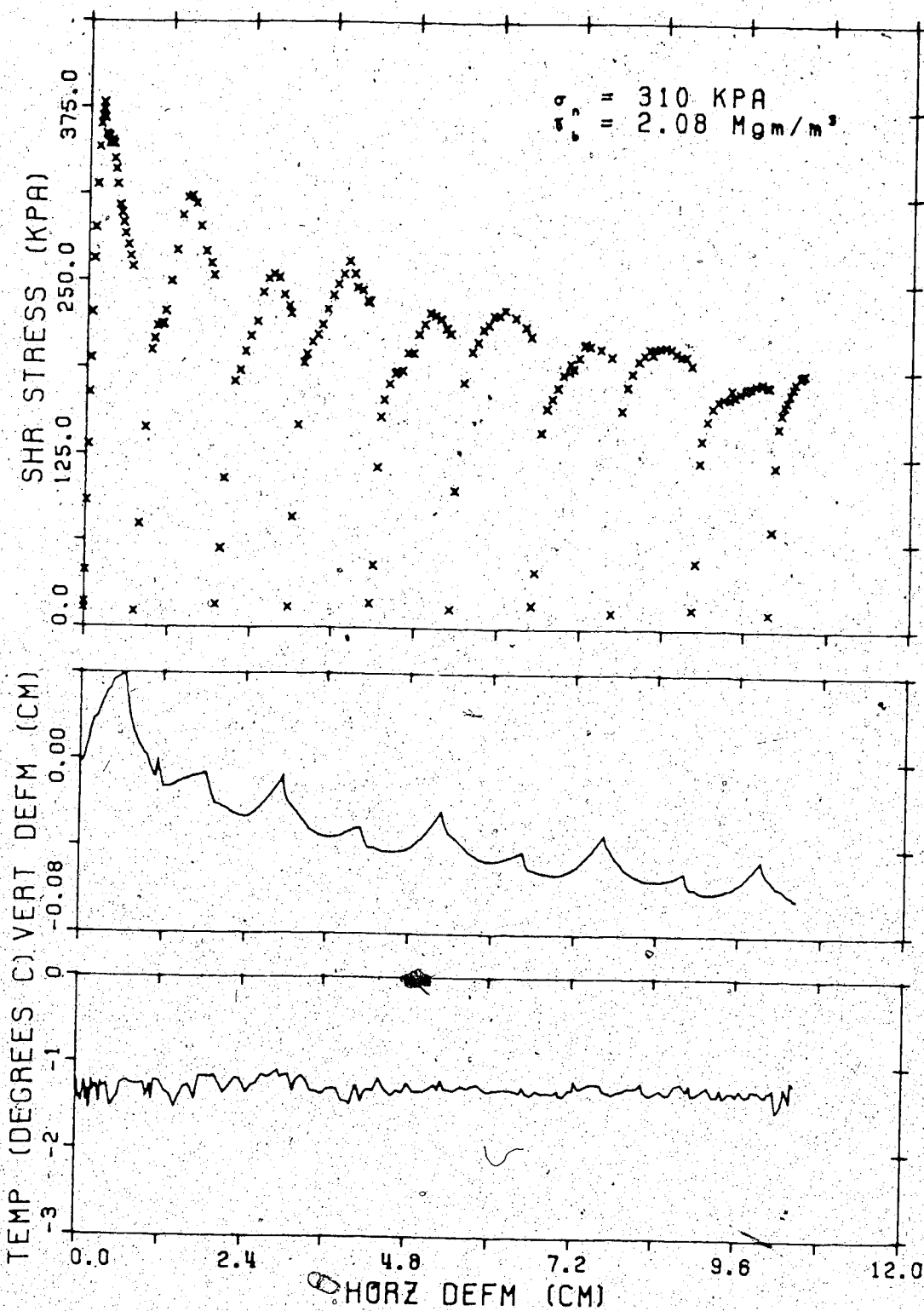


Figure D.4 Direct Shear Test 4 (frozen)

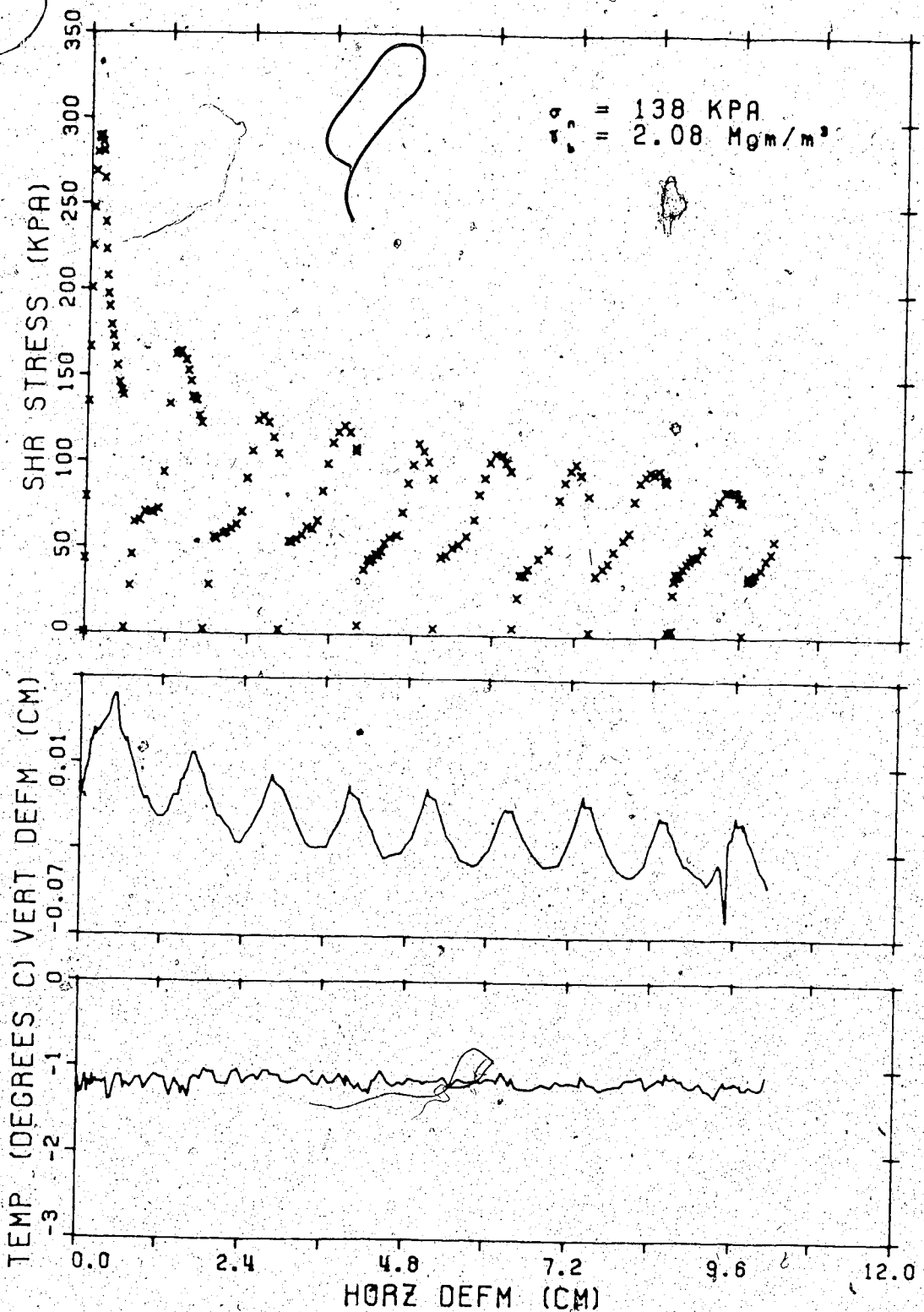


Figure D.5 Direct Shear Test 5 (frozen)

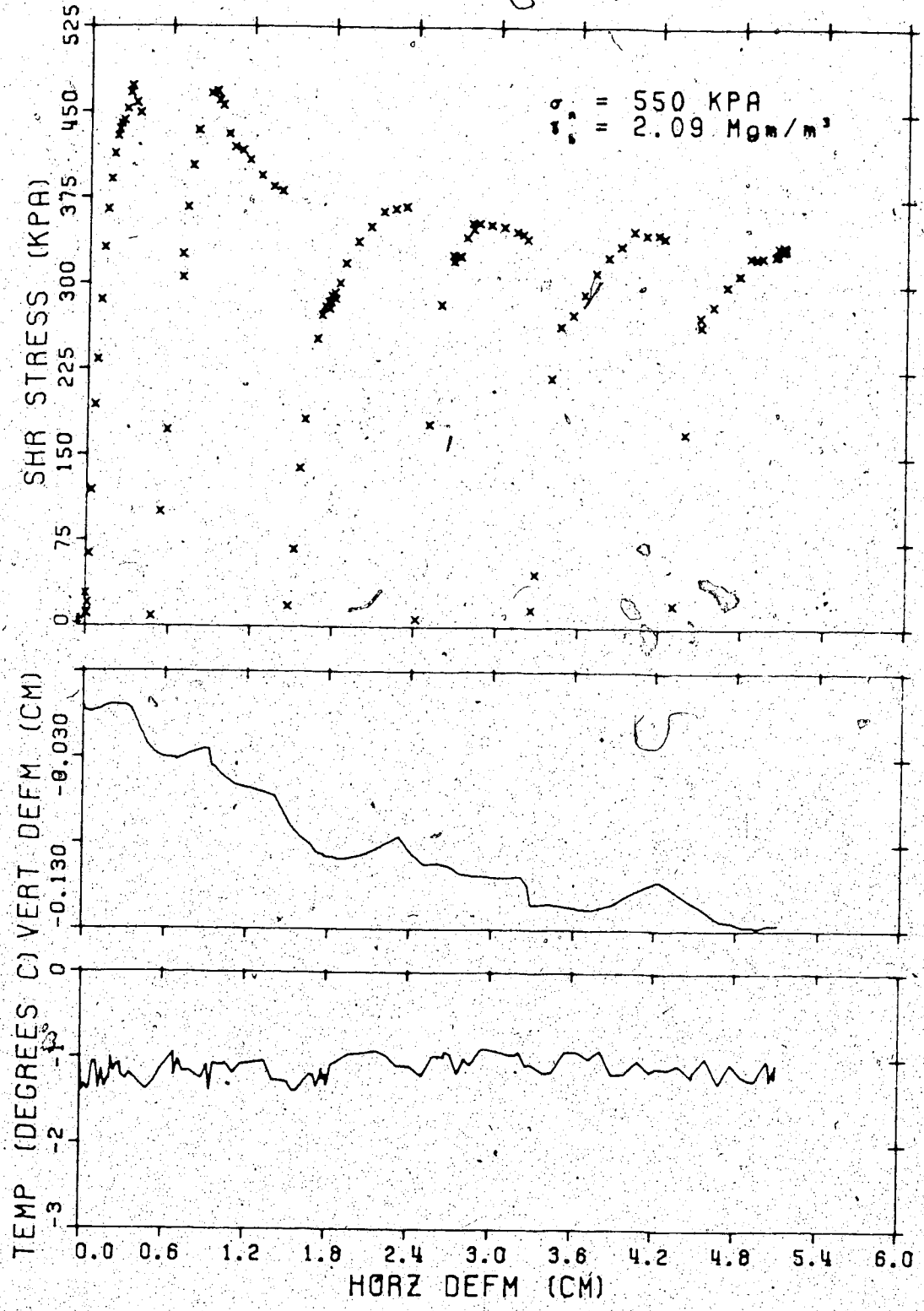


Figure D.6 Direct Shear Test 6 (frozen)

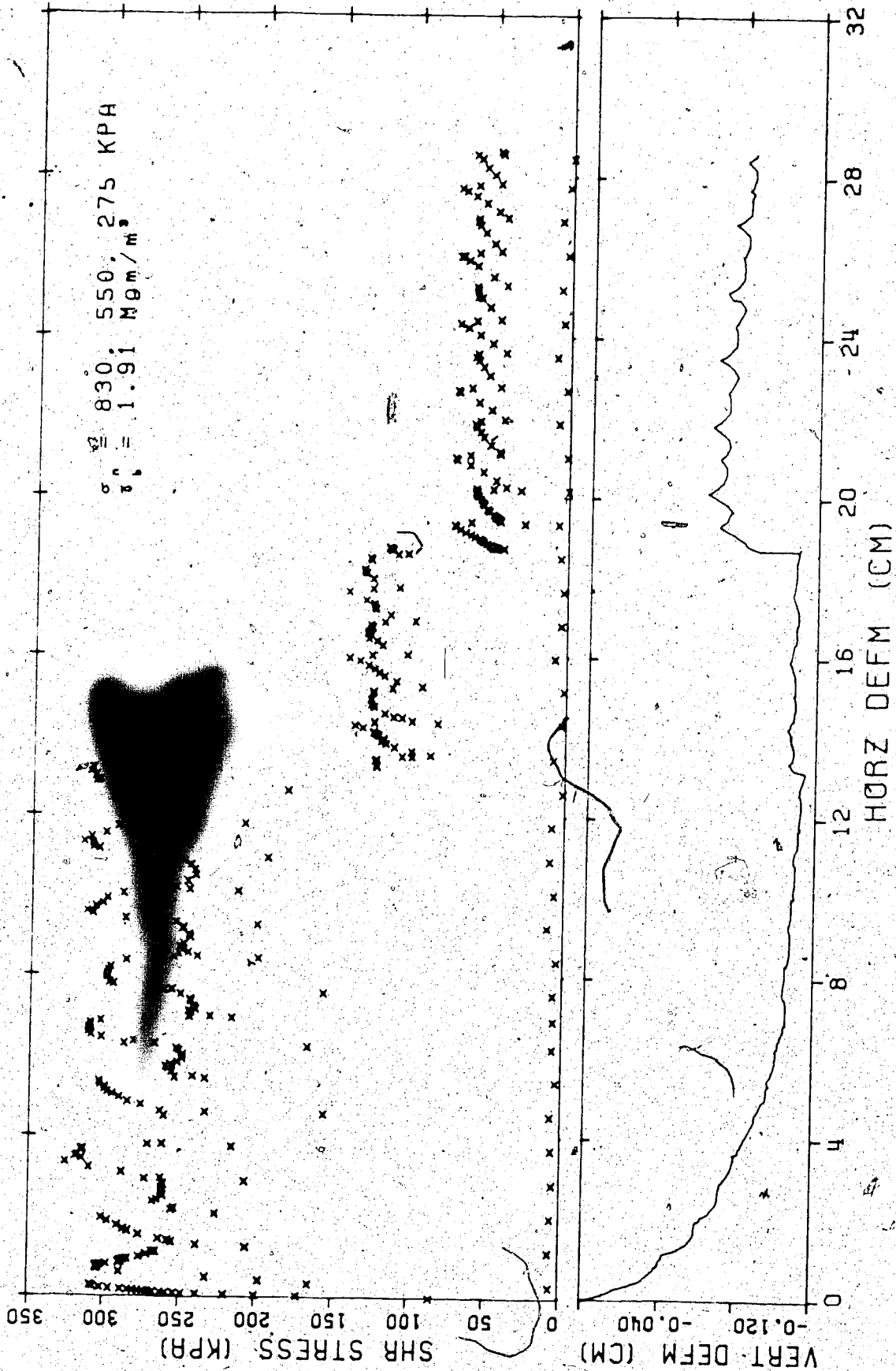


Figure 0.7 Direct Shear Test 7 (multistage)

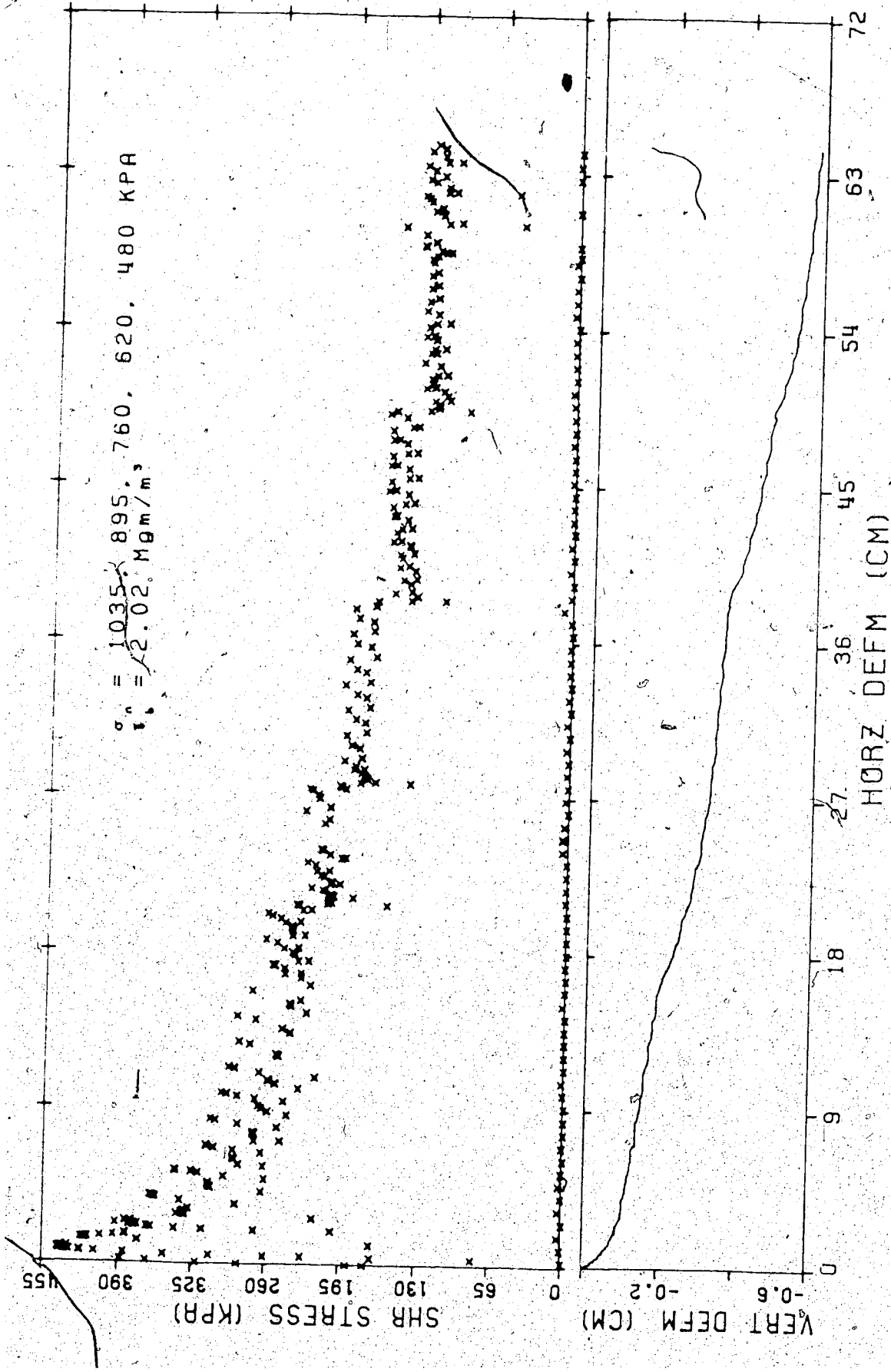


Figure D.8 Direct Shear Test 8 (multistage)

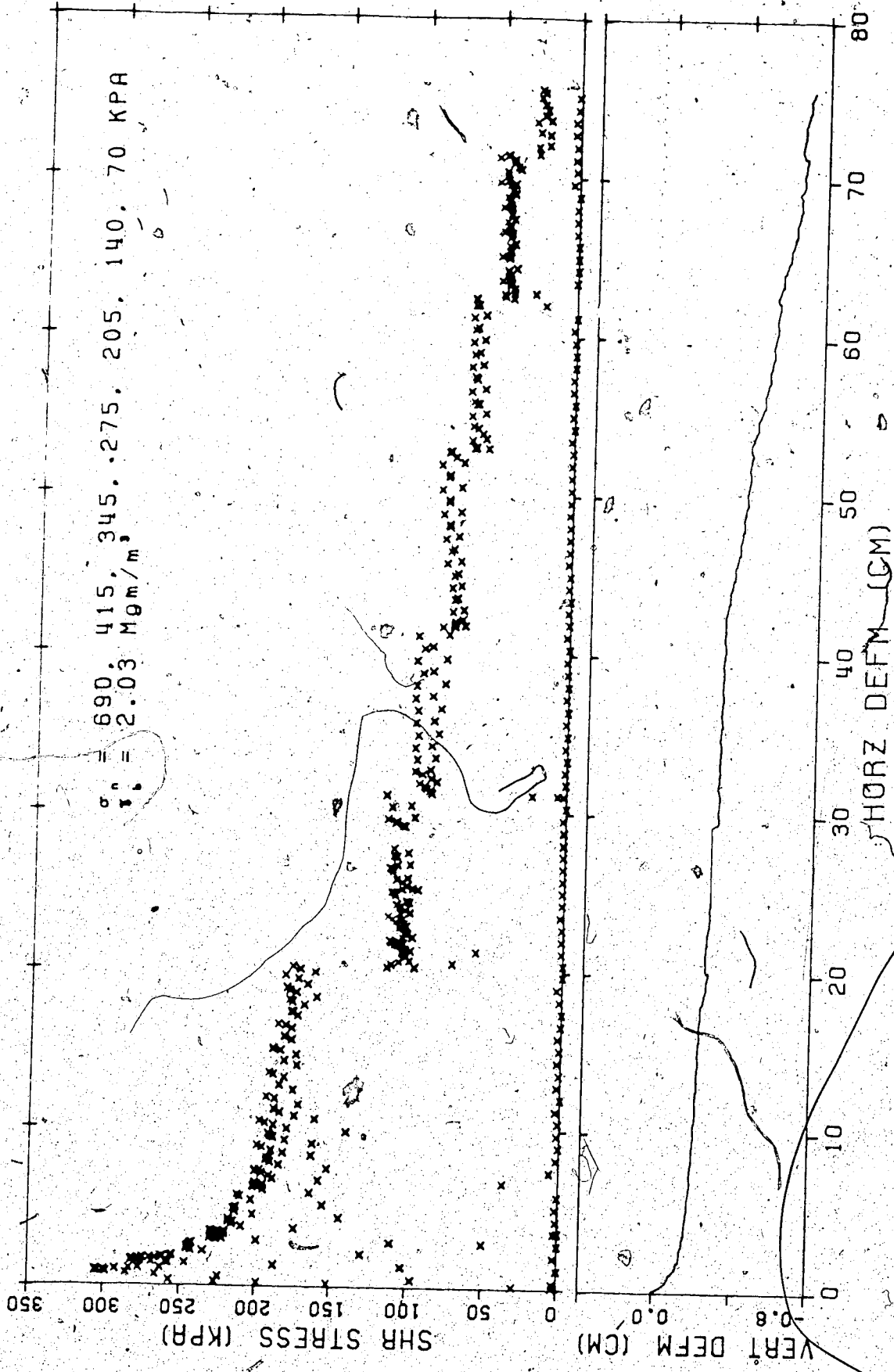


Figure 0.9 Direct Shear Test 9 (multistage)

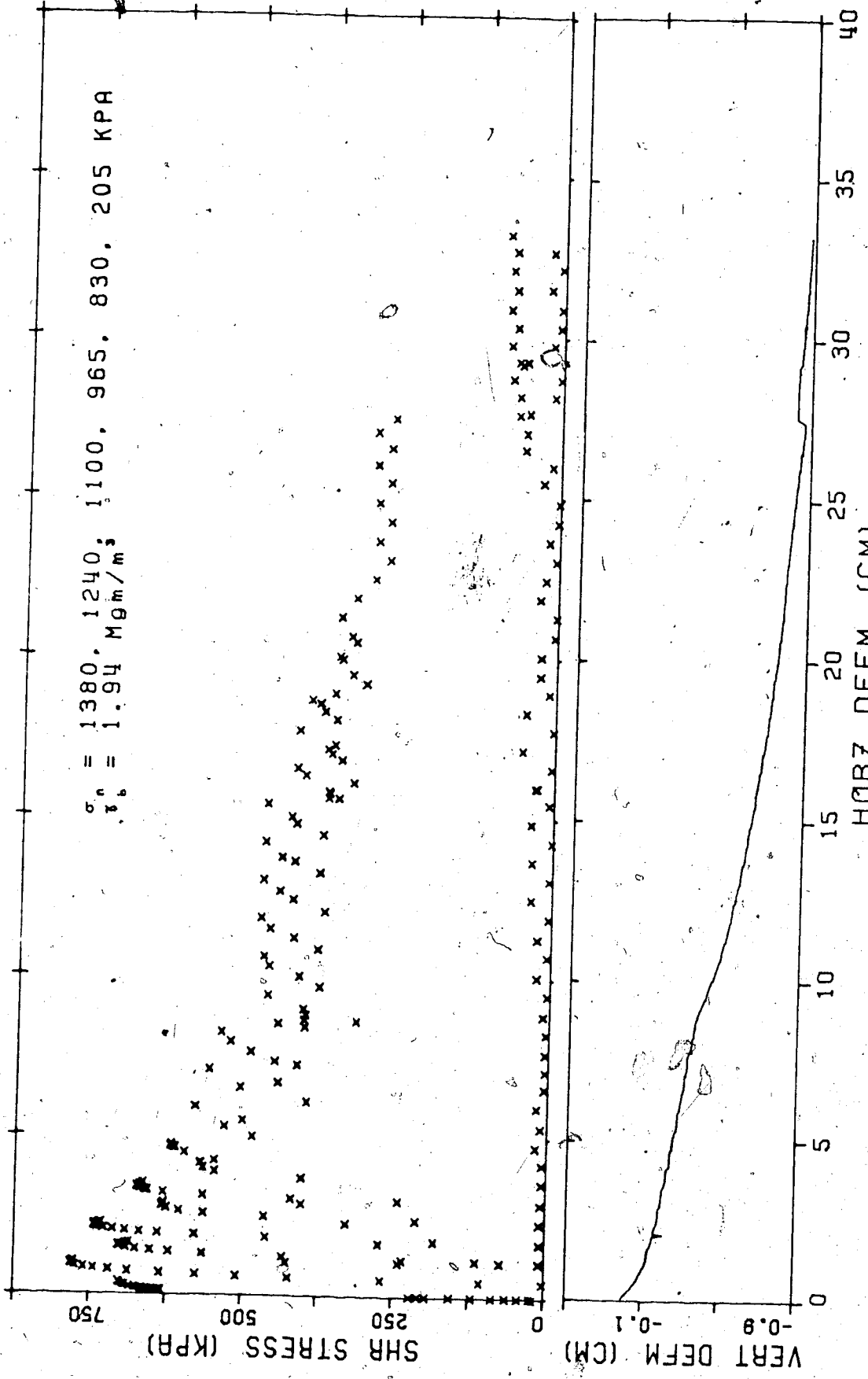


Figure D.10 Direct Shear Test 10 (multistage)



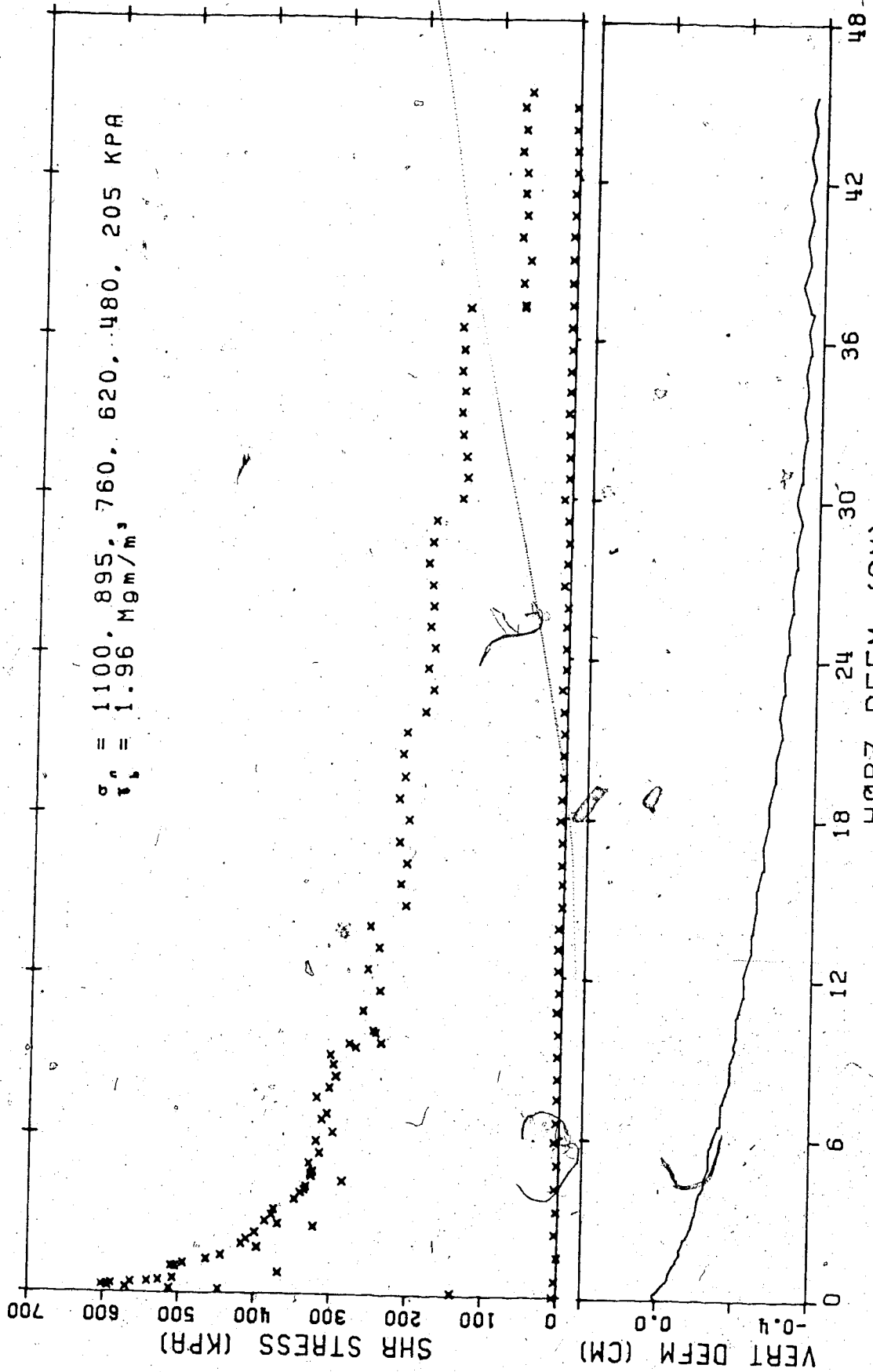


Figure D.11 Direct Shear Test 11 (multistage)

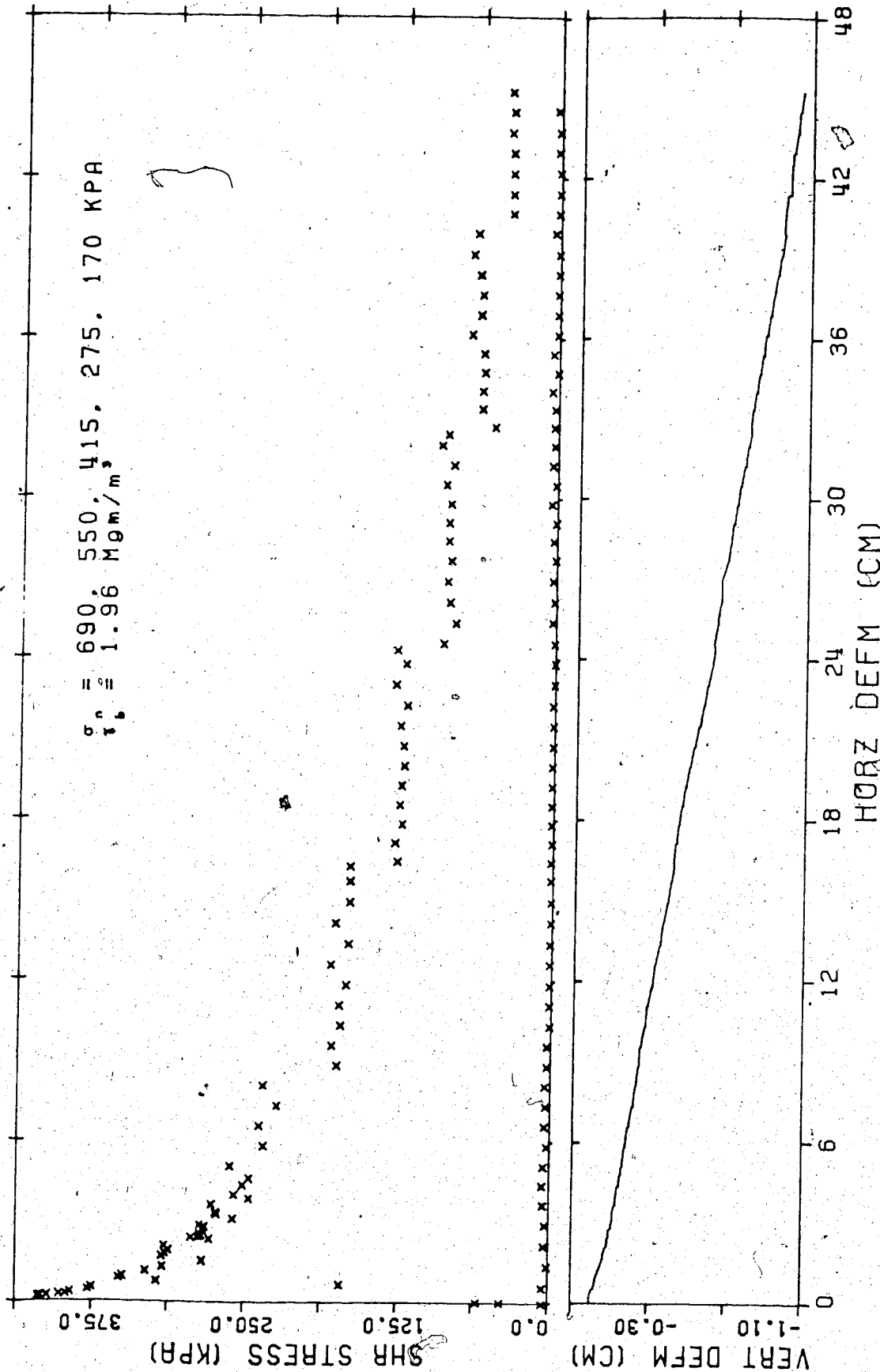


Figure D.12 Direct Shear Test 12 (multistage)

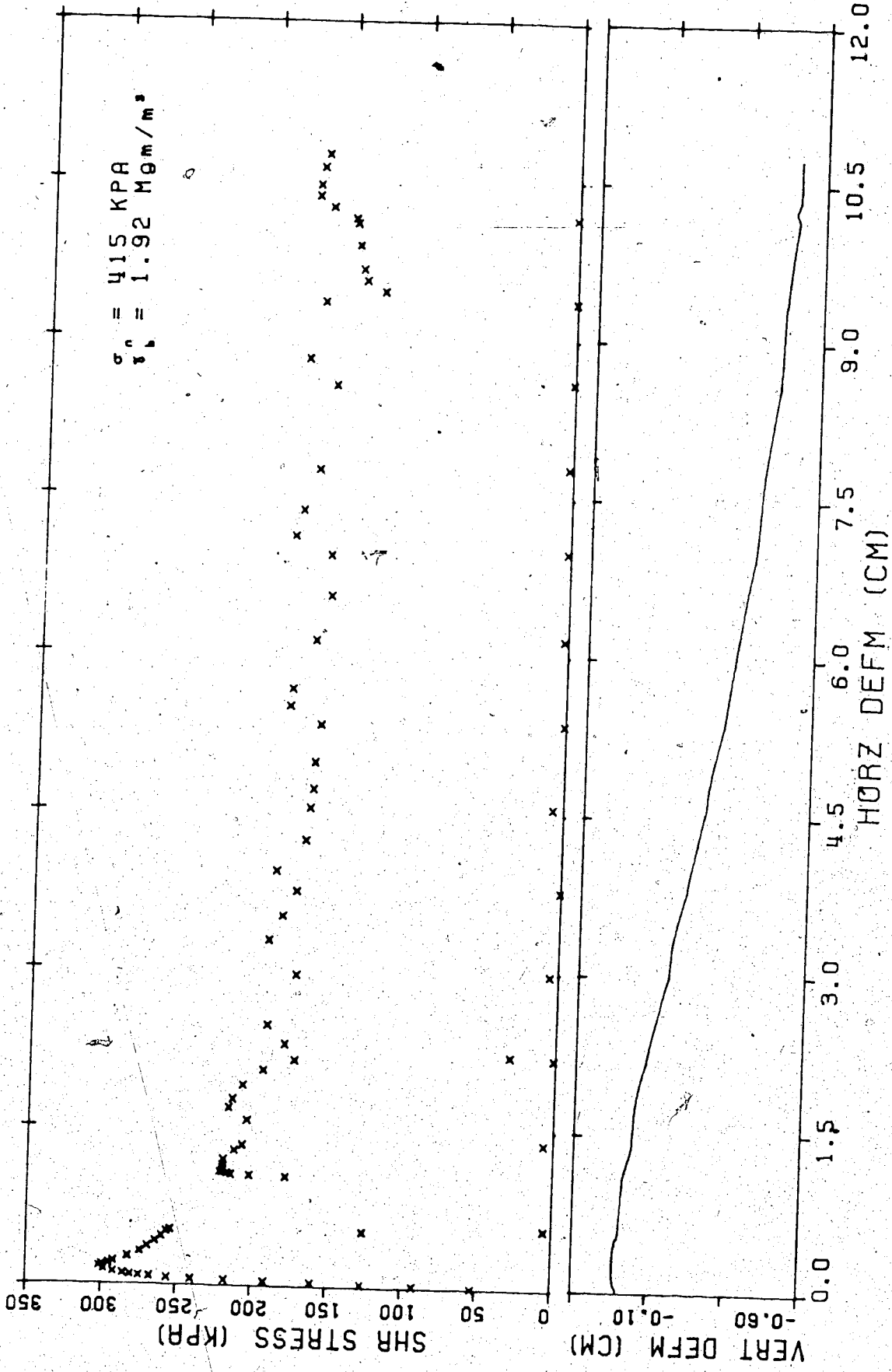


Figure D.13 Direct Shear Test 13

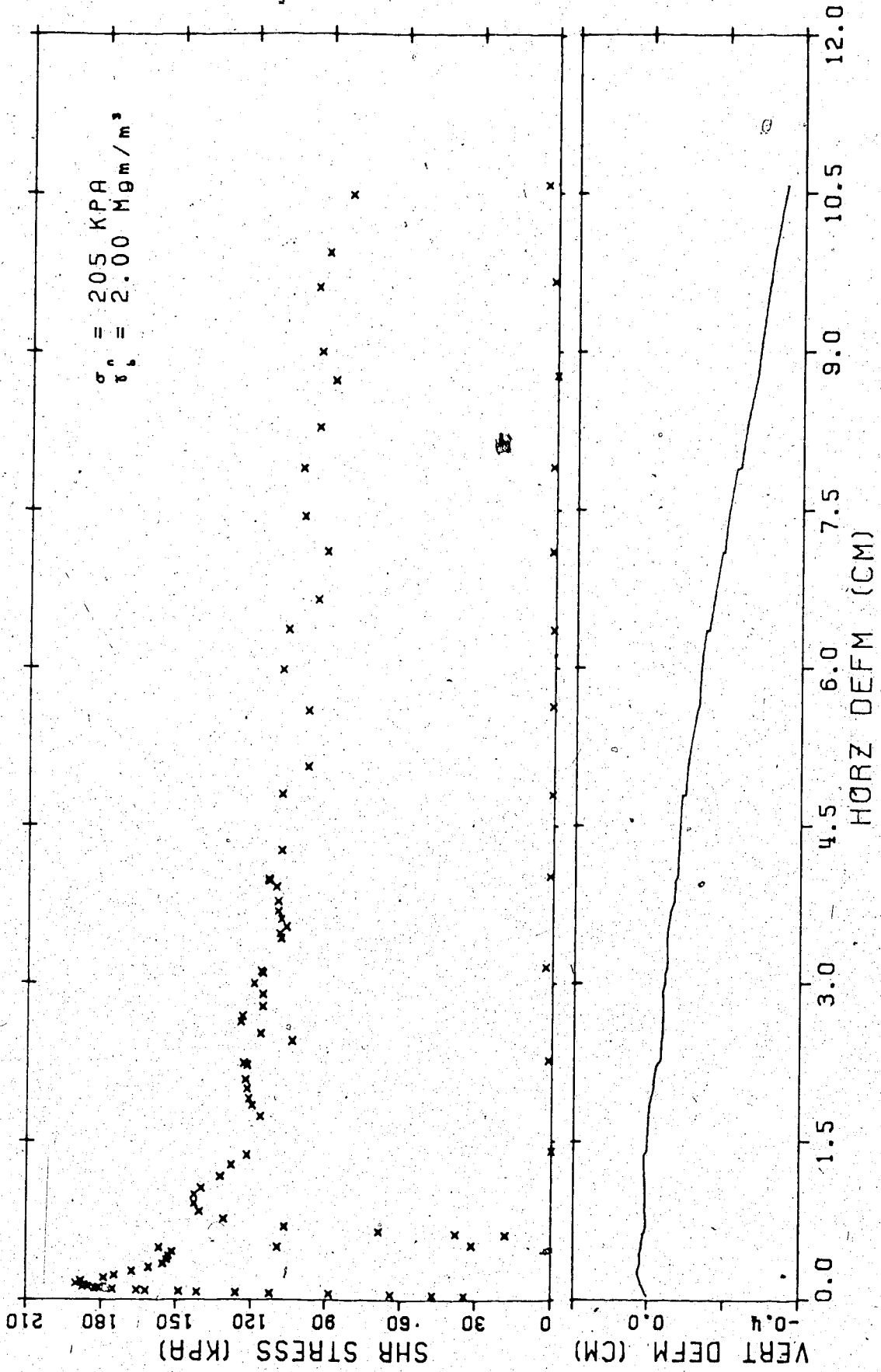


Figure D.14 Direct Shear Test 14

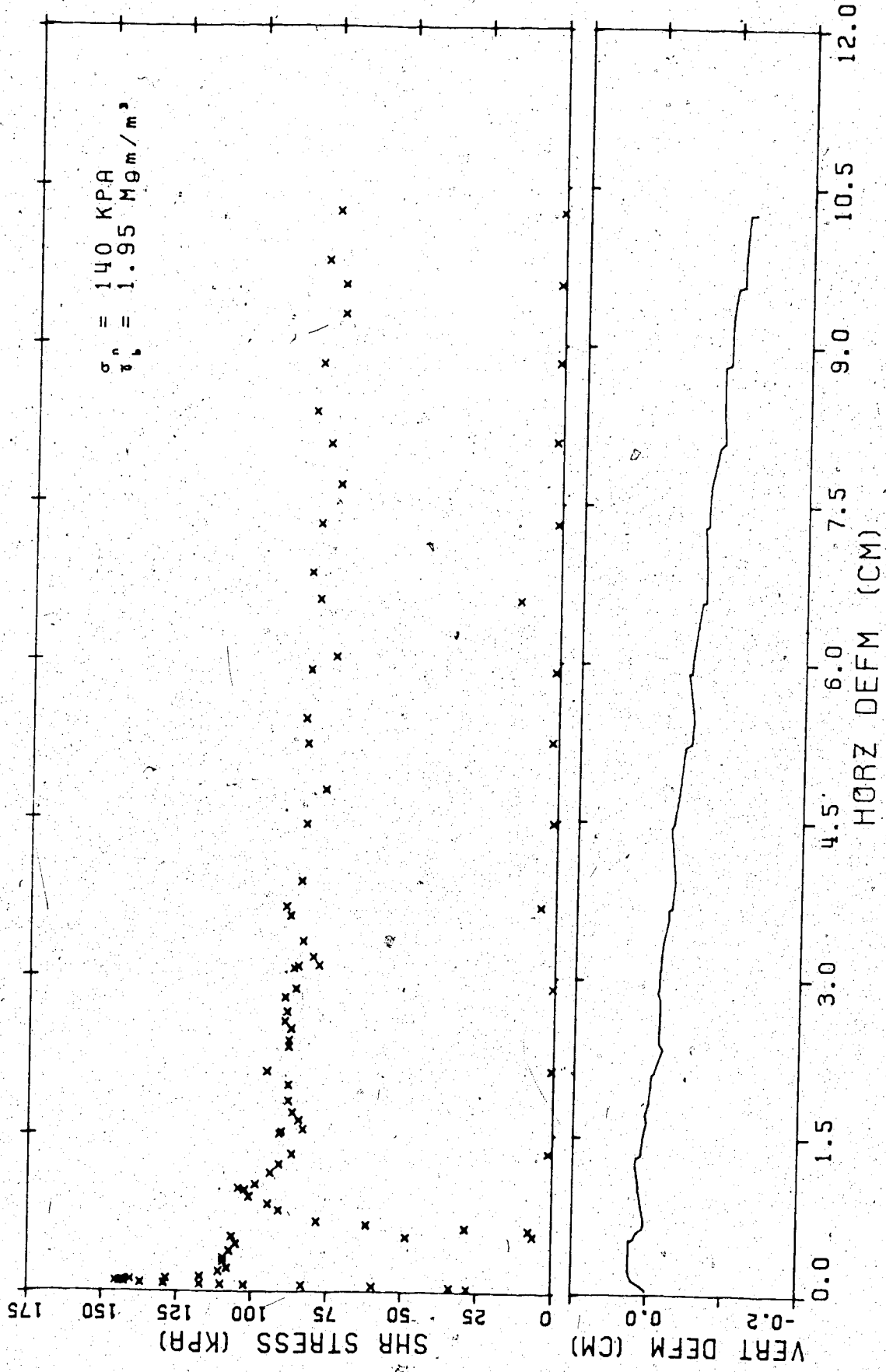


Figure D.15 Direct Shear Test 15

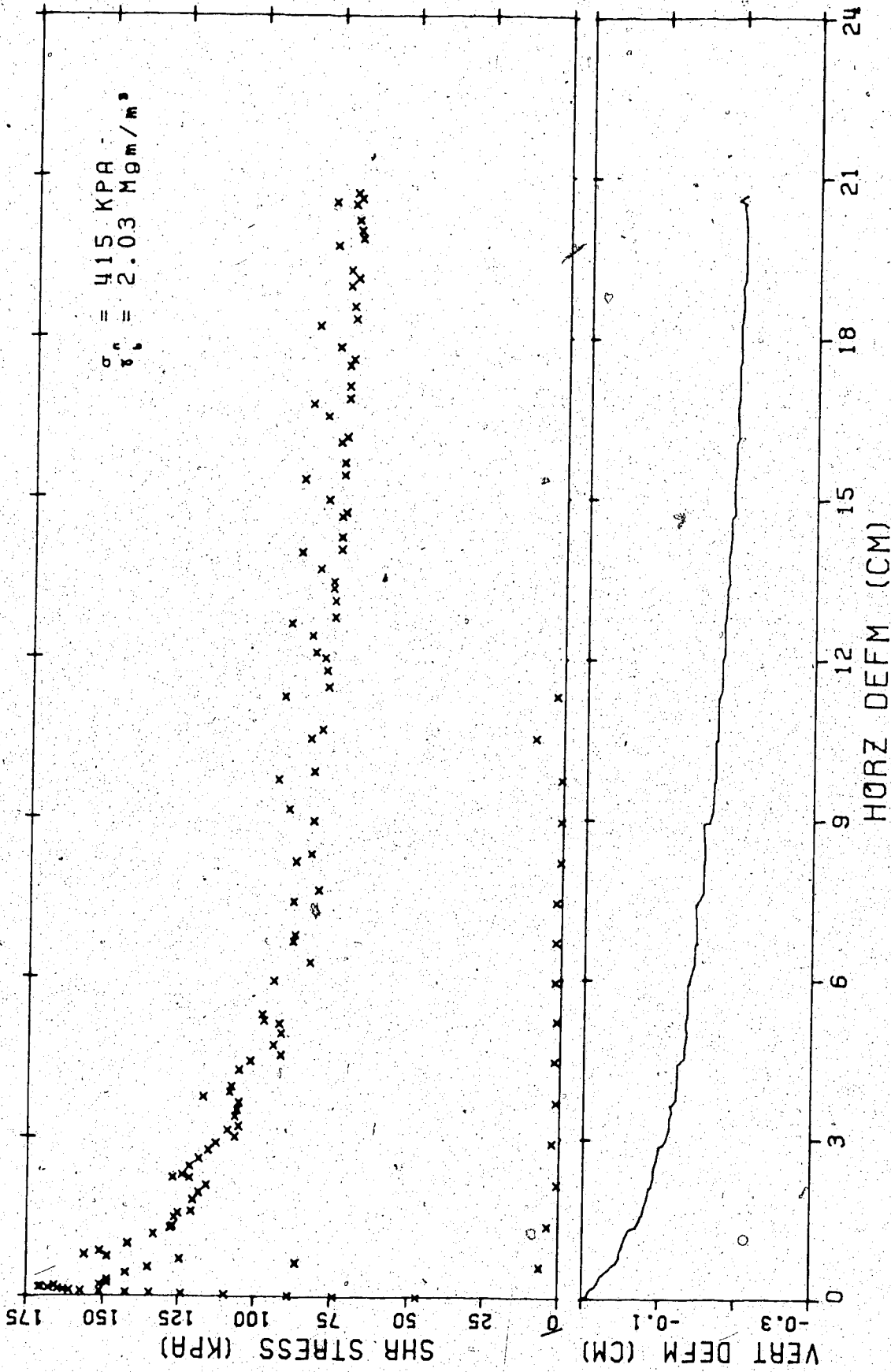


Figure D.16 Direct Shear Test 16

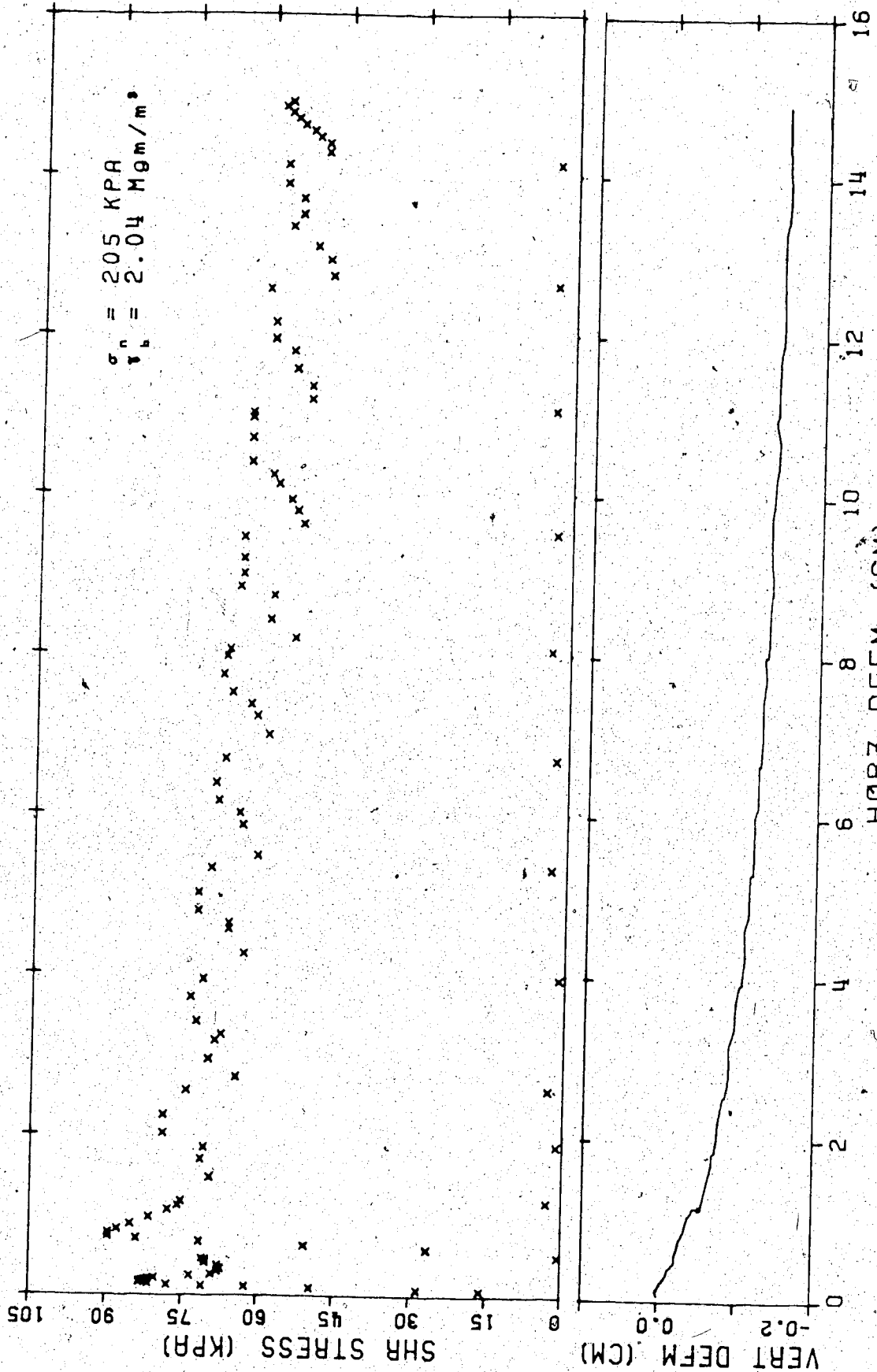


Figure D.17 Direct Shear Test 17

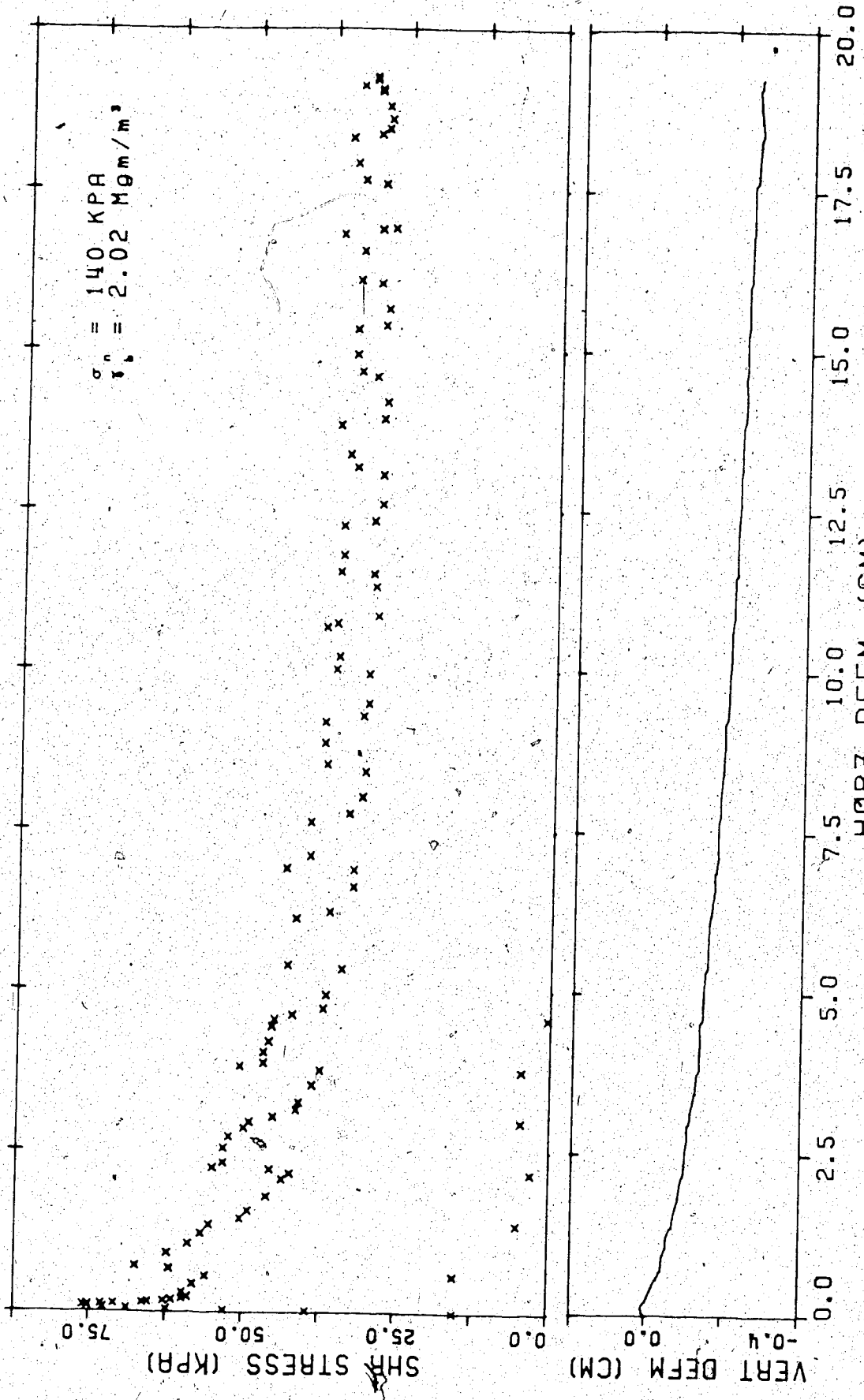


Figure D.18 Direct Shear Test 18



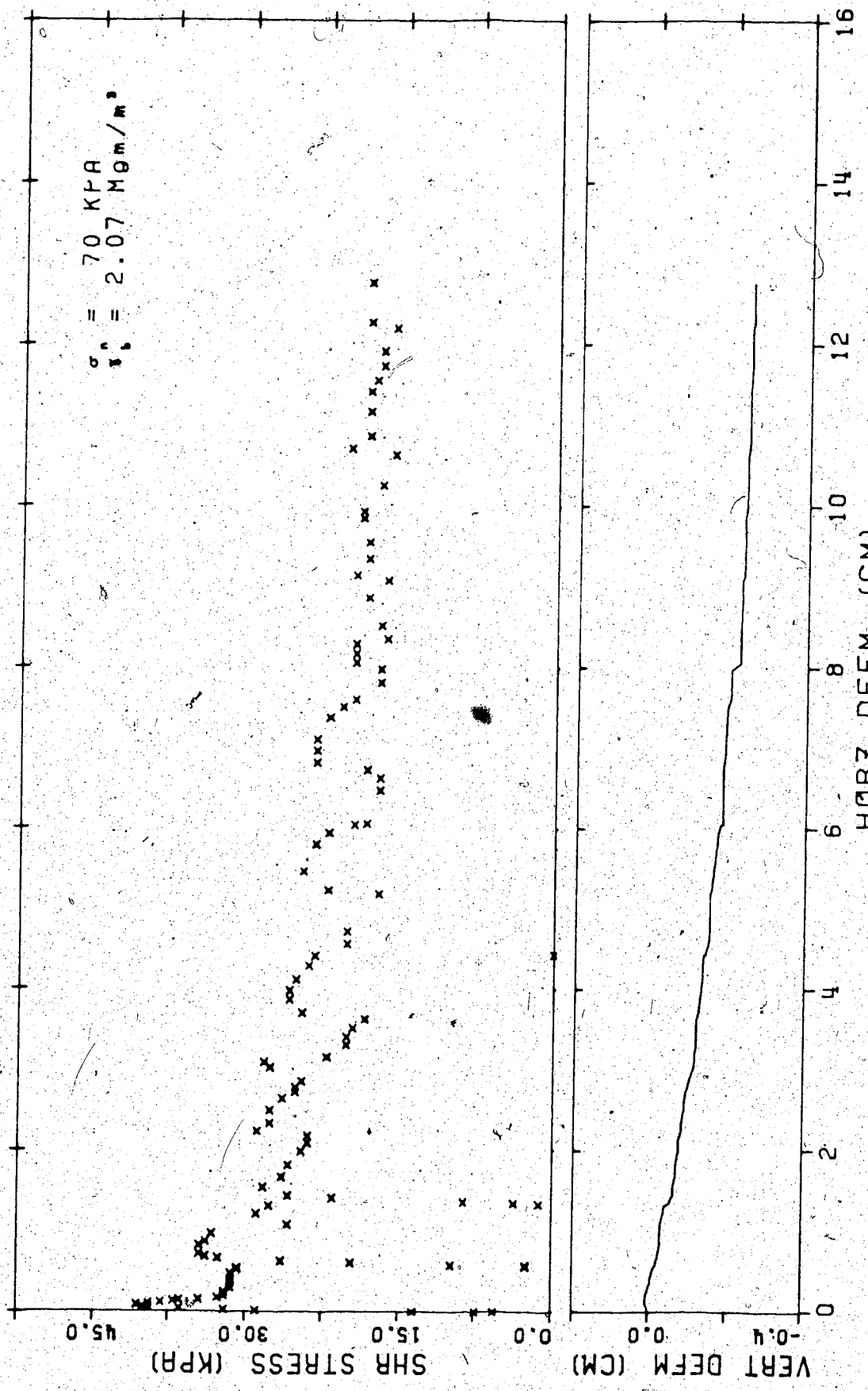


Figure D.19 Direct Shear Test 19

D.2 Triaxial Compression Tests



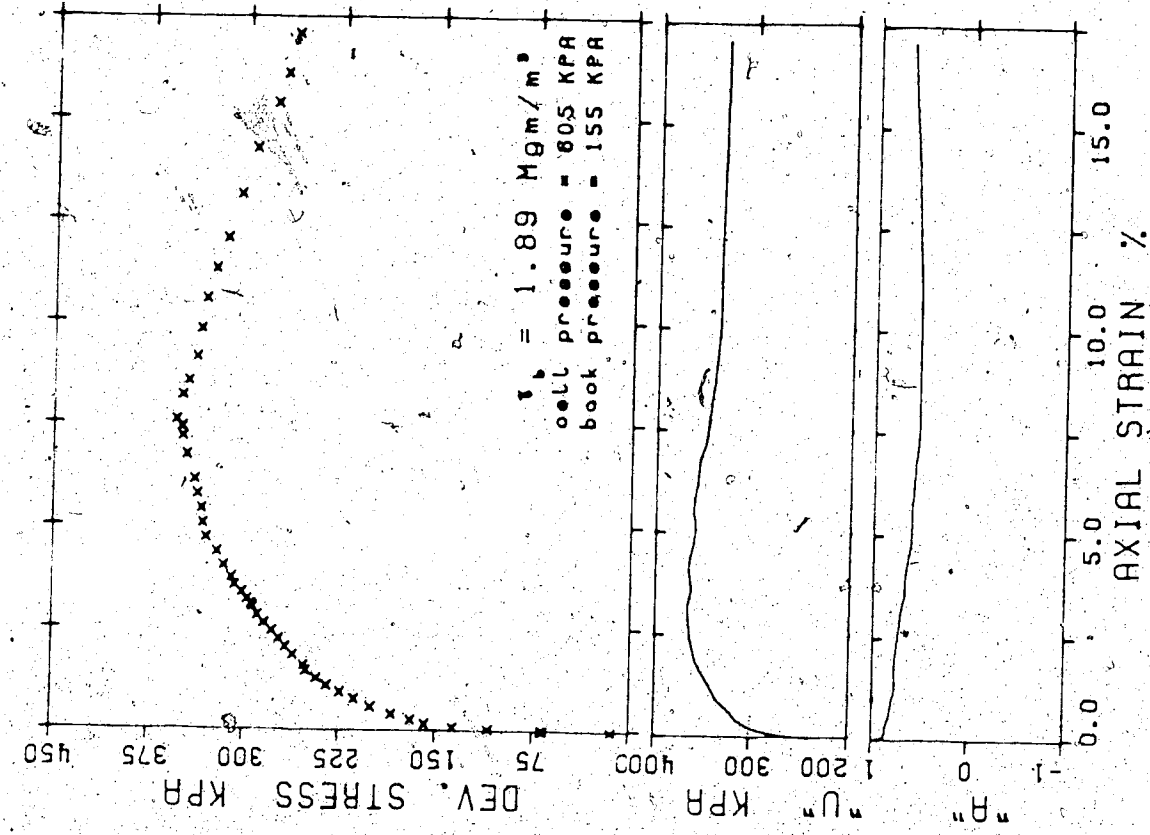


Figure D.20 Triaxial Compression Test 1

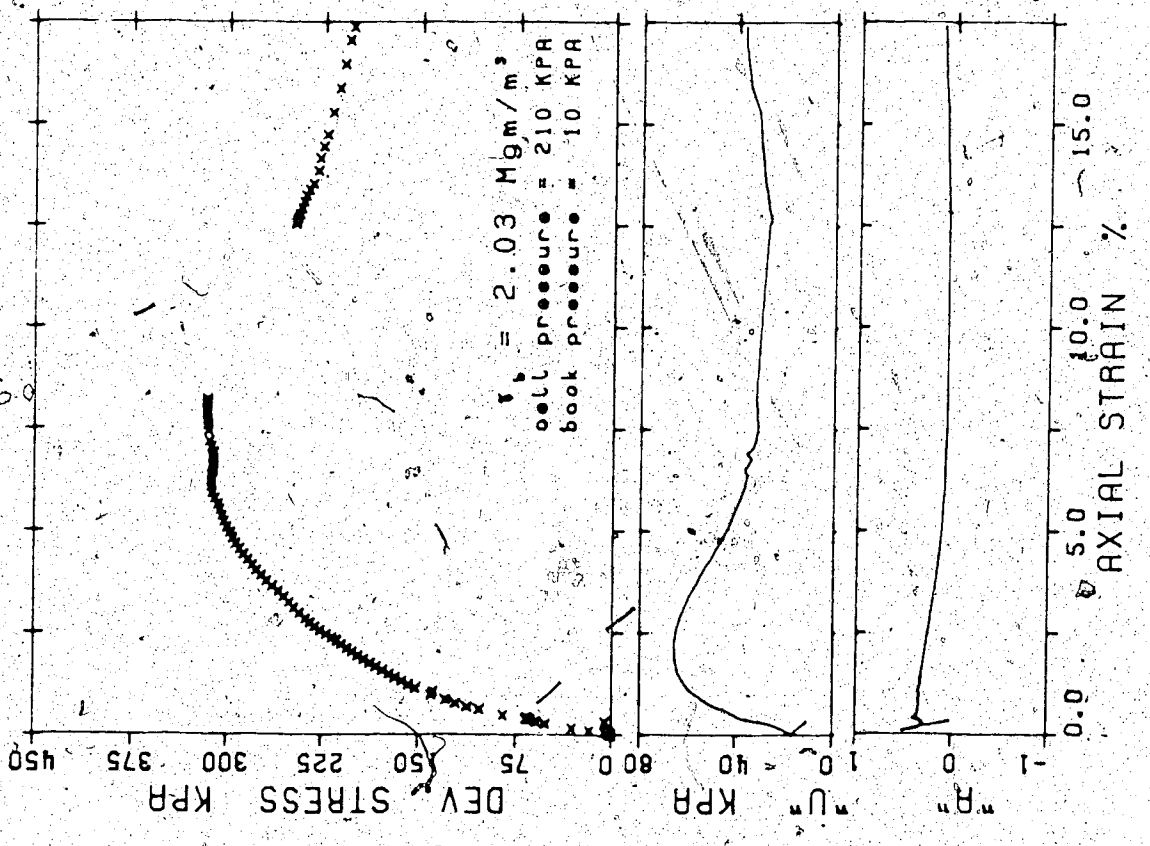


Figure D.21 Triaxial Compression Test 2

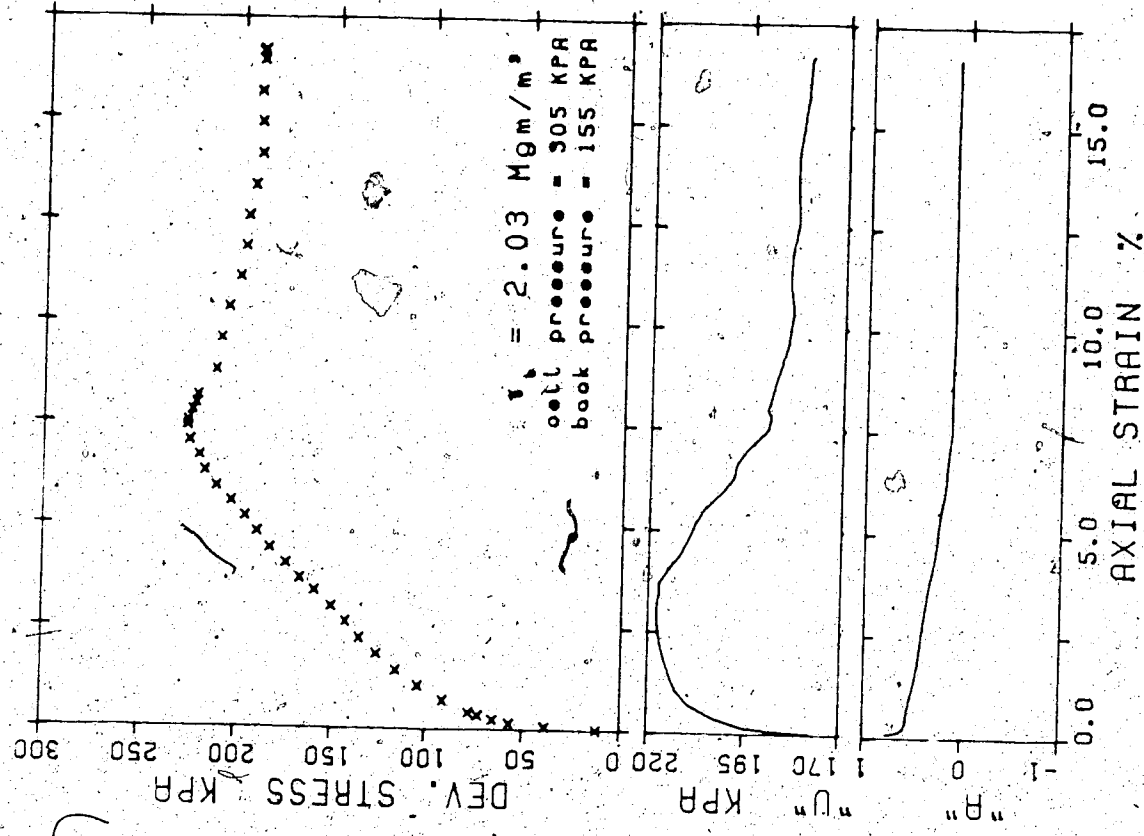


Figure D.22 Triaxial Compression Test 3

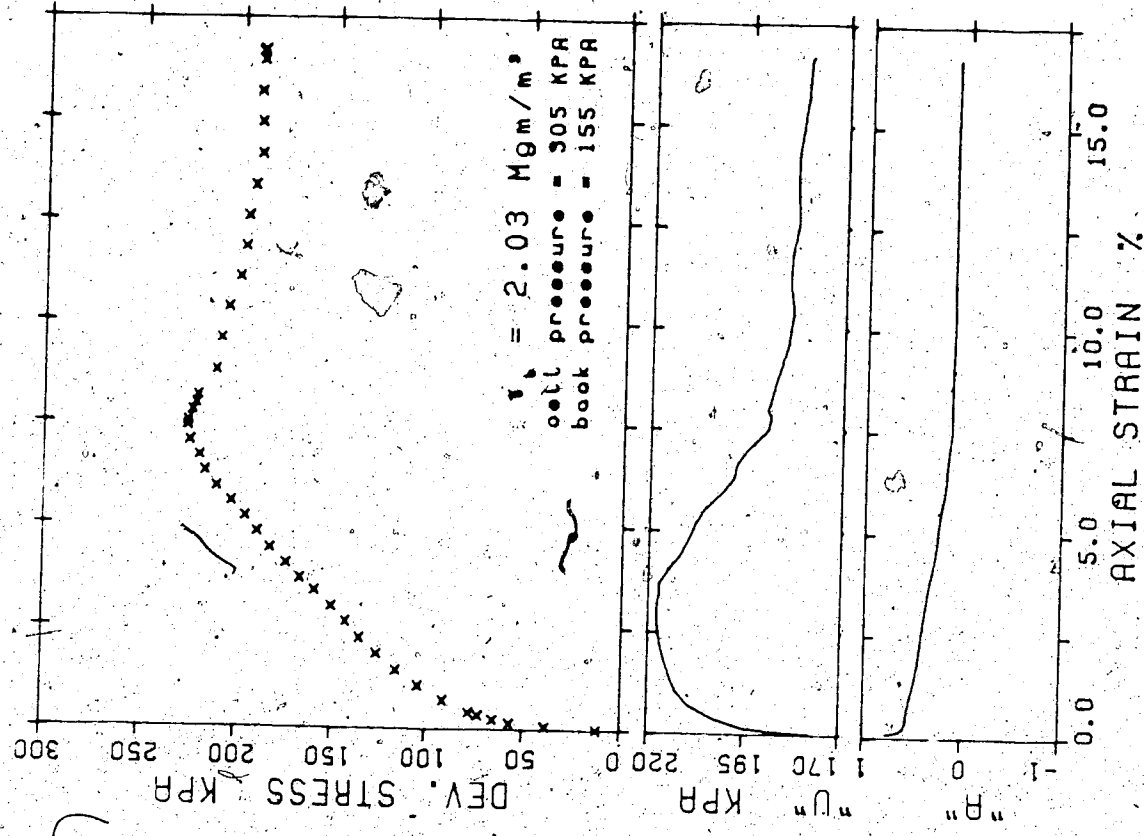


Figure D.23 Triaxial Compression Test 4

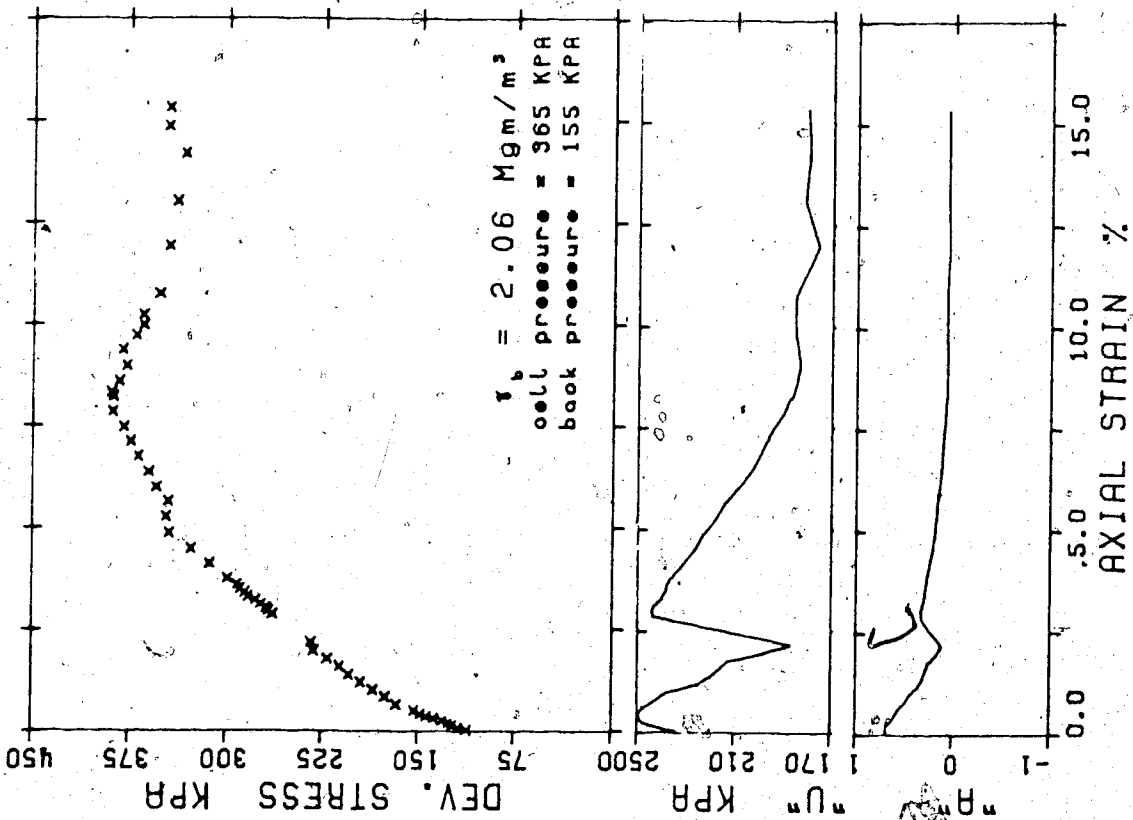


Figure D.24 Triaxial Compression Test 5

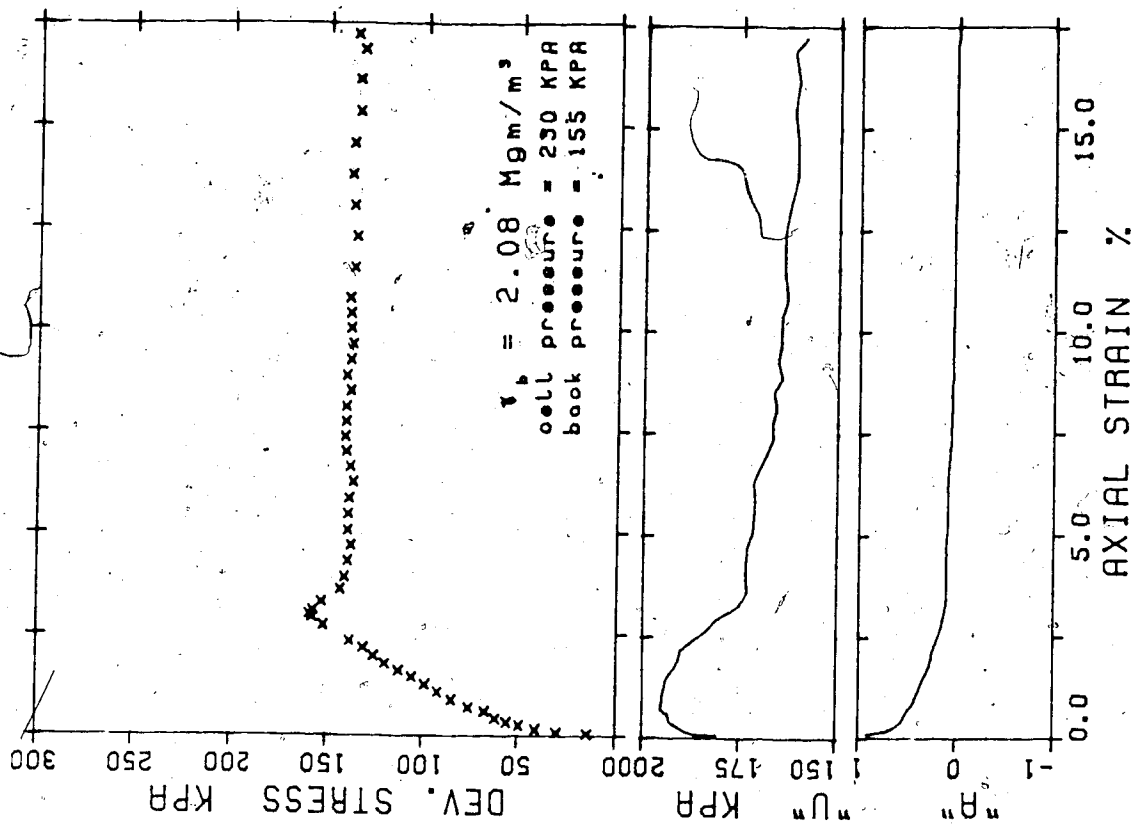


Figure D.25 Triaxial Compression Test 6

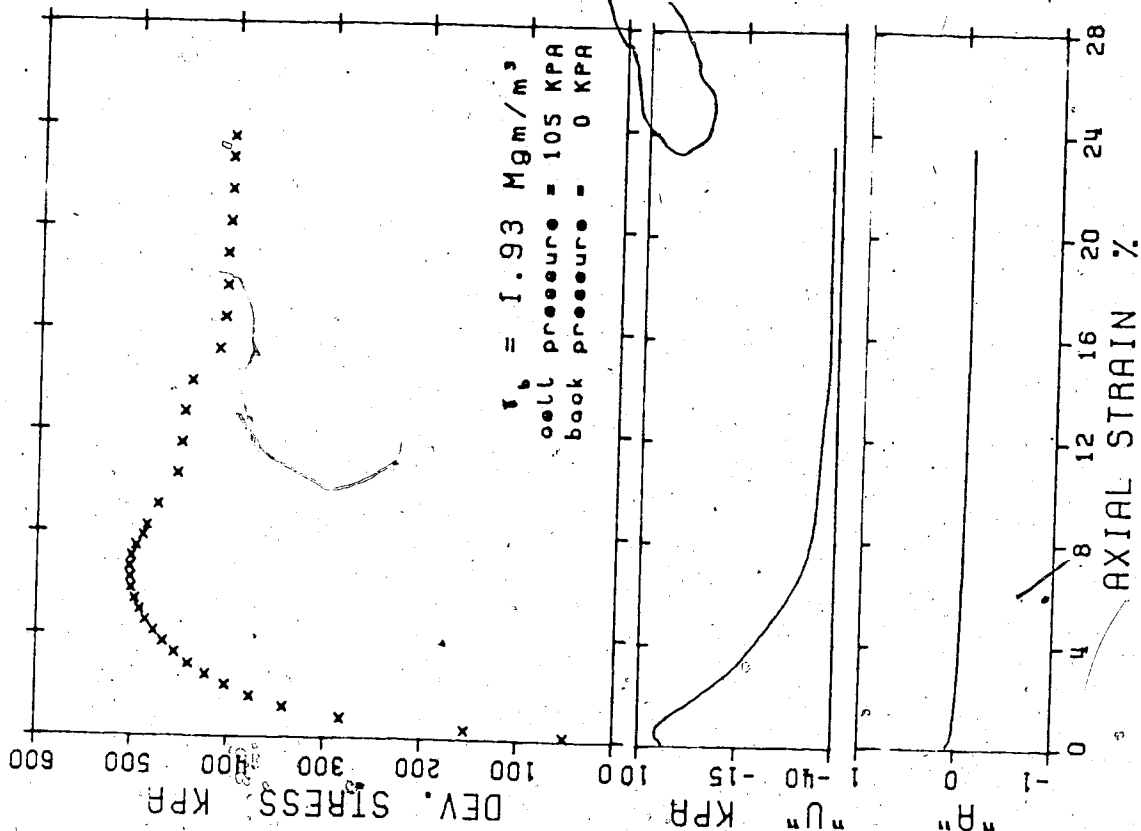


Figure D.27 Triaxial Compression Test 9

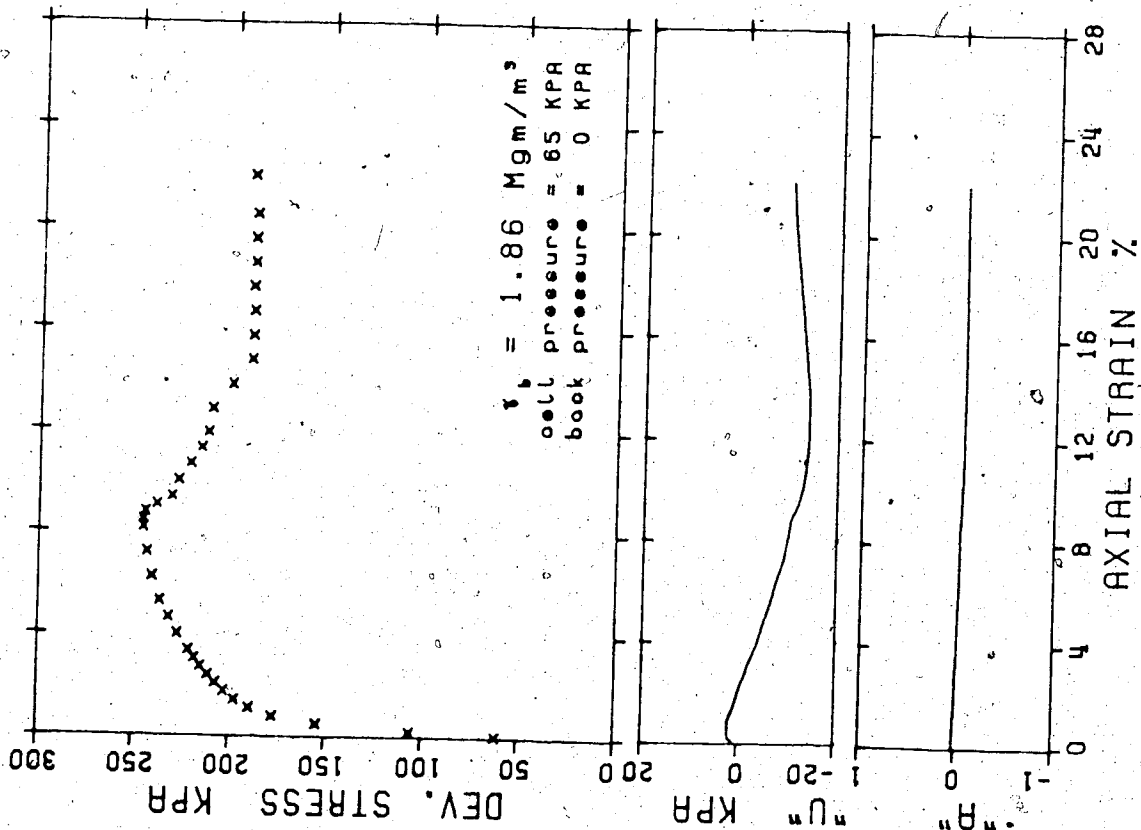


Figure D.26 Triaxial Compression Test 8

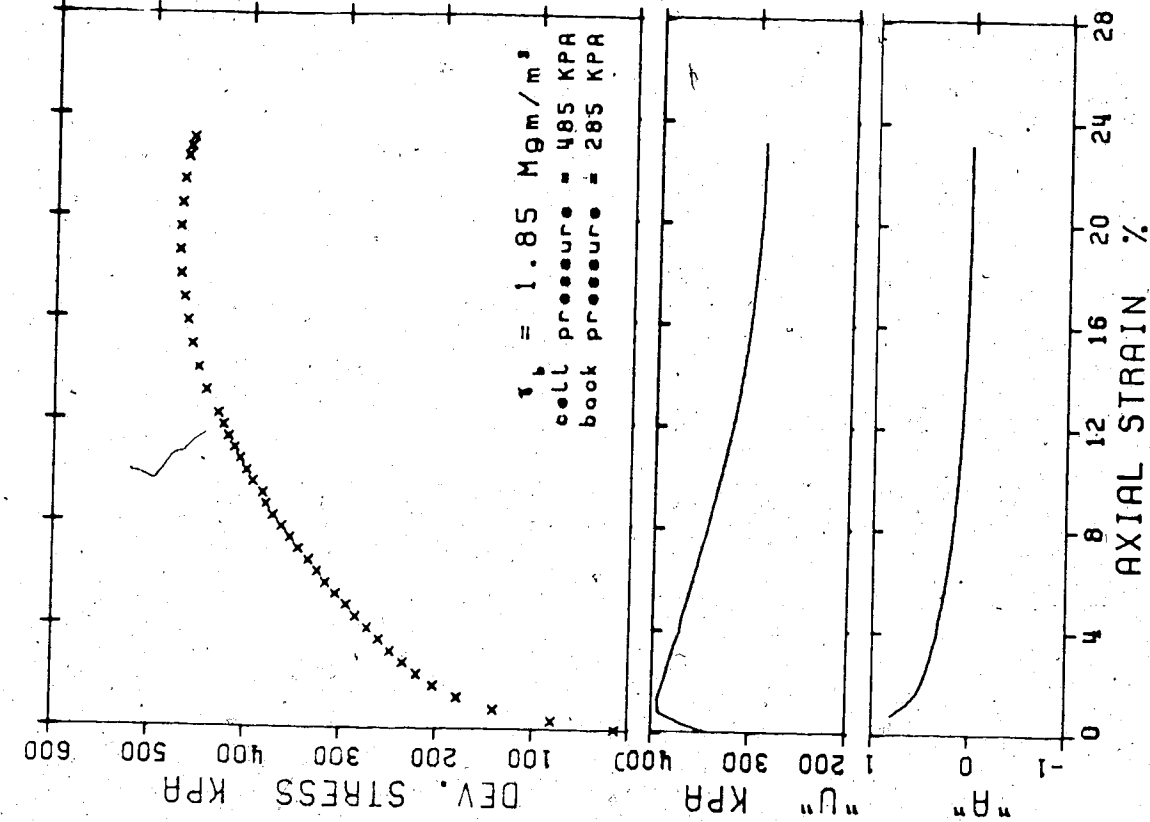


Figure D.29 Triaxial Compression Test II

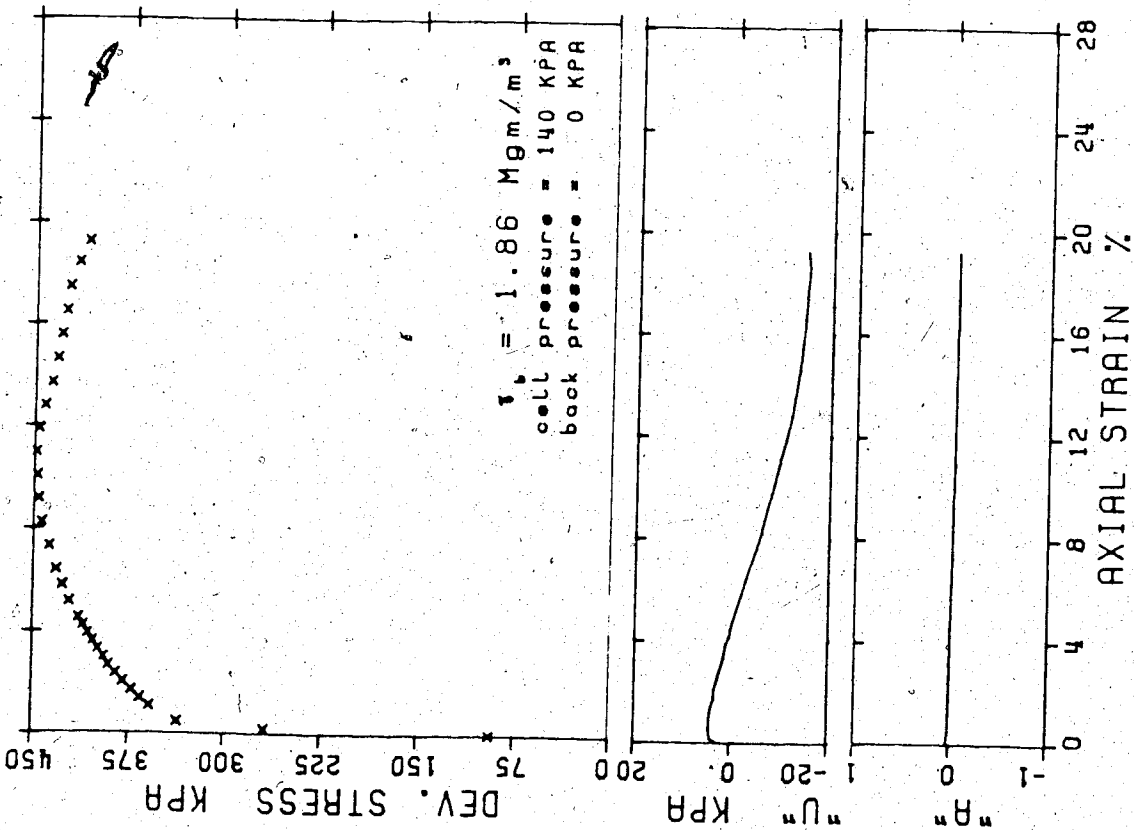


Figure D.28 Triaxial Compression Test 10



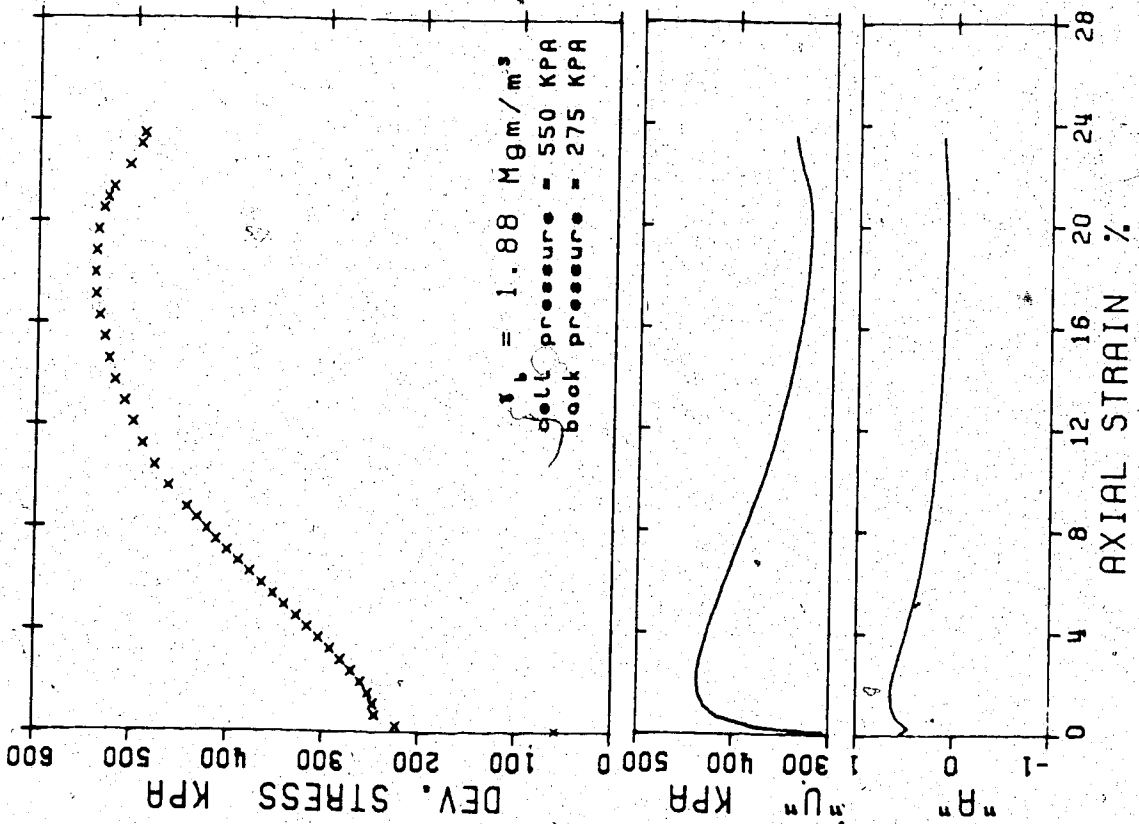


Figure D.30 Triaxial Compression Test 12

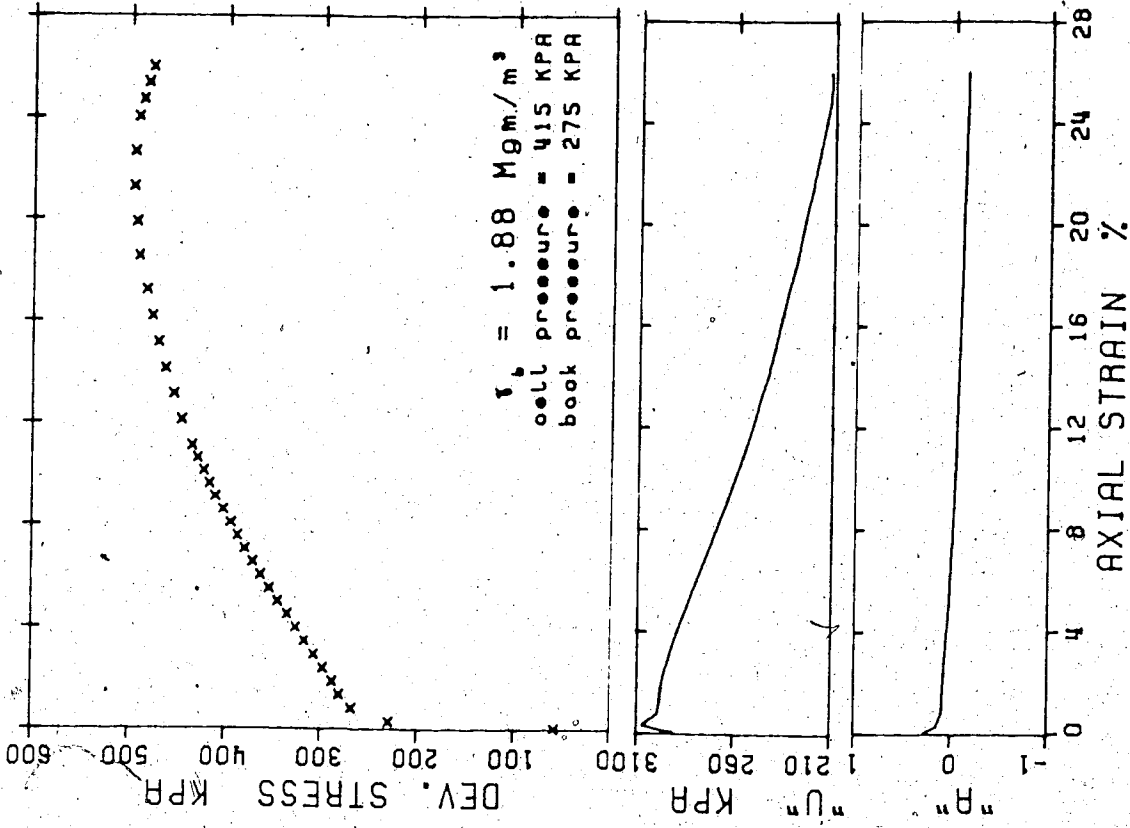


Figure D.31 Triaxial Compression Test 13

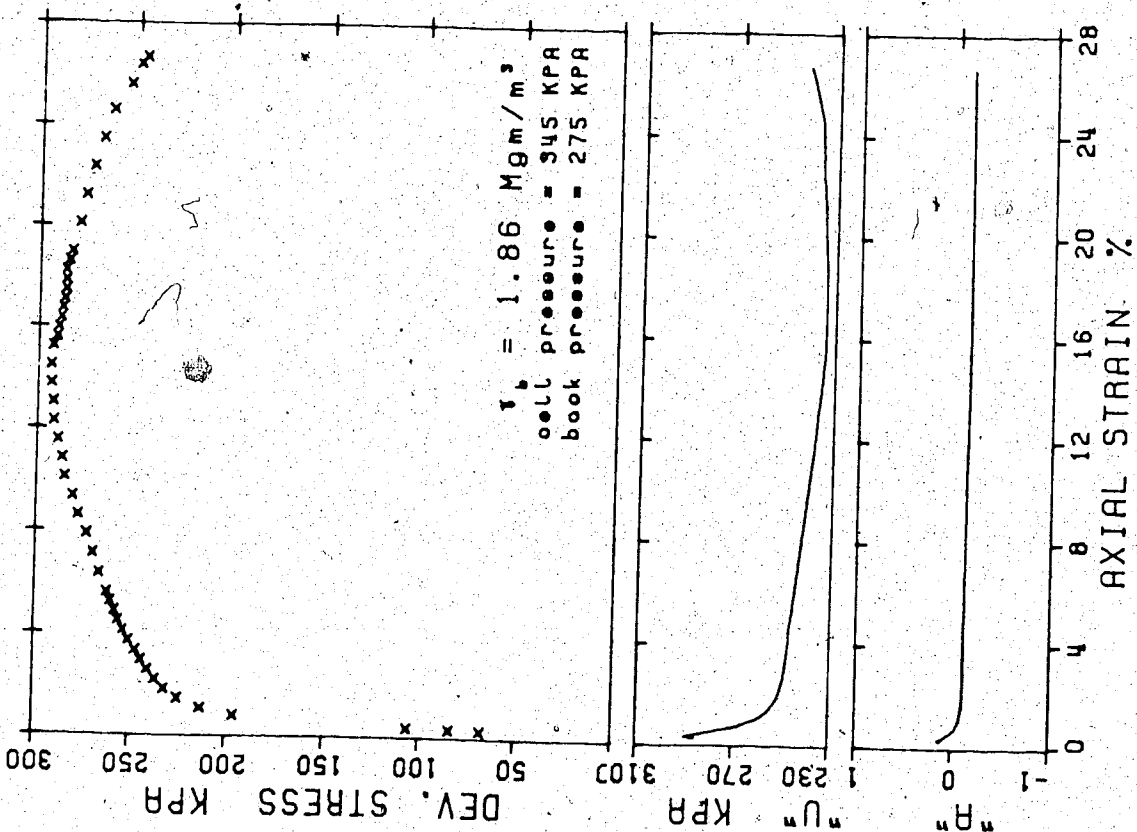


Figure D.32 Triaxial Compression Test 14

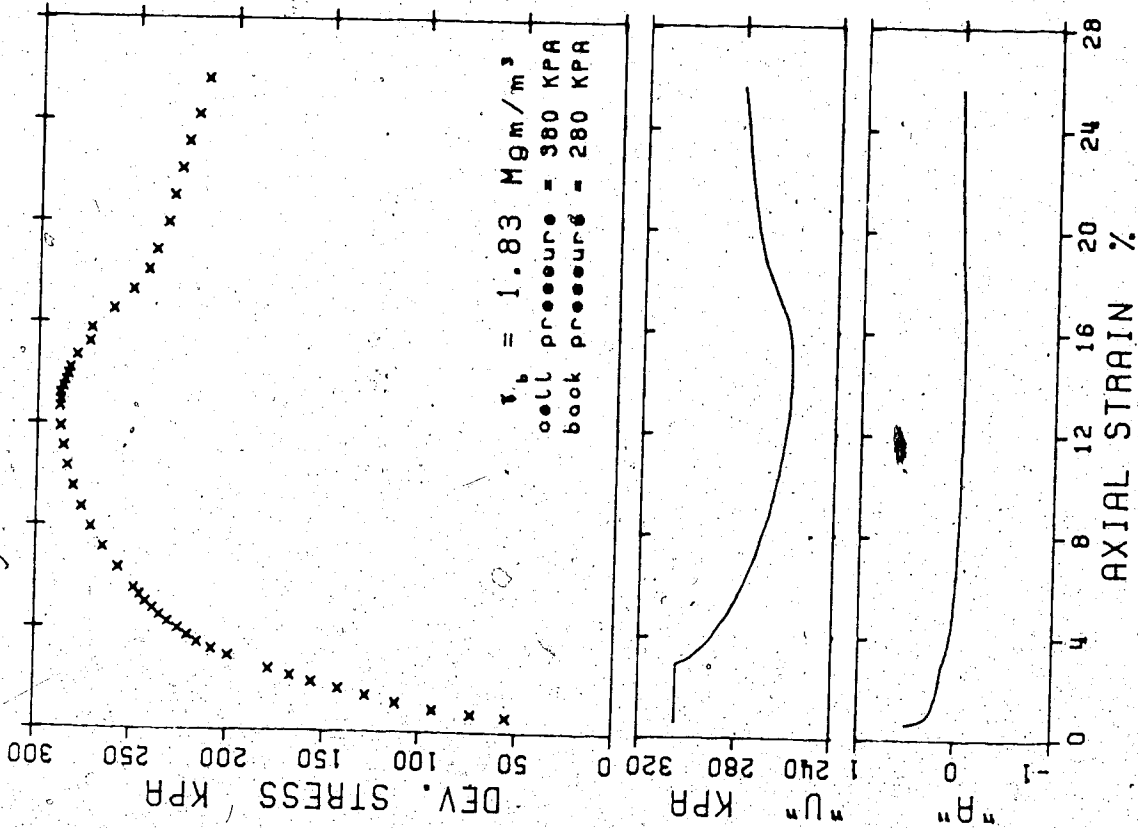


Figure D.33 Triaxial Compression Test 15

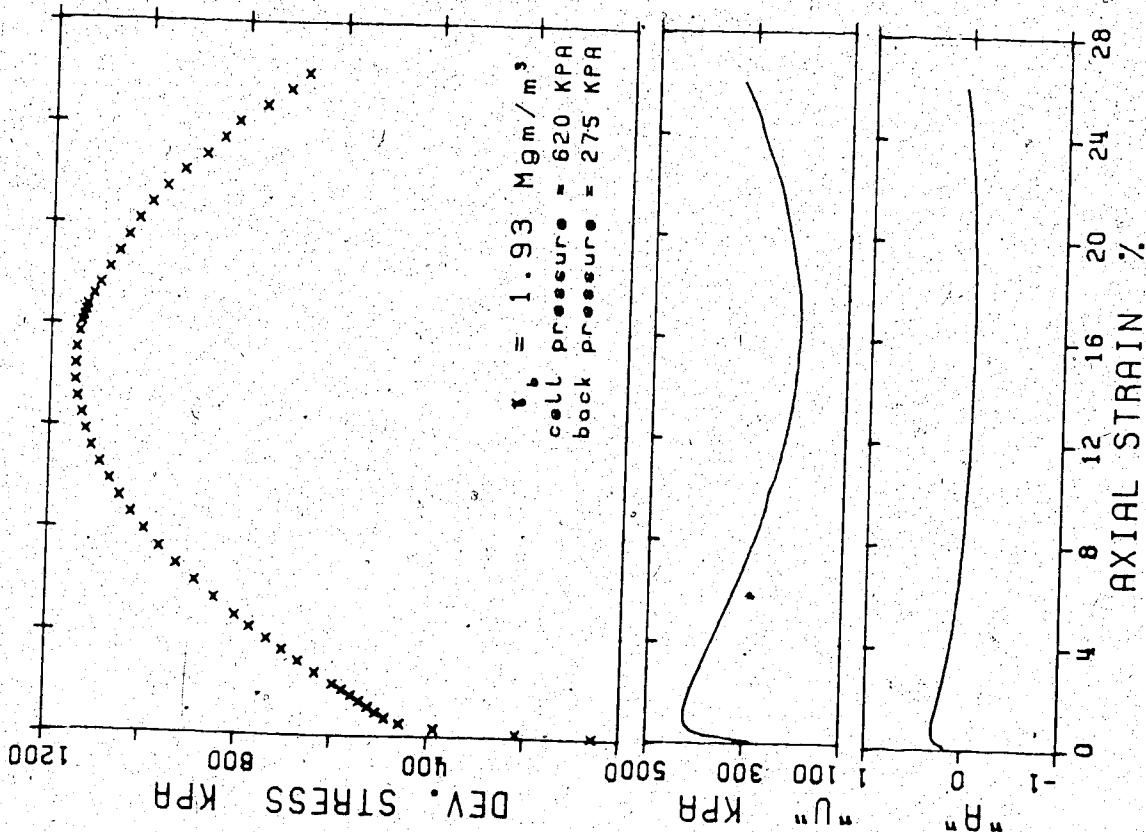


Figure D.34 Triaxial Compression Test 16

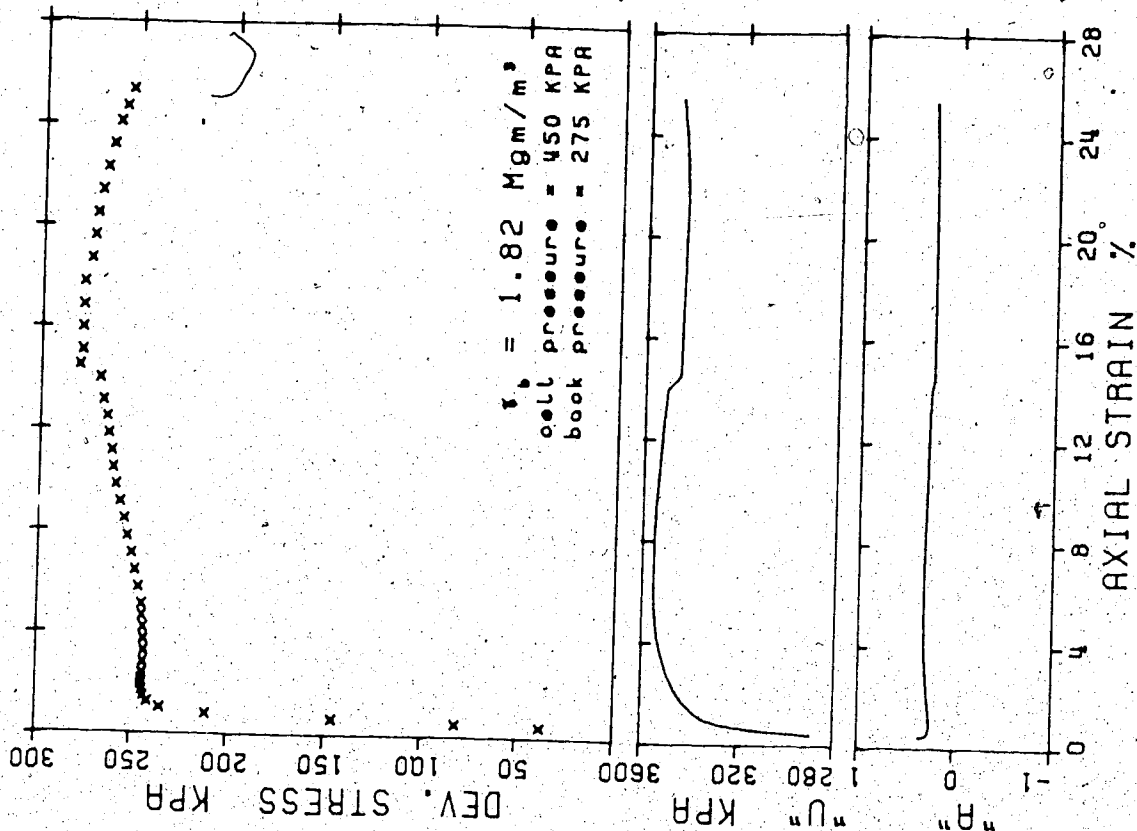


Figure D.35 Triaxial Compression Test 17

24

D.3 Triaxial Creep Tests

8

TABLE D.3  
ENGINEERING PROPERTIES OF CONSTANT STRESS TRIAXIAL CREEP TEST SAMPLES

TEST* NO.	SAMPLE NUMBER	AVERAGE DEPTH (m)	LENGTH (cm)	FROZEN BULK DENSITY (MG/m <sup>3</sup> )	SAND (%)	SILT (%)	CLAY (%)	LIQUID LIMIT (%)	PLASTIC LIMIT (%)
1	FN-1-53-5	31.1	25.4	1.78	0	58.6	41.4	46	21
2	FN-1-53-6	31.6	24.8	1.87	1.8	57.5	40.7	48	24
3	FN-1-57-3	33.8	28.7	1.93	0	46.8	53.2	46	23
4	FN-1-56-5	33.0	28.5	1.97	0	53.9	46.1	43	17
5	FN-1-58-5	34.7	28.6	1.89	0	47.2	52.8	51	22
6	FN-1-38-3	22.1	26.6	2.01	0	47.6	52.4	47	18
7	FN-1-32-7	24.9	29.0	2.06	2.0	44.6	53.4	49	23
8	FN-1-46-3	27.0	28.7	2.06	1.8	54.2	44.0	47	22
9	FN-1-43-2	25.7	28.7	2.05	3.4	59.0	37.6	47	20
10	FN-1-53-8	31.5	28.6	2.04	1.1	58.6	40.3	48	21
11	FN-2-3-3	1.4	28.6	1.52	2.7	41.1	56.1	54	22
12	FN-1-60-6	36.0	28.1	2.02	0	49.7	50.3	50	20
NES 3-11	GB3 C11	5.2	16.8	1.93	?	?	?	?	?
NES 3-8	GB3 C8	3.3	18.3	1.45	0	57.6	42.4	55	25
NES 3-10	GB3 C10	4.4	20.5	1.83	0	53.3	46.7	59	24

\*Tests 1 and 2 were destroyed in an equipment malfunction before being loaded.

TABLE D.4  
SUMMARY OF CONSTANT STRESS TRIAXIAL CREEP TEST DATA  
(PRIMARY STAGE)

TEST* NO.	TEMPERATURE (°C)	$\sigma_3$ (kpa)	$\sigma_1 - \sigma_3$ (kpa)	Y INTERCEPT $t = 10^6$ hours	$\alpha$ (-tan $\theta$ )	CORRELATION COEFFICIENT
1	-1.20	400	196	1.798	-0.71	0.913
2	-1.05	400	35	0.879	-0.52	0.988
3	-1.15	400	85	0.766	-0.90	0.995
4	-1.45	400	56	0.441	-0.82	0.978
7A	-1.30	400	35	0.056	-1.02	0.997
7B	-1.35	400	60	unacceptable	unacceptable	N/A
7C	-1.40	400	110	0.016	-0.57	0.998
8A	-1.20	400	35	0.056	-0.94	0.974
8B	-1.25	400	60	unacceptable	unacceptable	N/A
8C	-1.25	400	140	0.011	-0.61	0.993
9	-1.15	400	35	0.098	-0.92	0.999
10A	-1.05	400	35	0.311	-1.03	0.994
10B	-1.10	400	60	unacceptable	unacceptable	N/A
11	-1.15	400	35	0.874	-0.35	0.986
12A	-1.10	400	35	0.549	-1.07	0.967
12B	-1.10	400	75	0.023	-0.61	0.994
NES 3-11	-1.1	0	207	0.002	-1.03	0.982
NES 3-8	-1.0	0	138	0.004	-0.65	0.988
NES 3-10	-1.0	0	69	0.002	-0.67	0.991

\*Tests 1 and 2 were destroyed in an equipment malfunction before being loaded.

TABLE D.5  
SUMMARY OF CONSTANT STRESS TRIAXIAL CREEP TEST DATA  
(APPARENT SECONDARY STAGE)

TEST* NO.	TEMPER- ATURE (°C)	$\sigma_3$ (kPa)	$\sigma_1 - \sigma_3$ (kPa)	OBSERVED STRAIN RATE (%/HOUR x 10 <sup>-5</sup> )	STRAIN RATE (Year <sup>-1</sup> x 10 <sup>-4</sup> )	CRITICAL RATING	COMMENTS
1	-1.20	400	196	500000	4380000	Unaccept.	Failed in under 1 hr
2	-1.05	400	35	42000	368000	Unaccept.	Failed in 6 hours
3	-1.15	400	85	1600	14000	Unaccept.	Failed in 230 hrs (10 days)
4	-1.45	400	56	13000	114000	Unaccept.	Failed in 37 hrs (2 days)
5	-1.30	400	35	6.85	60.1	Fair	Load raised after 53 days
6	-1.35	400	60	10.10	88.5	Fair	Load raised after 53 days
7A	-1.40	400	110	69.30	607.0	Poor	Failed in 165 hrs (7 days)
7B	-1.20	400	35	13.86	121.0	Poor	Load raised after 53 days
7C	-1.25	400	60	12.80	112.0	Fair	Load raised after 53 days
8A	-1.25	400	140	15.87	139.0	Good	Test termin. after 167 days
8B	-1.15	400	35	65.38	573.0	Poor	Failed in 384 hrs (32 days)
8C	-1.05	400	35	14.28	125.0	Poor	Load raised after 45 days
9	-1.10	400	60	155.90	1370.0	Poor	Failed in 1217 hrs (51 days)
10A	-1.15	400	35	19000	16000	Unaccept.	Failed in 39 hrs (2 days)
10B	-1.10	400	35	14.47	127.0	Poor	Load raised after 58 days
11	-1.10	400	75	14.80	130.0	Good	Test term. after 165 days
12A	-1.10	400	75	14.80	130.0	Good	Test term. after 165 days
12B	-1.10	400	75	14.80	130.0	Good	Test term. after 165 days
NES							
3-11	-1.1	0	207	1.05	9.2	Good	Test term. after 96 days
3-8	-1.0	0	138	99.07	868.0	Good	Test term. after 113 days
3-10	-1.0	0	69	47.48	416.0	Poor	Test term. after 116 days

\*Tests 1 and 2 were destroyed in an equipment malfunction before being loaded.

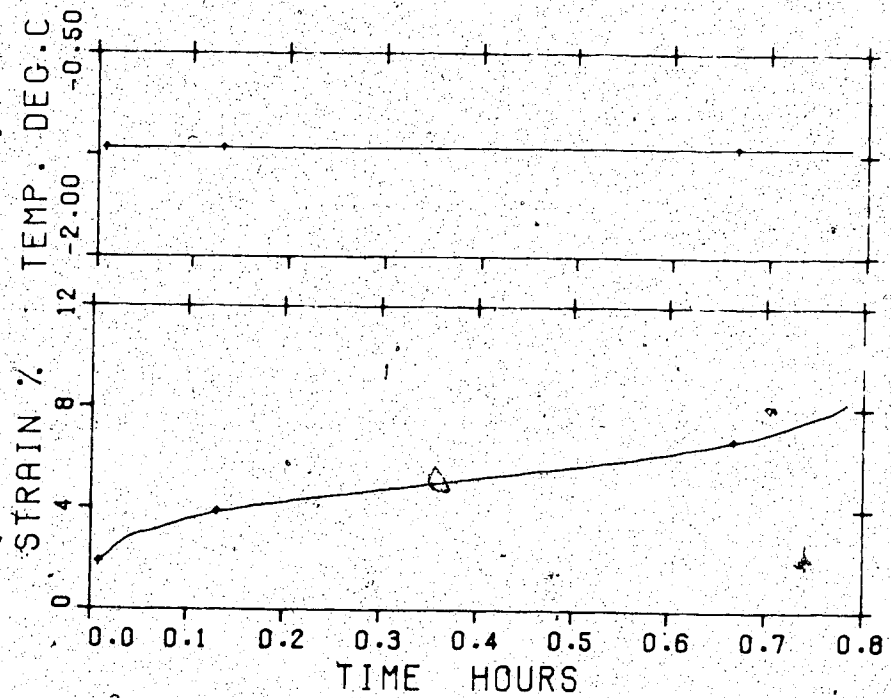
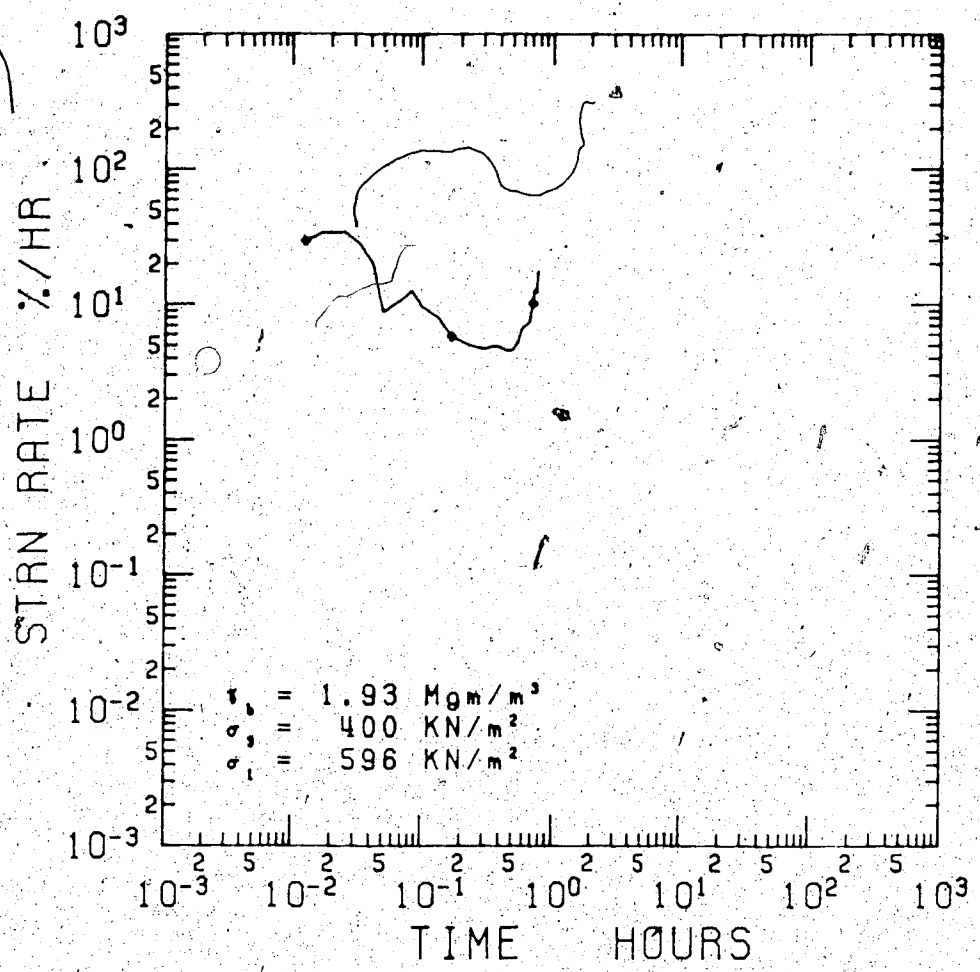


Figure D.36 Triaxial Creep Test 3



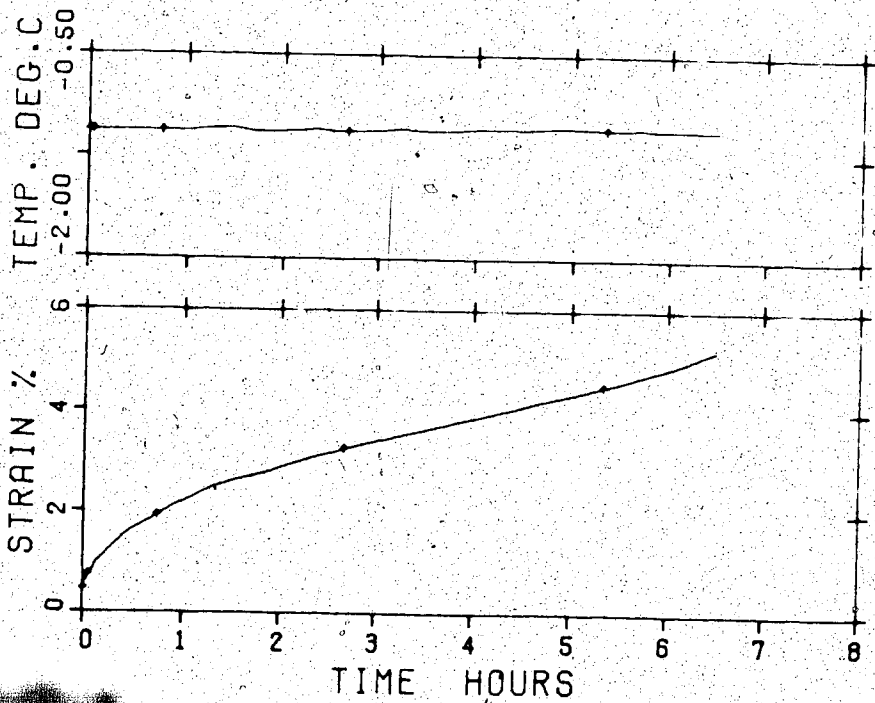
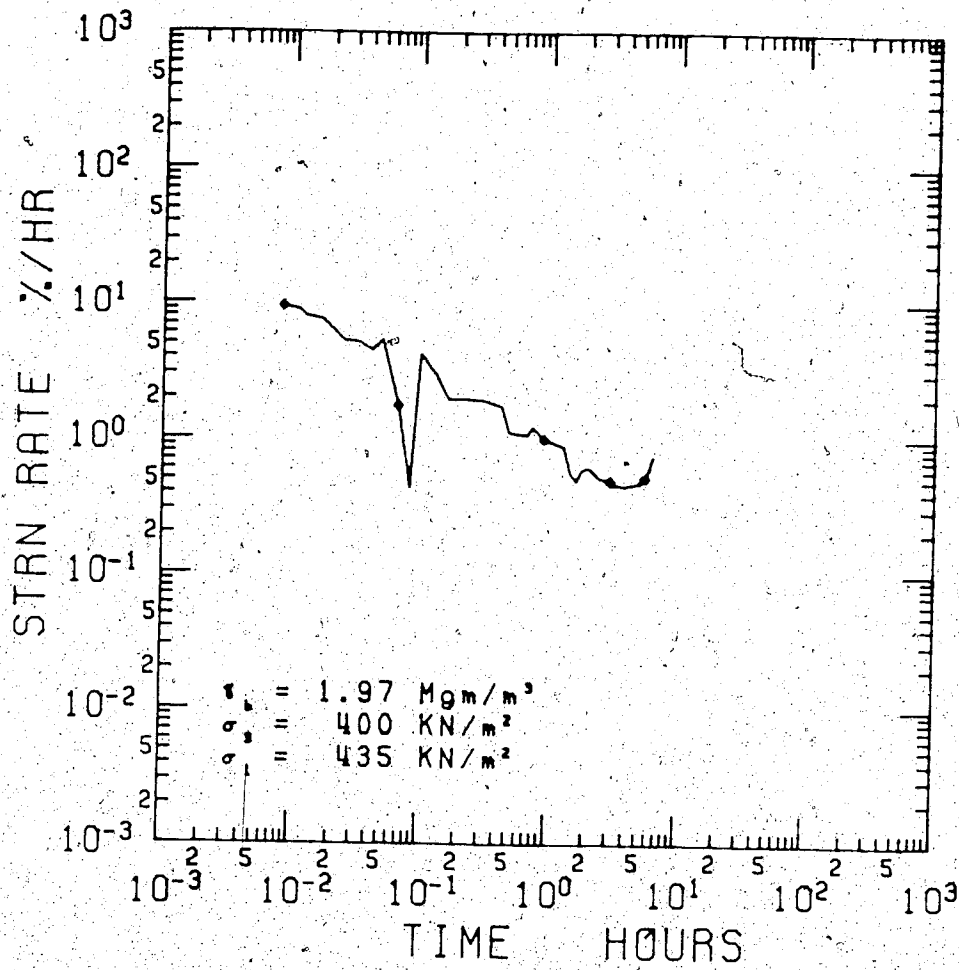


Figure D.37 Triaxial Creep Test 4

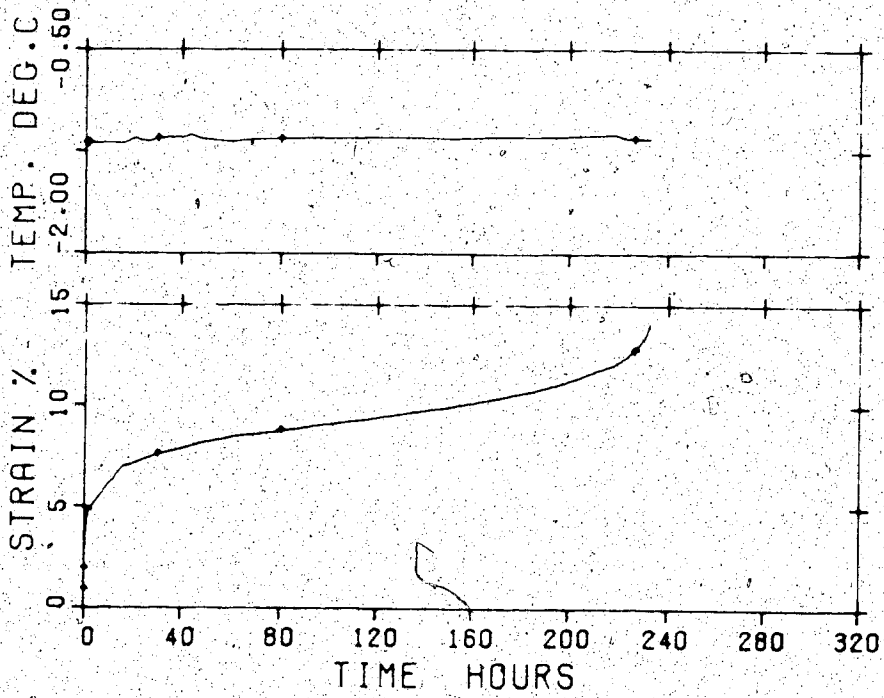
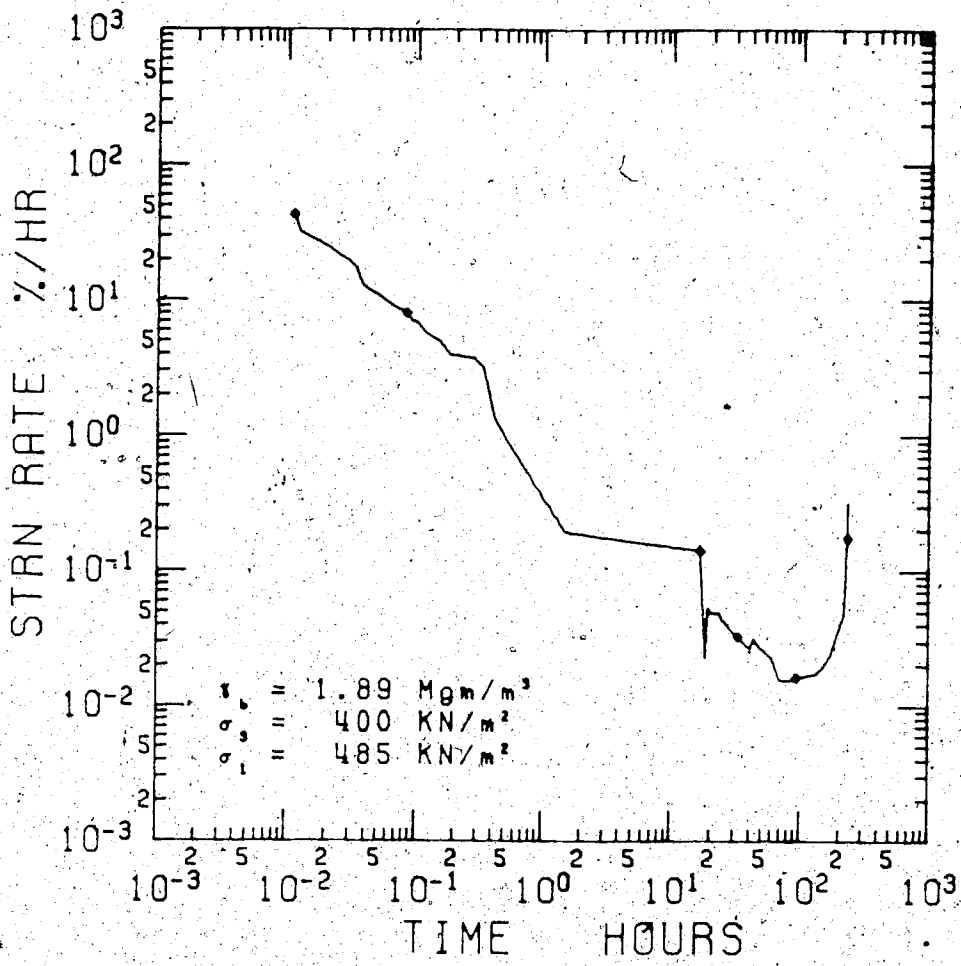


Figure D.38 Triaxial Creep Test 5

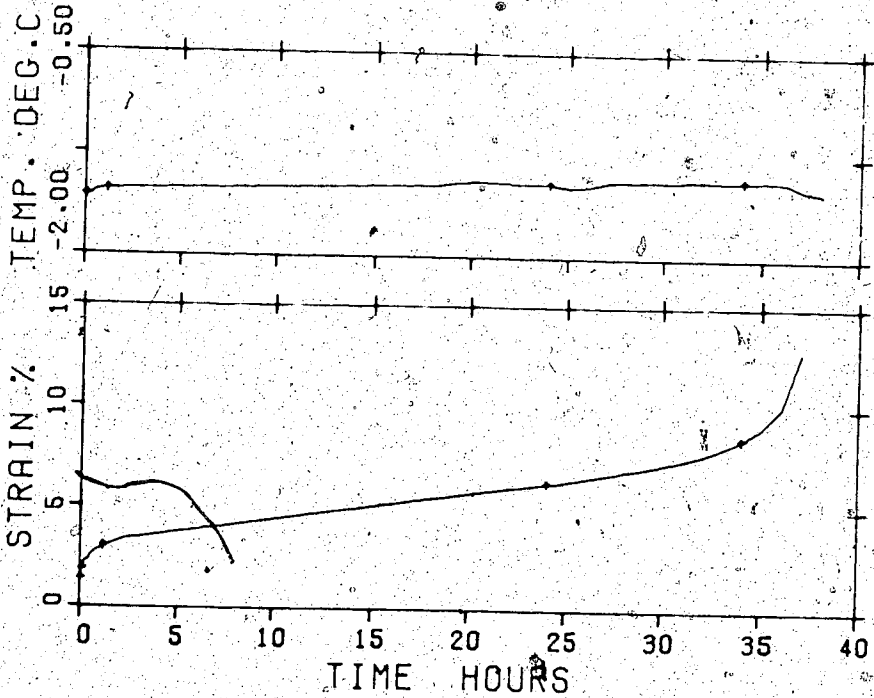
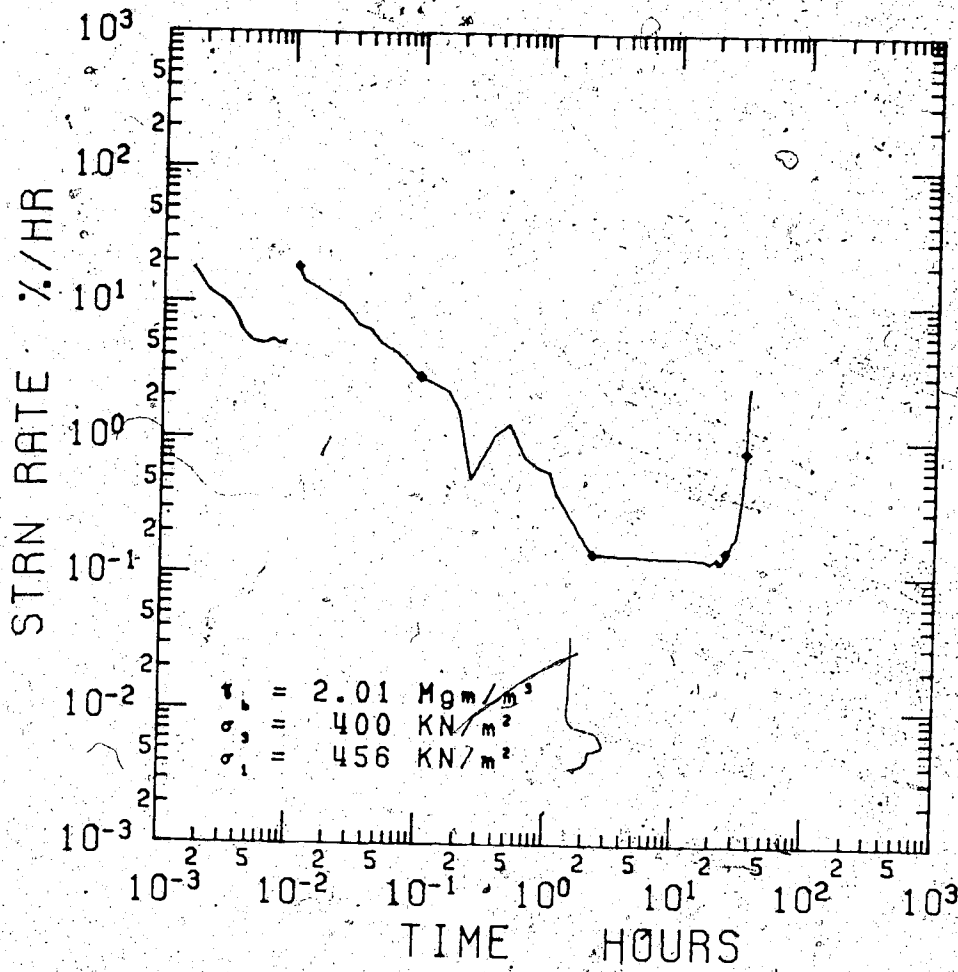


Figure D.39 Triaxial Creep Test 6

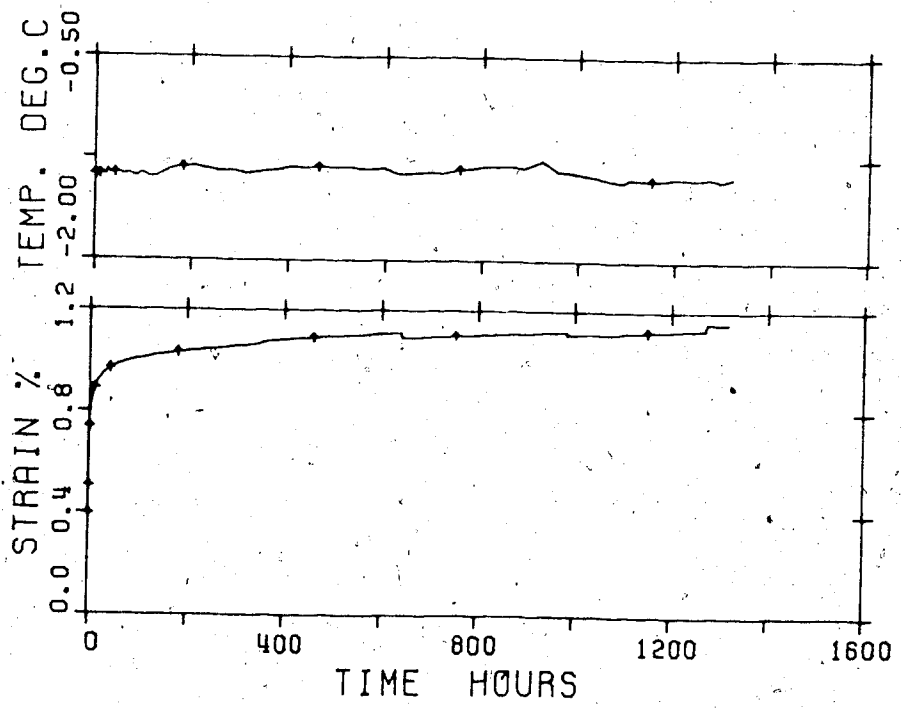
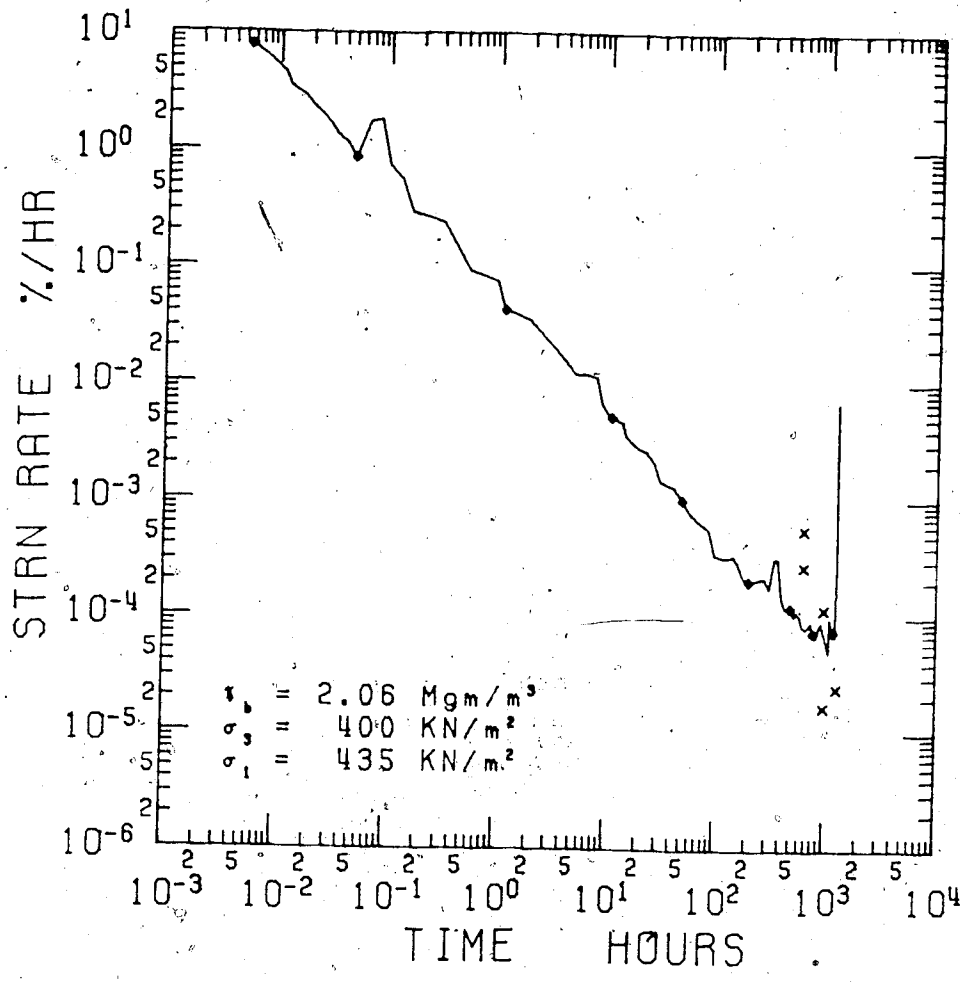


Figure D.40 Triaxial Creep Test 7 (stage one of three)

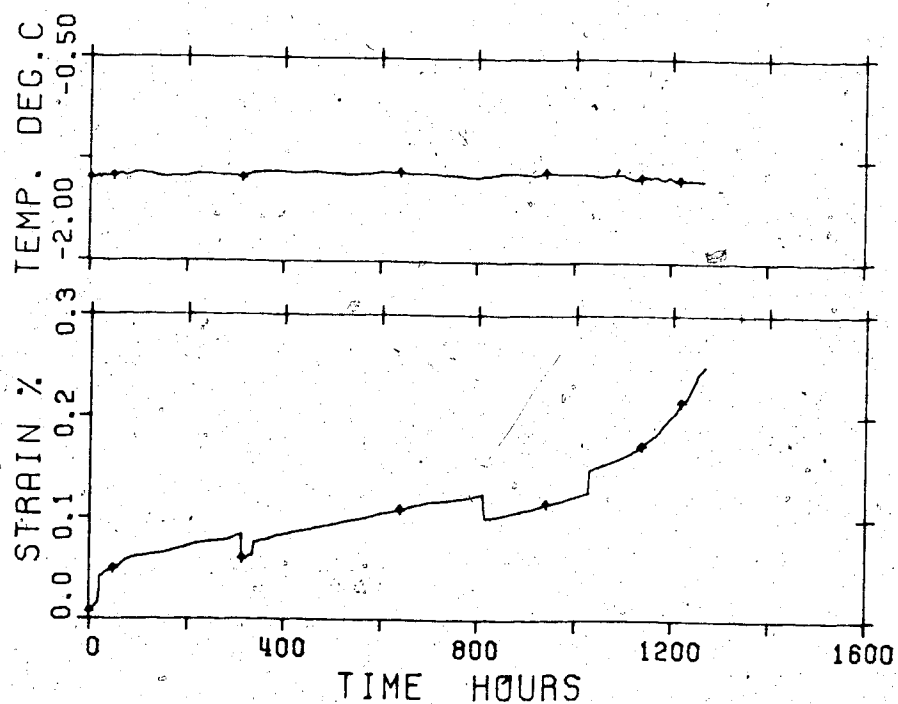
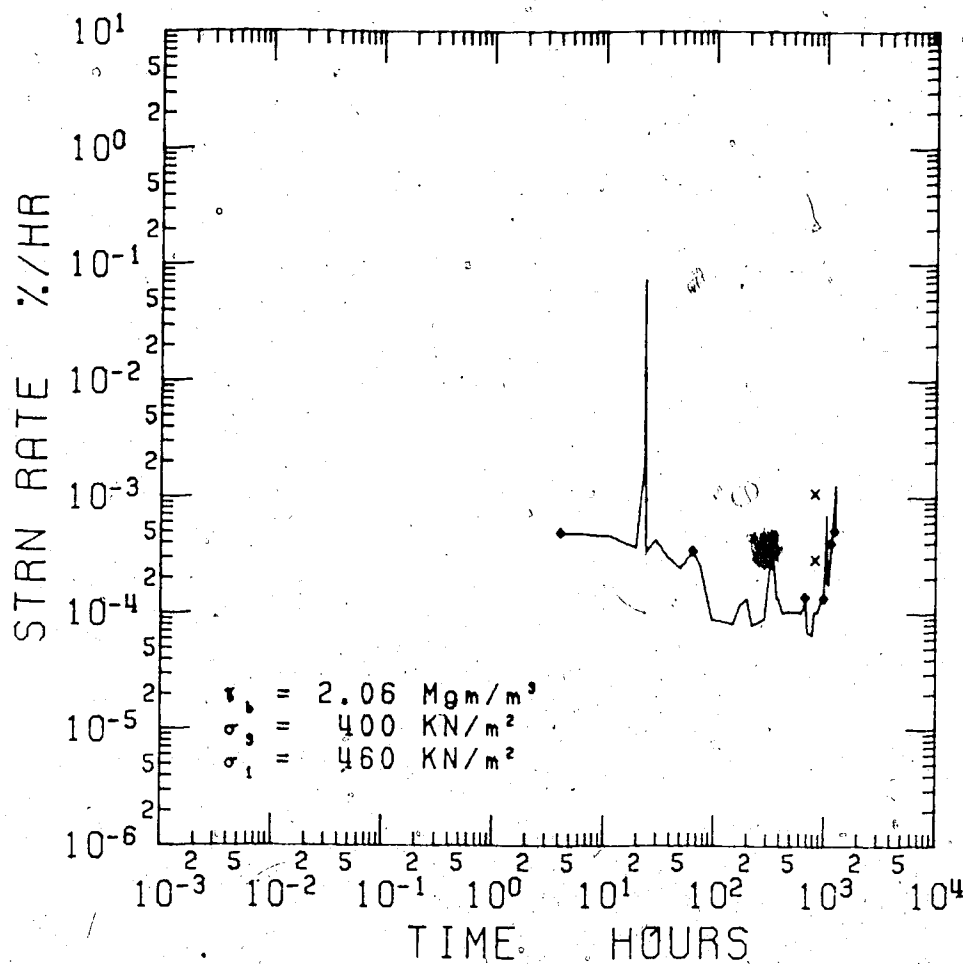


Figure D.41 Triaxial Creep Test 7 ( stage two of three)

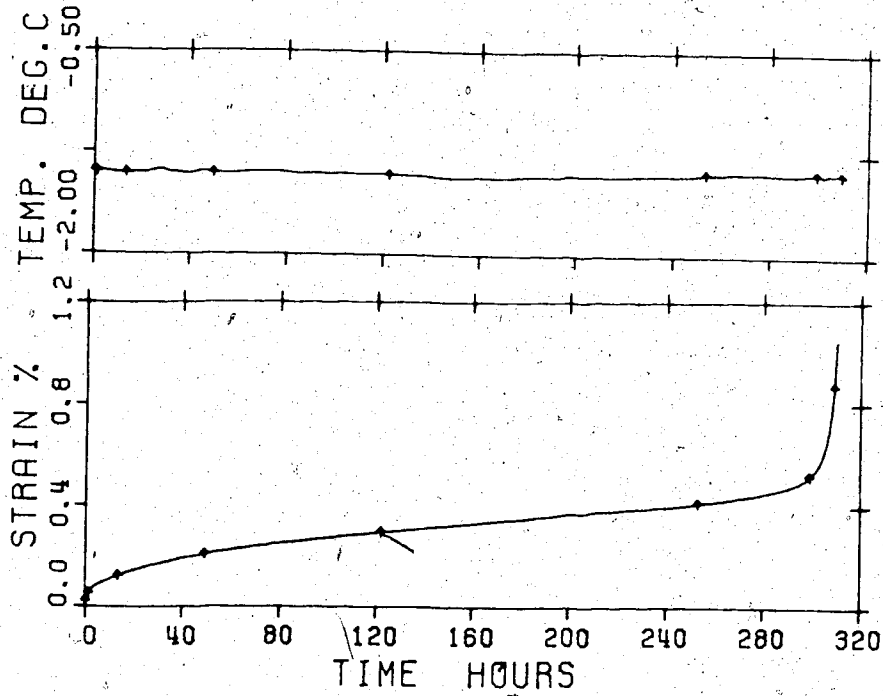
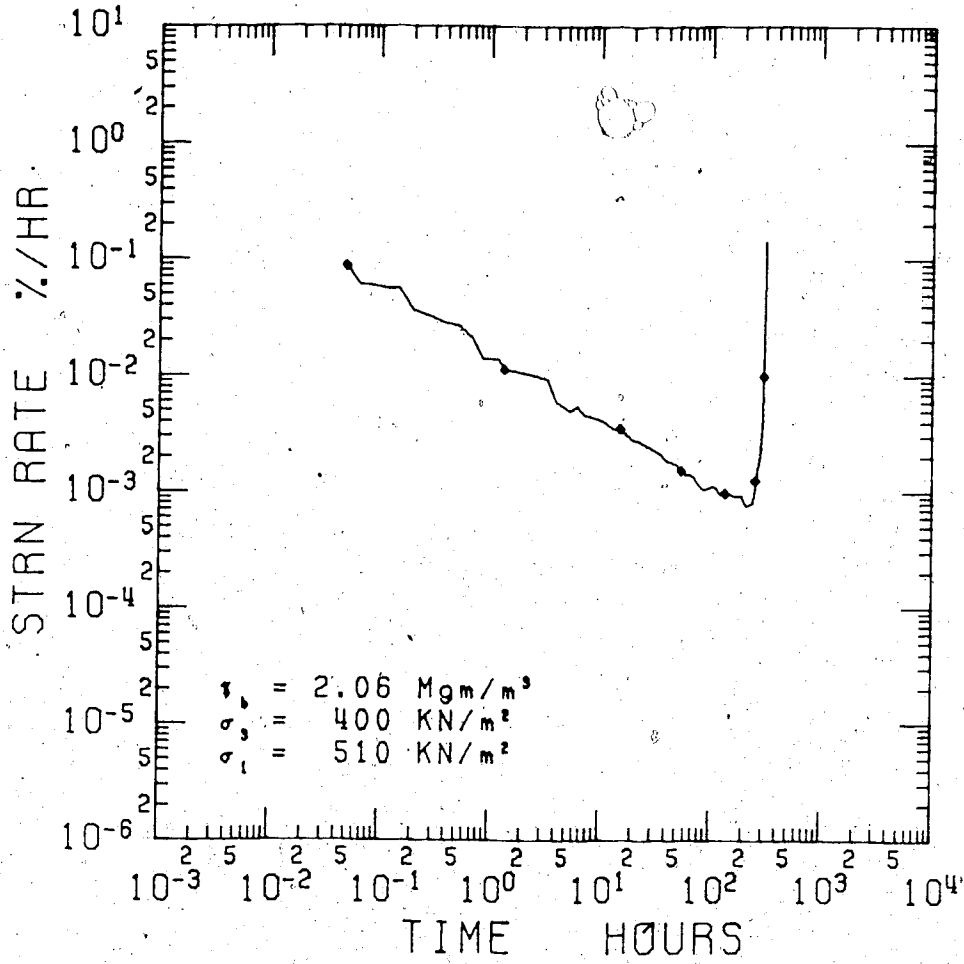


Figure D.42 Triaxial Creep Test 7 (stage three of three)

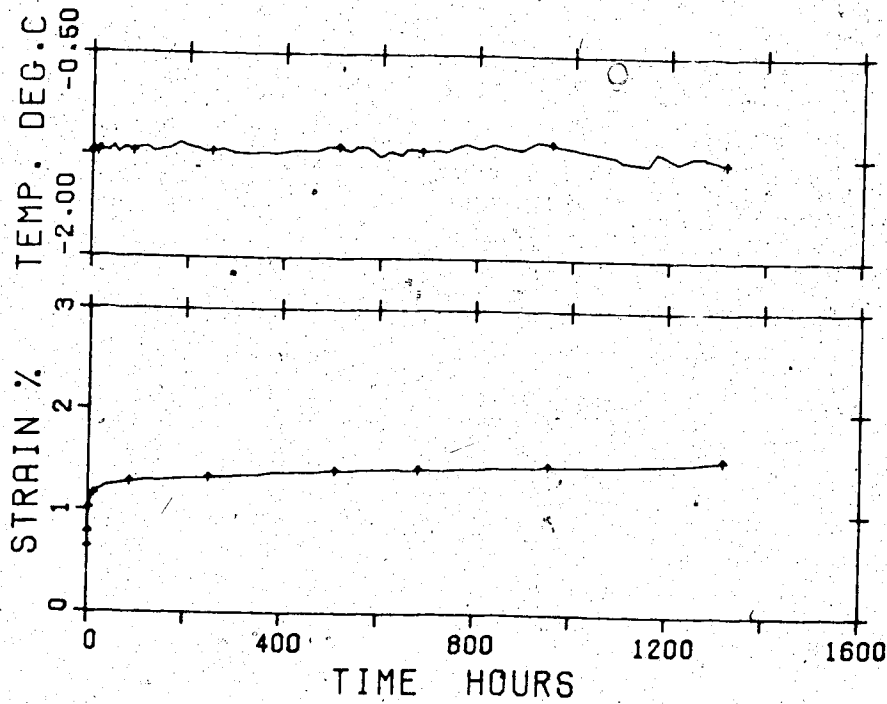
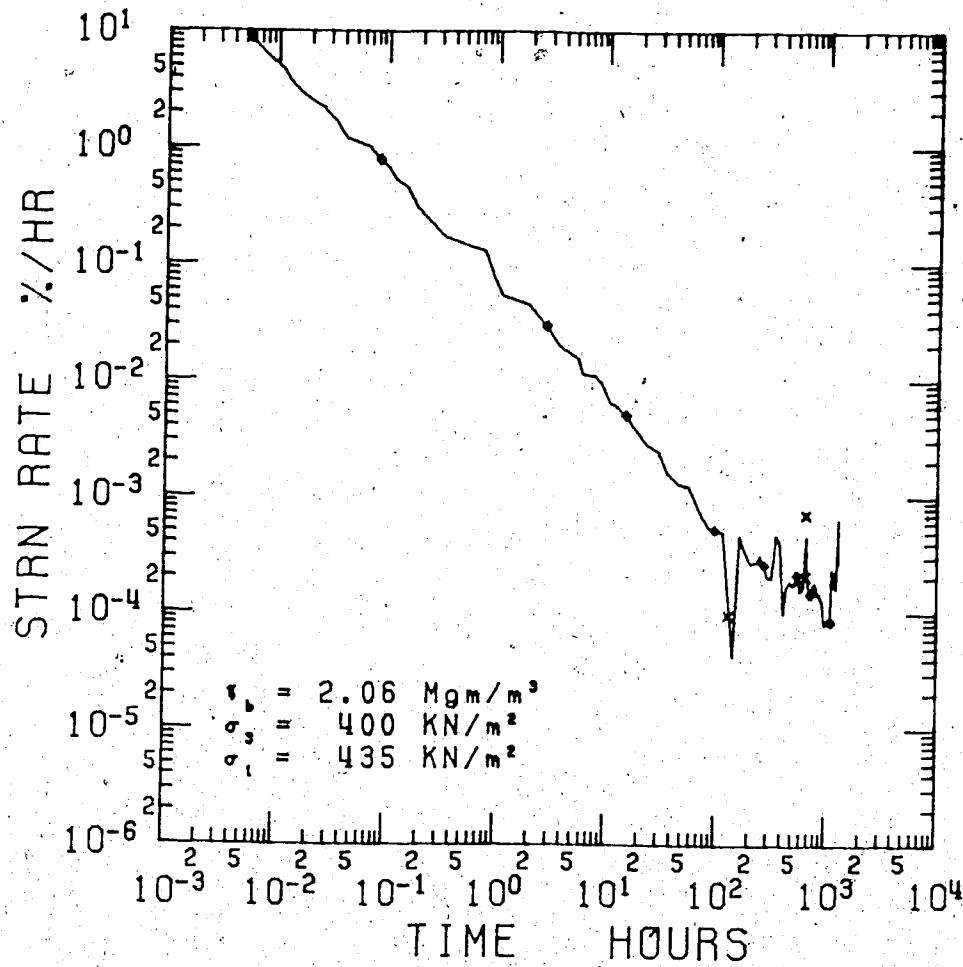


Figure D.43 Triaxial Creep Test 8 (stage one of three)

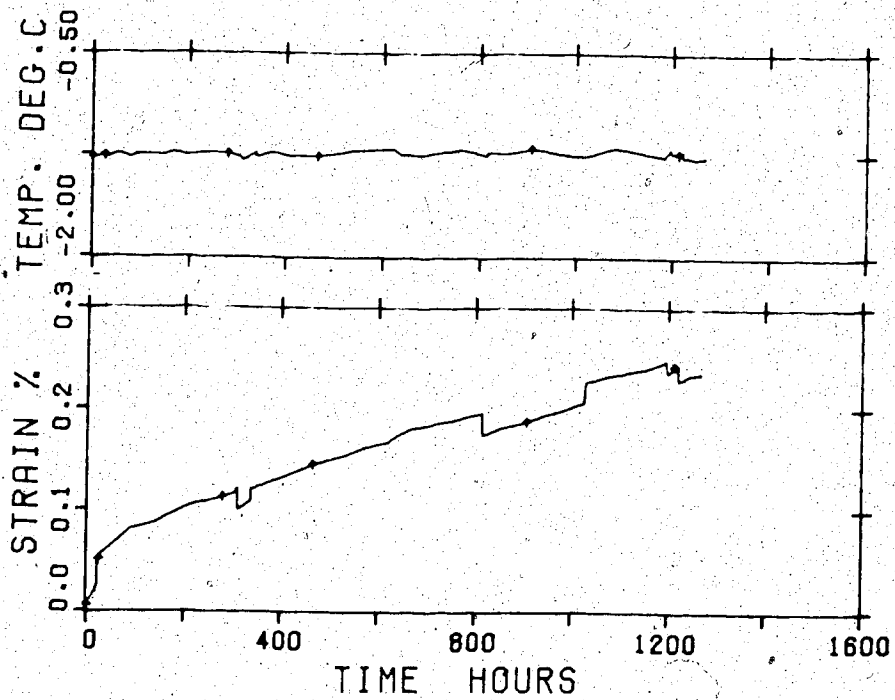
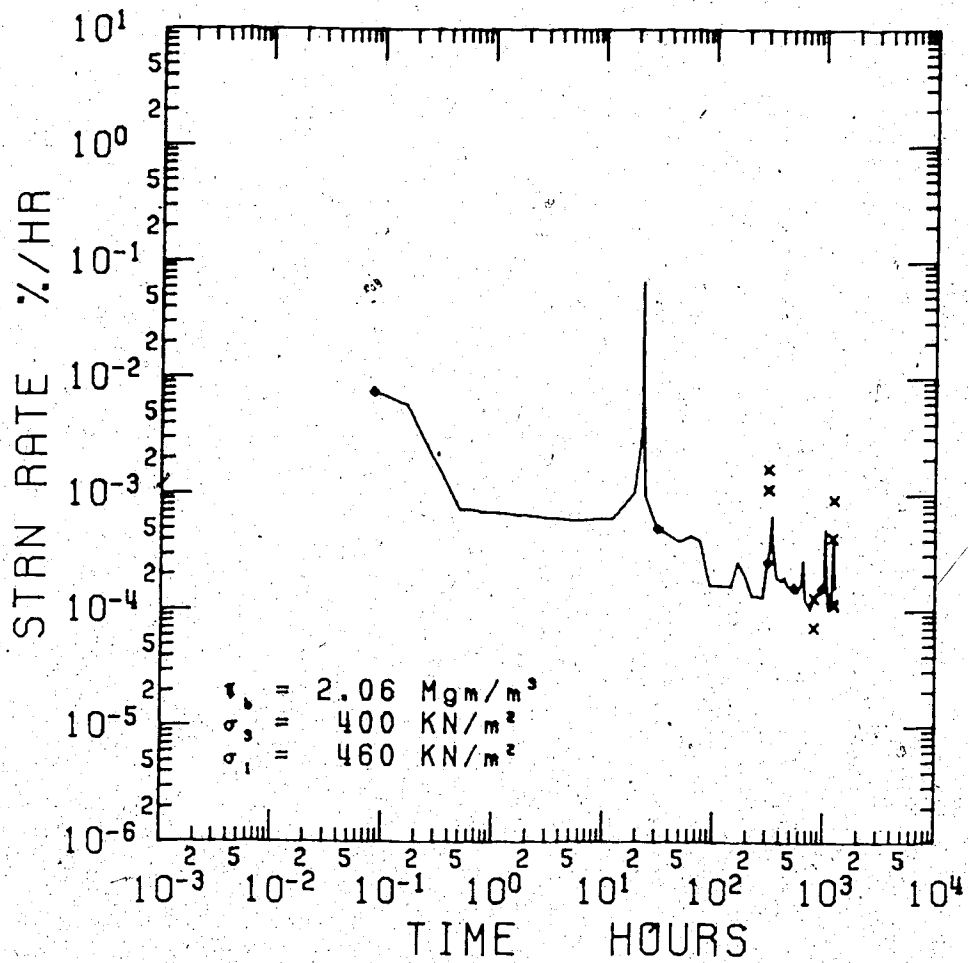


Figure D.44 Triaxial Creep Test 8 (stage two of three)



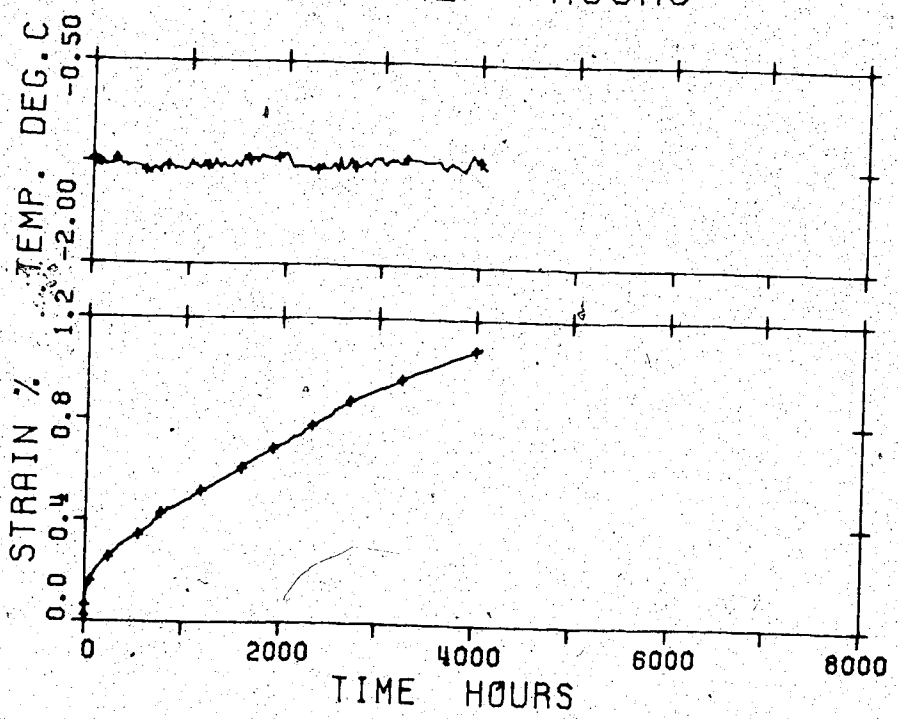
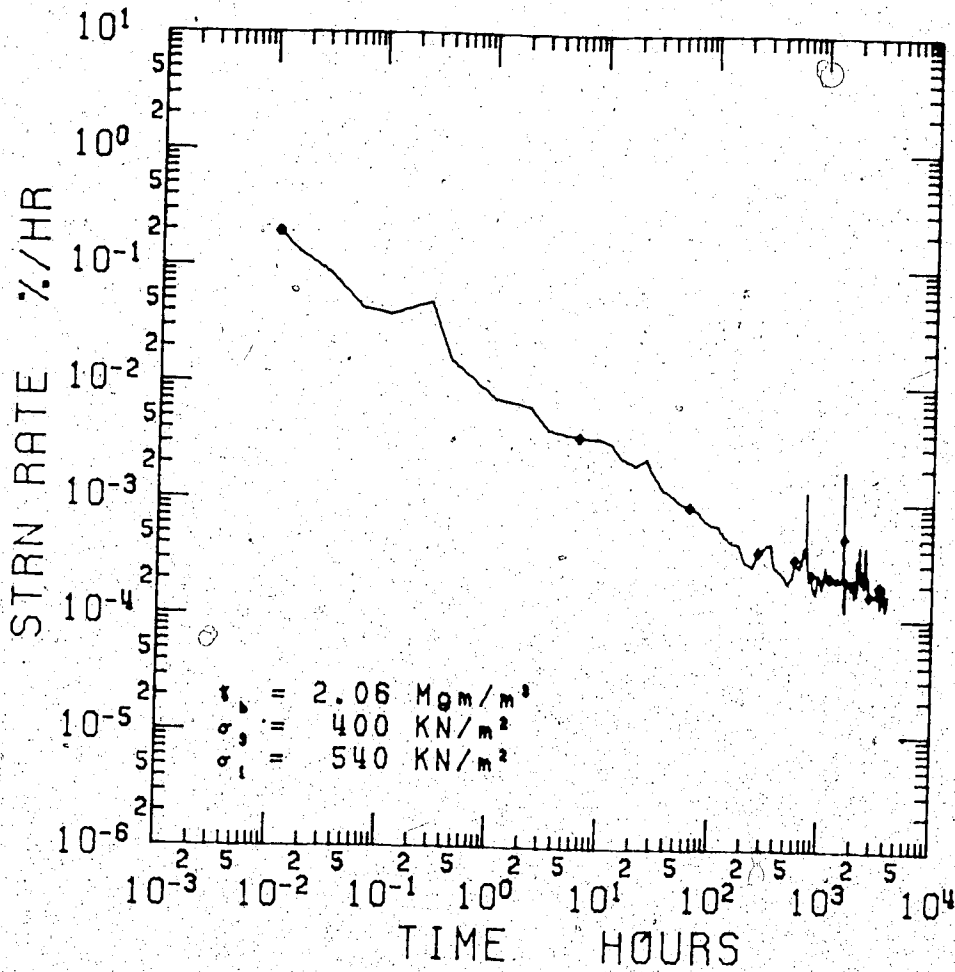


Figure D.45 Triaxial Creep Test 8 (stage three of three)

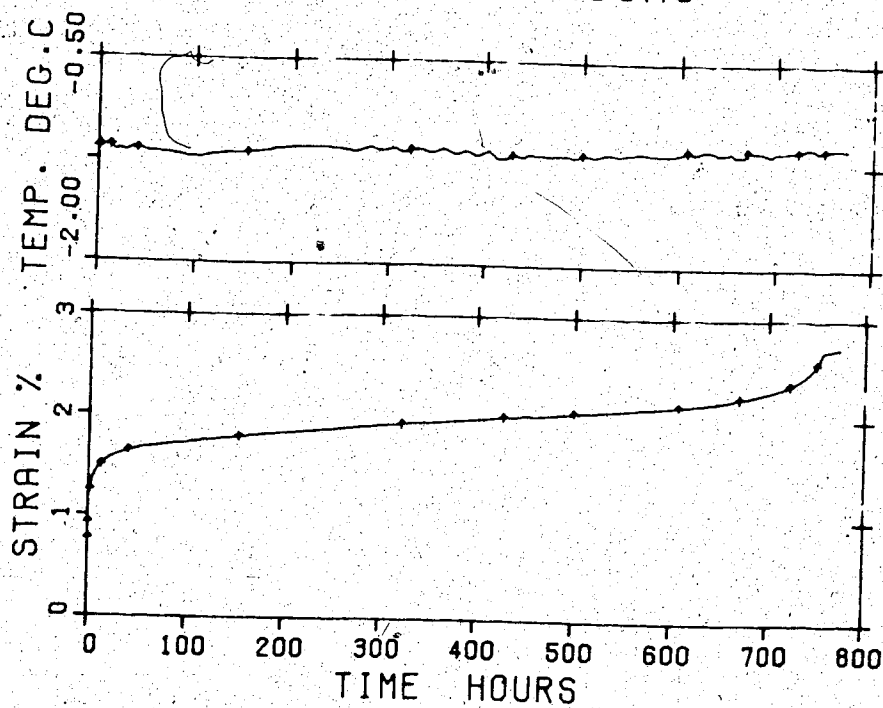
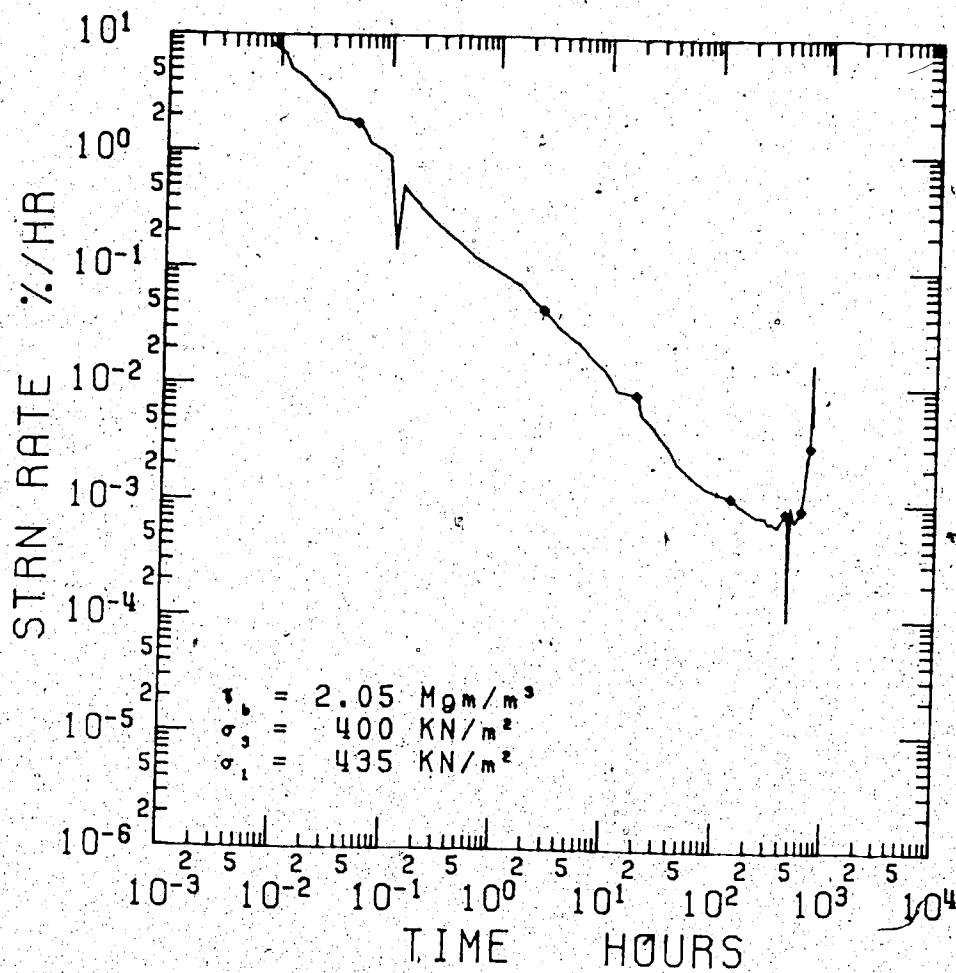


Figure D.46 Triaxial Creep Test 9

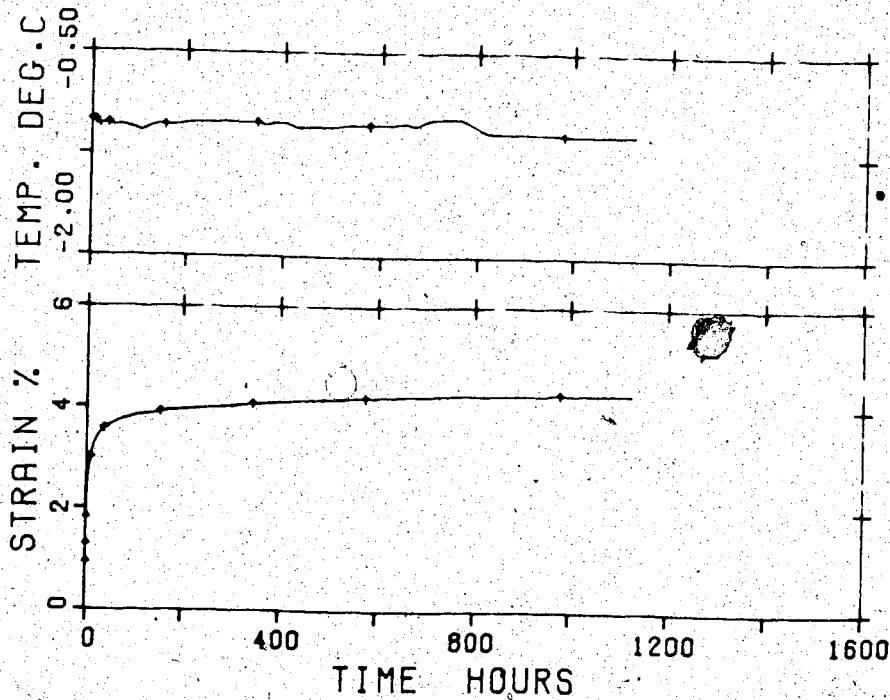
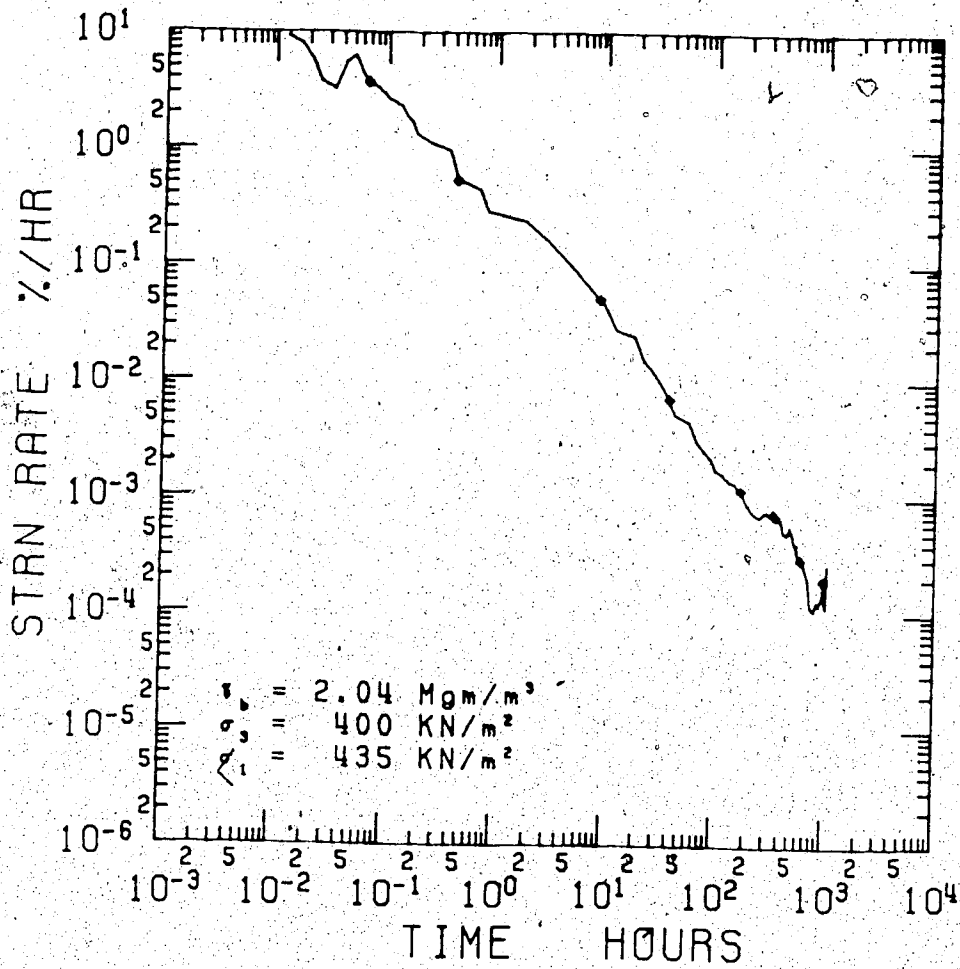


Figure D.47 Triaxial Creep Test 10 (stage one of two)

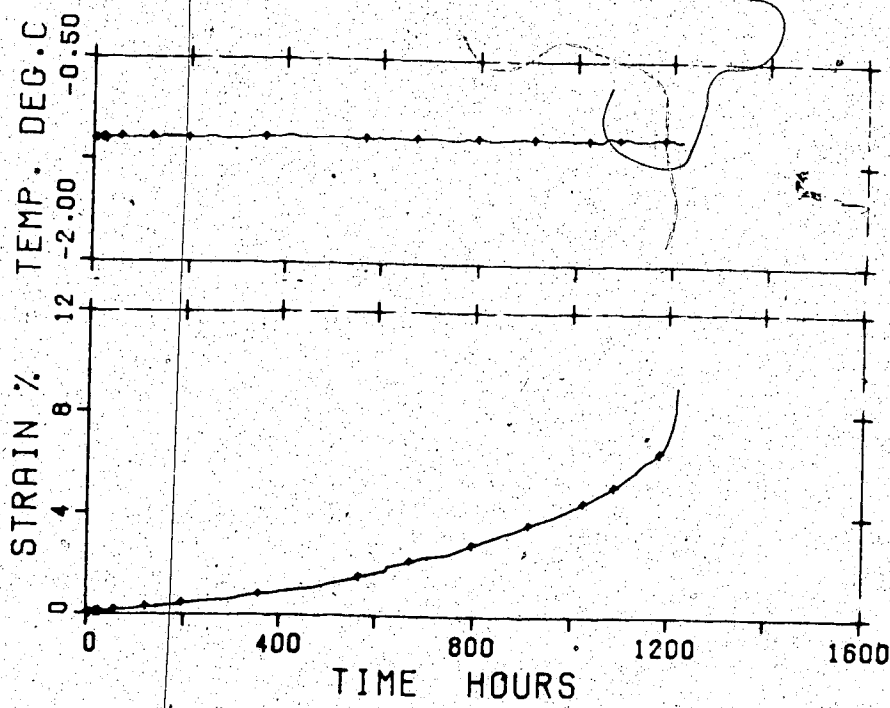
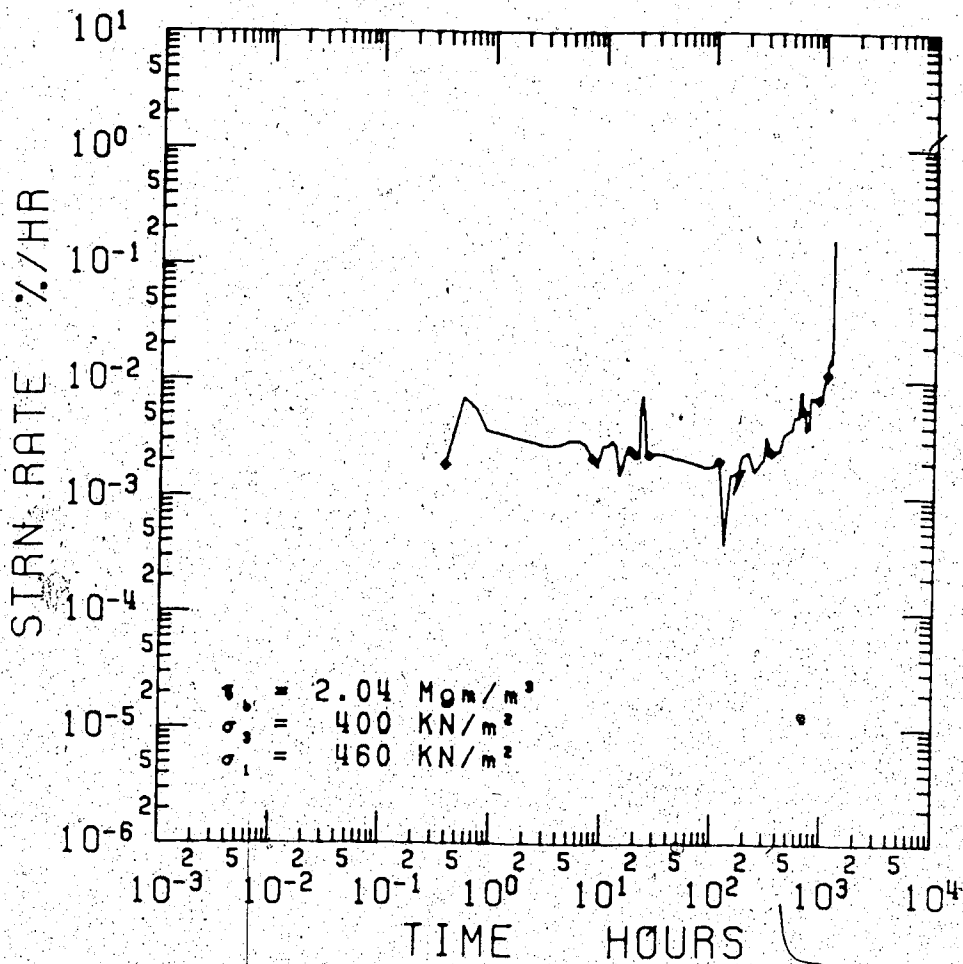


Figure D.48 Triaxial Creep Test 10 (stage two of two)

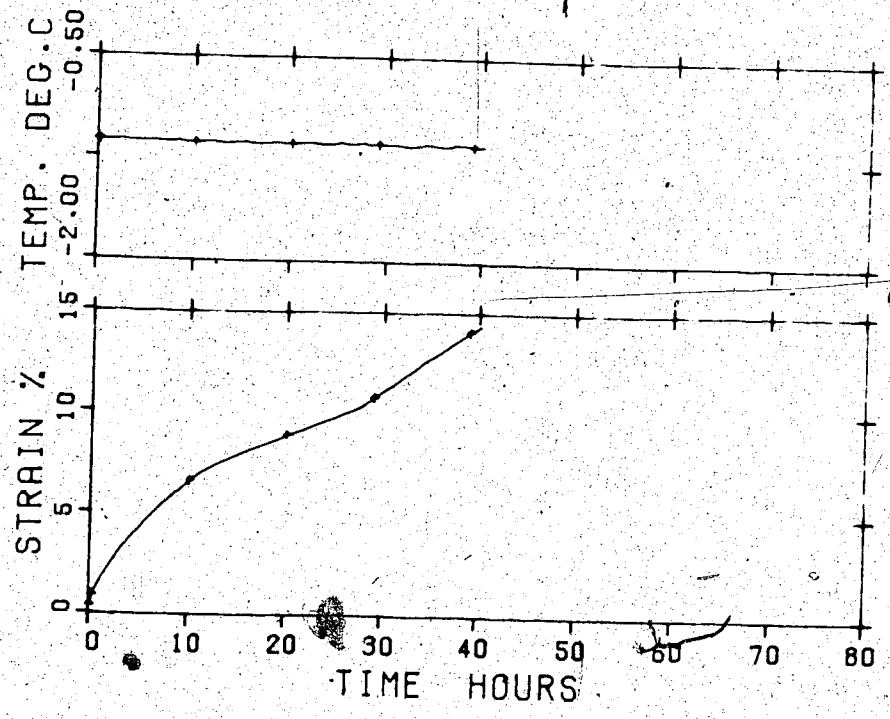
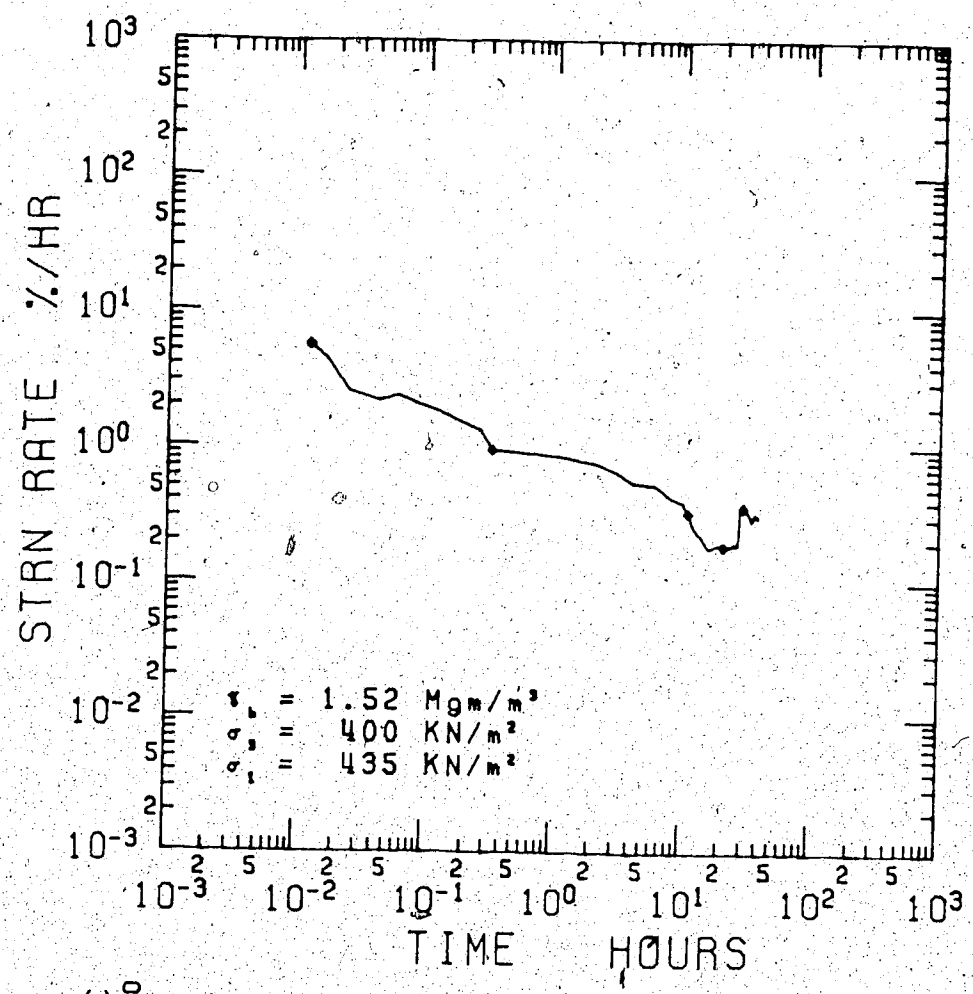


Figure D.49 Triaxial Creep Test 1

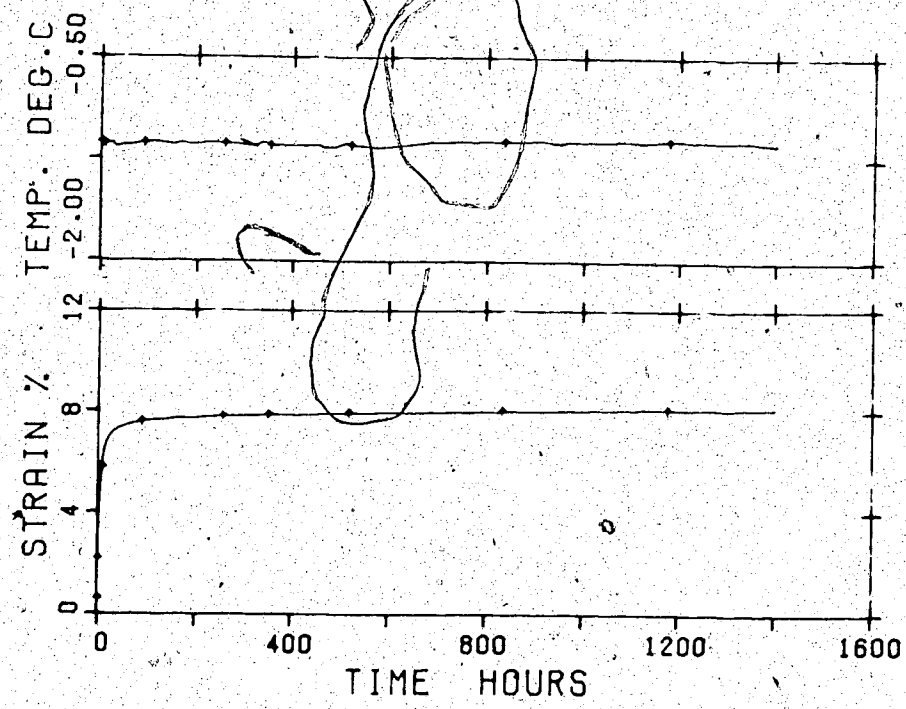
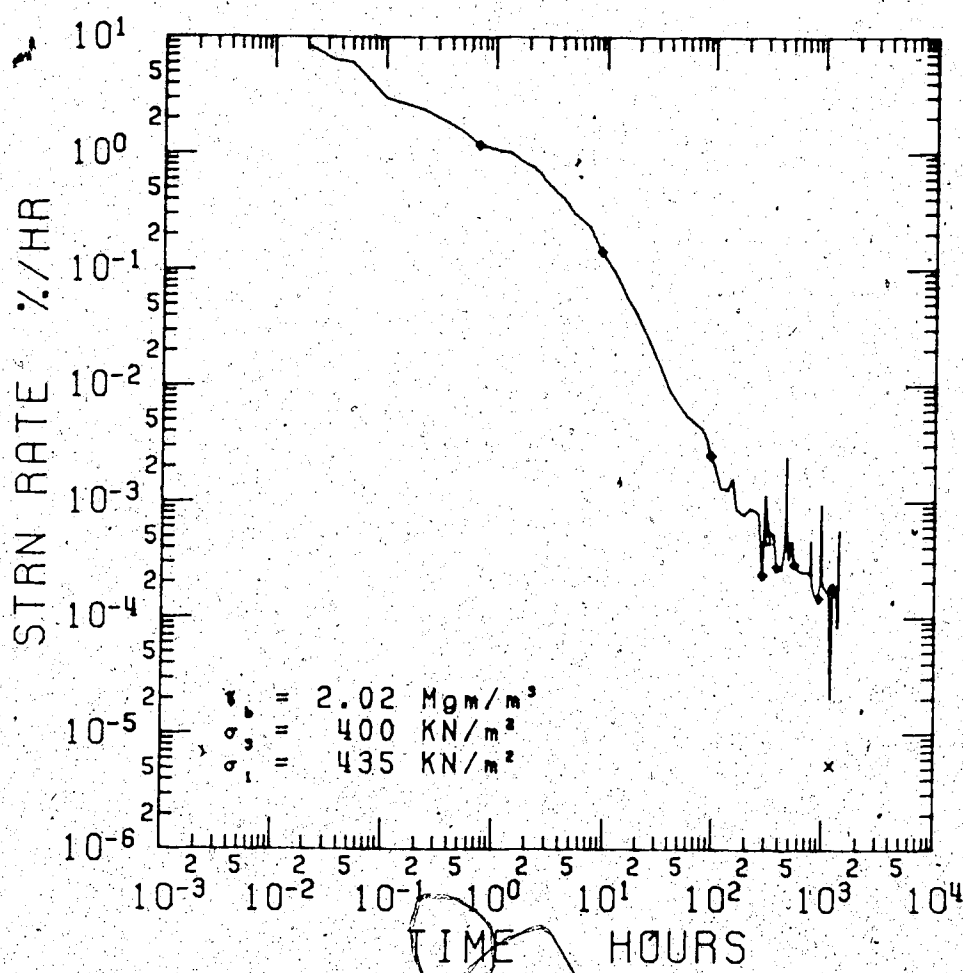


Figure D.50 Triaxial Creep Test 12 (stage one of two)

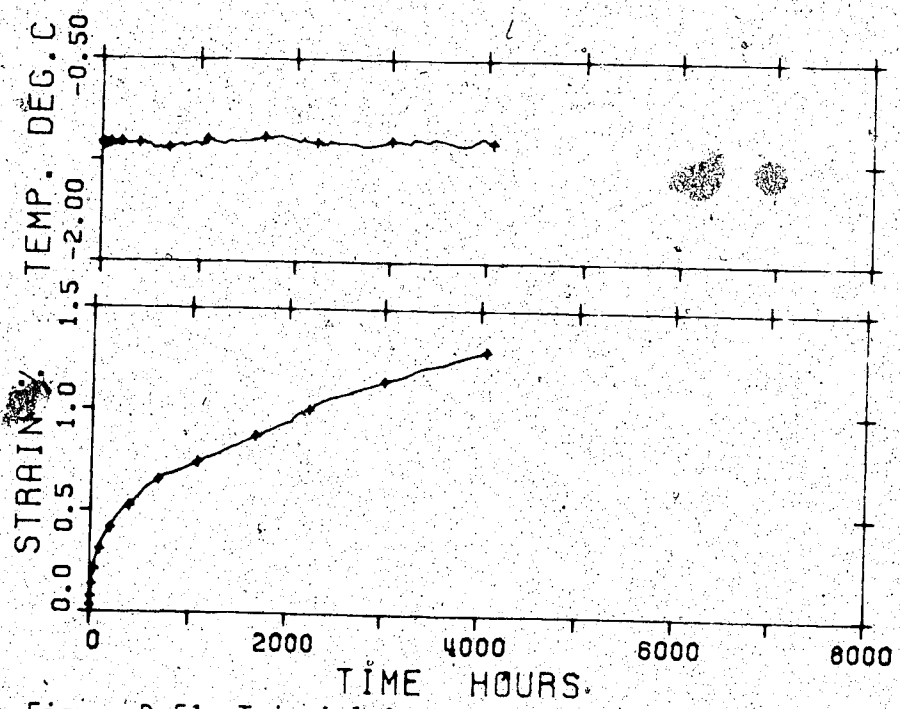
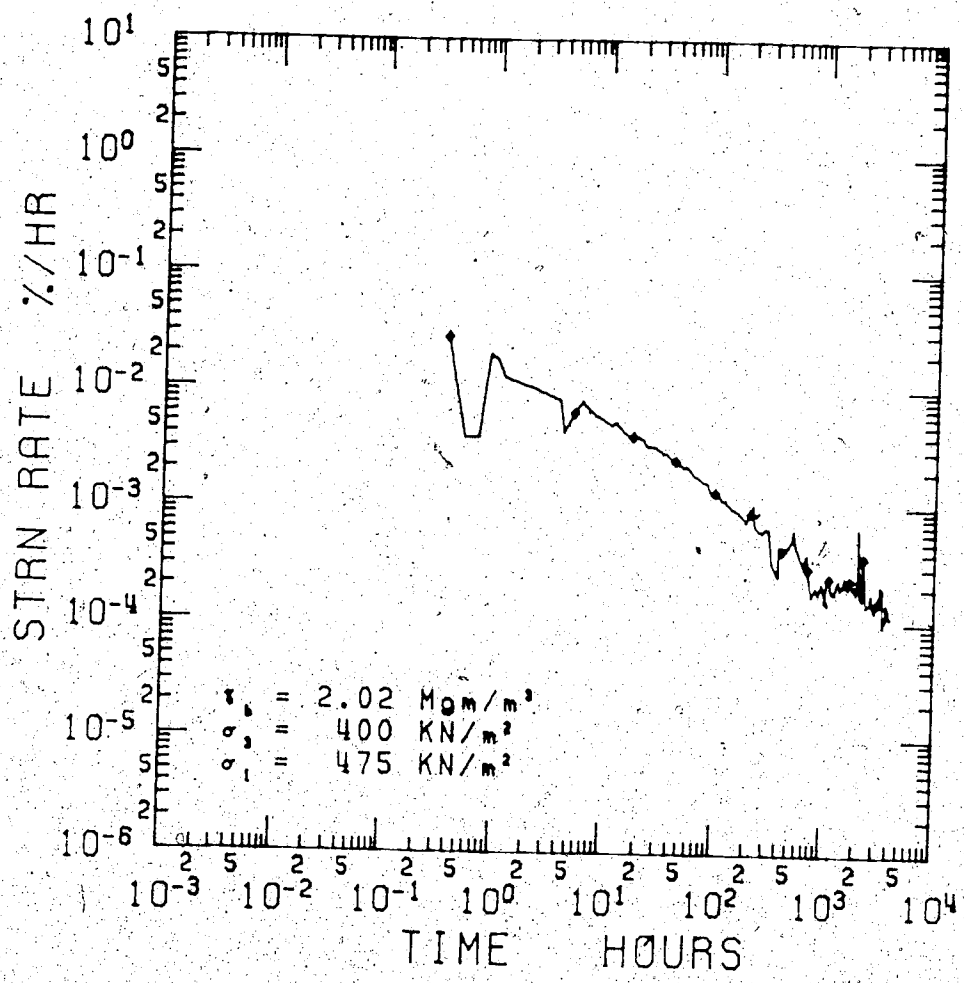


Figure D.51 Triaxial Creep Test 12 (stage two of two)

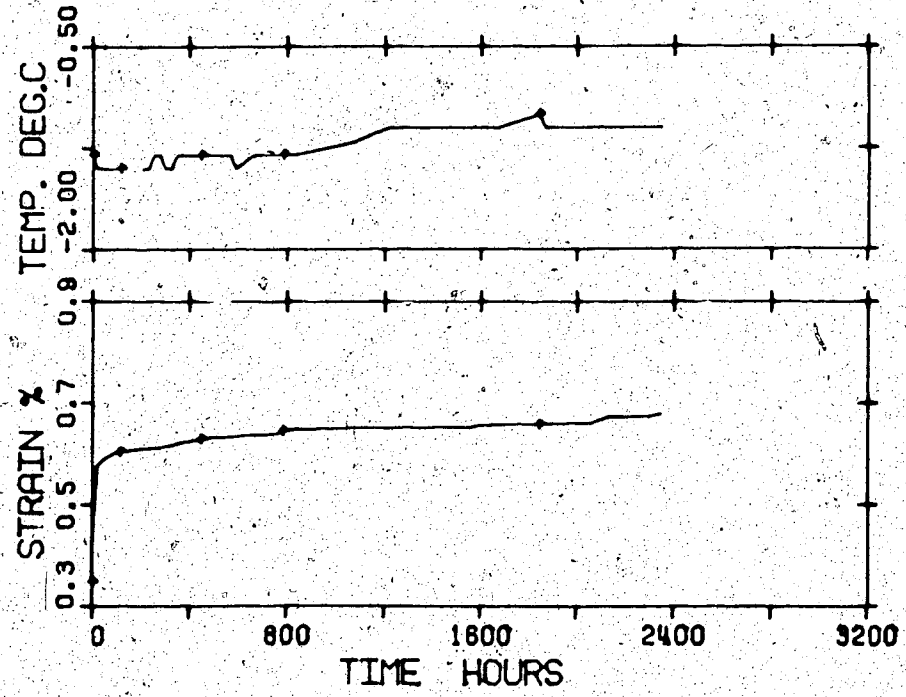
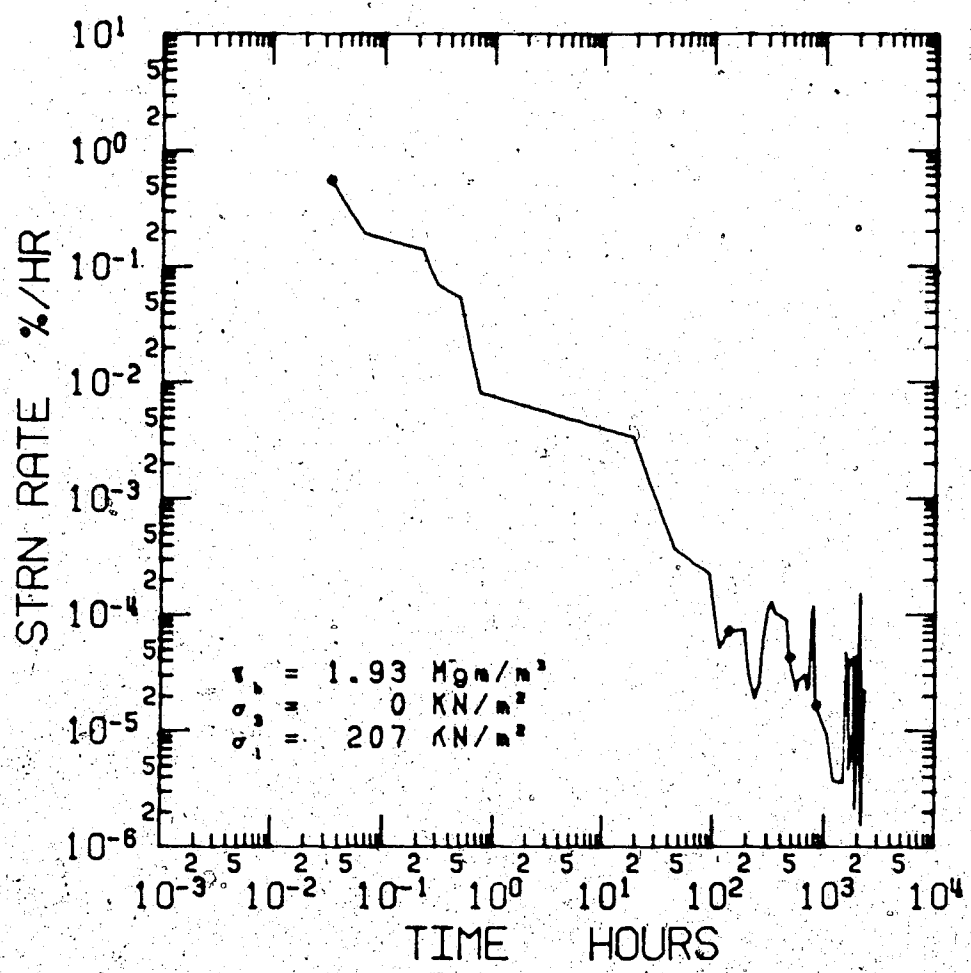


Figure D.52 Triaxial Creep Test NES 3-11



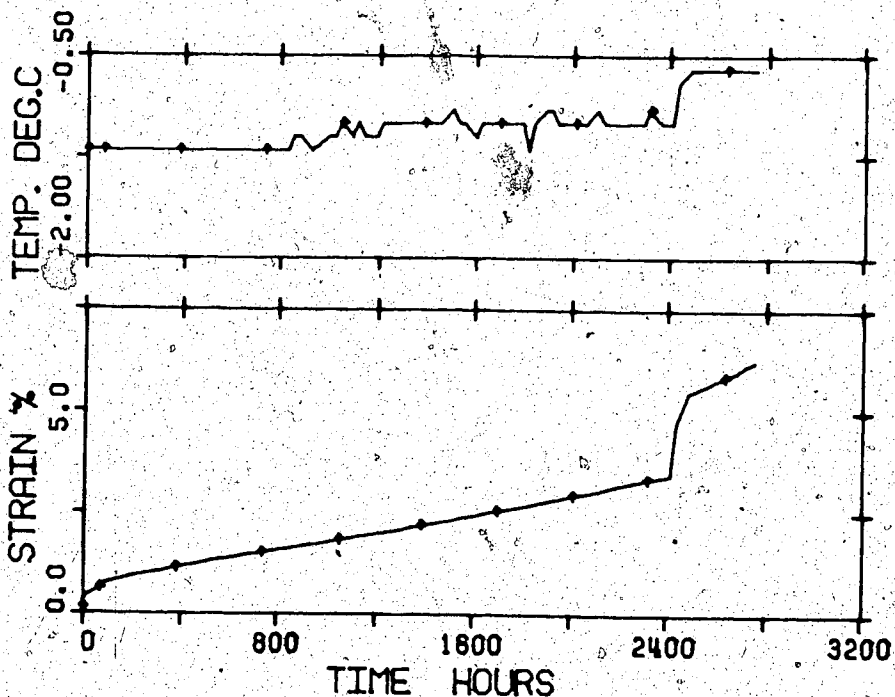
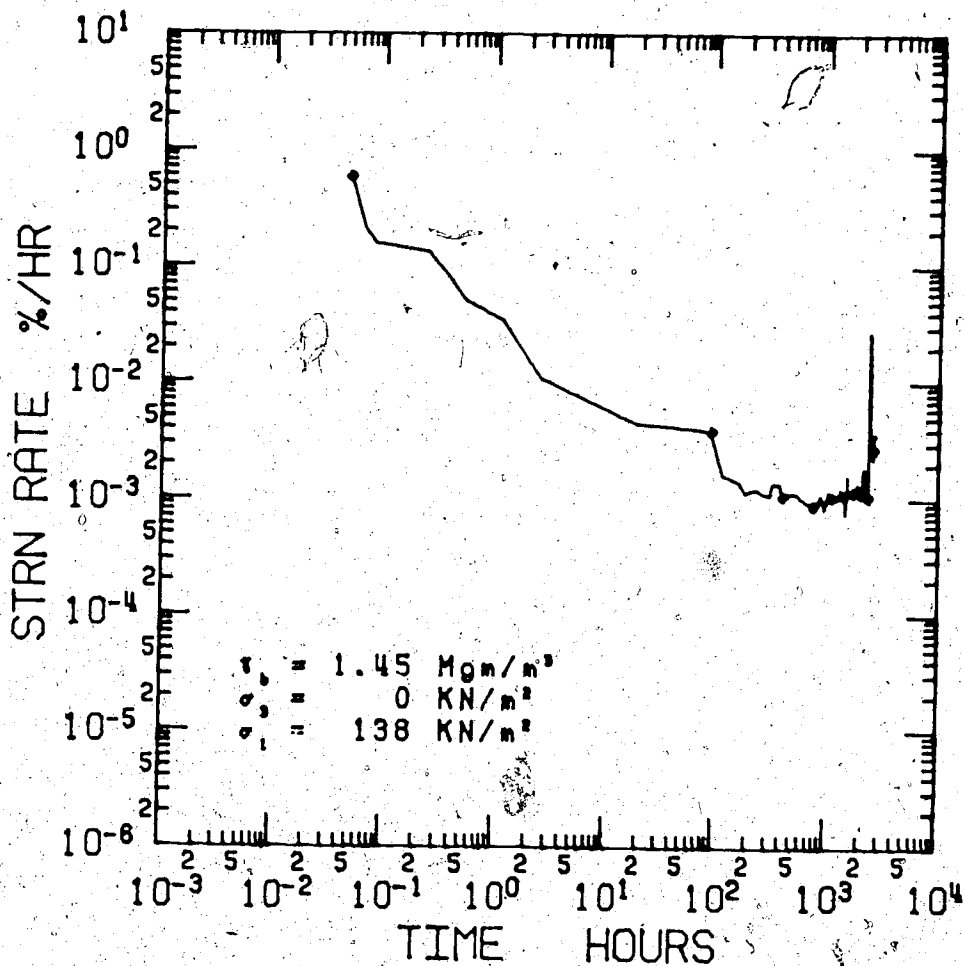


Figure D.53 Triaxial Creep Test NES 3-8

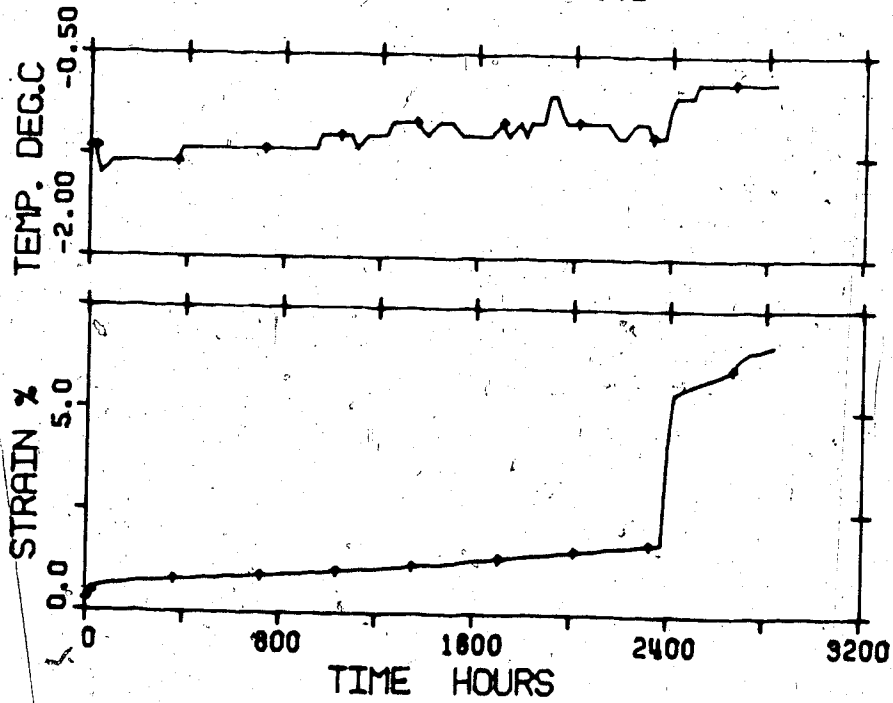
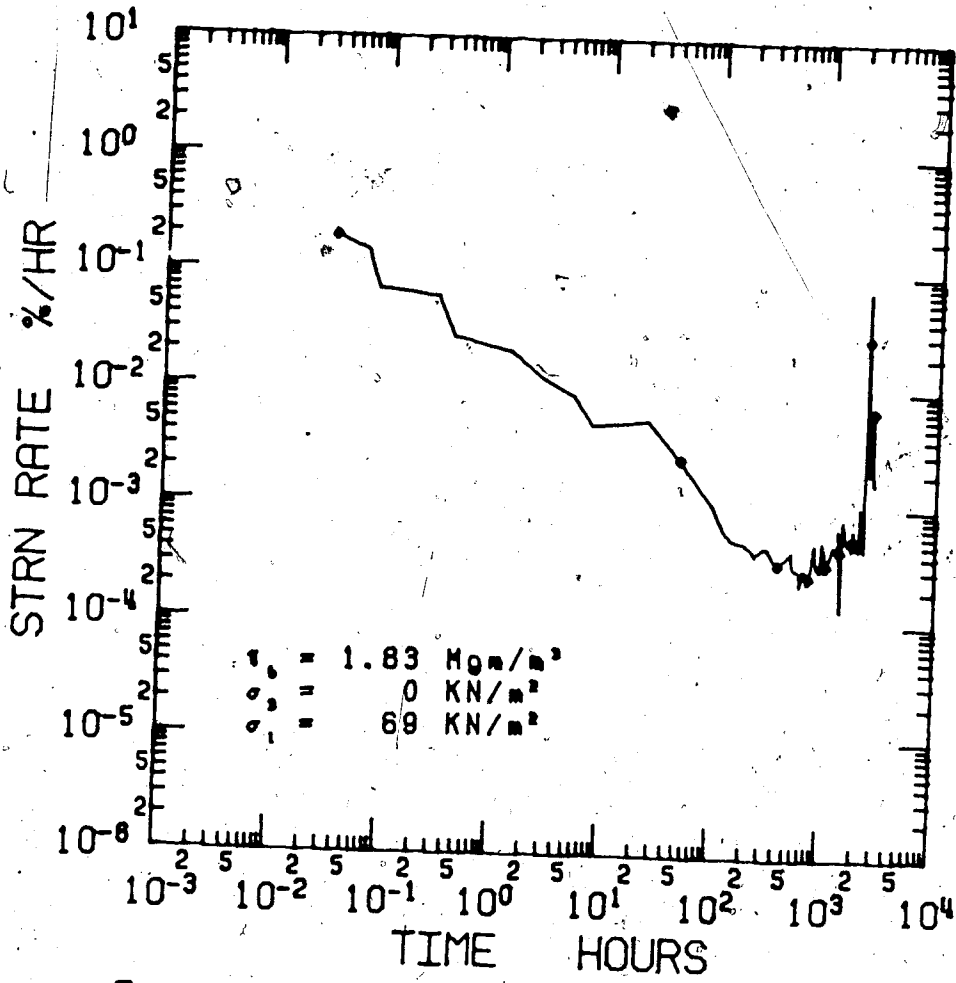


Figure D.54 Triaxial Creep Test NES 3-10